



**Politechnika  
Śląska**

**WYDZIAŁ CHEMICZNY  
KATEDRA CHEMII ORGANICZNEJ,  
BIOORGANICZNEJ I BIOTECHNOLOGII**

**ROZPRAWA DOKTORSKA**

Mgr inż. Mateusz Dawid Tomczyk

Promotor: Prof. dr hab. inż. Krzysztof Walczak

*Załącznik do rozprawy doktorskiej pt.*

**Synteza i właściwości biologiczne modyfikowanych  
interkalatorów i makrocycli**

**Publikacje P.1–P.6  
stanowiące monotematyczny cykl**

Gliwice 2023

## Publikacja P.1

Versatile synthesis of 2'-amino-2'-deoxyuridine derivatives with a 2'-amino group carrying linkers possessing a reactive terminal functionality.

Gondela, A.; **Tomczyk, M. D.**; Przypis, Ł.; Walczak, K. Z\*.

*Tetrahedron* **2016**, 72 (36), 5626–5632.



# Versatile synthesis of 2'-amino-2'-deoxyuridine derivatives with a 2'-amino group carrying linkers possessing a reactive terminal functionality

Andrzej Gondela<sup>†</sup>, Mateusz D. Tomczyk, Łukasz Przypis, Krzysztof Z. Walczak<sup>\*</sup>

Department of Organic Chemistry, Bioorganic Chemistry and Biotechnology, Silesian University of Technology, B. Krzywoustego 4, 44-100 Gliwice, Poland

## ARTICLE INFO

### Article history:

Received 20 February 2016

Received in revised form 8 July 2016

Accepted 25 July 2016

Available online 27 July 2016

### Keywords:

2,2'-Anhydrouridine

2'-Amino-2'-deoxyuridine

Isothiocyanates

Ring opening

Fluorophores

## ABSTRACT

2,2'-Anhydrouridine has been successfully converted into the appropriate 2'-amino-2'-deoxyuridine derivatives in a reaction with isothiocyanates obtained from amino acids or  $\alpha,\omega$ -diaminoalkanes. The initially formed oxazolidine-2-thione ring is cleaved under basic conditions into the corresponding 2'-amino(substituted)-2'-deoxyuridine derivatives. The implemented additional terminal functionality in the substituent attached to the 2'-amino group allows further modifications with e.g., fluorophore moiety.

© 2016 Elsevier Ltd. All rights reserved.

## 1. Introduction

Since the discovery of puromycin, an amino nucleoside that inhibits protein synthesis, the activity of nucleosides possessing an amino group in the sugar moiety is well documented and several methods of their synthesis have been developed. The activity of 2'-amino-2'-deoxynucleosides against bacteria, viruses and mycoplasma was ascertained in both the purine and pyrimidine series.<sup>1–6</sup> The analogues of 2'-amino-2'-deoxyuridine (2AU) containing a 3'- or 2'-hydroxyamino group are cytotoxic to murine leukaemia L1210 cells.<sup>7</sup> Novel ribozymes containing 2AU instead of uridine were more active in *in vitro* ligation of oligodeoxynucleotides.<sup>8–11</sup>

The analogues of 2AU 5'-diphosphate were considered to be agonists of the human P2Y6 receptor, a member of the G-protein coupled receptors.<sup>12–14</sup> Another practical application of amino nucleosides related to the presence of an amino group, is their usage as a conjugation site for the construction of linkers in oligonucleotides chemistry.<sup>15,16</sup> Using this strategy the 2-furanyl

moiety,<sup>17,18</sup> amino acids,<sup>19</sup> porphyrins<sup>20</sup> and coumarin<sup>21</sup> were incorporated into the sugar ring of 2AU and applied as components of antisense oligonucleotides able to improve drug efficacy by enhancement of resistance to chemical and enzymatic degradation.<sup>22,23</sup> Due to the importance of 2'-amino-2'-deoxynucleosides as potent therapeutics and reactants, several paths for their synthesis have been developed. Aside from the synthesis methods based on modifications of the monosaccharide molecule before coupling with the nucleobase, there are three independent methods for the synthesis of 2'-amino-2'-deoxynucleosides exploiting the transformation of uridine and its derivatives. The first one relies on substitution of a leaving group by the phthalimide ion, and subsequent cleavage with hydrazine.<sup>10,24</sup> In another approach, 2,2'-anhydrouridine upon treatment with sodium azide, afforded the 2'-azido-2'-deoxy-derivative. Catalytic reduction of the azido group gave the desired 2'-aminoderivative.<sup>25–28</sup> As both of these reactions occur with inversion of configuration on the atom bearing the leaving group the starting derivatives should possess the *D-arabino* configuration, which in the course of reaction is inverted into *D-ribo*. In the third method the 3'-OH group of 2,2'-anhydrouridine, under treatment with an excess of trichloroacetonitrile, afforded 3'-O-trichloroacetimidate, which under heating in the presence of catalytic amounts of triethylamine easily formed an intramolecular cyclic product, oxazoline.<sup>29–31</sup>

<sup>\*</sup> Corresponding author. Fax: +48 32 2372094; e-mail addresses: [agondela@gmail.com](mailto:agondela@gmail.com) (A. Gondela), [Krzysztof.Walczak@polsl.pl](mailto:Krzysztof.Walczak@polsl.pl) (K.Z. Walczak).

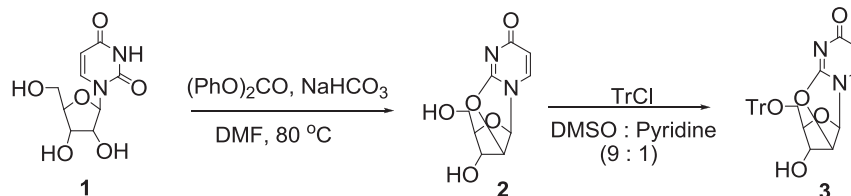
<sup>†</sup> Present address: Selvita S.A., Bobrzyńskiego 14, 30-348 Kraków, Poland.

The oxazoline when treated with ethanolic sodium hydroxide initially forms the 2'-*N*,3'-*O*-oxazolidin-2-one intermediate, which on prolonged heating gave 2'-amino-2'-deoxyuridine in 70–80% yield.<sup>30</sup>

In this report we present another approach involving the use of 5'-*O*-trityl-2,2'-anhydrouridine, which under basic conditions, upon treatment with the appropriate isothiocyanates (prepared from the methyl esters of amino acids or mono-protected  $\alpha,\omega$ -diaminoalkanes), afforded the corresponding tetrahydrofuro[3,4-*d*]-oxazole-2(3*H*)-thione derivatives. We explored two ways for the preparation of the final products. In the first one, tetrahydrofuro[3,4-*d*]-oxazole-2(3*H*)-thiones were transformed by a ring opening reaction into *N*-substituted 2'-amino-2'-deoxy-5'-*O*-trityluridine derivatives under basic conditions. In the case of amino acid derivatives under applied conditions, the methyl ester group is also hydrolysed. The opposite sequence of reactions was applied in the case of *N*-Boc derivatives; the trityl protection was done prior to the oxazole-2(3*H*)-thione ring cleavage. In both cases the yield of desired 2'-amino(substituted)-2'-deoxyuridine is satisfactory.

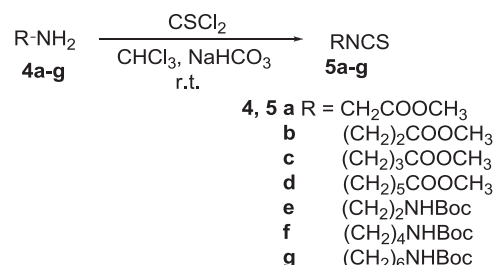
## 2. Results and discussion

The starting 2,2'-anhydrouridine **2** was prepared according to the known method<sup>30</sup> avoiding to use of HMPA. Commercially available uridine was reacted with diphenyl carbonate in the presence of sodium bicarbonate in DMF solution at 80 °C. Reaction occurred smoothly (2 h to complete) and **2** was isolated in 90% yield (Scheme 1). For the protection of the 5'-hydroxyl group, the trityl group was selected due to its stability under basic conditions. Tritylation was performed according to known reported method,<sup>32</sup> with slight modification. The reaction was carried out in a mixture of anhydrous DMSO and pyridine in the ratio 9 : 1 (*v* : *v*) at room temperature. The 5'-*O*-trityl-2,2'-anhydrouridine **3** was obtained in 73% yield. At the same time in parallel experiments the second reactants, isothiocyanates derived from the compounds possessing a primary amino group, were synthesized. There are several methods for the transformation of primary amines into isothiocyanates. Usually carbon disulphide<sup>33,34</sup> or thiophosgene<sup>35</sup> is used as a source of thiocarbonyl group. As the amino group donors we selected methyl esters of amino acids and  $\alpha,\omega$ -diaminoalkanes. In the latter, one of the amino groups was protected as the *N*-Boc derivative. Initially amino acids were reacted with methanol in the presence of thionyl chloride giving the methyl esters as their hydrochlorides in the crystal form.<sup>36</sup> Mono protected NH-*Boc*  $\alpha,\omega$ -diaminoalkanes were received from commercial sources.



Scheme 1. Synthesis of 5'-*O*-trityl-2,2'-anhydrouridine.

The preparation of isothiocyanates was performed in a two-phase system. A suspension of the selected amino compound **4a–g** in chloroform and an aqueous saturated solution of sodium bicarbonate, was treated with an excess of thiophosgene (1.5 equiv) at room temperature (Scheme 2). The progress of reaction was



Scheme 2. Synthesis of isothiocyanates derived from amino compounds.

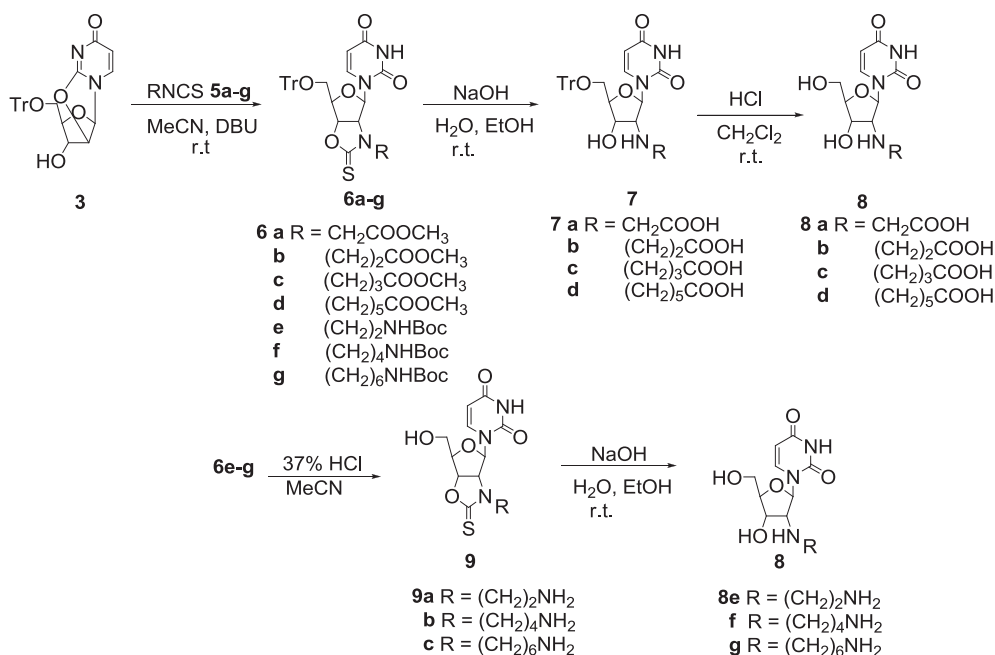
monitored by TLC (30% EtOAc : *n*-hexane) and after disappearance of the amino compounds the reaction mixture was diluted with cold water.

Work up and purification on silica gel gave the appropriate isothiocyanates **5a–g** in yields of 58%–75% and with sufficient purity for the next step. The reaction of 2, 2'-anhydrouridine **3** with isothiocyanates **5a–g** was carried out in a solution of acetonitrile in the presence of 1,8-diazabicyclo[5.4.0]undec-7-ene (DBU) as a base (Scheme 3). The isothiocyanates and base were used in a twofold excess with respect to anhydrouridine **3**. The reaction was carried out at room temperature and finished after disappearance of the uridine substrate (TLC, 5% MeOH : CHCl<sub>3</sub>).

Purification using column chromatography (20% MeOH : CH<sub>2</sub>Cl<sub>2</sub>) gave the desired tetrahydrofuro[3, 4-*d*]-oxazole-2(3*H*)-thione derivatives **6a–g** in yields of 54–87%. The key step of the synthetic pathway involved cleavage of the [3,4-*d*]-oxazole-2(3*H*)-thione ring in uridine derivative **6**. In the case of compounds **6a–d**, having a methyl alkanoate back bone, the oxazole-2(3*H*)-thione ring was easily opened when treated with an aqueous solution of sodium hydroxide at elevated temperature. Under these conditions the ester group present on the 2'-*N*-alkyl terminal position was also cleaved and **7** were obtained in satisfactory yields of 65–73%. Deprotection of the 5'-hydroxyl group was carried out at room temperature under acidic conditions giving the final products **8a–d** in good yield. For compounds **6e–g** we explored another approach for the preparation of the final products. According to our observation the oxazole-2(3*H*)-thione ring in **6** is resistant under acidic conditions at room temperature. This fact permits removal of both protecting groups, carbamate present in the *N*-Boc fragment of **6**, and the 5'-*O*-trityl ether simultaneously. When **6e–g** was treated with hydrochloric acid in acetonitrile solution at room temperature, both *N*-Boc and trityl protecting groups were removed and **9a–c** derivatives were isolated in good yield. The final products **8e–g** were obtained by

oxazole-2(3*H*)-thione ring opening in the presence of base in yields of 88%–92% (Scheme 3).

The formation of **6** can be explained as a result of reaction sequences initiated by the reaction of the 3'-OH group of the anhydrouridine with isothiocyanate. The initially formed



**Scheme 3.** Synthesis of 2'-(*N*-substituted)amino-2'-deoxyuridine derivatives.

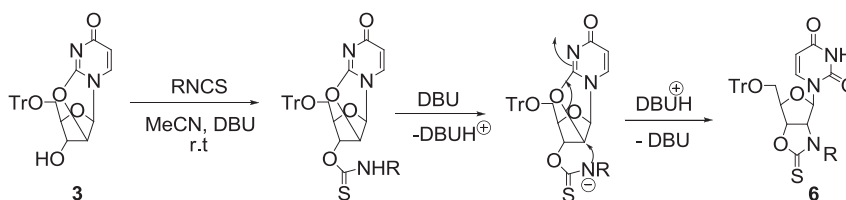
thiocarbamate is deprotonated by DBU resulting in intramolecular nucleophilic attack on the carbon C-2' of anhydrouridine. The *erythro* configuration of the 3'-OH group in **3** determines the side of attack by the deprotonated thiocarbamate unit and subsequent formation of the [3,4-*d*]-oxazole-2(3*H*)-thione ring (Scheme 4). A similar intermediate, namely tetrahydrofuro[3,4-*d*]oxazol-2(3*H*)-one was postulated in the reaction of 2,2'-anhydrouridine with *O*-benzyl hydroxylamine in the presence of *N,N'*-carbonyldiimidazole.<sup>29</sup> The resulting 3'-*O*-(benzyloxyamino)carbonyl derivative was converted into the corresponding 2'-(benzyloxyamino)-2'-*N*,3'-*O*-carbonyl derivative under treatment with catalytic amounts of DBU.

Finally we explored the usefulness of the obtained uridine derivatives **8** in the synthesis of conjugates with a common fluorophore (Scheme 5).<sup>37,38</sup> Thus **8g** reacted with benzo[*de*]

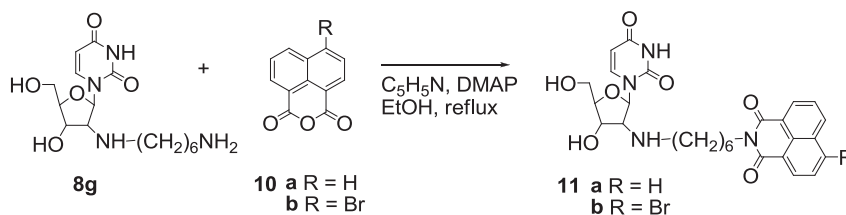
isochromene-1,3-dione **10a** and its 6-bromo derivative **10b** at elevated temperature to give the corresponding imide conjugates **11** in very good yield.

### 3. Conclusion

We have devised a new approach for the synthesis of 2'-amino-2'-deoxyuridine derivatives where the amino group bears a linker with an additional functional group located on the terminal carbon atom, either a carboxylic or amino group. By the choice of the order of deprotection steps is possible to selectively remove the trityl and *N*-Boc protecting groups and retain the oxazolidine-2-thione ring. Under basic conditions the oxazolidine-2-thione ring is cleaved together with the ester group present in the 2'-NH-linker, whereas the 5'-*O*-trityl and *N*-Boc groups are retained. The terminal



**Scheme 4.** Formation of tetrahydrofuro[3,4-*d*]-oxazole-2(3*H*)-thione derivatives.



**Scheme 5.** Introduction of fluorophore unit into 2'-aminofunctionalized uridine.

functional group can be used for further functionalization of the uridine e.g., conjugation with a fluorophore unit.

## 4. Experimental

### 4.1. General

All reagents and solvents were of analytical grade, obtained from commercial suppliers and used without further purification except for  $\text{CH}_2\text{Cl}_2$ , which was distilled prior to use and MeCN purified by distillation from  $\text{P}_2\text{O}_5$  and dried through storage over activated 3A molecular sieves. Anhydrous pyridine was dried over KOH pellets. Anhydrous  $\text{Et}_3\text{N}$  was dried through storage over activated 4A molecular sieves. All reactions were monitored by TLC using silica-gel-coated aluminium plates with a fluorescence indicator ( $\text{SiO}_2$  60,  $F_{254}$ ) and were visualized by UV light. Column chromatography was performed using silica gel packed columns (particle size 0.040–0.063 mm, Merck).  $^1\text{H}$  NMR spectra were recorded on a Varian 600 MHz System or Agilent 400 MHz Spectrometer;  $^{13}\text{C}$  NMR spectra were recorded at 150 MHz or 100 MHz, respectively. Chemical shifts were measured relative to residual non-deuterated solvent resonances. Melting points were determined using a Boethius M HMK hot-stage apparatus. IR spectra were recorded on Nicolet 6700 FTIR Spectrometer (Thermo Scientific). High-resolution electrospray ionisation mass spectroscopy (ESI-MS) experiments were performed using a Waters Xevo G2 QTOF instrument equipped with an injection system (cone voltage 50 V; source 120 °C).

2,2'-Anhydrouridine **2**<sup>30</sup> and 5'-*O*-trityl-2, 2'anhydrouridine **3**<sup>32</sup> was obtained in yields of 89% and 75%, respectively. Methyl esters of selected amino acids were prepared according to literature data.<sup>36</sup> *N*-Boc-1,4-butanediamine and *N*-Boc-1,6-hexanediamine were purchased from Sigma–Aldrich.

### 4.2. Typical procedure for preparation of isothiocyanates **5a–g**

To a mixture of sodium bicarbonate solution (10 mL, satd aq) and  $\text{CH}_2\text{Cl}_2$  (10 mL) the hydrochloride of amino acid methyl ester **5a–d** or *N*-Boc-mono-protected  $\alpha,\omega$ -diaminoalkane (15 mmol) **4e–g** was added. The reaction mixture was cooled down to 0 °C and a solution of thiophosgene (15 mmol) in  $\text{CH}_2\text{Cl}_2$  (5 mL) was added dropwise while stirring. After 30–60 min. TLC indicated a total disappearance of substrate (TLC, 30% EtOAc/*n*-hexane). The organic layer was separated and the aqueous layer was extracted with  $\text{CH}_2\text{Cl}_2$  (3 × 10 mL). The organic extracts were collected together, dried ( $\text{Na}_2\text{SO}_4$ ) and the solvent was evaporated under diminished pressure. The residual oil was purified on silica gel (30% EtOAc/*n*-hexane) and afforded the desired isothiocyanates as viscous yellow oils.

4.2.1. *Methyl 2-isothiocyanatoacetate* **5a**.<sup>39</sup> Yield 58% (1.24 g);  $\delta_{\text{H}}$  (600 MHz,  $\text{CDCl}_3$ ) 3.84 (s, 2H), 4.26 (s, 3H);  $\delta_{\text{C}}$  (150 MHz,  $\text{CDCl}_3$ ) 166.6 (C=O), 138.4 (C=S), 53.2, 46.3; MS (ESI)  $[\text{M}+\text{H}]^+$  calcd for  $\text{C}_4\text{H}_6\text{NO}_2\text{S}$  = 132.0119, Found 132.0126;  $R_f$  (30% EtOAc/*n*- $\text{C}_6\text{H}_{14}$ ) 0.52.

4.2.2. *Methyl 3-isothiocyanatopropanoate* **5b**.<sup>39</sup> Yield 59% (1.28 g);  $\delta_{\text{H}}$  (600 MHz,  $\text{CDCl}_3$ ) 2.71 (t, 6.6 Hz, 2H), 3.75 (s, 3H), 3.82 (t, *J* 6.6 Hz, 2H);  $\delta_{\text{C}}$  (150 MHz,  $\text{CDCl}_3$ ) 170.3, 126.9, 52.2, 40.8, 34.4; MS (ESI)  $[\text{M}+\text{H}]^+$  calcd for  $\text{C}_5\text{H}_8\text{NO}_2\text{S}$  = 146.0276, Found = 146.0281;  $R_f$  (30% EtOAc/*n*- $\text{C}_6\text{H}_{14}$ ) 0.49.

4.2.3. *Methyl 4-isothiocyanatobutanoate* **5c**.<sup>40</sup> Yield 75% (1.79 g);  $\delta_{\text{H}}$  (600 MHz,  $\text{CDCl}_3$ ) 2.00–2.05 (m, 2H), 2.48 (t, *J* 7.2 Hz, 2H), 3.64 (t, *J* 6.6 Hz, 2H), 3.70 (s, 3H);  $\delta_{\text{C}}$  (150 MHz,  $\text{CDCl}_3$ ) 172.5, 130.5, 51.7, 44.3,

30.5, 25.1; MS (ESI)  $[\text{M}+\text{Na}]^+$  calcd for  $\text{C}_6\text{H}_9\text{NO}_2\text{SNa}$  = 182.0252, Found = 182.0250;  $R_f$  (30% EtOAc/*n*- $\text{C}_6\text{H}_{14}$ ) 0.47.

4.2.4. *Methyl 6-isothiocyanatohexanoate* **5d**. Yield 71% (1.99 g); FTIR [ATR,  $\nu$   $\text{cm}^{-1}$ ] 2048, 1746, 436, 1208, 1150, 1054;  $\delta_{\text{H}}$  (600 MHz,  $\text{CDCl}_3$ ) 1.43–1.48 (m, 2H), 1.65–1.75 (m, 4H), 2.40 (t, *J* 7.8 Hz, 2H), 3.53 (t, *J* 6.6 Hz, 2H), 3.68 (s, 3H);  $\delta_{\text{C}}$  (150 MHz,  $\text{CDCl}_3$ ) 173.7, 128.0, 51.6, 44.9, 33.7, 26.1, 26.0, 24.1; MS (ESI)  $[\text{M}+\text{Na}]^+$  calcd for  $\text{C}_8\text{H}_{13}\text{NO}_2\text{SNa}$  = 210.2491, Found = 210.2490;  $R_f$  (30% EtOAc/*n*- $\text{C}_6\text{H}_{14}$ ) 0.46.

4.2.5. *t*-Butyl 2-isothiocyanatoethylcarbamate **5e**.<sup>41</sup> Yield 63% (1.91 g), white solid; Mp 63–64 °C [65 °C];<sup>41</sup> FTIR [ATR,  $\nu$   $\text{cm}^{-1}$ ] 2932, 2095, 1687, 1510, 1165;  $\delta_{\text{H}}$  (400 MHz,  $\text{CDCl}_3$ ) 1.46 (s, 9H), 3.41–3.36 (m, 2H), 3.65 (t, *J* 5.7 Hz, 2H), 4.93 (br s, 1H);  $\delta_{\text{C}}$  (100 MHz,  $\text{CDCl}_3$ ) 155.6, 132.3, 80.1, 45.4, 40.8, 28.3; MS (ESI)  $[\text{M}+\text{H}]^+$  calcd for  $\text{C}_8\text{H}_{15}\text{N}_2\text{O}_2\text{S}$  = 203.0854, Found = 203.0850;  $R_f$  (5% MeOH/ $\text{CHCl}_3$ ) 0.56.

4.2.6. *t*-Butyl 4-isothiocyanatobutylcarbamate **5f**.<sup>42</sup> Yield 60% (2.1 g) white semisolid;  $\delta_{\text{H}}$  (600 MHz,  $\text{CDCl}_3$ ) 1.45 (s, 9H), 1.58–1.65 (m, 2H), 1.70–1.77 (m, 2H), 3.16 (q, *J* 9.6 Hz, 2H), 3.59 (t, *J* 9.6 Hz, 2H), 4.63 (br s, 1H);  $\delta_{\text{C}}$  (150 MHz,  $\text{CDCl}_3$ ) 155.6, 132.3, 80.1, 45.4, 40.8; MS (ESI)  $[\text{M}+\text{H}]^+$  calcd for  $\text{C}_{10}\text{H}_{19}\text{N}_2\text{O}_2\text{S}$  = 231.1167, Found = 231.1158;  $R_f$  (5% MeOH/ $\text{CHCl}_3$ ) 0.62.

4.2.7. *t*-Butyl 6-isothiocyanatohexylcarbamate **5g**.<sup>42</sup> Yield 72% (2.8 g) white semisolid;  $\delta_{\text{H}}$  (600 MHz,  $\text{CDCl}_3$ ) 1.31–1.54 (m, 15H), 1.67–1.74 (m, 2H), 3.13 (q, *J* 6.4 Hz, 2H), 3.51 (t, *J* 6.4 Hz, 2H), 4.59 (br s, 1H);  $\delta_{\text{C}}$  (150 MHz,  $\text{CDCl}_3$ ) 155.9, 129.8, 79.0, 44.9, 40.3, 29.8, 29.6, 28.8, 26.2, 25.9; MS (ESI)  $[\text{M}+\text{H}]^+$  calcd for  $\text{C}_{12}\text{H}_{23}\text{N}_2\text{O}_2\text{S}$  = 259.1480, Found = 259.1493;  $R_f$  (5% MeOH/ $\text{CHCl}_3$ ) 0.74.

### 4.3. Typical procedure for preparation of compounds **6a–g**

To a suspension of 5'-*O*-trityl-2,2'-anhydro- $\beta$ -*D*-uridine **3** (1.7 mmol) in anhydrous MeCN (5 mL), isothiocyanates **5a–g** (3.4 mmol) and DBU (3.4 mmol) were added under argon. After completion of the reaction (TLC, 5% MeOH/ $\text{CHCl}_3$ ) the reaction mixture was washed with an aqueous solution of citric acid (10%, 2 × 10 mL). The aqueous layer was extracted with EtOAc (3 × 5 mL). The combined organic layers were washed with  $\text{H}_2\text{O}$  (5 mL), dried ( $\text{Na}_2\text{SO}_4$ ) and concentrated. Purification of the crude product by column chromatography (5% MeOH/ $\text{CHCl}_3$ ) gave the compound **6a–6g** as a white solid.

4.3.1. *Methyl 2-((3*aR*,4*R*,6*R*,6*aS*)-4-(2,4-dioxo-3,4-dihydropyrimidin-1(2*H*)-yl)-2-thioxo-6-(trityloxymethyl)tetrahydrofuro[3,4-*d*]oxazol-3(2*H*)-yl)acetate* **6a**. Yield 87% (0.89 g); Mp 147–149 °C; FTIR [ATR,  $\nu$   $\text{cm}^{-1}$ ] 2953, 1679, 1541, 1448, 1251, 1208, 1000;  $\delta_{\text{H}}$  (600 MHz,  $\text{CDCl}_3$ ) 3.52–3.54 (dd, *J* 11.4, 3.0 Hz, 1H), 3.60–3.63 (dd, *J* 11.4, 4.2 Hz, 1H), 3.70 (s, 3H), 3.89–3.95 (m, 2H), 4.56–4.62 (m, 1H), 4.83–4.86 (m, 1H), 5.41 (d, *J* 7.8 Hz, 1H), 5.45–5.46 (m, 1H), 6.06 (d, *J* 1.8 Hz, 1H), 7.27–7.36 (m, 15H), 7.67 (d, *J* 7.8 Hz, 1H), 9.25 (s, 1H);  $\delta_{\text{C}}$  (150 MHz,  $\text{CDCl}_3$ ) 188.0, 168.3, 163.1, 150.32, 142.7, 139.2, 128.5, 128.2, 127.7, 102.7, 90.5, 87.9, 86.2, 80.9, 71.6, 62.1, 52.7, 48.4; MS (ESI)  $[\text{M}+\text{H}]^+$  calcd for  $\text{C}_{32}\text{H}_{30}\text{N}_3\text{O}_7\text{S}$  = 600.1804, Found = 600.1802;  $R_f$  (5% MeOH/ $\text{CHCl}_3$ ) 0.40.

4.3.2. *Methyl 3-((3*aR*,4*R*,6*R*,6*aS*)-4-(2,4-dioxo-3,4-dihydropyrimidin-1(2*H*)-yl)-2-thioxo-6-(trityloxymethyl)tetrahydrofuro[3,4-*d*]oxazol-3(2*H*)-yl)propanoate* **6b**. Yield 54% (0.56 g); Mp 106–107 °C; FTIR [ATR,  $\nu$   $\text{cm}^{-1}$ ] 2925, 1683, 1447, 1258, 1202, 1001;  $\delta_{\text{H}}$  (600 MHz,  $\text{CDCl}_3$ ) 2.73–2.77 (m, 2H), 3.05–3.30 (m, 1H), 3.53–3.62 (m, 1H), 3.69 (s, 3H), 3.91–3.96 (m, 1H), 4.22–4.26 (m, 1H), 4.43–4.45 (m, 1H), 4.94–4.96 (m, 1H), 5.40 (d, *J* 7.8 Hz, 1H),

5.44–5.46 (m, 1H), 6.12 (d, *J* 1.8 Hz, 1H), 7.28–7.38 (m, 15H), 7.67 (d, *J* 7.8 Hz, 1H), 9.23 (s, 1H);  $\delta_C$  (150 MHz, CDCl<sub>3</sub>) 186.6, 172.9, 163.0, 150.2, 143.0, 139.9, 128.7, 128.30, 128.8, 103.4, 90.4, 87.9, 85.6, 80.9, 71.2, 62.5, 52.3, 42.7, 31.5; MS (ESI) [M+H]<sup>+</sup> calcd for C<sub>33</sub>H<sub>32</sub>N<sub>3</sub>O<sub>7</sub>S=614.1961, Found=614.1960; *R<sub>f</sub>* (5% MeOH/CHCl<sub>3</sub>) 0.45.

**4.3.3. Methyl 4-((3*a*R,4*R*,6*R*,6*a*S)-4-(2,4-dioxo-3,4-dihydropyrimidin-1(2*H*)-yl)-2-thioxo-6-(trityloxymethyl)tetrahydrofuro[3,4-*d*]oxazol-3(2*H*)-yl)butanoate **6c**.** Yield 69% (0.73 g); FTIR [ATR,  $\nu$  cm<sup>-1</sup>] 2927, 1683, 1446, 1256, 1201, 1003;  $\delta_H$  (600 MHz, CDCl<sub>3</sub>) 2.00–2.05 (m, 2H), 2.43–2.46 (m, 2H), 3.52 (dd, *J* 10.8, 3.6 Hz, 1H), 3.60 (dd, *J* 10.8, 3.0 Hz, 1H), 3.66 (s, 3H), 4.10–4.17 (m, 2H), 4.43–4.45 (m, 1H), 4.75 (dd, *J* 9.0, 1.8 Hz, 1H), 5.38 (dd, *J* 9.0, 4.8 Hz, 1H), 5.42 (dd, *J* 8.4, 2.4 Hz, 1H), 6.05 (d, *J* 2.4 Hz, 1H), 7.26–7.30 (m, 15H), 7.69 (d, *J* 7.8 Hz, 1H), 9.45 (s, 1H);  $\delta_C$  (150 MHz, CDCl<sub>3</sub>) 186.8, 173.7, 163.1, 150.2, 142.9, 139.9, 128.7, 128.3, 127.8, 103.2, 90.3, 87.9, 86.1, 80.6, 70.3, 62.4, 52.0, 46.5, 31.1, 21.4; MS (ESI) [M+H]<sup>+</sup> calcd for C<sub>34</sub>H<sub>34</sub>N<sub>3</sub>O<sub>7</sub>S=628.2117, Found=628.2115; *R<sub>f</sub>* (5% MeOH/CHCl<sub>3</sub>) 0.64.

**4.3.4. Methyl 6-((3*a*R,4*R*,6*R*,6*a*S)-4-(2,4-dioxo-3,4-dihydropyrimidin-1(2*H*)-yl)-2-thioxo-6-(trityloxymethyl)tetrahydrofuro[3,4-*d*]oxazol-3(2*H*)-yl)hexanoate **6d**.** Yield 81% (0.89 g); Mp 65–66 °C; FTIR [ATR,  $\nu$  cm<sup>-1</sup>] 2929, 1685, 1448, 1255, 1207, 1006;  $\delta_H$  (600 MHz, CDCl<sub>3</sub>) 1.39–1.40 (m, 2H), 1.65–1.69 (m, 4H), 2.31–2.34 (m, 2H), 3.55–3.60 (m, 4H), 3.65 (s, 3H), 4.42–4.44 (m, 1H), 4.62–4.64 (dd, *J* 9.0, 2.4 Hz, 1H), 5.39–5.40 (m, 2H), 6.06–6.07 (d, *J* 1.8 Hz, 1H), 7.27–7.37 (m, 15H), 7.70 (d, *J* 1.8 Hz, 1H), 9.55 (s, 1H);  $\delta_C$  (150 MHz, CDCl<sub>3</sub>) 186.5, 174.0, 163.0, 150.1, 142.8, 139.6, 128.6, 128.2, 127.7, 103.2, 89.8, 87.9, 86.0, 79.9, 70.5, 62.17, 51.6, 47.0, 33.8, 26.0, 25.6, 24.4; MS (ESI) [M+H]<sup>+</sup> calcd for C<sub>36</sub>H<sub>38</sub>N<sub>3</sub>O<sub>7</sub>S=656.2430, Found=656.2430; *R<sub>f</sub>* (5% MeOH/CHCl<sub>3</sub>) 0.65.

**4.3.5. *t*-Butyl 2-((3*a*R,4*R*,6*R*,6*a*S)-4-(2,4-dioxo-3,4-dihydropyrimidin-1(2*H*)-yl)-2-thioxo-6-(trityloxymethyl)tetrahydrofuro[3,4-*d*]oxazol-3(2*H*)-yl)ethylcarbamate **6e**.** Yield 65% (0.74 g); FTIR [ATR,  $\nu$  cm<sup>-1</sup>] 2934, 1686, 1449, 1254, 1159;  $\delta_H$  (400 MHz, DMSO-*d*<sub>6</sub>) 1.34 (s, 9H), 3.17–3.22 (m, 2H), 3.26 (dd, *J* 10.4, 4.4 Hz, 1H), 3.31–3.33 (br, 1H), 3.40–3.47 (m, 2H), 3.98–4.04 (m, 1H), 4.30 (dt, *J* 6.4, 4.4 Hz, 1H), 5.02 (d, *J* 8.0 Hz, 1H), 5.26 (dd, *J* 8.8, 4.8 Hz, 1H), 5.60 (dd, *J* 8.0, 2.0 Hz, 1H), 6.00 (d, *J* 2.4 Hz, 1H), 6.94 (t, *J* 6.0 Hz, 1H), 7.20 (d, *J* 8.0 Hz, 1H), 7.25–7.40 (m, 15H);  $\delta_C$  (100 MHz, DMSO-*d*<sub>6</sub>) 186.2, 163.1, 155.6, 150.1, 143.3, 142.2, 128.2, 127.9, 127.1, 102.1, 91.1, 86.3, 85.1, 82.2, 77.9, 68.3, 63.4, 46.3, 36.5, 28.1; HRMS (ESI) [M+H]<sup>+</sup> calcd for C<sub>36</sub>H<sub>39</sub>N<sub>3</sub>O<sub>7</sub>S=671.2539, Found=671.2534; *R<sub>f</sub>* (5% MeOH/CH<sub>2</sub>Cl<sub>2</sub>) 0.65.

**4.3.6. *t*-Butyl 4-((3*a*R,4*R*,6*R*,6*a*S)-4-(2,4-dioxo-3,4-dihydropyrimidin-1(2*H*)-yl)-2-thioxo-6-(trityloxymethyl)tetrahydrofuro[3,4-*d*]oxazol-3(2*H*)-yl)butylcarbamate **6f**.** Yield 87% (1.03 g); Mp 109–110 °C; FTIR [ATR,  $\nu$  cm<sup>-1</sup>] 2938, 1684, 1446, 1258, 1157, 740;  $\delta_H$  (600 MHz, DMSO-*d*<sub>6</sub>) 1.36–1.39 (m, 11H), 1.53–1.63 (m, 2H), 2.88–2.97 (m, 2H), 3.28 (dd, *J* 10.2, 4.2 Hz, 1H), 3.42 (dd, *J* 10.2, 6.6 Hz, 1H), 3.83–3.88 (m, 2H), 4.30 (dt, *J* 6.6, 4.8 Hz, 1H), 4.97 (dd, *J* 8.4, 2.4 Hz, 1H), 5.32 (dd, *J* 8.4, 4.8 Hz, 1H), 5.57 (d, *J* 7.8 Hz, 1H), 6.00 (d, *J* 1.8 Hz, 1H), 6.78 (t, *J* 5.4 Hz, 1H), 7.28–7.40 (m, 15H), 7.72 (d, *J* 7.8 Hz, 1H), 11.46 (s, 1H);  $\delta_C$  (150 MHz, DMSO-*d*<sub>6</sub>) 185.6, 163.0, 155.5, 150.2, 143.2, 141.9, 128.1, 127.9, 127.1, 101.9, 90.7, 86.3, 85.2, 81.6, 77.3, 68.1, 63.2, 46.0, 40.0, 28.2, 26.7, 22.5; MS (ESI) [M+H]<sup>+</sup> calcd for C<sub>38</sub>H<sub>43</sub>N<sub>3</sub>O<sub>7</sub>S=698.2774, Found=698.2770; *R<sub>f</sub>* (5% MeOH/CH<sub>2</sub>Cl<sub>2</sub>) 0.43.

**4.3.7. *t*-Butyl 6-((3*a*R,4*R*,6*R*,6*a*S)-4-(2,4-dioxo-3,4-dihydropyrimidin-1(2*H*)-yl)-2-thioxo-6-(trityloxymethyl)tetrahydrofuro[3,4-*d*]oxazol-3(2*H*)-yl)hexylcarbamate **6g**.** Yield 76%

(0.82 g); Mp 89–90 °C; FTIR [ATR,  $\nu$  cm<sup>-1</sup>] 2936, 1686, 1447, 1256, 1159, 748;  $\delta_H$  (600 MHz, DMSO-*d*<sub>6</sub>) 1.22–1.26 (m, 4H), 1.34–1.37 (m, 11H), 1.53–1.63 (m, 2H), 2.88 (dd, *J* 13.6, 6.6 Hz, 2H), 3.27 (dd, *J* 10.4, 4.1 Hz, 1H), 3.35 (dd, *J* 10.4, 6.6 Hz, 1H), 3.43–3.47 (m, 1H), 3.84 (ddd, *J* 13.8, 9.5, 6.8 Hz, 1H), 4.30 (dd, *J* 6.6, 4.1 Hz, 1H), 4.96 (dd, *J* 8.4, 2.4 Hz, 1H), 5.30 (dd, *J* 8.4, 4.1 Hz, 1H), 5.57 (dd, *J* 7.8, 2.2 Hz, 1H), 6.00 (d, *J* 2.2 Hz, 1H), 6.73 (t, *J* 5.4 Hz, 1H), 7.27–7.40 (m, 15H), 7.70 (d, *J* 7.8 Hz, 1H), 11.45 (d, *J* 2.2 Hz, 1H);  $\delta_C$  (150 MHz, DMSO-*d*<sub>6</sub>) 185.3, 163.1, 155.6, 150.2, 143.3, 141.8, 128.2, 128.0, 127.2, 102.1, 90.5, 86.4, 85.0, 81.6, 77.3, 68.1, 63.2, 46.3, 39.8, 29.3, 28.3, 25.9, 25.8, 25.2; MS (ESI) [M+H]<sup>+</sup> calcd for C<sub>40</sub>H<sub>47</sub>N<sub>3</sub>O<sub>7</sub>S=727.3165, Found=727.3164; *R<sub>f</sub>* (5% MeOH/CH<sub>2</sub>Cl<sub>2</sub>) 0.42.

#### 4.4. Preparation of 2'-amino-2'-deoxyuridine derivatives **7a–d** and **8e–g**

Compound **6a–d** or **9a–c** (0.5 mmol) was dissolved in aqueous ethanol (10 mL EtOH, 2 mL H<sub>2</sub>O) containing NaOH (10 mmol). The reaction mixture was refluxed for two hours (TLC, 10% MeOH : CHCl<sub>3</sub>). After disappearance of substrate, the reaction mixture was cooled down, portioned between EtOAc (50 mL) and H<sub>2</sub>O (20 mL) and neutralized with 20% aq HCl. The organic layer was separated, and the aqueous solution was extracted with EtOAc (2 × 10 mL). The organic extracts were combined, dried (MgSO<sub>4</sub>) and the volatiles were removed under diminished pressure. Purification of the residue on silica gel using gradient MeOH (10%–50% in CH<sub>2</sub>Cl<sub>2</sub>) gave the product **7a–d** or **8e–g** as a white semisolid.

**4.4.1. 2-((2*R*,3*R*,4*S*,5*R*)-2-(2,4-Dioxo-3,4-dihydropyrimidin-1(2*H*)-yl)-4-hydroxy-5-(trityloxymethyl)tetrahydrofuran-3-ylamino)ethanoic acid **7a**.** Yield 66% (0.18 g); FTIR [ATR,  $\nu$  cm<sup>-1</sup>] 3058, 1686, 1245, 1112, 1078, 763;  $\delta_H$  (600 MHz, DMSO-*d*<sub>6</sub>) 3.13–3.17 (m, 2H), 3.21–3.48 (m, 5H), 4.07 (d, *J* 3.0 Hz, 1H), 4.26–4.32 (m, 2H), 5.36 (d, *J* 8.0 Hz, 1H), 7.23–7.54 (m, 15H), 5.80 (s, 1H), 7.74 (d, *J* 8.0 Hz, 1H), 11.41 (s, 1H);  $\delta_C$  (150 MHz, DMSO-*d*<sub>6</sub>) 163.43, 151.06, 143.81, 140.77, 128.74, 128.44, 127.61, 101.88, 87.71, 86.92, 83.85, 74.07, 68.76, 64.11, 63.86, 55.33, 49.58; MS (ESI) [M+H]<sup>+</sup> calcd for C<sub>30</sub>H<sub>30</sub>N<sub>3</sub>O<sub>7</sub>=544.2084, Found=544.2082; *R<sub>f</sub>* (10% MeOH/CH<sub>2</sub>Cl<sub>2</sub>) 0.22.

**4.4.2. 3-((2*R*,3*R*,4*S*,5*R*)-2-(2,4-Dioxo-3,4-dihydropyrimidin-1(2*H*)-yl)-4-hydroxy-5-(trityloxy methyl)tetrahydrofuran-3-ylamino)propionic acid **7b**.** Yield 65% (0.18 g); FTIR [ATR,  $\nu$  cm<sup>-1</sup>] 3058, 1683, 1563, 1448, 1405, 1270, 1082, 772;  $\delta_H$  (600 MHz, DMSO-*d*<sub>6</sub>) 2.14–2.31 (m, 4H), 2.72 (t, *J* 6.2 Hz, 2H), 3.16–3.22 (m, 3H), 3.32 (dd, *J* 10.5, 4.9 Hz, 1H), 3.99 (d, *J* 3.6 Hz, 1H), 4.20–4.26 (m, 2H), 5.36 (d, *J* 8.1 Hz, 1H), 7.23–7.46 (m, 15H), 7.66 (d, *J* 8.1 Hz, 1H), 11.45 (s, 1H);  $\delta_C$  (150 MHz, DMSO-*d*<sub>6</sub>) 171.70, 170.79, 158.48, 151.24, 148.29, 136.13, 135.86, 135.04, 109.47, 94.86, 94.31, 91.45, 76.53, 71.80, 71.59, 52.00, 44.56; MS (ESI) [M+H]<sup>+</sup> calcd for C<sub>31</sub>H<sub>32</sub>N<sub>3</sub>O<sub>7</sub>=558.2240, Found=558.2238; *R<sub>f</sub>* (10% MeOH/CH<sub>2</sub>Cl<sub>2</sub>) 0.26.

**4.4.3. 4-((2*R*,3*R*,4*S*,5*R*)-2-(2,4-Dioxo-3,4-dihydropyrimidin-1(2*H*)-yl)-4-hydroxy-5-(trityloxy methyl)tetrahydrofuran-3-ylamino)butanoic acid **7c**.** Yield 73% (0.21 g); FTIR [ATR,  $\nu$  cm<sup>-1</sup>] 3058, 1686, 1557, 1447, 1404, 1270, 1082, 747;  $\delta_H$  (600 MHz, DMSO-*d*<sub>6</sub>) 1.56–1.66 (m, 2H), 2.16–2.25 (m, 2H), 2.56–2.58 (m, 2H), 3.17–3.25 (m, 2H), 3.33 (dd, *J* 10.5, 4.8 Hz, 1H), 4.00 (dd, *J* 7.9, 4.0 Hz, 1H), 4.18 (dd, *J* 5.1, 4.4 Hz, 1H), 5.35 (d, *J* 8.1 Hz, 1H), 5.71 (d, *J* 6.2 Hz, 1H), 7.24–7.43 (m, 15H), 7.67 (d, *J* 8.1 Hz, 1H), 11.34 (s, 1H);  $\delta_C$  (150 MHz, DMSO-*d*<sub>6</sub>) 162.8, 150.5, 143.3, 140.3, 128.2, 127.9, 127.1, 101.5, 87.0, 86.4, 83.7, 68.2, 63.54, 63.2, 46.6, 31.7, 25.0; MS (ESI) [M+H]<sup>+</sup> calcd for C<sub>32</sub>H<sub>34</sub>N<sub>3</sub>O<sub>7</sub>=572.2397, Found=572.2395; *R<sub>f</sub>* (10% MeOH/CH<sub>2</sub>Cl<sub>2</sub>) 0.26.

**4.4.4. 6-((2*R*,3*R*,4*S*,5*R*)-2-(2,4-Dioxo-3,4-dihydropyrimidin-1(2*H*)-yl)-4-hydroxy-5-(trityloxymethyl)tetrahydrofuran-3-ylamino)**

hexanoic acid **7d**. Yield 71% (0.21 g); FTIR [ATR,  $\nu$  cm<sup>-1</sup>] 3059, 1687, 1549, 1447, 1270, 1083, 765;  $\delta_{\text{H}}$  (600 MHz, DMSO-*d*<sub>6</sub>) 1.26 (dt, *J* 14.1, 7.1 Hz, 2H), 1.35–1.43 (m, 4H), 1.45–1.57 (m, 4H), 2.18 (t, *J* 7.3 Hz, 2H), 2.56 (dd, *J* 11.6, 5.2 Hz, 1H), 3.16–3.35 (m, 3H), 3.90–4.05 (m, 1H), 4.11–4.22 (m, 1H), 5.37 (d, *J* 8.0 Hz, 1H), 5.71 (d, *J* 5.2 Hz, 1H), 7.28–7.41 (m, 15H), 7.67 (d, *J* 8.0 Hz, 1H), 11.35 (s, 1H);  $\delta_{\text{C}}$  (150 MHz, DMSO-*d*<sub>6</sub>) 174.34, 162.83, 150.54, 143.33, 140.35, 128.23, 127.93, 127.14, 101.55, 87.52, 86.42, 83.75, 68.22, 63.57, 47.11, 33.61, 26.15, 24.37; MS (ESI) [M+H]<sup>+</sup> calcd for C<sub>34</sub>H<sub>38</sub>N<sub>3</sub>O<sub>7</sub>=600.2710, Found=600.2708; *R*<sub>f</sub> (10% MeOH/CH<sub>2</sub>Cl<sub>2</sub>) 0.31.

#### 4.5. Preparation of **8a–d** and **9a–c**

Protected derivative of uridine **7a–d** or **6e–g** (0.6 mmol) was dissolved in CH<sub>2</sub>Cl<sub>2</sub> (10 mL) and treated with concentrated HCl (0.3 mL, *d*=1.18 g/mL, 3.3 mmol) at room temperature. After completion of the reaction (TLC, 1% Et<sub>3</sub>N in 50%MeOH/CH<sub>2</sub>Cl<sub>2</sub>), H<sub>2</sub>O (10 mL) was added and the reaction mixture was neutralized with saturated NaHCO<sub>3</sub> solution. The water layer was washed with CH<sub>2</sub>Cl<sub>2</sub> (2×3 mL) and the organic layer discarded. The water was removed under diminished pressure and the residue was dissolved in minimal amounts of MeOH and purified by column chromatography (1% Et<sub>3</sub>N in 50%MeOH/CH<sub>2</sub>Cl<sub>2</sub>).

4.5.1. 2-((2*R*,3*R*,4*S*,5*R*)-2-(2,4-Dioxo-3,4-dihydropyrimidin-1(2*H*)-yl)-4-hydroxy-5-(hydroxymethyl)tetrahydrofuran-3-ylamino)acetic acid **8a**. Yield 93% (0.17 g) white semisolid; FTIR [ATR,  $\nu$  cm<sup>-1</sup>] 3224, 1687, 1581, 1396, 1271, 1094, 814;  $\delta_{\text{H}}$  (600 MHz, D<sub>2</sub>O) 3.84 (dd, *J* 12.7, 4.0 Hz, 1H), 3.90 (dd, *J* 12.7, 3.1 Hz, 1H), 3.92–3.96 (m, 1H), 4.00–4.05 (m, 1H), 4.24 (dd, *J* 6.7 Hz, 6.0 Hz, 1H), 4.31–4.34 (m, 1H), 4.67 (dd, *J* 6.0, 3.1 Hz, 1H), 5.97 (d, *J* 8.1 Hz, 1H), 6.37 (d, *J* 6.7 Hz, 1H), 7.92 (d, *J* 8.1 Hz, 1H);  $\delta_{\text{C}}$  (150 MHz, D<sub>2</sub>O) 169.23, 165.95, 151.78, 141.08, 103.06, 86.80, 85.66, 68.31, 62.06, 60.75, 47.22; MS (ESI) [M+H]<sup>+</sup> calcd for C<sub>11</sub>H<sub>16</sub>N<sub>3</sub>O<sub>7</sub>=302.0988, Found=302.0986; *R*<sub>f</sub> (30% MeOH/CH<sub>2</sub>Cl<sub>2</sub>) 0.28.

4.5.2. 3-((2*R*,3*R*,4*S*,5*R*)-2-(2,4-Dioxo-3,4-dihydropyrimidin-1(2*H*)-yl)-4-hydroxy-5-(hydroxymethyl)tetrahydrofuran-3-ylamino)propionic acid **8b**. Yield 89% (0.17 g) white semisolid; FTIR [ATR,  $\nu$  cm<sup>-1</sup>] 3229, 1682, 1575, 1396, 1273, 1107, 1052, 815;  $\delta_{\text{H}}$  (600 MHz, D<sub>2</sub>O) 2.53–2.62 (m, 2H), 3.15–3.25 (m, 2H), 3.85 (dd, *J* 12.6, 4.2 Hz, 1H), 3.91 (dd, *J* 12.6, 3.6 Hz, 1H), 3.92–3.94 (m, 1H), 4.29–4.31 (m, 1H), 4.62 (dd, *J* 6.0, 3.0 Hz, 1H), 5.98 (d, *J* 8.4 Hz, 1H), 6.20 (d, *J* 6.6 Hz, 1H), 7.95 (d, *J* 8.4 Hz, 1H);  $\delta_{\text{C}}$  (150 MHz, D<sub>2</sub>O) 170.3, 168.7, 154.5, 144.0, 105.5, 89.1, 71.1, 65.3, 63.6, 46.7, 36.6; MS (ESI) [M+H]<sup>+</sup> calcd for C<sub>12</sub>H<sub>18</sub>N<sub>3</sub>O<sub>7</sub>=316.1144, Found=316.1142; *R*<sub>f</sub> (30% MeOH/CH<sub>2</sub>Cl<sub>2</sub>) 0.29.

4.5.3. 4-((2*R*,3*R*,4*S*,5*R*)-2-(2,4-Dioxo-3,4-dihydropyrimidin-1(2*H*)-yl)-4-hydroxy-5-(hydroxymethyl)tetrahydrofuran-3-ylamino)butanoic acid **8c**. Yield 82% (0.16 g) white semisolid; FTIR [ATR,  $\nu$  cm<sup>-1</sup>] 3240, 1674, 1545, 1409, 1271, 1104, 1050, 815;  $\delta_{\text{H}}$  (600 MHz, D<sub>2</sub>O) 1.96 (dt, *J* 13.8, 7.0 Hz, 2H), 2.33 (t, *J* 7.0 Hz, 2H), 2.98–3.17 (m, 2H), 3.83 (dd, *J* 12.6, 4.2 Hz, 1H), 3.86 (dd, *J* 12.6, 3.6 Hz, 1H), 3.96–3.98 (t, *J* 6.4 Hz, 1H), 4.27 (dd, *J* 6.4, 3.1 Hz, 1H), 4.61 (dd, *J* 5.6, 2.8 Hz, 1H), 5.97 (d, *J* 8.1 Hz, 1H), 6.26 (d, *J* 7.1 Hz, 1H), 7.91 (d, *J* 8.1 Hz, 1H);  $\delta_{\text{C}}$  (150 MHz, D<sub>2</sub>O) 184.4, 168.6, 154.4, 143.9, 105.7, 89.1, 88.3, 71.0, 64.6, 63.6, 49.6, 37.4, 25.7; MS (ESI) [M+H]<sup>+</sup> calcd for C<sub>13</sub>H<sub>20</sub>N<sub>3</sub>O<sub>7</sub>=330.3137, Found=330.3135; *R*<sub>f</sub> (30% MeOH/CH<sub>2</sub>Cl<sub>2</sub>) 0.32.

4.5.4. 6-((2*R*,3*R*,4*S*,5*R*)-2-(2,4-Dioxo-3,4-dihydropyrimidin-1(2*H*)-yl)-4-hydroxy-5-(hydroxymethyl)tetrahydrofuran-3-ylamino)hexanoic acid **8d**. Yield 95% (0.20 g) white semisolid; FTIR [ATR,  $\nu$  cm<sup>-1</sup>] 3259, 1686, 1448, 1271, 1079, 812;  $\delta_{\text{H}}$  (600 MHz, D<sub>2</sub>O) 1.39–1.41 (m, 2H), 1.58–1.64 (m, 2H), 1.72–1.80 (m, 2H), 2.21 (t, *J* 7.4 Hz, 2H), 3.10–3.19

(m, 2H), 3.85 (dd, *J* 12.6, 4.0 Hz, 2H), 3.89 (dd, *J* 12.6, 3.2 Hz, 1H), 4.11 (dd, *J* 7.1, 6.0 Hz, 1H), 4.30–4.33 (m, 1H), 4.66 (dd, *J* 6.0, 2.6 Hz, 1H), 5.98 (d, *J* 8.1 Hz, 1H), 6.35 (d, *J* 7.1 Hz, 1H), 7.92 (d, *J* 8.1 Hz, 1H);  $\delta_{\text{C}}$  (150 MHz, D<sub>2</sub>O) 182.8, 165.9, 151.7, 144.2, 103.2, 86.8, 85.4, 68.4, 61.8, 60.9, 47.0, 36.6, 25.5, 25.4, 25.0; MS (ESI) [M+H]<sup>+</sup> calcd for C<sub>15</sub>H<sub>24</sub>N<sub>3</sub>O<sub>7</sub>=358.1614, Found: 358.1614; *R*<sub>f</sub> (30% MeOH/CH<sub>2</sub>Cl<sub>2</sub>) 0.30.

4.5.5. 1-((2*R*,3*R*,4*S*,5*R*)-3-(2-Aminoethylamino)-4-hydroxy-5-(hydroxymethyl)tetrahydrofuran-2-yl)pyrimidine-2,4(1*H*,3*H*)-dione **8e**. Yield 91% (0.15 g) white semisolid; FTIR [ATR,  $\nu$  cm<sup>-1</sup>] 3348, 1680, 1566, 1387, 1261;  $\delta_{\text{H}}$  (600 MHz, D<sub>2</sub>O) 2.89–2.95 (m, 2H), 3.28–3.33 (m, 2H), 3.84 (dd, *J* 12.6, 4.2 Hz, 1H), 3.90 (dd, *J* 12.6, 3.6 Hz, 1H), 3.95–3.98 (m, 2H), 4.27–4.30 (m, 2H), 4.60 (dd, *J* 6.0, 3.0 Hz, 1H), 5.97 (d, *J* 8.4 Hz, 1H), 6.22 (d, *J* 6.6 Hz, 1H), 7.98 (d, *J* 8.4 Hz, 1H);  $\delta_{\text{C}}$  (150 MHz, D<sub>2</sub>O) 169.8, 166.7, 153.2, 143.7, 105.2, 89.0, 712.0, 65.1, 63.2, 48.7, 43.6; MS (ESI) [M+H]<sup>+</sup> calcd for C<sub>11</sub>H<sub>19</sub>N<sub>4</sub>O<sub>5</sub>=287.1355, Found=287.1355; *R*<sub>f</sub> (40% MeOH/CH<sub>2</sub>Cl<sub>2</sub>) 0.20.

4.5.6. 1-((2*R*,3*R*,4*S*,5*R*)-3-(4-Aminobutylamino)-4-hydroxy-5-(hydroxymethyl)tetrahydrofuran-2-yl)pyrimidine-2,4(1*H*,3*H*)-dione **8f**. Yield 88% (0.17 g) white semisolid; FTIR [ATR,  $\nu$  cm<sup>-1</sup>] 3346, 1678, 1565, 1384, 1260;  $\delta_{\text{H}}$  (600 MHz, D<sub>2</sub>O) 1.38–1.44 (m, 2H), 1.54–1.58 (m, 2H), 2.61 (t, *J* 7.2 Hz, 2H), 3.03–3.11 (m, 2H), 3.83 (dd, *J* 12.6, 4.2 Hz, 1H), 3.88 (dd, *J* 12.6, 4.2 Hz, 1H), 3.96–3.97 (m, 2H), 4.28–4.29 (m, 2H), 4.61–4.64 (m, 1H), 5.97 (d, *J* 8.4 Hz, 1H), 6.24 (d, *J* 7.2 Hz, 1H), 7.92 (d, *J* 8.4 Hz, 1H);  $\delta_{\text{C}}$  (150 MHz, D<sub>2</sub>O) 168.5, 156.0, 144.1, 105.8, 89.6, 88.4, 71.2, 65.0, 63.9, 47.7, 44.2, 36.1, 26.7; MS (ESI) [M+H]<sup>+</sup> calcd for C<sub>13</sub>H<sub>23</sub>N<sub>4</sub>O<sub>5</sub>=315.1668, Found=315.1669; *R*<sub>f</sub> (40% MeOH/CH<sub>2</sub>Cl<sub>2</sub>) 0.22.

4.5.7. 1-((2*R*,3*R*,4*S*,5*R*)-3-(6-Aminohexylamino)-4-hydroxy-5-(hydroxymethyl)tetrahydrofuran-2-yl)pyrimidine-2,4(1*H*,3*H*)-dione **8g**. Yield 92% (0.19 g) white semisolid; FTIR [ATR,  $\nu$  cm<sup>-1</sup>] 3340, 1674, 1561, 1388, 1264;  $\delta_{\text{H}}$  (600 MHz, D<sub>2</sub>O) 1.32–1.39 (m, 2H), 1.42–1.46 (m, 2H), 1.62–1.66 (m, 4H), 2.58–2.62 (m, 2H), 3.05–3.12 (m, 2H), 3.80 (dd, *J* 12.6, 4.2 Hz, 1H), 3.86 (dd, *J* 12.6, 4.2 Hz, 1H), 3.92 (dd, *J* 12.6, 3.0 Hz, 1H), 4.28–4.31 (m, 2H), 4.61 (dd, *J* 6.0, 3.0 Hz, 1H), 5.95 (d, *J* 7.8 Hz, 1H), 6.23 (d, *J* 7.2 Hz, 1H), 7.92 (d, *J* 7.8 Hz, 1H);  $\delta_{\text{C}}$  (150 MHz, D<sub>2</sub>O) 168.7, 154.5, 144.2, 105.7, 89.4, 88.3, 71.2, 64.9, 63.8, 46.1, 44.9, 29.4, 27.5, 26.5, 26.2; MS (ESI) [M+H]<sup>+</sup> calcd for C<sub>15</sub>H<sub>27</sub>N<sub>4</sub>O<sub>5</sub>=343.1981, Found=343.1979; *R*<sub>f</sub> (40% MeOH/CH<sub>2</sub>Cl<sub>2</sub>) 0.25.

4.5.8. 1-((3*aR*,4*R*,6*R*,6*aS*)-3-(2-Aminoethyl)-6-(hydroxymethyl)-2-thioxohexahydrofuro[3,4-*d*]oxazol-4-yl)pyrimidine-2,4(1*H*,3*H*)-dione **9a**. Yield 86% (0.17 g) white semisolid; FTIR [ATR,  $\nu$  cm<sup>-1</sup>] 2938, 1682, 1631, 1489, 1447, 1266, 1102, 997;  $\delta_{\text{H}}$  (600 MHz, DMSO) 2.69–2.75 (m, 1H), 2.78–2.83 (m, 1H), 3.50–3.56 (m, 3H), 3.65 (dd, *J* 11.4, 4.8 Hz, 1H), 3.68 (dd, *J* 11.4, 4.8 Hz, 1H), 3.72 (ddd, *J* 14.4, 7.8, 6.6 Hz, 1H), 4.06 (ddd, *J* 14.4, 8.4, 6.0 Hz, 1H), 4.18 (dd, *J* 9.0, 4.2 Hz, 1H), 4.93 (dd, *J* 9.0, 3.0 Hz, 1H), 5.25 (dd, *J* 9.0, 4.2 Hz, 1H), 5.69 (d, *J* 7.8 Hz, 1H), 6.00 (d, *J* 3.0 Hz, 1H), 7.76 (d, *J* 7.8 Hz, 1H), 11.46 (d, *J* 1.8 Hz, 1H);  $\delta_{\text{C}}$  (150 MHz, DMSO) 185.9, 171.4, 163.4, 150.4, 141.7, 101.9, 90.5, 86.5, 82.2, 68.8, 60.5, 51.6, 42.2, 30.2; MS (ESI) [M+H]<sup>+</sup> calcd for C<sub>12</sub>H<sub>17</sub>N<sub>4</sub>O<sub>5</sub>S=329.0919, Found=329.0918; *R*<sub>f</sub> (20% MeOH/CH<sub>2</sub>Cl<sub>2</sub>) 0.10.

4.5.9. 1-((3*aR*,4*R*,6*R*,6*aS*)-3-(4-Aminobutyl)-6-(hydroxymethyl)-2-thioxohexahydrofuro[3,4-*d*]oxazol-4-yl)pyrimidine-2,4(1*H*,3*H*)-dione **9b**. Yield 89% (0.19 g) white solid; Mp 113–114 °C; FTIR [ATR,  $\nu$  cm<sup>-1</sup>] 2933, 1683, 1629, 1489, 1448, 1266, 1102, 998;  $\delta_{\text{H}}$  (600 MHz, DMSO-*d*<sub>6</sub>) 1.32 (qn, *J* 7.2 Hz, 2H), 1.52–1.56 (m, 4H), 2.53–2.55 (m, 3H), 3.49 (ddd, *J* 13.8, 9.0, 4.8 Hz, 1H), 3.66 (dd, *J* 12.0, 4.8 Hz, 1H), 3.69 (dd, *J* 12.0, 4.8 Hz, 1H), 3.86 (ddd, *J* 13.8, 9.6, 6.6 Hz, 1H), 4.19 (dd, *J* 9.0, 4.8 Hz, 1H), 4.44 (s, 1H), 4.92 (dd, *J* 9.0, 2.4 Hz, 1H), 5.27 (dd, *J* 8.4, 4.2 Hz, 1H), 5.67 (d, *J* 7.8 Hz, 1H), 5.97 (d, *J* 2.4 Hz, 1H), 7.76 (d, *J* 7.8 Hz, 1H);  $\delta_{\text{C}}$  (150 MHz, DMSO-*d*<sub>6</sub>) 185.8, 163.6, 150.6, 141.3,



102.1, 90.2, 86.6, 81.8, 68.3, 60.5, 46.4, 40.9, 29.8, 22.9; MS (ES)  $[M+H]^+$  calcd for  $C_{14}H_{21}N_4O_5S=357.1232$ , Found= $357.1230$ ;  $R_f$  (20% MeOH/CH<sub>2</sub>Cl<sub>2</sub>) 0.12.

**4.5.10. 1-((3aR,4R,6R,6aS)-3-(6-Aminoethyl)-6-(hydroxymethyl)-2-thioxohexahydrofuro[3,4-d]oxazol-4-yl)pyrimidine-2,4(1H,3H)-dione 9c.** Yield 85% (0.20 g) white solid; Mp: 99–100 °C; FTIR [ATR,  $\nu$  cm<sup>-1</sup>] 2934, 1682, 1632, 1489, 1449, 1261, 1100, 998;  $\delta_H$  (600 MHz, DMSO-*d*<sub>6</sub>) 1.22–1.31 (m, 6H), 1.42 (qn, *J* 7.2 Hz, 2H), 1.51–1.64 (m, 4H), 2.63 (t, *J* 7.2 Hz, 2H), 3.48 (ddd, *J* 13.8, 9.0, 4.8 Hz, 1H), 3.66 (dd, *J* 12.0, 4.8 Hz, 1H), 3.70 (dd, *J* 12.0, 4.8 Hz, 1H), 3.85 (ddd, *J* 13.8, 9.6, 6.6 Hz, 1H), 4.19 (dd, *J* 9.0, 4.8 Hz, 1H), 4.91 (dd, *J* 8.4, 2.4, 1H), 5.29 (dd, *J* 8.4, 4.2 Hz, 1H), 5.68 (d, *J* 7.8 Hz, 1H), 5.99 (d, *J* 2.4 Hz, 1H), 7.78 (d, *J* 7.8 Hz, 1H);  $\delta_C$  (150 MHz, DMSO) 185.6, 163.6, 150.6, 141.0, 102.0, 90.0, 86.4, 81.7, 68.3, 60.3, 46.3, 45.6, 29.9, 25.7, 25.6, 25.1; MS (ESI)  $[M+H]^+$  calcd for  $C_{16}H_{25}N_4O_5S=385.1545$ , Found= $385.1544$ ;  $R_f$  (20% MeOH/CH<sub>2</sub>Cl<sub>2</sub>) 0.13.

#### 4.6. Conjugation with anhydride of 1, 8-naphthalenedicarboxylic acid

A mixture of benzo[*de*]isochromene-1,3-dione **10a, b** (0.3 mmol) and **8g** (0.1 g, 0.26 mmol) in anhydrous ethanol (5 mL) containing pyridine (0.2 mL, 2.5 mmol) and 4-*N,N*-dimethyl-pyridine (0.1 g, 0.8 mmol) was refluxed under argon for 18 h and afterwards evaporated to dryness. The traces of pyridine were removed by co-evaporation with anhydrous toluene (2×5 mL). The residual oil was purified on silica gel packed column using a mixture of 10% MeOH/CHCl<sub>3</sub> as an eluent.

**4.6.1. 2-(6-((2R,3R,4S,5R)-2-(2,4-Dioxo-3,4-dihydropyrimidin-1(2H)-yl)-4-hydroxy-5-(hydroxymethyl)tetrahydrofuran-3-ylamino)hexyl)-1H-benzo[de]isoquinoline-1,3(2H)-dione 11a.** Yield 93% (0.13 g) yellowish solid; Mp 176–177 °C; FTIR [ATR,  $\nu$  cm<sup>-1</sup>] 3382, 2941, 1690, 1652, 1589, 1345, 1264, 1238, 1054, 779;  $\delta_H$  (600 MHz, DMSO-*d*<sub>6</sub>) 1.22 (s, 1H), 1.29–1.35 (m, 2H), 1.35–1.43 (m, 2H), 1.58–1.66 (m, 2H), 2.47–2.52 (m, 2H), 2.53–2.59 (m, 1H), 3.17 (dd, *J* 6.5, 5.7 Hz, 1H), 3.53–3.62 (m, 2H), 3.87 (dd, *J* 6.4, 3.4 Hz, 1H), 3.99–4.06 (m, 2H), 4.11 (dd, *J* 5.2, 2.7 Hz, 1H), 5.08 (t, *J* 4.9 Hz, 1H), 5.42 (s, 1H), 5.65 (d, *J* 8.0 Hz, 1H), 5.72 (d, *J* 7.1 Hz, 1H), 7.87 (dd, *J* 8.2, 7.2 Hz, 3H), 7.91 (d, *J* 8.1 Hz, 1H), 8.45 (dd, *J* 8.4, 1.0 Hz, 2H), 8.49 (dd, *J* 7.3, 1.1 Hz, 2H), 11.29 (s, 1H);  $\delta_C$  (150 MHz, DMSO-*d*<sub>6</sub>) 163.3, 162.9, 150.7, 140.6, 134.2, 131.2, 130.6, 127.2, 127.1, 122.0, 101.7, 86.6, 85.9, 68.4, 63.6, 61.1, 47.1, 39.5, 29.4, 27.4, 26.3, 26.2; MS (ESI)  $[M+H]^+$  calcd for  $C_{27}H_{31}N_4O_7=523.2192$ , Found= $523.2190$ ;  $R_f$  (10% MeOH/CHCl<sub>3</sub>) 0.15.

**4.6.2. 6-Bromo-2-(6-((2R,3R,4S,5R)-2-(2,4-dioxo-3,4-dihydropyrimidin-1(2H)-yl)-4-hydroxy-5-(hydroxymethyl)tetrahydrofuran-3-ylamino)hexyl)-1H-benzo[de]isoquinoline-1,3(2H)-dione 11b.** Yield 97% (0.15 g) yellowish solid; Mp 109–110 °C; FTIR [ATR,  $\nu$  cm<sup>-1</sup>] 3391, 2940, 1694, 1622, 1589, 1346, 1264, 1238, 1054, 779;  $\delta_H$  (600 MHz, DMSO-*d*<sub>6</sub>) 1.22 (s, 1H), 1.25–1.35 (m, 2H), 1.35–1.42 (m, 2H), 1.61 (dt, *J* 14.6, 7.3 Hz, 2H), 2.47–2.53 (m, 2H), 2.53–2.59 (m, 1H), 3.13–3.21 (m, 1H), 3.55 (dd, *J* 11.9, 3.2 Hz, 1H), 3.59 (dd, *J* 11.9, 3.7 Hz, 1H), 3.87 (dd, *J* 6.3, 3.4 Hz, 1H), 3.97–4.04 (m, 2H), 4.11 (dd, *J* 5.1, 2.7 Hz, 1H), 5.08 (s, 1H), 5.42 (s, 1H), 5.64 (d, *J* 8.0 Hz, 1H), 5.72 (d, *J* 7.1 Hz, 1H), 7.90 (d, *J* 7.1 Hz, 1H), 7.98 (dd, *J* 8.5, 7.3 Hz, 1H), 8.20 (d, 1H, *J* 7.8 Hz, 1H), 8.31 (d, *J* 7.8 Hz, 2H), 8.52 (dd, *J* 8.5, 1.1 Hz, 1H), 8.55 (dd, *J* 7.3, 1.1 Hz, 1H), 11.28 (s, 1H);  $\delta_C$  (150 MHz, DMSO-*d*<sub>6</sub>) 162.9, 162.7, 162.4, 150.7, 140.6, 132.5, 131.5, 131.2, 130.9, 129.7,

129.0, 128.7, 128.2, 122.7, 121.9, 101.7, 86.6, 85.9, 68.4, 63.6, 61.1, 47.1, 39.6, 29.4, 27.3, 26.3, 26.2; MS (ESI)  $[M+H]^+$  calcd for  $C_{27}H_{30}BrN_4O_7=601.1298$ ; 603.1277 Found= $601.1296$ ; 603.1275;  $R_f$  (10% MeOH/CHCl<sub>3</sub>) 0.13.

#### References and notes

- Iwai, Y.; Nakagawa, A.; Nagai, A.; Matsuyama, K.; Takahashi, Y.; Matsushita, M.; Hirano, A.; Omura, S. *J. Antibiot.* **1979**, *32*, 1367.
- Okawa, N.; Nakayama, H.; Ikeda, K.; Furihita, K.; Shimazu, A.; Otake, N.; Yonehara, Y. *Agric. Biol. Chem. (Tokyo)* **1980**, *44*, 1671.
- Taguchi, F.; Imatani, Y.; Nagaki, D.; Nakagawa, A.; Omura, S. *J. Antibiot.* **1981**, *34*, 313.
- Utogawa, T.; Morisawa, H.; Yamanaka, S.; Yamazaki, A.; Hirose, Y. *Agric. Biol. Chem.* **1985**, *49*, 2711.
- Sharma, R. A.; Bobek, M.; Bloch, A. *J. Med. Chem.* **1975**, *18*, 955.
- Lin, T. S.; Zhang, X. H.; Wang, Z. H.; Prusoff, W. H. *J. Med. Chem.* **1988**, *31*, 484.
- Osawa, A. A.; Tanaka, M.; Sasaki, T.; Matsuda, A. *J. Med. Chem.* **1998**, *41*, 5094.
- Vasil'eva, S. V.; Abramova, T. V.; Ivanova, T. M.; Shishkin, G. V.; Sil'nikov, V. N. *Russ. J. Bioorg. Chem.* **2004**, *30*, 234.
- Scherr, M.; Klebba, Ch.; Haener, R.; Ganser, A.; Engels, J. W. *Bioorg. Med. Chem. Lett.* **1997**, *7*, 1791.
- Das, S. R.; Fong, R.; Piccirilli, J. A. *Curr. Opin. Chem. Biol.* **2005**, *9*, 585.
- Teramoto, N.; Imanishi, Y.; Ito, Y. *J. Bioact. Compatible Polym.* **2000**, *15*, 297.
- Besada, P.; Shin, D. H.; Costanzi, S.; Ko, H.; Mathé, Ch.; Gagneron, J.; Gosselin, J. G.; Maddileti, S.; Harden, T. K.; Jacobson, K. A. *J. Med. Chem.* **2006**, *49*, 5532.
- Ivanov, A. A.; Ko, H.; Cosyn, L.; Maddileti, S.; Besada, P.; Ingrid Fricks, I.; Costanzi, S.; Harden, T. K.; Van Calenbergh, S.; Jacobson, K. A. *J. Med. Chem.* **2007**, *50*, 1166.
- Ko, H.; Carter, R. L.; Cosyn, L.; Petrelli, R.; de Castro, S.; Besada, P.; Zhou, Y.; Cappellacci, L.; Palmarisa Franchetti, P.; Grifantini, M.; Van Calenbergh, S.; Harden, T.; Jacobson, K. A. *Bioorg. Med. Chem.* **2008**, *16*, 6319.
- Winkler, J.; Urban, E.; Losert, D.; Wacheck, V.; Pehamberger, H.; Noe, Ch. R. *Nucleic Acids Res.* **2004**, *32*, 710.
- Ozaki, H.; Momiyama, S.; Yokotsuka, K.; Sawai, H. *Tetrahedron Lett.* **2001**, *42*, 677.
- Halila, S.; Velasco, T.; De Clercq, P.; Madder, M. *Chem. Commun.* **2005**, 936.
- de Beeck, M. O.; Madder, A. J. *Am. Chem. Soc.* **2011**, *133*, 796.
- Matulic-Adamic, J.; Beigelman, L.; Dudycz, L. W.; Gonzalez, C.; Usman, N. *Bioorg. Med. Chem. Lett.* **1995**, *5*, 2721.
- Sitaula, S.; Reed, S. M. *Bioorg. Med. Chem. Lett.* **2008**, *18*, 850.
- Mitsui, T.; Nakano, H.; Yamana, K. *Tetrahedron Lett.* **2000**, *41*, 2605.
- Kalra, N.; Parlato, M. C.; Parmar, V. S.; Wengel, J. *Bioorg. Med. Chem. Lett.* **2006**, *16*, 3166.
- Bugaut, A.; Bathany, K.; Schmitter, J. M.; Rayner, B. *Tetrahedron Lett.* **2005**, *46*, 687.
- Karpeisky, A.; Sweedler, D.; Haerberli, P.; Read, J.; Jarvis, K.; Beigelman, L. *Bioorg. Med. Chem. Lett.* **2002**, *12*, 3345.
- Walcher, G.; Pfeleiderer, W. *Helv. Chim. Acta* **1996**, *79*, 1067.
- Ikehara, M.; Maruyama, T.; Miki, H. *Tetrahedron Lett.* **1976**, *17*, 4485.
- Ranganathan, R. *Tetrahedron Lett.* **1977**, *18*, 1291.
- Verheyden, P. H.; Wagner, D.; Moffatt, J. G. *J. Org. Chem.* **1971**, *36*, 250.
- McGee, D. P. C.; Sebesta, D. P.; O'Rourke, S. S.; Martinez, R. L.; Jung, M. E.; Pieken, W. A. *Tetrahedron Lett.* **1996**, *37*, 1995.
- McGee, D. P. C.; Vaughn-Settle, A.; Vargeese, Ch; Zhai, Y. *J. Org. Chem.* **1996**, *61*, 781.
- Sebesta, D. P.; O'Rourke, S. S.; Martinez, R. L.; Pieken, W. A.; McGee, D. P. C. *Tetrahedron* **1996**, *52*, 14385.
- Faul, M. M.; Huff, B. E.; Dunlap, S. E.; Frank, S. A.; Fritz, J. E.; Kaldor, S. W.; LeTourneau, M. E.; Staszak, M. A.; Ward, J. A.; Werner, J. A.; Winneroski, L. L. *Tetrahedron* **1997**, *53*, 8085.
- Munch, H.; Hansen, J. S.; Pittelkow, M.; Christensen, J. B.; Ulrik Boas, U. *Tetrahedron Lett.* **2008**, *49*, 3117.
- Zhang, H.; Liu, R. Q.; Liu, K. Ch.; Li, Q. B.; Li, Q. Y.; Liu, S. Z. *Molecules* **2014**, *19*, 13631.
- Ulatowski, F.; Jurczak, J. *J. Org. Chem.* **2015**, *80*, 4235.
- Li, J.; Sha, Y. *Molecules* **2008**, *13*, 1111.
- Hwang, J. T.; Greenber, M. M. *Org. Lett.* **1999**, *1*, 2021.
- Kawai, K.; Kawabata, K.; Tojo, S.; Majima, T. *Bioorg. Med. Chem. Lett.* **2002**, *12*, 2363.
- Lebedev, A. V.; Lebedeva, A. B.; Sheludyakov, V. D.; Ovcharuk, S. N.; Kovaleva, E. A.; Ustinova, O. L. *Russ. J. Gen. Chem.* **2006**, *76*, 1069.
- Garmaise, D. L.; Schwartz, R.; McKay, A. F. *J. Am. Chem. Soc.* **1958**, *80*, 3332.
- Sureshbabu, V. N.; Naik, S. A.; Hemantha, H. P.; Narendra, N.; Das, U.; Guru Row, T. N. *J. Org. Chem.* **2009**, *74*, 5260.
- Gálcer, C. M.-O.; Roubert, P.; Sidhu, A.; Thurieau, Ch. PCT/FR2002/004055, 2004.

## **Publikacja P.2**

Anticancer activity and topoisomerase II inhibition of naphthalimides with  $\omega$ -hydroxylalkylamine side-chains of different lengths.

**Tomczyk, M. D.**; Byczek-Wyrostek, A.; Strama, K.; Wawzków, M.; Kasprzycki, P.; Walczak, Z. K\*.

*Medicinal Chemistry* **2019**, 15 (5), 550–560.

# Anticancer Activity and Topoisomerase II Inhibition of Naphthalimides with $\omega$ -Hydroxylalkylamine Side-Chains of Different Lengths

Mateusz D. Tomczyk<sup>a</sup>, Anna Byczek Wyrostek<sup>a</sup>, Klaudia Strama<sup>a</sup>, Martyna Wawszków<sup>a</sup>, Przemysław Kasprzycki<sup>b</sup> and Krzysztof Z. Walczak<sup>\*a</sup>

<sup>a</sup>Department of Organic Chemistry, Bioorganic Chemistry and Biotechnology, Faculty of Chemistry, Silesian University of Technology, Krzywoustego 4, 44-100 Gliwice, Poland

<sup>b</sup>Avantor Performance Materials Poland S.A., ul. Sowińskiego 11, 44-101 Gliwice, Poland

**Abstract:** 1,8-Naphthalimides (benzo[de]isoquinoline-1,3-diones) modified in various positions of chromophore, provided an effective method for enhancing their anticancer activity and reducing undesirable toxic effects. To accomplish this goal, several new 4- and 4,5-substituted 1,8-naphthalimides containing a  $\omega$ -hydroxylalkylamine side-chains of different length were obtained and evaluated in the report presented. Upon examination, it appeared that the replacement of the nitro groups in the chromophore slightly reduce its anticancer activities, whereas the presence of both nitro groups and  $\omega$ -hydroxylalkylamine chain resulted in seriously increased anticancer activities. Obtained compounds showed Topo II inhibitory activity, moreover, influence of the substitution pattern on the ability to inhibit Topo II activity and cancer cells proliferation was observed.

**Keywords:** Naphthalimide, Amonafide, Mitonafide, Anticancer, Topoisomerase II, DNA intercalator

## 1. INTRODUCTION

1,8-Naphthalimides are a representative family of DNA intercalators able to inhibit Topoisomerase II (Topo II) by stabilizing of covalent DNA-Topo II cleavage complex [1]. This interaction disrupt the cleavage-relegation equilibrium of Topo II, resulting in formation of broken strands of DNA. This lesions can trigger a series of cytotoxic events, which may eventually cause apoptotic cells death [2]. Amonafide and Mitonafide (Fig. 1) have been the two most extensively investigated 1,8-naphthalimide based intercalators and have been tested in clinical trials. Unfortunately, due to their high unexpected toxicity, e.g. neurotoxicity, hematotoxicity and limited efficiency, the clinical developments of these drugs were terminated [3-6]. Amonafide contains a free arylamine group, which causes it to be extensively metabolized *in vivo* by *N*-acetyl transferase-2 (NAT2) into a toxic metabolite and the nitro group of Mitonafide is responsible for causing toxic

effects [7-9]. In addition, differential level of *N*-acetylation among individuals also causes some difficulties in clinical evaluation [10]. However, existing research has shown that Amonafide derivatives, comprising 4-position free or substituted with amines, may retain the anticancer activities and avoid undesired toxic effects [11].

Much attention has been paid to substitution of 4-position over the last decades, and some promising anticancer results have been obtained in this matter. In the early 1970s, Brana *et al.* reported large series of derivatives modified with nitro, amine, alkyl, hydroxyl, alkoxy groups and halogen atoms at the 4-position [12, 13]. Since these reports many others have modified the 1,8-naphthalimide core with various functional groups such as straight-chain or cyclic amines, polyamines, pyrazoles, isoxazolidines and other at 4-position. Mostly all of these derivatives exhibited potent anticancer activity and some were even more active than Amonafide [14-17].

More recently, Wang *et al.* reported 1,8-naphthalimides modified with  $\omega$ -hydroxylalkylamine side-chains of different lengths and evaluated *in vitro* against Bel-7402 and HL-60 cancer cell lines [18]. Most of them exhibited significant *in vitro* activity with IC<sub>50</sub> values in the range of 5.57–9.17  $\mu$ M against Bel-7402 cell line. These types of derivatives contain side-chains with amine and terminal hydroxyl groups, able to form hydrogen bonds with DNA backbone.

Besides the mono-substituted derivatives, some studies have been focused on the bi-substituted derivatives. In 1985, Chang *et al.* reported a series of 3,6-dinitro and 4,5-diamino derivatives, which possess strong anticancer activities [19]. A several series of bi-substituted derivatives, that combine the aspects of both the nitro and the amino functional groups,

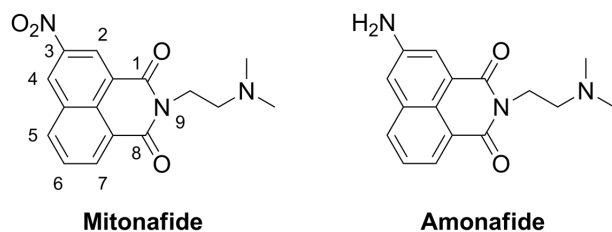


**Figure (1).** The structures of Mitonafide and Amonafide. Numbers in the structure of Mitonafide correspond to the position in the usual nomenclature of 1,8-naphthalimides.

\*Address correspondence to this author at the Department of Organic Chemistry, Bioorganic Chemistry and Biotechnology, Faculty of Chemistry, Silesian University of Technology, Gliwice 44-100, Poland; Tel/Fax: +48-32-237-13-08; +48-32-237-20-49; E-mail: krzysztof.walczak@polsl.pl

were reported. These derivatives were tested for their *in vitro* anticancer activity with the results showing that they exhibit higher activity than Amonafide.

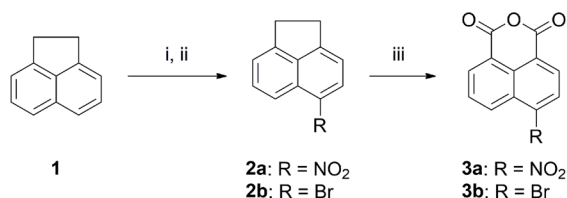
These studies indicate that modification of 1,8-naphthalimides with  $\omega$ -hydroxylalkylamine groups at the 4- or 4,5-positions may lead to improved binding into DNA, and as a result stronger anticancer activity. While most studies have examined a 3,6-substitution pattern, the aim of our study is to investigate the effect of 4- and 4,5-substituted derivatives. In an attempt to improve the anticancer activity, seven series of 1,8-naphthalimides were obtained with variations on the naphthalene rings and side-chains of various length at the imide nitrogen atom. Herein we present the preparation and interaction of selected derivatives with Topo II.

## 2. MATERIALS AND METHODS

$^1\text{H}$  NMR and  $^{13}\text{C}$  NMR spectra were recorded employing a Varian Mercury Plus 600 (600 MHz) and Agilent 400 MR (400 MHz) spectrometers, the chemical shifts are reported in ppm using TMS as an internal standard. The mass spectra were measured with a Mass Spectrometer AB Sciex 4000 QTRAP. Positive electrospray ionization (ESI) was used as the ionization source. Melting points were determined using a Boethius PHMK apparatus and are uncorrected. Column chromatography was performed using silica gel Geduran Si 60 (40-63  $\mu\text{m}$  mesh).

### 2.1. Synthesis of compounds 2a-12e:

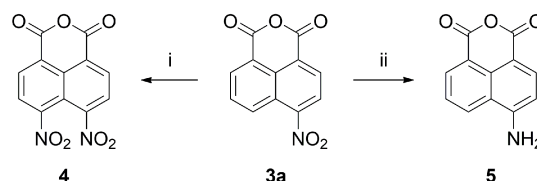
Compounds **2a-2b** were obtained from acenaphthene (**1**) under the conditions typical for aromatic electrophilic substitution reaction followed by oxidation to the corresponding anhydrides (**Scheme 1**). Thus, the 6-nitro derivative **2a** was prepared by nitration of acenaphthene (**1**) with concentrated nitric acid (65%) in glacial acetic acid at room temperature. Similarly, bromination of acenaphthene (**1**) was carried out under mild conditions to give the 6-bromo derivative **2b** in satisfactory yield. In the second step derivatives **2a-2b** were oxidized to the corresponding anhydrides **3a-3b** (**Scheme 1**). Since acenaphthene is resistant to most oxidizing reagents even in the presence of a catalysts, a potassium dichromate was applied as a reagent of choice [20].



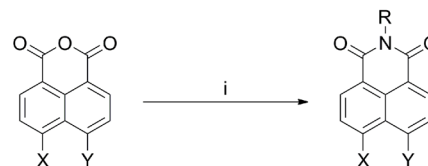
**Scheme (1).** Synthesis of compounds **2a-2b** and **3a-3b**. Reagents: (i)  $\text{HNO}_3$  (65%),  $\text{AcOH}$  (100%), rt, 3 h; (ii) NBS, anhydrous DMF, rt, 3 h; (iii)  $\text{K}_2\text{Cr}_2\text{O}_7$ ,  $\text{AcOH}$  (95%),  $90^\circ\text{C}$ , 4 h.

Then the compound **3a** was nitrated at a temperature not exceeding  $50^\circ\text{C}$  to the 4,5-dinitro anhydride **4**, which was recrystallized from glacial acetic acid. The reduction of the nitro group by treatment with tin(II) chloride, using ethanol (96%) as a solvent, allowed to obtain 6-amino anhydride **5** (**Scheme 2**).

The anhydrides **3a-5** obtained above were converted into the corresponding imide derivatives **6a-9e** by heating under reflux with one equivalent of appropriate amine alcohols in ethanolic (96%) solution (**Scheme 3**). This reactions easily

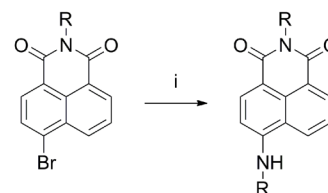


**Scheme (2).** Synthesis of compounds **4** and **5**. Reagents: (i)  $\text{HNO}_3$  (65%),  $\text{H}_2\text{SO}_4$  (98%),  $0-20^\circ\text{C}$ , then  $60^\circ\text{C}$ , 2 h; (ii)  $\text{SnCl}_2 \cdot 2\text{H}_2\text{O}$  (5 equiv),  $\text{EtOH}$  (96%), reflux, 4 h.



**3a:** X =  $\text{NO}_2$ ; Y = H  
**3b:** X = Br; Y = H  
**4:** X =  $\text{NO}_2$ ; Y =  $\text{NO}_2$   
**5:** X =  $\text{NH}_2$ ; Y = H  
**6a:** X =  $\text{NO}_2$ ; Y = H; R =  $(\text{CH}_2)_2\text{OH}$   
**6b:** X =  $\text{NO}_2$ ; Y = H; R =  $(\text{CH}_2)_3\text{OH}$   
**6c:** X =  $\text{NO}_2$ ; Y = H; R =  $(\text{CH}_2)_4\text{OH}$   
**6d:** X =  $\text{NO}_2$ ; Y = H; R =  $(\text{CH}_2)_5\text{OH}$   
**6e:** X =  $\text{NO}_2$ ; Y = H; R =  $(\text{CH}_2)_6\text{OH}$   
**7a:** X = Br; Y = H; R =  $(\text{CH}_2)_2\text{OH}$   
**7b:** X = Br; Y = H; R =  $(\text{CH}_2)_3\text{OH}$   
**7c:** X = Br; Y = H; R =  $(\text{CH}_2)_4\text{OH}$   
**7d:** X = Br; Y = H; R =  $(\text{CH}_2)_5\text{OH}$   
**7e:** X = Br; Y = H; R =  $(\text{CH}_2)_6\text{OH}$   
**8a:** X =  $\text{NO}_2$ ; Y =  $\text{NO}_2$ ; R =  $(\text{CH}_2)_2\text{OH}$   
**8b:** X =  $\text{NO}_2$ ; Y =  $\text{NO}_2$ ; R =  $(\text{CH}_2)_3\text{OH}$   
**8c:** X =  $\text{NO}_2$ ; Y =  $\text{NO}_2$ ; R =  $(\text{CH}_2)_4\text{OH}$   
**8d:** X =  $\text{NO}_2$ ; Y =  $\text{NO}_2$ ; R =  $(\text{CH}_2)_5\text{OH}$   
**8e:** X =  $\text{NO}_2$ ; Y =  $\text{NO}_2$ ; R =  $(\text{CH}_2)_6\text{OH}$   
**9a:** X =  $\text{NH}_2$ ; Y = H; R =  $(\text{CH}_2)_2\text{OH}$   
**9b:** X =  $\text{NH}_2$ ; Y = H; R =  $(\text{CH}_2)_3\text{OH}$   
**9c:** X =  $\text{NH}_2$ ; Y = H; R =  $(\text{CH}_2)_4\text{OH}$   
**9d:** X =  $\text{NH}_2$ ; Y = H; R =  $(\text{CH}_2)_5\text{OH}$   
**9e:** X =  $\text{NH}_2$ ; Y = H; R =  $(\text{CH}_2)_6\text{OH}$

**Scheme (3).** Synthesis of compounds **6a-9e**. Reagents: (i) appropriate  $\omega$ -hydroxyalkylamine (1 equiv),  $\text{EtOH}$  (96%), reflux, 4 h.

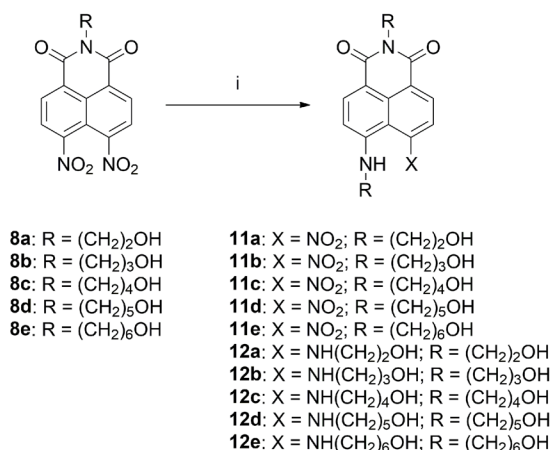


**7a:** R =  $(\text{CH}_2)_2\text{OH}$   
**7b:** R =  $(\text{CH}_2)_3\text{OH}$   
**7c:** R =  $(\text{CH}_2)_4\text{OH}$   
**7d:** R =  $(\text{CH}_2)_5\text{OH}$   
**7e:** R =  $(\text{CH}_2)_6\text{OH}$   
**10a:** R =  $(\text{CH}_2)_2\text{OH}$   
**10b:** R =  $(\text{CH}_2)_3\text{OH}$   
**10c:** R =  $(\text{CH}_2)_4\text{OH}$   
**10d:** R =  $(\text{CH}_2)_5\text{OH}$   
**10e:** R =  $(\text{CH}_2)_6\text{OH}$

**Scheme (4).** Synthesis of compounds **10a-10e**. Reagents: (i) appropriate  $\omega$ -hydroxyalkylamine (1 equiv), anhydrous DMF,  $90^\circ\text{C}$ , 4 h, then cooled to rt and poured into distilled water.

occurred and typically after 4 hours, anhydrides were fully consumed. After cooling, the formed precipitate was washed with plenty of water and recrystallized from ethanol (96%).

The mono- $\omega$ -hydroxylalkylamino imides **10a-10e** were synthesized by reaction of 4-bromo derivatives **7a-7e** with equimolar ratio of appropriate amine alcohol by heating in anhydrous DMF (**Scheme 4**). The bi- $\omega$ -hydroxylalkylamino derivatives **11a-12e** were obtained by reaction of 4,5-dinitro derivatives **8a-8e** with 2.5-fold molar excess of appropriate amine alcohol by heating in anhydrous DMF, precipitated by addition of water, dried in the air and purified using column chromatography (5%  $\text{MeOH}:\text{CHCl}_3$ ) (**Scheme 5**).



**Scheme (5).** Synthesis of compounds **11a-12e**. Reagents: (i) appropriate  $\omega$ -hydroxyalkylamine (2.5 equiv), EtOH (96%), reflux, 4 h.

**Compound 2a:** Nitric acid (65%, 4.6 ml, 72 mmol) was slowly added to a solution of acenaphthene (9.3 g, 60 mmol) in glacial acetic acid (90 ml) at -15°C. The reaction mixture was stirred at room temperature for 4 h, poured into twice its volume of distilled water (180 ml) and extracted with ethyl acetate (3x50 ml). The combined organic layer was washed with saturated solution of NaHCO<sub>3</sub>, dried over Na<sub>2</sub>SO<sub>4</sub> and filtrated. After evaporation, the crude grey solid was purified using column chromatography (10% MeOH-CHCl<sub>3</sub>) yielding 7.2 g (60%) of pure product. White solid. Mp: 102-103°C (lit. 101-102°C) [20]. <sup>1</sup>H NMR (CDCl<sub>3</sub>, 400 MHz):  $\delta$  3.34 (t,  $J = 7.4$  Hz, 4H), 7.39 (t,  $J = 7.6$  Hz, 1H), 7.55 (d,  $J = 8.0$  Hz, 1H), 7.72 (d,  $J = 7.6$  Hz, 1H), 7.93 (d,  $J = 8.0$  Hz, 1H), 8.44 (d,  $J = 7.6$  Hz, 1H). <sup>13</sup>C NMR (CDCl<sub>3</sub>, 400 MHz):  $\delta$  30.4, 30.6, 117.7, 119.9, 121.1, 125.1, 127.5, 131.3, 139.8, 140.1, 146.5, 147.1. ESI-MS ( $m/z$ ): 222.19 [M+Na]<sup>+</sup>.

**Compound 2b:** A solution of *N*-bromosuccinimide (9.5 g, 53 mmol) in DMF (50 ml) was added to a suspension of acenaphthene (8.2 g, 53 mmol) in DMF (30 ml) and stirred at room temperature for 4 h. The white suspension gradually turned yellow-green. After the completion of the reaction, as indicated by TLC (5% MeOH:CHCl<sub>3</sub>), the reaction mixture was poured into twice its volume of distilled water (100 ml). A pale yellow solid was filtered off, washed with plenty of water, dried and recrystallized from absolute ethanol. White solid. Yield 83%. Mp: 51°C (lit. 51-52°C) [21]. <sup>1</sup>H NMR (CDCl<sub>3</sub>, 400 MHz):  $\delta$  3.32-3.36 (m, 2H), 3.40-3.45 (m, 2H), 7.12 (d,  $J = 7.3$  Hz, 1H), 7.33 (d,  $J = 6.9$  Hz, 1H), 7.53-7.58 (m, 1H), 7.67 (d,  $J = 7.3$  Hz, 1H), 7.78 (d,  $J = 8.4$  Hz, 1H). <sup>13</sup>C NMR (CDCl<sub>3</sub>, 400 MHz):  $\delta$  29.8, 30.5, 116.5, 119.9, 120.1, 121.5, 124.1, 128.9, 130.7, 140.0, 145.7, 146.1. ESI-MS ( $m/z$ ): 256.09 [M+Na]<sup>+</sup>.

**Procedure for the synthesis of 3a-3b:** A mixture of the appropriate compounds **2a-2b** (15 mmol) and glacial acetic acid (25 ml) was added to a suspension of K<sub>2</sub>Cr<sub>2</sub>O<sub>7</sub> (11.4 g, 38.8 mmol) in glacial acetic acid (25 ml). After addition, the mixture was refluxed for about 4 h. After the completion of the reaction, as indicated by TLC (10% MeOH:CHCl<sub>3</sub>), the mixture was cooled and poured into distilled water with ice (300 ml). The resulting precipitate was then filtered off and washed with plenty of distilled water until a neutral pH was reached, dried for several days in the air and recrystallized twice from absolute ethanol to give pure products.

**Compound 3a:** Yellow solid. Yield 80.1%. Mp: 228-230°C (lit. 227-228°C) [21]. <sup>1</sup>H NMR (DMSO-*d*<sub>6</sub>, 400 MHz):  $\delta$  8.09 (t,  $J = 7.6$  Hz, 1H), 8.71 (d,  $J = 7.8$  Hz, 1H), 8.83 (d,  $J = 7.8$  Hz, 1H), 8.93 (d,  $J = 7.6$  Hz, 1H), 9.53 (d,  $J = 7.6$  Hz, 1H). <sup>13</sup>C NMR (DMSO-*d*<sub>6</sub>, 100 MHz):  $\delta$  119.8, 121.4, 124.2, 124.4, 129.5, 130.6, 130.8, 131.7, 135.4, 137.2, 145.8, 159.6, 159.8. ESI-MS ( $m/z$ ): 244.21 [M+H]<sup>+</sup>.

**Compound 3b:** White solid. Yield 75.6%. Mp: 220-222°C (lit. 218-220°C) [21]. <sup>1</sup>H NMR (DMSO-*d*<sub>6</sub>, 600 MHz):  $\delta$  7.90 (t,  $J = 8.0$  Hz, 1H), 8.09 (d,  $J = 8.4$  Hz, 1H), 8.19 (d,  $J = 8.4$  Hz, 1H), 8.39 (d,  $J = 8.0$  Hz, 1H), 8.45 (d,  $J = 8.0$  Hz, 1H). <sup>13</sup>C NMR (DMSO-*d*<sub>6</sub>, 150 MHz):  $\delta$  121.8, 122.6, 128.1, 128.6, 128.9, 129.6, 130.7, 131.2, 131.3, 132.3, 162.6, 162.7. ESI-MS ( $m/z$ ): 278.08 [M+H]<sup>+</sup>.

**Compound 4:** White solid. Yield 75.6%. Mp: 220-222°C (lit. 218-220°C) [22]. <sup>1</sup>H NMR (DMSO-*d*<sub>6</sub>, 600 MHz):  $\delta$  7.90 (t,  $J = 8.0$  Hz, 1H), 8.09 (d,  $J = 8.4$  Hz, 1H), 8.19 (d,  $J = 8.4$  Hz, 1H), 8.39 (d,  $J = 8.0$  Hz, 1H), 8.45 (d,  $J = 8.0$  Hz, 1H). <sup>13</sup>C NMR (DMSO-*d*<sub>6</sub>, 150 MHz):  $\delta$  121.8, 122.6, 128.1, 128.6, 128.9, 129.6, 130.7, 131.2, 131.3, 132.3, 162.6, 162.7. ESI-MS ( $m/z$ ): 278.08 [M+H]<sup>+</sup>.

**Compound 5:** A solution of compound **3a** (4.86 g, 20 mmol) in ethanol (96%, 50 ml) was added dropwisely to a vigorously stirred suspension of SnCl<sub>2</sub>·2H<sub>2</sub>O (22.6 g, 100 mmol) in ethanol (96%, 50 ml) and heated to reflux for 4 h. The mixture was then cooled to room temperature and the resulting precipitate was collected by filtration, washed with distilled water and dried in the air. The recrystallization from absolute ethanol gave 3.8 g of pure compound. Yellow solid. Yield 89%. Mp: >300°C (lit. >360°C) [23]. <sup>1</sup>H NMR (DMSO-*d*<sub>6</sub>, 400 MHz):  $\delta$  6.83 (d,  $J = 8.4$  Hz, 1H), 7.63 (t,  $J = 8.4$  Hz, 1H, H-6), 7.74 (s, 2H), 8.21 (d,  $J = 8.4$  Hz, 1H), 8.39 (d,  $J = 8.4$  Hz, 1H), 8.58 (d,  $J = 8.4$  Hz, 1H). <sup>13</sup>C NMR (DMSO-*d*<sub>6</sub>, 100 MHz):  $\delta$  107.6, 108.1, 119.3, 121.8, 123.7, 129.3, 129.6, 131.1, 133.5, 152.6, 162.9, 163.3. ESI-MS ( $m/z$ ): found 214.11 [M+H]<sup>+</sup>.

**Procedure for the synthesis of 6a-9e:** An appropriate amine alcohol (2 mmol) was added in on portion to a stirred solution of the corresponding anhydride **3a-5** (2 mmol) in ethanol (96%, 20 ml). The reaction mixture was refluxed for 4 h. After cooling to room temperature, the formed solid was filtrated off, washed with distilled water and recrystallized from absolute ethanol to give product of high purity.

**Procedure for the synthesis of 10a-10e:** A solution of appropriate compounds **7a-7e** (2 mmol) and amine alcohol (2 mmol) in anhydrous DMF (20 ml) was stirred and heated at 90°C for about 4 h. After total consumption of substrates, as indicated by TLC (10% MeOH:CHCl<sub>3</sub>), the mixture was poured into water (50 ml), the precipitate was filtered off, washed with distilled water and recrystallized from absolute ethanol to give product of high purity.

**Procedure for the synthesis of 11a-12e:** A solution of appropriate compounds **7a-7e** (2 mmol) and amine alcohol (5 mmol) in anhydrous DMF (20 ml) was stirred and heated at 90°C for 4 h. After total consumption of substrates **7a-7e**, the mixture was poured into distilled water (50 ml). Then the precipitate was filtered, washed with plenty of distilled water and dried in the air. Pure products were easily obtained using chromatography column (5% MeOH:CHCl<sub>3</sub>). Firstly, bi- and then mono-substituted derivatives were eluted.

**Compound 6a:** Yellow solid. Yield 72%. Mp: 185-186°C. <sup>1</sup>H NMR (DMSO-*d*<sub>6</sub>, 400 MHz): δ 3.59 (t, *J* = 6.6 Hz, 2H), 4.10 (t, *J* = 6.6 Hz, 2H), 4.81 (t, *J* = 6.0 Hz, 1H), 8.00 (t, *J* = 8.0 Hz, 1H), 8.48 (d, *J* = 8.0 Hz, 1H), 8.52-8.59 (m, 2H), 8.63 (d, *J* = 8.0 Hz, 1H). <sup>13</sup>C NMR (DMSO-*d*<sub>6</sub>, 100 MHz): δ 42.1, 57.6, 122.5, 122.6, 124.4, 126.8, 128.2, 128.6, 129.5, 130.0, 131.6, 149.0, 162.8, 162.9. ESI-MS (m/z): 287.25 [M+H]<sup>+</sup>.

**Compound 6b:** Yellow solid. Yield 82%. Mp: 165-166°C. <sup>1</sup>H NMR (DMSO-*d*<sub>6</sub>, 400 MHz): δ 1.79-1.85 (m, 2H), 3.52 (t, *J* = 6.8 Hz, 2H), 4.10 (t, *J* = 6.8 Hz, 2H), 4.51 (t, *J* = 5.0 Hz, 1H), 8.05 (t, *J* = 8.8 Hz, 1H), 8.49-8.64 (m, 4H). <sup>13</sup>C NMR (DMSO-*d*<sub>6</sub>, 100 MHz): δ 30.7, 38.0, 59.0, 122.6, 122.7, 124.2, 126.6, 128.2, 128.6, 129.5, 130.0, 131.6, 149.0, 162.1, 162.9. ESI-MS (m/z): 301.25 [M+H]<sup>+</sup>.

**Compound 6c:** Yellow solid. Yield 84%. Mp: 133-134°C. <sup>1</sup>H NMR (DMSO-*d*<sub>6</sub>, 400 MHz): δ 1.50-1.53 (m, 2H), 1.64-1.71 (m, 2H), 3.44 (t, *J* = 7.4 Hz, 2H), 4.05 (t, *J* = 7.4 Hz, 2H), 4.40 (t, *J* = 5.6 Hz, 1H), 8.03 (t, *J* = 8.4 Hz, 1H), 8.48 (d, *J* = 7.8 Hz, 1H), 8.52-8.56 (m, 2H), 8.61 (d, *J* = 8.4 Hz, 1H). <sup>13</sup>C NMR (DMSO-*d*<sub>6</sub>, 100 MHz): δ 24.3, 30.1, 40.1, 60.5, 122.4, 122.5, 124.3, 126.8, 128.3, 128.6, 129.7, 130.0, 131.4, 148.7, 162.1, 162.4. ESI-MS (m/z): 315.29 [M+H]<sup>+</sup>.

**Compound 6d:** Yellow solid. Yield 78%. Mp: 120-121°C. <sup>1</sup>H NMR (DMSO-*d*<sub>6</sub>, 600 MHz): δ 1.35-1.40 (m, 2H), 1.46-1.50 (m, 2H), 1.62-1.67 (m, 2H), 3.40 (t, *J* = 7.4 Hz, 2H), 4.01 (t, *J* = 7.4 Hz, 2H), 4.37 (br, 1H), 8.04 (t, *J* = 8.4 Hz, 1H), 8.50 (d, *J* = 7.8 Hz, 1H), 8.53-8.57 (m, 2H), 8.63 (d, *J* = 8.4 Hz, 1H). <sup>13</sup>C NMR (DMSO-*d*<sub>6</sub>, 150 MHz): δ 23.0, 27.2, 32.2, 40.0, 60.5, 122.6, 122.7, 124.2, 126.5, 128.2, 128.6, 129.5, 130.0, 131.6, 149.0, 162.0, 162.8. ESI-MS (m/z): 329.26 [M+H]<sup>+</sup>.

**Compound 6e:** Yellow solid. Yield 78%. Mp: 112-113°C. <sup>1</sup>H NMR (DMSO-*d*<sub>6</sub>, 400 MHz): δ 1.33-1.35 (m, 4H), 1.40-1.43 (m, 2H), 1.61-1.65 (m, 2H), 3.38 (t, *J* = 7.6 Hz, 2H), 4.01 (t, *J* = 7.4 Hz, 2H), 4.38 (br, 1H), 8.06 (t, *J* = 8.8 Hz, 1H), 8.45-8.58 (m, 2H), 8.56 (d, *J* = 8.4 Hz, 1H), 8.65 (d, *J* = 8.4 Hz, 1H). <sup>13</sup>C NMR (DMSO-*d*<sub>6</sub>, 100 MHz): δ 25.2, 26.4, 27.4, 32.4, 40.2, 60.6, 122.6, 122.7, 124.2, 126.4, 128.3, 128.6, 129.6, 130.0, 131.6, 149.0, 162.1, 162.8. ESI-MS (m/z): 343.22 [M+H]<sup>+</sup>.

**Compound 8a:** Orange solid. Yield 60%. Mp: 230-231°C. <sup>1</sup>H NMR (DMSO-*d*<sub>6</sub>, 400 MHz): δ 3.60 (t, *J* = 6.6 Hz, 2H), 4.10 (t, *J* = 6.6 Hz, 2H), 4.76 (t, *J* = 5.8 Hz, 1H), 8.64-8.73 (m, 4H). <sup>13</sup>C NMR (DMSO-*d*<sub>6</sub>, 100 MHz): δ 42.2, 57.8, 113.9, 126.9 (x2), 127.4 (x2), 129.3, 131.1 (x2), 147.1 (x2), 162.0 (x2). ESI-MS (m/z): 332.23 [M+H]<sup>+</sup>.

**Compound 8b:** Orange solid. Yield 56%. Mp: 218-219°C. <sup>1</sup>H NMR (DMSO-*d*<sub>6</sub>, 400 MHz): δ 2.46-2.56 (m, 2H), 4.20 (t, *J* = 6.2 Hz, 2H), 4.80 (t, *J* = 7.4 Hz, 2H), 5.20 (t, *J* = 5.0 Hz, 1H), 9.36-9.41 (m, 4H). <sup>13</sup>C NMR (DMSO-*d*<sub>6</sub>, 100 MHz): δ 30.6, 40.2, 58.9, 114.1, 127.2 (x2), 127.6 (x2), 129.5, 131.0 (x2), 147.1 (x2), 161.7 (x2). ESI-MS (m/z): 346.22 [M+H]<sup>+</sup>.

**Compound 8c:** Orange solid. Yield 60%. Mp: 207-208°C. <sup>1</sup>H NMR (DMSO-*d*<sub>6</sub>, 400 MHz): δ 1.64-1.92 (m, 4H), 3.72 (t, *J* = 6.6 Hz, 2H), 4.04 (t, *J* = 7.4 Hz, 2H), 4.34 (br, 1H), 8.64-8.72 (m, 4H). <sup>13</sup>C NMR (DMSO-*d*<sub>6</sub>, 100 MHz): δ 24.4, 30.6, 40.1, 60.7, 114.3, 127.2 (x2), 127.7 (x2),

129.5, 131.0 (x2), 147.0 (x2), 161.5 (x2). ESI-MS (m/z): 360.30 [M+H]<sup>+</sup>.

**Compound 8d:** Orange solid. Yield 53%. Mp: 191-192°C. <sup>1</sup>H NMR (DMSO-*d*<sub>6</sub>, 400 MHz): δ 1.36-1.40 (m, 2H), 1.44-1.52 (m, 2H), 1.59-1.67 (m, 2H), 3.39 (t, *J* = 7.0, 2H), 4.04 (t, *J* = 7.2 Hz, 2H), 4.35 (t, *J* = 5.2 Hz, 1H), 8.67-8.73 (m, 4H). <sup>13</sup>C NMR (DMSO-*d*<sub>6</sub>, 100 MHz): δ 22.94, 27.09, 32.2, 40.3, 60.4, 114.1, 127.1 (x2), 127.5 (x2), 129.5, 131.1 (x2), 147.1 (x2), 161.1 (x2). ESI-MS (m/z): 374.10 [M+H]<sup>+</sup>.

**Compound 8e:** Orange solid. Yield 53%. Mp: 175-176°C. <sup>1</sup>H NMR (DMSO-*d*<sub>6</sub>, 400 MHz): δ 1.32-1.41 (m, 4H), 1.42-1.45 (m, 2H), 1.62 (m, 2H), 3.36 (t, *J* = 7.2 Hz, 2H), 4.06 (t, *J* = 7.4 Hz, 2H), 4.32 (t, *J* = 5.0 Hz, 1H), 8.69-8.74 (m, 4H). <sup>13</sup>C NMR (DMSO-*d*<sub>6</sub>, 100 MHz): δ 24.9, 25.7, 27.0, 32.2, 40.1, 60.5, 116.9, 126.6(x2), 127.3 (x2), 129.4, 133.1 (x2), 145.1 (x2), 169.0 (x2). ESI-MS (m/z): 388.11 [M+H]<sup>+</sup>.

**Compound 9a:** Red solid. Yield 84%. Mp: 208-209°C. <sup>1</sup>H NMR (DMSO-*d*<sub>6</sub>, 400 MHz): δ 3.60 (q, *J* = 6.4 Hz, 2H), 4.10 (t, *J* = 6.4 Hz, 2H), 4.45 (s, 1H), 6.83 (d, *J* = 8.4 Hz, 1H), 7.40 (s, 2H), 7.63 (t, *J* = 8.4 Hz, 1H), 8.21 (d, *J* = 8.8 Hz, 1H), 8.39 (d, *J* = 8.2 Hz, 1H), 8.58 (d, *J* = 8.2 Hz, 1H). <sup>13</sup>C NMR (DMSO-*d*<sub>6</sub>, 100 MHz): δ 42.1, 57.6, 107.6, 108.1, 119.3, 121.8, 123.7, 129.3, 129.6, 131.1, 133.5, 152.6, 162.9, 163.3. ESI-MS (m/z): 257.27 [M+H]<sup>+</sup>.

**Compound 9b:** Orange solid. Yield 88%. Mp: 199-200°C. <sup>1</sup>H NMR (DMSO-*d*<sub>6</sub>, 400 MHz): δ 1.72-1.79 (m, 2H), 3.47 (t, *J* = 7.6 Hz, 2H), 4.06 (t, *J* = 7.6 Hz, 2H), 4.45 (s, 1H), 6.83 (d, *J* = 8.4 Hz, 1H), 7.40 (s, 2H), 7.63 (t, *J* = 8.4 Hz, 1H), 8.17 (d, *J* = 8.8 Hz, 1H), 8.40 (d, *J* = 8.0 Hz, 1H), 8.58 (d, *J* = 8.0 Hz, 1H). <sup>13</sup>C NMR (DMSO-*d*<sub>6</sub>, 100 MHz): δ 31.2, 36.9, 59.0, 107.6, 108.1, 119.3, 121.8, 123.9, 129.2, 129.6, 130.9, 133.9, 152.6, 162.9, 163.8. ESI-MS (m/z): 271.22 [M+H]<sup>+</sup>.

**Compound 9c:** Orange solid. Yield 83%. Mp: 188-189°C. <sup>1</sup>H NMR (DMSO-*d*<sub>6</sub>, 400 MHz): δ 1.46-1.53 (m, 2H), 1.60-1.70 (m, 2H), 3.42 (t, *J* = 7.4 Hz, 2H), 4.07 (t, *J* = 7.6 Hz, 2H), 4.39 (br, 1H), 6.85 (d, *J* = 8.4 Hz, 1H), 7.46 (s, 2H), 7.64 (t, *J* = 7.6 Hz, 1H), 8.18 (d, *J* = 8.4 Hz, 1H), 8.41 (d, *J* = 8.0 Hz, 1H), 8.58 (d, *J* = 8.0 Hz, 1H). <sup>13</sup>C NMR (DMSO-*d*<sub>6</sub>, 100 MHz): δ 24.2, 31.0, 40.1, 60.5, 107.6, 108.0, 119.0, 122.0, 123.9, 129.2, 129.7, 131.0, 133.8, 152.6, 162.9, 163.5. ESI-MS (m/z): 285.29 [M+H]<sup>+</sup>.

**Compound 9d:** Yellow solid. Yield 87%. Mp: 178-179°C. <sup>1</sup>H NMR (DMSO-*d*<sub>6</sub>, 600 MHz): δ 1.33-1.38 (m, 2H), 1.45-1.50 (m, 2H), 1.59-1.64 (m, 2H), 3.41 (t, *J* = 6.6 Hz, 2H), 4.01 (t, *J* = 7.5 Hz, 2H), 4.37 (br, 1H), 6.86 (d, *J* = 8.4 Hz, 1H), 7.43 (s, 2H), 7.65 (t, *J* = 7.5 Hz, 1H), 8.20 (d, *J* = 8.4 Hz, 1H), 8.42 (d, *J* = 7.2 Hz, 1H), 8.62 (d, *J* = 7.2 Hz, 1H). <sup>13</sup>C NMR (DMSO-*d*<sub>6</sub>, 150 MHz): δ 23.1, 27.6, 32.3, 39.1, 60.5, 107.6, 108.1, 119.4, 121.8, 123.9, 129.2, 129.6, 130.9, 133.9, 152.6, 162.9, 163.7. ESI-MS (m/z): 299.27 [M+H]<sup>+</sup>.

**Compound 9e:** Yellow solid. Yield 85%. Mp: 159-160°C. <sup>1</sup>H NMR (DMSO-*d*<sub>6</sub>, 600 MHz): δ 1.30-1.42 (m, 6H), 1.56-1.60 (m, 2H), 3.66 (t, *J* = 6.4 Hz, 2H), 3.98 (t, *J* = 7.2 Hz, 2H), 4.32 (br, 1H), 6.83 (d, *J* = 8.0 Hz, 1H), 7.61 (s, 2H), 7.63 (t, *J* = 8.0 Hz, 1H), 8.17 (d, *J* = 8.4 Hz, 1H), 8.40 (d, *J* = 8.0 Hz, 1H), 8.60 (d, *J* = 8.0 Hz, 1H). <sup>13</sup>C NMR

(DMSO-*d*<sub>6</sub>, 150 MHz):  $\delta$  25.2, 26.5, 27.7, 32.4, 40.2, 60.6, 107.6, 108.1, 119.3, 121.8, 123.9, 129.2, 129.6, 130.9, 133.8, 152.6, 162.9, 163.7. ESI-MS (m/z): 313.34 [M+H]<sup>+</sup>.

**Compound 10a:** Yellow solid. Yield 84%. Mp: 199-200°C. <sup>1</sup>H NMR (DMSO-*d*<sub>6</sub>, 400 MHz): 3.36-3.60 (m, 4H), 3.64 (t, *J* = 5.6 Hz, 2H), 4.11 (t, *J* = 6.4 Hz, 2H), 4.79 (t, *J* = 6.0 Hz, 1H), 4.92 (t, *J* = 5.0 Hz, 1H), 6.75 (d, *J* = 8.8 Hz, 1H), 7.67 (t, *J* = 7.8 Hz, 1H), 7.75 (t, *J* = 6.6 Hz, 1H), 8.25 (d, *J* = 8.8 Hz, 1H), 8.41 (d, *J* = 7.2 Hz, 1H), 8.66 (d, *J* = 8.8 Hz, 1H). <sup>13</sup>C NMR (DMSO-*d*<sub>6</sub>, 100 MHz):  $\delta$  41.8, 46.02, 57.8, 58.5, 103.7, 106.5, 120.0, 121.7, 124.2, 128.3, 129.4, 130.4, 133.9, 151.0, 160.9, 162.6. ESI-MS (m/z): 301.31 [M+H]<sup>+</sup>.

**Compound 10b:** Yellow solid. Yield 80%. Mp: 155-156°C. <sup>1</sup>H NMR (DMSO-*d*<sub>6</sub>, 600 MHz):  $\delta$  1.75-1.79 (m, 4H), 1.86-1.90 (m, 4H), 3.35-3.59 (m, 4H), 4.47 (br, 1H), 4.64 (br, 1H), 6.77 (d, *J* = 9.0 Hz, 1H), 7.67 (t, *J* = 7.8 Hz, 1H), 7.75 (t, *J* = 5.4 Hz, 1H), 8.25 (d, *J* = 9.0 Hz, 1H), 8.42 (d, *J* = 7.2 Hz, 1H), 8.66 (d, *J* = 9.0 Hz, 1H). <sup>13</sup>C NMR (DMSO-*d*<sub>6</sub>, 150 MHz):  $\delta$  31.1, 31.2, 37.0, 40.1, 58.5, 59.0, 103.7, 107.5, 120.1, 121.8, 124.2, 128.4, 129.4, 130.6, 134.2, 150.7, 162.9, 163.7. ESI-MS (m/z): 329.34 [M+H]<sup>+</sup>.

**Compound 10c:** Yellow solid. Yield 80%. Mp: 120-121°C. <sup>1</sup>H NMR (DMSO-*d*<sub>6</sub>, 400 MHz):  $\delta$  1.46-1.53 (m, 8H), 1.63-1.78 (m, 4H), 3.64 (t, *J* = 7.6 Hz, 2H), 3.97 (t, *J* = 7.6 Hz, 2H), 4.33 (br, 1H), 4.40 (br, 1H), 6.72 (d, *J* = 8.4 Hz, 1H), 7.61 (t, *J* = 7.8 Hz, 1H), 7.75 (t, *J* = 5.4 Hz, 1H), 8.25 (d, *J* = 8.4 Hz, 1H), 8.41 (d, *J* = 7.2 Hz, 1H), 8.64 (d, *J* = 8.2 Hz, 1H). <sup>13</sup>C NMR (DMSO-*d*<sub>6</sub>, 100 MHz):  $\delta$  24.3, 24.8, 30.1, 31.2, 40.0, 41.1, 60.4, 60.6, 104.1, 108.0, 119.9, 121.4, 124.3, 128.2, 129.8, 131.1, 134.9, 150.2, 162.2, 162.3. ESI-MS (m/z): 357.41 [M+H]<sup>+</sup>.

**Compound 10d:** Yellow solid. Yield 81%. Mp: 89-90°C. <sup>1</sup>H NMR (DMSO-*d*<sub>6</sub>, 400 MHz):  $\delta$  1.31-1.57 (m, 8H), 1.60-1.72 (m, 4H), 3.24-3.45 (m, 4H), 3.66 (t, *J* = 7.4 Hz, 2H), 3.99 (t, *J* = 7.6 Hz, 2H), 4.33 (t, *J* = 6.0 Hz, 1H), 4.41 (t, *J* = 5.4 Hz, 1H), 6.79 (d, *J* = 8.4 Hz, 1H), 7.62 (t, *J* = 7.8 Hz, 1H), 7.71 (t, *J* = 5.4 Hz, 1H), 8.28 (d, *J* = 8.4 Hz, 1H), 8.44 (d, *J* = 7.4 Hz, 1H), 8.69 (d, *J* = 8.0 Hz, 1H). <sup>13</sup>C NMR (DMSO-*d*<sub>6</sub>, 100 MHz):  $\delta$  23.0, 23.3, 27.3, 28.0, 32.2, 32.3, 38.9, 41.7, 60.4, 60.6, 103.5, 107.5, 120.2, 121.5, 124.2, 128.3, 129.4, 130.3, 134.0, 151.0, 161.6, 162.6. ESI-MS (m/z): 385.47 [M+H]<sup>+</sup>.

**Compound 10e:** Yellow solid. Yield 86%. Mp: 84-85°C. <sup>1</sup>H NMR (DMSO-*d*<sub>6</sub>, 400 MHz):  $\delta$  1.31-1.51 (m, 12H), 1.60-1.66 (m, 4H), 3.23-3.46 (m, 4H), 3.68 (t, *J* = 7.4 Hz, 2H), 3.98 (t, *J* = 7.6 Hz, 2H), 4.31-4.36 (m, 2H), 6.72 (d, *J* = 8.4 Hz, 1H), 7.62 (t, *J* = 7.4 Hz, 1H), 7.74 (t, *J* = 5.4 Hz, 1H), 8.22 (d, *J* = 8.4 Hz, 1H), 8.40 (d, *J* = 7.2 Hz, 1H), 8.61 (d, *J* = 8.2 Hz, 1H). <sup>13</sup>C NMR (DMSO-*d*<sub>6</sub>, 100 MHz):  $\delta$  24.3, 25.0, 26.1, 26.3, 27.4, 27.5, 31.8, 31.9, 41.0, 43.5, 60.5, 60.6, 103.1, 108.0, 120.3, 121.3, 124.4, 128.3, 129.1, 130.4, 134.5, 150.1, 162.5, 162.6. ESI-MS (m/z): 413.42 [M+H]<sup>+</sup>.

**Compound 11a:** Red solid. Yield 28%. Mp: 191-192°C. <sup>1</sup>H NMR (DMSO-*d*<sub>6</sub>, 400 MHz):  $\delta$  3.34 (q, *J* = 5.6 Hz, 2H), 3.60 (q, *J* = 6.4 Hz, 2H), 3.66 (q, *J* = 5.6 Hz, 2H), 4.11 (t, *J* = 6.4 Hz, 2H), 4.79 (t, *J* = 6.0 Hz, 1H), 4.97 (t, *J* = 5.0 Hz, 1H), 6.04 (t, *J* = 4.8 Hz, 1H), 7.10 (d, *J* = 8.8 Hz, 1H), 8.70 (d, *J* = 8.0 Hz, 1H), 8.36 (d, *J* = 8.8 Hz, 1H), 8.48 (d, *J* = 8.0 Hz, 1H). <sup>13</sup>C NMR (DMSO-*d*<sub>6</sub>, 100 MHz):  $\delta$  41.8, 46.0, 57.8, 58.5, 108.7, 109.7, 110.6, 120.4, 125.0, 131.1, 134.3,

137.2, 148.2, 150.4, 162.5, 162.7. ESI-MS (m/z): 346.28 [M+H]<sup>+</sup>.

**Compound 11b:** Red solid. Yield 27%. Mp: 187-188°C. <sup>1</sup>H NMR (DMSO-*d*<sub>6</sub>, 400 MHz):  $\delta$  1.75 (m, 2H), 1.85 (m, 2H), 3.25-3.29 (m, 2H), 3.42 (q, *J* = 6.6 Hz, 2H), 3.62-3.64 (m, 2H), 4.01 (t, *J* = 7.2 Hz, 2H), 4.42 (t, *J* = 5.2 Hz, 1H), 4.70 (t, *J* = 5.2 Hz, 1H), 6.19 (t, *J* = 5.0 Hz, 1H), 7.09 (d, *J* = 8.4 Hz, 1H), 8.07 (d, *J* = 8.0 Hz, 1H), 8.33 (d, *J* = 8.8 Hz, 1H), 8.49 (d, *J* = 8.0 Hz, 1H). <sup>13</sup>C NMR (DMSO-*d*<sub>6</sub>, 100 MHz):  $\delta$  31.0, 31.4, 40.3, 41.5, 59.0, 59.1, 108.7, 110.2, 111.1, 121.1, 124.4, 131.4, 134.2, 137.6, 148.5, 150.3, 163.0, 163.3. ESI-MS (m/z): 374.23 [M+H]<sup>+</sup>.

**Compound 11c:** Red solid. Yield 26%. Mp: 179-180°C. <sup>1</sup>H NMR (DMSO-*d*<sub>6</sub>, 400 MHz):  $\delta$  1.48-1.72 (m, 8H), 3.24-3.45 (m, 6H), 4.05 (t, *J* = 6.8 Hz, 2H), 4.31-4.36 (m, 2H), 6.19 (t, *J* = 5.0 Hz, 1H), 7.09 (d, *J* = 8.4 Hz, 1H), 8.07 (d, *J* = 8.0 Hz, 1H), 8.33 (d, *J* = 8.8 Hz, 1H), 8.49 (d, *J* = 8.0 Hz, 1H). <sup>13</sup>C NMR (DMSO-*d*<sub>6</sub>, 100 MHz):  $\delta$  24.3, 24.6, 30.1, 30.2, 40.1, 41.3, 60.4, 60.6, 109.0, 109.8, 110.8, 121.2, 125.2, 131.3, 134.2, 137.3, 148.5, 150.5, 162.3, 162.5. ESI-MS (m/z): 402.40 [M+H]<sup>+</sup>.

**Compound 11d:** Red solid. Yield 29%. Mp: 114-115°C. <sup>1</sup>H NMR (DMSO-*d*<sub>6</sub>, 400 MHz):  $\delta$  1.28-1.30 (m, 2H), 1.35-1.42 (m, 6H), 1.43-1.48 (m, 2H), 1.68-1.72 (m, 2H), 3.17-3.32 (m, 2H), 3.36-3.46 (m, 6H), 4.33 (t, *J* = 6.0 Hz, 1H), 4.41 (t, *J* = 5.4 Hz, 1H), 6.10 (t, *J* = 4.8 Hz, 1H), 7.08 (d, *J* = 8.4 Hz, 1H), 8.71 (d, *J* = 8.0 Hz, 1H), 8.34 (d, *J* = 8.4 Hz, 1H), 8.49 (d, *J* = 8.0 Hz, 1H). <sup>13</sup>C NMR (DMSO-*d*<sub>6</sub>, 100 MHz):  $\delta$  23.1, 23.3, 27.5, 28.0, 32.2, 32.3, 40.2, 42.9, 60.5, 60.6, 108.5, 110.0, 110.8, 121.7, 124.5, 134.1, 137.5, 148.1, 150.1, 163.0, 163.2. ESI-MS (m/z): 430.41 [M+H]<sup>+</sup>.

**Compound 11e:** Red solid. Yield 27%. Mp: 110-111°C. <sup>1</sup>H NMR (DMSO-*d*<sub>6</sub>, 400 MHz):  $\delta$  1.33-1.48 (m, 12H), 1.61-1.65 (m, 4H), 3.24-3.44 (m, 6H), 3.98 (t, *J* = 7.0 Hz, 2H), 4.31-4.36 (m, 2H), 6.21 (t, *J* = 4.8 Hz, 1H), 7.06 (d, *J* = 8.4 Hz, 1H), 8.07 (d, *J* = 8.0 Hz, 1H), 8.34 (d, *J* = 8.8 Hz, 1H), 8.47 (d, *J* = 8.0 Hz, 1H). <sup>13</sup>C NMR (DMSO-*d*<sub>6</sub>, 100 MHz):  $\delta$  25.2 (x2), 26.4, 26.5, 27.5, 27.7, 32.4, 32.5, 40.2, 43.6, 60.6, 60.7, 108.3, 109.1, 111.0, 121.8, 124.8, 130.3, 134.3, 137.1, 148.5, 150.7, 162.3, 162.7. ESI-MS (m/z): 458.50 [M+H]<sup>+</sup>.

**Compound 12a:** Red solid. Yield 32%. Mp: 175-176°C. <sup>1</sup>H NMR (DMSO-*d*<sub>6</sub>, 400 MHz):  $\delta$  3.31-3.35 (m, 4H), 3.53-3.58 (m, 4H), 3.73-3.76 (m, 4H), 4.06-4.11 (m, 3H), 6.83 (d, *J* = 8.8 Hz, 2H), 7.22 (t, *J* = 5.0 Hz, 2H), 8.20 (d, *J* = 8.8 Hz, 2H). <sup>13</sup>C NMR (DMSO-*d*<sub>6</sub>, 100 MHz):  $\delta$  46.3, 51.4 (x2), 63.3, 64.2 (x2), 111.8 (x2), 114.9 (x2), 115.4, 137.1, 138.3 (x2), 158.2 (x2), 168.6 (x2). ESI-MS (m/z): 360.22 [M+H]<sup>+</sup>.

**Compound 12b:** Red solid. Yield 31%. Mp: 151-152°C. <sup>1</sup>H NMR (DMSO-*d*<sub>6</sub>, 400 MHz):  $\delta$  1.76 (q, *J* = 6.8 Hz, 2H), 1.88 (t, *J* = 6.4 Hz, 2H), 3.29-3.31 (m, 4H), 3.45 (t, *J* = 6.0 Hz, 4H), 3.61-3.63 (m, 4H), 4.03 (t, *J* = 7.2 Hz, 2H), 4.44 (t, *J* = 5.2 Hz, 1H), 4.72 (t, *J* = 5.0 Hz, 2H), 6.79 (d, *J* = 8.8 Hz, 2H), 7.27 (t, *J* = 8.8 Hz, 2H), 8.20 (d, *J* = 8.8 Hz, 2H). <sup>13</sup>C NMR (DMSO-*d*<sub>6</sub>, 100 MHz):  $\delta$  30.9 (x2), 31.3, 40.2, 41.7 (x2), 59.0, 59.2 (x2), 105.9 (x2), 109.2 (x2), 109.7, 131.9, 133.1 (x2), 153.0 (x2), 163.4 (x2). ESI-MS (m/z): 402.20 [M+H]<sup>+</sup>.

**Compound 12c:** Red solid. Yield 33%. Mp: 131-132°C. <sup>1</sup>H NMR (DMSO-*d*<sub>6</sub>, 400 MHz):  $\delta$  1.64-1.97 (m, 14H), 3.72 (t, *J* = 5.6 Hz, 4H), 4.04 (t, *J* = 7.4 Hz, 6H), 4.34 (br, 1H),

4.38-4.41 (m, 2H), 6.79 (d,  $J = 8.8$  Hz, 2H), 7.25 (t,  $J = 8.8$  Hz, 2H), 8.19 (d,  $J = 8.8$  Hz, 2H).  $^{13}\text{C}$  NMR (DMSO- $d_6$ , 100 MHz):  $\delta$  24.2 (x2), 24.4, 30.5, 30.7 (x2), 40.0, 40.1 (x2), 60.3, 60.5 (x2), 105.9 (x2), 111.2 (x2), 111.6, 135.2, 137.0 (x2), 159.0 (x2), 166.9 (x2). ESI-MS (m/z): 444.45 [M+H] $^+$ .

**Compound 12d:** Red solid. Yield 37%. Mp: 111-112°C.  $^1\text{H}$  NMR (DMSO- $d_6$ , 400 MHz):  $\delta$  1.28-1.32 (m, 2H), 1.42-1.61 (m, 12H), 1.68-1.76 (m, 4H), 3.17-3.22 (m, 4H), 3.63-3.46 (m, 6H), 3.96 (t,  $J = 7.4$  Hz, 2H), 4.32-4.34 (m, 1H), 4.38-4.41 (m, 2H), 6.80 (d,  $J = 8.8$  Hz, 2H), 7.14 (t,  $J = 5.0$  Hz, 2H), 8.19 (d,  $J = 8.8$  Hz, 2H).  $^{13}\text{C}$  NMR (DMSO- $d_6$ , 100 MHz):  $\delta$  23.1, 23.3 (x2), 27.7, 28.1 (x2), 32.3, 32.4 (x2), 40.2, 43.9 (x2), 60.5, 60.6 (x2), 106.5 (x2), 109.7 (x2), 110.2, 131.8, 133.1 (x2), 153.6 (x2), 163.3 (x2). ESI-MS (m/z): 486.51 [M+H] $^+$ .

**Compound 12e:** Red solid. Yield 35%. Mp: 89-90°C.  $^1\text{H}$  NMR (DMSO- $d_6$ , 400 MHz):  $\delta$  1.30-1.49 (m, 24H), 1.62-1.65 (m, 4H), 3.35 (t,  $J = 7.2$  Hz, 4H), 4.06 (t,  $J = 7.4$  Hz, 4H), 4.33 (t,  $J = 5.0$  Hz, 1H), 4.38-4.41 (m, 2H), 6.80 (d,  $J = 8.8$  Hz, 2H), 7.14 (t,  $J = 5.0$  Hz, 2H), 8.19 (d,  $J = 8.8$  Hz, 2H).  $^{13}\text{C}$  NMR (DMSO- $d_6$ , 100 MHz):  $\delta$  25.2, 26.4 (x2), 26.5, 27.5 (x2), 27.7, 28.7 (x2), 32.4, 32.5 (x2), 40.2, 43.6 (x2), 60.6, 60.7 (x2), 106.5 (x2), 109.7 (x2), 110.2, 131.8, 133.1 (x2), 153.6 (x2), 163.3 (x2). ESI-MS (m/z): 528.69 [M+H] $^+$ .

## 2.2. MTT assay:

Cytotoxicity was estimated using the MTT assay (Sigma-Aldrich, Germany), according to the reported protocol [24]. 24h before addition of the tested compounds, the cells were plated in 96-well plates (Nunc, Germany) at the density of 2000 per well. Assays were performed after 72 h of continuous exposure to varying concentrations of the derivatives tested. Each compound was tested in ten different concentrations in a single experiment, which was repeated at least three times. Viability of cells was expressed as a percentage compared to a non-treated control.  $\text{IC}_{50}$  values were defined as a concentration of a compound at which cells viability decreased by 50%. This value was counted with the statistic of median-effect [25].

## 2.3. Topoisomerase II assay:

Decatenation assay was carried out using Topo II Assay Kit and human Topo II $\alpha$  (TopoGEN, USA) according to the manufacturer's instruction books. This assay utilizes the kinetoplast DNA from insect *Crithidia fasciculata*, since it forms an aggregate of interlocked (catenated) DNA circles (mostly 2.5 kb) that form extremely large networks of high molecular weight. Topo II decatenates the circles from the network. While the catenated circles are unable to enter an agarose gel, upon decatenation the free circles are detected as a discrete band on the gel.

## 2.4. Cell lines:

HCT 116 human colon cancer cells, A-549 human non-small cell lung cancer cells and non-tumorigenic BEAS-2B human bronchial epithelium cells were purchased from the ATCC (Manassas, VA, USA). Cells were grown in high-glucose containing DMEM medium (Sigma-Aldrich, DK) supplemented with 10% (v/v) fetal bovine serum (GIBCO Invitrogen, UK) and 40  $\mu\text{g}/\text{ml}$  gentamicin sulphate (Sigma-Aldrich, DK) at 37°C in the presence of 5%  $\text{CO}_2$ .

## 3. RESULTS AND DISCUSSION

### 3.1. Antiproliferative activity:

The preliminary antiproliferative activity of synthesized 1,8-naphthalimides **6a-12e** against two human cell lines was performed using a 72-hours standard MTT (tetrazolium dye) assay [24]. Obtained results were shown in **Table 1**, while Amonafide and Mitonafide were performed as positive control. The human cancer HCT 116 human colon cancer cells and human non-small cell lung epithelial cells A549 were used to assess cytotoxic activity of the 1,8-naphthalimides derivatives. All experiments were performed at least three times. Half-maximal inhibitory concentration ( $\text{IC}_{50}$ ) values are presented as mean  $\pm$  standard deviation (SD). The  $\text{IC}_{50}$  values of Amonafide and Mitonafide against HCT 116 and A549 cell lines presented in the study are in good agreement with other data reported in the literature [26, 27]. Most of the

**Table (1).** Antiproliferative activities of selected compounds against HCT 116 human colon cancer cells, human non-small cell lung cells A549 and non-tumorigenic BEAS-2B human bronchial epithelium cells.

Compound	HCT 116 wt $\text{IC}_{50}$ [ $\mu\text{M}$ ]	A549 $\text{IC}_{50}$ [ $\mu\text{M}$ ]	BEAS-2B $\text{IC}_{50}$ [ $\mu\text{M}$ ]
Amonafide	1.7 $\pm$ 0.4	7.0 $\pm$ 0.1	3.9 $\pm$ 0.1
Mitonafide	1.1 $\pm$ 0.1	1.8 $\pm$ 0.2	0.6 $\pm$ 0.1
<b>6a</b>	6.7 $\pm$ 0.9	7.8 $\pm$ 1.6	8.3 $\pm$ 1.5
<b>6b</b>	5.2 $\pm$ 1.9	6.2 $\pm$ 1.0	6.4 $\pm$ 1.7
<b>6c</b>	3.3 $\pm$ 0.1	4.6 $\pm$ 1.1	4.5 $\pm$ 0.5
<b>6d</b>	4.1 $\pm$ 2.5	9.8 $\pm$ 1.7	1.4 $\pm$ 0.3
<b>6e</b>	2.9 $\pm$ 0.5	3.8 $\pm$ 0.1	5.5 $\pm$ 0.2
<b>8a</b>	1.7 $\pm$ 0.2	2.8 $\pm$ 0.8	NT
<b>8b</b>	1.0 $\pm$ 0.1	2.5 $\pm$ 0.2	2.5 $\pm$ 1.1
<b>8c</b>	2.3 $\pm$ 0.3	3.5 $\pm$ 0.5	NT
<b>8d</b>	0.5 $\pm$ 0.1	3.1 $\pm$ 0.4	1.4 $\pm$ 0.1
<b>8e</b>	1.7 $\pm$ 0.1	2.2 $\pm$ 0.2	0.8 $\pm$ 0.1
<b>9a</b>	46.9 $\pm$ 0.7	>100	NT
<b>9b</b>	39.5 $\pm$ 7.1	>100	52.6 $\pm$ 8.4
<b>9c</b>	55.2 $\pm$ 1.2	>100	NT
<b>9d</b>	65.4 $\pm$ 1.7	>100*	>100*
<b>9e</b>	>50*	>50*	>50*
<b>10a</b>	>50*	>50*	>50*
<b>10b</b>	>50*	>50*	>50*
<b>10c</b>	46.9 $\pm$ 2.9	57.5 $\pm$ 0.1	103.4 $\pm$ 3.4
<b>10d</b>	39.2 $\pm$ 2.8	91.7 $\pm$ 11.0	70.2 $\pm$ 0.8
<b>10e</b>	29.0 $\pm$ 1.5	55.8 $\pm$ 6.5	55.5 $\pm$ 2.1
<b>11a</b>	1.3 $\pm$ 0.1	1.8 $\pm$ 0.1	1.9 $\pm$ 0.1
<b>11b</b>	1.3 $\pm$ 0.1	1.6 $\pm$ 0.1	2.1 $\pm$ 0.2
<b>11c</b>	1.1 $\pm$ 0.1	1.3 $\pm$ 0.2	1.6 $\pm$ 0.1
<b>11d</b>	2.1 $\pm$ 0.3	1.1 $\pm$ 0.1	1.5 $\pm$ 0.1
<b>11e</b>	1.2 $\pm$ 0.1	2.4 $\pm$ 0.1	1.0 $\pm$ 0.1
<b>12a</b>	>100	>100	NT
<b>12b</b>	64.3 $\pm$ 10.0	64.1 $\pm$ 3.4	44.3 $\pm$ 5.8
<b>12c</b>	>100	>100	NT
<b>12d</b>	>100	>100	>100
<b>12e</b>	>100	>100	>100

\* The compound precipitated in the medium in this concentration. We could not calculate  $\text{IC}_{50}$  values. NT – compound not tested.



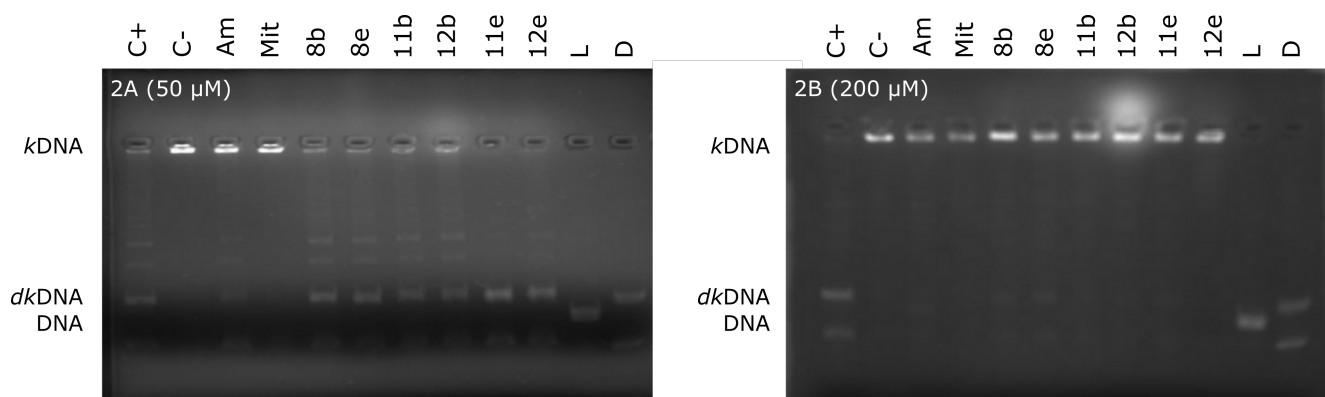


**Figure (2).** Decatenation of *kDNA* was assayed by monitoring the appearance of decatenated *dkDNA* in the presence of target compounds of different concentrations. “C+” refers to *kDNA* in the presence of Topo II as positive control, “C-” refers to *kDNA* in the absence of Topo II as negative control, “Am” refers to Amonafide, “Mit” refers to Mitonafide, “L” refers to linear DNA form marker and “D” refers to decatenated *dkDNA* form marker. (2A) Inhibition of Topo II-mediated *kDNA* decatenation by indicated compounds at concentration of 50  $\mu\text{M}$  or (2B) at concentration of 200  $\mu\text{M}$ .

newly synthesized compounds exhibited moderate to good antiproliferative activity, especially compounds **8a-8e** and **11a-11e** with at least one nitro group at the chromophore, compared to the control group. For a better understanding of structure-activity relationship and the effect of rigidity and flexibility of the compounds obtained, different lengths of side-chains were introduced in order to investigate their role in biological activity.

The most important is a type of substituents present on the naphthalene rings. Among all compounds tested, two series of nitro-substituted derivatives, **8a-8e** and **11a-11e**, demonstrated the highest cytotoxicity in the low micromolar range ( $\text{IC}_{50} = 0.5 - 3.5 \mu\text{M}$ ). The reason may be the presence of electron-withdrawing nitro groups may strongly enhance electrostatic interaction between intercalator and base pairs, which may greatly improve biological activities [28-30]. Furthermore, when there is more than one nitro group at the chromophore, as in the case of compounds **8a-8e** containing two neighboring nitro groups at 4- and 5-positions, a slight increase in antiproliferative activity can be observed. These conclusions are also in good agreement with literature data [19]. Interestingly, the compounds **11a-11e** with both nitro group and  $\omega$ -hydroxyalkylamine side-chain at 4,5-positions also showed fairly potent activity with the  $\text{IC}_{50}$  values of 1.1 to 2.4  $\mu\text{M}$ . To the best of our knowledge, this substitution pattern of 1,8-naphthalimides is presented here for the first time. The compounds **12a-12d** with two side-chains at the 4,5-positions, in contrast to **11a-11e**, showed no cytotoxic activity up to 100  $\mu\text{M}$ . Only a compound **12b** with a short side-chains, showed  $\text{IC}_{50}$  value of 64.3  $\mu\text{M}$ , probably due to less steric hindrance.

As shown in **Table 1**, there are no significant differences between the anticancer activity of compounds and respective series. In good agreement with another report on 4-alkylendiamine substituted 1,8-naphthalimides [31] are the findings indicating that the length of the side-chains have only weak effects on the anticancer properties. From the preliminary *in vitro* antiproliferative assay, we concluded that only the nitro substituted derivatives **8a-8e**, **11a-11e** and **12a-12e** showed good antiproliferative activities against HCT 116 and A549 cell lines. Thus, afterwards it was examined whether these compounds, especially the derivatives **8b**, **8e**, **11b** and **11e**,

may affect the activity of Topo II. The compounds **12b** and **12e** were used to study the significance of the side-chains length, as well as of the presence/absence of nitro groups.

### 3.2. Topoisomerase II activity:

According to the literature data, Amonafide is one of the most active 1,8-naphthalimide anticancer agent, which may intercalate into DNA and form a stable tertiary complex of intercalator–DNA–Topo II. Since the compounds presented herein are structurally similar to Amonafide (they contain a flat aromatic naphthalene system and flexible side-chains), their impact in the activity of Topo II with catenated DNA (*kDNA*) assay was tested, as described earlier [32]. Active Topo II can release free DNA minicircles from the extremely high molecular weight *kDNA* and thus enable migration that can be observed in agarose gel electrophoresis.

At concentration of 50  $\mu\text{M}$  of the tested compounds (**Fig. 2A**), only decatenation of *kDNA* by Topo II was at the same level as of Amonafide and Mitonafide. For compounds **8b**, **8e**, **11b** and **12b**, catenated and decatenated DNA (*dkDNA*) forms were observed. Compounds **11e** and **12e**, carrying the longest side-chains were not sufficient to inhibit the catalytic activity of Topo II, only decatenated form of DNA occurred. Subsequently, we tested the influence of the concentration of mentioned derivatives on the increase of the concentration of decatenated DNA form (**Fig. 2B**). It was demonstrated that upon treatment with concentration of 200  $\mu\text{M}$ , all derivatives display Topo II inhibitory activity, which may be compared with activity of Amonafide. However, no increase in linear DNA form was observed in the concentration up to 200  $\mu\text{M}$ , thus we conclude that tested compounds **8b**, **8e**, **11b**, **11e**, **12b** and **12e** act as the catalytic inhibitors rather than as the poison of Topo II.

## 4. CONCLUSION

We synthesized seven new series of 1,8-naphthalimides with differently substituted naphthalimide rings on 4- and 5-positions with  $\omega$ -hydroxyalkylamine side-chains in order to improve activity of these derivatives against cancer cells. The compounds investigated exhibited moderate to good cytotoxic activity against human cancer HCT-116 and A549 cells, mostly with an  $\text{IC}_{50}$  values in the one-digit micromolar

range, comparable to that of Amonafide. The activities of the derivatives were greatly affected by the chemical alternations at the 4,5-positions. Derivatives **9a-9e**, **10a-10e** and **12a-12e** which lack nitro groups at these positions exhibited much decreased cytotoxic activity, whereas, derivatives **6a-6e**, **8a-8e** and **11a-11e** containing at least one nitro group exhibited fairly potent cytotoxic activity. Considering that Amonafide and most of its derivatives are slightly more or equally active against cancer cells over normal cells, the newly-synthesed compounds were evaluated against the normal BEAS-2B human bronchial epithelium cells. Comparable cytotoxicity against the normal cell line and the cancer cell lines suggests that these compounds showed the low level of selectivity and search for new 1,8-naphthalimides with improved anticancer properties is necessary.

The influence of compounds **8b**, **8e**, **11b**, **11e**, **12b** and **12e** on the decatenation activity of Topo II was tested with *k*DNA assay. The results indicated that selected compounds completely inhibit Topo II catalytic activity, however, in a relatively high concentration of 200  $\mu$ M. Besides, it was also observed that there is no clear relationship between Topo II inhibition and cytotoxicity of the selected compounds. The compounds **12b** and **12e**, which did not display cytotoxicity at 100  $\mu$ M, inhibited Topo II activity at 200  $\mu$ M. Since they were not typical DNA intercalators in structure – **12b** and **12e** contain three flexible  $\omega$ -hydroxylalkylamine chains that can limit intercalation into DNA and thereby formation of a stable tertiary complex with Topo II. The obtained results do not preclude another possibility where compounds **12b** and **12e** could inhibit Topo II directly before formation of their complex with DNA. The confirmation of such behavior will be continued in another research program.

## CONFLICT OF INTEREST

The authors declare no conflict of interest.

## ACKNOWLEDGEMENTS

The authors would like to thank the Faculty of Chemistry of Silesian University of Technology for financial support.

## REFERENCES

- Hsiang, Y.H.; Jiang, J.B.; Liu, L.F. Topoisomerase II-Mediated DNA Cleavage by Amonafide and Its Structural Analogs. *Mol. Pharmacol.*, **1989**, *36*, 371–376.
- Kaina, B. DNA damage-triggered apoptosis: critical role of DNA repair, double-strand breaks, cell proliferation and signaling. *Biochem. Pharmacol.*, **2003**, *66*(8), 1547–1554.
- Hsiang, Y.H.; Jiang, J.B.; Liu, L.F. Naphthalimides Induce G2 Arrest Through the ATM-Activated Chk2-Executed Pathway in HCT116 Cells. *Neoplasia*, **2009**, *11*(11), 1226–1234.
- Rosell, R.; Carles, J.; Abad, A.; Ribelle, N.; Barnadas, A.; Benavides, A.; Miguel, M. Phase study of mitonafide in 120 hour continuous. *Invest. New Drugs*, **1992**, *10*(3), 171–175.
- Díaz-Rubio, E.; Martín, M.; López-Vega, J.M.; Casado, A.; Benavides, A. Phase I study of mitonafide with a 3-day administration schedule: early interruption due to severe central nervous system toxicity. *Invest. New Drugs*, **1994**, *12*(4), 277–281.
- Miller, A.A.; Case, D.; Harmon, M.; Savage, P.; Lesser, G.; Hurd, D.; Melin, S.A.J. Phase I study of lenalidomide in solid tumors. *J. Thorac. Oncol.*, **2007**, *2*(5), 445–449.
- Felder, T.B.; McLean, M.A.; Vestal, M.L.; Lu, K.; Farquhar, D.; Legha, S.S.; Shah, R.; Newman, R.A. Pharmacokinetics and metabolism of the antitumor drug amonafide (NCS308847) in humans. *Drug Metab. Dispos.*, **1987**, *15*(6), 773–778.
- Taningher, M.; Malacarne, D.; Izzotti, A.; Ugolini, D.; Parodi, S. Drug metabolism polymorphisms as modulators of cancer susceptibility. *Mutat. Res.*, **1999**, *436*(3), 227–261.
- Innocenti, F.; Iyer, L.; Ratain, M.J. Pharmacogenetics of anticancer agents: lessons from amonafide and irinotecan. *Drug Metab. Dispos.*, **2001**, *29*(4), 596–600.
- Ratain, M.J.; Mick, R.; Berezin, F.; Janisch, L.; Schilsky, R.L.; Vogelzang, N.J.; Lane, L.B. Phase I study of amonafide dosing based on acetylator phenotype. *Cancer Res.*, **1993**, *53*(10), 2304–2308.
- Norton, J.T.; Witschi, M.A.; Luong, L.; Kawamura, A.; Ghosh, S.; Stack, M.S.; Sim, E.; Avram, M.J.; Appella, D.H.; Huang, S. Synthesis and anticancer activities of 6-amino amonafide derivatives. *Anticancer Drugs*, **2008**, *19*(1), 23–36.
- Braña, M.F.; Castellano, J.M.; Jimenez, A.; Llombart, A.; Rabadan, F.P.; Roldan, M.; Roldan, C.; Santos, A.; Vazquez, D. Synthesis, cytostatic activity and mode of action of a new series of imide derivatives of 3-nitro-1,8-naphthalic acid. *Curr. Chemother.*, **1978**, *2*, 1216–1217.
- Braña, M.F.; Castellano, J.M.; Roldán, C.M.; Santos, A.; Vazquez, D.; Jimenez, A. Synthesis and mode(s) of action of a new series of imide derivatives of 3-nitro-1,8-naphthalic acid. *Cancer Chemother. Pharmacol.*, **1980**, *4*(1), 61–66.
- Wang, K.; An, H.; Wang, Y.; Yan, X.; Li, R.; Chen, H.; Zhang, P.; Li, J.; Li, X.; Zhang, J. Synthesis, DNA Binding Properties and Bioactivity of Naphthalimide Polyethylene imine Conjugates. *Chinese J. Org. Chem.*, **2012**, *32*(4), 696–702.
- Chen, Z.; Liang, X.; Zhang, H.; Xie, H.; Liu, J.; Xu, Y.; Zhu, W.; Wang, Y.; Wang, X.; Tan, S.; Kuang, D.; Qian, X. A new class of naphthalimide-based antitumor agents that inhibit topoisomerase II and induce lysosomal membrane permeabilization and apoptosis. *J. Med. Chem.*, **2010**, *53*(6), 2589–2600.
- Li, S.; Xu, S.; Tang, Y.; Ding, S.; Zhang, J.; Wang, S.; Zhou, G.; Zhou, C.; Li, X. Synthesis, anticancer activity and DNA-binding properties of novel 4-pyrazolyl-1,8-naphthalimide derivatives. *Bioorg. Med. Chem. Lett.*, **2014**, *24*(2), 586–590.
- Kokosza, K.; Andrei, G.; Schols, D.; Snoeck, R.; Piotrowska, D.G. Design, antiviral and cytostatic properties of isoxazolidine-containing amonafide analogues. *Bioorg. Med. Chem.*, **2015**, *23*(13), 3135–3146.
- Wang, K.; Wang, Y.; Yan, X.; Chen, H.; Ma, G.; Zhang, P.; Li, J.; Li, X.; Zhang, J. DNA binding and anticancer activity of naphthalimides with 4-hydroxyl-alkylamine side chains at different lengths. *Bioorg. Med. Chem. Lett.*, **2012**, *22*(2), 937–941.
- Zee-Cheng, R.K.; Cheng, C.C. N-(Aminoalkyl)imide antineoplastic agents. Synthesis and biological activity. *J. Med. Chem.*, **1985**, *28*(9), 1216–1222.
- Khosravi, A.; Moradian, S.; Gharanjig, K.; Taromi, F.A. Synthesis and spectroscopic studies of some naphthalimide based disperse azo dyestuffs for the dyeing of polyester fibres. *Dye. Pigment.*, **2006**, *69*(1–2), 79–92.
- Qin, J.C.; Yan, J.; Wang, B.D.; Yang, Z.Y. Rhodamine-naphthalene conjugate as a novel ratiometric fluorescent probe for recognition of Al<sup>3+</sup>. *Tetrahedron Lett.*, **2016**, *57*(17), 1935–1939.
- Zhu, M.; Zhang, J.; Yu, G.; Chen, H.; Huang, J.; Liu, Y. Dialkyl-14H-benzo[4,5]isoquino[2,3-a]perimidin-14-one-3,4,10,11-tetracarboxylic diimides: A New Family of n-Type Organic Semiconductors. *Chem. Asian J.*, **2012**, *7*(10), 2208–2212.
- Yuan, D.; Brown, R.G.; Hepworth, J.D.; Alexiou, M.S.; Tyman, J.H.P. The synthesis and fluorescence of novel N-substituted-1,8-naphthylimides. *J. Heterocycl. Chem.*, **2008**, *45*(2), 397–404.
- Berridge, M.V.; Tan, A.S.; McCoy, K.D.; Wang, R. The biochemical and cellular basis of cell proliferation assays that use tetrazolium salts. *Biochemica*, **1996**, *4*(1), 15–19.
- Lombardo, T.; Anaya, L.; Kornblihtt, L.; Blanco, G. In: *Flow Cytometry – Recent Perspectives*, Schmid, I. Ed.; Intech Open Science, **2012**, Chapter 20, 393–420.
- Van Quaquebeke, E.; Mahieu, T.; Dumont, P.; Dewelle, J.; Ribaucour, F.; Simon, G.; Sauvage, S.; Gaussin, J.F.; Tuti, J.; El Yazidi, M.; Van Vynckt, F.; Mijatovic, T.; Lefranc, F.; Darro, F.; Kiss, R. 2,2,2-Trichloro-N-({2-[2-(dimethylamino)ethyl]-1,3-dioxo-2,3-dihydro-1H-benzo[de]isoquinolin-5-yl} carbamoyl)acetamide (UNBS3157), a novel nonhematotoxic naphthalimide derivative with potent antitumor activity. *J. Med. Chem.*, **2007**, *50*(17), 4122–4134.
- Wang, K.R.; Qian, F.; Sun, Q.; Ma, C.L.; Rong, R.X.; Cao, Z.R.; Wang, X.M.; Li, X.L. Substituent Effects on Cytotoxic Activity, Spectroscopic Property, and DNA Binding Property of

- Naphthalimide Derivatives. *Chem. Biol. Drug Des.*, **2016**, 87(5), 664–672.
- [28] Sharma, M.C.; Sharma, S.; Sharma, P.; Kumar, A. Comparative QSAR and pharmacophore modeling of substituted 2-[2'-(dimethylamino) ethyl]-1, 2-dihydro-3H-dibenz[de,h]isoquinoline-1,3-diones derivatives as anti-tumor activity. *Med. Chem. Res.*, **2013**, 22(12), 5772–5788.
- [29] Quintana-Espinoza, P.; Martín-Acosta, P.; Amesty, Á.; Martín-Rodríguez, P.; Lorenzo-Castrillejo, I.; Fernández-Pérez, L.; Machín, F.; Estévez-Braun, A. 5-Ethynylarylnaphthalimides as antitumor agents: Synthesis and biological evaluation. *Bioorg. Med. Chem.*, **2017**, 25(6), 19760–1983.
- [30] Johnson, C.A.; Hudson, G.A.; Hardebeck, L.K.E.; Jolley, E.A.; Ren, Y.; Lewis, M.; Znosko, B.M. Effect of intercalator substituent and nucleotide sequence on the stability of DNA- and RNA-naphthalimide complexes. *Bioorg. Med. Chem.*, **2015**, 23(13), 3586–3591.
- [31] Wang, K.R.; Qian, F.; Yang, Z.B.; An, H.W.; Han, D.; Chen, H.; Zhang, P.Z.; Li, X.L. Anticancer Activity and DNA Binding of 4-Alkylenediamines Modified Naphthalimide Derivatives. *Lett. Drug Des. Discov.*, **2014**, 11(6), 742–748.
- [32] Pourpak, A.; Landowski, T.H.; Dorr, R.T. Ethonafide-Induced Cytotoxicity Is Mediated by Topoisomerase II Inhibition in Prostate Cancer Cells. *J. Pharmacol. Exp. Ther.*, **2007**, 321(3), 1109–1117.

## Publikacja P.3

Polyamine–oligonucleotide conjugates: 2'-OMe-triazole-linked 1,4,7,10-tetra-azacyclododecane and intercalating dyes and their effect on the thermal stability of DNA duplexes.

Gondela, A.; **Tomczyk, M. D.**; Przypis, Ł.; Walczak, K. Z\*.

*Pharmaceutics* **2022**, *15* (5), 66.

## Article

# Polyamine–Oligonucleotide Conjugates: 2'-OMe-Triazole-Linked 1,4,7,10-Tetraazacyclododecane and Intercalating Dyes and Their Effect on the Thermal Stability of DNA Duplexes

Mateusz D. Tomczyk <sup>1</sup>, Mariusz Zalewski <sup>2</sup> , Per T. Jørgensen <sup>3</sup> , Jesper Wengel <sup>3</sup>  and Krzysztof Walczak <sup>1,\*</sup> 

- <sup>1</sup> Department of Organic Chemistry, Bioorganic Chemistry and Biotechnology, Silesian University of Technology, Krzywoustego 4, 44-100 Gliwice, Poland; mateusz.d.tomczyk@polsl.pl
- <sup>2</sup> Department of Chemical Organic Technology and Petrochemistry, Silesian University of Technology, Krzywoustego 4, 44-100 Gliwice, Poland; mariusz.zalewski@polsl.pl
- <sup>3</sup> BioNEC Center, Department of Physics, Chemistry and Pharmacy, University of Southern Denmark, Campusvej 55, 5230 Odense M, Denmark; ptj@sdu.dk (P.T.J.); jwe@sdu.dk (J.W.)
- \* Correspondence: krzysztof.walczak@polsl.pl

**Abstract:** Oligonucleotides with the sequences 5'-GTG AU<sup>P</sup>A TGC, 5'-GCA TAU<sup>P</sup> CAC and 5'-GU<sup>P</sup>G ATA U<sup>P</sup>GC, where U<sup>P</sup> is 2'-O-propargyl uridine, were subjected to post-synthetic Cu(I)-catalyzed azide–alkyne cycloaddition to attach 1,4,7,10-tetraazacyclododecane (cyclen) and two well-known DNA intercalating dyes: thioxanthone and 1,8-naphthalimide. We propose a convenient cyclen protection–deprotection strategy that allows efficient separation of the resulting polyamine–oligonucleotide conjugates from the starting materials by RP-HPLC to obtain high-purity products. In this paper, we present hitherto unknown macrocyclic polyamine–oligonucleotide conjugates and their hybridization properties reflected in the thermal stability of thirty-two DNA duplexes containing combinations of labeled strands, their unmodified complementary strands, and strands with single base pair mismatches. Circular dichroism measurements showed that the B-conformation is retained for all dsDNAs consisting of unmodified and modified oligonucleotides. An additive and destabilizing effect of cyclen moieties attached to dsDNAs was observed. *T<sub>m</sub>* measurements indicate that placing the hydrophobic dye opposite to the cyclen moiety can reduce its destabilizing effect and increase the thermal stability of the duplex. Interestingly, the cyclen-modified U showed significant selectivity for TT mismatch, which resulted in stabilization of the duplex. We conclude the paper with a brief review and discussion in which we compare our results with several examples of oligonucleotides labeled with polyamines at internal strand positions known in the literature.

**Keywords:** oligonucleotide conjugates; duplex stability; thioxanthone; 1,8-naphthalimide; cyclen



**Citation:** Tomczyk, M.D.; Zalewski, M.; Jørgensen, P.T.; Wengel, J.; Walczak, K. Polyamine–Oligonucleotide Conjugates: 2'-OMe-Triazole-Linked 1,4,7,10-Tetraazacyclododecane and Intercalating Dyes and Their Effect on the Thermal Stability of DNA Duplexes. *Pharmaceutics* **2022**, *14*, 66. <https://doi.org/10.3390/pharmaceutics14010066>

Academic Editors: Tina Kauss, Philippe Barthélémy and Gabriele Candiani

Received: 21 November 2021

Accepted: 25 December 2021

Published: 28 December 2021

**Publisher's Note:** MDPI stays neutral with regard to jurisdictional claims in published maps and institutional affiliations.



**Copyright:** © 2021 by the authors. Licensee MDPI, Basel, Switzerland. This article is an open access article distributed under the terms and conditions of the Creative Commons Attribution (CC BY) license (<https://creativecommons.org/licenses/by/4.0/>).

## 1. Introduction

Macrocyclic polyamines and their transition metal complexes are attracting increasing interest due to their clinical potential in cancer and virus treatment and in magnetic resonance imaging. Chemical modifications involving covalent attachment of polyamines to oligonucleotides (ON) create zwitterionic functional groups that can significantly improve their biological and biophysical properties, such as target affinity and cell penetration, in a manner similar to polyamine transfection agents. The introduction of such modifications was carried out using several different strand positions, including the 3' and 5'-positions of the phosphate backbone, the 2' and 4'-positions on the ribose ring, and within the nucleobase itself [1,2]. In contrast to the 3' and 5'-positions, the stability of both oligonucleotides and duplexes is more sensitive to modifications of the ribose ring structure and conformation, although it is the 2'-position of the ribose ring that is particularly suitable for the covalent attachment of large molecules, such as polyamines, with minimal disruption of the base-pairing potential. There are many examples of polyamine–oligonucleotide conjugates,

but in most studies, polyamines are linear, while examples of macrocyclic polyamines that can form stable complexes with transition metals are rarer, and information on their effect on duplex stability is often lacking. Dubey et al. showed that cyclen-based transition metal complexes attached to the 5'-position of an oligo(dT) are able to hydrolyze the target oligo(dA) more efficiently; however, the effect of the cyclen moiety on the thermal stability of the duplex has not been described [3]. Steward et al. demonstrated a four-arm, lattice-bearing, single-stranded DNA bound to the central Ni(II)–cyclen complex, which improves self-assembly at the supramolecular level, but its effect on duplexes is also unknown [4]. On the other hand, it is known that macrocyclic polyamines such as 1,4,7,10-tetraazacyclododecane (cyclen) are potential artificial nucleases, and their derivatives can cleave double-stranded DNA (dsDNA), even without metal ions, through hydrolysis or oxidative cleavage [5–9]. Thus, covalent attachment of a macrocyclic amine to ssDNA may provide new and useful models for studying the function and *in vitro* use of artificial nucleic acid-based nucleases.

The second type of modification that we introduced, intercalating dyes, have a considerable position in the chemistry of nucleic acids [10]. These planar and aromatic molecules can intercalate between the nucleobases of dsDNA changing its topology but can also be explored as fluorescent probes for *in vitro* applications. Typically, oligonucleotide-based probes consist of covalently attached fluorescent dyes, including perylene [11], pyrene and phenanthroline [12–15], or fluorescein [16], which are known to exhibit high fluorescence and can interact noncovalently with dsDNA, e.g., by intercalation or groove-binding, leading to its stabilization. We have previously shown that covalent attachment of a carbazole moiety to the 5'-end of a 9-mer sequence increases the thermal stability of the resulting 9-mer/15-mer dsDNA by +4.2 °C [17]. To date, the effect of the combined attachment of both molecules, an intercalator and cyclen, to double-stranded oligonucleotides on their thermal stability has not been investigated. The knowledge of the stabilizing (or destabilizing) effect will be helpful in the preparation of cyclen-containing oligonucleotides with tailored stability of the resulting hybridized duplexes. Telser et al. prepared several dsDNAs with covalently attached labels, e.g., anthraquinone or pyrene, placed at the internal positions of both strands and showed that both label–duplex and label–label interactions affect the thermal stability of the resulting duplexes [18,19]. Following the above studies, we also examined the mutual influence of the introduced modifications on the stability of duplexes.

Herein, we present a preliminary study of a new methodology for the covalent attachment of cyclen moieties to oligonucleotides and the assessment of their effect on the thermal stability of the resulting DNA duplexes. For this purpose, we developed a new procedure for introducing *N*-TFA-protected cyclen via a 2'-OMe-triazole linkage, followed by purification and deprotection of the resulting conjugate to obtain a high-purity product that is well separated from the initial oligonucleotide. We were also interested in the mutual influence of the different labels placed on opposite positions of complementary strands on their stabilizing properties, which turn out to be of significant importance in the case of cyclen groups. In summary, we tested seven labeled oligonucleotides on examples of thirty-two dsDNA combinations formed between the labeled strands, their unmodified complementary strands, and strands with a single base pair mismatch.

## 2. Materials and Methods

### 2.1. Chemical Synthesis and Analysis

All reagents and anhydrous solvents were obtained from commercial sources and used without further purification except phenol distillation. Anhydrous solvents were dried over 4 Å molecular sieves and checked using a Karl Fisher titrator to determine if the water concentration was below 12 ppm before use. The progress of the chemical reactions was monitored by thin layer chromatography (TLC) on silica gel 60 F254 plates (Merc, Darmstadt, Germany). Spots on the TLC plate were visualized under UV light at 254 nm or by heating the plate after treatment with ninhydrin reagent made by dissolving

1.5 g of ninhydrin in 100 mL of *n*-butanol and adding 3.0 mL of acetic acid. Column chromatography was performed on Merck silica gel 60 (40–63  $\mu\text{m}$ ). Recycling preparative HPLC (prep-HPLC) was performed on a JAI LaboACE 5060 (Japan Analytic Industry, Tokyo, Japan). Depending on the type of compound to be purified, a tandem set of GPC JAIGEL-2HR+2.5 HR columns ( $\text{O}20\text{ mm} \times 600\text{ mm}$ ) or a silica-based RP JAIGEL-ODS-AP-L SP-120-10 column ( $\text{O}20\text{ mm} \times 500\text{ mm}$ , 10  $\mu\text{m}$ ) was used for prep-HPLC.  $^1\text{H-NMR}$  and  $^{13}\text{C-NMR}$  spectra were recorded on a Varian NMR system 600 spectrometer (Agilent Technologies, Santa Clara, CA, USA) at 600 and 150 MHz, respectively. Peak multiplicity is expressed as follows: s = singlet, d = doublet, t = triplet, q = quartet, dd = doublet of doublets, ddd = doublet of doublets of doublets, m = multiplet. NMR chemical shifts are reported in ppm ( $\delta$ ), relative to residual nondeuterated solvents as internal standard and coupling constants ( $J$ ) are given in Hz. Melting points (Mp) were determined using a Boethius microscope HMK type (Franz Küstner, Dresden, Germany). High-resolution electrospray ionization mass spectroscopy (HR-ESI-MS) analyses were performed on a Waters Xevo G2 QTOF apparatus (Waters-Micromass, Manchester, UK). Microwave-assisted reactions were carried out in a Biotage Initiator microwave reactor (Stockholm, Sweden) using 0.5–2.0 mL vials under the following conditions: 2 h, 90  $^\circ\text{C}$ , prestirring 30 s, high adsorption.

### 2.2. Ultraviolet Thermal Melting Studies

To determine the melting temperature ( $T_m$ ) of the obtained duplexes, UV melting studies were performed on a Lambda 35 UV/Vis Spectrometer (Perkin-Elmer, Norwalk, CT, USA) using 10 mm path length Hellma SUPRASIL quartz cuvettes (Müllheim, Germany), monitoring at 260 nm with a complementary DNA/DNA strands concentration of 2.5  $\mu\text{M}$  and a volume of 1.0 mL. Samples were prepared as follows: The modified strands and their corresponding complementary strands were mixed 1:1 (*n/n*) in 2.0 mL Eppendorf tubes before medium salt buffer (2 $\times$ , 11.7 mM sodium phosphate, pH 7.0, 200 mM NaCl, 0.20 mM EDTA, pH 7.0, 500  $\mu\text{L}$ ) was added, which was completed in 1.0 mL using Milli-Q water. Thus, all samples were dissolved in 1 $\times$  buffer condition (5.8 mM sodium phosphate, pH 7.0, 100 mM NaCl, and 0.10 mM EDTA). The samples were denatured by heating to 90  $^\circ\text{C}$  in a water bath and then slowly cooled to rt before transferring them to cuvettes. The absorbance at 260 nm was recorded as a function of time with a linear temperature increase from 6 to 80  $^\circ\text{C}$  at a rate of 1.0  $^\circ\text{C}/\text{min}$  programmed by a Peltier temperature controller. Two separate melting curves were measured, and  $T_m$  values were calculated with the UV-WinLab software, taking the mean of the two melting curves with a deviation of no more than 0.5  $^\circ\text{C}$ .

### 2.3. Circular Dichroism Studies

Samples were prepared in the same way as for the  $T_m$  measurement. The background spectrum of the buffer was recorded and subtracted from the corresponding spectra. Measurements were performed on a JASCO J-815 spectrometer (Tokyo, Japan) at 20  $^\circ\text{C}$  using quartz optical cells with a path length of 5 mm and a total volume of 1.0 mL. All CD spectra were recorded from 200–400 nm with a scan rate of 100 nm/min, employing 5 scans.

### 2.4. Synthesis of

*1,1',1''-(1,4,7,10-Tetraazacyclododecane-1,4,7-triyl)tris(2,2,2-trifluoroethan-1-one); 1*

TFAEt (18.0 mL, 150 mmol) was added dropwise to a stirred solution of cyclen (6.55 g, 38.0 mmol) and  $\text{Et}_3\text{N}$  (5.27 mL, 38.0 mmol) in MeOH (40 mL) at rt for 30 min and left at rt overnight. All volatiles were evaporated in vacuo and the residual oil was suspended in AcOEt (10 mL), evaporated onto 10 times its weight of silica gel and purified by silica gel column ( $\text{O}50\text{ mm} \times 200\text{ mm}$ ), eluting with 100% AcOEt. The fractions at  $R_f$  0.35 (TLC, 100% AcOEt), which became slightly stained in ninhydrin reagent, were evaporated to give **1** as a white foam (15.7 g, 85%). Mp = 79–80  $^\circ\text{C}$ .  $^1\text{H-NMR}$  (600 MHz,  $\text{DMSO-d}_6$ ):  $\delta$  3.91–3.78 (m, 4H), 3.66–3.42 (m, 8H), 2.82–2.67 (m, 4H), 2.33 (q,  $J$  = 8.3 Hz, 1H).  $^{13}\text{C-NMR}$  (150 MHz,  $\text{DMSO-d}_6$ ):  $\delta$  156.78–156.24 (m), 117.53 (q,  $J$  = 286.4 Hz), 55.28–43.00 (m). HR-ESI-MS:

$m/z$  calcd. for  $C_{14}H_{18}F_9N_4O_3$  461.1235  $[M+H]^+$ ; found 461.1134. The proton-decoupled  $^{13}C$ -NMR spectra of TFA-protected cyclen and its derivatives are complicated by the C–F coupling and the presence of conformers at rt.

2.5. Synthesis of 1,1',1''-(10-(5-Bromopentanoyl)-1,4,7,10-tetraazacyclododecane-1,4,7-triyl)tris(2,2,2-trifluoroethan-1-one); 2

An amount of 5-Bromovaleryl chloride (562  $\mu$ L, 4.23 mmol) was added to a stirred solution of **1** (1.77 g, 3.84 mmol) in DCM (20 mL) with  $K_2CO_3$  (585 mg, 4.23 mmol) and stirred for 40 min in an ice-water bath. The progress of the reaction was monitored by TLC (5% MeOH- $CHCl_3$ ,  $v/v$ ) for the appearance of a new spot at  $R_f$  0.42, which turned pale brown after ninhydrin treatment, and disappearance of the substrate. After the substrate spot was completely consumed, the reaction mixture was washed with water (20 mL) and the organic layer was dried over  $Na_2SO_4$ . The filtrate was evaporated, and the oil residue was purified on a silica gel column ( $\varnothing$ 15 mm  $\times$  400 mm) eluting with 50% AcOEt-hexane ( $v/v$ ). The fractions at  $R_f$  0.22 (TLC, 50% AcOEt-hexane,  $v/v$ ) were combined and evaporated to give **2** as a viscous oil (1.94 g, 81%).  $^1H$ -NMR (600 MHz,  $DMSO-d_6$ ):  $\delta$  3.84–3.67 (m, 16H), 3.55 (t,  $J$  = 6.6 Hz, 2H), 2.38–2.31 (m, 2H), 1.85–1.81 (m, 2H), 1.65–1.63 (m, 2H).  $^{13}C$ -NMR (150 MHz,  $DMSO-d_6$ ):  $\delta$  172.92, 156.59–156.01 (m), 116.04 (q,  $J$  = 286.5 Hz), 48.02–45.11 (m), 40.04, 34.74, 31.72, 23.23, 23.16.

2.6. Synthesis of 1,1',1''-(10-(5-Azidopentanoyl)-1,4,7,10-tetraazacyclododecane-1,4,7-triyl)tris(2,2,2-trifluoroethan-1-one); 3

$NaN_3$  (130 mg, 2.00 mmol) was added to a solution of **2** (623 mg, 1.00 mmol) in DMF (10 mL) and stirred for 24 h at rt. TLC analysis (50% AcOEt-hexane,  $v/v$ ) showed a new spot of **3** at  $R_f$  0.45, near the substrate at  $R_f$  0.40, which stains darker on heating with ninhydrin than the substrate spot. The mixture was partitioned between AcOEt (20 mL) and water (80 mL), the organic layer was dried over  $Na_2SO_4$  and evaporated to give a viscous oil, which was purified by prep-HPLC (JAIGEL-ODS-AP-L, 100% MeOH, flow rate 7.0 mL/min). The fraction at a  $t_R$  26.8 min was collected and evaporated to give **3** (115 mg, 94%).  $^1H$ -NMR (600 MHz,  $CD_3OD$ ):  $\delta$  3.89–3.73 (m, 16H), 3.34 (t,  $J$  = 6.6 Hz, 2H), 2.46–2.42 (m, 2H), 1.71–1.69 (m, 2H), 1.65–1.62 (m, 2H).  $^{13}C$ -NMR (150 MHz,  $CD_3OD$ ):  $\delta$  174.88, 157.84–157.05 (m), 116.27 (q,  $J$  = 285.8), 50.79, 47.07–46.28 (m), 32.12, 28.01, 22.05.

2.7. Synthesis of 2-Hydroxy-9H-thioxanthen-9-one; 4

Freshly distilled phenol (9.00 g, 97.3 mmol) was added portionwise to a suspension of thiosalicylic acid (5.00 g, 32.4 mmol) at concd.  $H_2SO_4$  (96%, 60 mL) and the mixture was heated at 90  $^\circ C$  for 18 h. After cooling to rt, the mixture was gently poured into 500 mL of water with crushed ice to give a yellow precipitate, which was filtrated off and dried to give a yellow solid. The crude solid was dissolved in  $CHCl_3$  (50 mL) and evaporated onto 10 times its weight of silica gel, applied to a silica gel column ( $\varnothing$ 50 mm  $\times$  200 mm), and eluted using 5% MeOH- $CHCl_3$  ( $v/v$ ). The fractions visible on TLC as yellow spots at  $R_f$  0.32 was evaporated together to give **4** as a yellow solid (3.41 g, 46%). Mp = 245–246  $^\circ C$ .  $^1H$ -NMR (600 MHz,  $CD_3OD$ ):  $\delta$  10.22 (s, 1H), 8.52 (ddd,  $J$  = 7.8, 1.2, 0.6, 1H), 7.93 (d,  $J$  = 2.4, 1H), 7.65–7.70 (m, 2H), 7.57 (d,  $J$  = 9.0, 1H), 7.50 (ddd,  $J$  = 8.4, 6.0, 1.8, 1H), 7.25 (dd,  $J$  = 9.0, 3.0, 1H).  $^{13}C$ -NMR (150 MHz,  $CD_3OD$ ):  $\delta$  179.30, 156.53, 137.98, 137.45, 132.08, 129.86, 129.00, 128.12, 127.29, 125.90, 125.75, 122.32, 113.12. HR-ESI-MS:  $m/z$  calcd. for  $C_{13}H_7O_2S$  227.0172  $[M-H]^-$ ; found 227.0167.

2.8. Synthesis of 2-(4-Bromobutoxy)-9H-thioxanthen-9-one; 5

An amount of 1,4-dibromobutane (1.40 mL, 11.9 mmol) was added in one portion to a mixture of  $K_2CO_3$  (900 mg, 56.6 mmol) and **4** (680 mg, 2.98 mmol) in DMF (15 mL) and stirred at 100  $^\circ C$  for 48 h. The mixture was cooled to rt, diluted with AcOEt to 40 mL, and washed with water (100 mL). The organic layer was dried over  $Na_2SO_4$ , filtered off, and evaporated to give a yellow oil, which crystallized over time. The crude solid was purified



by silica gel chromatography ( $\varnothing$ 15 mm  $\times$  450 mm) eluting with 100% CHCl<sub>3</sub>. The fractions at  $R_f$  0.75 (TLC, 100% CHCl<sub>3</sub>) were evaporated to give **5** as a light-yellow solid (922 mg, 85%).  $M_p$  = 122–123 °C. <sup>1</sup>H-NMR (600 MHz, CDCl<sub>3</sub>):  $\delta$  8.61 (ddd,  $J$  = 7.8, 1.2, 0.6 Hz, 1H), 8.04 (d,  $J$  = 2.4 Hz, 1H), 7.60 (ddd,  $J$  = 7.2, 6.6, 1.2 Hz, 1H), 7.57 (ddd,  $J$  = 8.4, 1.8, 0.6 Hz, 1H), 7.48 (d,  $J$  = 9.0 Hz, 1H), 7.47 (ddd,  $J$  = 7.2, 6.6, 1.2 Hz, 1H), 7.24 (dd,  $J$  = 8.4, 2.4 Hz, 1H), 4.13 (t,  $J$  = 6.0 Hz, 2H), 3.50 (t,  $J$  = 6.6 Hz, 2H), 2.19–2.07 (m, 2H), 2.02–1.97 (m, 2H). <sup>13</sup>C-NMR (150 MHz, CDCl<sub>3</sub>):  $\delta$  179.59, 157.62, 137.47, 131.99, 130.20, 129.85, 129.14, 128.57, 127.29, 126.05, 125.95, 122.88, 111.08, 67.33, 33.29, 29.44, 27.78.

### 2.9. Synthesis of 2-(4-Azidobutoxy)-9H-thioxanthen-9-one; **6**

The reaction of NaN<sub>3</sub> (130 mg, 2.00 mmol) with solution of **5** (363 mg, 1.00 mmol) in DMF (15 mL) was performed similar to that of **3**. The crude product was purified on a silica gel column ( $\varnothing$ 15 mm  $\times$  450 mm) and the eluates at  $R_f$  0.95 (100% CHCl<sub>3</sub>), turning grey on heating with ninhydrin, were evaporated and purified by prep-HPLC (JAIGEL-2HR+2.5HR, 100% DCM, flow rate 7.0 mL/min). The fraction at a  $t_R$  36.3 min was evaporated to give **6** (310 mg, 95%) as a yellow oil, which crystallized over time.  $M_p$  = 77–78 °C. <sup>1</sup>H-NMR (600 MHz, DMSO-d<sub>6</sub>):  $\delta$  8.46 (ddd,  $J$  = 8.4, 1.8, 0.6 Hz, 1H), 7.89 (d,  $J$  = 3.0 Hz, 1H), 7.80 (ddd,  $J$  = 8.4, 1.8, 0.6 Hz, 1H), 7.75 (ddd,  $J$  = 7.2, 6.6, 1.2 Hz, 1H), 7.73 (d,  $J$  = 9.0 Hz, 1H), 7.57 (ddd,  $J$  = 7.2, 6.6, 1.2 Hz, 1H), 7.39 (dd,  $J$  = 8.4, 3.0 Hz, 1H), 4.12 (t,  $J$  = 6.0 Hz, 2H), 3.44 (t,  $J$  = 6.6 Hz, 2H), 1.84–1.81 (m, 2H), 1.76–1.71 (m, 2H). <sup>13</sup>C-NMR (150 MHz, DMSO-d<sub>6</sub>):  $\delta$  178.80, 157.80, 137.19, 133.07, 129.86, 129.48, 128.58, 128.39, 128.16, 126.90, 126.87, 123.02, 111.46, 67.84, 50.85, 26.28, 25.51.

### 2.10. Synthesis of 2-(4-Bromobutyl)-1H-benzo[de]isoquinoline-1,3(2H)-dione; **7**

To a stirred suspension of 1,8-naphthalimide (1.12 g, 5.68 mmol) in dry DMF (20 mL), NaH (80% dispersion in mineral oil; 341 mg, 11.36 mmol) was added portionwise. The suspension was allowed to stir at rt for 1 h. Then, 1,4-dibromobutane (2.37 mL, 22.72 mmol) was added to the reaction mixture in one portion and stirred overnight at rt. The reaction mixture was then poured into a 5% HCl solution and the resulting white precipitate was filtered off and air dried. The crude solid was purified by silica gel chromatography ( $\varnothing$ 15 mm  $\times$  450 mm) eluting with 100% CHCl<sub>3</sub>. Fractions with  $R_f$  0.90 (TLC, 100% CHCl<sub>3</sub>) were evaporated to afford **7** as a white solid (1.40 g, 74%).  $M_p$  = 115–116 °C. <sup>1</sup>H-NMR (400 MHz, CDCl<sub>3</sub>):  $\delta$  8.58 (dd,  $J$  = 7.2, 1.2 Hz, 2H), 8.21 (dd,  $J$  = 8.4, 1.2 Hz, 2H), 7.75 (dd,  $J$  = 8.2, 7.4 Hz, 2H), 4.22 (t,  $J$  = 7.0 Hz, 2H), 3.48 (t,  $J$  = 6.6 Hz, 2H), 1.96–2.03 (m, 2H), 1.86–1.95 (m, 2H). <sup>13</sup>C-NMR (100 MHz, CDCl<sub>3</sub>):  $\delta$  164.11, 133.92, 131.53, 131.24, 128.11, 126.96, 122.57, 39.30, 33.11, 30.22, 26.94.

### 2.11. Synthesis of 2-(4-Azidobutyl)-1H-benzo[de]isoquinoline-1,3(2H)-dione; **8**

The reaction of NaN<sub>3</sub> (474 mg, 7.28 mmol) with solution of **7** (1.21 g, 3.64 mmol) in DMF (20 mL) was performed similar to that of **3**. The crude product was purified on a silica gel column ( $\varnothing$ 15 mm  $\times$  450 mm) and the eluates at  $R_f$  0.95 (100% CHCl<sub>3</sub>), turning grey on heating with ninhydrin, were evaporated and purified by prep-HPLC (JAIGEL-2HR + 2.5HR, 100% DCM, flow rate 7.0 mL/min). The fraction at a  $t_R$  32.1 min was evaporated to give **8** (980 mg, 91%) as a white solid.  $M_p$  = 73–74 °C. <sup>1</sup>H-NMR (600 MHz, CDCl<sub>3</sub>):  $\delta$  8.58 (dd,  $J$  = 7.2, 1.1 Hz, 2H), 8.20 (dd,  $J$  = 8.3, 1.0 Hz, 2H), 7.76–7.73 (m, 2H), 4.21 (t,  $J$  = 7.4 Hz, 2H), 3.35 (t,  $J$  = 6.9 Hz, 2H), 1.86–1.81 (m, 2H), 1.74–1.69 (m, 2H). <sup>13</sup>C-NMR (150 MHz, CDCl<sub>3</sub>):  $\delta$  164.14, 133.93, 131.56, 131.23, 128.12, 126.90, 122.56, 51.16, 39.61, 26.49, 25.37.

### 2.12. Oligonucleotides Purification and Analysis

RP-HPLC purification of crude oligonucleotides was performed by Waters 600 HPLC System with a Waters XBridge BEH C18-column ( $\varnothing$ 19 mm  $\times$  100 mm, 5  $\mu$ m). Elution was performed by isocratic hold of A-buffer for 5.0 min, followed by a linear gradient to 70% of B-buffer for 16.5 min at a flow rate of 5.0 mL/min (A-buffer: 0.05 M TEAA buffer, pH 7.4;

B-buffer: 25% A-buffer, 75% MeCN). IE-HPLC purification of oligonucleotides was carried on a DIONEX Ultimate 3000 system with a DNAPac PA100 Semi-Preparative column ( $\varnothing 9$  mm  $\times$  250 mm, 13  $\mu$ m) at 60 °C (Thermo Fisher Scientific, Darmstadt, Germany). Elution was performed with an isocratic hold of 10% C-buffer in Milli-Q water, starting with hold on 2% D-buffer in Milli-Q water for 2.0 min, followed by a linear gradient to 25% of D-buffer in Milli-Q water for 20.0 min at a flow rate of 2.0 mL/min (C-buffer: 0.25 M Tris-Cl, pH 8.0; D-buffer: 1.0 M NaClO<sub>4</sub>). After purification, the appropriate fractions were combined and concentrated by purging with N<sub>2</sub> at 55 °C, and the obtained samples were dissolved in Milli-Q water (100  $\mu$ L), then desalted with an addition of NaClO<sub>4</sub> solution (5.0 M, 15  $\mu$ L), suspended in cold ethanol (1.5 mL) and stored at –20 °C for 1–2 h. After centrifugation (13,200 rpm, 5 min, 4 °C), the supernatant was filtered off and the pellet was washed with cold ethanol (2  $\times$  1.0 mL), dried under N<sub>2</sub> flow at 55 °C, and dissolved in Milli-Q water (1.0 mL). Analytical RP-HPLC was performed on a Merck-Hitachi 7000 system (Hitachi Instruments, Tokyo, Japan) equipped with a Waters XBridge OBD C18-column ( $\varnothing 10$  mm  $\times$  50 mm, 2.5  $\mu$ m) at 60 °C. Elution was started with an isocratic hold of A-buffer for 2 min followed by a linear gradient to 85% of B-buffer for 30 min, keeping the flow rate at 1.3 mL/min. The structure and composition of oligonucleotides was verified by the MALDI-TOF MS method performed on an Ultraflex Extreme mass spectrometer (Bruker Daltonics, Bremen, Germany). Finally, the purified oligonucleotides were quantified by measuring OD as the absorbance at 260 nm of the sample in 1.0 mL of water in a 10 mm path length cuvette. The excitation coefficients for DNAs at 260 nm were estimated to be  $1 \times 10^4$  M cm<sup>–1</sup> residue<sup>–1</sup>.

### 2.13. Synthesis and Purification of ON1–ON5

Target **ON1–ON5** were synthesized at the 1.0  $\mu$ mol scale on polystyrene beads (Amersham Biosciences, Piscataway, NJ, USA) using an automated synthesizer Expedite 8909 (PerSeptive Biosystems, Framingham, MA, USA) according to the manufacturer's standard protocol, except for the introduction of 2'-O-propargyl-uridine (U<sup>P</sup>) into the **ON3–ON5** sequence by the so-called "hand-coupling procedure", previously used by Wengel's group [17]. The stepwise coupling efficiencies were >95% for standard conditions and ~85% for hand-coupling. Cleavage from the beads and nucleobase deprotection were performed by incubation with concd. aq. NH<sub>3</sub> in a screw cap vial at 55 °C overnight. The supernatant was filtered and evaporated to remove NH<sub>3</sub> by heating the filtrate to 55 °C and purging with N<sub>2</sub> for 4 h. The crude samples were purified DMT-on by RP-HPLC and the 5'-DMT group was cleaved with 2% aq. trifluoroacetic acid. The deprotected oligonucleotides were eluted with a 30% MeCN soln. in water (*v/v*) and purified by IE-HPLC, then the composition of the collected fractions was assessed by MALDI-TOF MS. Unmodified and 2'-O-propargylated oligonucleotides were isolated in overall yields of 80–88% and were >98% pure by IE-HPLC analysis.

### 2.14. Synthesis and Purification of ON9-ON12, ON13 and ON14

To a 2.0 mL Ar purged microwave vial containing **ON3** (203 nmol in 800  $\mu$ L of dH<sub>2</sub>O) in a mixture of TEAA buffer (250  $\mu$ L, 1.0 M, pH 7.4) and DMSO (400  $\mu$ L), azide-functionalized **3** (51.0  $\mu$ L, 10.0 mM DMSO soln.), freshly prepared CuSO<sub>4</sub>–TBTA equimolar complex (80.0  $\mu$ L, 10.0 mM DMSO–dH<sub>2</sub>O mixture, 3:7, *v/v*) and sodium ascorbate (201  $\mu$ L, 25.0 mM dH<sub>2</sub>O soln.) were subsequently added. The resulting mixture was vortexed and centrifuged after adding each of the reagents. The vial was equipped with a magnetic stirrer, purged with Ar, sealed with a Teflon-lined septum cap, and microwaved. After completion of the reaction, the volume was made up to 2.0 mL with dH<sub>2</sub>O and divided into two equal parts. Each sample was desalted through a NAP-10 column (GE Healthcare, Little Chalfont, UK) following manufacturer's protocol. The resulting solution contains a mixture of two major products, tris-*N*-TFA-protected **ON6** and partially deprotected bis-*N*-TFA-protected **ON6'**. During RP-HPLC purification, the fractions ranging from *t*<sub>R</sub> 12.2 to 17.2 min were collected, evaporated together under a stream of N<sub>2</sub>, and used as a mixture in the next step. The

resulting sample was incubated with 1.0 mL of satd. aq.  $\text{NH}_3$  at 55 °C overnight and then evaporated by gentle blowing with  $\text{N}_2$  at 30 °C for 4 h. The crude sample after deprotection was purified by IE-HPLC to give **ON13** in 41% overall yield and 98% purity.

The synthesis of the intercalator-labeled **ON9–ON12** and cyclen-labeled **ON14** was performed under the same conditions as for **ON13**. After desalting through an NAP-10 column, **ON9–ON12** samples were evaporated under a stream of  $\text{N}_2$  and purified by RP-HPLC. These samples were obtained in high yield and purity (Table 1) and did not require further purification by IE-HPLC. After coupling **3** with **ON4**, a mixture of intermediates **ON7'** was obtained which was purified by RP-HPLC by collecting the fractions at  $t_R$  from 12.2 to 17.2 min. After their joint deprotection and purification of the resulting sample by IE-HPLC, the **ON14** conjugate was obtained in an overall yield of 40% and 98% purity.

### 2.15. Synthesis and Purification of ON15

For the synthesis of the double-functionalized **ON15**, the same procedure was used as for **ON13**, except that the following reaction system was used: **ON5** (83 nmol in 480  $\mu\text{L}$  of  $\text{dH}_2\text{O}$ ) in a mixture of TEAA buffer (150  $\mu\text{L}$ , 1.0 M, pH 7.4) and DMSO (240  $\mu\text{L}$ ), azide-functionalized **3** (42.0  $\mu\text{L}$ , 10.0 mM DMSO soln.), freshly prepared  $\text{CuSO}_4$ –TBTA equimolar complex (33.0  $\mu\text{L}$ , 10.0 mM DMSO– $\text{dH}_2\text{O}$  mixture, 3:7, *v/v*) and sodium ascorbate (164  $\mu\text{L}$ , 25.0 mM  $\text{dH}_2\text{O}$  soln.). The fractions ranging from  $t_R$  12.7 to 17.5 min were collected by RP-HPLC and evaporated together under a stream of  $\text{N}_2$ . After complete deprotection, a single peak was observed at  $m/z$  3428.227 in the MALDI-TOF MS spectra assigned to **ON15** (calcd. as  $m/z$  3428.957) and a single peak in the RP-chromatogram at  $t_R$  8.39 min. This fraction was collected and purified by IE-HPLC to give **ON15** in 38% overall yield and 95% purity.

**Table 1.** Overall yields and MADI-TOF mass spectra of the obtained conjugates.

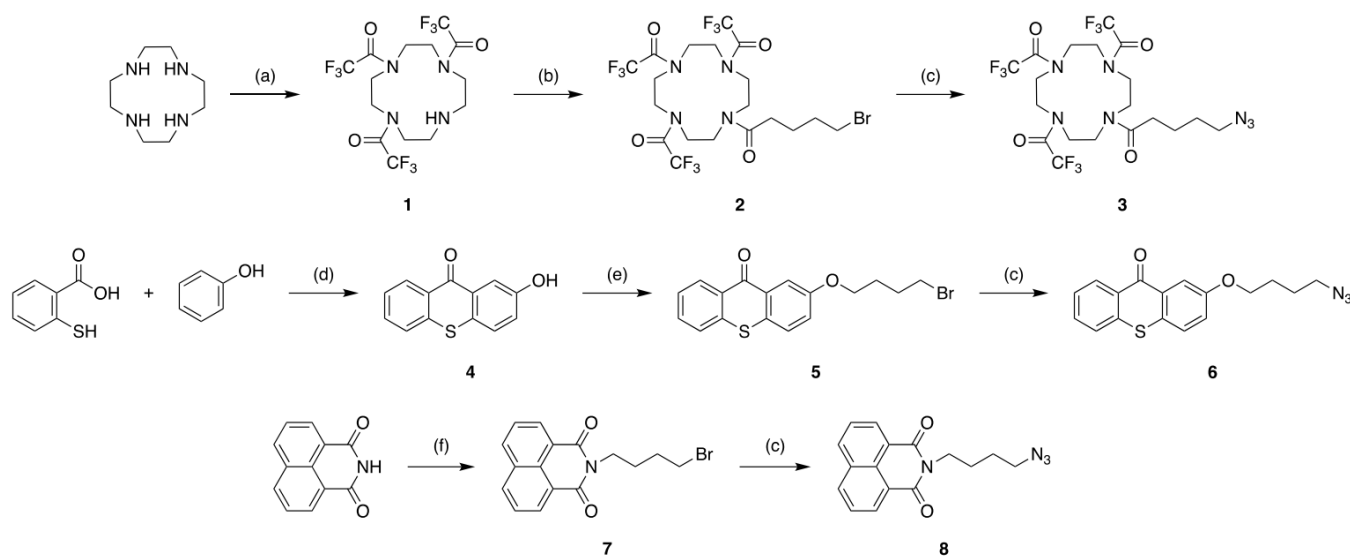
No	Sequence	MALDI-TOF MS		Yield	IE-Purity
		Calcd. $m/z$ [M+H] <sup>+</sup>	Found $m/z$		
<b>ON6</b>	5'-GTG AU <sup>3TFA</sup> A TGC	3379.303	3379.920		
<b>ON6'</b>	5'-GTG AU <sup>2TFA</sup> A TGC	3283.295	3283.192		
<b>ON9</b>	5'-GTG AU <sup>T</sup> A TGC	3119.595	3118.754	56%	98%
<b>ON10</b>	5'-GCA TAU <sup>T</sup> CAC	3048.222	3048.840	52%	99%
<b>ON11</b>	5'-GTG AU <sup>N</sup> A TGC	3088.618	3088.722	58%	86%
<b>ON12</b>	5'-GCA TAU <sup>N</sup> CAC	3017.618	3016.764	61%	83%
<b>ON13</b>	5'-GTG AU <sup>C</sup> A TGC	3091.278	3091.684	41%	98%
<b>ON14</b>	5'-GCA TAU <sup>C</sup> CAC	3020.734	3020.739	40%	98%
<b>ON15</b>	5'-GU <sup>C</sup> G ATA U <sup>C</sup> GC	3428.957	3428.227	38%	95%

## 3. Results

### 3.1. Chemical Synthesis of Labels

The structures of cyclen and selected intercalating dyes do not provide suitable functional groups for direct attachment to oligonucleotides, so we first synthesized their derivatives having an azide-terminated linker. The synthesis is shown in Scheme 1 and performed according to well-known methods with some modifications. First, three of the four cyclen amino groups were selectively *N*-protected as trifluoroacetamides (*N*-TFA) using ethyl trifluoroacetate (TFAEt) and purified by column chromatography in accordance with the method described previously [20]. The trifluoroacetamide protecting groups were chosen because of their easy and efficient removal in the last step of conjugate synthesis. During further steps, amine **1** was reacted with commercially available 5-bromovaleryl chloride in dry  $\text{CH}_2\text{Cl}_2$ , followed by treatment with  $\text{NaN}_3$  in DMSO to form azide-terminated **3** with a 65% overall yield. Then, 2-Hydroxy-9*H*-thioxanthen-9-one **4** was synthesized by the reaction of phenol with thiosalicylic acid, which proceeds through successive EAS reactions and culminates in intramolecular Friedel–Crafts cyclization to form a tricyclic thioxanthone core [21]. Reaction of **4** and 1,8-naphthalimide with 1,4-dibromobutane led to

5 and 7, respectively, in good yields. Further substitution of the terminal bromine for the azide group led to the formation of target compounds 6 and 8 with overall yield of 37 and 76%, respectively. The introduced linkers are expected to move the labels far enough and provide them sufficient flexibility to be close to the duplex backbone. The final products were purified by preparative HPLC before their conjugation with oligonucleotides.



**Scheme 1.** Synthesis of azide-functionalized labels. Reagents and conditions: (a) TFAEt, Et<sub>3</sub>N, MeOH, rt, overnight; (b) 5-bromovaleryl chloride, K<sub>2</sub>CO<sub>3</sub>, dry CH<sub>2</sub>Cl<sub>2</sub>, 0 °C, 40 min; (c) NaN<sub>3</sub>, DMSO, rt, 24 h; (d) concd. H<sub>2</sub>SO<sub>4</sub>, 90 °C, 18 h; (e) 1,4-dibromobutane, K<sub>2</sub>CO<sub>3</sub>, DMF, 90 °C, 48 h; (f) NaH, dry DMF, rt, 1 h; then 1,4-dibromobutane, rt, overnight.

### 3.2. Synthesis and Modification of Oligonucleotides

Scheme 2 shows a labeling method by post-synthetic coupling of azide-functionalized labels to 2'-*O*-propargylated oligonucleotides using Cu(I)-catalyzed azide-alkyne cycloaddition (CuAAC). Target oligonucleotides were prepared at the 1.0 μmol scale using an automated synthesizer and standard solid phase phosphoramidite chemistry. The 2'-*O*-propargyl-U (U<sup>P</sup>) units were incorporated into the growing chains of ON3–ON5 in a sequence-specific manner using the so-called “hand-coupling protocol”, which involves manual injection of U<sup>P</sup> phosphoramidite and increasing the coupling time to 25 min [22]. Covalent functionalization of mono-alkyne-modified ON3 and ON4 was carried out by microwave-assisted CuAAC using 0.4-fold molar ratio of CuSO<sub>4</sub>–TBTA complex with sodium ascorbate (*n/n*, 1:1:2.5) and a 4-fold ratio of azide-functionalized label to oligonucleotide [23]. Using the same reaction conditions to functionalize the di-alkyne analogue, ON5, did not give the expected double-clicked adduct, ON8", even after doubling the concentration of the catalyst system and azide label and increasing the MW reaction time to 6 h. We then sought to determine whether Cu(I)–THPTA or Cu(I)–BPS complexes could force the reaction to the double-clicked adduct better than Cu(I)–TBTA. We found that using THPTA instead of TBTA and BPS as a ligand, at the same molar ratio of the catalytic system, could promote the dual coupling of ON5, but showed no improvement in the single coupling of ON3 or ON4.

RP-HPLC analysis of the crude sample obtained after conjugation of 3 with ON3 followed by desalting on a NAP-column show the presence of two new fractions (shaded in gray in Figure 1a), well separated from each other and from the starting ON3. We collected both fractions separately and found that the one at *t*<sub>R</sub> 13.1 min gives a signal at *m/z* 3283.192, corresponding to ON6' (calcd. as *m/z* 3283.295) with a partially deprotected cyclen moiety, while the fraction at *t*<sub>R</sub> 16.3 min gives a signal at *m/z* 3379.920, corresponding to ON6 (calcd. as *m/z* 3379.303) with a fully protected cyclen moiety. Regardless of whether these

fractions were collected and deprotected separately or together, in the RP-chromatogram, we observed the presence of only one fraction at  $t_R$  8.4 min with a signal at  $m/z$  3091.684, coming from **ON13** (calcd. as  $m/z$  3091.278) having a fully deprotected cyclen moiety. After final IE-HPLC purification, **ON13** was obtained in a total yield of 41% and a purity of 98% by IE-analysis (Supplementary Materials Figure S1).

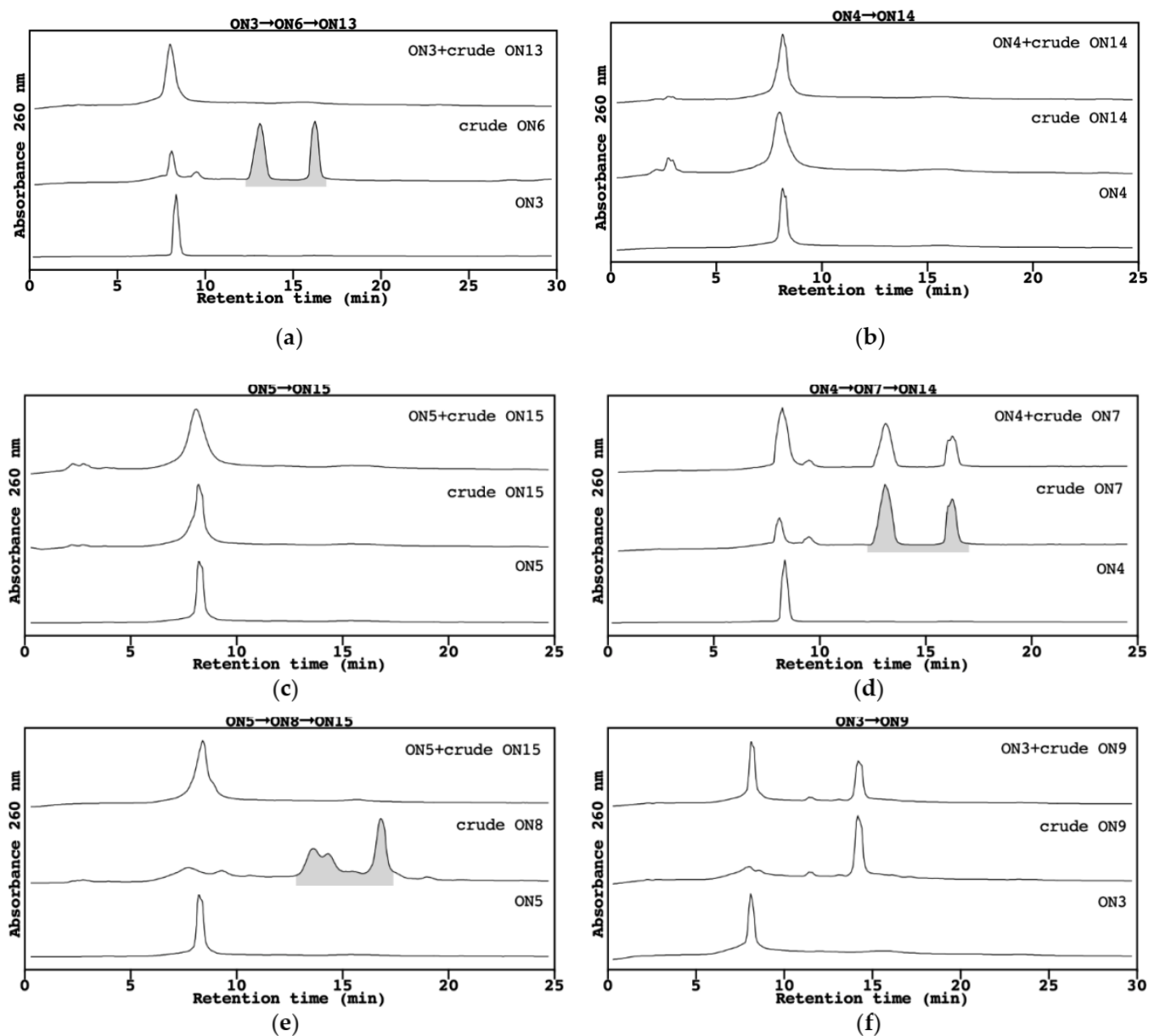
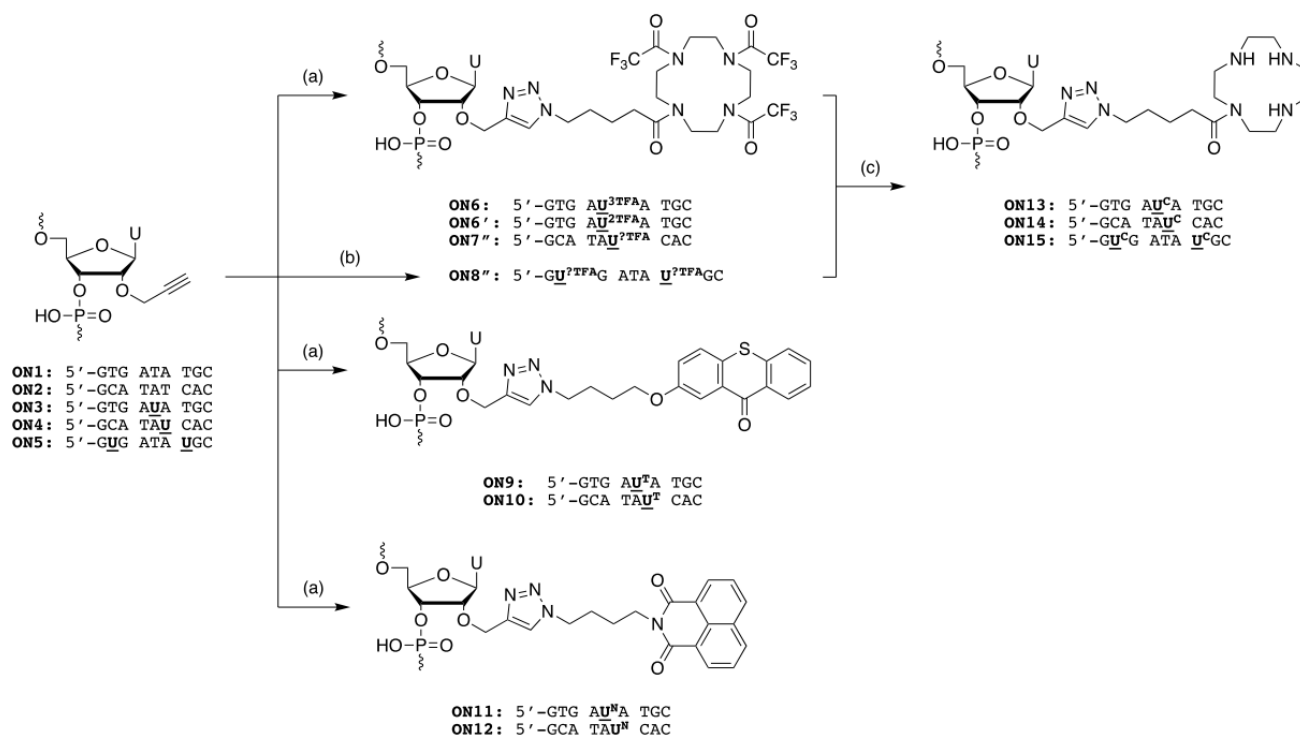


**Figure 1.** The overlay of analytical RP-HPLC chromatograms from the subsequent stages of the synthesis of modified oligonucleotides: (a) **ON13** by separation of **ON6''**, (b) **ON14** without separation of **ON7''**, (c) **ON15** without separation of **ON8''**, (d) **ON7''**, (e) **ON15** by separation of **ON8''**, (f) **ON9**. RP-HPLC conditions: XBridge BEH C18-column ( $\varnothing$ 19 mm  $\times$  100 mm, 5  $\mu$ m); mobile phase: A: 0.05 M TEAA buffer, pH 7.4; B: 25% A, 75% MeCN; isocratic hold of A for 5.0 min, followed by a linear gradient to 70% B for 16.5 min; flow rate 5.0 mL/min; rt.



**Scheme 2.** A post-synthetic approach for the synthesis of 2'-labeled oligonucleotides. Reagents and conditions: (a)  $\text{CuSO}_4$ -TBTA, sodium ascorbate ( $n/n$  1:1:2.5), TEAA buffer/DMSO, Ar, microwave, 90 °C, 2 h; (b)  $\text{CuSO}_4$ -THPTA complex, sodium ascorbate ( $n/n$  1:1:2.5), TEAA buffer/DMSO, Ar, microwave, 90 °C, 2 h; (c) concd. aq.  $\text{NH}_3$  (35%), 55 °C, overnight. 3TFA: tris-*N*-TFA-protected cyclen; 2TFA: bis-*N*-TFA-protected cyclen; ?TFA: unknown degree of cyclen protection. **ON6'**: RP-HPLC separated fraction of the conjugate with bis-*N*-TFA-protected cyclen moiety. **ON7''**, **ON8''**: Unseparated mixture of conjugates with differentially *N*-TFA-protected cyclen moieties.

The overlay of RP-chromatograms in Figure 1a–e shows that omitting the isolation of the *N*-TFA-protected cyclen–oligonucleotide conjugates from the crude **ON6**–**ON8** samples and proceeding directly to the deprotection step prevented further separation of the fully deprotected conjugates from the starting alkynylated oligonucleotides by RP-HPLC. In all cases, the retention time of the fully deprotected conjugates is almost equal to that of the starting alkynylated oligonucleotides and only a single peak is visible after the coinjection of both samples. IE-HPLC analysis of **ON14** obtained by this procedure showed at least 17% content of the remaining fractions (Figure S2). In turn, when **ON14** was prepared by the same procedure as for **ON13**, i.e., by collecting fractions of differently protected **ON7''** conjugates (shaded in gray in Figure 1d) and deprotecting them together, we could easily obtain the final product in 41% overall yield and significant higher 98% purity (Figure S3). We then applied this procedure to obtain **ON15** by bifunctionalization of **ON5**, which, unlike monofunctionalization, resulted in a mixture of several overlapping fractions of differentially protected **ON8''** conjugates, seen in the RP-chromatogram at  $t_R$  of 12.5 to 18.2 min (shaded in gray in Figure 1e). When these fractions were collected and deprotected together (Figure S4), a single fraction was observed by RP-analysis at  $t_R$  8.4 min with a signal at  $m/z$  3428.227 corresponding to **ON15** (calcd. as  $m/z$  3428.957).

Coupling of the thioxanthone derivative **6** to **ON3** gave only one RP-fraction at  $t_R$  14.4 min with a signal at  $m/z$  3118.754 corresponding to **ON9** (calcd. as  $m/z$  3119.595); this was accompanied by the disappearance of the initial **ON3** peak at  $t_R$  8.4 min (Figure 1f). Purification by RP-HPLC gave **ON9** with a purity of 98% and an overall yield of 56%; according to IE-analysis, the sample was sufficiently pure to be used in further duplex stabilization studies without the need for additional IE-HPLC purification (Figure S5). A similar situation occurs for the conjugation of the 1,8-naphthalimide derivative **9** with **ON3**

and for other intercalating dyes; the products of these reactions are well separated from the starting materials and, after RP-HPLC purification, can be used directly for further studies (see Supplementary Materials, Figures S6–S8 show the results of IE-analysis for the remaining conjugates).

### 3.3. Circular Dichroism Studies

Figure 2 shows circular dichroism (CD) spectra recorded to find possible changes in the secondary structure of the labeled duplexes. For all of them, the CD spectra showed intense negative and positive amplitudes at ~250 nm and ~280 nm, respectively, with no major differences relative to unmodified **DU1** DNA duplex (black line in Figure 2a). The intensity of the bands also did not change significantly relative to unmodified **DU1**, suggesting that all modifications introduced do not induce any changes in the overall B-type duplex structure.

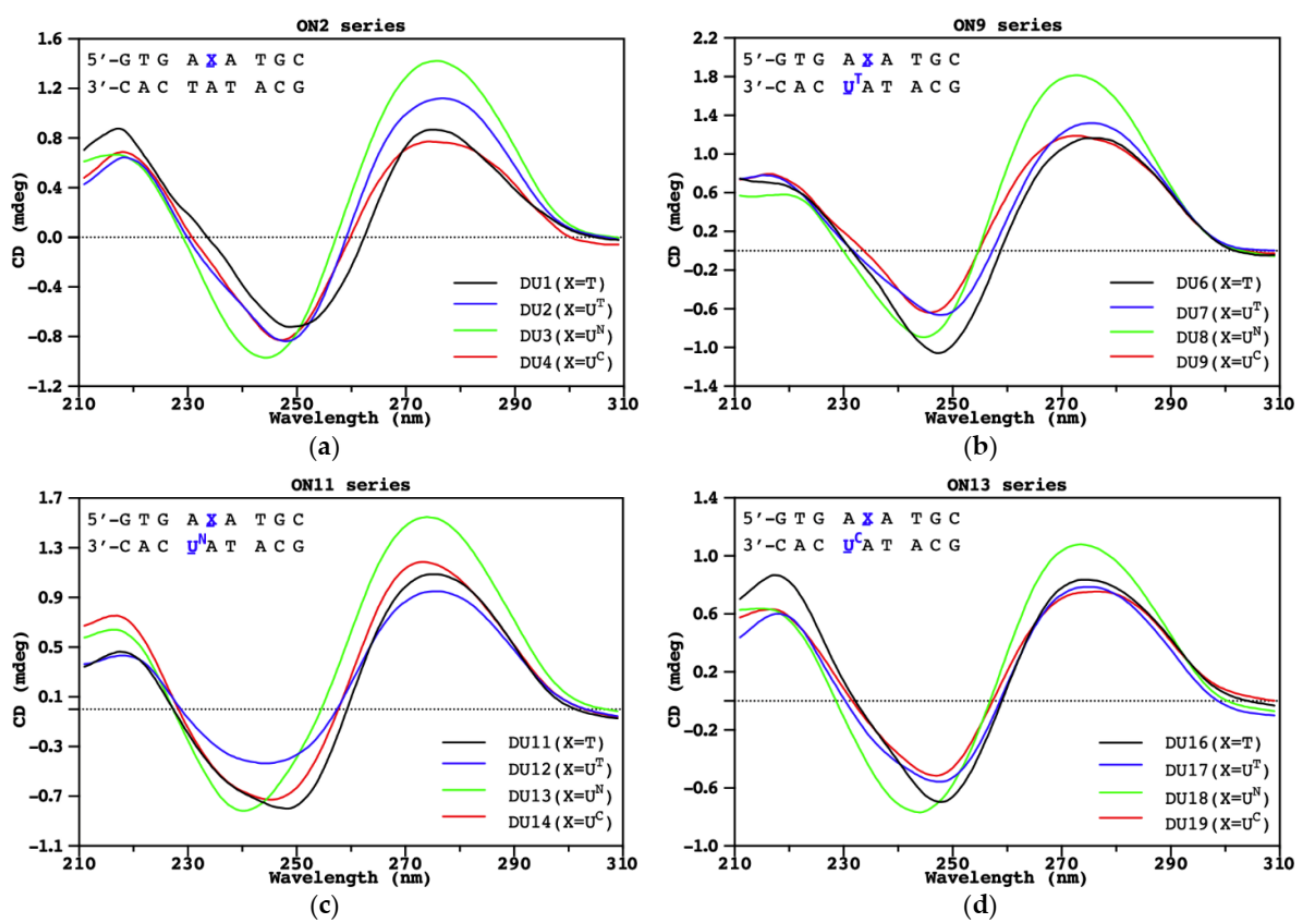


**Figure 2.** Circular dichroism spectra at rt of (a) **DU1–DU4**, (b) **DU6–DU9**, (c) **DU11–DU14**, and (d) **DU16–DU19**. The experiments were performed in a medium salt buffer 5.8 mM  $\text{NaH}_2\text{PO}_4/\text{Na}_2\text{HPO}_4$  buffer (pH 7.0), containing 100 mM NaCl and 0.10 mM EDTA. The concentration of oligonucleotide: Watson–Crick complementary strand = 2.5:2.5  $\mu\text{M}$ .

### 3.4. Ultraviolet Thermal Melting Studies

Figure 3 summarizes the duplex sequences along with the relative changes in melting temperatures ( $\Delta T_m$ ) compared to the corresponding references. The unmodified duplex **D1** has a reference  $T_m$  of 32.5 °C, which is consistent with literature data [24]. In general, oligonucleotides with attached intercalating dyes have a positive effect on the thermal stability of all duplexes obtained, especially duplexes containing mismatches on one of the strands. The magnitude of this effect depends on the position and type of intercalating

dye attached; in the case of duplexes containing only one modified strand, the highest increase in melting temperature was observed for **DU6** and **DU11**, in which intercalator-labeled  $U^T$  and  $U^N$  were adjacent to the GC base pair. For most duplexes containing two intercalator-labeled strands, an additive stabilizing effect was observed, although its magnitude depended on the combination and position of the labeled nucleotides. The largest stabilizing effect was observed for **DU8**, for which  $\Delta T_m$  is  $+10$  °C. Interestingly, in the case of **DU12** with an interchanged dye arrangement, compared to **DU8**, despite the stabilization of  $+5$  °C compared to unmodified **DU1**, an antagonistic effect of lowering  $T_m$  by  $-5$  °C compared to **DU8** was observed.

	ON1	ON9	ON11	ON13	ON15
ON2	5'-GTG ATA TGC 3'-CAC TAT ACG DU1: ref. 32.5 °C	5'-GTG A $U^T$ A TGC 3'-CAC TAT ACG DU2: +3.0 °C	5'-GTG A $U^N$ A TGC 3'-CAC TAT ACG DU3: +3.0 °C	5'-GTG A $U^C$ A TGC 3'-CAC TAT ACG DU4: -4.0 °C	5'-G $U^C$ G ATA $U^C$ G C 3'-CAC TAT ACG DU5: -13.0 °C
ON10	5'-GTG ATA TGC 3'-CAC $U^T$ AT ACG DU6: +4.5 °C	5'-GTG A $U^T$ A TGC 3'-CAC $U^T$ AT ACG DU7: +9.0 °C	5'-GTG A $U^N$ A TGC 3'-CAC $U^T$ AT ACG DU8: +10.0 °C	5'-GTG A $U^C$ A TGC 3'-CAC $U^T$ AT ACG DU9: +1.0 °C	5'-G $U^C$ G ATA $U^C$ G C 3'-CAC $U^T$ AT ACG DU10: -4.0 °C
ON12	5'-GTG ATA TGC 3'-CAC $U^N$ AT ACG DU11: +6.0 °C	5'-GTG A $U^T$ A TGC 3'-CAC $U^N$ AT ACG DU12: +5.0 °C	5'-GTG A $U^N$ A TGC 3'-CAC $U^N$ AT ACG DU13: +7.0 °C	5'-GTG A $U^C$ A TGC 3'-CAC $U^N$ AT ACG DU14: +1.0 °C	5'-G $U^C$ G ATA $U^C$ G C 3'-CAC $U^N$ AT ACG DU15: -9.0 °C
ON14	5'-GTG ATA TGC 3'-CAC $U^C$ AT ACG DU16: -5.5 °C	5'-GTG A $U^T$ A TGC 3'-CAC $U^C$ AT ACG DU17: -2.5 °C	5'-GTG A $U^N$ A TGC 3'-CAC $U^C$ AT ACG DU18: -0.5 °C	5'-GTG A $U^C$ A TGC 3'-CAC $U^C$ AT ACG DU19: -5.0 °C	5'-G $U^C$ G ATA $U^C$ G C 3'-CAC $U^C$ AT ACG DU20: -18.0 °C
MM1	5'-GTG ATA TGC 3'-CAC T $C$ T ACG DU21: ref. 17.0 °C	5'-GTG A $U^T$ A TGC 3'-CAC T $C$ T ACG DU22: +7.5 °C	5'-GTG A $U^N$ A TGC 3'-CAC T $C$ T ACG DU23: +6.0 °C	5'-GTG A $U^C$ A TGC 3'-CAC T $C$ T ACG DU24: -4.0 °C	ND
MM2	5'-GTG ATA TGC 3'-CAC T $T$ T ACG DU25: ref. 17.5 °C	5'-GTG A $U^T$ A TGC 3'-CAC T $T$ T ACG DU26: +7.0 °C	5'-GTG A $U^N$ A TGC 3'-CAC T $T$ T ACG DU27: +5.5 °C	5'-GTG A $U^C$ A TGC 3'-CAC T $T$ T ACG DU28: +1.0 °C	ND
MM3	5'-GTG ATA TGC 3'-CAC T $G$ T ACG DU29: ref. 23.0 °C	5'-GTG A $U^T$ A TGC 3'-CAC T $G$ T ACG DU30: +5.0 °C	5'-GTG A $U^N$ A TGC 3'-CAC T $G$ T ACG DU31: +7.0 °C	5'-GTG A $U^C$ A TGC 3'-CAC T $G$ T ACG DU32: -5.0 °C	ND

**Figure 3.** Heat map of the relative changes in melting temperatures ( $\Delta T_m$ ) of the modified duplexes compared to their respective controls.  $\Delta T_m$  values are the average of three measurements. **DU1** is reference for **DU2–DU20**, **DU21** is reference for **DU22–DU24**, **DU25** is reference for **DU26–DU28**, **DU29** is reference for **DU30–DU32**. Red indicates an increase in the thermal stability of the duplex, blue indicates a decrease. ND: not detected. Conditions: 2.5  $\mu$ M of each strand in a medium salt buffer 5.8 mM  $NaH_2PO_4/Na_2HPO_4$  buffer (pH 7.0), containing 100 mM NaCl and 0.10 mM EDTA. The  $T_m$  values reflect the average of two measurements.  $\Delta T_m$  values for mismatches were calculated as the difference in  $T_m$  values between unmodified mismatched and modified mismatched duplexes.

The second regularity observed in almost all duplexes is a decrease in melting temperature by approximately the same value in the range from  $-4.0$  to  $-5.5$  °C, caused by the presence of a cyclen-labeled  $U^C$  in one of the strands. The destabilizing effect of  $U^C$  is additive and increases with increasing number of cyclen moieties attached to a single strand and their total number in the duplex, with  $\Delta T_m$  averaging  $-6$  °C for each  $U^C$  introduced. However, there are two exceptions to this regularity; one of which is **DU28**, where some selectivity against mismatch TT was observed, as evidenced by  $\Delta T_m$  of  $+1$  °C. This result is not necessarily surprising, as previous work on Zn(II)–cyclen complexes has shown that cyclen is able to selectively recognize thymine by forming hydrogen bonds between the carbonyl oxygens of thymine and the cyclen amino groups [25,26]. The second exception is **DU19**, where two  $U^C$  units are adjacent on complementary strands of the duplex, however, their destabilizing effect is not additive. In this case, only a thermal destabilization of  $-5$  °C was observed, corresponding to the introduction of one  $U^C$  unit instead of two. The ability of covalently coupled polyamines to thermally destabilize short duplexes has been reported and is discussed below. For mixed duplexes, consisting of one strand with a cyclen-modified  $U^C$  and the other strand with an intercalator attached, additive effects affecting the thermal stability were also observed.



#### 4. Discussion

Typically, when linear polyamines are introduced at the 2' or 4'-position of the ribose ring, either an adverse or no effect on the thermal stability of the DNA duplex is observed. Sund et al. showed that the introduction of C-branched spermine via ara-U-2'-phosphate (six-atom linker; the length of the linker is counted from the first atom attached to the ribose ring to the first polyamine atom) in the middle of **DU33** (Figure 4) decreases the thermal stability of the duplex by as much as  $-28.5$  °C, but the same study also showed that if spermine is attached to the 3' or 5'-end, then the thermal stability increases by  $+0.5$  to  $+2.5$  °C [27]. Winkler et al. attached linear polyamines via a 2'-N-succinylamido linker (four atoms long) to the internal and terminal nucleotides of **DU34** (Figure 4), which also reduced the thermal stability by  $-4.5$  °C [28]. Moreover, the introduction of further polyamine moieties into the internal positions of the 18-mer only led to further destabilization of the resulting duplexes. In contrast, Wengel's group has reported many examples of DNA oligonucleotides modified with linear or branched polyamines attached through 2'-amino-LNA motifs, including **DU35–DU37** (Figure 4), which increase the thermal stability from  $+7.0$  to  $+8.5$  °C when present in the middle of the strand [23,29,30]. The modifications present in **DU36** and **DU37** are of particular interest to us because of their sequential and structural similarity to the duplexes obtained in this work, in particular to **ON13**. The cyclen-labeled U<sup>C</sup> present in **DU4** consists of three protonable amine groups, similar to the spermidine moiety in **DU37**, and a 2'-methoxy-triazolyl-butyl linker is the same length (nine atoms long) as the linkers in **DU36** and **DU37**. Despite these similarities, **DU4** shows reduced thermal stability by  $-4.0$  °C, while **DU36** and **DU37** show increased stabilization by  $+8.5$  °C. The stabilization effect of  $+7.0$  °C is also maintained by a shorter propanamide linker (three atoms long) conjugated with the piperazine ring in **DU35**, and even by the mere presence of the 2'-amino-LNA motif in **D38**, resulting in  $\Delta T_m$  of  $+4.0$  °C. The results discussed here may suggest that the 2'-amino-LNA motif helps to adopt the correct conformation of the ribose ring, which may be critical for duplex stabilization by polyamines, especially when they are covalently attached to the internal positions of the strands.

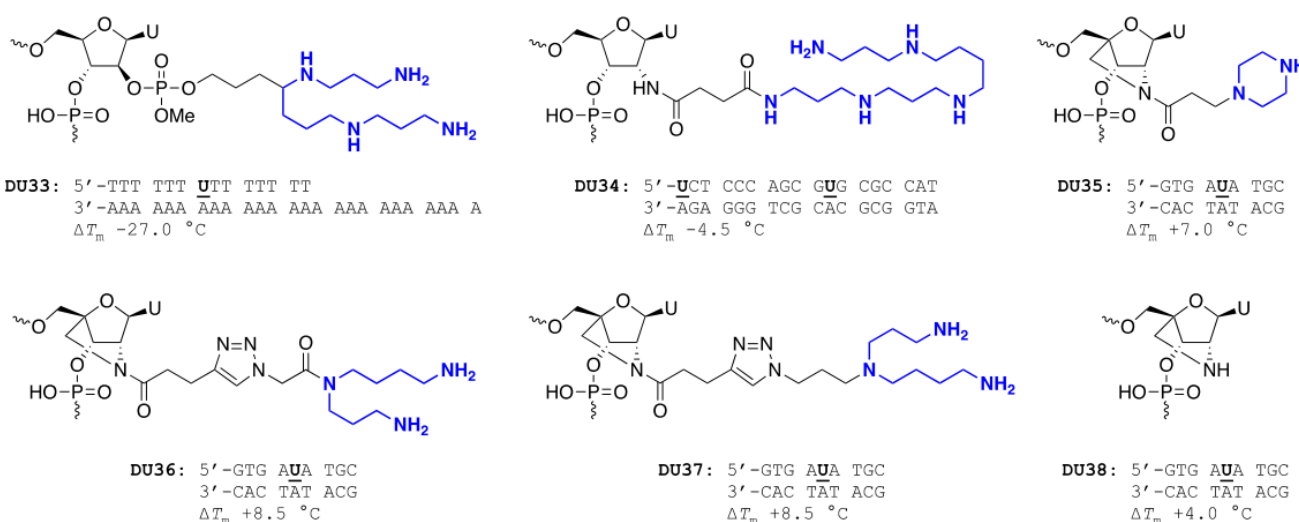


**Figure 4.** Structures and melting temperatures of polyamine–oligonucleotide conjugates known from literature. All conjugates shown are modified at the 2'-position of the ribose and are located on internal strand positions. The attached polyamines are marked in blue.

The results obtained for **DU4** with those from the literature indicated a lower destabilization effect of cyclen in comparison with reported data for linear polyamines. The exceptions are polyamine–LNA conjugates, such as **DU36** and **DU37**, unambiguously confirming the stabilizing effect of the LNA motif. Our study shows that the incorporation

of cyclen-labeled  $U^C$  in the middle of **DU4** and other related duplexes led to a decrease in the thermal stability by an average value of  $-6.0$  °C. An interesting exception to this rule is the introduction of two  $U^C$  units directly opposite to each other on complementary strands, which causes much less duplex destabilization than would appear from the number of polyamines attached. Such an arrangement can be used to maximize the number of polyamines introduced with the least effect on the thermal stability of the duplex. Another exception to this rule is the presence of  $U^C$  opposite the TT mismatch on a complementary strand; in this case, we observed a slight stabilization of the duplex, which can be used to design mismatch-selective DNA binders as useful models for understanding and modulating the action of DNA repair enzymes. We also showed that the presence of  $U^T$  and  $U^N$  modifications has a strong thermostabilizing effect on duplex formation, and the proximity of both modifications to each other and  $U^C$  does not disturb their interaction with the duplex. This property can be useful to overcome the thermostabilizing effect of cyclen moiety and to design hybrids possessing two functionalities. Shedding more light on the source of the observed effects will require additional studies on the interaction of polyamines with duplexes but will provide valuable insight into the key design requirements for such conjugates and their future applications in biological systems.

## 5. Conclusions

We have developed a new protocol for the synthesis of cyclen-containing oligonucleotides by post-synthetic coupling of azide-functionalized labels to 2'-*O*-propargylated oligonucleotides using Cu(I)-catalyzed azide–alkyne cycloaddition. All dye-containing oligonucleotides have a positive effect on the thermal stability of the obtained duplexes, especially those containing mismatches on one of the strands. The  $T_m$  amplitude depends on the number and position of the attached dye molecules. The presence of the cyclen moiety in one of the strands decreases the melting temperature by approximately the same value in the range from  $-4.0$  to  $-5.5$  °C. This destabilization effect can, however, be diminished by the presence of a dye molecule in the complementary strand. Compensating for the destabilizing effect of cyclen (and possibly other polyamines) on dsDNA by inclusion of an intercalating dye is a promising tool for adjusting the thermal stability of polyamine-labeled DNA duplexes.

**Supplementary Materials:** The following supporting information can be downloaded at: <https://www.mdpi.com/article/10.3390/pharmaceutics14010066/s1>, Figure S1. (a) Semi-preparative RP-HPLC ( $t_R$  10.489 min), (b) analytical IE-HPLC ( $t_R$  8.31 min) and (c) MALDI-MS (calcd.  $m/z$  [M+H]<sup>+</sup> 3091.278) of ON13; Figure S2. Analytical IE-HPLC of ON14 ( $t_R$  9.28 min) obtained directly from ON4, without separation of *N*-TFA protected byproducts ON7''; Figure S3. (a) Semi-preparative RP-HPLC ( $t_R$  10.173 min), (b) MALDI-MS (calcd.  $m/z$  [M+H]<sup>+</sup> 3020.734) of ON14 obtained by separating a mixture of ON7'' byproducts and their joint deprotection and (c) analytical IE-HPLC ( $t_R$  8.31 min) of ON14; Figure S4. (a) Semi-preparative RP-HPLC of ON8'' byproducts ( $t_R$  14.476, 14.876 and 16.694 min) containing cyclen moieties with a different degree of *N*-TFA protection. These fractions were collected and deprotected together to yield the final conjugate ON15. (b) MALDI-MS of ON15; Figure S5. (a) Semi-preparative RP-HPLC ( $t_R$  15.906 min), (b) analytical IE-HPLC ( $t_R$  11.42 min) and (c) MALDI-MS (calcd.  $m/z$  [M+H]<sup>+</sup> 3119.595) of ON9; Figure S6. (a) Semi-preparative RP-HPLC ( $t_R$  15.959 min), (b) analytical IE-HPLC ( $t_R$  11.87 min) and (c) MALDI-MS (calcd.  $m/z$  [M+H]<sup>+</sup> 3048.222) of ON10; Figure S7. (a) Analytical IE-HPLC ( $t_R$  10.84 min) and (b) MALDI-MS (calcd.  $m/z$  [M+H]<sup>+</sup> 3088.618) of ON11; Figure S8. (a) Analytical IE-HPLC ( $t_R$  10.95 min) and (b) MALDI-MS (calcd.  $m/z$  [M+H]<sup>+</sup> 3017.618) of ON12.

**Author Contributions:** Conceptualization, M.D.T. and P.T.J.; methodology, M.D.T. and P.T.J.; investigation, M.D.T. and M.Z.; writing—original draft preparation, M.D.T.; writing—review and editing, K.W.; supervision, K.W. and J.W.; funding acquisition, M.D.T. All authors have read and agreed to the published version of the manuscript.

**Funding:** This research was funded by the Rector's grant in the area of scientific research and development works. Silesian University of Technology, grant number 04/020/RGJ20/0119.

**Institutional Review Board Statement:** Not applicable.

**Informed Consent Statement:** Not applicable.

**Data Availability Statement:** The data presented in this study are available upon request from the corresponding author.

**Conflicts of Interest:** The authors declare no conflict of interest.

## References

1. Sharma, V.K.; Sharma, R.K.; Singh, S.K. Antisense oligonucleotides: Modifications and clinical trials. *MedChemComm* **2014**, *5*, 1454–1471. [\[CrossRef\]](#)
2. Wan, W.B.; Seth, P.P. The Medicinal Chemistry of Therapeutic Oligonucleotides. *J. Med. Chem.* **2016**, *59*, 9645–9667. [\[CrossRef\]](#) [\[PubMed\]](#)
3. Dubey, I.; Dubey, L.; Piletska, E.; Piletsky, S. Metal complexes of 1, 4, 7-triazacyclononane and their oligonucleotide conjugates as chemical nucleases. *Ukr. Bioorg. Acta* **2007**, *1*, 11–19.
4. Stewart, K.M.; McLaughlin, L.W. Four-Arm Oligonucleotide Ni(II)–Cyclam-Centered Complexes as Precursors for the Generation of Supramolecular Periodic Assemblies. *J. Am. Chem. Soc.* **2004**, *126*, 2050–2057. [\[CrossRef\]](#)
5. Wan, S.-H.; Liang, F.; Xiong, X.-Q.; Yang, L.; Wu, X.-J.; Wang, P.; Zhou, X.; Wu, C.-T. DNA hydrolysis promoted by 1,7-dimethyl-1,4,7,10-tetraazacyclododecane. *Bioorganic Med. Chem. Lett.* **2006**, *16*, 2804–2806. [\[CrossRef\]](#)
6. Wang, M.-Q.; Zhang, J.; Zhang, Y.; Zhang, D.-W.; Liu, Q.; Liu, J.-L.; Lin, H.-H.; Yu, X.-Q. Metal-free cleavage efficiency toward DNA by a novel PNA analog-bridged macrocyclic polyamine. *Bioorganic Med. Chem. Lett.* **2011**, *21*, 5866–5869. [\[CrossRef\]](#)
7. Li, J.; Zhang, J.; Lu, Q.-S.; Yue, Y.; Huang, Y.; Zhang, D.-W.; Lin, H.-H.; Chen, S.-Y.; Yu, X.-Q. Hydrolytic cleavage of DNA by urea-bridged macrocyclic polyamines. *Eur. J. Med. Chem.* **2009**, *44*, 5090–5093. [\[CrossRef\]](#)
8. Zhang, Y.; Wang, M.-Q.; Zhang, J.; Zhang, D.-W.; Lin, H.-H.; Yu, X.-Q. Synthesis, DNA Binding, and Cleavage Studies of Novel PNA Binding Cyclen Complexes. *Chem. Biodivers.* **2011**, *8*, 827–840. [\[CrossRef\]](#)
9. Lu, Q.-S.; Huang, Y.; Li, J.; Zhang, Z.-W.; Lin, H.-H.; Yu, X.-Q. The Effect of an Amino-Acid Bridge on Binding Affinity and Cleavage Efficiency of Pyrenyl-Macrocyclic Polyamine Conjugates toward DNA. *Chem. Biodivers.* **2009**, *6*, 1273–1282. [\[CrossRef\]](#)
10. Asseline, U. Development and Applications of Fluorescent Oligonucleotides. *Curr. Org. Chem.* **2006**, *10*, 491–518. [\[CrossRef\]](#)
11. Bag, S.S.; Saito, Y.; Hanawa, K.; Kodate, S.; Suzuka, I.; Saito, I. Intelligent fluorescent nucleoside in sensing cytosine base: Importance of hydrophobic nature of perylene fluorophore. *Bioorganic Med. Chem. Lett.* **2006**, *16*, 6338–6341. [\[CrossRef\]](#)
12. Langenegger, S.M.; Häner, R. Remarkable Stabilization of Duplex DNA Containing an Abasic Site by Non-Nucleosidic Phenanthroline and Pyrene Building Blocks. *ChemBioChem* **2005**, *6*, 848–851. [\[CrossRef\]](#)
13. Crockett, A.O.; Wittwer, C.T. Fluorescein-Labeled Oligonucleotides for Real-Time PCR: Using the Inherent Quenching of Deoxyguanosine Nucleotides. *Anal. Biochem.* **2001**, *290*, 89–97. [\[CrossRef\]](#)
14. Lee, H.J.; Kim, B.H. Detection of AAG repeats through DNA triplex-induced G-cluster formation. *Chem. Commun.* **2019**, *55*, 7526–7529. [\[CrossRef\]](#)
15. Podder, A.; Lee, H.J.; Kim, B.H. Fluorescent Nucleic Acid Systems for Biosensors. *Bull. Chem. Soc. Jpn.* **2021**, *94*, 1010–1035. [\[CrossRef\]](#)
16. Lee, H.J.; Kim, B.H. Pyrene-Modified Guanine Cluster Probes Forming DNA/RNA Hybrid Three-Way Junctions for Imaging of Intracellular MicroRNAs. *ACS Appl. Bio Mater.* **2021**, *4*, 1668–1676. [\[CrossRef\]](#)
17. Gouda, A.S.; Przepis, Ł.; Walczak, K.; Jørgensen, P.T.; Wengel, J. Carbazole modified oligonucleotides: Synthesis, hybridization studies and fluorescence properties. *Org. Biomol. Chem.* **2020**, *18*, 6935–6948. [\[CrossRef\]](#)
18. Telser, J.; Cruickshank, K.A.; Schanze, K.S.; Netzel, T.L. DNA oligomers and duplexes containing a covalently attached derivative of tris(2,2'-bipyridine)ruthenium(II): Synthesis and characterization by thermodynamic and optical spectroscopic measurements. *J. Am. Chem. Soc.* **1989**, *111*, 7221–7226. [\[CrossRef\]](#)
19. Telser, J.; Cruickshank, K.A.; Morrison, L.E.; Netzel, T.L.; Chan, C.K. DNA duplexes covalently labeled at two sites: Synthesis and characterization by steady-state and time-resolved optical spectroscopies. *J. Am. Chem. Soc.* **1989**, *111*, 7226–7232. [\[CrossRef\]](#)
20. Yang, W.; Giandomenico, C.M.; Sartori, M.; Moore, D.A. Facile N-1 protection of cyclam, cyclen and 1,4,7-triazacyclononane. *Tetrahedron Lett.* **2003**, *44*, 2481–2483. [\[CrossRef\]](#)
21. Wutzel, H.; Jarvid, M.; Bjuggren, J.M.; Johansson, A.; Englund, V.; Gubanski, S.; Andersson, M. Thioxanthone derivatives as stabilizers against electrical breakdown in cross-linked polyethylene for high voltage cable applications. *Polym. Degrad. Stab.* **2015**, *112*, 63–69. [\[CrossRef\]](#)
22. Astakhova, I.K.; Wengel, J. Interfacing Click Chemistry with Automated Oligonucleotide Synthesis for the Preparation of Fluorescent DNA Probes Containing Internal Xanthene and Cyanine Dyes. *Chem. Eur. J.* **2013**, *19*, 1112–1122. [\[CrossRef\]](#)
23. Danielsen, M.B.; Christensen, N.J.; Jørgensen, P.T.; Jensen, K.J.; Wengel, J.; Lou, C. Polyamine-Functionalized 2'-Amino-LNA in Oligonucleotides: Facile Synthesis of New Monomers and High-Affinity Binding towards ssDNA and dsDNA. *Chem. Eur. J.* **2020**, *27*, 1416–1422. [\[CrossRef\]](#)
24. Singh, S.K.; Nielsen, P.; Koshkin, A.; Wengel, J. LNA (locked nucleic acids): Synthesis and high-affinity nucleic acid recognition. *Chem. Commun.* **1998**, *4*, 455–456. [\[CrossRef\]](#)

25. Zhu, Z.; Wang, S.; Wei, D.; Yang, C. Zn<sup>2+</sup>-cyclen-based complex enable a selective detection of single-stranded thymine-rich DNA in aqueous buffer. *Biosens. Bioelectron.* **2016**, *85*, 792–797. [[CrossRef](#)]
26. Kimura, E.; Katsube, N.; Koike, T.; Shiro, M.; Aoki, S. Effects of Bis(aromatic) Pendants on Recognition of Nucleobase Thymine by Zn<sup>2+</sup>-1,4,7,10-tetraazacyclododecane (Zn<sup>2+</sup>-cyclen). *Supramol. Chem.* **2002**, *14*, 95–102. [[CrossRef](#)]
27. Sund, C.; Puri, N.; Chattopadhyaya, J. Synthesis of C-branched spermine tethered oligo-DNA and the thermal stability of the duplexes and triplexes. *Tetrahedron* **1996**, *52*, 12275–12290. [[CrossRef](#)]
28. Winkler, J.; Saadat, K.; Díaz-Gavilán, M.; Urban, E.; Noe, C.R. Oligonucleotide–polyamine conjugates: Influence of length and position of 2'-attached polyamines on duplex stability and antisense effect. *Eur. J. Med. Chem.* **2009**, *44*, 670–677. [[CrossRef](#)] [[PubMed](#)]
29. Lou, C.; Vester, B.; Wengel, J. Oligonucleotides containing a piperazino-modified 2'-amino-LNA monomer exhibit very high duplex stability and remarkable nuclease resistance. *Chem. Commun.* **2015**, *51*, 4024–4027. [[CrossRef](#)] [[PubMed](#)]
30. Lou, C.; Samuelsen, S.V.; Christensen, N.J.; Vester, B.; Wengel, J. Oligonucleotides Containing Aminated 2'-Amino-LNA Nucleotides: Synthesis and Strong Binding to Complementary DNA and RNA. *Bioconjugate Chem.* **2017**, *28*, 1214–1220. [[CrossRef](#)] [[PubMed](#)]

## Publikacja P.4

Synthesis and *in vitro* cytotoxic activity of dye-linker-macrocycle conjugates with variable linker length and components

**Tomczyk, M. D.\***; Matczak, K.; Skonieczna, M.; Chulkin, P.; Denel-Bobrowska, M.; Różycka, D.; Rykowski, S.; Olejniczak, A. B.; Walczak, K.

*Bioorganic Chemistry* **2023**, 106782.



## Synthesis and *in vitro* cytotoxic activity of dye-linker-macrocycle conjugates with variable linker length and components

Mateusz D. Tomczyk <sup>a,\*</sup>, Karolina Matczak <sup>b</sup>, Magdalena Skonieczna <sup>c</sup>, Pavel Chulkin <sup>d</sup>, Marta Denel-Bobrowska <sup>e</sup>, Daria Różycka <sup>e</sup>, Sebastian Rykowski <sup>e</sup>, Agnieszka B. Olejniczak <sup>e</sup>, Krzysztof Walczak <sup>a</sup>

<sup>a</sup> Department of Organic Chemistry, Bioorganic Chemistry and Biotechnology, Faculty of Chemistry, Silesian University of Technology, Krzywoustego 4, Gliwice 44-100, Poland

<sup>b</sup> Department of Medical Biophysics, University of Łódź, Pomorska 141/143, Łódź 90-236, Poland

<sup>c</sup> Department of Systems Biology and Engineering, Silesian University of Technology, Akademicka 16, Gliwice 44-100, Poland

<sup>d</sup> Department of Physical Chemistry and Technology of Polymers, Silesian University of Technology, Strzody 9, Gliwice 44-100, Poland

<sup>e</sup> Institute of Medical Biology, Polish Academy of Sciences, Lodowa 106, Łódź 93-232, Poland

### ARTICLE INFO

#### Keywords:

Cytotoxic activity  
Thioxanthone  
1,8-Naphthalimide  
Cyclic polyamines  
Crown ethers

### ABSTRACT

The study investigated the structure–activity relationship of newly synthesized dye-linker-macrocycle (DLM) conjugates and the effects of each component on various biological properties, including cytotoxicity, cellular uptake, intracellular localization, interaction with DNA, and photodynamic effects. The conjugates were synthesized by combining 1,8-naphthalimide and thioxanthone dyes with 1,4,7,10-tetraazacyclododecane (cyclen) and 1-aza-12-crown-4 (1A12C4) using alkyl linkers of different lengths. The results revealed significant differences in biological activity among the various series of conjugates. Particularly, 1A12C4 conjugates exhibited notably higher cytotoxicity compared to cyclen conjugates. The conjugation with 1A12C4 proved to be an effective strategy for increasing cellular uptake and cytotoxicity of small-molecule conjugates. In addition, the results highlighted the critical role of linker length in modulating the biological activity of DLM conjugates. It became clear that the choice of each component (dye, macrocycle and linker) could significantly alter the biological activity of the conjugates.

### 1. Introduction

The term “theranostic” was first introduced by John Funkhouser in 1998, denoting the integration of diagnostic and therapeutic functions within a single agent [1]. These agents typically consist of two to three covalently linked components: (1) a cytotoxic drug (cargo), (2) an imaging agent (dye) to visualize the tumor microenvironment and provide feedback on therapeutic efficacy, and (3) a vector and/or receptor for precise and targeted delivery of chemotherapeutics to cancer cells [2,3]. Funkhouser’s concept emphasizes the close relationship between diagnostic and therapeutic agents, often sharing similar structural features or even identical counterparts. Examples include molecular probes with a dye-linker-receptor design [4–6] and anticancer drugs with a vector-linker-cargo design [7,8] (Fig. 1). In both scenarios, small

molecule dyes/vectors or receptors/cargoes can serve dual functions, acting as both imaging units with intrinsic targeting capabilities or therapeutic units with intrinsic imaging capabilities, resulting in “1 + 1” type theranostic molecules.

However, the structural similarities often observed among therapeutic and diagnostic agents, and thus their similar chemical properties, may not always align with their intended use and expected biological effects. While theranostics used in anticancer therapies are specifically designed to combine cytotoxicity with other functions, molecular probes should remain non-cytotoxic to prevent interference with the activity of test drugs and cellular functions. Therefore, it is important to identify specific structural features that make these agents suitable for use as anticancer drugs or molecular probes. To address this issue, we synthesized three series of dye-linker-macrocycle (DLM) conjugates

**Abbreviations:** 1A12C4, 1-Aza-12-crown-4; C2, 1,2-Ethylene linker; C4, 1,4-Butylene linker; C6, 1,6-Hexylene linker; CC<sub>50</sub>, Concentration of cytotoxicity 50%; Clog P, Computed log P; CT-DNA, Calf Thymus DNA; cyclen, 1,4,7,10-Tetraazacyclododecane; DLM, Dye-linker-macrocycle; EtBr, Ethidium bromide; FHA, Fast halo assay; NDF, Nuclear diffusion factor; NPI, 1,8-Naphthalimide; ROS, Reactive oxygen species; TFA, Trifluoroacetic acid; THX, Thioxanthone

\* Corresponding author.

E-mail address: [mateusz.d.tomczyk@polsl.pl](mailto:mateusz.d.tomczyk@polsl.pl) (M.D. Tomczyk).

<https://doi.org/10.1016/j.bioorg.2023.106782>

Received 1 June 2023; Received in revised form 7 August 2023; Accepted 8 August 2023

0045-2068/© 20XX

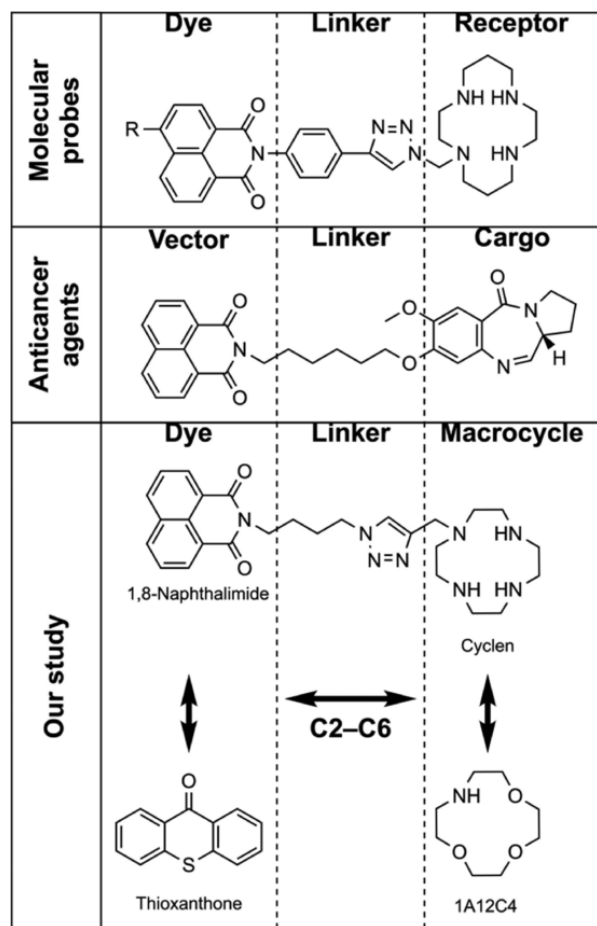


Fig. 1. Schematic representation of common architecture and constituent elements in the synthesis of molecular probes [9] and anticancer agents [10].

(Fig. 1) and tested them for specific biological properties. This approach allowed us to study the structure–activity relationship and provided valuable insights into the impact of individual components on their biological effects.

As the imaging agent in this study, we utilized two fluorescent dyes with intrinsic cytotoxicity and tumor-targeting capabilities, namely 1,8-naphthalimide and thioxanthone. Recently, 1,8-naphthalimides have gained increasing attention as imaging agents due to their exceptional brightness, photostability, and ease of modifying their properties through substitution [11–13]. Additionally, these compounds have been extensively explored as versatile scaffolds for developing anticancer agents [14,15]. Thioxanthenes, in addition to their strong fluorescent properties [16,17], also exhibit remarkable anticancer properties due to their photodynamic activity [18]. After absorbing light of a certain wavelength, thioxanthenes generate reactive oxygen species (ROS) that cause damage to DNA, proteins and lipids, ultimately leading to cell death in the targeted area.

However, the development of molecular probes and anticancer agents based on fluorescent dyes can pose challenges to their utility in biological systems. One of the major challenges is the limited solubility of conjugates containing polyaromatic dyes in aqueous media. To overcome this limitation, the conjugate structure can be optimized by incorporating hydrophilic polar groups, thereby increasing solubility. In addition, non-specific binding to biological targets can lead to inaccurate results or low cellular uptake. To address this problem, functional groups such as polyamines or polyethers can be incorporated into the conjugate to increase selectivity to specific biomolecules (e.g. DNA), cellular receptors (e.g. PAT) or organelles (e.g. nuclei or liposomes).

In the context of theranostics, polyamines and polyethers can serve all three functions while also improving the bioavailability and cellular uptake of the resulting conjugates. For instance, Xu et al. showed that incorporating branched chains with tertiary ammonium groups into perylene improved its solubility and DNA staining ability [19,20]. Additionally, Phanstiel et al. showed that attaching linear polyamines to anthracene facilitated the delivery of conjugates into cells via polyamine transporters [21–24]. Furthermore, Cao et al. reported that conjugating doxorubicin with polyethylene glycol led to increased cellular uptake and broadened distribution of small drug molecules within cells [25].

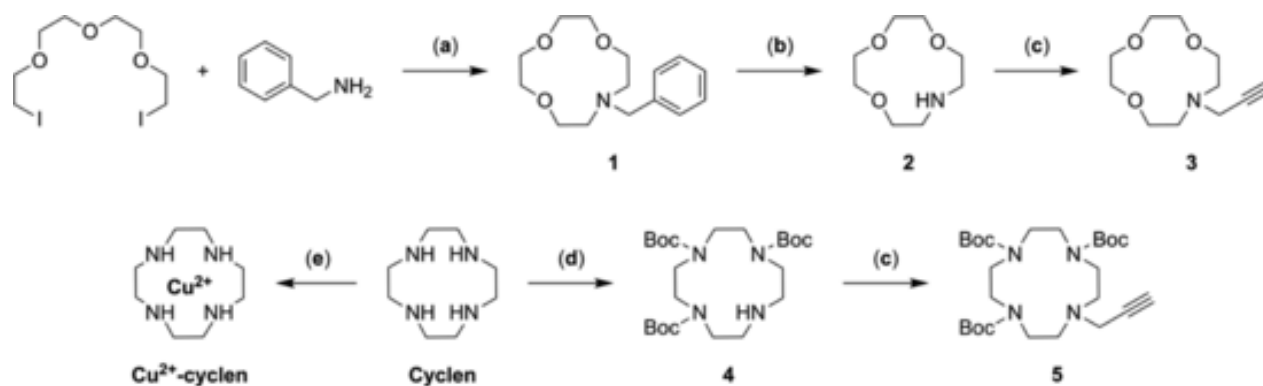
Cyclic polyamines (azamacrocycles) and crown ethers are commonly used as receptors in molecular probes due to their unique chelating properties [26–28]. These macrocycles also exhibit notable biological properties; for instance, azamacrocycles complexes can catalyze DNA hydrolysis [29], while crown ethers demonstrate strong cytotoxicity due to their ionophoric properties [30]. As a result, there is a growing interest in employing macrocycles as components in anti-cancer agents. However, while extensive studies have explored the effects of linear polyamines on conjugates' interactions with DNA, cellular uptake, and other biological aspects, the corresponding effects of cyclic polyamines remain less explored [31,32]. Even less is known about conjugates with crown ethers and their aza-derivatives. Our study addresses this gap and provides valuable insights into the biological effects resulting from the conjugation of macrocycles with fluorescent dyes and intercalating agents.

## 2. Results and discussion

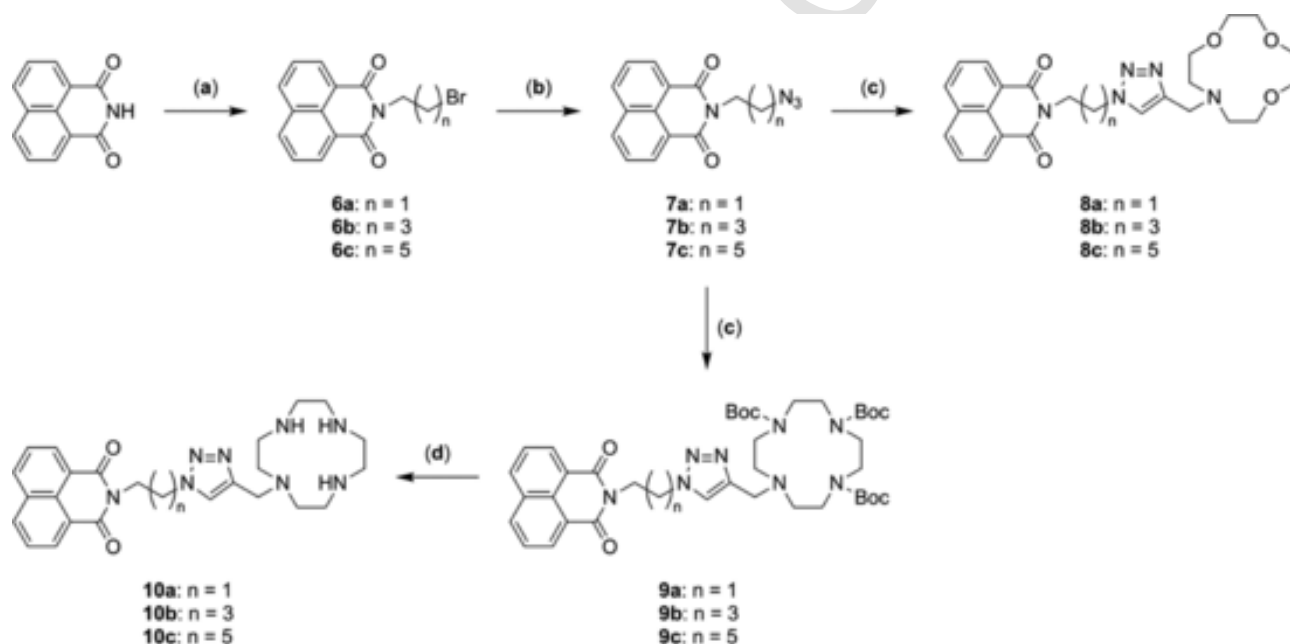
### 2.1. Chemistry

In this study, we employ a versatile synthetic strategy to create a diverse library of DLM conjugates by using click chemistry to combine *N*-propargylated macrocycles with azide-containing intercalating dyes (Scheme 1). Cyclen and 1-aza-12-crown-4 (2) were chosen as suitable scaffolds because of their readily functionalized amino groups and distinct chemical properties. To synthesize 1-aza-12-crown-4, we employed a [2:1] cyclization strategy as previously described [33]. Specifically, we reacted 1,11-diiodo-3,6,9-trioxaundecane with benzylamine under high dilution conditions to generate the *N*-protected intermediate 1, which was then deprotected by hydrogenolysis to give 1-aza-12-crown-4 in 59% yield, based on intermediate 1. The resulting 1-aza-12-crown-4 was then functionalized with propargyl bromide and purified by column chromatography to give compound 3 in 89% yield. To synthesize compound 4, we used commercially available cyclen and selectively protected three out of four amino groups using di-*tert*-butoxydicarbonate ( $\text{Boc}_2\text{O}$ ). This strategy took advantage of the steric hindrance effect of the bulky *tert*-butyloxycarbonyl (Boc) group, allowing the selective introduction of only three protecting groups in a relatively small macrocycle of cyclen. The reaction proceeded with an almost quantitative yield of 95%. The unprotected amino group was then reacted with propargyl bromide to yield the monofunctionalized *N*-propargyl derivative 5 in 73% yield.

Azide-functionalized 1,8-naphthalimides 7a–c were synthesized by replacing the bromine atoms in compounds 6a–c with azide groups, with yields in the range of 76–88% (Scheme 2). *N*-alkylated derivatives 6a–c were obtained by reacting commercially available 1,8-naphthalimide with a 1.5-fold excess of NaH and a 4-fold excess of the appropriate dibromoalkane, with satisfactory yields in the 75–80% range. The synthesis of 2-hydroxy-9*H*-thioxanthen-9-one (11) involved a multi-step reaction sequence, starting with the reaction of phenol with thiosalicylic acid, followed by successive electrophilic aromatic substitutions and intramolecular Friedel–Crafts cyclization, resulting in a moderate yield of 29% (Scheme 3) [34]. Compound 11 was then reacted with a 4-fold excess of the corresponding dibromoalkane in the



**Scheme 1.** General synthetic route to obtain propargylated macrocyclic ligands **3** and **5**. Synthesis of  $\text{Cu}^{2+}$ -cyclen. Conditions and reagents: (a) Benzylamine (1.1 eq),  $\text{K}_2\text{CO}_3$  (3 eq), MeCN, reflux, 24 h; (b) cat. 5% Pd/C,  $\text{H}_2$  (3 bar), EtOH, rt, 8 h, (c) propargyl bromide (80% in toluene, 1.1 eq)  $\text{K}_2\text{CO}_3$  (1.5 eq), MeCN, reflux, 8 h; (d)  $\text{Boc}_2\text{O}$  (3.5 eq) in 4 h,  $\text{Et}_3\text{N}$  (3.5 eq),  $\text{CHCl}_3$ , rt, 24 h; (e)  $\text{CuCl}_2$  (2 eq), EtOH, rt, 24 h.



**Scheme 2.** Synthesis of 1,8-naphthalimide conjugates **8a-c** and **10a-c**. Conditions and reagents: (a) NaH (1.5 eq), anhydrous DMF, rt, 30 min; then  $\text{Br}(\text{CH}_2)_n\text{Br}$  (4 eq), rt, 24 h; (b)  $\text{NaN}_3$  (2 eq), DMF, rt, 24 h; (c) propargyl-derivative (1 eq),  $\text{CuSO}_4 \cdot 5\text{H}_2\text{O}$  (0.1 eq), sodium ascorbate (0.2 eq), THF: $\text{H}_2\text{O}$  mixture (7:3, v/v), rt, 24 h; (d) TFA (50 eq),  $\text{CH}_2\text{Cl}_2$ , rt, 24 h.

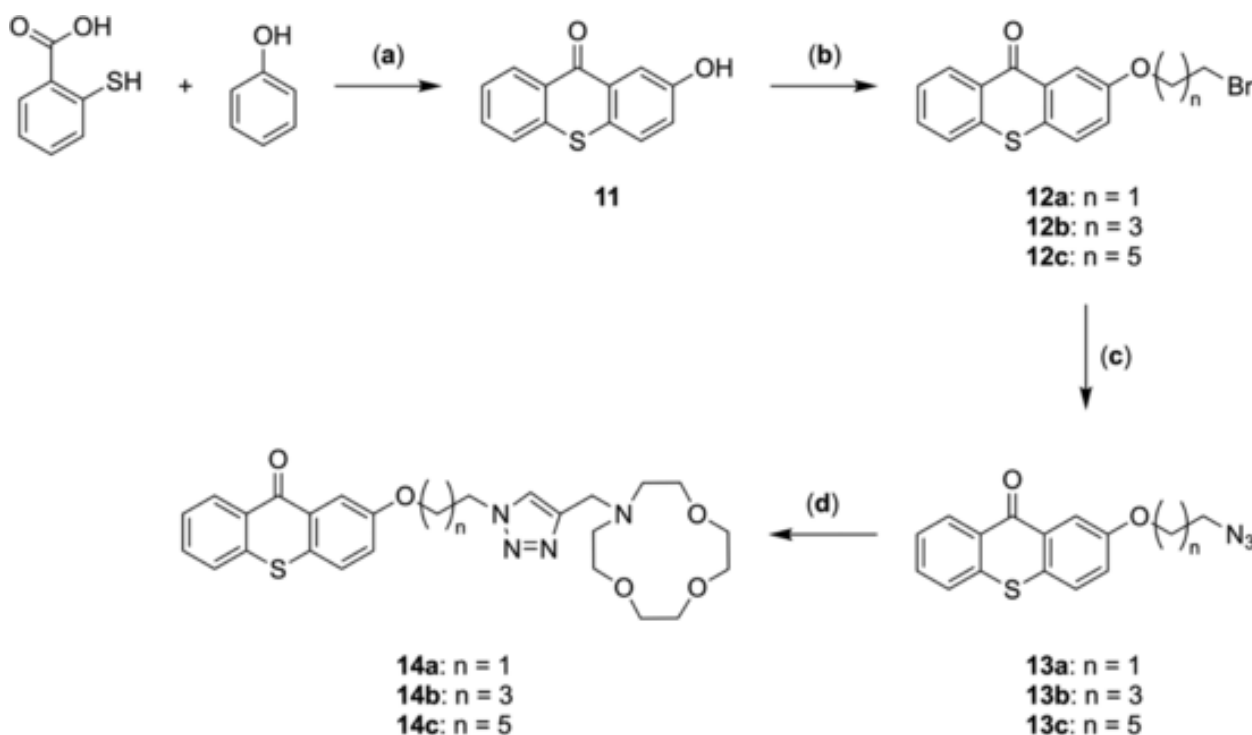
presence of a base to generate *O*-alkylated derivatives **12a-c**, with yields of 31–38%. Finally, the substitution of the terminal bromine with azide ions led to the synthesis of azide functionalized thiox-anthones **13a-c** with high yield of 90–96%.

The click chemistry reaction was performed by combining equimolar amounts of both substrates in a mixture of THF and water (7:3, v/v), along with copper salt ( $\text{CuSO}_4 \cdot 5\text{H}_2\text{O}$ ) and sodium ascorbate. To remove excess ascorbate and copper salts, the reaction mixture was divided between  $\text{CHCl}_3$  and saturated EDTA solution. This step was particularly important for conjugates containing cyclen (**13a-c**) because copper salts can form complexes with cyclen. The organic layer was isolated and washed with water to remove any remaining impurities. *N*-Boc deprotection of **13a-b** was achieved by stirring them with an excess of TFA in  $\text{CH}_2\text{Cl}_2$ . After completion of the reaction, excess TFA and solvent were removed under vacuum, and the resulting products were purified by aluminum gel column chromatography. By this method, we obtained three series of DLM conjugates for further analysis: (a) conjugates of 1,8-naphthalimide and 1-aza-12-crown-4, **8a-c**; (b) conjugates of 1,8-naphthalimide and cyclen, **10a-c**; and (c) conjugates of thioxanthone and 1-aza-12-crown-4, **14a-c**.

## 2.2. Photoluminescence

All compounds under investigation exhibit photoluminescent properties, as shown in Fig. 2. The 2D color-gradient graphs in Fig. 2a provide a detailed visualization of the photoluminescent activity of the compounds on a wavelength scale. The graphs depict the intensity of emission at various excitation light wavelengths, with a straight line visible in the upper left portion of each graph indicating the equality between excitation and emission wavelength (when the reflected light from the source is measured by the detector). Excitation and emission profiles representing the maximal photoluminescence intensity are displayed in Fig. 2b. Within each series, Fig. 2b focuses specifically on compounds **8a**, **10a**, and **14a** due to the similarity observed in their spectra. Compounds **8a-c** and **10a-c** are insensitive to external light with a wavelength  $>380$  nm and are most effectively excited with UV light at  $350 \pm 5$  nm. Compounds **14a-c** can be excited not only with UV light, but also with violet and dark-blue light in the range of 360–440 nm, with maximum excitation at  $410 \pm 5$  nm. All compounds exhibit a single emission maximum, occurring at about 390 nm for **8a-c** and **10a-c**, corresponding to violet color emission. For **14a-c**, the





**Scheme 3.** Synthesis of thioxanthone conjugates **14a–c**. Conditions and reagents: (a) Thioisalicic acid:phenol (1:3, n/n), conc.  $\text{H}_2\text{SO}_4$  (96%), 90 °C, 18 h; (b)  $\text{K}_2\text{CO}_3$  (2 eq),  $\text{Br}(\text{CH}_2)_n\text{Br}$  (4 eq), DMF, 90 °C, 24 h; (c)  $\text{NaN}_3$  (2 eq), DMF, rt, 24 h; (d) propargyl-derivative (1 eq),  $\text{CuSO}_4 \cdot 5\text{H}_2\text{O}$  (0.1 eq), sodium ascorbate (0.2 eq), THF-water mixture (7:3, v/v), rt, 24 h.

emission maximum is observed at about 480 nm, corresponding to blue-green color emission.

### 2.3. Cytotoxicity assay

One of the main objectives of this study was to evaluate the potential of newly synthesized DLM conjugates for cancer treatment by assessing their cytotoxicity on a panel of normal (Vero, LLC-MK2, NCTC 929, MRC-5) and cancer (HeLa, A549, HepG2) cell lines. The results, summarized in Table 1, showed significant differences in cytotoxic activity between the various series of conjugates. The graphs presented in Fig. 3 provide a visual representation of the data used to determine the  $\text{CC}_{50}$  values for each series of tested compounds.

The 1,8-naphthalimide-cyclen conjugates (**10a–c**) showed the lowest cytotoxicity of all the tested conjugates. The cytotoxicity of the conjugates with C2 and C4 linkers was similar, with none of them reaching  $\text{IC}_{50}$  values below 500  $\mu\text{M}$ , as shown in Fig. 3. However, derivative **10c**, with the longest C6 linker, showed significantly higher cytotoxicity ( $\text{CC}_{50}$  156.70–269.15  $\mu\text{M}$ ) against some normal cell lines (Vero, NCTC 929, MRC-5) and cancer cell lines (HeLa, HepG2), but without apparent selectivity against a specific panel. Interestingly, the parent compound cyclen also showed cytotoxicity against the same cell lines as **10c**, but at slightly higher levels ( $\text{CC}_{50}$  63.45–159.10  $\mu\text{M}$ ). However, when complexed with copper,  $\text{Cu}^{2+}$ -cyclen significantly reduced its cytotoxic activity against all tested cell lines ( $\text{CC}_{50} > 500 \mu\text{M}$ ).

In the case of the 1,8-naphthalimide-1A12C4 conjugates (**8a–c**), compound **8a** with the shortest C2 linker showed moderate cytotoxicity only against the non-cancerous Vero cell line ( $\text{CC}_{50} = 244.4 \mu\text{M}$ ), which was also the most sensitive cell line to all synthesized conjugates. On the other hand, compounds **8b** and **8c**, with longer C4 and C6 linkers, respectively, showed much higher but comparable activity against both normal cell lines ( $\text{CC}_{50}$  44.78–195.10  $\mu\text{M}$ ) and cancer cell lines ( $\text{CC}_{50}$  63.40–202.80  $\mu\text{M}$ ), without selectivity against a specific cell line. As for the 1,8-naphthalimide conjugates, there is a clear tendency for cytotoxicity to increase with increasing linker length (C6 > C4 > C2),

along with the lipophilicity of the macrocycle (1A12C4 > cyclen >  $\text{Cu}^{2+}$ -cyclen). This observation, along with the lack of selectivity towards a specific panel and cell line, suggests a similar mechanism of cellular uptake and cytotoxic activity among these conjugates.

As shown in Fig. 3, a similar trend of increased cytotoxicity with linker extension is observed in a series of thioxanthone-1A12C4 conjugates (**14a–c**). This series of conjugates showed several to tens of times higher cytotoxicity compared to the corresponding 1,8-naphthalimide conjugates (**8a–c**), both on normal cell lines (median  $\text{CC}_{50}$  14.49 vs 111.16  $\mu\text{M}$ ) and cancer cell lines (median  $\text{CC}_{50}$  17.73 vs 193.40  $\mu\text{M}$ ). As with the 1,8-naphthalimide series, the thioxanthone conjugates also lacked noticeable selectivity against cancer cells, making them non-selective agents. The most active compound in this series was **14c** with  $\text{CC}_{50}$  values in the range of 7.15–13.60  $\mu\text{M}$  against normal cell lines (Vero, LLC-MK2, NCTC, MRC-5) and  $\text{CC}_{50}$  values in the range of 1.36–10.50  $\mu\text{M}$  against cancer cell lines (HeLa, A549, HepG2).

### 2.4. Intracellular localization

As mentioned earlier, the cytotoxicity of the DLM conjugates appears to be related with their cellular uptake. To better understand the factors contributing to their cytotoxicity, we investigated their intracellular localization. In this study, A549 cells were treated with 10  $\mu\text{M}$  of the selected compounds, and their localization in the cells was examined based on their intrinsic fluorescence properties (Figs. 4 and 5). The results showed that none of the tested compounds localized within the cell nucleus. Moreover, cyclen conjugates **10a–c** (Fig. 5), and the parent compound **6c** (Fig. 4a) were not detected inside the cells at all. In contrast, 1A12C4 conjugates, **8a–c** and **14a–c**, were able to penetrate cells, although their distribution was mainly uniform in the cytoplasm (Fig. 4b). Interestingly, the compounds with the highest cytotoxicity, **14b–c**, also showed increased accumulation near the cell nucleus. The observation of different levels of cellular uptake provides a potential explanation for the higher cytotoxicity of 1A12C4 conjugates compared to cyclen conjugates.

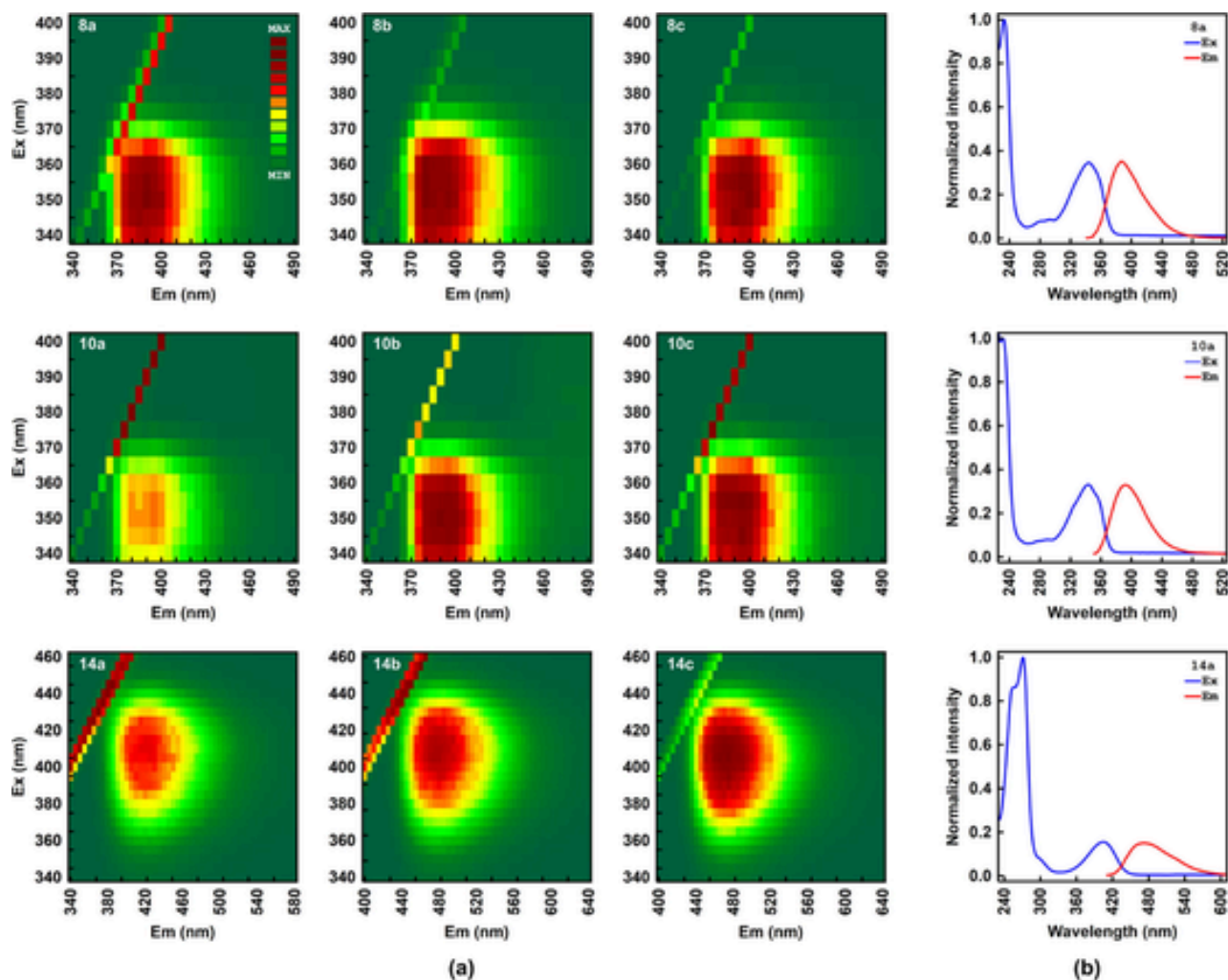


Fig. 2. Fluorescence excitation-emission matrices (a) and normalized excitation and fluorescence emission spectra (b) of studied conjugates. Location of the peak maxima: **8a–c** and **10a–c** (Ex. 350 nm/Em. 390 nm), and **14a–c** (Ex. 410 nm/Em. 480 nm).

Table 1

Cytotoxicity results of compounds at concentrations from 0.1 to 1000  $\mu\text{M}$  on Vero (Monkey African Green kidney), LLC-MK2 (Monkey Rhesus kidney), NCTC 929 (Mouse connective tissue), MRC-5 (Human foetal lung), HeLa (Human cervix epitheloid carcinoma), A549 (Human lung carcinoma) and HepG2 (Human hepatocyte carcinoma) cells.

Compound	Non-cancer cell lines				Cancer cell lines			
	Vero	LLC-MK2	NCTC 929	MRC-5	HeLa	A549	HepG2	
Cyclen	159.10 $\pm$ 5.55	>500	63.45 $\pm$ 3.56	>500	123.80 $\pm$ 4.62	>500	42.63 $\pm$ 1.17	
Cu <sup>2+</sup> -cyclen	>500	>500	>500	>500	>500	>500	>500	
10a	>500	>500	>500	>500	>500	>500	>500	
10b	>500	>500	>500	>500	>500	>500	>500	
10c	225.90 $\pm$ 10.76	>500	416.80 $\pm$ 18.49	162.90 $\pm$ 7.03	156.70 $\pm$ 5.76	>500	269.15 $\pm$ 19.61	
8a	244.40 $\pm$ 22.79	>500	>500	>500	>500	>500	>500	
8b	54.76 $\pm$ 7.90	120.22 $\pm$ 7.84	152.60 $\pm$ 23.40	195.10 $\pm$ 6.99	193.40 $\pm$ 9.95	202.80 $\pm$ 19.09	120.20 $\pm$ 10.70	
8c	47.88 $\pm$ 6.89	66.05 $\pm$ 5.28	69.71 $\pm$ 8.62	69.16 $\pm$ 5.52	63.40 $\pm$ 3.00	121.50 $\pm$ 7.58	71.51 $\pm$ 10.22	
14a	83.17 $\pm$ 7.30	162.00 $\pm$ 9.06	120.00 $\pm$ 10.55	72.76 $\pm$ 2.77	126.90 $\pm$ 5.07	179.50 $\pm$ 9.25	91.00 $\pm$ 10.65	
14b	15.38 $\pm$ 1.82	11.03 $\pm$ 0.78	6.91 $\pm$ 0.76	19.19 $\pm$ 0.65	11.76 $\pm$ 0.44	17.73 $\pm$ 1.18	42.73 $\pm$ 3.58	
14c	10.36 $\pm$ 1.35	7.15 $\pm$ 0.47	8.09 $\pm$ 0.91	13.60 $\pm$ 0.80	1.36 $\pm$ 0.03	7.07 $\pm$ 0.49	10.50 $\pm$ 0.86	

## 2.5. Interaction with DNA

1,8-Naphthalimide and thioxanthone derivatives are well-known for their strong intercalation properties, which play a key role in their biological activity [14,35]. These compounds interfere with DNA processing enzymes, resulting in DNA damage and cell death [36,37]. It is worth noting that modifications to the structure of an intercalator can

significantly influence its binding to DNA. Previous studies have demonstrated that conjugating fluorescent dyes with linear polyamines enhances their binding to DNA and facilitates accumulation in the cell nucleus [19,20,38]. However, in our study of cell internalization, we observed that none of the tested compounds tended to localize to the cell nucleus, despite their known intercalation properties. This observation prompted us to investigate the compounds' interaction with DNA

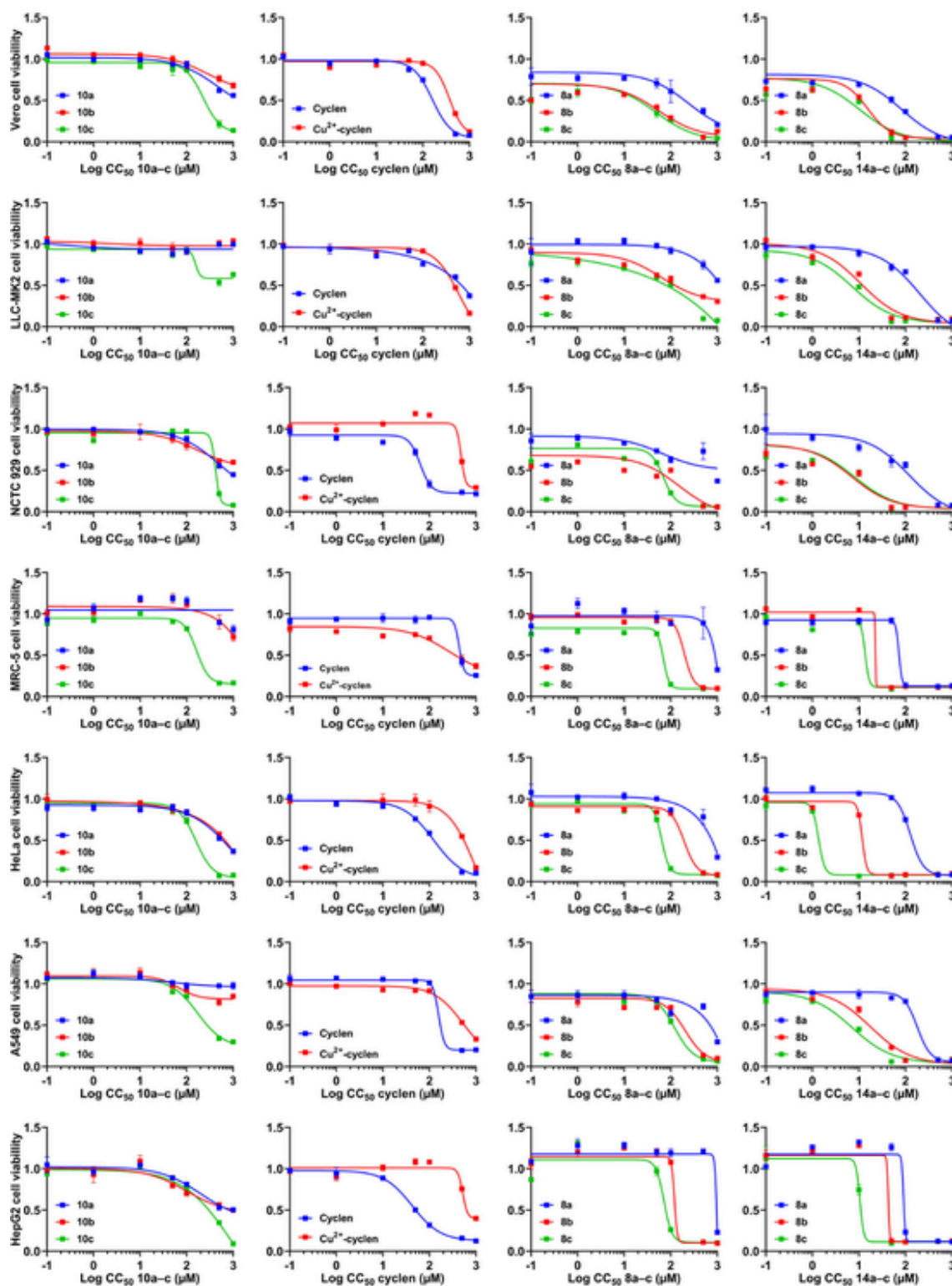
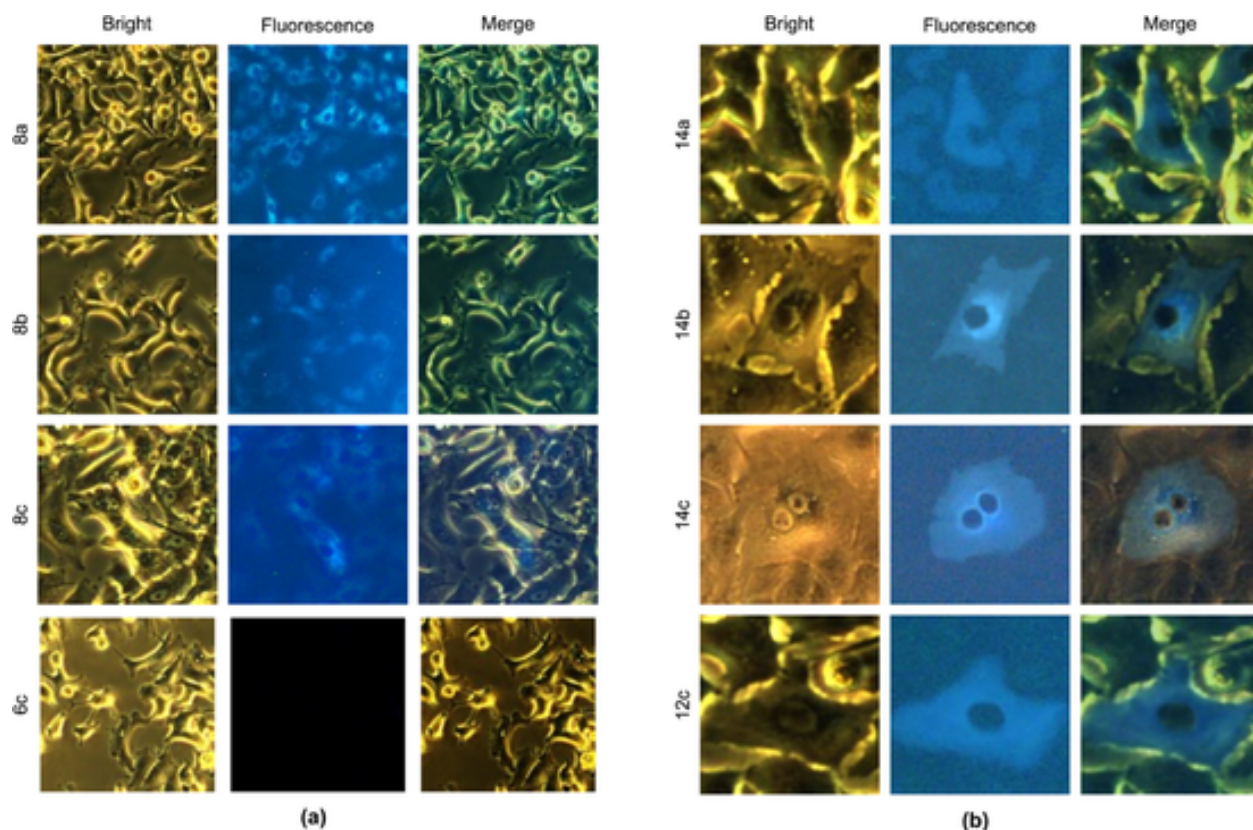


Fig. 3. Log  $CC_{50}$  values against the Vero, LLC-MK2, NCTC 929, MRC-5, HeLa, A549 and HepG2 cells. To enhance clarity, the data point representing the control sample, with a fixed concentration of 0.01  $\mu\text{M}$  and a cell viability of 1 in each case, has been omitted from the graphs.

using three gold standards methods: (1) measuring the melting temperature ( $T_m$ ) of DNA, (2) examining circular dichroism (CD) spectra, and (3) evaluating DNA viscosity. For this study, we selected 1A12C4 conjugates, **8a-c** and **14a-c**, due to their significant cytotoxicity and ability to effectively penetrate the cell.

## 2.6. Test compounds have no effect on $T_m$ of CT-DNA

As the sample temperature increases, the DNA double helix gradually unwinds, causing the base pairs to separate, and this leads to an increase in absorbance at 260 nm. The temperature at which half of the DNA is melted is  $T_m$ . When small molecule ligands are added and interact with DNA, they can either stabilize or destabilize the double helix,



**Fig. 4.** Example photomicrographs of A549 cells incubated with: (a) **8a–c** and **6c**, (b) **14a–c** and **12c** at 10  $\mu\text{M}$  after 2 h of incubation time. The left panel shows bright field images, middle panel shows fluorescence, and right panel shows merged images of all channels on the same cells. Cells were analyzed with an inverted fluorescence microscope at 150 $\times$  magnification.

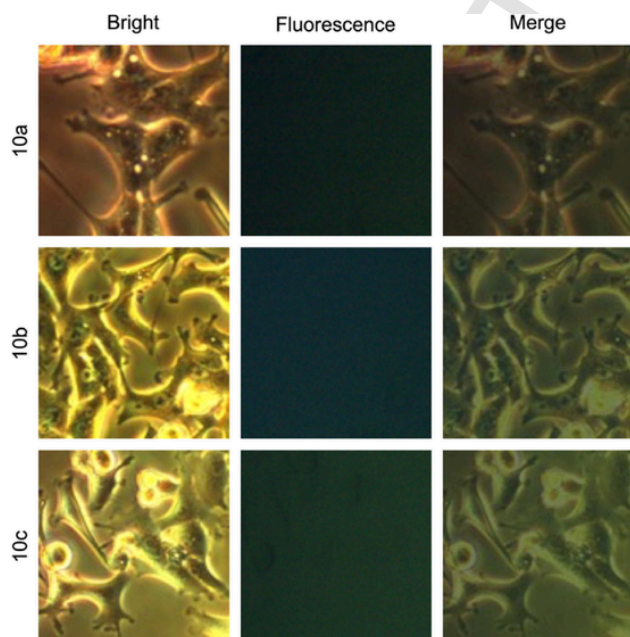


**Fig. 5.** Example photomicrographs of A549 cells incubated with **10a–c** at 10  $\mu\text{M}$  after 2 h of incubation time. The left panel shows bright field images, middle panel shows fluorescence, and right panel shows merged images of all channels on the same cells. Cells were analyzed with an inverted fluorescence microscope at 150 magnification.

resulting in changes to  $T_m$ . Intercalators typically increase  $T_m$  by stabilizing the double helix structure, which makes it harder for the DNA strands to separate, requiring a higher temperature for melting [14].

To investigate the interaction between the studied compounds and double-stranded DNA, we measured the melting temperature of calf thymus DNA (CT-DNA) in the presence or absence of each compound. We found that the  $T_m$  values obtained in the presence of 1,8-naphthalimides **8a–c** (Fig. 6a) and thioxanthenes **14a–c** (Fig. 6b) were not significantly different ( $<1.0$   $^{\circ}\text{C}$ ) from the  $T_m$  of the control CT-DNA (75.33  $^{\circ}\text{C}$ ). These results indicate that the tested compounds do not affect the thermal stability of CT-DNA and suggest that either they do not intercalate into DNA, or if they do, the interaction may not be strong enough to cause a significant stabilization of the double helix structure. It should be noted, however, that the lack of  $T_m$  shift does not exclude the possibility of other types of interactions between compounds and CT-DNA, such as groove binding or electrostatic interactions, which do not affect the  $T_m$  of DNA.

#### 2.7. Test compounds do not disrupt CT-DNA conformation

CD spectroscopy is a highly effective technique for monitoring conformational changes in dsDNA resulting from complex formation. This is due to the sensitivity of the positive band at 275 nm and the negative band at 248 nm to interactions between dsDNA and small molecules, which indicate base stacking and right-handed helicity, respectively. The groove binding mode and electrostatic interactions between small molecules and dsDNA generally do not perturb these bands significantly, while the intercalation mode increases the intensity of both bands by stabilizing the right-handed B conformation of CT-DNA. This has been observed with classical intercalators such as methylene blue [39].

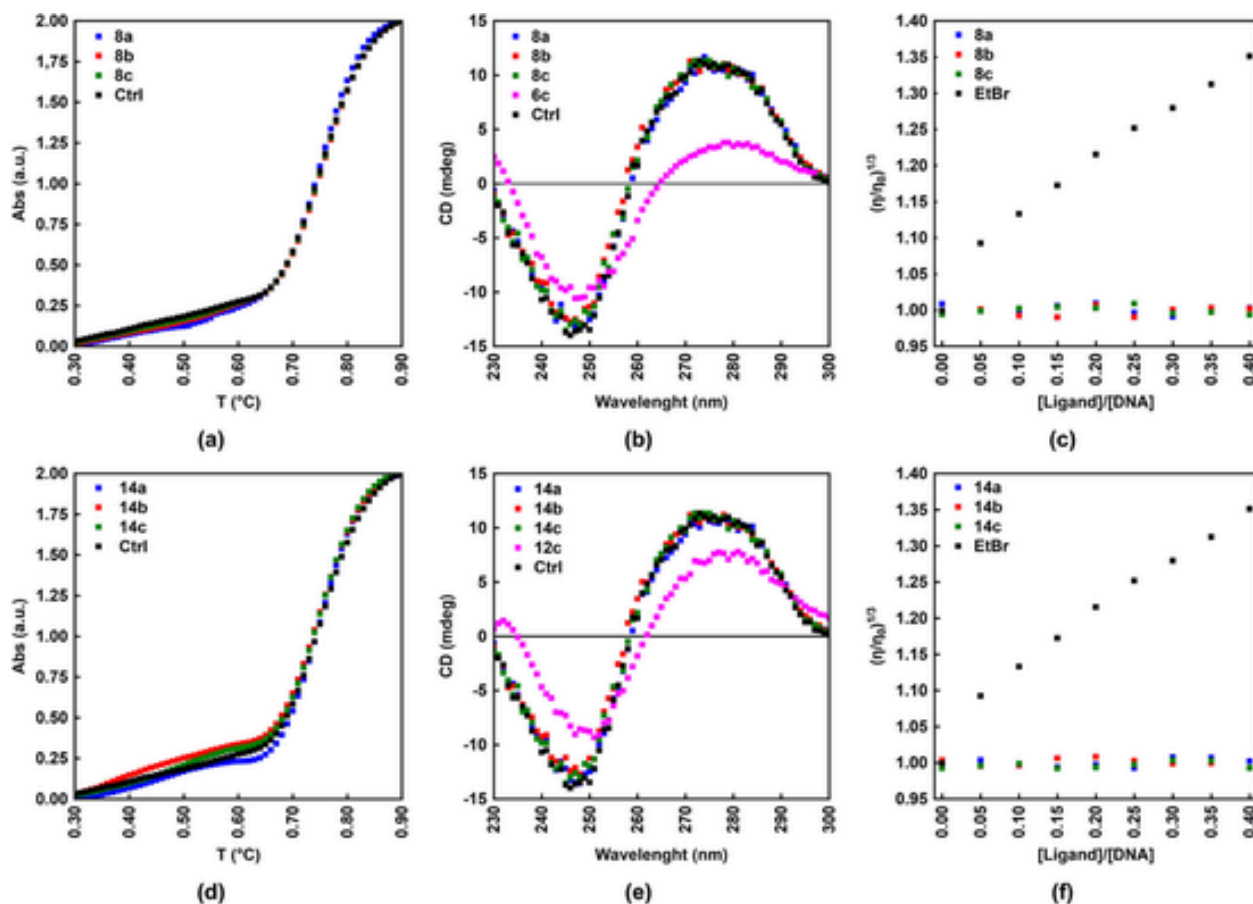


**Fig. 6.** UV melting curves of CT-DNA (20  $\mu$ M) (a) **8a–c** and (b) **14a–c** in 20 mM cacodylate buffer, pH 7.0; [ligand]/[DNA] = 0.30. CD spectra of CT-DNA (200  $\mu$ M) in the absence and presence of (c) **8a–c** and **6c**, and (d) **14a–c** and **12c** in 5 mM Tris–HCl, 50 mM NaCl, pH 7.0 at 25  $^{\circ}$ C; [ligand]/[DNA] = 0.30. Effect of increasing amounts of (e) **8a–c**, (f) **14a–c** and EtBr on the relative viscosity of CT-DNA (200  $\mu$ M) in 5 mM Tris–HCl, 50 mM NaCl, pH 7.0 at 25  $^{\circ}$ C; [ligand]/[DNA] = 0, 0.05, 0.10, 0.15, 0.20, 0.25, 0.30, 0.35, 0.40. All values reported are mean of three independent experiments.

Treatment of CT-DNA with parent compound **6c** (Scheme 2) led to a reduction in the negative band at 247 nm and an even more significant decrease in the positive band at 275 nm in the CD spectrum (Fig. 6c). Additionally, a bathochromic shift of the negative band to around 250 nm was observed with the addition of **6c**. Similar changes were observed in the CD spectrum when the parent compound **12c** was added to the CT-DNA (Fig. 6d), although the positive band was reduced to a slightly lesser extent. These findings indicate that both **6c** and **12c** have the ability to intercalate into dsDNA and cause its unwinding, leading to a reduction in helicity. The greater reduction in CD bands induced by **6c** suggests that it binds more strongly to dsDNA than **12c** and is therefore more effective at disturbing the secondary structure of DNA at the same concentration. In contrast, treatment of CT-DNA with **8a–c** (Fig. 6c) and **14a–c** (Fig. 6d) did not cause any significant changes in the CD spectrum, suggesting that these compounds do not intercalate into dsDNA.

## 2.8. Test compounds have no effect on CT-DNA length

Viscosity measurement is another method for studying how the ligand-DNA complex interacts. In the case of the intercalation binding mode, the DNA helix length increases due to the separation of base pairs, resulting in increased DNA viscosity. On the other hand, if the ligand interacts with DNA via electrostatic or groove binding mode, the viscosity of the DNA solution does not change significantly.

Fig. 6e–f shows that as the amount of ethidium bromide (EtBr) added to the CT-DNA solution increases, the viscosity of the solution also increases due to intercalation of EtBr into CT-DNA [40]. In con-

trast, the addition of **8a–c** (Fig. 6e) and **14a–c** (Fig. 6f) to the CT-DNA solution does not cause any change in viscosity, indicating that the functionalization of 1,8-naphthalimide and thioxanthone with 1A12C4 reduces their ability to intercalate into DNA.

## 2.9. Photodynamic effect

The presence of a fluorophore in the tested compounds suggests that they may exhibit distinct biological properties when cells are exposed to light of an appropriate wavelength. Both thioxanthone [18] and 1,8-naphthalimide [41,42] derivatives are known photosensitizers and have been investigated for their potential use in photodynamic therapy. To explore this possibility, we compared the cytotoxicity of these compounds against A549 cells under non-irradiated and irradiated conditions. The study showed that only thioxanthone conjugates, **14a–c**, showed a significant increase in cytotoxicity after irradiating the cells (Fig. 7). As shown in Table 2, the  $IC_{50}$  values for irradiated cells were 37–56% lower compared to non-irradiated cells. In contrast, the other compounds did not show comparable effects.

In addition, we examined genotoxic properties in the absence of light and in cells subjected to irradiation. The study showed that only the thioxanthone derivatives exhibited genotoxic properties, with the highest level of damage observed in cells treated with compound **14c**. Both single-stranded (SSBs) and double-stranded DNA breaks (DSBs) were observed in nuclear DNA. Irradiating the cells also had a significant effect on the amount of DNA damage that occurred, with 20–40% more damage observed in irradiated cells compared to cells incubated without light. However, an intracellular localization assay showed that

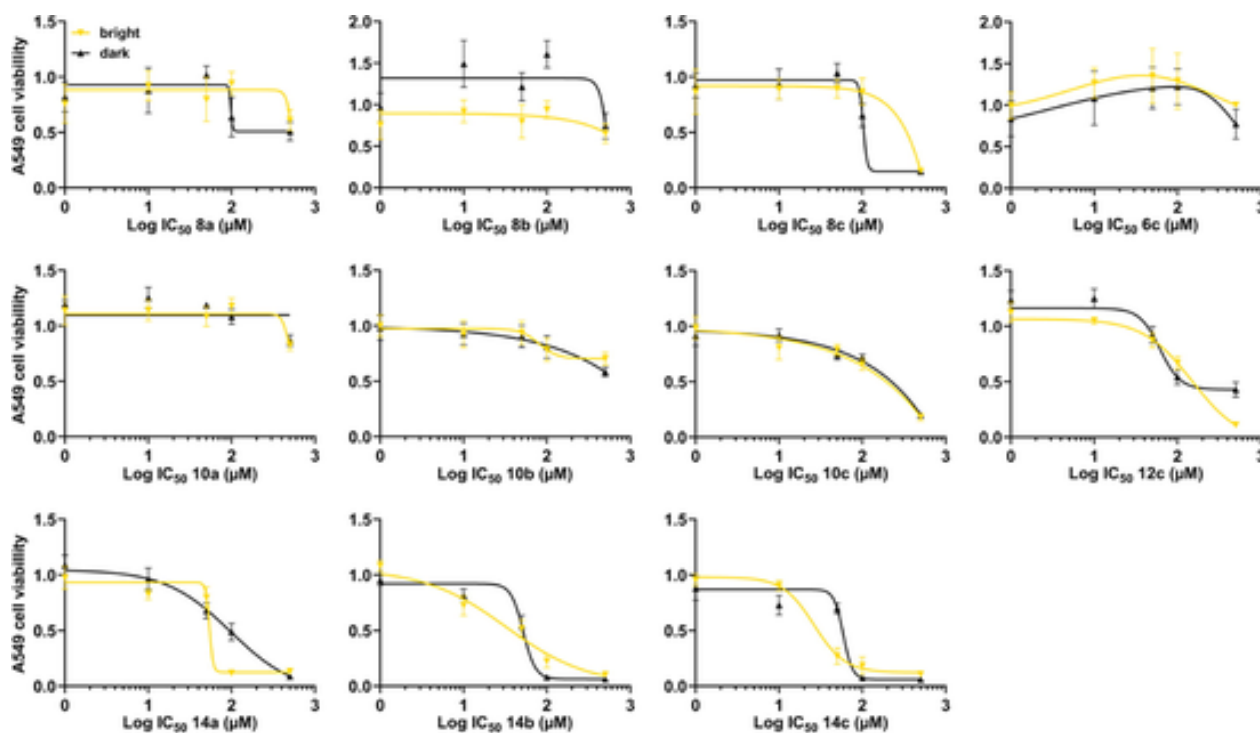


Fig. 7. Log  $IC_{50}$  values against the A547 cell line under dark (black  $\blacktriangle$ ) and bright (yellow  $\blacktriangledown$ ) conditions. To enhance clarity, the data point representing the control sample, with a fixed concentration of 0.1  $\mu\text{M}$  and a cell viability of 1.0 in each case, has been omitted from the graphs. (For interpretation of the references to color in this figure legend, the reader is referred to the web version of this article.)

Table 2  
Cytotoxicity and fast halo assay results on A549 cells under dark and bright conditions.

Compound	Cytotoxicity ( $IC_{50}$ $\mu\text{M}$ )		DNA damage in cells (NDF)					
	Dark	Bright	Dark			Bright		
			DSBs	SSBs	Total	DSBs	SSBs	Total
10a	>500	>500						
10b	>500	>500						
10c	200.54 $\pm$ 11.66	175.99 $\pm$ 13.76						
8a	>500	>500	1.30 $\pm$ 0.09	0.32 $\pm$ 0.13	1.62 $\pm$ 0.10	1.24 $\pm$ 0.07	0.48 $\pm$ 0.12	1.72 $\pm$ 0.10
8b	>500	>500	1.20 $\pm$ 0.02	0.19 $\pm$ 0.02	1.40 $\pm$ 0.02	1.29 $\pm$ 0.09	0.25 $\pm$ 0.12	1.54 $\pm$ 0.09
8c	102.55 $\pm$ 9.83	301.98 $\pm$ 33.97	1.54 $\pm$ 0.09	0.01 $\pm$ 0.12	1.55 $\pm$ 0.10	1.39 $\pm$ 0.11	0.14 $\pm$ 0.11	1.53 $\pm$ 0.11
6c	>500	>500	1.10 $\pm$ 0.01	0.10 $\pm$ 0.01	1.20 $\pm$ 0.01	1.10 $\pm$ 0.02	0.01 $\pm$ 0.04	1.11 $\pm$ 0.03
Ctrl			1.00 $\pm$ 0.01	0.10 $\pm$ 0.06	1.10 $\pm$ 0.06	1.02 $\pm$ 0.01	0.08 $\pm$ 0.05	1.10 $\pm$ 0.02
14a	96.66 $\pm$ 6.96	54.24 $\pm$ 4.48	2.48 $\pm$ 0.13	2.50 $\pm$ 0.14	4.98 $\pm$ 0.07	2.95 $\pm$ 0.06	3.02 $\pm$ 0.10	5.98 $\pm$ 0.08
14b	51.91 $\pm$ 4.06	32.68 $\pm$ 2.84	2.52 $\pm$ 0.07	1.43 $\pm$ 0.07	3.95 $\pm$ 0.03	2.93 $\pm$ 0.04	2.58 $\pm$ 0.07	5.51 $\pm$ 0.06
14c	59.05 $\pm$ 6.10	26.26 $\pm$ 1.39	3.52 $\pm$ 0.06	2.40 $\pm$ 0.07	5.92 $\pm$ 0.04	4.51 $\pm$ 0.10	3.46 $\pm$ 0.11	7.97 $\pm$ 0.06
12c	61.50 $\pm$ 6.81	149.70 $\pm$ 9.87	1.52 $\pm$ 0.12	1.41 $\pm$ 0.12	2.94 $\pm$ 0.02	1.51 $\pm$ 0.03	2.01 $\pm$ 0.10	3.52 $\pm$ 0.10
Ctrl			1.15 $\pm$ 0.06	0.13 $\pm$ 0.10	1.02 $\pm$ 0.09	1.15 $\pm$ 0.06	0.03 $\pm$ 0.01	1.19 $\pm$ 0.06

The cells were incubated in the dark for 2 h with compounds, followed by irradiation with a benchtop LED reactor with an appropriate wavelength and an energy density of 20 J/cm<sup>2</sup>. The wavelength used for compounds 6c, 8a–c and 10a–c was 340 nm, while for compounds 12c, 14a–c, it was 400 nm. The cells were then further incubated in the dark for 46 h. The data are expressed as the mean value  $\pm$  SD from three independent experiments.

none of the compounds tested penetrated into the cell nucleus. It can therefore be hypothesized that the observed damage is not directly due to interaction with DNA, but rather as an effect of ROS.

Both groups of tested compounds can generate ROS through two mechanisms used in the type-I and the type-II photodynamic therapy (PDT). In the first case, electron or hydrogen atom transfer occurs between the excited photosensitizer and an adjacent substrate, resulting in the generation of reactive radical ions that consequently damage biomolecules. Type II PDT is based on the generation of singlet oxygen ( $^1O_2$ ) as a result of energy transfer from the excited photosensitizer to molecular oxygen in the ground state. [43,44].

### 3. Conclusions

The present study aimed to investigate the structure–activity relationship of the tested conjugates, providing valuable insights into their biological activity. Through a comparative analysis, several important conclusions can be drawn regarding the cytotoxicity and behavior of each series of conjugates:

- 1A12C4 conjugates, 8b–c and 14a–c, exhibited the highest cytotoxicity against both normal (Vero, LLC-MK2, NCTC 929, MRC-5) and cancer (HeLa, A549, HepG2) cell lines. Both series of 1A12C4 conjugates showed significantly higher cytotoxicity and cell permeability compared to cyclen conjugates, 10a–c,

which showed minimal biological activity and were unable to penetrate the cells.

2. Thioxanthone conjugates, **14a–c**, exhibited significantly higher cytotoxicity than 1,8-naphthalimide conjugates, **8a–c** and **10a–c**, against all tested cell lines.
3. The cytotoxicity of the tested conjugates showed a positive correlation with increasing linker length (C2 > C4 > C6) against all tested cell lines. Moreover, none of the investigated conjugates showed any specificity towards a particular panel or cell line.
4. 1A12C4 conjugates, **8a–c** and **14a–c**, did not bind or intercalate to DNA, unlike their parent compounds, **6c** and **12c**, respectively. The absence of interaction with DNA was also reflected in their lack of localization in the cell nucleus.
5. Thioxanthone conjugates, **14a–c**, induced significant damage to cellular DNA under light conditions, while 1,8-naphthalimide conjugates, **8a–c**, did not cause such damage. The observed increase in non-specific DNA damage suggests that it may be triggered by ROS production.

The structure–activity relationship analysis of DLM conjugates revealed a positive correlation between their lipophilicity, cellular uptake and cytotoxicity. Additionally, the observed lack of cellular selectivity indicates that their biological activity may primarily involve simple diffusion across cell membranes. Increasing the length of the linker (C6 > C4 > C2) and replacing the protonable cyclen moiety (clog P = -0.85) with the neutral and more lipophilic 1A12C4 moiety (clog P = 0.11) led to a significant increase in their cell permeability and cytotoxicity. Our findings align with previous literature reports, demonstrating that conjugation with lipids is an effective strategy for enhancing cell permeability and bioactivity of compounds not involved in active transport. For example, Tan et al. showed that incorporating a pendant *n*-octyl chain into 1,8-naphthalimide-cyclam conjugates significantly increased their cytotoxicity compared to derivatives with shorter alkyl chains [37]. Similarly, Morstein et al. conjugated fluorescein, which has low intrinsic cell permeability, with medium or long saturated lipid chains (C10–C18), resulting in a > 100-fold increase in cellular fluorescence. In this context, our study demonstrated that aza-crown ethers can serve as versatile vehicles to enhance cellular transport and activity of small molecule compounds.

The cytotoxicity of the conjugates was found to be highly dependent on the type of fluorescent dye used. Conjugates based on 1,8-naphthalimide showed low cytotoxicity, while those based on thioxanthone exhibited high cytotoxicity. In our recent studies, we observed a significant increase in DNA stability upon attaching 1,8-naphthalimide and thioxanthone units to oligonucleotides. In this study, we demonstrated that conjugating fluorescent dyes with aza-crown ether limited their interaction with DNA. None of the 1A12C4 conjugates intercalated into DNA or localized within the cell nucleus. These findings are consistent with several other studies indicating that the conjugation of intercalators with crown ethers resulted in the destabilization of the tertiary ligand-DNA complex [45–47]. Therefore, the cytotoxicity of the examined conjugates likely does not arise from their interaction with DNA.

By carefully selecting individual components, we successfully manipulated the biological activity of DLM conjugates. The choice of a specific macrocycle moiety allowed us to control cellular internalization, while the selection of the dye moiety contributed to the cytotoxic activity of the conjugates. For instance, 1,8-naphthalimide conjugates containing the 1A12C4 moiety and a short linker, particularly **8a** (CC<sub>50</sub> > 500 μM), exhibited minimal cytotoxicity and did not induce genotoxic damage in cells, making them potential candidates for molecular probes. 1,8-Naphthalimide conjugates containing cyclen, **10a–b**, not only exhibited negligible cytotoxicity (CC<sub>50</sub> > 500 μM) but also showed limited cellular internalization, making them promising molecular probes for extracellular applications. In contrast, conjugates bear-

ing the thioxanthone moiety and longer linkers exhibited strong cytotoxicity, as demonstrated by **14c** (CC<sub>50</sub> = 1.49–24.91 μM), which also induced significant genotoxic damage upon light irradiation. These conjugates show promising applications as theranostatic drugs, particularly in photodynamic therapy. Further studies are needed to elucidate the structural features of DLM conjugates that may affect their intracellular localization and enhance selectivity against cancer cells.

## 4. Experimental

### 4.1. Chemical synthesis

All reagents and solvents were obtained from commercial sources and used without further purification. Reactions were monitored by TLC analysis using silica gel 60 F254 plates (Merc, Darmstadt, Germany). Column chromatography was performed on silica gel 60 (Merc, Darmstadt, Germany). <sup>1</sup>H and <sup>13</sup>C NMR spectra were performed on a Varian NMR system 600 spectrometer (Agilent Technologies, Santa Clara, CA, USA) at 600 and 151 MHz, respectively; 400 and 101 MHz spectra were performed on a Bruker AM-400 spectrometer (Bruker-BioSpin Corp., Coventry, UK). Peak multiplicity is expressed as follows: s = singlet, d = doublet, t = triplet, dd = doublet of doublets. NMR chemical shifts are given in ppm (δ), relative to residual non-deuterated solvents as internal standard, coupling constants (*J*) are given in Hz. Melting points (mp) were determined using a Boethius PHMK apparatus (Franz Küstner, Dresden, Germany) and were not corrected. High resolution electrospray ionization mass spectroscopy (ESI-HRMS) analyses were performed using a Waters Xevo G2 Q-TOF apparatus (Waters-Micromass, Manchester, UK).

#### 4.1.1. Synthesis of compound 3

A stirred solution of 1,11-diiodo-3,6,9-trioxaundecane (10.0 g, 24.2 mmol) and ben-zylamine (2.85 g, 26.6 mmol) in dry MeCN (400 mL) containing powdered anhydrous Na<sub>2</sub>CO<sub>3</sub> (10.0 g, 72.4 mmol) was refluxed under Ar for 24 h. After cooling to rt, the mixture was decanted and filtered to remove the solid. The filtrate was concentrated under vacuum using a rotary evaporator. The resulting oily residue was partitioned between water (300 mL) and Et<sub>2</sub>O (150 mL). The aqueous layer was extracted twice with Et<sub>2</sub>O (2 × 150 mL). The combined organic layers were washed with brine (100 mL) and dried over Na<sub>2</sub>SO<sub>4</sub>. After evaporating Et<sub>2</sub>O, the residue was distilled through a short path, collecting the volatile material at a pressure of 0.05 mmHg and a boiling point of 135–140 °C (lit. [33] bp 140–143 °C). The resulting distillate was further used without characterization or purification. The distillate (3.82 g) was dissolved in anhydrous EtOH (50 mL), and a catalytic amount of 5% Pd/C (500 mg) was added to the reaction vessel. The mixture was then placed in a Parr apparatus and shaken with hydrogen at a pressure of about 3.0 bar at rt for 8 h. After completion of the reaction, the catalyst was removed by filtering the reaction mixture through a tissue paper filter. The filtrate was then concentrated under vacuum using a rotary evaporator and further used without characterization or purification. Next, the oily residue of 1-aza-12-crown-4 (3.20 g, 18.3 mmol) was dissolved in MeCN (100 mL) and reacted with propargyl bromide (80% in toluene; 1.80 mL, 20.1 mmol) in the presence of K<sub>2</sub>CO<sub>3</sub> (3.79 g, 27.4 mmol) under reflux for 8 h. Completion of the reaction was indicated by silica gel TLC using 10% MeOH-AcOEt as the eluent. The mixture was then evaporated and purified by silica gel column chromatography using 10% MeOH-AcOEt as the eluent. After evaporation of the product fraction, compound **3** was obtained in 89% yield, based on 1-aza-12-crown-4.

#### 4.1.2. 10-(prop-2-yn-1-yl)-1,4,7-trioxa-10-azacyclododecane (**3**)

Yield: 89%; yellow, hygroscopic oil; <sup>1</sup>H NMR (600 MHz, CD<sub>3</sub>OD) δ 3.67–3.62 (m, 12H), 3.42 (d, *J* = 2.4 Hz, 2H), 2.78–2.76 (m, 4H), 2.54 (t, *J* = 2.4 Hz, 1H); <sup>13</sup>C NMR (151 MHz, CD<sub>3</sub>OD) δ 78.45, 72.55, 70.37,

69.93, 68.93, 53.41, 43.93. HRMS (ESI-TOF):  $m/z$  calc. for  $C_{11}H_{20}NO_3$  [M+H]<sup>+</sup> 214.1443, found: 214.1475.

#### 4.1.3. Synthesis of compound 4

A solution of cyclen (2.20 g, 12.8 mmol) and triethylamine (6.2 mL, 44.8 mmol) in  $CHCl_3$  (100 mL) was stirred at rt. Di-*tert*-butyl dicarbonate (22.4 mL, 44.8 mmol) was added dropwise to the stirred solution over 4 h. The reaction mixture was stirred for an additional 24 h at rt, and the completion of the reaction was indicated by TLC using 25% AcOEt/hexane as the eluent and staining the plate with ninhydrin solution. The solvent was then evaporated under vacuum using a rotary evaporator, and the remaining residue was purified by silica gel column chromatography using 25% AcOEt/hexane as the eluent. The product fraction was collected and evaporated to yield compound 4 as a colorless oil.

#### 4.1.4. Tri-*tert*-butyl 1,4,7,10-tetraazacyclododecane-1,4,7-tricarboxylate (4)

Yield: 95%; colorless oil; m.p. 65–67 °C; HRMS (ESI-TOF):  $m/z$  calc. for  $C_{23}H_{45}N_4O_6$  [M+H]<sup>+</sup> 473.3339, found: 473.1952.

#### 4.1.5. Synthesis of compound 5

To a stirred solution of compound 4 (1.95 g, 4.13 mmol) in MeCN (50 mL),  $K_2CO_3$  (1.14 g, 8.25 mmol) and propargyl bromide (80% in toluene; 552  $\mu$ L, 4.95 mmol) were added. The mixture was heated under reflux for 16 h. The reaction completion was confirmed by TLC using 50% AcOEt-hexane as the eluent, and the plate was stained with ninhydrin solution. The insoluble residues were removed by filtration, and the solvent was removed under vacuum using a rotary evaporator. The resulting oily residue was purified by silica gel column chromatography using 50% AcOEt-hexane as the eluent. The product fraction was combined and evaporated, and compound 5 was obtained as a white foam in 73% yield.

#### 4.1.6. Tri-*tert*-butyl 10-(prop-2-yn-1-yl)-1,4,7,10-tetraazacyclododecane-1,4,7-tricarboxylate (5)

Yield: 73%; white foam; m.p. 126–128 °C; HRMS (ESI-TOF):  $m/z$  calc. for  $C_{26}H_{47}N_4O_6$  [M+H]<sup>+</sup> 511.3496, found: 511.3488.

#### 4.1.7. Synthesis of compounds 6a–c

A solution of 1,8-naphthalimide (2.0 mmol) in 10 mL of dry DMF was cooled in an ice bath. Then, NaH (80% dispersion in mineral oil; 3.0 mmol) was added slowly in small portions. The mixture was left in the ice bath for 30 min, and after hydrogen evolution stopped, an appropriate dibromoalkane (8.0 mmol) was added in one portion. The mixture was stirred at rt for 24 h. The completion of the reaction was confirmed by silica gel TLC using  $CHCl_3$  as the eluent. The reaction mixture was poured into about 50 mL of 5% HCl, and the resulting precipitate was filtered. The precipitate was washed with water until neutral pH was achieved, and then left to dry. The crude product of 6a and 6b was purified by silica gel column chromatography using  $CHCl_3$  as the eluent, and 6c was purified using DCM.

#### 4.1.8. 2-(2-Bromoethyl)-1H-benzo[de]isoquinoline-1,3(2H)-dione (6a)

Yield: 75%; white solid; m.p. 215–216 °C; <sup>1</sup>H NMR (600 MHz,  $CDCl_3$ )  $\delta$  8.62 (dd,  $J$  = 7.2, 1.2 Hz, 2H), 8.23 (dd,  $J$  = 8.3, 1.2 Hz, 2H), 7.77 (dd,  $J$  = 8.2, 7.2 Hz, 2H), 4.62 (t,  $J$  = 7.2 Hz, 2H), 3.68 (t,  $J$  = 7.2 Hz, 2H); <sup>1</sup>H NMR (151 MHz,  $CDCl_3$ )  $\delta$  163.98, 134.27, 131.65, 131.55, 128.24, 127.02, 122.34, 41.24, 41.21, 41.19, 27.78.

#### 4.1.9. 2-(4-Bromobutyl)-1H-benzo[de]isoquinoline-1,3(2H)-dione (6b)

Yield: 85%; white solid; m.p. 114–115 °C; <sup>1</sup>H NMR (600 MHz,  $CDCl_3$ )  $\delta$  8.59 (dd,  $J$  = 7.2, 1.1 Hz, 2H), 8.20 (dd,  $J$  = 8.4, 1.1 Hz, 2H), 7.74 (dd,  $J$  = 8.2, 7.2 Hz, 2H), 4.24–4.22 (m, 2H), 3.49–3.47 (m, 2H), 2.01–1.98 (m, 2H), 1.93–1.91 (m, 2H); <sup>13</sup>C NMR (151 MHz,  $CDCl_3$ )  $\delta$

164.17, 133.97, 131.57, 131.27, 128.14, 126.93, 122.57, 39.34, 33.14, 30.25, 26.89.

#### 4.1.10. 2-(6-Bromohexyl)-1H-benzo[de]isoquinoline-1,3(2H)-dione (6c)

Yield: 80%; white solid; m.p. 92–93 °C; <sup>1</sup>H NMR (600 MHz,  $CDCl_3$ )  $\delta$  8.59 (dd,  $J$  = 7.2, 1.2 Hz, 2H), 8.20 (dd,  $J$  = 8.4, 1.2 Hz, 2H), 7.75 (dd,  $J$  = 8.2, 7.2 Hz, 2H), 4.20–4.16 (m, 2H), 3.41 (t,  $J$  = 6.8 Hz, 2H), 1.93–1.85 (m, 2H), 1.81–1.71 (m, 2H), 1.57–1.43 (m, 4H); <sup>13</sup>C NMR (151 MHz,  $CDCl_3$ )  $\delta$  164.17, 133.86, 131.58, 131.18, 128.14, 126.92, 122.70, 40.24, 33.80, 32.69, 27.91, 27.89, 26.28.

#### 4.1.11. Synthesis of compounds 7a–c

A solution of the starting substrate (1.00 mmol) in 10 mL of DMF was treated with  $NaN_3$  (2.0 mmol) and stirred at rt for 24 h. The completion of the reaction was confirmed by TLC using  $CHCl_3$  as the eluent and staining the plate with ninhydrin solution. The azido derivatives were visible more than the bromo derivatives under ninhydrin staining, resulting in brown-colored spots. The reaction mixture was extracted with water (100 mL) and  $CHCl_3$  (50 mL), and the organic layer was dried over  $Na_2SO_4$ . After evaporation of the solvent, the crude product was purified by silica gel column chromatography using  $CHCl_3$  as the eluent.

#### 4.1.12. 2-(2-Azidoethyl)-1H-benzo[de]isoquinoline-1,3(2H)-dione (7a)

Yield: 88%; white solid; m.p. 174–175 °C; <sup>1</sup>H NMR (600 MHz,  $CDCl_3$ )  $\delta$  8.62 (d,  $J$  = 7.2 Hz, 2H), 8.23 (d,  $J$  = 8.4 Hz, 2H), 7.77 (t,  $J$  = 7.8 Hz, 2H), 4.45 (t,  $J$  = 6.3 Hz, 2H), 3.67 (t,  $J$  = 6.3 Hz, 2H). <sup>13</sup>C NMR (151 MHz,  $CDCl_3$ )  $\delta$  164.19, 134.24, 131.63, 131.53, 128.25, 126.99, 122.32, 48.87, 38.82.

#### 4.1.13. 2-(4-Azidobutyl)-1H-benzo[de]isoquinoline-1,3(2H)-dione (7b)

Yield: 76%; white solid; m.p. 73–74 °C; <sup>1</sup>H NMR (600 MHz,  $CDCl_3$ )  $\delta$  8.58 (dd,  $J$  = 7.3, 1.1 Hz, 2H), 8.20 (dd,  $J$  = 8.2, 1.1 Hz, 2H), 7.74 (dd,  $J$  = 8.2, 7.3 Hz, 2H), 4.12 (t,  $J$  = 7.2 Hz, 2H), 3.35 (t,  $J$  = 6.9 Hz, 2H), 1.88–1.79 (m, 2H), 1.76–1.67 (m, 2H); <sup>13</sup>C NMR (151 MHz,  $CDCl_3$ )  $\delta$  164.16, 133.95, 131.58, 131.25, 128.14, 126.92, 122.58, 51.17, 39.62, 26.50, 25.38.

#### 4.1.14. 2-(6-Azidohexyl)-1H-benzo[de]isoquinoline-1,3(2H)-dione (7c)

Yield: 81%; white solid; m.p. 94–95 °C; <sup>1</sup>H NMR (600 MHz,  $CDCl_3$ )  $\delta$  8.58 (dd,  $J$  = 7.3, 1.1 Hz, 2H), 8.20 (dd,  $J$  = 8.2, 1.1 Hz, 2H), 7.74 (dd,  $J$  = 8.2, 7.3 Hz, 2H), 4.18 (t,  $J$  = 7.2 Hz, 2H), 3.41 (t,  $J$  = 6.8 Hz, 1H), 1.92–1.84 (m, 2H), 1.80–1.72 (m, 2H), 1.56–1.46 (m, 2H), 1.49–1.42 (m, 2H); <sup>13</sup>C NMR (151 MHz,  $CDCl_3$ )  $\delta$  164.15, 133.86, 131.57, 131.17, 128.13, 126.91, 122.69, 40.24, 33.80, 32.69, 27.91, 27.89, 26.28.

#### 4.1.15. Synthesis of compounds 8a–c

A solution of starting substrate (1.0 mmol) and compound 3 (1.0 mmol) in 10 mL of a THF-water mixture (7:3, v/v) was treated with sodium ascorbate (0.2 mmol) followed by  $CuSO_4 \cdot 5H_2O$  (0.1 mmol) after stirring for about 10 min. The reaction mixture was stirred at rt for 24 to 48 h. The completion of the reaction was confirmed by the disappearance of the substrate fraction on the TLC plate using 5% MeOH- $CHCl_3$  as the eluent and staining the plate with ninhydrin solution. The reaction mixture was then extracted with  $CHCl_3$  (50 mL) and a saturated solution of EDTA (100 mL). The organic layer was extracted twice with EDTA solution (2  $\times$  100 mL) and dried over  $Na_2SO_4$ . After evaporation of the solvent, a yellow oil was obtained. The crude product was purified using silica gel column chromatography with 5% MeOH- $CHCl_3$  as the eluent.



#### 4.1.16. 2-(2-(4-((1,4,7-Trioxa-10-azacyclododecan-10-yl)methyl)-1H-1,2,3-triazol-1-yl)ethyl)-1H-benzo[de]isoquinoline-1,3(2H)-dione (**8a**)

Yield: 67%; yellow, viscous oil;  $^1\text{H}$  NMR (400 MHz,  $\text{CDCl}_3$ )  $\delta$  8.53 (dd,  $J = 7.3$ , 1.1 Hz, 2H), 8.22 (dd,  $J = 8.4$ , 1.1 Hz, 2H), 7.75 (t,  $J = 7.6$ , 2H), 7.27 (s, 1H), 4.77 (t,  $J = 6.0$  Hz, 2H), 4.67 (t,  $J = 6.0$  Hz, 2H), 3.82 (s, 2H), 3.71–3.62 (m, 4H), 3.63–3.47 (m, 4H), 3.52 (t,  $J = 4.8$ , Hz, 4H), 2.66 (t,  $J = 4.8$ , Hz, 4H);  $^{13}\text{C}$  NMR (101 MHz,  $\text{CDCl}_3$ )  $\delta$  163.92, 145.61, 134.30, 131.66, 131.49, 128.32, 126.97, 123.44, 122.18, 70.90, 70.63, 69.59, 54.31, 50.76, 47.86, 39.88. HRMS (ESI-TOF):  $m/z$  calc. for  $\text{C}_{25}\text{H}_{30}\text{N}_5\text{O}_5$   $[\text{M}+\text{H}]^+$  480.2247, found: 480.2236.

#### 4.1.17. 2-(4-(4-((1,4,7-Trioxa-10-azacyclododecan-10-yl)methyl)-1H-1,2,3-triazol-1-yl)butyl)-1H-benzo[de]isoquinoline-1,3(2H)-dione (**8b**)

Yield: 91%; yellow, viscous oil;  $^1\text{H}$  NMR (600 MHz,  $\text{CDCl}_3$ )  $\delta$  8.59 (dd,  $J = 7.2$ , 1.1 Hz, 2H), 8.22 (dd,  $J = 8.2$ , 1.1 Hz, 2H), 7.76 (t,  $J = 7.2$  Hz, 2H), 7.74 (s, 1H), 4.44 (t,  $J = 7.2$  Hz, 2H), 4.24 (t,  $J = 7.2$ , 2H), 3.88 (s, 2H), 3.71–3.58 (m, 12H), 2.79–2.73 (m, 4H), 2.06–1.98 (m, 2H), 1.84–1.75 (m, 2H);  $^{13}\text{C}$  NMR (151 MHz,  $\text{CDCl}_3$ )  $\delta$  164.18, 134.06, 131.58, 131.29, 128.14, 126.95, 123.05, 122.50, 70.85, 70.60, 69.54, 54.44, 50.90, 49.70, 39.26, 27.76, 25.06. HRMS (ESI-TOF):  $m/z$  calc. for  $\text{C}_{27}\text{H}_{34}\text{N}_5\text{O}_5$   $[\text{M}+\text{H}]^+$  508.2560, found: 508.1239.

#### 4.1.18. 2-(6-(4-((1,4,7-Trioxa-10-azacyclododecan-10-yl)methyl)-1H-1,2,3-triazol-1-yl)hexyl)-1H-benzo[de]isoquinoline-1,3(2H)-dione (**8c**)

Yield: 87%; yellow, viscous oil;  $^1\text{H}$  NMR (400 MHz,  $\text{CDCl}_3$ )  $\delta$  8.59 (dd,  $J = 7.3$ , 1.1 Hz, 2H), 8.21 (dd,  $J = 8.4$ , 1.1 Hz, 2H), 7.75 (t,  $J = 7.6$  Hz, 2H), 7.67 (s, 1H), 4.33 (t,  $J = 7.2$  Hz, 2H), 4.17 (t,  $J = 7.6$  Hz, 2H), 3.86 (s, 2H), 3.73–3.58 (m, 8H), 3.61 (t,  $J = 4.8$  Hz, 4H), 2.76 (t,  $J = 4.8$  Hz, 4H), 1.99–1.87 (m, 2H), 1.80–1.68 (m, 2H), 1.54–1.35 (m, 4H);  $^{13}\text{C}$  NMR (101 MHz,  $\text{CDCl}_3$ )  $\delta$  164.19, 145.58, 133.93, 131.61, 131.21, 128.17, 126.95, 122.69, 122.68, 70.93, 70.67, 69.70, 54.53, 51.09, 50.17, 40.12, 30.13, 27.82, 26.47, 26.19. HRMS (ESI-TOF):  $m/z$  calc. for  $\text{C}_{29}\text{H}_{38}\text{N}_5\text{O}_5$   $[\text{M}+\text{H}]^+$  536.2873, found: 536.2476.

#### 4.1.19. Synthesis of compounds **9a–c**

To synthesize compounds **9a–c**, we employed the same synthetic procedure that was used for the preparation of compounds **8a–c**. Tri-tert-butyl 10-((1-(2-(1,3-dioxo-1H-benzo[de]isoquinolin-2(3H)-yl)ethyl)-1H-1,2,3-triazol-4-yl)methyl)-1,4,7,10-tetraazacyclododecane-1,4,7-tricarboxylate (**9a**). Yield: 95%; white foam; m.p. 114–115 °C;  $^1\text{H}$  NMR (600 MHz,  $\text{DMSO}-d_6$ )  $\delta$  8.46 (d,  $J = 8.2$  Hz, 2H), 8.41 (d,  $J = 7.7$  Hz, 2H), 8.09 (s, 1H), 7.85 (t,  $J = 7.7$  Hz, 2H), 4.73 (t,  $J = 5.7$  Hz, 2H), 4.49 (t,  $J = 5.7$  Hz, 2H), 3.83 (s, 2H), 3.58–3.09 (m, 12H), 2.49–2.32 (m, 4H), 1.45–1.30 (m, 27H). HRMS (ESI-TOF):  $m/z$  calc. for  $\text{C}_{40}\text{H}_{57}\text{N}_8\text{O}_8$   $[\text{M}+\text{H}]^+$  777.4299, found: 777.4286.

#### 4.1.20. Tri-tert-butyl 10-((1-(4-(1,3-dioxo-1H-benzo[de]isoquinolin-2(3H)-yl)butyl)-1H-1,2,3-triazol-4-yl)methyl)-1,4,7,10-tetraazacyclododecane-1,4,7-tricarboxylate (**9b**)

Yield: 95%; white foam; m.p. 97–98 °C;  $^1\text{H}$  NMR (600 MHz,  $\text{CD}_3\text{OD}$ )  $\delta$  8.46 (dd,  $J = 7.3$ , 1.1 Hz, 2H), 8.27 (d,  $J = 8.2$  Hz, 2H), 7.97 (s, 1H), 7.75 (t,  $J = 7.8$  Hz, 2H), 4.51 (t,  $J = 7.2$  Hz, 2H), 4.16 (t,  $J = 7.2$  Hz, 2H), 3.95 (s, 2H), 3.58 (br, 4H), 3.39 (br, 8H), 2.62–2.56 (m, 4H), 2.05–1.96 (m, 2H), 1.74–1.66 (m, 2H), 1.51–1.37 (m, 27H). HRMS (ESI-TOF):  $m/z$  calc. for  $\text{C}_{42}\text{H}_{61}\text{N}_8\text{O}_8$   $[\text{M}+\text{H}]^+$  805.4612, found: 805.2639.

#### 4.1.21. Tri-tert-butyl 10-((1-(6-(1,3-dioxo-1H-benzo[de]isoquinolin-2(3H)-yl)hexyl)-1H-1,2,3-triazol-4-yl)methyl)-1,4,7,10-tetraazacyclododecane-1,4,7-tricarboxylate (**9c**)

Yield: 91%; white foam; m.p. 92–93 °C;  $^1\text{H}$  NMR (600 MHz,  $\text{CDCl}_3$ )  $\delta$  8.60 (dd,  $J = 7.3$ , 1.1 Hz, 2H), 8.22 (dd,  $J = 8.2$ , 1.1 Hz, 2H), 7.76

(dd,  $J = 8.2$ , 7.3 Hz, 2H), 7.45 (s, 1H), 4.33 (t,  $J = 7.3$  Hz, 2H), 4.20–4.15 (m, 2H), 3.90 (s, 2H), 3.66–3.50 (m, 4H), 3.48–3.24 (m, 8H), 2.84–2.52 (m, 4H), 1.97–1.88 (m, 2H), 1.79–1.71 (m, 2H), 1.52–1.37 (m, 31H). HRMS (ESI-TOF):  $m/z$  calc. for  $\text{C}_{44}\text{H}_{65}\text{N}_8\text{O}_8$   $[\text{M}+\text{H}]^+$  833.4925, found: 833.2695.

#### 4.1.22. Synthesis of compounds **10a–c**

The *N*-Boc-protected conjugate (1.0 mmol) was dissolved in  $\text{CH}_2\text{Cl}_2$  (30 mL) and TFA (50.0 mmol) was added in one portion. The mixture was left stirring at rt for 24 h. The solution was then evaporated to dryness under vacuum on a rotary evaporator, and the residue was divided between a 1.0 M NaOH solution (15 mL) and  $\text{CH}_2\text{Cl}_2$  (30 mL). The aqueous layer was extracted with  $\text{CH}_2\text{Cl}_2$  twice ( $2 \times 30$  mL). The combined organic layers (about 45 mL) were washed with brine (15 mL) and dried over  $\text{Na}_2\text{SO}_4$ . The solvent was evaporated under vacuum on a rotary evaporator and the obtained residue was purified on an aluminum gel column chromatography using 30% MeOH- $\text{CHCl}_3$  as the eluent. The fractions containing the product were combined and evaporated to yield a yellowish oily residue, which eventually crystallized as a foam.

#### 4.1.23. 2-(2-(4-((1,4,7,10-Tetraazacyclododecan-1-yl)methyl)-1H-1,2,3-triazol-1-yl)ethyl)-1H-benzo[de]isoquinoline-1,3(2H)-dione (**10a**)

Yield: 90%; yellow foam; m.p. 69–70 °C;  $^1\text{H}$  NMR (600 MHz,  $\text{CD}_3\text{OD}$ )  $\delta$  8.41 (dd,  $J = 7.2$ , 1.2 Hz, 2H), 8.29 (dd,  $J = 8.2$ , 1.2 Hz, 2H), 7.95 (s, 1H), 7.75 (dd,  $J = 8.2$ , 7.2 Hz, 2H), 4.83–4.74 (m, 2H), 4.67–4.52 (m, 2H), 3.76 (s, 2H), 2.89–2.70 (m, 4H), 2.63–2.55 (m, 4H), 2.55–2.49 (m, 4H), 2.49–2.41 (m, 4H);  $^{13}\text{C}$  NMR (151 MHz,  $\text{CD}_3\text{OD}$ )  $\delta$  165.25, 144.58, 135.68, 133.16, 132.27, 129.29, 128.13, 125.71, 123.26, 51.09, 47.29, 46.48, 45.04, 40.91. HRMS (ESI-TOF):  $m/z$  calc. for  $\text{C}_{25}\text{H}_{33}\text{N}_8\text{O}_2$   $[\text{M}+\text{H}]^+$  477.2729, found: 477.2740.

#### 4.1.24. 2-(4-(4-((1,4,7,10-Tetraazacyclododecan-1-yl)methyl)-1H-1,2,3-triazol-1-yl)butyl)-1H-benzo[de]isoquinoline-1,3(2H)-dione (**10b**)

Yield: 87%; yellow foam; m.p. 52–53 °C;  $^1\text{H}$  NMR (400 MHz,  $\text{CD}_3\text{OD}$ )  $\delta$  8.44 (dd,  $J = 7.3$ , 1.1 Hz, 2H), 8.27 (dd,  $J = 8.2$ , 1.1 Hz, 2H), 7.94 (s, 1H), 7.74 (dd,  $J = 8.2$ , 7.3 Hz, 2H), 4.48 (t,  $J = 7.2$  Hz, 2H), 4.15 (t,  $J = 7.2$  Hz, 2H), 3.78 (s, 2H), 2.87–2.69 (m, 4H), 2.69–2.59 (m, 4H), 2.59–2.48 (m, 8H), 2.06–1.95 (m, 2H), 1.77–1.66 (m, 2H);  $^{13}\text{C}$  NMR (101 MHz,  $\text{CD}_3\text{OD}$ )  $\delta$  165.45, 145.20, 135.48, 133.07, 132.09, 129.11, 128.12, 125.06, 123.48, 51.56, 50.86, 49.56, 47.21, 46.40, 45.03, 40.35, 28.78, 26.09. HRMS (ESI-TOF):  $m/z$  calc. for  $\text{C}_{27}\text{H}_{37}\text{N}_8\text{O}_2$   $[\text{M}+\text{H}]^+$  505.3040, found: 505.3162.

#### 4.1.25. 2-(6-(4-((1,4,7,10-Tetraazacyclododecan-1-yl)methyl)-1H-1,2,3-triazol-1-yl)hexyl)-1H-benzo[de]isoquinoline-1,3(2H)-dione (**10c**)

Yield: 92%; yellow foam; m.p. 45–46 °C;  $^1\text{H}$  NMR (600 MHz,  $\text{CD}_3\text{OD}$ )  $\delta$  8.45 (dd,  $J = 7.3$ , 1.1 Hz, 2H), 8.26 (dd,  $J = 8.2$ , 1.1 Hz, 2H), 7.91 (s, 1H), 7.74 (t,  $J = 7.8$  Hz, 2H), 4.39 (t,  $J = 7.2$  Hz, 1H), 4.07 (t,  $J = 7.2$  Hz, 2H), 3.78 (s, 2H), 2.75–2.70 (m, 4H), 2.67–2.61 (m, 4H), 2.60–2.55 (m, 4H), 2.55–2.50 (m, 4H), 1.97–1.89 (m, 2H), 1.72–1.64 (m, 2H), 1.48–1.35 (m, 4H);  $^{13}\text{C}$  NMR (151 MHz,  $\text{CD}_3\text{OD}$ )  $\delta$  165.45, 145.32, 135.44, 133.10, 132.06, 129.13, 128.13, 124.81, 123.57, 51.66, 51.26, 49.66, 47.23, 46.41, 45.06, 41.04, 31.03, 28.82, 27.43, 27.14. HRMS (ESI-TOF):  $m/z$  calc. for  $\text{C}_{29}\text{H}_{42}\text{N}_8\text{O}_2$   $[\text{M}+2\text{H}]^{2+}$  267.1716, found: 267.1718.

#### 4.1.26. Synthesis of compound **11**

Freshly distilled phenol (9.00 g, 97.3 mmol) was added dropwise to a suspension of thiosalicylic acid (5.00 g, 32.4 mmol) in concentrated sulfuric acid (96%, 60 mL) and the mixture was heated at 90 °C for 18 h. After cooling to rt, the reaction mixture was gently poured into a mixture of crushed ice and water (500 mL) to yield a yellow precipitate, which was filtered and dried to obtain a yellow solid. The crude solid was suspended in  $\text{CHCl}_3$  (50 mL) and evaporated onto 10 times its

weight of silica gel. The mixture was then applied to a silica gel column and eluted using 5% MeOH-CHCl<sub>3</sub>. The fractions containing product were evaporated together to give compound **4** as a yellow solid in 29% yield.

#### 4.1.27. 2-hydroxy-9H-thioxanthen-9-one (**11**)

Yield: 29%; yellow solid; m.p. 226–227 °C; <sup>1</sup>H NMR (600 MHz, CD<sub>3</sub>OD): δ 8.55–8.50 (m, 1H), 7.93 (d, *J* = 2.8 Hz, 1H), 7.73–7.65 (m, 2H), 7.57 (d, *J* = 8.8 Hz, 1H), 7.50 (ddd, *J* = 8.2, 6.0, 2.1 Hz, 1H), 7.25 (dd, *J* = 8.8, 2.8 Hz, 1H); <sup>13</sup>C NMR (150 MHz, CD<sub>3</sub>OD): δ 156.56, 138.01, 132.10, 129.02, 127.31, 125.92, 125.77, 122.34, 113.14. HR-ESI-MS: *m/z* calc. for C<sub>13</sub>H<sub>7</sub>O<sub>2</sub>S 228.0245 [M]<sup>+</sup>, found: 228.9468.

#### 4.1.28. Synthesis of compounds **12a–c**

In this step, a suspension of compound **11** (1.0 mmol) and K<sub>2</sub>CO<sub>3</sub> (2.0 mmol) in DMF (20 mL) was reacted with the appropriate dibromoalkane (4.0 mmol) in a single addition, and the reaction mixture was heated at 90 °C for 24 h. After cooling, the mixture was separated into water (100 mL) and AcOEt (200 mL) layers. The organic layer was dried over Na<sub>2</sub>SO<sub>4</sub> and concentrated under vacuum using a rotary evaporator, resulting in a yellow solid. The crude product was then purified using silica gel column chromatography with CHCl<sub>3</sub> as the eluent. The fractions containing the product were combined and evaporated to yield the final product as a yellow solid.

#### 4.1.29. 2-(2-bromoethoxy)-9H-thioxanthen-9-one (**12a**)

Yield: 38%; yellow solid; m.p. 169–171 °C; <sup>1</sup>H NMR (600 MHz, DMSO-*d*<sub>6</sub>) δ 8.46 (dd, *J* = 8.1, 1.5 Hz, 1H), 7.91 (d, *J* = 3.0 Hz, 1H), 7.88–7.78 (m, 2H), 7.75 (ddd, *J* = 8.3, 7.0, 1.5 Hz, 1H), 7.57 (ddd, *J* = 8.1, 7.0, 1.2 Hz, 1H), 7.46 (dd, *J* = 8.8, 3.0 Hz, 1H), 4.46 (t, *J* = 5.4 Hz, 2H), 3.85 (t, *J* = 5.4 Hz, 2H); <sup>13</sup>C NMR (151 MHz, DMSO-*d*<sub>6</sub>) δ 178.87, 157.26, 137.21, 133.28, 129.94, 129.55, 129.25, 128.74, 128.18, 127.10, 127.01, 123.16, 112.00, 68.68, 31.67.

#### 4.1.30. 2-(4-bromobutoxy)-9H-thioxanthen-9-one (**12b**)

Yield: 31%; yellow solid; m.p. 95–96 °C; <sup>1</sup>H NMR (600 MHz, CDCl<sub>3</sub>) δ 8.62 (ddd, *J* = 8.2, 1.5, 0.7 Hz, 1H), 8.04 (d, *J* = 3.0 Hz, 1H), 7.60 (ddd, *J* = 8.2, 6.7, 1.5 Hz, 1H), 7.57 (ddd, *J* = 8.2, 1.5, 0.7 Hz, 1H), 7.48 (d, *J* = 8.8 Hz, 1H), 7.47 (ddd, *J* = 8.2, 6.7, 1.5 Hz, 1H), 7.24 (dd, *J* = 8.8, 3.0 Hz, 1H), 4.13 (t, *J* = 6.6 Hz, 2H), 3.50 (t, *J* = 6.6 Hz, 2H), 2.13–2.05 (m, 2H), 2.03–1.96 (m, 2H); <sup>13</sup>C NMR (151 MHz, CDCl<sub>3</sub>) δ 179.62, 157.64, 137.49, 132.01, 130.22, 129.86, 129.16, 128.59, 127.30, 126.07, 125.97, 122.89, 111.10, 67.34, 33.29, 29.45, 27.78.

#### 4.1.31. 2-((6-bromohexyl)oxy)-9H-thioxanthen-9-one (**12c**)

Yield: 35%; yellow solid; m.p. 90–91 °C; <sup>1</sup>H NMR (600 MHz, CDCl<sub>3</sub>) δ 8.63 (ddd, *J* = 8.2, 1.4, 0.7 Hz, 1H), 8.06 (d, *J* = 3.0 Hz, 1H), 7.61 (ddd, *J* = 8.2, 6.6, 1.4 Hz, 1H), 7.58 (ddd, *J* = 8.2, 1.7, 0.7 Hz, 1H), 7.49 (d, *J* = 8.8 Hz, 1H), 7.48 (ddd, *J* = 8.2, 6.6, 1.7 Hz, 1H), 7.26 (dd, *J* = 8.8, 3.0 Hz, 1H), 4.11 (t, *J* = 6.4 Hz, 2H), 3.43 (t, *J* = 6.4 Hz, 2H), 1.96–1.82 (m, 2H), 1.56–1.50 (m, 2H); <sup>13</sup>C NMR (151 MHz, CDCl<sub>3</sub>) δ 179.72, 157.87, 137.55, 132.01, 130.25, 129.89, 128.99, 128.63, 127.28, 126.07, 126.00, 123.03, 111.12, 68.22, 33.74, 32.69, 28.95, 27.93, 25.30.

#### 4.1.32. Synthesis of compounds **13a–c**

To synthesize compounds **13a–c**, we employed the same synthetic procedure that was used for the preparation of compounds **7a–c**.

#### 4.1.33. 2-(2-azidoethoxy)-9H-thioxanthen-9-one (**13a**)

Yield: 91%; yellow solid; m.p. 131–133 °C; <sup>1</sup>H NMR (600 MHz, DMSO-*d*<sub>6</sub>) δ 8.45 (dd, *J* = 8.2, 1.4 Hz, 1H), 7.92 (d, *J* = 2.9 Hz, 1H), 7.83–7.78 (m, 2H), 7.75 (ddd, *J* = 8.2, 6.9, 1.5 Hz, 1H), 7.56 (ddd, *J* = 8.2, 7.0, 1.2 Hz, 1H), 7.43 (dd, *J* = 8.8, 2.9 Hz, 1H), 4.31 (t, *J* = 4.8, 2H), 3.70 (t, *J* = 4.8, 2H); <sup>13</sup>C NMR (151 MHz, DMSO-*d*<sub>6</sub>) δ

178.87, 157.33, 137.21, 133.26, 129.94, 129.54, 129.18, 128.72, 128.18, 127.08, 127.00, 123.00, 111.87, 67.76, 49.96.

#### 4.1.34. 2-(4-azidobutoxy)-9H-thioxanthen-9-one (**13b**)

Yield: 96%; yellow solid; m.p. 77–78 °C; <sup>1</sup>H NMR (600 MHz, DMSO-*d*<sub>6</sub>) δ 8.46 (ddd, *J* = 8.1, 1.5, 0.6 Hz, 1H), 7.89 (d, *J* = 2.9 Hz, 1H), 7.80 (ddd, *J* = 8.1, 1.3, 0.6 Hz, 1H), 7.75 (ddd, *J* = 8.2, 7.0, 1.5 Hz, 1H), 7.73 (d, *J* = 8.8 Hz, 1H), 7.57 (ddd, *J* = 8.2, 6.9, 1.2 Hz, 1H), 7.39 (dd, *J* = 8.8, 2.9 Hz, 1H), 4.12 (t, *J* = 6.3 Hz, 2H), 3.44 (t, *J* = 6.8 Hz, 2H), 1.86–1.80 (m, 2H), 1.76–1.70 (m, 2H); <sup>13</sup>C NMR (151 MHz, DMSO-*d*<sub>6</sub>) δ 178.33, 157.32, 136.71, 132.59, 129.38, 129.00, 128.10, 127.91, 127.68, 126.42, 126.39, 122.53, 110.98, 67.35, 50.36, 25.79, 25.02.

#### 4.1.35. 2-((6-azidoheptyl)oxy)-9H-thioxanthen-9-one (**13c**)

Yield: 90%; yellow solid; m.p. 69–71 °C; <sup>1</sup>H NMR (600 MHz, CDCl<sub>3</sub>) δ 8.63 (ddd, *J* = 8.2, 1.5, 0.6 Hz, 1H), 8.06 (d, *J* = 2.9 Hz, 1H), 7.60 (ddd, *J* = 8.0, 6.6, 1.4 Hz, 1H), 7.58 (ddd, *J* = 8.1, 1.7, 0.6 Hz, 1H), 7.49 (d, *J* = 8.8 Hz, 1H), 7.47 (ddd, *J* = 8.2, 6.6, 1.6 Hz, 1H), 7.25 (dd, *J* = 8.8, 2.9 Hz, 1H), 4.11 (t, *J* = 6.4 Hz, 2H), 3.29 (t, *J* = 6.9 Hz, 2H), 1.85 (dt, *J* = 14.6, 6.5 Hz, 2H), 1.65 (dt, *J* = 14.3, 7.0 Hz, 2H), 1.58–1.43 (m, 4H); <sup>13</sup>C NMR (151 MHz, CDCl<sub>3</sub>) δ 179.70, 157.87, 137.54, 132.00, 130.25, 129.89, 128.99, 128.63, 127.28, 127.27, 126.06, 125.99, 123.01, 111.11, 77.24, 68.21, 51.39, 28.99, 28.81, 26.51, 25.68.

#### 4.1.36. Synthesis of compounds **14a–c**

To synthesize compounds **14a–c**, we employed the same synthetic procedure that was used for the preparation of compounds **8a–c**.

#### 4.1.37. 2-(2-(4-((1,4,7-trioxa-10-azacyclododecan-10-yl)methyl)-1H-1,2,3-triazol-1-yl)ethoxy)-9H-thioxanthen-9-one (**14a**)

Yield: 48%; yellow oil; <sup>1</sup>H NMR (600 MHz, CDCl<sub>3</sub>) δ 8.61 (dd, *J* = 8.2, 1.5 Hz, 1H), 8.05 (d, *J* = 2.9 Hz, 1H), 7.92 (s, 1H), 7.62 (ddd, *J* = 8.3, 6.8, 1.5 Hz, 1H), 7.58 (dd, *J* = 8.1, 1.4 Hz, 1H), 7.50 (d, *J* = 8.8 Hz, 1H), 7.48 (ddd, *J* = 8.2, 6.8, 1.4 Hz, 1H), 7.26 (dd, *J* = 8.8, 2.9 Hz, 1H), 4.81 (t, *J* = 5.1 Hz, 2H), 4.52 (t, *J* = 5.1 Hz, 2H), 3.91 (s, 2H), 3.69 (td, *J* = 3.7, 2.0 Hz, 4H), 3.65 (td, *J* = 3.7, 2.1 Hz, 4H), 3.62 (t, *J* = 4.7 Hz, 4H), 2.78 (t, *J* = 4.7 Hz, 4H); <sup>13</sup>C NMR (151 MHz, CDCl<sub>3</sub>) δ 179.43, 156.65, 137.36, 132.18, 130.21, 130.08, 129.88, 128.51, 127.58, 126.23, 126.00, 124.06, 122.59, 111.52, 70.84, 70.61, 69.47, 66.69, 54.47, 50.98, 49.51. HRMS (ESI-TOF): *m/z* calc. for C<sub>26</sub>H<sub>31</sub>N<sub>4</sub>O<sub>5</sub>S [M+H]<sup>+</sup> 511.2016, found: 505.0685.

#### 4.1.38. 2-(4-(4-((1,4,7-trioxa-10-azacyclododecan-10-yl)methyl)-1H-1,2,3-triazol-1-yl)butoxy)-9H-thioxanthen-9-one (**14b**)

Yield: 55%; yellow oil; <sup>1</sup>H NMR (600 MHz, CDCl<sub>3</sub>) δ 8.62 (ddd, *J* = 8.1, 1.5, 0.6 Hz, 1H), 8.03 (d, *J* = 2.9 Hz, 1H), 7.83 (s, 1H), 7.61 (ddd, *J* = 8.1, 6.7, 1.5 Hz, 1H), 7.58 (ddd, *J* = 8.1, 1.6, 0.7 Hz, 1H), 7.49 (d, *J* = 8.7 Hz, 1H), 7.47 (ddd, *J* = 8.2, 6.6, 1.6 Hz, 1H), 7.24 (dd, *J* = 8.8, 2.9 Hz, 1H), 4.46 (t, *J* = 7.1 Hz, 2H), 4.13 (t, *J* = 6.1 Hz, 2H), 3.93 (s, 2H), 3.72–3.62 (m, 12H), 2.81 (br, 4H), 2.27–2.10 (m, 2H), 1.99–1.81 (m, 2H); <sup>13</sup>C NMR (151 MHz, CDCl<sub>3</sub>) δ 179.60, 157.54, 137.50, 132.06, 130.22, 129.86, 129.26, 128.58, 127.37, 126.10, 126.00, 123.25, 122.83, 111.15, 70.83, 70.69, 69.30, 67.42, 54.43, 50.82, 49.92, 27.16, 26.15. HRMS (ESI-TOF): *m/z* calc. for C<sub>28</sub>H<sub>35</sub>N<sub>4</sub>O<sub>5</sub>S [M+H]<sup>+</sup> 539.2328, found: 539.2349.

#### 4.1.39. 2-((6-(4-((1,4,7-trioxa-10-azacyclododecan-10-yl)methyl)-1H-1,2,3-triazol-1-yl)hexyl)oxy)-9H-thioxanthen-9-one (**14c**)

Yield: 44%; yellow oil; <sup>1</sup>H NMR (400 MHz, CDCl<sub>3</sub>) δ 8.67–8.58 (m, 1H), 8.04 (d, *J* = 2.8 Hz, 1H), 7.75 (s, 1H), 7.66–7.56 (m, 2H), 7.53–7.44 (m, 2H), 7.25 (dd, *J* = 8.8, 2.8 Hz, 1H), 4.36 (t, *J* = 7.2 Hz, 2H), 4.09 (t, *J* = 6.4 Hz, 2H), 3.90 (s, 2H), 3.81–3.57 (m, 14H), 2.89–2.70 (m, 4H), 1.96 (p, *J* = 7.2 Hz, 3H), 1.90–1.78 (m, 2H),

1.66–1.49 (m, 2H), 1.42 (tt,  $J = 10.6, 6.2$  Hz, 2H);  $^{13}\text{C}$  NMR (101 MHz,  $\text{CDCl}_3$ )  $\delta$  179.70, 157.82, 137.55, 132.03, 130.22, 129.87, 129.03, 128.61, 127.31, 126.08, 126.01, 123.12, 122.99, 111.13, 70.74, 70.55, 69.36, 68.11, 54.42, 50.97, 50.18, 30.19, 28.87, 26.26, 25.54. HRMS (ESI-TOF):  $m/z$  calc. for  $\text{C}_{30}\text{H}_{39}\text{N}_4\text{O}_5\text{S}$   $[\text{M}+\text{H}]^+$  566.2563, found: 566.2537.

#### 4.1.40. Synthesis of $\text{Cu}^{2+}$ -cyclen

Cyclen (300 mg, 1.74 mmol) and  $\text{CuCl}_2$  (234 mg, 1.74 mmol) were separately dissolved in EtOH (5 mL) and then mixed together. The mixture was heated to boiling, then cooled to rt and stirred overnight. The resulting precipitate was filtered and washed with EtOH. The green precipitate obtained after drying was used for further studies. HRMS (ESI-TOF):  $m/z$  calc. for  $\text{C}_8\text{H}_{20}\text{CuN}_4$   $[\text{M}]^{2+}$  117.5492, found: 117.4794;  $m/z$  calc. for  $\text{C}_8\text{H}_{20}\text{ClCuN}_4$   $[\text{M}+\text{Cl}]^+$  270.0673, found: 269.9572.

## 4.2. Photoluminescence

To investigate the photoluminescent properties of the compounds, diluted ( $10^{-4}$  M) aqueous solutions of pH 7.4 PBS buffer were prepared. Fluorescence measurements were carried out in 3.5 mL fluorescence glass cuvettes with a 10 mm path length (LAB4US; Thermo Fisher Scientific, Cleveland, OH, USA). The spectra were recorded and processed using a laser-coupled Fluorometer System (Camlin Ltd, Lisburn, UK) equipped with FluoroSENS Application Software. To optimize the signal acquisition, the following measurement parameters were adjusted: a 100 ms integration time, 100 k gain, and 2 mm slits width. A xenon lamp was used as a high-intensity broad-spectrum light source.

## 4.3. Cytotoxicity assay

### 4.3.1. Cell culture

Cancer cell lines A549 (ATCC CCL-185, Human lung carcinoma cells), HepG2 (ATCC HB-8065, Human hepatocellular carcinoma), and HeLa (ATCC CCL-2, Human cervix adenocarcinoma cells) and non-cancer cell lines Vero (ATCC CCL-81, Cercopithecus aethiops normal kidney cells), LLCMK2 (ATCC CCL-7, Macaca mulatta normal kidney cells), NCTC clone 929 (ATCC CCL-1, Mus musculus normal subcutaneous connective tissue cells), and MRC-5 (ATCC CCL-171, Human lung normal fibroblasts) were purchased from ATCC. The cells were cultured in Minimum Essential Medium Eagle (MEM) supplemented with 10% fetal bovine serum (FBS) and antibiotics. The cells were incubated overnight at 37 °C in a humidified atmosphere containing 5%  $\text{CO}_2$ .

### 4.3.2. Drug treatment

Stock solutions of the investigated compounds were prepared in DMSO at 100 mM and diluted with medium supplemented with 10% FBS. The final content of DMSO in solutions did not exceed 0.1%. A549, HepG2, HeLa, Vero, LLC-MK2, NCTC clone 929, and MRC-5 cells were seeded into 96-well microplates at a density of  $2 \times 10^5$  cells/mL. After overnight incubation, the culture medium was removed, and the cells were treated with 100  $\mu\text{L}$  of freshly prepared solution of compounds diluted with the growth medium supplemented with 10% FBS to obtain concentrations ranging from 0.1 to 1000  $\mu\text{M}$ . All experiments were performed in triplicate.

### 4.3.3. Cytotoxicity assay

After incubation with the drugs for 48 h, the cytotoxicity of the investigated compounds was observed microscopically, and cell viability was determined using the 3-(4,5-dimethylthiazol-2-yl)-2,5-diphenyltetrazolium bromide (MTT) assay. The cells were treated with 25  $\mu\text{L}$  of MTT dye solution (5 mg/mL) for 2 h and lysed with 100  $\mu\text{L}$  of solvent solution containing 45 mL of dimethylformamide (DMF), 13.5 g of sodium dodecylsulfate (SDS), and 55 mL of distilled water [48]. After overnight incubation at 37 °C, the optical density at 550 nm

with a reference wavelength of 670 nm was measured using an ELISA reader (VarioskanLux, Thermo Fisher Scientific, Waltham, MA, USA). The curves used to determine the  $\text{CC}_{50}$  values (50% cytotoxic concentration) and the calculation of these values were performed using GraphPad Prism 9 software.

## 4.4. $T_m$ measurements

The experiment involved adding aliquots of DMSO stock solution of the tested compounds to 20 mM cacodylate buffer, pH 7.0. The final DMSO content in the solution ranged from 0.29% to 0.34%, depending on the sample.  $T_m$  curves were collected at a [ligand]/[DNA] ratio of 0.3 to ensure the dominant binding mode. The thermal melting curves were plotted by measuring the absorption change at 260 nm as a function of temperature using a Cintra10 UV-Vis spectrometer (GBC Scientific Equipment, Dandenong, Victoria, Australia) equipped with a GBC Scientific Equipment Peltier Thermocell. The measurements were carried out using a 1 cm pathway quartz cell. The absorbance of the samples was monitored from 25 to 90 °C with a heating rate of 1 °C  $\text{min}^{-1}$ . The  $T_m$  values were determined from the midpoint of the transition curves of the maximum or the first derivative. The  $\Delta T_m$  values were calculated by subtracting the  $T_m$  of free CT-DNA from the  $T_m$  of CT-DNA in the presence of the sample. All  $T_m$  values were measured in triplicate, and the error in  $\Delta T_m$  was  $\pm 0.5$  °C.

## 4.5. Circular dichroism measurements

The CD spectra were obtained using a JASCO J-500 spectropolarimeter with a JASCO DP-500 data processor (Jasco, Tokyo, Japan). To ensure the accuracy of the measurements, the polarimeter was purged with a continuous flow of nitrogen (99.999%), and the experiments were conducted at 25 °C using 1 cm pathway quartz cells. The CD spectra were recorded from 320 to 220 nm at a speed of 20 nm  $\text{min}^{-1}$ , and the buffer background was subtracted automatically. Data were collected at an interval of 1 nm. The CD spectrum of CT-DNA alone (200 mM) was recorded as a control experiment.

## 4.6. Viscosity measurements

The experiment involved conducting viscosity measurements using a Cannon-Ubbelohde viscometer (model no: 9721-K56; ColeParmer Instrument Co., Vernon Hills, IL, USA) equipped in a viscometer bath set at 25 °C. The flow time of each sample was measured using a digital stopwatch and repeated three times to calculate the average time. The results were presented as  $(\eta/\eta_0)^{1/3}$  versus [ligand]/[DNA] concentration ratios, where  $\eta$  represents the viscosity of CT-DNA in the presence of the ligand, and  $\eta_0$  represents the viscosity of CT-DNA in the absence of the ligand. The samples were prepared by adding aliquots of DMSO stock solution of the tested compounds to 5 mM TRIS-HCl, 50 mM NaCl, pH 7.0. The final DMSO content in the solution ranged from 0.30% to 0.35%, depending on the sample.

## 4.7. Fast halo assay

To assess DNA damage in cells, we followed the methodology outlined by Sestili *et al* [49]. We employed the non-denaturing fast Halo assay (FHA) to quantitatively determine the levels of DNA double-strand breaks (DSBs) while avoiding interference from single-strand breaks (SSBs) in the background DNA. The non-denaturing FHA specifically detects DNA DSBs, whereas the denaturing FHA can detect both SSBs and DSBs. Therefore, by subtracting the DSBs from the total DNA damage, we were able to calculate the level of SSBs.

#### 4.8. Cell culture and drug treatment

A549 cells were seeded into 24-well plates at a density of  $2.5 \times 10^5$  cells per well. After overnight incubation at 37 °C, the culture medium was replaced with fresh medium containing investigated compounds at a concentration of 5  $\mu$ M. The plates were incubated in the dark for 2 h, followed by irradiation using a Well Plate Illuminator (Luzchem Research Inc., Ottawa, Ontario, Canada) benchtop reactor with LEDs centered at the appropriate wavelength. 1,8-Naphthalimide derivatives **8a–c** were irradiated at 340 nm (dose of 20 J/cm<sup>2</sup>), while thioxanthone derivatives **14a–c** were irradiated at 400 nm (dose of 20 J/cm<sup>2</sup>). After irradiation, the plates were further incubated in the dark for another 46 h. Control plates (not irradiated) were incubated in the dark for 48 h. The curves used to determine the IC<sub>50</sub> values (50% inhibitory concentration) and the calculation of these values were performed using GraphPad Prism 9 software.

#### 4.9. Preparation of slides for DNA damage analysis

Following treatment, cells were resuspended in 50  $\mu$ L of ice-cold pH 7.4 PBS. This cell suspension was then mixed with an equal amount of 2% low-melting agarose in PBS and placed immediately between an agarose-coated slide and a coverslip. The slides were left to gel on ice, and once fully gelled, the coverslips were removed. The slides were then treated with FHA. For denaturing FHA, the slides were incubated in 0.3 M NaOH at rt for 20 min. For non-denaturing FHA, the slides were soaked in a lysis solution containing 0.15 M NaOH, 0.1 M NaH<sub>2</sub>PO<sub>4</sub>, 1 mM EDTA and 1% Triton X100 (v/v) at pH 10.1 for 10 min before being incubated for an additional 15 min in pH 7.4 PBS containing 0.1 mg/mL RNase (bovine pancreas Type 1A). Staining of halos for brightfield microscopy was performed using a commercial Wright's staining solution with methylene blue and eosin freshly diluted 1:1 (v/v) with pH 7.4 PBS. Digital images were captured using a PC connected to a digital camera (Olympus IX70, Tokyo, Japan), and were then processed using ImageJ software.

#### Declaration of Competing Interest

The authors declare that they have no known competing financial interests or personal relationships that could have appeared to influence the work reported in this paper.

#### Data availability

Data will be made available on request.

#### Appendix A. Supplementary data

Supplementary data to this article can be found online at <https://doi.org/10.1016/j.bioorg.2023.106782>.

#### References

- S.S. Kelkar, T.M. Reineke, Theranostics: combining imaging and therapy, *Bioconjug. Chem.* 22 (10) (2011) 1879–1903, <https://doi.org/10.1021/bc200151q>.
- R. Kumar, W.S. Shin, K. Sunwoo, W.Y. Kim, S. Koo, S. Bhuniya, J.S. Kim, Small conjugate-based theranostic agents: an encouraging approach for cancer therapy, *Chem. Soc. Rev.* 44 (19) (2015) 6670–6683, <https://doi.org/10.1039/C5CS00224A>.
- R. Zhang, L. Hao, P. Chen, G. Zhang, N. Liu, Multifunctional small-molecule theranostic agents for tumor-specific imaging and targeted chemotherapy, *Bioorg. Chem.* 137 (2023) 106576, <https://doi.org/10.1016/j.bioorg.2023.106576>.
- Y. Fu, N.S. Finney, Small-molecule fluorescent probes and their design, *RSC Adv.* 8 (51) (2018) 29051–29061, <https://doi.org/10.1039/C8RA02297F>.
- J.K. Wong, M.H. Todd, P.J. Rutledge, Recent advances in macrocyclic fluorescent probes for ion sensing, *Molecules* 22 (2) (2017) 200, <https://doi.org/10.3390/molecules22020200>.
- G. Prabakaran, C.I. David, R. Nandhakumar, A review on pyrene based chemosensors for the specific detection on D-transition metal ions and their various applications, *J. Environ. Chem. Eng.* 11 (3) (2023) 109701, <https://doi.org/10.1016/j.jece.2023.109701>.
- S. Mohamad Reza Nazifi, H. Sadeghi-aliabadi, A. Fassihi, L. Saghale, Structure-activity relationship of polyamine conjugates for uptake via polyamine transport system, *Struct. Chem.* 30 (1) (2019) 175–184.
- I.G. Tucker, Drug delivery to the brain via the blood-brain barrier: a review of the literature and some recent patent disclosures, *Ther. Deliv.* 2 (3) (2011) 311–327, <https://doi.org/10.4155/tde.11.3>.
- M. Yu, S. Ast, Q. Yu, A.T.S. Lo, R. Flehr, M.H. Todd, P.J. Rutledge, Incorporating a piperidinyl group in the fluorophore extends the fluorescence lifetime of click-derived cyclam-naphthalimide conjugates, *PLoS ONE* 9 (7) (2014) 100761, <https://doi.org/10.1371/journal.pone.0100761>.
- A. Kamal, B.S.N. Reddy, G.S.K. Reddy, G. Ramesh, Design and synthesis of C-8 linked pyrrolobenzodiazepine-naphthalimide hybrids as anti-tumour agents, *Bioorg. Med. Chem. Lett* 12 (15) (2002) 326–334, [https://doi.org/10.1016/S0960-894X\(02\)00326-8](https://doi.org/10.1016/S0960-894X(02)00326-8).
- C. Geraghty, C. Wynne, R.B.P. Elmes, 1,8-Naphthalimide based fluorescent sensors for en-zymes, *Coord. Chem. Rev.* 437 (2021) 213713, <https://doi.org/10.1016/j.ccr.2020.213713>.
- T.B. Wei, H.Q. Dong, X.Q. Ma, Q.Y. Yang, Y.F. Zhang, Y.J. Sun, Q. Lin, 1,8-Naphthalimide-based fluorescent chemosensors: recent advances and perspectives, *J. Mater. Chem. C* 8 (39) (2020) 13501–13529, <https://doi.org/10.1039/D0TC03681A>.
- S. Kagitkar, D. Sunil, A systematic review on 1,8-naphthalimide derivatives as emissive materials in organic light-emitting diodes, *J. Mater. Sci.* 57 (2020) 105–139, <https://doi.org/10.1007/s10853-021-06602-w>.
- M.D. Tomczyk, K.Z. Walczak, 1,8-Naphthalimide based DNA intercalators and anticancer agents. A systematic review from 2017, *Eur. J. Med. Chem.* 159 (2007) (2007) 363–422, <https://doi.org/10.1016/j.ejmech.2018.09.055>.
- S. Banerjee, E.B. Veale, C.M. Phelan, S.A. Murphy, G.M. Tocci, L.J. Gillespie, D.O. Primannsson, J.M. Kelly, T. Gunnlaugsson, Recent advances in the development of 1,8-naphthalimide based DNA targeting binders, anticancer and fluorescent cellular imaging agents, *Chem. Soc. Rev.* 42 (4) (2013) 1601.
- J.C. Dalton, F.C. Montgomery, Solvent effects on thioxanthone fluorescence, *J. Am. Chem. Soc.* 96 (19) (1974) 6230–6232, <https://doi.org/10.1021/ja00826a072>.
- C.N. Dansholm, A.K.R. Junker, L.G. Nielsen, N. Kofod, R. Pal, T.J. Sørensen,  $\pi$ -Expanded thioxanthenes – engineering the triplet level of thioxanthone sensitizers for lanthanide-based luminescent probes with visible excitation, *ChemPlusChem* 84 (12) (2019) 1778–1788, <https://doi.org/10.1002/cplu.201900309>.
- N.F. Nikitas, P.L. Gkizis, C.G. Kokotos, Thioxanthone: A powerful photocatalyst for organic reactions, *Org. Biomol. Chem.* 19 (24) (2021) 5237–5253, <https://doi.org/10.1039/d1ob00221j>.
- Z. Xu, K. Guo, J. Yu, H. Sun, J. Tang, J. Shen, M. Yin, A unique perylene-based DNA intercalator: localization in cell nuclei and inhibition of cancer cells and tumors, *Small* 10 (20) (2014) 4087–4092, <https://doi.org/10.1002/sml.201401262>.
- Z. Xu, W. Cheng, K. Guo, J. Yu, J. Shen, J. Tang, M. Yin, Molecular size, shape, and electric charges: essential for perylene bisimide-based DNA intercalator to localize in cell nuclei and inhibit cancer cell growth, *ACS Appl. Mater. Interfaces* 7 (18) (2015) 9784–9791, <https://doi.org/10.1021/acsami.5b01665>.
- R.A. Gardner, J.G. Delcros, F. Konate, F. Breitbeil, B. Martin, M. Sigman, M. Huang, N1-substituent effects in the selective delivery of polyamine conjugates into cells containing active polyamine transporters, *J. Med. Chem.* 47 (24) (2004) 6055–6069, <https://doi.org/10.1021/jm0497040>.
- C. Wang, J.G. Delcros, J. Biggerstaff, O. Phanstiel, Molecular requirements for targeting the polyamine transport system: synthesis and biological evaluation of polyamineanthracene conjugates, *J. Med. Chem.* 46 (13) (2003) 2672–2682, <https://doi.org/10.1021/jm020598g>.
- C. Wang, J.G. Delcros, L. Cannon, F. Konate, H. Carias, J. Biggerstaff, R.A. Gardner, O. Phanstiel, Defining the molecular requirements for the selective delivery of polyamine conjugates into cells containing active polyamine transporters, *J. Med. Chem.* 46 (24) (2003) 5129–5138, <https://doi.org/10.1021/jm030223a>.
- O. Phanstiel, N. Kaur, J.G. Delcros, Structure-activity investigations of polyamine-anthracene conjugates and their uptake via the polyamine transporter, *Amino Acids* 33 (2) (2007) 305–313, <https://doi.org/10.1007/s00726-007-0527-y>.
- N. Cao, S.S. Feng, Doxorubicin conjugated to D- $\alpha$ -tocopheryl polyethylene glycol 1000 succinate (TPGS): conjugation chemistry, characterization, in vitro and in vivo evaluation, *Biomaterials* 29 (28) (2008) 3856–3865, <https://doi.org/10.1016/j.biomaterials.2008.05.016>.
- B. Verdejo, M. Inclán, M.P. Clares, I. Bonastre-Sabater, M. Ruiz-Gasent, E. García-España, Fluorescent chemosensors based on polyamine ligands. A review, *Chemosensors* 10 (1) (2022) 1, <https://doi.org/10.3390/chemosensors10010001>.
- G.W. Gokel, Lariat ethers: from simple sidearms to supramolecular systems, *Chem. Soc. Rev.* 21 (1) (1992) 39–47, <https://doi.org/10.1039/CS9922100039>.
- J. Li, D. Yim, W.D. Jang, J. Yoon, Recent progress in the design and applications of fluorescence probes containing crown ethers, *Chem. Soc. Rev.* 46 (9) (2017) 2437–2458, <https://doi.org/10.1039/C6CS00619A>.
- M. D. Tomczyk, N. Kuźnik, K. Walczak, Cyclen-based artificial nucleases: Three decades of development (1989–2022). Part a – Hydrolysis of phosphate esters, *Coord. Chem. Rev.* 481 (2023) 215047, <https://doi.org/10.1016/j.ccr.2023.215047>.
- R.R. Hendrixson, M.P. Mack, R.A. Palmer, A. Ottolenghi, R.G. Ghirardelli, Oral toxicity of the cyclic polyethers-12-crown-4, 15-crown-5, and 18-crown-6- in mice, *Toxicol. Appl. Pharmacol.* 44 (2) (1978) 263–268, [https://doi.org/10.1016/0041-008X\(78\)90188-6](https://doi.org/10.1016/0041-008X(78)90188-6).

- [31] N. Umezawa, Y. Horai, Y. Imamura, M. Kawakubo, M. Nakahira, N. Kato, A. Muramatsu, Y. Yoshikawa, K. Yoshikawa, T. Higuchi, Structurally diverse polyamines: solid-phase synthesis and interaction with DNA, *ChemBioChem* 16 (12) (2015) 1811–1819, <https://doi.org/10.1002/cbic.201500121>.
- [32] A. Dobrovolskaite, R.A. Gardner, J.G. Delcros, O. Phanstiel, Development of polyamine lassos as polyamine transport inhibitors, *ACS Med. Chem. Lett.* 13 (2) (2022) 319–326, <https://doi.org/10.1021/acsmchemlett.1c00557>.
- [33] M.J. Calverley, J. Dale, 1,4,7-Trioxa-10-azacyclododecane and some N-substituted derivatives; synthesis and cation complexing, *Acta Chem. Scand. B* 36b (1982) 241–247, <https://doi.org/10.3891/acta.chem.scand.36b-0241>.
- [34] H. Wutzel, M. Jarvid, J.M. Bjuggren, A. Johansson, V. Englund, S. Gubanski, M.R. Andersson, Thioxanthone derivatives as stabilizers against electrical breakdown in cross-linked polyethylene for high voltage cable applications, *Polym. Degrad. Stab.* 112 (2015) 63–69.
- [35] Y.S. Kurniawan, K.T.A. Priyanga, Jumina, H.D. Pranowo, E.N. Sholikhah, A.K. Zulkarnain, H.A. Fatimi, J. Julianus, An update on the anticancer activity of xanthone derivatives. A review, *Pharmaceuticals* 14 (11) (2021) 1144, <https://doi.org/10.3390/ph14111144>.
- [36] M.D. Tomczyk, A. Byczek-Wyrostek, K. Strama, M. Wawszkó, P. Kasprzycki, K.Z. Walczak, Anticancer activity and topoisomerase II inhibition of naphthalimides with  $\omega$ -hydroxylalkylamine side-chains of different lengths, *Med. Chem.* 15 (5) (2019) 550–560, <https://doi.org/10.2174/1573406414666180912105851>.
- [37] S. Tan, D. Sun, J. Lyu, X. Sun, F. Wu, Q. Li, Y. Yang, J. Liu, X. Wang, Z. Chen, H. Li, X. Qian, Y. Xu, Antiproliferative and apoptosis-inducing activities of novel naphthalimide-cyclam conjugates through dual topoisomerase (Topo) I/II inhibition, *Bioorg. Med. Chem.* 23 (17) (2015) 5672–5680, <https://doi.org/10.1016/j.bmc.2015.07.011>.
- [38] S.G. König, R. Krämer, Polyamine-modified near-infrared cyanine dyes for targeting the nuclei and nucleoli of cells, *Dyes Pigm.* 145 (2017) 80–94, <https://doi.org/10.1016/j.dyepig.2017.05.041>.
- [39] B. Nordén, F. Tjerneld, Structure of methylene blue–DNA complexes studied by linear and circular dichroism spectroscopy, *Biopolymers* 21 (9) (1982) 1713–1734, <https://doi.org/10.1002/bip.360210904>.
- [40] X.B. Fu, D.D. Liu, Y. Lin, W. Hui, Z.W. Mao, X.Y. Le, Water-soluble DNA minor groove binders as potential chemotherapeutic agents: synthesis, characterization, DNA binding and cleavage, antioxidation, cytotoxicity and HSA interactions, *Dalton Trans.* 43 (23) (2014) 8721–8737, <https://doi.org/10.1039/C3DT53577K>.
- [41] L. Gopala, Y. Cha, M.H. Lee, Versatile naphthalimides: their optical and biological behavior and applications from sensing to therapeutic purposes, *Dyes Pigm.* 201 (2022) 110195, <https://doi.org/10.1016/j.dyepig.2022.110195>.
- [42] N.B. Morozova, M.A. Pavlova, A.D. Plyutinskaya, A.A. Pankratov, K.T. Efendiev, A.S. Semkina, O.A. Fedorova, Photodiagnosis and photodynamic effects of bacteriochlorin-naphthalimide conjugates on tumor cells and mouse model, *J. Photochem. Photobiol. B* 223 (2021) 112294, <https://doi.org/10.1016/j.jphotobiol.2021.112294>.
- [43] V.N. Nguyen, S. Qi, S. Kim, N. Kwon, G. Kim, Y. Yim, J. Yoon, An emerging molecular design approach to heavy-atom-free photosensitizers for enhanced photodynamic therapy under hypoxia, *J. Am. Chem. Soc.* 141 (41) (2019) 16243–16248, <https://doi.org/10.1021/jacs.9b09220>.
- [44] V.N. Nguyen, G. Baek, S. Qi, S. Heo, Y. Yim, J. Yoon, A lysosome-localized thionaphthalimide as a potential heavy-atom-free photosensitizer for selective photodynamic therapy, *Dyes Pigm.* 177 (2020) 108265, <https://doi.org/10.1016/j.dyepig.2020.108265>.
- [45] T. Ihara, S. Sueda, A. Inenaga, R. Fukuda, M. Takagi, Synthetic DNA ligands conjugated with metal binding moiety. regulation of the interaction with DNA by metal ions and the ligand effect on metal assisted DNA cleaving, *J. Supramol. Chem.* 8 (2) (1997) 93–111, <https://doi.org/10.1080/10610279708233974>.
- [46] R. Fukuda, S. Takenaka, M. Takagi, Metal ion assisted DNA-intercalation of crown ether-linked acridine derivatives, *J. Chem. Soc., Chem. Commun.* 15 (1990) 1028–1030, <https://doi.org/10.1039/C39900001028>.
- [47] A. Basac, H. Dugas, Design and synthesis of DNA intercalating crown ether molecules, *Tetrahedron Lett.* 27 (1) (1986) 3–6, [https://doi.org/10.1016/S0040-4039\(00\)83924-6](https://doi.org/10.1016/S0040-4039(00)83924-6).
- [48] Z.J. Leśnikowski, E. Paradowska, A.B. Olejniczak, M. Studzińska, P. Seekamp, U. Schüssler, D. Gabel, R.F. Shinazi, J. Plešek, Towards new boron carriers for boron neutron capture therapy: metallacarboranes and their nucleoside conjugates, *Bioorg. Med. Chem.* 13 (13) (2005) 4168–4175, <https://doi.org/10.1016/j.bmc.2005.04.042>.
- [49] P. Sestili, The fast-halo assay for the assessment of DNA damage at the single-cell level, *Methods Mol. Biol.* 521 (2009) 517–533, [https://doi.org/10.1007/978-1-60327-815-7\\_30](https://doi.org/10.1007/978-1-60327-815-7_30).

## **Publikacja P.5**

1,8-Naphthalimide based DNA intercalators and anticancer agents. A systematic review from 2007 to 2017

**Tomczyk, M. D.; Walczak, K. Z.\***

*Medicinal Chemistry* **2018**, *159*, 393–422.



## Review article

# 1,8-Naphthalimide based DNA intercalators and anticancer agents. A systematic review from 2007 to 2017

Mateusz D. Tomczyk, Krzysztof Z. Walczak\*

Department of Organic Chemistry, Bioorganic Chemistry and Biotechnology, Silesian University of Technology, B. Krzywoustego 4, 44-100, Gliwice, Poland

## ARTICLE INFO

## Article history:

Received 10 April 2018

Received in revised form

17 September 2018

Accepted 20 September 2018

Available online 24 September 2018

## Keywords:

1,8-Naphthalimides

DNA intercalators

Amonafide

Mitonafide

Anticancer agents

## ABSTRACT

In this review, we describe a detailed investigation about the structural variations and relative activity of 1,8-naphthalimide based intercalators and anticancer agents. The 1,8-naphthalimides binds to the DNA via intercalation, and exert their antitumor activities through Topoisomerase I/II inhibition, photoinduced DNA damage or related mechanism. Here, our discussion focused on works published over the last ten years (2007–2017) related to therapeutic applications, in the order of cancer treatment followed by other properties of 1,8-naphthalimides. In preparing for this review, we considered that several seminal reviews have appeared over the last fifteen years and focused on closely related subjects, however, none of them is exhaustive.

© 2018 Elsevier Masson SAS. All rights reserved.

## Contents

1. Introduction .....	393
2. 1,8-Naphthalimide intercalators .....	394
2.1. Mono-intercalators .....	394
2.2. Fused-ring-extended 1,8-naphthalimides .....	402
2.3. 1,8-Naphthalimides as photonucleases .....	404
2.4. Bifunctional 1,8-naphthalimide conjugates .....	406
2.5. Organometallic complexes .....	413
3. Conclusions and perspectives .....	417
Supplementary data .....	418
References .....	418

## 1. Introduction

In this review, we will focus on small polyaromatic molecules that bind with double stranded DNA (ds-DNA) by intercalating between adjacent base pairs, thereby altering the DNA backbone conformation and also interfering with DNA-protein interaction. DNA is considered to be one of the most important target for the development of new chemotherapeutic drugs, which can change

DNA conformation and inhibit duplication or transcription, and thus inhibit cancer cell growth. There are three major ways for reversible binding of small molecules with ds-DNA, which are significantly different: (i) interactions with anionic backbone of DNA (which are generally nonspecific), (ii) interactions with the edges of base-pairs in either of the (major or minor) grooves of DNA, and (iii) intercalation of planar polyaromatic ring system between stacked base pairs. In fact, this classification for DNA interactive compounds is somewhat simple and schematic since the most known intercalators contain non-intercalating moieties (e.g. sugars, peptides). The non-intercalative moieties placed in the major or minor groove contribute to complex stabilization.

\* Corresponding author.

E-mail address: [krzysztof.walczak@polsl.pl](mailto:krzysztof.walczak@polsl.pl) (K.Z. Walczak).

Intercalators are generally grouped into three major classes: (i) classical intercalators, (ii) threading intercalators and (iii) multifunctional intercalators (Fig. 1). Details of interaction processes as well as structural requirements of intercalators are now well understood and have been extensively reviewed [1–3].

Though there is a relationship between cytotoxic activity and the DNA-intercalator complex stability, biological activity is not only result of intercalation binding energy to *ds*-DNA; there are many noncytotoxic intercalators which strongly bind with DNA. Formation of a DNA-intercalator complex is often a necessary first step in the whole process that underline cytotoxicity. Since intercalators do not cause strand breaks in purified DNA [4], it was suggested that the double-strand breaks (DSBs) observed in cellular DNA may result from the action of enzymes responding to topological perturbations of DNA caused by intercalation [5–7]. To be effective, an intercalator must poison Topo II, an enzyme responsible for maintaining the correct topological properties of DNA in cells, by stabilizing the ternary DNA-intercalator-Topo complex. Finally, once the ternary complex forms, interference of the intercalator molecule with Topo II initiates DNA damage, e.g. protein associated DNA double-strand breaks, correlates with cytotoxicity [6,7].

Here, our discussion focuses on articles and patents published between 2007 and 2017 with special attention paid to selectivity and structure-activity relationships of 1,8-naphthalimides. Most of these compounds have been well-described as DNA intercalating agents; however, there are several reports of anticancer activity which lack information regarding the specific mode of action, in particular whether it is an intercalation into DNA. Because these compounds displayed a high degree of structural similarities it is often assumed that they have a similar mechanism of action; this review attempts to summarize also such reports.

## 2. 1,8-Naphthalimide intercalators

### 2.1. Mono-intercalators

In the early 1970s, the team of Brana published the first series of 1,8-naphthalimides **1a-d** possessing good cytotoxicity towards HeLa and KB cancer cells (Fig. 2) [8–10]. Later, several series of 1,8-naphthalimide derivatives with different substituents at the *N*-imide and C3 positions were synthesized and extensive SAR studies were performed in order to investigate the substituents effects [11–13]. Studies revealed that the presence of a terminal amine functionality in the *N*-imide side chain was important and greatly increased the cytotoxicity of these compounds. Specific substituent types on the naphthalic ring also might increased the cytotoxicity; for example, 3-amino, 3-nitro or 3-methoxy groups gave the best



Fig. 1. Different types of intercalators: (left) classical mono-intercalator with positively charged side chain(s), (center) threading intercalator with groove-binding moieties and (right) multifunctional intercalator with side chain covalently attached to DNA.

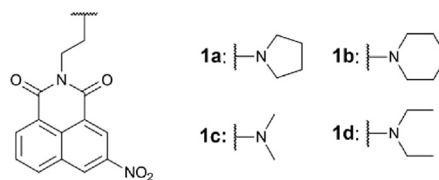


Fig. 2. First 1,8-naphthalimides obtained by Brana.

results. Activity was maximized when the amino group in side chain was two to three methylene groups from the 1,8-naphthalimide unit. Moreover, substitution at the C3 position of the naphthalic ring instead of C2 or C4 gave optimal results. According to the CPK model, the 3-nitro group lies in or nearer to the naphthalic ring plane compared with a more sterically hindered nitro group at the C4 position which rotates out of the plane [14]. This structure difference helps explain the stronger binding of the 3-nitro relative to the 4-nitro-1,8-naphthalimide derivatives with DNA [15].

Two of these compounds, Amonafide and Mitonafide (Fig. 3) have entered phase II clinical trials. Amonafide showed activity towards breast and prostate cancer [16,17]. Amonafide acts as a Topo II poison by perturbing the cleavage-religation equilibrium, which results in accumulation of DNA-Topo II covalent adducts [18]. Arresting the religation step after DNA cleavage generates of double-strand breaks. Similarly, Mitonafide primarily targets DNA; this compound shows DNA synthesis inhibitory activity and induces Topo II mediated DNA DSBs [19].

Despite its activity, Amonafide is no longer in clinical trials because of unpredicted toxicity caused by one of its metabolite, *N*-acetyl-amonafide (Fig. 4) Metabolite production by *N*-acetyltransferase 2 was the major determinant of myelosuppression in individuals with a fast acetylator phenotype [20,21]. Generally, slow acetylators, where drugs may accumulate in cells, are more likely to suffer and die due to adverse drug effects. The opposite situation was observed for Amonafide; this was due to impaired CYP1A2-mediated oxidation in fast acetylators. *In vitro* studies demonstrated that Amonafide undergoes CYP1A2 oxidation to *N*-oxide-amonafide and toxicity appears when the *N*-acylated metabolite inhibits CYP1A2 metabolism [22]. The mechanism through which Amonafide exerts its cytotoxic activity has been extensively revived [23].

The 1,8-naphthalimide derivatives synthesized before 2007 were described in 2001 by Brana et al. [24]. In the last few years, several other reviews have appeared. Since the subject has been widely reviewed by Kiss et al. in 2009, only the salient features of that work will be mentioned here [25]. The same year Xu et al. published a similar review focused on SAR studies with mono- and some examples of bis-intercalators [26]. In 2013 Kelly et al. reviewed 1,8-naphthalimide based intercalators and fluorescent cell imaging dyes [27]. In 2013 Kamal et al. reviewed numerous important patents published from 2006 to 2011 which focused on

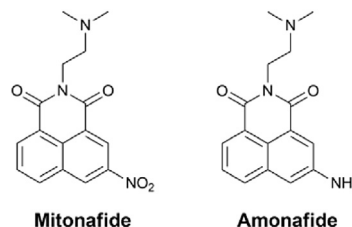


Fig. 3. Structure of mitonafide and amonafide.



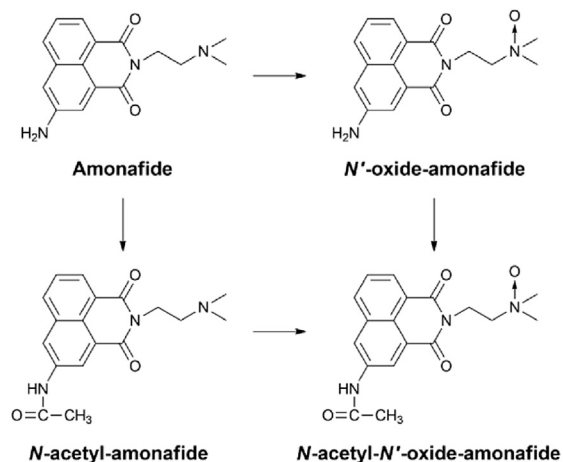


Fig. 4. Biotransformation pathways of Amonafide in humans.

1,8-naphthalimides as potential cancer therapeutics [28]. In 2016, Gellerman summarized recent developments in the synthesis and SAR studies of Amonafide derivatives [29].

In 2007 Quaquebeke et al. develop five groups of derivatives by modifying the 3-amine group of Amonafide (Fig. 5) [30]. As discussed above, clinical studies showed that due to presence of free amine group Amonafide is converted to *N*-acetyl derivative. To improve its activity and to avoid the metabolism that provoke the hematotoxicity such groups as amides (2a–k), ureas (3a–j), thioamides (4a–d), amines (5a–g), and imines (6a–g) were tested. The most active compound 7 showed a 4-fold higher maximum tolerated dose compared with Amonafide and did not provoke hematotoxicity in mice at doses that exhibited potent antitumor effects. Interestingly, compound 7 demonstrates 5-fold weaker intercalating strength than Amonafide, it does not seem to be a Topo II poison, it is however, able to inhibit its strand-passage activity. Most compounds from this series showed potent *in vivo* anticancer activity against different human cancer cell lines.

A detailed analysis of the mechanism of action revealed that compound 7 rapidly hydrolyzes to unsubstituted urea 8 (Fig. 5) without formation of Amonafide [31]. Compound 8 showed pan-antagonist activity towards CXCL chemokine expression which has anticancer effects in PC-3 cell line. The mechanism in which compound 8 antagonizes CXCL chemokine expression remains unknown, but it does seem that this antagonism does not occur at the level of CXCL chemokine receptors.

In 2008 Antonini et al. reported a series of 1,8-naphthalimide derivatives 9a–m (Fig. 6) prepared to determine the effects of side chain modifications on biological activity and DNA binding [32]. All of these derivatives showed high antiproliferative activity with  $IC_{50} = 0.06–2.10 \mu M$  against the HT-29 cell line, with the exception of derivative 9l, which has the longest side chains and an amino group replacing the nitro group in the chromophore. The apparent

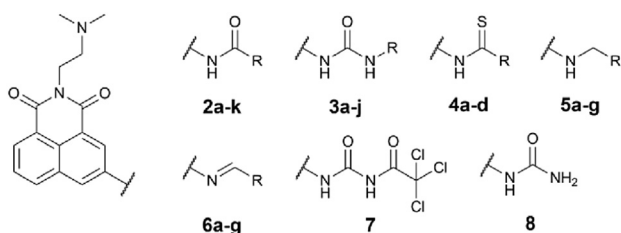


Fig. 5. 3-*N*-Substituted derivatives 2a–8.

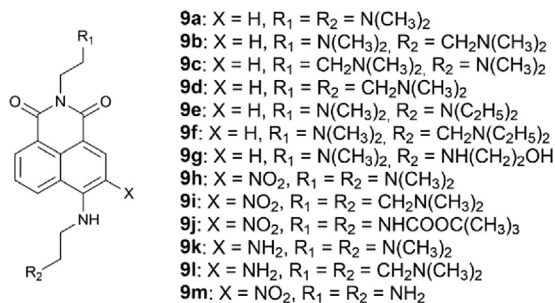


Fig. 6. 4,9-*N,N'*-Disubstituted 1,8-naphthalimides 9a–m.

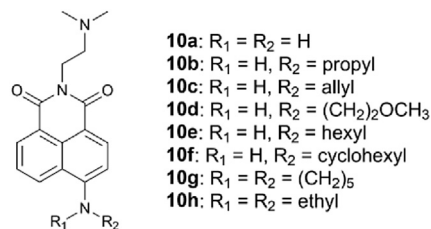


Fig. 7. 4-*N*-substituted derivatives 10a–h.

binding constant  $K_{app}^1 = 1.3–7.7 \times 10^7 M^{-1}$ , which indicated that these derivatives strongly bind to DNA; however, there is no simple linear correlation between anticancer activity and ability to bind to DNA. This study also demonstrated that a second side chain at C4 enhanced the anticancer activity despite the lack of a nitro group at the C3 position. Also, the nature of the side chain influenced activity; this effect is stronger in 9a–g without the nitro group. For 9h–m, the influence of the side chain had less of an impact on their cytotoxicity.

In 2008 Norton et al. synthesized compounds 10a–h (Fig. 7), possessing different aminoalkyl groups at the C4 position instead of the C3 position [33]. These derivatives (named Numonafides) had similar *in vitro* potency as Amonafide but interestingly were not *N*-acetylated by NAT2; therefore, they retain their anticancer activity and avoid toxic effects. These new derivatives showed activities on the order of  $10^{-6}$  to  $10^{-7} M$ , similar to Amonafide; however, they equal or even suppress the potency of inhibiting normal cells growth over cancer cells, this trend is most notable for the more hydrophobic derivatives 10e–g. Changes in hydro-philicity also led to changes in the subcellular location; while most of the derivatives were localized in the nucleus, the most hydrophobic derivatives 10e–h localized to cytoplasmic puncta. Although these derivatives intercalate into DNA, they do not stabilize *in vitro* DNA-Topo II cleavable complexes.

Qazi et al. patented a method of preparation of 11a–g (Fig. 8) and their usage in cancer treatment [34]. Derivatives 11b and 11f, both bearing nitro group at the C4 position showed the highest cytotoxicity ( $IC_{50} = 0.3–1.9 \mu M$ ) against HL-60 and U-937 cell lines. The major mode of cells death was shown to be apoptosis. However, the molecular interactions between these compounds and DNA were not clearly established.

In 2009 Xie et al. synthesized and evaluated a series of eight 3-

<sup>1</sup>  $K_{app}$ : Apparent binding constant is relative DNA binding affinity, which based on a competitive fluorometric ethidium bromide (EtBr) displacement method.  $K_{app(drug)} = C_{EtBr-DNA} / C_{50} \times K_{app(EtBr)}$ , where  $C_{EtBr-DNA}$  is concentration of EtBr in EtBr-DNA complex,  $C_{50}$  is concentration of drug that is required to reduce the fluorescence by 50%, and  $K_{app(EtBr)}$  is EtBr DNA binding constant taken as  $10^7 M^{-1}$ .

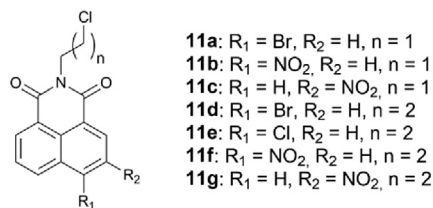


Fig. 8. 9-*N*-( $\omega$ -chloroalkyl)-1,8-naphthalimides **11a-g**.

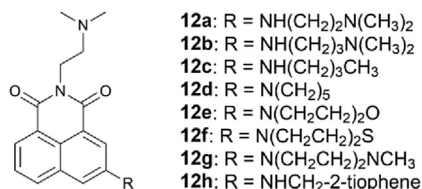


Fig. 9. 3-*N*-alkylated derivatives **12a-h**.

alkylamino substituted Amonafides (Fig. 9) [35]. Most of these compounds exhibited good cytotoxicity on the order of  $10^{-7}$  M; among them, **12a** and **12b** were the most active against the P388 and HeLa cells ( $IC_{50} = 0.23\text{--}0.83\ \mu\text{M}$ ). DNA-binding studies revealed that **12a-h** binding to DNA ( $K_b^2 = 0.79\text{--}2.48 \times 10^{-5}\ \text{M}^{-1}$ ) was comparable over Amonafide ( $K_b = 1.05 \times 10^{-5}\ \text{M}^{-1}$ ).

In the same year, Wu et al. synthesized a series of Amonafide derivatives **13a-b**, **14a-e** and **15a-c** to investigate their biological activities; these derivatives featured various linkers between the naphthalic ring and the terminal aryl groups (Fig. 10) [36]. Most of these compounds have antitumor activity similar to Amonafide ( $IC_{50}$  values in the range of 1.27 to over  $50\ \mu\text{M}$ ). Moreover, the same authors showed that **15a** can induce G<sub>2</sub>/M phase cell cycle arrest by inhibiting the PI3 K/Akt signaling pathway and had a potent effect on Topo II and led to DNA DSBs [37]. Compound **15a** caused a decrease in the level of Cyclin B1 and Cdk1 and induced cell cycle arrest and apoptosis in p53 and NH- $\kappa$ B in an independent manner.

Qian et al. developed two sets of conjugates **16a-c** and **17a-c** with a L-leucine moiety (Fig. 11) [38]. *In vitro* studies showed moderate to good antitumor activity against A-375, A-549, P388, HL-60, MCF-7, HCT 8 and HeLa cell lines with  $IC_{50}$  values from 6.51 to over  $50\ \mu\text{M}$ . Generally, compounds **16a-c**, with a diamine backbone at the C4 position showed better cytotoxic activity and DNA intercalating abilities than **17a-c**. Compound **16c** exhibited the highest cytotoxic activities and the association constant with ct-DNA was  $K_a = 4.92 \times 10^{-4}\ \text{M}^{-1}$ .

In 2010, Mukherje et al. reported a series of derivatives **18a-j** with an *N*-( $\omega$ -hydroxyalkyl) chains of various lengths (Fig. 12) [40,41]. They are structurally similar to the previously described derivatives **11a-11g**. *In vitro* studies on HL-60 and U-937 cells revealed no significant differences in cytotoxic activities among derivatives with a terminal -Cl and -OH group. The more active compounds **11b**, **11f** ( $IC_{50} = 0.3\text{--}1.95\ \mu\text{M}$ ) and corresponding compounds **18d** and **18i** ( $IC_{50} = 0.7\text{--}1.8\ \mu\text{M}$ ) exhibited almost identical cytotoxicities. A cell cycle analysis of **18i** showed a rise in G1 fraction, which suggest that it affects the DNA duplication before

mitosis. It was proved by inhibition of H<sup>3</sup>-uridine uptake in S-180 cells, which imply suppression of DNA synthesis.

Qian and co. designed and evaluated **19a-l** (Fig. 13), built up from long alkyl chains and weakly basic tertiary amines to make these derivatives similar to lysosomotropic detergents possesses potent anticancer activities [42]; they are well-known as LMP-inducing (Lysosomal Membrane Permeabilization) agents and are in preclinical trials [43]. Most of the compounds from series **19a-l** displayed moderate activities ( $IC_{50} = 2.41\text{--}46.43\ \mu\text{M}$ ) comparable to Amonafide, but with a distinct mode of action. These compounds were weak DNA binders; however, they were able to inhibit Topo II modestly. Antiproliferative activity was correlated with ability to induce LMP. The more active **19a-d**, with the polyamine chain at *N*-imide position, induced LMP. It is worth mentioning that, in contrast to **19a-d**, compounds with the polyamine chain at the C4 position, **19e-h**, showed much weaker LMP induction.

A series of 1,8-naphthalimide derivatives **20a-e** with various 4-(*N*-( $\omega$ -hydroxyalkylamine) substituents (Fig. 14) were studied using fluorescence spectroscopy ( $K_{SV} = 1.15\text{--}7.12 \times 10^3\ \text{M}^{-1}$ ), UV-Vis ( $K_b = 0.74\text{--}1.44 \times 10^4\ \text{M}^{-1}$ ), CD technique and thermal denaturation experiments ( $\Delta T_m = 2.6\text{--}3.8\ ^\circ\text{C}$ ) [44]. Compounds **20a-e** were tested for their anticancer activity against Bel-7402 and HL-60 cell lines ( $IC_{50} = 5.57\text{--}38.53\ \mu\text{M}$ ). Results suggested a relationship between side chain elongation and cytotoxicities. The activities of compounds with short side chain, **20a** and **20b**, was weaker than the activities of compounds **20c** and **20d** with longer side chains. However, when 6-hydroxyaminohexyl was a C4 substituent, the activity of compound **20e** decreased.

The series of 3-aryl and 3-(2-hetaryl) substituted compounds **21a-g** was prepared via a Suzuki coupling reaction and evaluated for their anticancer activities (Fig. 15) [45,46]. It was postulated that electron-withdrawing groups attached to naphthalic ring may improve binding with DNA and thus anticancer activity. *In vitro* activity of these compounds showed cytotoxicity similar ( $IC_{50} = 3.70\text{--}6.04\ \mu\text{M}$ ) to that of Amonafide ( $IC_{50} = 6.45\ \mu\text{M}$ ) against the HeLa cells. The DNA-binding studies suggested that **21a-g** intercalate into DNA in different fashion with  $K_b$  values ranging from  $10.75\text{--}14.85 \times 10^5\ \text{M}^{-1}$ , stronger than its parent compound Amonafide ( $K_b = 1.05 \times 10^5\ \text{M}^{-1}$ ).

Sharma et al. reported a series of bioactive 1,8-naphthalimide derivatives modified by the introduction of isothiocyanate or carbamimidothioate groups on the terminal atom of the *N*-alkyl chains **22a-d** and **23a-b**, respectively (Fig. 16) [47]. Both series effectively induced apoptosis in UACC-903, A-375, 1205Lu and SK-MEL-37 human melanoma cell lines, with  $IC_{50}$  values in the range of 1.67–11.48  $\mu\text{M}$ , except for **23b** with  $IC_{50}$  values of 6.95–39.47  $\mu\text{M}$ . In addition, no adverse systemic toxicological changes were found. Generally, a slight increase in activity was observed with an extension of the *N*-alkyl side chain length and introduction of a nitro group at the 3-position for the series of isothiocyanates **22a-d**. Finally, it was shown that **22a-d** inhibited Akt pathway.

In 2012, the synthesis and biological activity of three series of 2-, 3- and 4-non-amino substituted derivatives **24a-n** (Fig. 17) were reported [48]. Studies with *S. cerevisiae* showed that these compounds produced DNA DSBs *in vitro* and *in vivo*. These compounds strongly bind to DNA via intercalation and inhibit Topo II activity at concentrations from 30 to 100  $\mu\text{M}$ . Generally, derivatives **24d-n** with a benzene ring at the C3 position exhibit higher antiproliferative activities than C2 and C4 substituted derivatives. The presence of electron-withdrawing group in the aryl moiety of **24h** and **24j** contributed to an activity increase (in both cases  $IC_{50} = 1.2\ \mu\text{M}$ ) against SKBR-3 cells. In contrast, the presence of a donor group with a hydrogen bond, **24i** and **24k**, leads to a decrease ( $IC_{50} = 4.4$  and  $14.2\ \mu\text{M}$  respectively) in its anticancer activity.

<sup>2</sup>  $K_b$ : Scatchard binding constant which was calculated based on the fluorescence or absorbance quenching techniques. The equilibrium between free and bound intercalator molecules is given by equation:  $r/C_f = Kn - Kr$ , where  $r$  is the ratio of bound intercalator per base,  $C_f$  is the free intercalator concentration,  $n$  is the number of binding sites per base and  $K$  is the intrinsic association constant to a site [39].

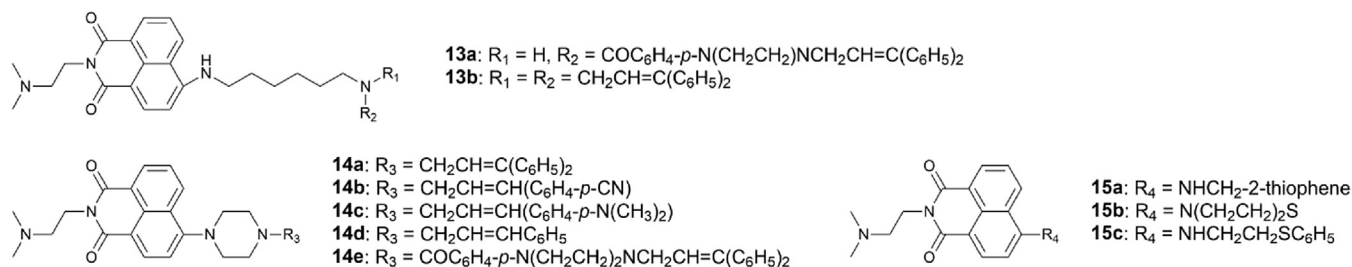


Fig. 10. 4-N-substituted derivatives 13a-b, 14a-e and 15a-c.

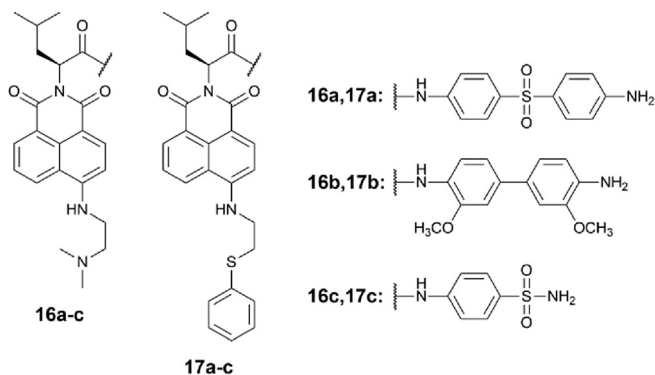


Fig. 11. Structures of derivatives 16a-c and 17a-c.

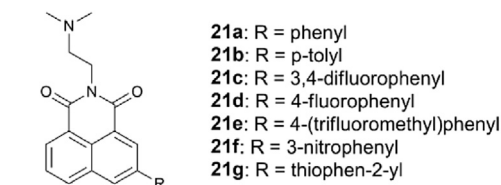


Fig. 15. 3-Aryl and 3-(2-hetaryl)-1,8-naphthalimides 21a-g.

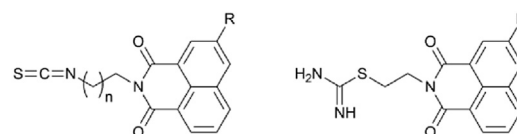


Fig. 16. Structures of compounds 22a-d and 23a-b.

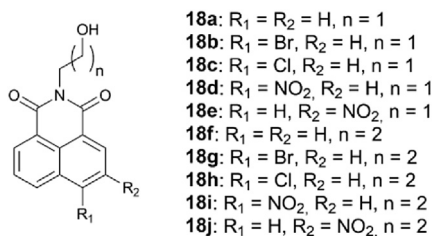
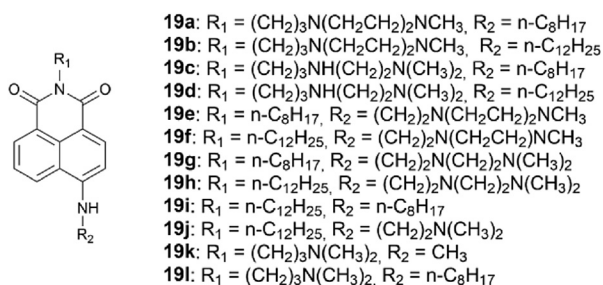
Fig. 12. 3,4-Disubstituted-9-N-( $\omega$ -hydroxyalkyl) derivatives 18a-j.

Fig. 13. 4,9-N,N'-Disubstituted derivatives 19a-l.

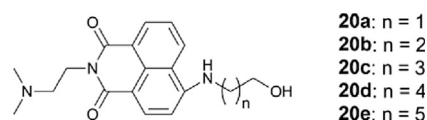
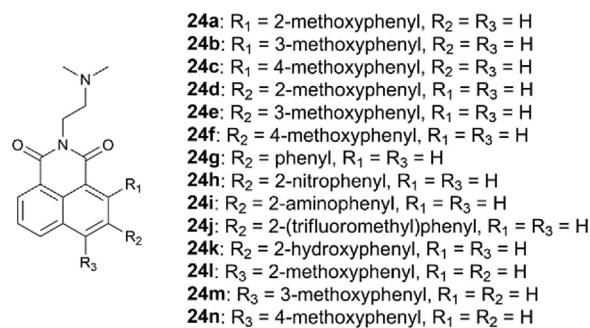
Fig. 14. 4-( $\omega$ -Hydroxyalkylamino)-1,8-naphthalimides 20a-e.

Fig. 17. Structures of compounds 24a-n.

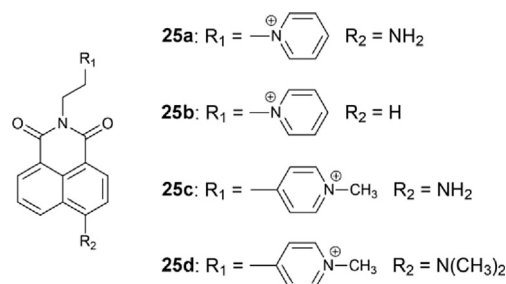


Fig. 18. 4-Pyridinium-1,8-naphthalimides 25a-d.

Kelly et al. reported the synthesis and evaluate DNA-binding of pyridinium derivatives **25a-d** (Fig. 18) [49,50]. Compared to unsubstituted **25b** ( $K_b = 2.0 \times 10^4 \text{ M}^{-1}$ ) [51], C4 amino derivatives possess higher binding affinity towards *st*-DNA (salmon testes DNA) with  $K_b$  ranging between  $1.38\text{--}1.85 \times 10^5 \text{ M}^{-1}$ . Compound **25c** showed the highest DNA-binding properties and showed an affinity six times larger towards AT-rich regions, as determined for [poly(dA-dT)]<sub>2</sub> ( $K_b = 5.15 \times 10^5 \text{ M}^{-1}$ ) than for [poly(dG-dC)]<sub>2</sub> ( $K_b = 0.82 \times 10^5 \text{ M}^{-1}$ ). The positively charged pyridinium moiety likely binds electrostatically within the groove and thus makes a significant contribution in the ligand binding process. This effect has been confirmed by increasing the ionic strength of the buffer, which caused a significant decrease of binding constant.

As structural analogues of compounds **20a-e**, which contain a flexible spacer, the same length of side chains and terminal free amino group, **26a-d** (Fig. 19), have shown slightly potent activity towards tested cell lines [52]. In this case, changing the hydroxyl group to an amino group did not induce significant improvement in the activity or DNA binding.

Amonafide derivatives **27a-h** (Fig. 20) acetylated by amino acids of different lengths and containing an additional terminal dichloroacetamide functionality were synthesized by Wang et al. [53]. Sodium dichloroacetate was shown to be promising drug to modulate cancer metabolic processes and reached phase II trials for the treatment of brain cancer. The results of antiproliferative trials using **27a-h** against cancer cells showed moderate activity towards HeLa ( $\text{IC}_{50} = 21.5\text{--}47.4 \mu\text{M}$ ), A-549 ( $\text{IC}_{50} = 4.7\text{--}28.1 \mu\text{M}$ ) and K-562 ( $\text{IC}_{50} = 8.5\text{--}60.5 \mu\text{M}$ ) cell lines. However, these activities were generally weaker than the respective activities of Amonafide. Fluorescence, CD and thermal denaturation studies have showed that compounds **27a-h** intercalate into *ct*-DNA with  $K_b = 1.15\text{--}5.1 \times 10^5 \text{ M}^{-1}$ .

In 2013, Seliga et al. reported a series of a 1,8-naphthalimide pyridine conjugates **28a-c** and **29a-c** (Fig. 21). These derivatives were evaluated against Jurkat, HeLa, MCF-7 and A-549 human cancer cell lines and showed activity almost exclusively against Jurkat (human leukemia) cells with  $\text{IC}_{50} = 5.58\text{--}11.02 \mu\text{M}$  [54]. Among them, only **28c** and **29a** exhibited activity against A-549 and MCF-7 cells with  $\text{IC}_{50} = 5.67\text{--}11.02 \mu\text{M}$ , while HeLa cells were resistant to these compounds. Interestingly, the apparent binding constant of **28c** ( $K_{\text{app}} = 3.1 \times 10^6 \text{ M}^{-1}$ ) indicates that these derivatives intercalate moderately.

In 2015 Luo et al. synthesized a series of 1,8-naphthalimides containing a 4-(2-mercaptobenzimidazolyl) substituents and *N*-(4-triazole or triazolium)butyl substituent (**30a-i**, **31a-h**, **32a-d** and **33a-d**; Fig. 22); these compounds were all tested for their antimicrobial activity [55]. Some earlier work of Li et al. indicated that an attachment of a 1,2,4-triazole moiety to the *N*-alkyl chain of 1,8-naphthalimides might contribute to enhance their activity against cancer cells [56]. UV-Vis and fluorescence quenching spectra suggested that cationic compound **31g** bind to DNA via intercalation; however, there is no data on the interaction of the rest of compounds with DNA. Compound **31g**, as well as other triazolium salts in the series also exhibited significantly higher antimicrobial activity against all tested bacteria strains with MIC ranging from 2 to 19  $\mu\text{g}/\text{mL}$ . Compared with them, the derivatives **30a-f** lacked a positively charged triazole moiety showed much

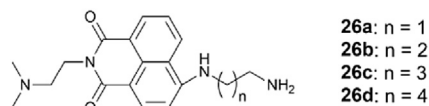


Fig. 19. 4-( $\omega$ -Aminoalkylamino)-1,8-naphthalimides **26a-d**.

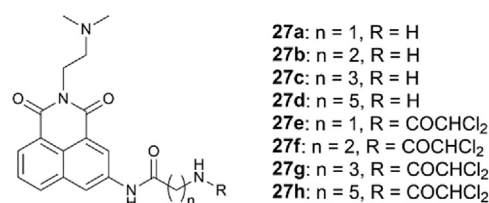


Fig. 20. 3-*N*-Acetylated derivatives **27a-h**.

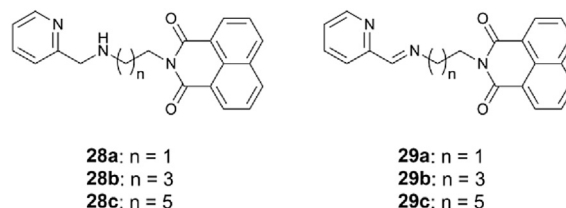


Fig. 21. 1,8-Naphthalimide pyridyl conjugates **28a-c** and **29a-c**.

lower activity with MIC value higher than 512  $\mu\text{g}/\text{mL}$ . The main reason triazolium salts exhibit significantly better activity than their precursor triazoles is due to the fact that the quaternization of help improve solubility and membrane permeability.

Li et al. synthesized a series of 4-pyrazolyl derivatives **34a-l** (Fig. 23) and evaluated their DNA-binding and cytotoxic activity [57]. These derivatives showed cytotoxicity ( $\text{IC}_{50} = 0.51\text{--}17.01 \mu\text{M}$ ) comparable to Amonafide ( $\text{IC}_{50} = 1.68\text{--}13.0 \mu\text{M}$ ) towards MCF-7, HeLa and A-549 cell lines. Among them, the most active derivative was **34j** containing 3,4,5-trimethoxyphenyl fragment. This derivative intercalate into *ct*-DNA ( $K_b = 1.01 \times 10^4 \text{ M}^{-1}$ ), an order of magnitude lower than Amonafide ( $K_b = 1.05 \times 10^5 \text{ M}^{-1}$ ).

Nyab et al. synthesized 1,8-naphthalimide based Schiff bases **35a-c** (Fig. 24) and evaluate their DNA-binding and free radical scavenging ability [58]. These compounds were shown to bind with *ct*-DNA via intercalative mode with the following binding constants ( $K_b$ ): **35a** ( $2.25 \times 10^4 \text{ M}^{-1}$ ), **35b** ( $3.33 \times 10^4 \text{ M}^{-1}$ ) and **35c** ( $2.0 \times 10^4 \text{ M}^{-1}$ ). Antioxidant evaluation by the hydrogen peroxide and DPPH assay revealed that all the tested compound showed scavenging activity. It was observed that **35b** has highest DPPH and hydroxyl radical scavenging activity with  $\text{IC}_{50}$  of 1.28 and 1.06  $\text{mg}/\text{mL}$ , followed by **35a** with  $\text{IC}_{50}$  at 1.43 and 1.17  $\text{mg}/\text{mL}$  respectively. The highest scavenging activity of compound **35b** can be attributed to the content of phenolic group, which is ideal donor of hydrogen to the radical. Compound **35c** with the lowest value of binding constant and scavenging activity, however, was found to be very promising antimicrobial agent. Among all the compounds screened, **35c** displayed significantly higher activity with MIC value as low as 0.031  $\text{mg}/\text{mL}$  against *E. coli* and 0.062  $\text{mg}/\text{mL}$  against both *S. typhimurium* and *S. aureus*. These results could be explained by the presence of additional methoxy group that causes an increase of lipophilicity, which enhances the transport into the lipid membrane and restricts further growth of the microorganism.

Zhou et al. studied the effect of an amino group exchange for guanidine group in the 1,8-naphthalimides **36a-e** (Fig. 25) [59]. Since the guanidine group possesses strong basicity and usually bears a positive charge, it is often introduced to the intercalators to enhance their binding properties towards DNA. Fluorescence titration showed that these compounds bind strongly with DNA; their binding affinities were compared with the concentration of *ds*-DNA needed to 50% of the maximal fluorescence decrease ( $\text{DC}_{50\text{DNA}}$ ). The DNA-binding decreases in strength in series **36e** > **36c** > **36a** > **36b** > **36d**. Their  $\text{IC}_{50}$  values against MCF-7 cells

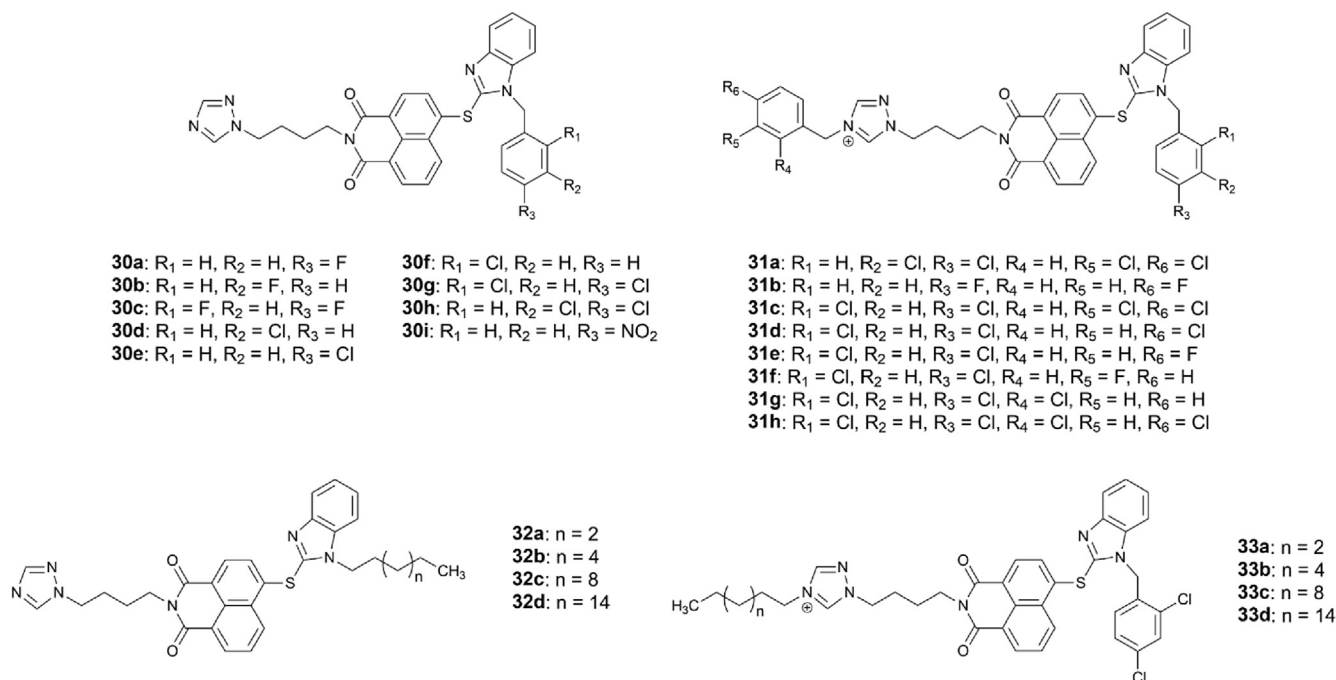


Fig. 22. Structures of triazole **30a-i**, **32a-d** and triazolium **31a-h**, **33a-d** derivatives.

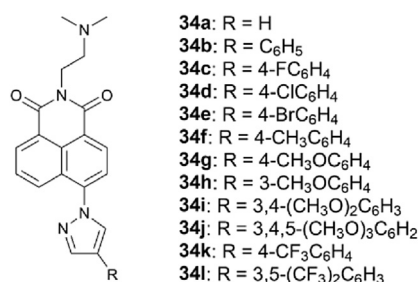


Fig. 23. 4-(Pyrazol-1-yl)-1,8-naphthalimides **34a-l**.

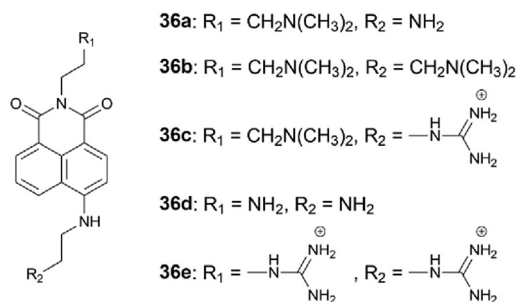


Fig. 25. 4,9-*N,N'*-Disubstituted derivatives **36a-e**.



Fig. 24. Schiff base containing derivatives **35a-c**.

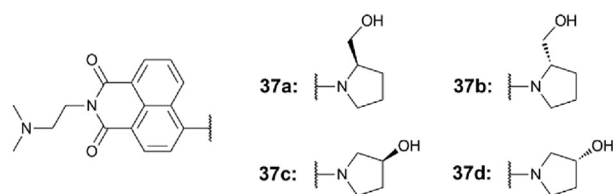


Fig. 26. 4-Pyrrolidine-1,8-naphthalimides **37a-d**.

were estimated to be  $2.04 \pm 0.02$ ,  $10.41 \pm 0.12$  and  $56.62 \pm 0.08 \mu M$  for **36b**, **36c** and **36a**, respectively, whereas compounds **36d** and **36e** were not cytotoxic. The presence of the guanidine groups in the side chain increased the binding ability with nucleic acids, however, did not favor cell permeability and cytotoxicity.

In 2014, Wang et al. reported derivatives **37a-d** modified with chiral pyrrolidinols. They showed significant *in vitro* cytotoxic activity against HeLa, MCF-7, SGC-7901 and A-549 ( $IC_{50} = 0.87-3.85 \mu M$ ) (Fig. 26) [60]. These compounds were shown to bind to *ct*-DNA by intercalation with  $K_b = 1.8-6.7 \times 10^4 M^{-1}$ . The *R/S* configuration of the pyrrolidine moiety did not show a definitive impact on their anticancer activity. The binding strength to DNA and cytotoxicity can be connected with the distance of hydroxyl group and pyrrolidine ring. Compounds **37c-d** are slightly more potent against cell lines tested than **37a-b** with a hydroxymethyl substituent.

In 2015, Verma et al. reported a series of derivatives disubstituted at the C4 position, **38a-n** (Fig. 27), incorporating a variety of substituents [61]. Thermal melting experiments demonstrated that these derivatives act as DNA intercalators and increased the melting temperature of DNA by as much as  $18.2^\circ C$ . The cytotoxicity results from NCI's *in vitro* screening panel revealed that only compounds substituted with cyclic amines, especially **38b**, showed significant anticancer activity. Compound **38b** exhibited inhibition towards more than 60% of all the cancer cell lines at a concentration of  $10 \mu M$ . Primary amines showed less than 40% of growth inhibition at this same concentration. Compound **38b** was also more potent than Oxaliplatin, an approved chemotherapeutic drug.

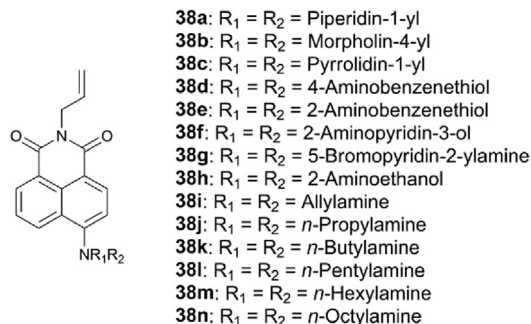


Fig. 27. 4-*N,N*-Disubstituted-9-(2-propenyl) derivatives **38a-n**.

Other derivatives with chiral configurations were obtained by Kokosza et al. Compounds **39a-40d** (Fig. 28) possessing *cis*- and *trans*-isoxazolidine moiety containing phosphonate group were joined by a carbamoyl linker to the 1,8-naphthalimide unit [62]. Earlier studies showed that isoxazolidines joined with substituted phenyls was able to suppress proliferation of three human cancer cell lines with IC<sub>50</sub> values in the range of 120–228 μM. These derivatives combined properties of two biologically active moieties (isoxazolidines and 1,8-naphthalimides) and were designed.

To receive conjugated drugs. It was interesting to check if variation in the chirality of the isoxazolidine moiety influenced the binding affinity to DNA. Compounds **39a-f** were active against a large variety of DNA and RNA viruses with moderate activity, while none of compounds **40a-d** were found to be active toward tested viruses, except for a weak activity against the *Punta Toro* strain. Among derivatives **39a-f**, *trans*-**39d** and *trans*-**39f** showed the highest activities with EC<sub>50</sub> values comparable to Ganciclovir (antiviral agent used as the reference compound). Moreover, the tested compounds were not cytotoxic towards HeLa cell line (in which the tested viruses were replicated) at concentrations up to 100 μM.

Noro et al. synthesized a number of 1,8-naphthalimides with structures **41a-47c** (Fig. 29) [63]. In these compounds, the side chain at *N*-imide position contain two to four carbon atoms and different terminal groups which include amino, imino, pyrrole, ureas and *p*-nitrobenzene. *In vitro* studies on different cell lines revealed that there is an indirect relationship between length of the chain and activity. For compounds **41a-c**, **43a-b** and **47a-c**, which bear amino, imino and triazole groups, derivatives with shorter chains showed higher cytotoxicity. Elongation of the side chains resulted in a loss of activity. However, a different trend was observed for compounds bearing a *p*-nitrobenzene. In this case,

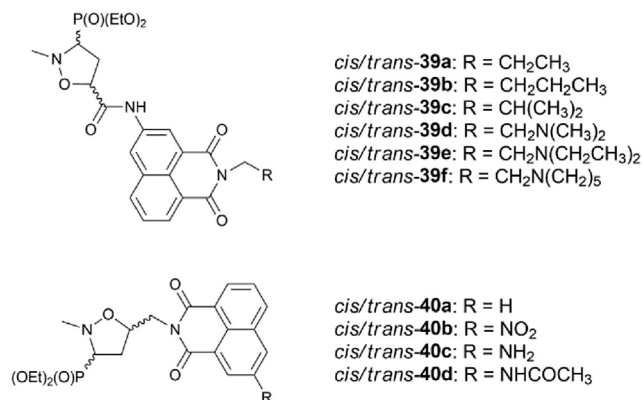


Fig. 28. Isoxazolidine containing derivatives **39a-f** and **40a-d**.

compounds contain four carbon atom chain were the most active against tested cell lines. Because of solubility limitations, it was not possible to determine IC<sub>50</sub> values for all compounds, but most active compounds showed IC<sub>50</sub> values from 2.44 to over 5 μM against CF-7 and HCT 15. In comparison with non-tumor cells, these compounds showed no cytotoxicities against BMMØ and THP1 cell lines even at relatively high concentrations (such as 10–50 μM).

Compounds **48a-t** (Fig. 30) are examples of derivatives where the aromaticity of the naphthalic ring is extended by the unfused aromatic conjugated system [64]. For this purpose, the naphthalic ring was substituted at the C4 position by an electron-donating 5-phenyl-pyrazol-1-yl fragment. Compounds **48a-t** are not fully planar; the pyrazole with benzene substituent deviates from the plane due to steric hindrance. *In vitro*, these derivatives showed cytotoxic activity against A-549, HeLa and MCF-7 cell lines with IC<sub>50</sub> values of 5.06–25.33 μM, comparable to Amonafide and cisplatin. Compounds **48o-t** containing two or three substituents showed lower cytotoxicity compared to compounds with only one substituent.

In 2016, Wang et al. obtained and evaluated a series of novel 1,8-naphthalimides **49a-e** (Fig. 31), which contained piperazine and piperidine ring [65]. It was found that, **49a** and **49b**, which contained a piperazine ring, binds stronger to DNA due to the additional nitrogen atom that contributed to the enhanced binding interaction with the backbone of DNA. Cytotoxic tests showed that the piperazine-modified derivatives, **49a** and **49b**, showed higher activity against HeLa, SGC-7901 and A-459 cell lines with IC<sub>50</sub> values lower than 7.0 μM, comparable to the control drug Amonafide. The interactions with *ct*-DNA by intercalation were confirmed by UV-Vis spectroscopy and binding constants were obtained as 0.47 to 3.8 × 10<sup>5</sup> M<sup>-1</sup>. Furthermore, the binding mode was also confirmed by 2D NOESY NMR spectroscopy, where clear NOE cross-peaks between the naphthalic protons and the protons of the nucleobases of DNA were observed.

Triazole derivatives have been studied extensively because of their ease of synthesis and promising biological activity. In 2016, Glowacka et al., inspired by some earlier studies, synthesized and

evaluated the antiviral activities and cytotoxicities of a thirty-six compound series, **50a-aj** (Fig. 32), contained both 1,2,3-triazole and phosphonate groups attached at the *N*-imide position of 1,8-naphthalimides [66]. Among them, derivatives having bromine atom at the C4 position were the most cytotoxic towards the four tested cell lines at concentrations as low as 14 μM. On the other hand, compounds having a free amine group at the C3 position were noncytotoxic (IC<sub>50</sub> > 250 μM) against all tested cell lines. Antiproliferative activity correlated well with antiviral activity; compounds with bromine atoms proved to be the most effective. Moreover, structural features of compounds **50a-aj** may suggest they primarily act as DNA intercalators as well as activation or termination of DNA synthesis agents.

Discussing the 1,8-naphthalimide based DNA intercalators, the 1,4,5,8-naphthalenediimide derivatives require mention; they are usually considered as G-quadruplex ligands [67,68], but are sometimes referred to as intercalators. Suseela et al. synthesized imidazolyl-naphthalenediimide “threading” intercalators, **51a-g**, with imidazole fragments on both sides of a naphthalenediimide moiety with variable linker lengths and charge on the imidazole ring (Fig. 33) [69]. The interaction of imidazolium cation, which works like groove binders, with the negatively charged backbone of DNA was designed to enhance enthalpy change, which in turn enhances DNA-binding affinity. Competitive binding analysis showed that **51d** and **51e** most significantly release DNA from their complexes with EtBr, indicating their higher DNA-binding affinity than this typical DNA intercalator. Similar behavior was observed for DNA-Hoechst complexes despite their different binding modes

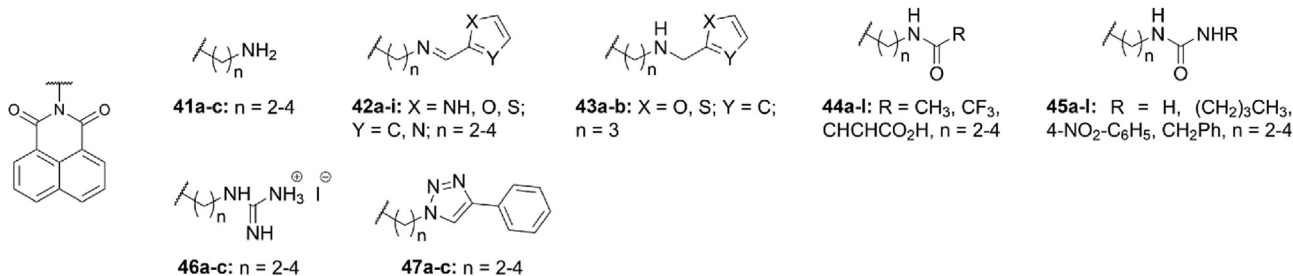


Fig. 29. Structures of compounds 41a–47c.

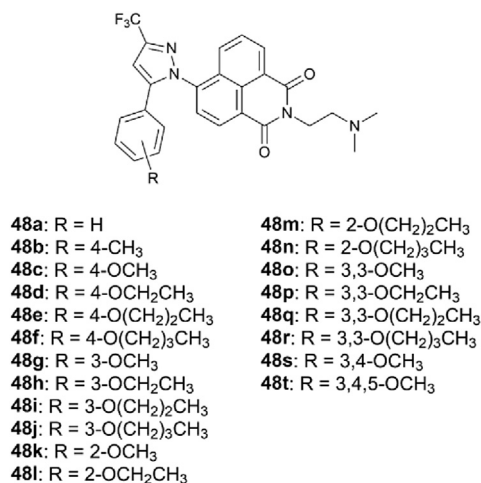


Fig. 30. 4-(Pyrazol-1-yl)-9-N-substituted derivatives 48a–t.

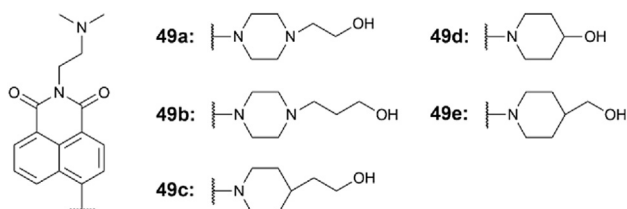


Fig. 31. 4-N-Substituted derivatives 49a–e.

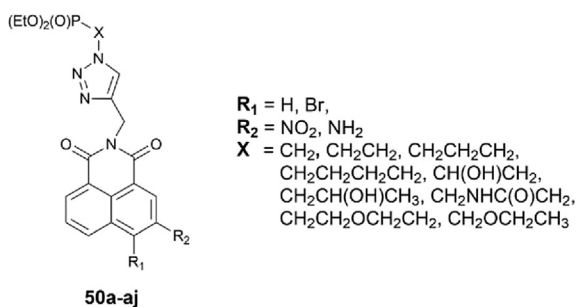


Fig. 32. 1,2,3-Triazole containing derivatives 50a–aj.

toward DNA; these stains are usually located in DNA's minor groove. Determined by calorimetric methods, the binding affinity of **51e** for *ct*-DNA was  $9.53 \times 10^6 \text{ M}^{-1}$ . Compared to **51e**, derivatives **51a**, **51c** and **51f** exhibited about two times less affinity for *ct*-DNA. In the case of derivatives **51a** and **51c**, the flexibility introduced by glycine

linker reduced their abilities to bind DNA. Among others, only derivatives **51b**, **51d** and **51f** were found to be cytotoxic to HeLa cells. The others compounds in this group were non-cytotoxic. Moreover, **51b**, **51d** and **51e** also affected Topo I activity which correlated with intercalation ability; the most efficient intercalating compound **51d** was also the most cytotoxic one.

A several series of 1,2,3-triazole derivatives [70], and a series of 1,2,4-triazoles [71], have been reported earlier by Zhou et al. Derivatives **52a–c** and **54a–i** were found to bind with *ct*-DNA by an intercalative mode with  $K_{SV}$  in the range of  $10^4 \text{ M}^{-1}$  (Fig. 34). These derivatives displayed weak or no activities to the tested bacterial and fungal strains, except for derivatives **54a–h** with a differently halogenated benzene ring, which exhibited moderate to good activities against *E. coli* ( $\text{MIC} = 1\text{--}8 \mu\text{g/mL}$ ), almost equal to those antibiotic Norfloxacin.

The analogous 1,2,4-triazoles **53e–h** and **55e–m** (Fig. 34) and related imidazoles **53a–d** and **55a–d**, possesses similar structural features to compounds previously mentioned [71]. Among tested compounds, salts **55a–m** showed the highest antifungal activities against all the tested strains ( $\text{MIC} = 1.0\text{--}32 \mu\text{g/mL}$ ), while their corresponding precursors, **53a–h**, showed the least activities even ( $\text{MIC} = 16\text{--}128 \mu\text{g/mL}$ ) at much higher concentrations ( $\text{MIC} > 256 \mu\text{g/mL}$ ).

In 2017, Quintana-Espinoza et al., synthesized 3-ethynylaryl-naphthalimides **56a–j** (Fig. 35) using Sonogashira coupling [72]. All prepared compounds showed cytotoxic activity with an  $\text{IC}_{50}$  in range of  $0.1\text{--}21.7 \mu\text{M}$  against SKBr-3, HL-60 and HEL cell lines; however, no relationship was observed between structure and activity. Among them, the most potent was **56g**, which bore the electron-withdrawing group  $\text{CF}_3$ . Though it had the best anti-proliferative activity, compound **56g** also showed a significantly lower inhibition of Topo II ( $<20\%$ ) as compared to compounds **56a**, **56i** and **56j** ( $>80\%$ ) which possessed an unsubstituted aryl ring. Finally, these compounds caused DNA damages *in vivo* in a dose-response manner in the model organism *S. cerevisiae*.

A series of hydrochlorides **57a–h** (Fig. 36) was obtained and evaluated for their anti-hepatocellular carcinoma activity [73]. Among these compounds, only **57a** and **57b** possessed moderate activity against SC-7721, Hep-G2, HCT 116 and K-562 cell lines ( $\text{IC}_{50} = 13.7\text{--}46.8 \mu\text{M}$ ); compounds bearing long aliphatic side chains showed only low activity ( $\text{IC}_{50} > 50 \mu\text{M}$ ).

Interesting *in vitro* and *in vivo* anticancer activities against B16F10 murine melanoma cells were observed with benzazole derivatives **58a–f** (Fig. 37) reported by Lu et al. [74]. Among them, **58e** and **58f** were shown to powerfully suppress murine B16F10 lung metastasis with no visible signs of general toxicity. Cytotoxic activity of these compounds depended highly on the structure of the side chain. The presence of a terminal amino group contributed positively to an increase in anticancer activity. Derivatives **58a–d** did not show cytotoxic activity even at high concentration such as  $40 \mu\text{M}$ , while derivatives **58e** ( $\text{IC}_{50} = 7.8 \mu\text{M}$ ) and **58f** ( $\text{IC}_{50} = 4.5 \mu\text{M}$ )

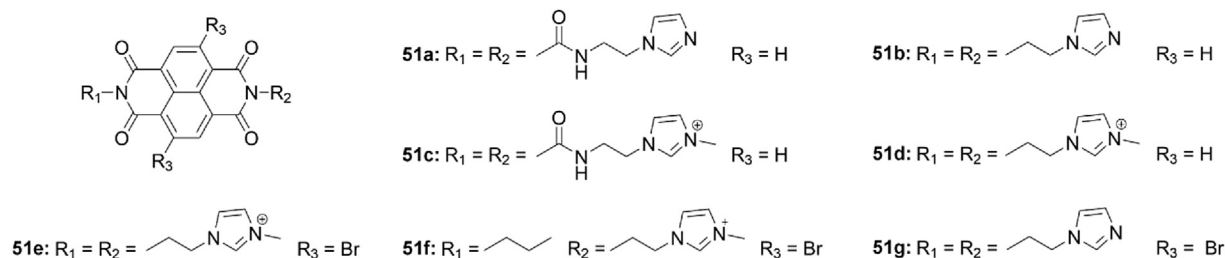


Fig. 33. Structures of naphthalenediimide derivatives 51a-g.

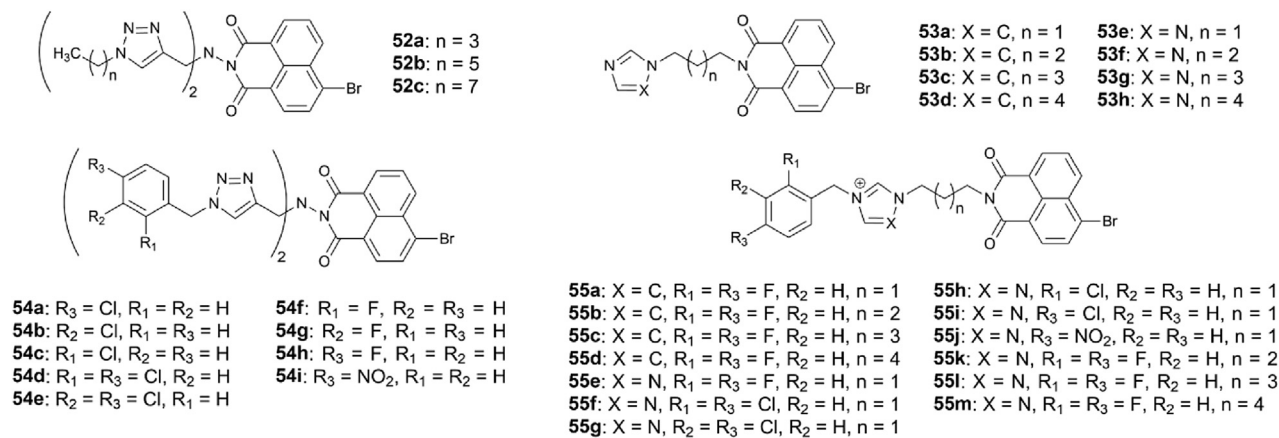


Fig. 34. Structures of compounds 52a-c, 53a-h, 54a-i, 55a-m.

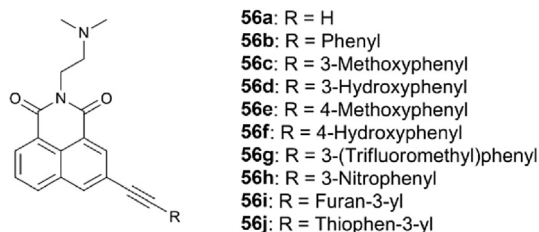


Fig. 35. 3-Ethynylaryl-1,8-naphthalimides 56a-j.

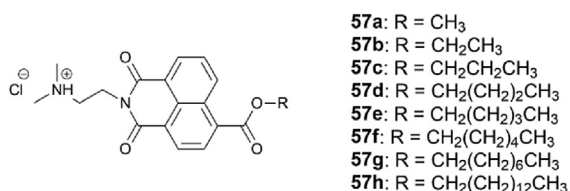


Fig. 36. Structures of compounds 57a-h.

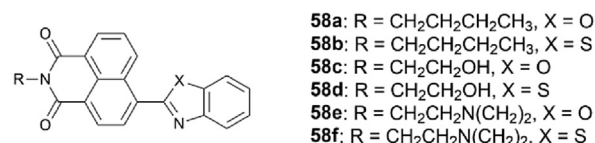


Fig. 37. Benzazole containing derivatives 58a-f.

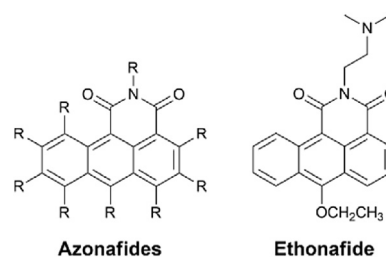


Fig. 38. Structures of azonafides and ethonafide.

showed activities comparable to Amonafide ( $\text{IC}_{50} = 6.7 \mu\text{M}$ ).

## 2.2. Fused-ring-extended 1,8-naphthalimides

One of the most common approach to enhance DNA-binding properties of mono-naphthalimides involved the introduction of an extra benzene ring or heterocyclic ring fused with naphthalene chromophore. In general, additional rings led to the formation of a larger aromatic system and therefore increase stacking forces and intercalation abilities of the extended chromophore.

This approach was initiated in 1993 with anthracene-based derivatives, later named Azonafides, in which the naphthalic ring system was extended to an anthracene ring system (Fig. 38) [75]. As a result of this modification, more than a hundred derivatives of Azonafide, having different functionalities in all positions of.

The anthracene and different side chains, were obtained [76–78]. Most of these derivatives proved to be considerably more potent cytotoxic agents than the parent compound Amonafide against a broad panel of human cancer cell lines. Among them, Ethonafide (6-ethoxyazonafide; Fig. 38), displayed the greatest cytotoxicity with  $\text{IC}_{50}$  values from the low  $\mu\text{M}$  to nM range. A quantitative structure-activity relationship (QSAR) study showed



that DNA-binding properties influenced cytotoxic activity, with compound lipophilicity increasing DNA-binding while large substituents decreased DNA-binding [77]. Quantum-chemical calculations showed that a high HOMO energy value negatively affected the DNA-binding [79]. Electron-donating groups in the anthracene ring, such as methoxy or alkylamino group, lead to increases in the energy of the HOMO orbital, whereas electron-withdrawing groups, e.g. nitro group, lower the energy of the HOMO orbital. Higher polarizability corresponds to a low energy gap between the HOMO and LUMO and favors electrostatic interactions of intercalator with DNA. Thus, designing intercalators containing electron-withdrawing groups should improve DNA-binding and thus cytotoxicity. For more details on the synthesis, anticancer activity and preclinical tests of Azonafide derivatives, we refer the reader to the 2009 review by Ingrassia et al. [80].

Pourak et al. confirmed that from a mechanistic point of view, Ethonafide bound with DNA and acted as a Topo II poison that stabilized the cleavable DNA-Topo II complex, which involved both Topo II $\alpha$  and - $\beta$  isoforms and led to the generation of DNA DSBs [81]. Although Ethonafide poisons both Topo II $\alpha$  and II $\beta$ , results suggested that the  $\alpha$  isoform of the enzyme is the primary cytotoxic target. Congdon et al. also independently confirmed that the cytotoxicity of Ethonafide is associated with Topo II $\alpha$  expression and its activity [82]. Increasing Topo II $\alpha$  expression through inhibition of proteasomal degradation increased DNA DSBs and enhanced the cytotoxic activity of Ethonafide. Finally, it was demonstrated that Ethonafide, such as other well-known Topo II poisons, induced a potent G2 cell cycle arrest.

In 2000, a series of tetrahydroazonafides, phenantrenes and azaphenantrenes were reported [83]. A general overview of the structures of the derivatives and substitution positions, that have been explored are shown in Fig. 39. In general, phenantrenes and azaphenantrenes, both of which contain a bent ring system, did not demonstrate much improvement in potency over linear azonafides. The tetrahydroazonafide analogs displayed potency between Amonafide and Azonafides.

Brana et al. have recently reported a few new azaphenantrene derivatives, in which the pyridine was replaced by a much more  $\pi$ -deficient pyrazine bearing electron-withdrawing CF<sub>3</sub> groups in attempt to increase the DNA-binding and cytotoxic activities of **59a-b** (Fig. 40) [84]. Their results showed little improvement in the cytotoxicity for these derivatives. Derivatives **59a-b** showed similar activities against HeLa cell line to Amonafide with IC<sub>50</sub> values of 1.9 and 3.8  $\mu$ M, respectively. The decrease in activity for derivative **59b** suggested that CF<sub>3</sub> groups probably produce a steric hindrance limitation. In thermal denaturation studies, **59a** increased the melting point of DNA by 3.9 °C which suggested a strong interaction. Moreover, compound **59a** strongly inhibited the activity of the Topo II, which resulted in DNA double strand breaks.

While most examples of chromophore size expansion involve modifications in the naphthalene system, Verma et al. decided to fuse a benzimidazole ring to the imide system of naphthalimide to

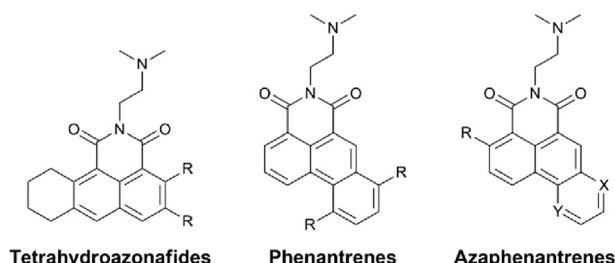


Fig. 39. Tetrahydroazonafides, phenantrenes and azaphenantrenes.

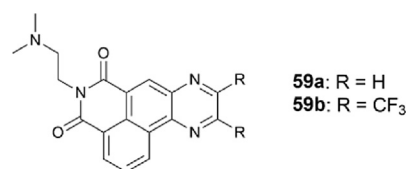


Fig. 40. Azaphenantrene derivatives **59a-b**.

obtain **60a-k** (Fig. 41) [85]. These compounds were tested by NCI for their *in vitro* cytotoxicity and were tested against sixty different human cancer cell lines. Among them, compound **60d**, bearing a 4-amino-phenylsulfanyl, exhibited the greatest growth inhibition with a GI<sub>50</sub> value of 5.05  $\mu$ M. DNA binding studies of **60d** revealed that from a mechanistic point of view it acted as an intercalator and to bind DNA and was confirmed by an increase in the melting temperature of 8.2 °C. Biological studies did not define a molecular target for this compounds; however, *in silico* studies indicate that the target may be one of the enzymes (Topo I, Topo II or ribonucleotide reductase) involved in the DNA replication mechanism.

Recently, Rozovsky et al. reported on the synthesis of a series of Amonafide analogues conjugated with carbazole moiety, **61a-i** (Fig. 42), providing useful method of synthesis and these agents showed low  $\mu$ M activity [86]. Among them, the most cytotoxic derivative was **61c** bearing phenolic group at the carbazole ring, which showed more than an order of magnitude better activity (IC<sub>50</sub> = 0.80  $\mu$ M) over Amonafide (IC<sub>50</sub> = 11.2  $\mu$ M) against the HTC-116 cell line.

Ge et al. reported the development of a two 1,8-naphthalimide series, **62a-e**, with a thiazole fragment fused to naphthalic ring, and **63a-h** with ester substituent at the C4 position (Fig. 43) [87]. Compounds **62a-e** generally showed better anticancer activities than the corresponding 4-formates **63a-h** (IC<sub>50</sub> > 50  $\mu$ M). The most active derivative in this series was **62a**, which exerted very potent *in vivo* effects against two H22 transplant models (solid and pulmonary metastasis tumors) without obvious toxicity. The *in vitro* studies with K-562, HCT 116, SMMC-7721 and Hep-G2 cell lines showed that **62a** and **62c** displayed the best inhibition activity against two hepatoma cell lines with IC<sub>50</sub> values ranging from 1.61 to 9.33  $\mu$ M. Finally, compound **62a** induced a G2/M phase arrest and strongly up-regulated the expression of CCNB1, CDK1 and p21 proteins. Among the 4-formate derivatives only, **63a** and **63b**, with the shortest alkyl chains showed IC<sub>50</sub> < 50  $\mu$ M against SMMC-7721 (IC<sub>50</sub> = 22.06 and 13.66  $\mu$ M) and Hep-G2 (IC<sub>50</sub> = 22.11 and 25.85  $\mu$ M) cell lines.

In 2012, Li et al. reported the synthesis and cytotoxicity study of a series of triazolo-naphthalimide conjugates **64a-l**, where the 1,8-naphthalimide fragment was fused with a 1,2,3-triazole ring, and unfused derivatives **65a-b** (Fig. 44) [88]. These derivatives usually showed slightly higher activities (IC<sub>50</sub> = 0.13–4.77  $\mu$ M) than Amonafide (IC<sub>50</sub> = 1.41–8.83  $\mu$ M) towards five cancer cell lines, with the exception of derivatives **64f** and **64g**, which had IC<sub>50</sub> values of

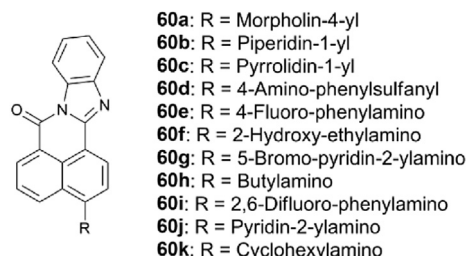
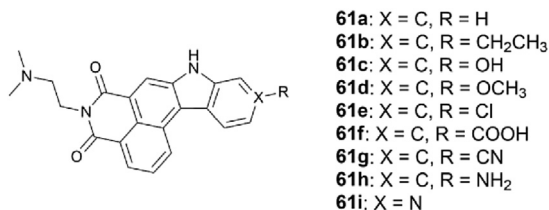
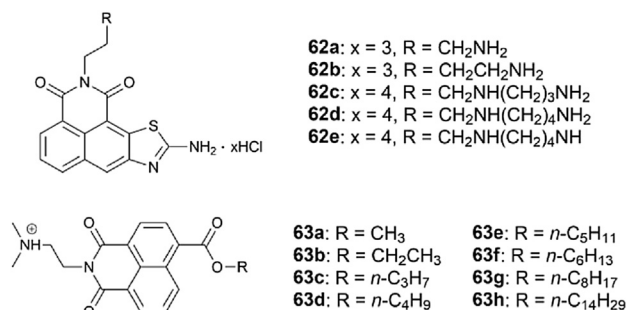
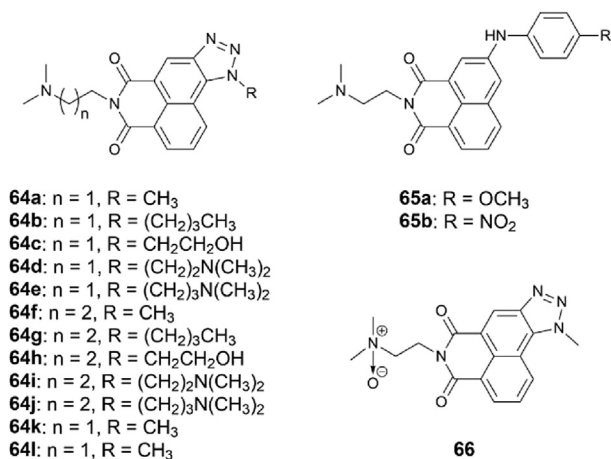
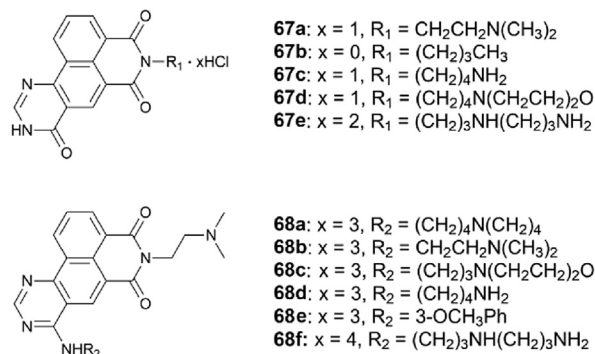


Fig. 41. Benzimidazole fused derivatives **60a-k**.

Fig. 42. Amonafide carbazole conjugates **61a-i**.Fig. 43. Structures of compounds **62a-e** and **63a-h**.Fig. 44. Structures of compounds **64a-l**, **65a-b** and **66**.

4.31–24.98  $\mu\text{M}$ . Among them, compounds **64d** and **64e**, with two  $\omega$ -aminoalkyl side chains, showed the highest cytotoxicity ( $\text{IC}_{50} = 0.13\text{--}0.73\ \mu\text{M}$ ). To reduce any undesirable toxicity, *N*-oxide **66**, a prodrug of **64a**, was prepared; this agent was expected to be activated under the hypoxic conditions often present in cancerous tissues. Compared with **64a**, compound **66** showed much lower *in vitro* activity both in cancer and healthy human cells; however, *N*-oxide **66** did exhibit potent anticancer activity *in vivo* in S180-bearing mice. These results showed that **66** is a promising anticancer agent.

Wang et al. filed a patent (CN 106083850), where a series of 1,8-naphthalimides **67a-e** and **68a-f** (Fig. 45) were evaluated for their activity against SMMC-7721, Hep-G2 and MDA-MB-231 cancer cells [89]. These derivatives contain a pyrimidine moiety fused to the naphthalimide ring system. After the modification with polyamines, the anticancer activity of **68a-d** ( $\text{IC}_{50} = 1.12\text{--}24.0\ \mu\text{M}$ ) was greatly improved as compared to **67a-e** ( $\text{IC}_{50} = 2.64$  to over  $100\ \mu\text{M}$ ); compounds **68b** and **68f** were substantially more potent against all tested cell lines with  $\text{IC}_{50}$  values of 1.12–4.53 and 1.57–3.90  $\mu\text{M}$ ,

Fig. 45. Structures of compounds **67a-e** and **68a-f**.

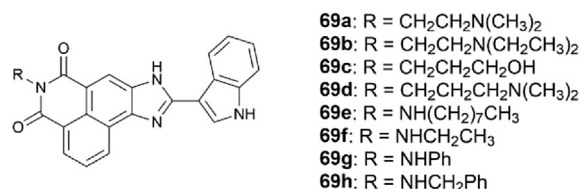
respectively.

The more extended 1,8-naphthalimide derivatives containing fused imidazolium naphthalimide ring with unfused indole ring **69a-h** are depicted in Fig. 46 [90]. These compounds showed only moderate anticancer activities against BGC-823, HL-7702 and MCF-7 cell lines with  $\text{IC}_{50}$  values between  $10^{-6}$  and  $10^{-7}$  M. Among them, compound **69b** showed the highest activity with the  $\text{IC}_{50} = 8.2\text{--}23.7\ \mu\text{M}$  against tested cell lines.

### 2.3. 1,8-Naphthalimides as photonucleases

Several attempts of additional heterocyclic ring attachment to the parent 1,8-naphthalimide chromophore have been performed. The many variations in heterocyclic structures obtained in this manner often show bioactivity improvement. The presence of extra heteroatoms in the modified chromophore very often results in additional and an important feature, namely photosensitization. The vast majority of compounds discussed below will be referred to as photosensitizing agents; these are defined as compounds whose excitation by photon absorption may initiate a series of reactions which ultimately lead to DNA damage with or without causing a strand break. Photocleavage of DNA often involves an initial oxidative reaction with either nucleobase or sugar residue. An excellent review devoted to photocleavage of nucleic acids was published in 1998 by Armitage [91], where a comprehensive presentation of the mechanism of action and examples of photocleavage agents are described.

In 2007, Qian et al. reported the synthesis and cytotoxicity of 1,8-naphthalimides **70a-b** and **71a-f** containing a fused thiazole ring (Fig. 47) [92]. The linear compounds **71a-f** were far more active than their angular isomers **70a-b** against A-549 and P388 cell lines. The relatively high cytotoxicity of **71a-f** ( $\text{IC}_{50} = 0.8\text{--}88.0\ \mu\text{M}$ ) as compared to Amonafide ( $\text{IC}_{50} = 1100$  and  $200\ \mu\text{M}$ ) has been attributed to the presence of the linearly fused thiazole ring. Replacing the amino group of the most active derivative, **71a**, with other substituents resulted in a cytotoxicity decreasing. Previously, these authors also reported that **70a-b**, with a linear chromophore, have far higher DNA-binding affinity and photo-cleaving activity

Fig. 46. Structures of compounds **69a-h**.

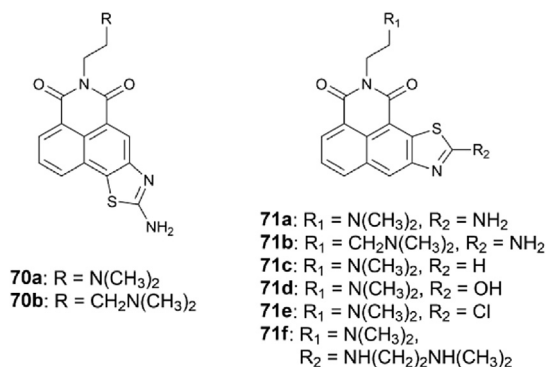


Fig. 47. Thiazole fused derivatives **70a-b** and **71a-f**.

than ones with an angular chromophore [93]. Interestingly, the intercalating ability of **71b** ( $K_b = 4.7 \times 10^{-4} \text{ M}^{-1}$ ) with a longer side chain, was higher than **71a** ( $K_b = 2.6 \times 10^{-4} \text{ M}^{-1}$ ) with a shorter side chain; however, compound **71a** with shorter side chain showed better cytotoxicity. Furthermore, compounds **71a-b** (at 100  $\mu\text{M}$ ) caused photocleavage of plasmid pBR322 under irradiation, while angular isomers **70a-b** have not shown such activity. The aminoalkyl side chain probably transfers an electron from nucleobase to the chromophore, then to an oxygen atom to form superoxide anions ( $\text{O}_2^-$ ), which are responsible for cleavage of the plasmid pBR322. The quantum calculations also suggested that electron transfer might be responsible for photo-cleavage activity. In excited state both nitrogen and sulfur atoms in the thiazole ring of **71a-b** have low electron density, so they could attract the electron more strongly, the electron might be more readily transfer from the side chain to the thiazole moiety and then to oxygen to form superoxide anions.

This study was further extended to develop several series of 1,8-naphthalimide derivatives **72a-j**, **73a-c**, **74a-b** and **75a-d** by introducing a fused imidazole ring connected with unfused aryl or heteroaryl ring (Fig. 48) [94]. The insertion of larger aromatic systems with conformationally flexible, unfused aromatic rings led to the formation of compounds with enhanced DNA-binding as well as cytotoxic activities as compared to Amonafide. The most active compounds all had  $\text{IC}_{50}$  values 5.4 to over 30-fold lower than the values found for Amonafide. These compounds were shown to intercalate, as demonstrated by their abilities to stabilize DNA against heat denaturation ( $\Delta T_m = 4.0\text{--}13.3^\circ\text{C}$ ). However, there is no clear relationship between substituent type, DNA-binding and

cytotoxicity. Results indicated that DNA is a potential, but not a unique, target for antitumor activity.

In 2011, Li et al. reported two series of 1,2,3-triazoles, **76a-j** and **77a-e**, substituted at C3 and C4 positions (Fig. 49) [95,96]. Compounds from both series containing aminoalkyl side chains exhibited similar intercalating ability ( $10^{-5} \text{ M}^{-1}$ ) and cytotoxicity ( $\text{IC}_{50} = 0.30\text{--}2.55 \mu\text{M}$ ) that are comparable to Amonafide ( $\text{IC}_{50} = 1.68\text{--}4.27 \mu\text{M}$ ) against all tested cell lines. In the absence of an amino group in the side chain, a drastic cytotoxicity decrease ( $\text{IC}_{50} = 19.51$  to over  $100 \mu\text{M}$ ) was observed. In addition to their cytotoxic activity and DNA-binding, these compounds cleaved plasmid pBR322 into open circular form under UV irradiation. In general, C4 substituted derivatives showed slightly better DNA-binding affinity, as demonstrated by the model derivatives **76a** ( $K_b = 5.10 \times 10^5 \text{ M}^{-1}$ ) and **77a** ( $K_b = 2.95 \times 10^5 \text{ M}^{-1}$ ). This may be a result of steric requirements which favor linear derivatives.

Yang et al. reported several heterocyclic-fused series of 1,8-naphthalimides, **78a-f**, **79a-c**, and **80a-c** (Fig. 50), with a chiral (*S*)-(-)- or (*R*)-(+)-aminopyrrolidine fragment attached to the *N*-imide nitrogen by a methylene linker and their racemic mixtures [97]. The binding constants between the obtained derivatives and DNA showed that the *S*-enantiomers intercalated more efficient into DNA than the *R*-enantiomers and the racemic mixtures. The relationship between the structure and the binding constant for compounds was related to the presence of a sulfur atom in order **79a-c** > **80a-c** > **78d-f** > **78a-c**, and *S* > *X* > *R* for configuration. Compound **78a** showed the strongest DNA-binding (the binding constants ranged from 0.82 to  $10.0 \times 10^5 \text{ M}^{-1}$ ) as well as far better

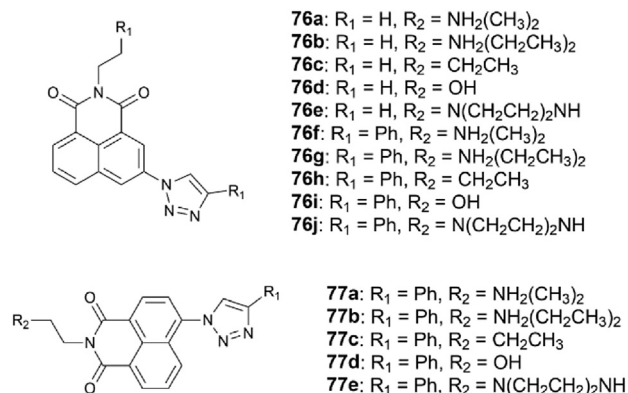


Fig. 49. Structures of compounds **76a-j** and **77a-e**.

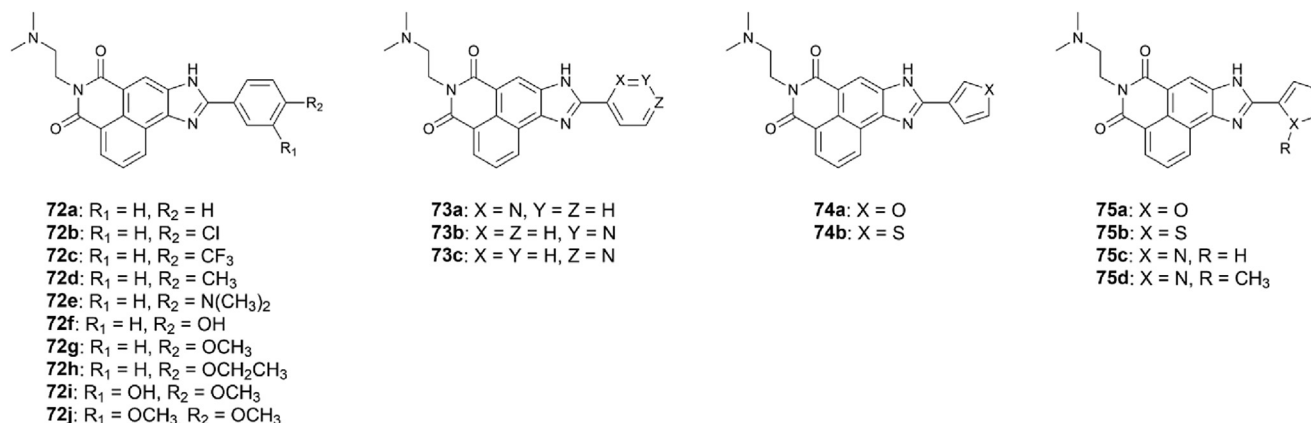


Fig. 48. Structures of compounds **72a-j**, **73a-c**, **74a-b** and **75a-d**.

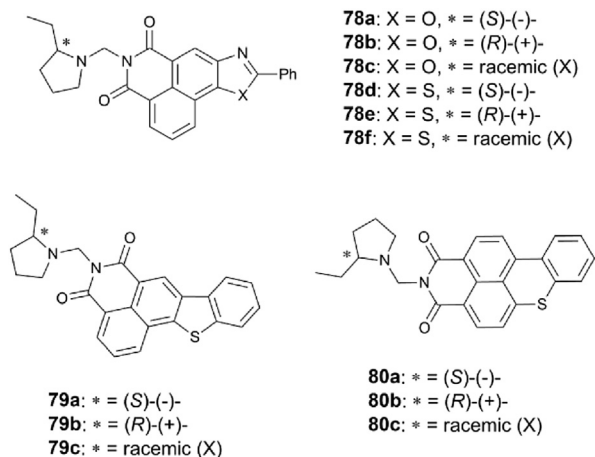


Fig. 50. Structures of compounds **78a-f**, **79a-c** and **80a-c**.

cleavage ability than other compounds. The order of cleavage efficiency by these derivatives nearly paralleled their binding abilities. All these derivatives showed very strong cytotoxicity towards A-549 and P388 cell lines in low  $\mu\text{M}$  concentration ( $\text{IC}_{50} = 0.07\text{--}8.84 \mu\text{M}$  and  $0.47\text{--}13.9 \mu\text{M}$ ). Even if there is no clear correlation between the extent of DNA-binding and activity, the interaction with DNA seems to be necessary for cytotoxicity. Finally, *S/R*-enantiomers behaved quite differently in terms of cytotoxic activity towards tested cell lines. Compound **78b** was found to be most cytotoxic ( $\text{IC}_{50} = 0.07 \mu\text{M}$ ) against A-549 cells, while the  $\text{IC}_{50}$  value of the *S*-enantiomer **78a** was  $0.23 \mu\text{M}$ . It is also interesting that the cytotoxic activities of racemic mixtures were both lower and higher than those of the corresponding pure *S*- and *R*-enantiomers alone, which may suggest there might be mechanisms, which strengthen or weaken the activity of racemic mixtures.

Not only can the incorporation of a fused heterocycles lead to photocytotoxicity, Ott et al. showed significant photocleavage activity of closed supercoiled DNA with a series of non-fused 1,8-naphthalimides **81a-f** (Fig. 51) [98]. These compounds have simple thioalkyl substituents at the C4 position in the naphthalic ring and showed enhanced photocleaving properties after UV irradiation. Moreover, these compounds also displayed cytotoxic activities under non-irradiation conditions with  $\text{IC}_{50} = 2.6\text{--}4.4 \mu\text{M}$  against the MCF-7 cell line. The cytotoxic activity of these compounds has been assigned to their ability to intercalate DNA and inhibit the expression of Topo II $\alpha$ .

Three series of oxygen containing heterocycles **82a-f**, **83a-d** and **84a-d** (Fig. 52) were synthesized by Tan et al. and evaluated *in vitro* against cancer cell lines, Topo I and II [99]. Derivatives with the larger, five-membered chromophore, **83a-d** and **84a-d**, provided better cytotoxicity than the oxazolo derivatives **82a-f**. Compounds **83a** and **84a** bearing a  $\text{CH}_2\text{CH}_2\text{N}(\text{CH}_3)_2$  side chain showed higher cytotoxicity towards A-549 ( $\text{IC}_{50} = 0.61$  and  $0.36 \mu\text{M}$ ) and P388 ( $\text{IC}_{50} = 1.11$  and  $0.65 \mu\text{M}$ ) cell lines than their analogues with other

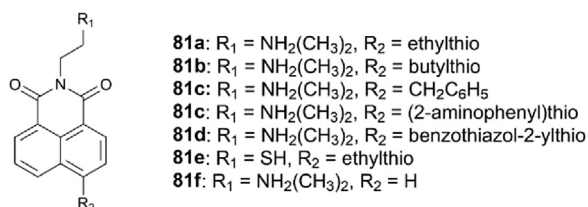


Fig. 51. 4-Thioalkyl-1,8-naphthalimides **81a-f**.

side chain. These compounds intercalated into DNA with  $K_b = 1.5$  and  $2.9 \times 10^5 \text{ M}^{-1}$ , respectively; however, they were weaker intercalators than Amonafide. In comparison with the previously mentioned thiazole analogues, **70a-b** and **71a-f** (Fig. 47), they intercalated stronger, which was consistent with their cytotoxic superiority. Compounds **83a** and **84a** caused significant inhibition of both Topo I and Topo II enzymes; such dual inhibition may contribute to enhanced anticancer selectivity and drug resistance.

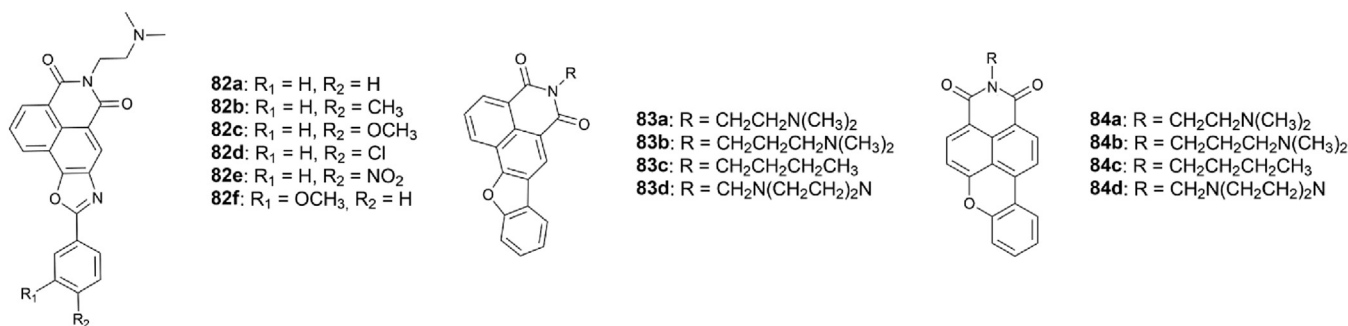
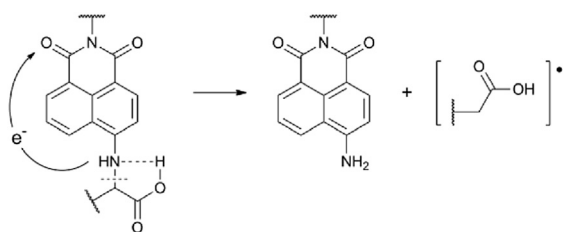
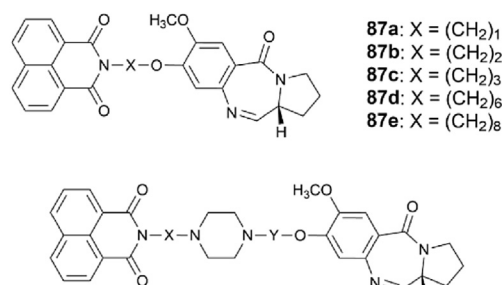
Recently, two interesting groups of 1,8-naphthalimides, **85a-g** and **86a-h** (Fig. 54), with photocleavage abilities were reported by Zhou et al. [100]. Compounds containing a 4-lysine group, **85a-g**, showed strong photocleavage activities after irradiation; which led to ICT from the 4-amino group to the imide system which resulted in the cleavage of the C-N bond of the  $\alpha$ -amino acid. However, 4-amino-derived **86a-h**, without an  $\alpha$ -carboxyl group, do not undergo photocleavage. This activity difference was explained by the transition state of the 4-amino compounds in which the formation of a five-membered-ring from an intra-molecular hydrogen-bond (Fig. 53) appears to be crucial for the photocleavage of 4- $\alpha$ -amino acid containing 1,8-naphthalimides. Photocleavage reaction of **85a-g** produced a radicals of amino acid residues, which in contact with dissolved oxygen generate singlet oxygen responsible for DNA damage.

#### 2.4. Bifunctional 1,8-naphthalimide conjugates

This section will discuss bifunctional DNA-binding agents in which the two functionalities coupled to each other possess two different mechanisms of DNA interaction. In the past ten years, any efforts have been made to increase the DNA recognition abilities of 1,8-naphthalimides and anticancer activities by the coupling of a DNA intercalator, usually by a flexible spacer, to molecules such as groove binders and crosslinkers. The composition of two anticancer moieties with different modes of action might carry a significant advantage in anticancer therapy since tumor growth is usually caused by multiple mutations. Therefore, activation of more than one signaling pathway can often define cancerous cell phenotype and possibly augment the potency of both coupled moieties and/or reduce side-effects and drug resistance development.

Recently, there has been growing interest in the designing of DNA crosslinking agents conjugated with the 1,8-naphthalimide intercalating unit to enhance the cancer cells selectivity. In view of the interesting biological activity shown by pyrrolo[2,1-c] [1,4] benzodiazepines (PBDs) Kamal et al. reported several works on PDB-naphthalimide conjugates, coupled through flexible alkane spacers [101,102]. A series of novel compounds, **88a-e** (Fig. 55), was obtained as a continuation of the previously reported **87a-e** [103], with promising anticancer activity in trials performed by NCI. Compound **87c**, in particular, showed excellent cell killing activity at a concentration of  $37.5 \text{ mg/kg}$  dose in several selected cell lines. Compounds **88a-e** were coupled through a piperazine ring with either a symmetrical or unsymmetrical spacer to a PBD unit. Thermal denaturation studies revealed that the compounds obtained significantly stabilize *ds*-DNA with  $\Delta T_m$  values ranging from  $12.9$  to  $26.5 \text{ }^\circ\text{C}$ , which demonstrate that **88a-e** have strong DNA-binding ability. Compounds **88b** and **88c** bind to DNA the strongest and exhibited the highest cytotoxicity with  $\text{IC}_{50}$  values of  $0.5\text{--}1.0 \mu\text{M}$  against all cell lines tested. Studies on the DNA-binding of the above mentioned conjugates were further carried out with a combination of 2D NMR, spectroscopic, calorimetric and molecular dynamic methods and support intercalative mode of binding [104,105].

In 2009, Kamal et al. reported 1,8-naphthalimide conjugated with coumarins **89a-g** and diimides **90a-g** (Fig. 56) linked by an

Fig. 52. Structures of compounds **82a-f**, **83a-d** and **84a-d**.Fig. 53. The photocleavage mechanism of compounds **85a-g**.Fig. 55. Pyrrolo[2,1-c][1,4]benzodiazepine derivatives **87a-e** and **88a-e**.

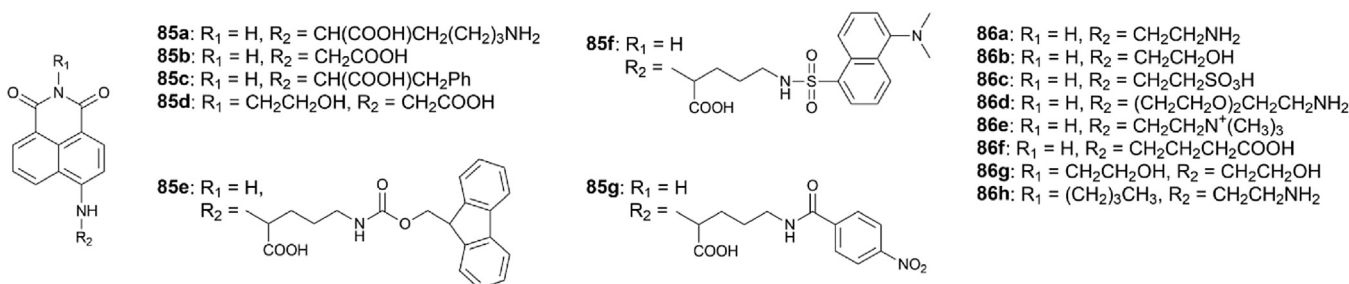
aminothiazolyl moiety [106]. Most of these compounds showed moderate activity towards tested cell lines, while compound **89e** showed the greatest activity with IC<sub>50</sub> values between 0.19 and 31 μM. In general, monoimides demonstrated better activity than the corresponding diimides except for **90a** and **90b**, which exhibited substantial activity against the A2780 cells (IC<sub>50</sub> < 0.1 μM). All of these compounds elevated the melting temperature of *ct*-DNA ( $\Delta T_m = 0.1$ – $24.3$  °C), although there is no direct correlation with cytotoxicity. Interestingly, **90c**, with moderate activity, showed the greatest  $\Delta T_m = 24.3$  °C, while the most cytotoxic compound, **89e** showed  $\Delta T_m = 3.8$  °C. These compounds were tested against gram positive (*S. aureus* and *S. epidermidis*) and gram negative bacterial strains (*P. aeruginosa* and *E. coli*). These compounds demonstrated equipotent inhibition of bacterial growth with MIC values between 18.75 and 75 μg/mL as compared to Ciprofloxacin (MIC = 18.75 μg/mL).

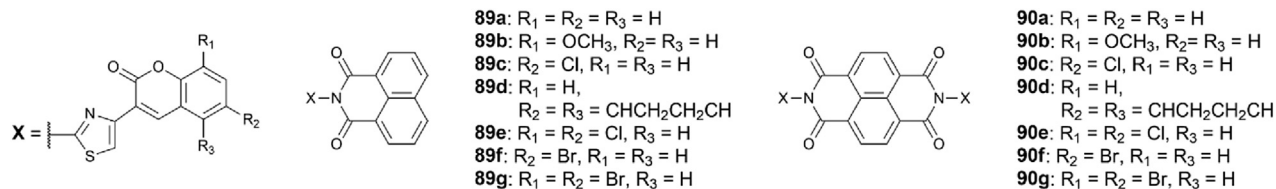
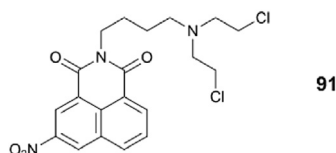
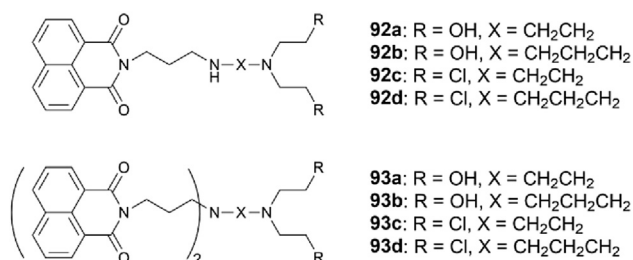
Nitrogen mustard are one of the oldest of the DNA-alkylating classes of anticancer agents and were one of the widely used in anticancer treatment; however, current treatment with potent nitrogen mustard are associated with adverse effects such as cutaneous atrophy and contact dermatitis [107]. For this reason, research is conducted to limit them while maintaining high anticancer activity. Nitrogen mustard species reacts with DNA and alkylated mostly the guanine on nitrogen N7. These alkylating

agents, due to their high reactivity and lack of specific affinity toward DNA, may also react with other cellular nucleophiles, before reaching the target DNA, which results in undesired side reactions. To overcome these serious drawbacks, a number of bifunctional 1,8-naphthalimides with a nitrogen mustard moiety have been reported in the literature.

Recently, Xie et al. reported 3-nitro-1,8-naphthalimide and nitrogen mustard moiety conjugate **91** (Fig. 57), which exhibited significant activities, both *in vitro* and *in vivo*, against four HCC cell lines (IC<sub>50</sub> = 1.90–3.40 μM) [108]. Fluorescence titration showed that this compound displace ethidium bromide, from its complex with DNA, suggesting that DNA might be at least one molecular target.

Further studies by Xie et al. led to the synthesis of mono- and 1,4,5,8-naphthalimides, **92a-d** and **93a-d** (Fig. 58), containing nitrogen mustard functionality at the *N*-imide position connected via polyamine chain [109]. These compounds showed moderate to significant cytotoxic activity against various cancer cell lines. The

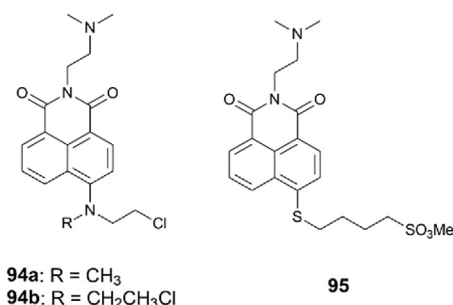
Fig. 54. Structures of compounds **85a-g** and **86a-h**.

Fig. 56. Coumarin naphthalimide conjugates **89a-g** and **90a-g**.Fig. 57. Nitrogen mustard conjugate **91**.Fig. 58. Nitrogen mustard derivatives **92a-d** and **93a-d**.

activity of compound **93d** was the highest with  $IC_{50}$  values ranging between 0.35 and 1.01  $\mu M$ , while compound **92d** showed similar cytotoxic activity ( $IC_{50} = 1.40$ – $5.59 \mu M$ ) to the control, Amonafide. In general, nitrogen mustards, **92d** and **93d**, showed better cytotoxicity than related **92b** ( $IC_{50} = 6.96$ – $69.97 \mu M$ ) and **93b** ( $IC_{50} = 0.82$ – $3.33 \mu M$ ). Compounds **92a** ( $>40 \mu M$ ) and **93a** ( $>15 \mu M$ ) showed a much weaker cytotoxicity.

To strengthen the activity and selectivity of the bifunctional derivatives **94a-b** and **95** (Fig. 59), Brider et al. left the original *N,N*-dimethylamino terminal group present in Amonafide, which is crucial for additional interactions with DNA backbone [110]. Compounds **94a-b** were more cytotoxic ( $IC_{50} = 1.9$ – $12.3 \mu M$ ) than the methyl sulfonate derivative **95** ( $IC_{50} = 11.7$ – $44.6 \mu M$ ) against HTC-116 and PANC-1 cell lines; their cytotoxicity were similar to that of Amonafide ( $IC_{50} = 2.7$ – $13.8 \mu M$ ). Moreover, it has been shown that there is no significant difference between activity of mono-alkylating agent **94a** and cross-linking **94b**.

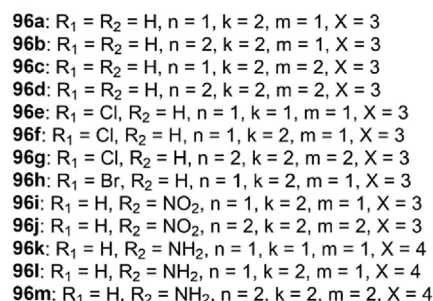
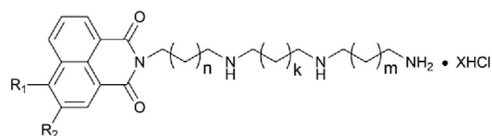
Another popular strategy for the development of selective and

Fig. 59. Structures of compounds **94a-b** and **95**.

effective bifunctional 1,8-naphthalimides focused on conjugates with polyamine molecular vectors. Both natural and synthetic polyamines are identified as such vectors and could elevated the affinity for cancer cells via polyamine transport system (PTS). This is due to fact that fast growing cancer cells types often have a more active PTS for the sufficient uptake of exogenous poly-amines than resting ones. In fact, many anticancer agents with a polyamines, e.g. chlorambucil-spermidine conjugate [111], one of the most cited polyamine conjugate, are many times stronger against cancer cells than their parent precursors and reaches their molecular targets with far greater specificity. For more detailed information on the utilization of polyamines, we refer the reader to the excellent review by Xie et al. [112].

When combining DNA intercalator fragment with polyamine, a synergistic effect is often achieved. The polyamine may serves not only as a molecular vector, but may also increase the DNA-binding and Topo II inhibitory activity of the resulting conjugate. Recently, a novel series of 1,8-naphthalimides **96a-m** (Fig. 60) conjugated with various polyamines at the *N*-imide position has been reported by Tian et al. [113,114]. The incorporation of the polyamine chain significantly affected the selectivity against the Bel-7402 cancer cells ( $IC_{50} = 1.06$ – $33.91 \mu M$ ) and the normal QSG-7701 cells ( $IC_{50} > 50 \mu M$ ). Moreover, the results from the Hep-G2 cells treated with DMFO (which facilitates the import of exogenous polyamines via PAT) and spermidine (antagonist for PTS-selective drug uptake) confirmed that upregulation of PTS-mediated processes helped the drugs distinguish between cancer cells and normal ones (having a less active polyamine transport system). For example, compound **96a**, showed better biological activity in the presence of DMFO and elevated the cytotoxicity while the spermidine decreased the cytotoxicity; this suggested that these conjugates are PTS-selective agents.

Tian et al. synthesized a series of naphthalimide-polyamine conjugates **97**, **98a-e** (Fig. 61) and previously obtained **96a** (not

Fig. 60. Structures of compounds **96a-m**.

shown in Fig. 61) to evaluate the effect of polyamine length on the interaction between conjugates and DNA [115]. The binding constant values  $K_b$  ranged from  $1.910 \times 10^3 \text{ M}^{-1}$  to  $1.146 \times 10^4 \text{ M}^{-1}$ , and decreased in the following order **96a** > **98e** > **98d** > **98c** > **98b** > **98a** > **97**; this revealed that triamine conjugate **96a** inter-acted more efficiently with DNA than diamine conjugates. The presence of the bulky *N,N*-dimethylamino terminal group in **97** reduced the binding strength relative to diamines **98a–e**; though as the number of methylene groups increased, so did the binding strength. The calculated thermodynamic parameters showed that hydrogen bonds and hydrophobic forces play dominant roles in the interaction between compounds **98a–e** and DNA. Similarly, the effects of ionic intensity on the  $K_b$  exclude an electrostatic interaction mode. In quenching studies with iodide, this highly negative quencher due to repulsion by the DNA backbone is expected to quench only free aqueous ligands of groove binders. Iodide quenching effects decreased when compounds **97**, **98b–e** and **96a** were bound to DNA, which imply that these compounds intercalate into DNA. However, compound **98a** might bind DNA in the groove because its decreasing rate  $K_b$  of iodide ion in the absence and presence of DNA was very small. Compound **98a** interacted with DNA by intercalation because it displaced EtBr from its EtBr–DNA complexes. Furthermore, the results of CD studies showed that these conjugates are not the classical DNA intercalator but have also the possibility of binding to DNA by groove, especially **98a**.

In 2014, Tian et al. reported a series of polyamine conjugates **98a–99g**, (Fig. 62), which differed in the length of polyamine chain [116,117]. These compounds were tested *in vitro* for their DNA binding and cytotoxicity against K-562, HCT 116 and 7701 cell lines. Among these conjugates, compound **99c** was the most cytotoxic ( $\text{IC}_{50} = 5.45\text{--}19.69 \mu\text{M}$ ) against the tested cells; most of these conjugates showed moderate activity. These derivatives also showed  $K_b$  values similar to **98a–c**; for example, the binding constant of **99c** with DNA were  $6.059 \times 10^3 \text{ M}^{-1}$ . Compound **99c** induced cell cycle arrest at the G2/M phase in the Hep-G2 cells and triggered apoptosis.

Further studies on the effect of the spermidine conjugate **99c** on apoptosis induction in HeLa cell line revealed that apoptosis correlated to both caspase-dependent intrinsic pathway and AIF-related caspase-independent pathway related to sustaining intracellular ROS accumulation [118]. These studies showed that the concentration of  $9 \mu\text{M}$  of **99c** was sufficient to induce apoptosis in HeLa cells line. Furthermore, GSH (reduced form of glutathione) pool depletion followed by ROS increases induced the increase of **99c**, and the up-regulation of PAO activity was likely the source of ROS concentration increases.

Kerang et al. synthesized 1,8-naphthalimides **100a–c** (Fig. 63) with a polyamine chain at the C4 position and a side chain like Amonafide [119]. These molecules showed high binding affinity with *ct*-DNA via intercalation and stabilized *ct*-DNA in thermal denaturation experiments with  $\Delta T_m = 11.77\text{--}13.02 \text{ }^\circ\text{C}$ . Despite the

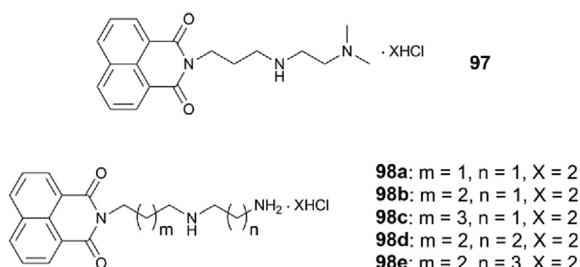


Fig. 61. 9-N-Polyamine-1,8-naphthalimides **97** and **98a–e**.

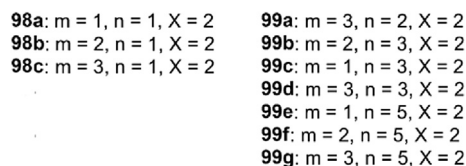
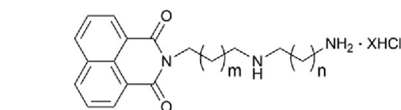


Fig. 62. 9-N-Polyamine-1,8-naphthalimides **98a–c** and **99a–g**.

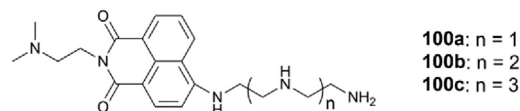


Fig. 63. 9-N-Polyamine derivatives **100a–c**.

high binding affinity to DNA, these compounds showed only moderate activity against HL-60, A-549 and HeLa cell lines with  $\text{IC}_{50}$  values of  $13.08\text{--}109.38 \mu\text{M}$ . Among them, **100a** was the most active member of the series, with superior activity against the A-549 cell line ( $\text{IC}_{50} = 3.16 \mu\text{M}$ ).

Wang et al. investigated the C3 position for the synthesis of Amonafide-polyamine conjugates **101a–f** with an amide and a urea moieties **102a–g** (Fig. 64) as the linkers [120]. The *in vitro* trials showed that compounds **101a–g** with a urea linker were not active against all tested cell lines ( $\text{IC}_{50} > 50 \mu\text{M}$ ). Among them, only derivative **102c** showed even moderate activity ( $\text{IC}_{50} = 8.62\text{--}18.54 \mu\text{M}$ ) against the K-562, HCT 116 and SMMC-7721 cell lines. For comparison, derivatives **101a–f**, with an amide linker showed cytotoxic activity with  $\text{IC}_{50}$  values of  $6.42\text{--}35.59 \mu\text{M}$ . Compound **101f** as a representative and most cytotoxic *in vitro* was tested *in vivo* with the H22 cancer transplant model and was as potent as Amonafide. Furthermore, the combination of **101f** with aspirin displayed better toxicological profile and resulted in significant upregulation cancer growth inhibition.

The amide linker was also used by Li et al. to synthesize conjugates **103a–d** (Fig. 65) with polyamine at the *N*-imide position [121]. These compounds showed good to moderate activity with  $\text{IC}_{50}$  values from 2.86 to over  $50 \mu\text{M}$  against several cancer cell lines.

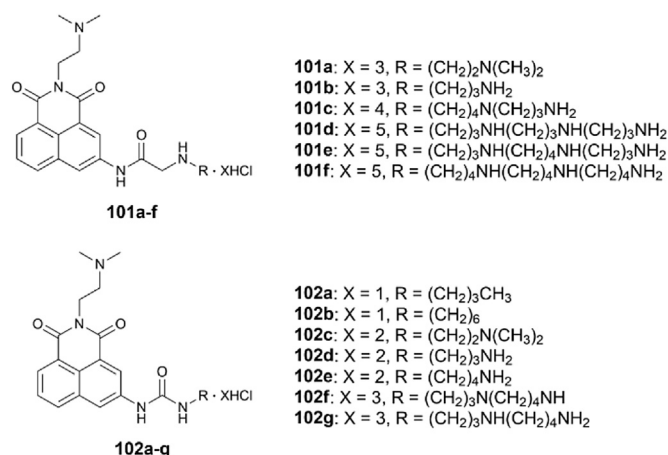
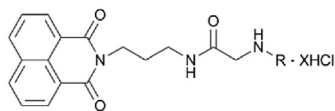


Fig. 64. 3-N-Acetylated-1,8-naphthalimides **101a–f** and **102a–g**.



- 103a:** X = 2, R = (CH<sub>2</sub>)<sub>3</sub>NH<sub>2</sub>  
**103b:** X = 3, R = (CH<sub>2</sub>)<sub>3</sub>NH(CH<sub>2</sub>)<sub>3</sub>NH<sub>2</sub>  
**103c:** X = 4, R = (CH<sub>2</sub>)<sub>3</sub>NH(CH<sub>2</sub>)<sub>4</sub>NH(CH<sub>2</sub>)<sub>3</sub>NH<sub>2</sub>  
**103d:** X = 4, R = (CH<sub>2</sub>)<sub>4</sub>NH(CH<sub>2</sub>)<sub>4</sub>NH(CH<sub>2</sub>)<sub>4</sub>NH<sub>2</sub>

Fig. 65. 9-N-Polyamine-1,8-naphthalimides **103a-d**.

Compound **103c** proved to be most cytotoxic, possessing an IC<sub>50</sub> values ranging from 2.86 to 11.98 μM against HTC-116, Hep-G2, K-562 and MDA-MB-231 cell lines. Compound **103c** induced apoptosis via ROS-mediated mitochondrial dysfunction in Hep-G2 cell line. This compound reduced the tumor growth of H22 transplanted tumors *in vivo* by 70.92% at a dose of 1 mg/kg compared to controls; while administration of a 5 mg/kg dose of Amonafide resulted in 43.73% tumor growth suppression.

Conjugates **104a-g** (Fig. 66) related to **100a**, differing in the length of *n*-alkyl side chains at the *N*-imide position have been synthesized in order to achieve Topo II inhibition, induction of LMP and apoptosis [122]. These compounds inhibited Topo II activity; among them, **104a**, **104d-g** showed inhibitory potency comparable to Amonafide at 100 μM. In addition, the structure-activity relationship of these conjugates showed that, where the length of the alkyl chains significantly influenced the cytotoxic activity. Compounds **104d-f** exhibited much better activity with IC<sub>50</sub> values primarily in the 1.0–10.0 μM range against HL-60, MDA-MB-231 and A-549 cells and comparable with Amonafide (IC<sub>50</sub> = 0.9–4.4 μM). These compounds inhibited Topo II and enhanced selectivity towards cancer cells; less cytotoxicity was observed towards normal cells of L-02 and GES-1 lines. The rest of the series showed weaker activities with IC<sub>50</sub> values of 17.0–31.3 μM. Interestingly, CD spectra indicated that all compounds were weaker DNA intercalators than conventional Amonafide derivatives according. These studies indicated for the first time that compounds **104e** and **104f** inhibited various angiogenesis-related RTKs, including VEGFR2, PDGFRα and FGFR1 in the low μM range.

Other common conjugate types are intercalator-groove binder hybrids, which can associate with DNA by both major or minor groove-binding along the backbone and by intercalation between adjacent base pairs. Considering this type of conjugate, it should be noted that in contrast to intercalators, typical groove binders show selectivity towards AT-rich regions (which provide more hydrogen bond donors/acceptors) and binding constants which range from 10<sup>5</sup> – 10<sup>9</sup> M<sup>-1</sup>; they are generally much higher than the binding constant of typical intercalator (10<sup>4</sup>–10<sup>5</sup> M<sup>-1</sup>) [123]. For this purpose, the main part of DNA-binding forces of such conjugates comes from groove binder segment, while the intercalation part may be responsible for the binding selectivity.

This strategy was used in 2007 by Davis-Cordonnier et al. for the synthesis of oligopyrrole carboxamide conjugates of groove binders connected with a variety of intercalators, which included 1,8-naphthalimides **105a-d** (Fig. 67) [124]. Thermal melting

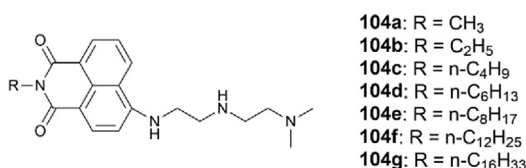


Fig. 66. 9-N-Polyamine derivatives **104a-g**.

experiments and DNA relaxations performed in the presence of Topo I demonstrated that these compounds bind with *ct*-DNA; however, bis-pyrrole **105b** and **105d** showed significantly higher affinity for *ct*-DNA ( $\Delta T_m = 5.7$  °C) and especially for AT-rich sequences ( $\Delta T_m = 18.2$ – $20.4$  °C). The presence of a nitro group on the chromophore does not change the relative DNA binding affinity for *ct*-DNA or [poly(dA-dT)]<sub>2</sub>. A direct poisoning of the Topo I (using gels pre-stained with ethidium bromide) was not detected for these compounds; however, at 50 mM, compound **105c** qualified as mildly effective Topo II poison.

Pedersen et al. published a WO patent (WO 2009/135890) for the preparation and use of oligonucleotide conjugates **106a-b** and **107** (Fig. 68) that contained a general formula consisting of two oligonucleotide sequences covalently attached to the intercalator unit [125]. These conjugates bound specifically to *ds*-DNA and stabilized DNA or RNA triplexes and duplexes as indicated by the extraordinary high thermal melting stability of the corresponding complexes.

Kamal et al. published a WO patent (WO 2009/110000) in which they described a series of benzimidazole conjugates **108a-e** (Fig. 69) as anticancer compounds [126]. In this study, two types of linkers were incorporated for SAR evaluation. All compounds were to be potential anticancer agents towards 60 human cancer cell lines. Conjugates **108a-b** displayed cytotoxicity with an IC<sub>50</sub> values ranged from 0.11 to 10.0 μM, while **108c-e** displayed GI = 50–99% at concentration of 10 μM.

Wu et al. reported 1,8-naphthalimides **109a-i** conjugated with 4-[4-(3,3-diphenylallyl)piperazin-1-yl]benzoic acid with IC<sub>50</sub> in the range of 10<sup>-6</sup> to 10<sup>-5</sup> M against several cancer cell lines (Fig. 70) [127]. Compound **109i** had the highest cytotoxicity against HeLa, P388 and A-375 cells with IC<sub>50</sub> values of 6.7–10.5 μM. These derivatives effectively induced arrest in G<sub>2</sub>/M phase of the cell cycle and progress towards apoptosis in HL-60 cells after treatment with IC<sub>50</sub> concentrations. However, the mechanism of action and biological targets of these compounds remain far from being understood since they had less interaction with DNA and weaker inhibition of Topo II than Amonafide.

The same authors reported naphthalimides **110a-d** (Fig. 71) conjugated with indomethacin, which showed moderate activity with IC<sub>50</sub> values of 13.9–76.3 μM against several cancer cells [128]. Recent studies showed that indomethacin can induce G<sub>1</sub> phase arrest and apoptosis of human colorectal cancer cells by influencing the Wnt/β-catenin signaling pathway and inhibiting angiogenesis [129,130]. Derivatives **110b** and **110d**, with amide linker, had better activities (IC<sub>50</sub> = 13.9–44.2 μM) as compared to their ester analogs (IC<sub>50</sub> = 27.4–76.3 μM); the ester analogs showed preference for hypoxic cytotoxicity against HeLa cells. For **110a** and **110c**, the hypoxic cytotoxicity ratios were 1.3 and 3.0, respectively, while **110b** and **110d** showed no hypoxic cytotoxicity. This effect might be used to design a pro-mising prodrugs against hypoxic cancer cells. Compounds with amide linkers were also the most efficient apoptosis-inducing agents; the most active among them was **110d**, which induced apoptosis in 49.8% of HeLa cells. This result demonstrated that there was no straight relationship between cytotoxicity and pro-apoptotic activity.

In 2015, Tan et al. reported two series of cyclams (1,4,8,11-

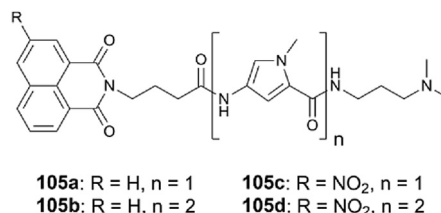


Fig. 67. Structures of compounds **105a-d**.



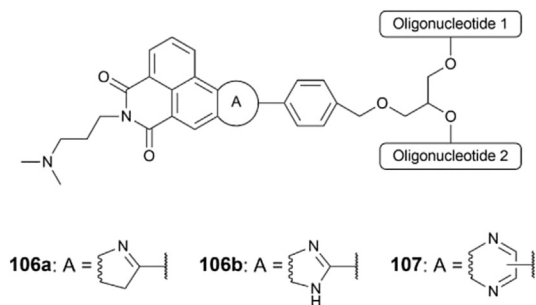
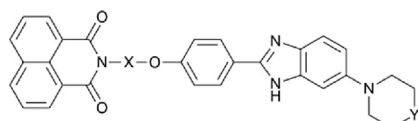
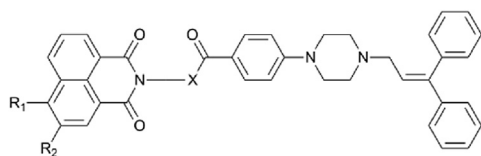


Fig. 68. Structures of compounds 106a-b and 107.



- 108a: X = (CH<sub>2</sub>)<sub>3</sub>, Y = NCH<sub>3</sub>  
 108b: X = (CH<sub>2</sub>)<sub>4</sub>, Y = O  
 108c: X = (CH<sub>2</sub>)<sub>4</sub>N(CH<sub>2</sub>CH<sub>2</sub>)<sub>2</sub>N(CH<sub>2</sub>)<sub>4</sub>, Y = NCH<sub>3</sub>  
 108d: X = (CH<sub>2</sub>)<sub>4</sub>N(CH<sub>2</sub>CH<sub>2</sub>)<sub>2</sub>N(CH<sub>2</sub>)<sub>4</sub>, Y = O  
 108e: X = (CH<sub>2</sub>)<sub>5</sub>N(CH<sub>2</sub>CH<sub>2</sub>)<sub>2</sub>N(CH<sub>2</sub>)<sub>5</sub>, Y = O

Fig. 69. Structures of compounds 108a-e.



- 109a: X = CH<sub>2</sub>CH<sub>2</sub>O, R<sub>1</sub> = NHCH<sub>2</sub>-2-thiophene, R<sub>2</sub> = H  
 109b: X = CH<sub>2</sub>CH<sub>2</sub>O, R<sub>1</sub> = N(CH<sub>2</sub>CH<sub>2</sub>)<sub>2</sub>S, R<sub>2</sub> = H  
 109c: X = CH<sub>2</sub>CH<sub>2</sub>O, R<sub>1</sub> = N(CH<sub>2</sub>CH<sub>2</sub>)<sub>2</sub>S, R<sub>2</sub> = NO<sub>2</sub>  
 109d: X = CH<sub>2</sub>CH<sub>2</sub>O, R<sub>1</sub> = NHCH<sub>2</sub>CH<sub>2</sub>N(CH<sub>3</sub>)<sub>2</sub>, R<sub>2</sub> = H  
 109e: X = CH<sub>2</sub>CH<sub>2</sub>O, R<sub>1</sub> = NHCH<sub>2</sub>CH<sub>2</sub>SC<sub>6</sub>H<sub>5</sub>, R<sub>2</sub> = H  
 109f: X = *p*-C<sub>6</sub>H<sub>4</sub>-SO<sub>2</sub>NH, R<sub>1</sub> = NHCH<sub>2</sub>-2-thiophene, R<sub>2</sub> = H  
 109g: X = *p*-C<sub>6</sub>H<sub>4</sub>-SO<sub>2</sub>NH, R<sub>1</sub> = N(CH<sub>2</sub>CH<sub>2</sub>)<sub>2</sub>S, R<sub>2</sub> = H  
 109h: X = *p*-C<sub>6</sub>H<sub>4</sub>-SO<sub>2</sub>NH, R<sub>1</sub> = N(CH<sub>2</sub>CH<sub>2</sub>)<sub>2</sub>S, R<sub>2</sub> = NO<sub>2</sub>  
 109i: X = *p*-C<sub>6</sub>H<sub>4</sub>-SO<sub>2</sub>NH, R<sub>1</sub> = NHCH<sub>2</sub>CH<sub>2</sub>N(CH<sub>3</sub>)<sub>2</sub>, R<sub>2</sub> = H

Fig. 70. Trisubstituted 1,8-naphthalimides 109a-i.

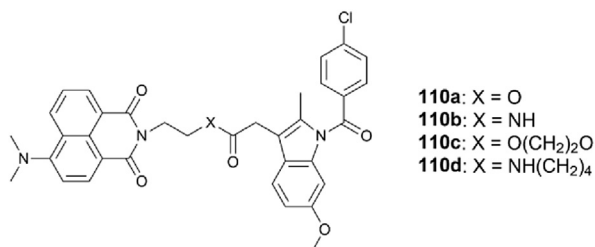


Fig. 71. Structures of compounds 110a-d.

tetraazaacrocycles) linked with a 1,8-naphthalimide, **111a-d** and **112a-d** (Fig. 72) [131]. Usually, the azamacrocycles, especially tetraazamacrocycles and triazamacrocycles (TACN) are studied as metal complexes for the diagnosis and treatment of tumors [132]. Some of them, TACN derivatives in particular, have the ability to cleave DNA [133]. There are also examples of TACN-intercalator conjugates that promote the cleavage of DNA [134]. For the

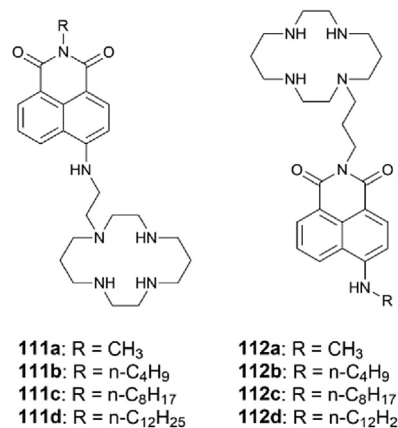


Fig. 72. Cyclam 1,8-naphthalimide conjugates 111a-d and 112a-d.

presented compounds, incorporation of the cyclam unit resulted in no cleavage activity, but binding with the negatively charged backbone of DNA instead, as indicated by CD spectra and molecular modeling. Almost all these conjugates had better activities (IC<sub>50</sub> = 9.4–38.9 μM) than cyclam alone (>50 μM), and cytotoxicity increased with elongation of the aliphatic side chain length. Both types of substitutions exhibited no obvious difference in cytotoxicity compared to their analogs. Similarly, for the Topo II inhibition, no obvious difference was observed between the activities of compounds **111a-d** and **112a-d**; their activities were similar to Amonafide. Interestingly, compounds **111a-d** were more potent than **112a-d** for inhibition of Topo I; compounds **111a-d** were also more efficient Topo I inhibitors than both Camptothecin and Amonafide.

Ryan et al. synthesized and evaluated the binding affinity of 1,8-naphthalimide dipyrido[3,2-a:2',3'-c]phenazine conjugates **113** and **114a-b** (Fig. 73) to DNA [135]. In this work, binding of conjugates to DNA was noted both through groove binding and intercalation, where the positively charged bipyridine fragment was expected to result in electrostatic interaction with natively charged backbone of DNA, while the 1,8-naphthalimide moiety may intercalate between adjacent base pairs. UV-Vis studies of **113** and **114a-b** in the presence and absence of DNA showed an absorbance decrease as the concentration of DNA increased; this suggested the mode of action was intercalation. Further support for intercalation was obtained from EtBr displacement studies which showed release of EtBr from its complex followed by a decrease in the fluorescence of the EtBr-DNA complex. Large binding constant

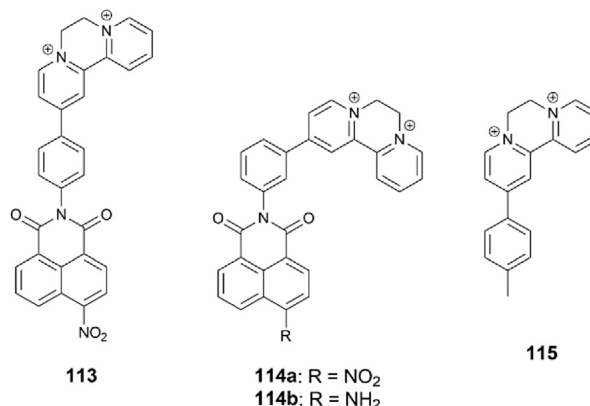


Fig. 73. Structures of compounds 113, 114a-b and 115.

values  $K$  were observed, which followed the trend: **113** ( $1.7 \times 10^7 \text{ M}^{-1}$ ) > **114a** ( $6.5 \times 10^6 \text{ M}^{-1}$ ) > reference **115** ( $2.8 \times 10^6 \text{ M}^{-1}$ ) > **114b** ( $2.3 \times 10^6 \text{ M}^{-1}$ ). Moreover, these conjugates did not display any marked sequence selectivity in their binding modes. Thermal denaturation studies of **113** and **114a-b** showed large changes in the melting point of [poly(dA-dT)]<sub>2</sub> which also supported the intercalation pathway. The greatest changes were observed for **114a** ( $\Delta T_m = 23 \text{ }^\circ\text{C}$ ), and indicated the possibility of groove binding due to the wedged shape of this molecule. This was further supported by ionic strength studies where conjugates **113** and **114a-b** showed partial displacement followed by a large decrease in the melting temperature. The greatest changes were observed for **114a** ( $\Delta T_m = 11 \text{ }^\circ\text{C}$ ). Circular dichroism confirmed that derivatives **113** and **114a-b** binds to DNA via intercalation to alternating [poly(dA-dT)]<sub>2</sub> as well as [poly(dA-dT)]<sub>2</sub> duplexes; linear dichroism (LD) studies supported stronger groove binding for compound **114a**.

Pain et al. reported 1,8-naphthalimides bearing a nitrosourea functionality **116a-d** (Fig. 74) as a DNA alkylating agents [136]. Nitrosoureas are an important class of chemotherapeutic agents, among which the methylnitrosourea class is best represented by compound **117** (named Streptozotocin; Fig. 74). Streptozotocin has been in clinical use since 1967 and finds many application in the carcinoid and endocrine tumors of the pancreas. Compounds **116a-d** were screened for their *in vitro* cytotoxicity against four cell lines including SiHa cervix, T-47D breast, SNB-78 CNS and Hop62 lung with Lomustine (another alkylating agent used for treating brain cancers) and Mitonafide as reference. Compounds **116a-d** did not reach an IC<sub>50</sub> value at a concentration of 10  $\mu\text{M}$ . None of these compounds exhibited curative *in vivo* anticancer activity in S-180 and EAC cancer cell lines. The optimum dose for **116a** was found to be 40.0 mg/kg on a schedule of 1–7 days with T/C values of 140 and 134 for S-180 and EAC respectively. However, Mitonafide and Lomustine have showed better *in vivo* activity in S-180 (T/C values of 187 and > 279, respectively) and EAC (T/C value > 240 for Lumostine) lines. Exposure of tumors cells to **116a-d** at 8  $\mu\text{M}$  resulted in moderate inhibition of DNA (max 65% for **116a**) and RNA (max 60% for **116a**) synthesis; both inhibition values are less than those of Lomustine (64% and 90%, respectively) and Mitonafide (99% and 94%, respectively) at the same concentration.

Recently, Kang et al. reported a series of metronidazole 1,8-naphthalimide conjugates **118a-g** (Fig. 75) [137]. Metronidazole is commonly used in current clinical practice for the treatment of infectious diseases. The new compounds were developed as antibacterial agents that overcome antibiotic resistance and for steric protection of the nitro group, which may be reduced *in vivo* and leads to adverse effects. These compounds showed moderate to good antibacterial activity. Among them, ethylamino derivative

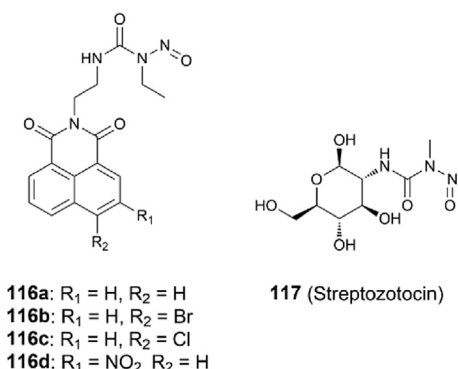


Fig. 74. Nitrosourea containing derivatives **116a-d** and **117**.

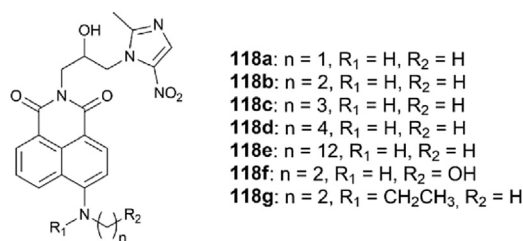


Fig. 75. Metronidazole 1,8-naphthalimide conjugate **118a-g**.

**118b** showed the strongest activity against all strains, especially against *P. vulgaris* and *S. dysenteriae* with excellent MIC values of 0.002 and 0.01  $\mu\text{M}/\text{mL}$ , respectively. Moreover, it was shown that MRSA was more difficult to develop resistance against the most active derivative **118b** than for Norfloxacin. Compound **118b** possessed significant *in vitro* anticancer activity against MCF-7 cell lines with IC<sub>50</sub> = 8.51  $\mu\text{M}$ . UV-Vis spectra of **118b** indicated an absorption decrease as the *ct*-DNA concentration, and suggested that this derivative could intercalate into *ct*-DNA. Moreover, compound **118b** was effectively transported by HAS, a main carrier protein for a variety of endogenous and exogenous substances in the body, via the formation a 1:1 protein-molecule complex through hydrogen bonding and hydrophobic effects. Molecular modeling studies indicated that **118b** could form a complex with Topo II.

Kamal et al. reported 1,8-naphthalimide dihydropyrimidone conjugates **119a-l** (Fig. 76) [138]. These compounds showed significant *in vitro* activity against the Gram-positive bacteria *S. aureus* and *S. epidermidis* (15–21 mm zone of inhibition) similar to Streptomycin at 50  $\mu\text{g}/\text{mL}$  (21 and 23 mm zone, respectively). These compounds also showed significant activity against Gram-negative organisms *P. aeruginosa* and *E. coli* (12–25 mm zone) similar to Streptomycin (24 and 29 mm zone, respectively). It has been observed that most of these compounds showed significant activities against fungal strains *A. niger*, *C. albicans*, *R. oryzae*, *S. cerevisiae* (12–20 mm zone) and were similar to Clotrimazole at 100  $\mu\text{g}/\text{mL}$  (22–24 mm zone).

Hariprakash et al. synthesized compounds **120a-j** (Fig. 77) that bears two different DNA-binding molecules connected by a flexible alkyl linker and evaluated their biological activity [139]. Imidazoacridones have shown very good anticancer activity and anti-MDR activity against a number of human cancer cell lines via DNA intercalation [140]. Position R<sub>1</sub> of the imidazoacridone ring can undergo metabolic hydroxylation; this in turn causes a negative effects on the *in vivo* anticancer activity. To overcome this limitation, positions R<sub>1</sub> and R<sub>2</sub> in the previously synthesized compound **120j** was substituted with CH<sub>3</sub> and OCH<sub>3</sub> groups and F atoms [141,142]. All these conjugates showed superior activity against HCT 116, HT-29 and Hep-G2 (GI<sub>50</sub> = 1.0–22.0 nM) cell lines. Interestingly, although the cytotoxicity of these conjugates is similar, their

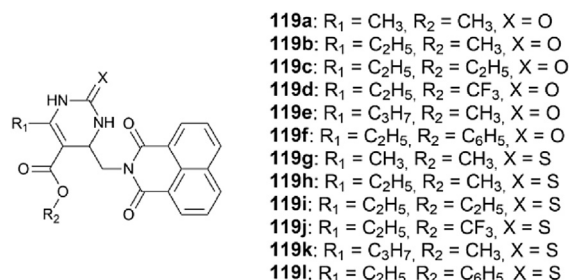
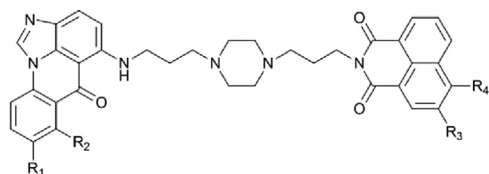


Fig. 76. Structures of compounds **119a-l**.



- 120a:** R<sub>1</sub> = F, R<sub>2</sub> = H, R<sub>3</sub> = NO<sub>2</sub>, R<sub>4</sub> = H  
**120b:** R<sub>1</sub> = OCH<sub>3</sub>, R<sub>2</sub> = H, R<sub>3</sub> = NO<sub>2</sub>, R<sub>4</sub> = H  
**120c:** R<sub>1</sub> = CH<sub>3</sub>, R<sub>2</sub> = H, R<sub>3</sub> = NO<sub>2</sub>, R<sub>4</sub> = H  
**120d:** R<sub>1</sub> = H, R<sub>2</sub> = CH<sub>3</sub>, R<sub>3</sub> = NO<sub>2</sub>, R<sub>4</sub> = H  
**120e:** R<sub>1</sub> = H, R<sub>2</sub> = H, R<sub>3</sub> = H, R<sub>4</sub> = H  
**120f:** R<sub>1</sub> = OCH<sub>3</sub>, R<sub>2</sub> = H, R<sub>3</sub> = H, R<sub>4</sub> = H  
**120g:** R<sub>1</sub> = H, R<sub>2</sub> = H, R<sub>3</sub> = H, R<sub>4</sub> = NO<sub>2</sub>  
**120h:** R<sub>1</sub> = OCH<sub>3</sub>, R<sub>2</sub> = H, R<sub>3</sub> = H, R<sub>4</sub> = NO<sub>2</sub>  
**120i:** R<sub>1</sub> = F, R<sub>2</sub> = H, R<sub>3</sub> = NH<sub>2</sub>, R<sub>4</sub> = H  
**120j:** R<sub>1</sub> = H, R<sub>2</sub> = H, R<sub>3</sub> = NO<sub>2</sub>, R<sub>4</sub> = H

Fig. 77. Imidazoacridone containing derivatives **120a-j**.

ability to kill cancer cells (LD<sub>50</sub>) varies greatly depending on the substitution pattern. The presence of the nitro group at the C3 position, as in derivatives **120a-d** and **120j**, was necessary to maintain the cell-killing activity. A similar effects were observed in the absence of substituents at the R<sub>1</sub> and R<sub>2</sub> in the imidazoacridone ring. Elimination of both substituents led to an approximately 10-fold reduction in LC<sub>50</sub>. Compounds **120g** and **120h** with a nitro group at position C4 rather than C3 had much lower LD<sub>50</sub>. After introduction of the OCH<sub>3</sub> group in R<sub>1</sub> of **120b**, a significant improvement of *in vitro* and *in vivo* potency was observed. An activity comparison of **120j** and **120b** in the NCI 60 human tumor cell line screen, showed a 30-fold higher cell killing activity of compound **120b** (median LC<sub>50</sub> value of 0.67 μM compared to 19.9 μM for **120j**). Finally it was shown that compound **120b** needed a much shorter incubation time to shown cytotoxic activity.

## 2.5. Organometallic complexes

The covalent attachment of organic intercalators to transition metal coordination complexes, yielding organometallic ligands, are being increasingly used as building blocks for the design of new metallodrugs. Furthermore, organometallic complexes may associate with *ds*-DNA; because of the relatively high stability of their metal-carbon bonds and established syntheses methods, the popularity of these intercalators has dramatically increased during the last decade. Promising biological effects have been observed with several transition metals, in particular with gold, ruthenium and platinum. For example, the anticancer activity of *cis*- and *trans*-diamine Pt(II) complexes are drastically enhanced by incorporating of σ-bonded intercalator moiety [143]. In the this section we will focus on 1,8-naphthalimide-transition metal complexes that act as intercalators.

In 2009, Ott et al. prepared a Au(I) phosphine complex **121** (Fig. 78) with a 1,8-naphthalimide to enhance anticancer activity of Au(I) complexes [144]. Compound **121** showed cytotoxicity against MCF-7 and HT-29 cell lines with IC<sub>50</sub> values of 5.3 and 2.6 μM,

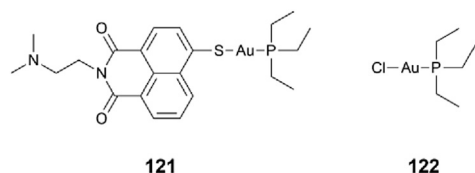


Fig. 78. Gold(I) based complexes **121** and **122**.

respectively. However, these values were slightly lower than those for Et<sub>3</sub>PAuCl (**122**, IC<sub>50</sub> = 3.2 and 1.3 μM) used as a reference compound. On the other hand, the non-naphthalimide Et<sub>3</sub>PAuCl complex showed a significant lower cellular uptake of gold in the nuclei of cancer cells compared to compound **121** (up to 27 times lower), thus the 1,8-naphthalimide system could be a useful vector to facilitate transport of gold ions into nuclei.

In 2013, Banerjee et al. reported the Pt(II) based complex **123** with 4-amino-1,8-naphthalimide and terpyridine moiety (Fig. 79) [145]. Although Pt(II) organometallic species are relatively well understood, there are only a few studies using 1,8-naphthalimide as one of the ligand. The presence of the 1,8-naphthalimide unit in **123** significantly increased the binding constant with *st*-DNA ( $K_b = 4.73 \times 10^5 \text{ M}^{-1}$ ), which is even higher than binding constants reported for other Pt(II) species such as [Pt(terpy)(4-picoline)]<sup>2+</sup> ( $K_b = 5.3 \times 10^4 \text{ M}^{-1}$ ) [146]. Similarly, *in vitro* cytotoxicity assay have shown that **123** displayed higher activity (IC<sub>50</sub> = 16.6 μM) than [Pt(terpy)(4-picoline)]<sup>2+</sup> (IC<sub>50</sub> > 100 μM) against the MCF-7 cell line. A possible mechanism of action for the **123** is covalent binding to DNA by the guanosine nucleoside.

Several reports indicated that selenium compounds had higher anticancer potency than their sulfur analogues or additional properties in some aspects. Zhao et al. reported selenium analogues **124a-h** (Fig. 80) of described sulfur containing compounds **15b** and **15c** (Fig. 10) [147]. Most of these analogues showed good cytotoxic activities against HeLa, HCT 116, K-562, MCF-7 and A-549 cell lines (IC<sub>50</sub> = 5.3–22.3 μM) except **124f**, which had lowest activity (IC<sub>50</sub> > 25 μM). The activity was very similar to that of the sulfur analogues. Binding constants with *ct*-DNA for **15c** and **124b** were  $8.26 \times 10^4$  and  $2.43 \times 10^4 \text{ M}^{-1}$ , respectively. The authors suggested that this difference in binding abilities can be explained by the steric hindrance associated with larger size of selenium atoms as compared to sulfur.

Another example of selenium containing compounds **125a-d** and **126a-b** (Fig. 81) with anti-melanoma activity were reported by Karelia et al. [148]. The structure of these derivatives consists of two moieties; one of them contains an isoselenocyanate group, which mimics naturally occurring isothiocyanates that inhibited melanoma tumor growth by targeting the Akt signaling pathway. The second fragment is a 1,8-naphthalimide unite that is known from the Topo II inhibitor Mitonafide. These structural features result in a dual Akt pathway and Topo II inhibitory activities. In general, compounds of series **125a-d** (IC<sub>50</sub> = 0.8–28.4 μM) are more potent than the compounds of series **126a-b** (IC<sub>50</sub> = 5.2 to >50 μM) against four different human melanoma cell lines. The most active compound, **125c**, was further evaluated for Topo II inhibitory activity and showed a response similar to Mitonafide for inhibiting Topo IIα activity. Compound **125c** efficiently inhi-bited phosphorylation of Akt in a dose dependent manner.

A new series of organoselenocyanates **127a-e** (Fig. 82) with additional intercalating fragment have been developed to reveal their protective efficacy against the cellular toxicity imparted by cyclophosphamide (CP) and mechanism of protection [149–151]. CP is a oxazaphosphorine alkylating agent that is clinically used to

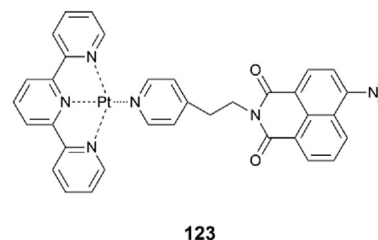
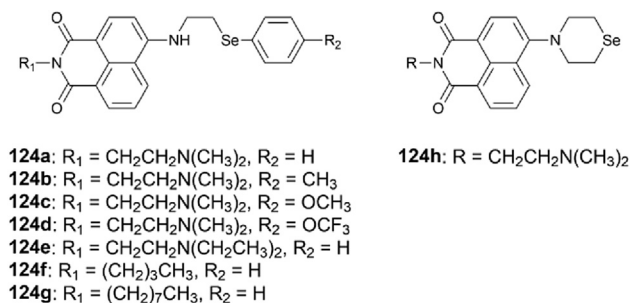
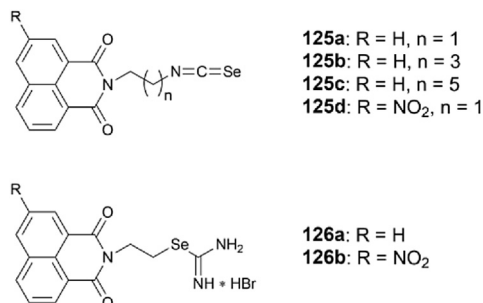
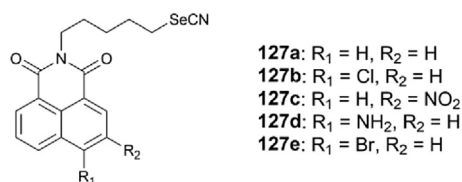


Fig. 79. Platinum(II) based complexes **123**.

Fig. 80. Selenium containing derivatives **124a-h**.Fig. 81. Isoselenocyanate derivatives **125a-d** and **126a-b**.Fig. 82. Selenocyanate derivatives **127a-e**.

treat neoplastic diseases or as a primary immunosuppressant after whole organ transplantation. However, CP may cause DNA damage and chromosomal aberrations through the generation of free radicals and alkylating DNA. In evaluating of the protective properties of compounds **127a-d** against CP-induced cellular toxicity, pretreatment with these compounds gave better results. Among them, amine containing group derivative **127d**, showed the best host protective properties. From a mechanistic point of view, these derivatives act as groove binders that fit into a minor groove. Due to the type of mechanistic action, these derivatives act as minor groove binders. This mechanism was confirmed by compound **127e** in studies with *ct*-DNA. In addition, compound **127e** preferentially bound to AT-rich sequence of DNA.

1,8-Naphthalimide based *N*-heterocyclic carbenes **128a-c** and their complexes **129a-c**, **130a-c** and **131a-c** are shown in Fig. 83. Except for unstable copper-based **129a-c**, these complexes are moderately effective DNA intercalators with  $K_b = 5.4 \times 10^3 \text{ M}^{-1}$  for Rh(II) **130b** and  $8.0 \times 10^4 \text{ M}^{-1}$  for Ru(I) complex **131b**, which is 15-fold higher than the constants for the metal-free analogues **128a-c** [152]. Ruthenium complexes are known to bind with the N7 nitrogen of guanine. It was showed that Rh(II) based complex **130b** and Ru(I) based complex **131b** were able to covalently bind the model nucleobase 9-ethylguanine in addition to intercalation binding. These complexes also showed only moderate anticancer activity against MCF-7 and HT-29 cells with  $\text{IC}_{50}$  values between 2.0 and  $>50 \mu\text{M}$ . However, compared to the reference compounds

**128a-c**, the activity increase was 3- to 10-fold. The most active were Rh(II) based complex **130a-c** with  $\text{IC}_{50}$  values under  $10 \mu\text{M}$  against tested cell lines. Among them, complexes with an ethyl side chain usually exhibited the low or no activity, while methyl derivatives exhibited moderate activity. In contrast, complexes containing benzyl ring on the imidazole showed relatively high cytotoxic activity.

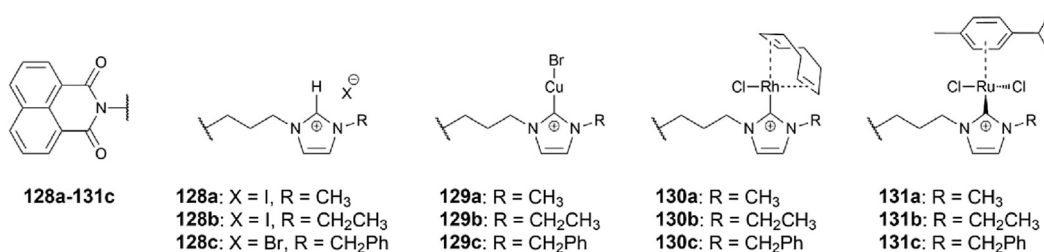
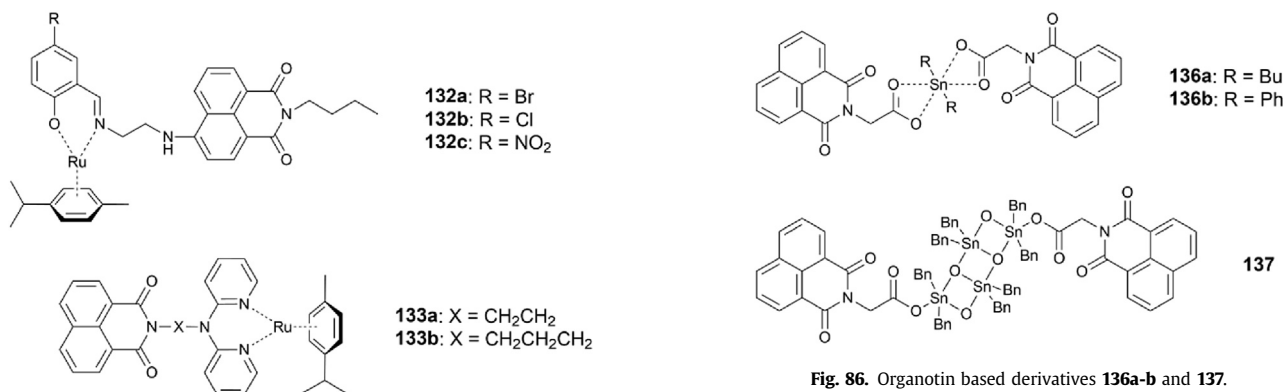
In 2015 Ghebreyessus et al. reported a series of Ru(II) based complexes **132a-c** and **133a-b** (Fig. 84) with potent anticancer properties against CRL7687 human melanoma cancer cell line ( $\text{IC}_{50} = 0.62\text{--}1.01 \mu\text{M}$ ) [153]. These compounds demonstrated poor to medium selectivity against cancer CRL7687 cells versus the healthy CA-M75 skin cells ( $\text{IC}_{50} = 0.61\text{--}1.02 \mu\text{M}$ ). Among them, only compound **132b** displayed higher selectivity towards cancer cells ( $\text{IC}_{50} = 1.01 \mu\text{M}$ ) over health cells ( $\text{IC}_{50} = 19.7 \mu\text{M}$ ). UV-Vis and fluorescence studies revealed that these compounds bind to DNA through intercalation with a  $K_b = 1.0\text{--}6.0 \times 10^4 \text{ M}^{-1}$  which indicated the presence of a moderate interaction between DNA and the ligands.

Ryan et al. reported the synthesis of four novel ruthenium(II) complexes **134a-b**, **135a-b** (Fig. 85) and their evaluation upon interaction with *ds*-DNA [154,155]. Derivatives **134a-b** showed strong hypochromism (up to 34%) upon titration with *ds*-DNA, indicating the intercalative mode of binding. These derivatives intercalated into DNA with  $K_b$  values of  $4.5$  and  $3.0 \times 10^6 \text{ M}^{-1}$  for **134a** and **134b**, respectively. Intercalation was further supported with EtBr displacement assay studies, which showed release of EtBr from its EtBr-DNA complexes and with thermal melting studies. Moreover, both **134a** and **134b** exhibited DNA cleavage upon light irradiation ( $>390 \text{ nm}$ ), during which supercoiled DNA was converted to nicked and linear DNA forms. Derivative **134b** with amine group at C4 was far more effective than **134a**. Similar results were observed for complexes **135a** and **135b**. Significant hypochromism (37% and 56%) and bathochromic shifts, were observed upon DNS addition which suggested intercalation of these complexes into DNA. The binding constants of these interactions were checked as  $9.0 \times 10^6$  and  $15.0 \times 10^6 \text{ M}^{-1}$ , respectively. Increases in the melting temperatures of DNA were observed during thermal denaturation studies for **135a** ( $\Delta T_m = 6.8 \text{ }^\circ\text{C}$ ) and **135b** ( $\Delta T_m = 2.0 \text{ }^\circ\text{C}$ ); these results support the intercalation mode of binding. However, a much smaller stabilization observed with bis-naphthalimide **135b** which indicated that this complex may bind partially by intercalation and groove binding. Upon light irradiation, **135a** was shown to effectively cleaved plasmid DNA while **135b** showed only poor cleavage.

Recently, anticancer properties of organotin based derivatives, **136a-b** and **137** (Fig. 86), were evaluated against the MCF-7 and Hep-G2 cell lines [156]. Preliminary results indicated that these derivatives were more cytotoxic against tested cells ( $\text{IC}_{50} = 0.62\text{--}1.13 \mu\text{g/mL}$ ) than cis-platinum ( $\text{IC}_{50} = 19.51$  and  $67.23 \mu\text{g/mL}$ , respectively).

Kilpin et al. reported biologically active ruthenium(II) arene complexes with 1,8-naphthalimide **138a-c** and **139a-d** and their precursors **140a-b** (Fig. 87) [157]. All complexes showed high cytotoxicity ( $\text{IC}_{50} = 2.0\text{--}49 \mu\text{M}$ ) toward A2780 and A2780R (cisplatin-sensitive and -resistant, respectively) human cell lines, and toward HEK cells (a model for healthy cells). Among them, derivatives **138a**, **139a** and **140a** substituted at the C4 position of 1,8-naphthalimide showed much higher cytotoxicities than non-substituted derivatives, which indicated the important role intercalation play in biological activity. The imidazoles **139a-d** showed slightly less cytotoxic activity and selectivity towards cancer cells than **138a-c**. Mechanistic studies showed a double mode of binding, the 1,8-naphthalimide part is responsible for intercalation into DNA while the ruthenium(II) center preferentially binds to proteins, rather than react with DNA.

Meyer et al. reported that Au(I) 1,8-naphthalimide complexes **141a-d** and their precursors **142a-d** (Fig. 88) were active against

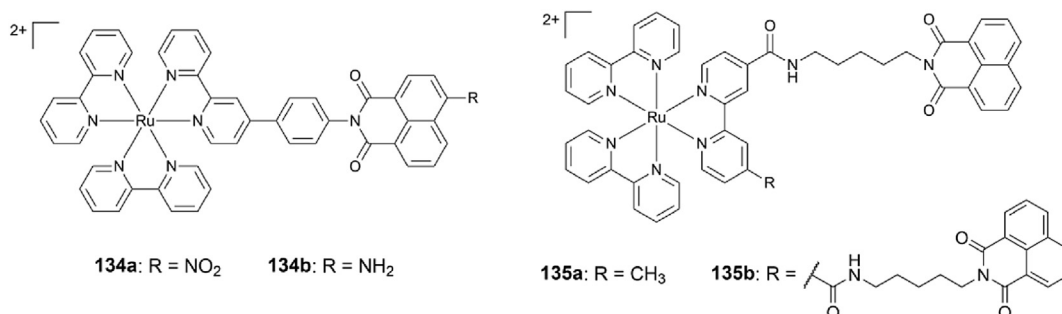
Fig. 83. Structures of compounds **128a-c**, **129a-c**, **130a-c** and **131a-c**.Fig. 84. Ruthenium(II) based complexes **132a-c** and **133a-b**.

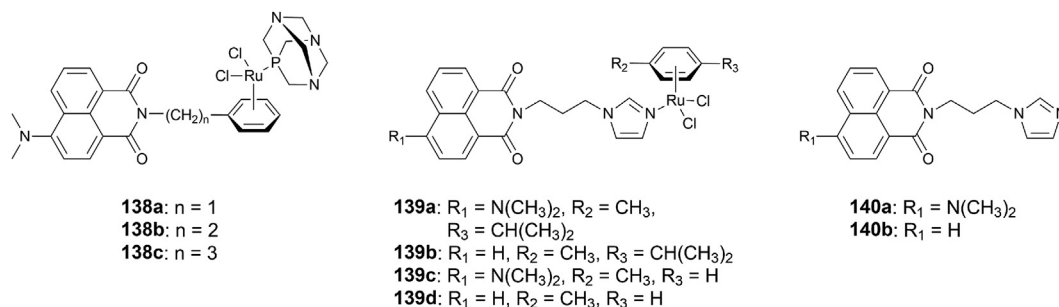
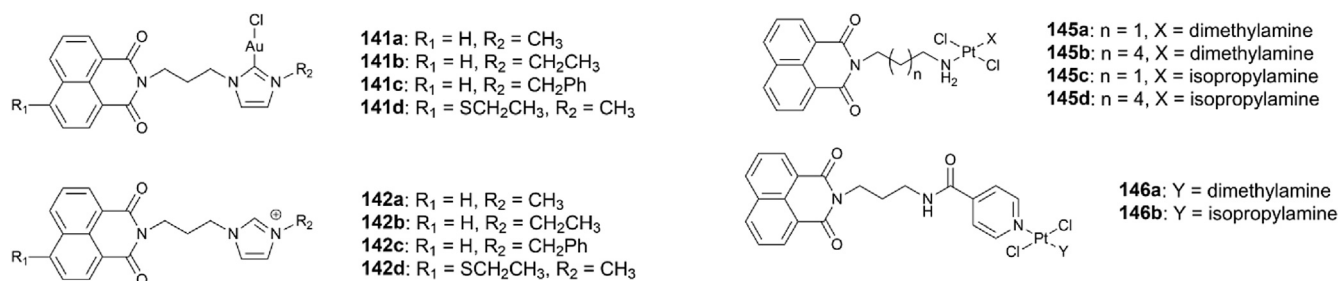
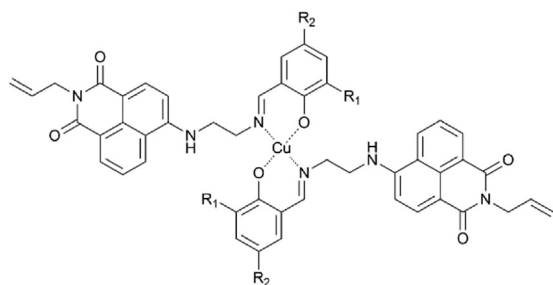
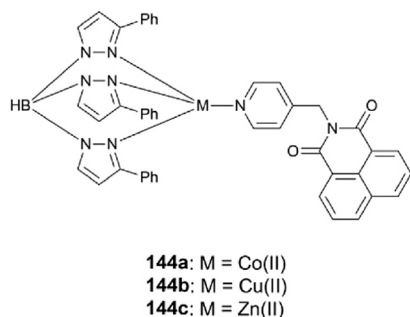
MCF-7 and HT-29 cancer cells in the low  $\mu\text{M}$  range [158]. The study revealed that incorporation of the Au(I) moiety in **141a-d** enhanced anticancer activity ( $\text{IC}_{50} = 1.9\text{--}18.2\ \mu\text{M}$ ) as compared to the corresponding gold-free imidazolium salts **142a-d** ( $\text{IC}_{50} = 4.6\text{--}56.8\ \mu\text{M}$ ). Thermal stability experiments showed that both **141a-d** and **142a-d** greatly increased the melting temperature of ( $\Delta T_m = 3\text{--}11\ ^\circ\text{C}$ ) *ct*-DNA with no apparent differences between the two groups of derivatives. Among them, **141a** and **142c** were the strongest intercalators. Finally, it was shown that complexes **141a** and **141d** both effectively inhibit TrxR activities with  $\text{IC}_{50}$  values of  $0.28 \pm 0.12\ \mu\text{M}$  and  $0.40 \pm 0.13\ \mu\text{M}$ , respectively. The corresponding gold-free derivatives **142a** and **142d** did not show any TrxR-inhibitory activities, even at  $1.0\ \mu\text{M}$ . Moreover, these complexes selectively inhibit the tumor-relevant enzyme TrxR, but not glutathione reductase, which was inhibited by **141a** and **141d** only at much higher concentrations ( $\text{IC}_{50} = 221.2$  and  $15.6\ \mu\text{M}$ , respectively).

Recently, Mao et al. reported the synthesis of Schiff bases in the form of their complexes with copper(II) ions **143a** and **143b** (Fig. 89) and evaluated their DNA-interactions and antioxidant activity [159,160]. The binding of the Cu(II) complexes and the free

ligands with *ct*-DNA were investigated using fluorescence titration, absorption titration, and viscosity measurements. The results indicated that in both cases, the free ligands of **143a** and **143b** bind to DNA stronger than the copper(II) complexes. With the addition of DNA, the free ligands showed hypochromism of 19.3%, while the copper(II) species exhibited hypochromism of 14.9%. The spectroscopic studies revealed that both free ligands and their complexes exhibit strong affinity to intercalate into adjacent *ct*-DNA base pairs. For the absorption titration studies, the  $K_b$  values of the free ligands were  $1.20 \times 10^3\ \text{M}^{-1}$  and  $2.36 \times 10^5\ \text{M}^{-1}$  for **143a** and **143b**, respectively. The binding constants for the complexes measured in the same experiments were  $6.40 \times 10^3\ \text{M}^{-1}$  and  $1.60 \times 10^5\ \text{M}^{-1}$  for **143a** and **143b**. These results were also supported by viscosity and fluorescence quenching studies with the EtBr-DNA displacement assay. In addition, both copper(II) species and free ligands show significant scavenging activity for  $\text{O}_2^{\cdot-}$ ; however, it was shown copper(II) complexes display much stronger activity than their free ligands.

A large amount of work has recently been devoted to metal complexes that have ability to cleave DNA under physiological conditions. Roy et al. provided examples of complexes **144a-c** (Fig. 90) which consist of a 1,8-naphthalimide intercalator and

Fig. 85. Structures of ruthenium(II) complexes **134a-b** and **135a-b**.

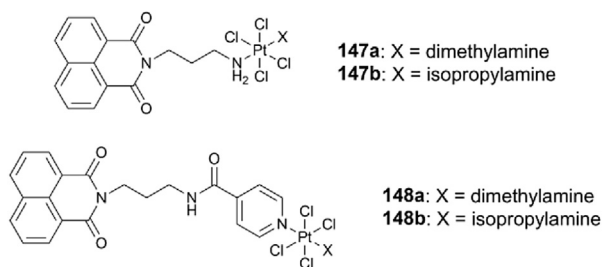
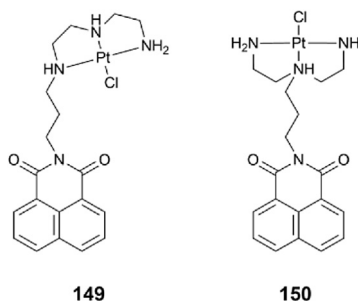
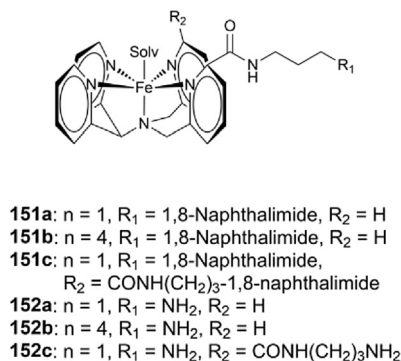
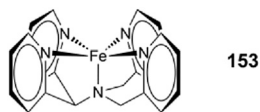
Fig. 87. Structures of ruthenium(II) complexes **138a-c**, **139a-d** and **140a-b**.Fig. 91. Platinum(II) based complexes **145a-d** and **146a-b**.Fig. 88. Structures of compounds **141a-d** and **142a-d**.Fig. 89. Copper(II) based dimer complexes **143a-b**.Fig. 90. Structures of compounds **144a-c**.

tris(3-phenylpyrazolyl)borate chelator with Co(II), Cu(II) and Zn(II) ions [161]. Under physiological conditions and without light excitation, these complexes showed no cleavage of DNA; however, excitation with UV-A light led to the appearance of moderate cleavage of DNA for all tested complexes. Moreover, Cu(II) complex **144b** also display DNA cleavage activity in red light (647 and

676 nm) and near-IR light (>750 nm). This study suggested that hydroxyl radicals formation led to DNA cleavage. The Cu(II) complex **144b** showed moderate cytotoxicity in the dark and much better cytotoxicity after exposure to UV-A light ( $IC_{50} = 29.7$  and  $18.6 \mu M$ , respectively). Similar behavior was observed for the Co(II) based complex **144a**; cytotoxicity in the UV-A light was  $IC_{50} = 32.0 \mu M$ , but no activity in the dark was observed. The Zn(II) based complex **144c** did not show DNA or protein cleavage activity in the dark, nor was there any DNA cleavage activity observed in visible light.

A series of platinum(II) based complexes **145a-d** and **146a-b** (Fig. 91) bearing aliphatic amines were tested for cytotoxicities against sensitive A2780 and cisplatin resistant A2780cisR cells [162]. The activities of complexes **145c**, **145d** and **146b**, which contained isopropylamine as the ligand showed the lowest  $IC_{50}$  values from 0.26 to  $7.18 \mu M$ ; this surpassed the cytotoxicities of the dimethylamine series, **145b** and **146a**, by more than a factor of 10 ( $IC_{50} = 11.21$ – $55.10 \mu M$ ) and was even more active than cisplatin ( $IC_{50} = 1.51$ – $13.33 \mu M$ ). Complexes **145a** and **146a** showed the best activities towards both A2780 and A2780cisR cancer cell lines. Intercalation of complexes **145a-d** and **146a-b** into *ds*-DNA was further suggested by the ability to unwind the supercoiled plasmid DNA. Among them, **145a** and **145c** showed best intercalating abilities as indicated by the highest unwinding angle degree of DNA.

The same authors later investigated the effect of Pt(IV) incorporation instead of Pt(II) to overcome its limitation by slowing down its reactivity [163]. Compounds **147a-b** and **148a-b** (Fig. 92) were designed as prodrugs, activated *in vivo* via reduction of Pt(IV) to Pt(II) with the loss of the two axial ligands, which then act as the corresponding compounds **145a**, **145b**, **146a** and **146b** (Fig. 91). Such a reduction takes place by the assistance of agents present in living cells, e.g. ascorbic acid and glutathione, or may be effect of hypoxic conditions in the tumoral microenvironment. However, *in vitro* studies with **147a-b** and **148a-b** have yielded surprising results. The  $IC_{50}$  values of the Pt(IV) complexes ( $0.06$ – $2.50 \mu M$ ) were even higher than those for corresponding Pt(II) complexes ( $IC_{50} = 0.26$ – $13.6 \mu M$ ). The authors explain that the higher activity of the Pt(IV) complexes might be related to their higher

Fig. 92. Platinum(II) based complexes **147a-b** and **148a-b**.Fig. 93. Platinum(II) based complexes **149** and **150**.Fig. 94. Structures of iron(II) complexes **151a-c** and **152a-c**.Fig. 95. Structures of iron(II) complex **153**.

lipophilicity, which obviously will increase the uptake in comparison to the Pt(II) complexes.

Davey et al. described Pt(II) complexes **149** and **150** (Fig. 93) as anticancer agents having a naphthalimide moiety and showing DNA intercalating abilities [164]. Cytotoxicities of **149** and **150** towards A2780 and A2780cisR after treatment for 72 h were 4- and 5-fold higher than cisplatin, respectively. Complexes **149** and **150** showed IC<sub>50</sub> values of 0.25 and 0.18 μM against A2780 cells and IC<sub>50</sub> values of 0.48 and 0.32 against A2780cisR cells. Such high cytotoxicities were not largely due to the intercalating activity itself, since it was shown that the naphthalimide moiety alone yields a much lower activity with IC<sub>50</sub> values of 55.3 and 96.3 μM for A2780 and A2780cisR cell lines, respectively. In addition, while cisplatin is still significantly toxic to the healthy HaCaT cell model (IC<sub>50</sub> of

3.6 μM), which corresponds to ~3.6-fold decrease as compared to that for the A2780 cells; complexes **149** and **150** were approximately 74-fold (IC<sub>50</sub> = 18.4 μM) and 149-fold (IC<sub>50</sub> = 26.8 μM) less cytotoxic to healthy HaCaT cells, respectively. After a 3-day incubation of **149** and **150** with DNA, adducts were formed in which 6 to 8 adducts belong to 10<sup>4</sup> base pairs of DNA.

Li et al. reported Fe(II) complexes containing ligands **151a-c** and **152a-c** (Fig. 94) and evaluated their iron catalyzed oxidative cleavage of supercoiled plasmid DNA [165]. This study showed that all Fe(II) complexes can very efficiently cleave supercoiled DNA with 47%–73% conversions within 5 min. What is more, with few exceptions, all supercoiled DNA was consumed after 40 min; that was followed by an increase in the fraction of nicked DNA (68%–88%) and formation of linear DNA (8%–32%). Mechanistic studies showed that complexes **151a**, **151c**, **152a** and **152c** with Fe(II) are strong single-strand DNA cleaving agents; while for **151b** and **152b** complexes, only single-strand cleavage occurs initially, but double-strand cleavage also takes place at a later stage. However, under the same conditions, none of these complexes were more active than Bleomycin complex with Fe(II), a natural antibiotic produced by bacteria *S. verticillus* that cleaves DNA in the presence of Fe(II) ions and O<sub>2</sub>, which is used clinically for the treatment of tumors.

Further developing the above mentioned studies, the same authors investigated the relationship between the efficiency of complex **153** (Fig. 95) with Fe(II) towards cleavage of DNA in the presence of the 1,8-naphthalimides [166]. Under UV light and in the presence of 5 equivalents of 1,8-naphthalimide, DNA cleavage was significantly increased. Surprisingly, the addition of ROS scavengers led to an increase in DNA cleavage activity, which is explained by the possibility of inhibition of <sup>3</sup>Ni\* state quenching, thus making PET between the <sup>3</sup>Ni\* chromophore and Fe(III)N4Py complex more efficient. As a result, the reduction to Fe(II) and the further formation of a more reactive iron complex by reaction with a ROS occurs. The role of the scavenger is in this case to maintain an optimal level of the ROS.

### 3. Conclusions and perspectives

After the spectacular success of the first 1,8-naphthalimides prepared in the early 1980s by a team led by prof. Brana and promising results of clinical trials involving Amonafide and Mitonafide, the use of 1,8-naphthalimides in the treatment of cancer reached peak interest in the mid-late 1990s. Fig. 96 provides an overview of the cumulative number of publications and patents on 1,8-naphthalimides reported from 1980 to 2017. The graph shows that from 1980 to 1996 there was a significant increase in the total number of publications; almost every second publication involving naphthalimides concerned their anticancer activity. This was followed by a slight decrease after 1996, likely due to several reports of adverse drug reactions. Some of these challenges have been met, but with limited success. The search for “better 1,8-naphthalimides” continues. In the past 10 years, interest in 1,8-naphthalimides has noticeably increased, which apart from their photophysical properties, is also largely related to their use in cancer treatments and the development of new diagnostic tools for medicinal usage, e.g. molecular probes.

Recently, there has been great interest in 1,8-naphthalimides that have been designed to achieve both increased DNA damage and better delivery into the cancer cells. Different strategies have been employed in the design of naphthalimides. Among these derivatives, apart from the classical intercalators built upon the basic or extended chromophore of 1,8-naphthalimide and side chains, a large and interesting group are bifunctional conjugates that combine two molecules with differing biological properties as well as organometallic complexes or 1,8-naphthalimides with

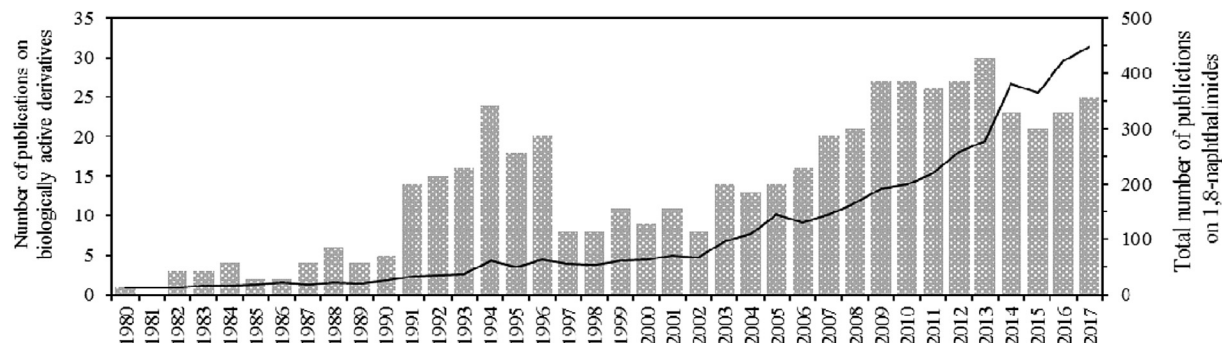


**Fig. 96.** Growth rates for journal articles and patents on 1,8-naphthalimides published between 1980 and 2017 derived using data from SciFinder from Chemical Abstracts and Google Scholar. The graph represents the total number of abstracts for each year (black line) and the number of publications on biological properties, especially anticancer activities and examples of interaction with DNA (grey bars).

photosensitizing properties. In particular, these last three groups enjoy increasing interest and offer great opportunities to create new and more effective 1,8-naphthalimides that have stronger anticancer activities and fewer side effects. The coming years will tell us more about the direction in studies on naphthalimides and the possibility of using them in the treatment of cancer.

#### Appendix A. Supplementary data

Supplementary data to this article can be found online at <https://doi.org/10.1016/j.ejmech.2018.09.055>.

#### References

- [1] R. Martínez, L. Chacón-García, The search of DNA-intercalators as antitumor drugs: what it worked and what did not work, *Curr. Med. Chem.* 12 (2005) 127–151. <https://doi.org/10.2174/0929867053363414>.
- [2] D. Reha, M. Kabeláč, F. Ryjáček, J. Šponer, J.E. Šponer, M. Elstner, S. Suhai, P. Hobza, Intercalators. 1. Nature of stacking interactions between intercalators (ethidium, Daunomycin, Ellipticine, and 4',6-Diaminide-2-phenylindole) and DNA base pairs. Ab Initio quantum chemical, density functional theory, and empirical potential study, *Eur. J. Med. Chem.* 124 (2002) 3366–3376. <https://doi.org/10.1021/ja011490d>.
- [3] A. Rescifina, C. Zagni, M.G. Varrica, V. Pistaà, A. Corsaro, Recent advances in small organic molecules as DNA intercalating agents: synthesis, activity, and modeling, *Eur. J. Med. Chem.* 74 (2014) 95–115. <https://doi.org/10.1016/j.ejmech.2013.11.029>.
- [4] G. Capranico, F. Zunino, K.W. Kohn, Y. Pommier, Sequence-selective topoisomerase II inhibition by anthracycline derivatives in SV40 DNA: relationship with DNA binding affinity and cytotoxicity, *Biochemistry* 29 (1990) 562–569. <https://doi.org/10.1021/bi00454a033>.
- [5] W.E. Ross, M.O. Bradley, DNA double-strand breaks in mammalian cells after exposure to intercalating agents, *Biochim. Biophys. Acta Nucleic Acids Protein Synth.* 654 (1981) 129–134. [https://doi.org/10.1016/0005-2787\(81\)90145-3](https://doi.org/10.1016/0005-2787(81)90145-3).
- [6] R.T. Dorr, W. Bellamy, J.D. Liddil, A. Baker, K.W. Bair, Correlation of cytotoxicity and protein-associated DNA strand breaks for 2-(arylmethylamino)-1,3-propanediols, *Anticancer Drug Des.* 13 (1998) 825–835.
- [7] Y. Pommier, L.A. Zwelling, C.-S. Kao-Shan, J. Whang-Peng, M.O. Bradley, Correlations between intercalator induced DNA strand breaks and sister chromatid exchanges, mutations, and cytotoxicity in Chinese hamster cells, *Canc. Res.* 45 (1985) 3143–3149.
- [8] M.C. Roldan, M.F. Brana, J.M.C. Berlanga, 4-acylamino-n-phenylbutyramides - Useful as Pharmaceuticals, 1973. DE 23181136.
- [9] M.F. Brana, J.M. Castellano, A. Jimenez, A. Lombart, F.P. Rabadan, M.C. Roldan, A. Santos, D. Vazquez, Synthesis, cytostatic activity and mode of action of a new series of imide derivatives of 3-nitro-11 $\alpha$  naphthalic acid, *Current Chemother.* 2 (1978) 1216–1217.
- [10] C.M. Roldan, M.F. Brana, J.M.C. Berlanga, N-Aminoethyl-substituted-3-nitronaphthalimides, 1979. US 4416720.
- [11] M.F. Brana, A.M. Sanz, R.P. Alvarez-Ossorio, C.M. Roldan, C.R. Fernandez de Gamboa, N(Aminoalkyl)-naphthalimides and Their Derivatives, 1980. US 4204063.
- [12] M.F. Braña, J.M. Castellano, C.M. Roldán, A. Santos, D. Vázquez, A. Jiménez, Synthesis and mode(s) of action of a new series of imide derivatives of 3-nitro-1,8 naphthalic acid, *Cancer Chemother. Pharmacol.* 4 (1980) 61–66. <https://doi.org/10.1007/BF00255461>.
- [13] M.F. Braña, J.M. Castellano, A.M. Sanz, Synthesis and cytostatic activity of benzo(de)isoquinolin-1,3-diones. Structure-activity relationship, *Eur. J. Med. Chem.* 3 (1981) 207–212. <https://doi.org/10.1002/chin.198140185>.
- [14] K.D. Paull, M. Nasr, V.L. Narayanan, Computer Assisted Structure-Activity Correlations. Evaluation of benzo(de)isoquinoline-1,3-diones and related compounds as antitumor agents, *Arzneim.-Forsch./Drug Res.* 34 (1984) 1243–1246.
- [15] National Cancer Institute, Clinical Brochure, Nafidimide, NSC 308847, November 1984, pp. 6–22.
- [16] M.E. Costanza, D. Berry, I.C. Henderson, M.J. Ratain, K. Wu, C. Shapiro, D. Duggan, J. Kalra, I. Berkowitz, A.P. Lyss, Amonafide: an active agent in the treatment of previously untreated advanced breast cancer—a cancer and leukemia group B study (calgb 8642), *Clin. Canc. Res.* 1 (1995) 699–704.
- [17] M.E. Marshall, B. Blumenstein, E.D. Crawford, I.M. Thompson, J.B. Craig, M. Eisenberger, F. Ahmann, Phase II trial of amonafide for the treatment of advanced, hormonally refractory carcinoma of the prostate, *Am. J. Clin. Oncol.* 17 (1994) 514–515. <https://doi.org/10.1097/00000421-199412000-00013>.
- [18] P. De Isabella, F. Zunino, G. Capranico, Base sequence determinants of amonafide stimulation of topoisomerase II DNA cleavage, *Nucleic Acids Res.* 23 (1995) 223–229. <https://doi.org/10.1093/nar/23.2.223>.
- [19] A. Nishio, E.M. Uyeki, Induction of DNA strand breaks and chromosome abnormalities by an imide derivative of 3-Nitro-1,8-naphthalic acid (mitonafide) in Chinese hamster ovary cells, *J. Natl. Cancer Inst.* 70 (1983) 1097–1102. <https://doi.org/10.1093/jnci/70.6.1097>.
- [20] T.B. Felder, M.A. McLean, M.L. Vestal, K. Lu, D. Farquhar, S.S. Legha, R. Shah, R.A. Newnan, Pharmacokinetics and metabolism of the antitumor drug amonafide (NSC-308847) in humans, *Drug Metab. Dispos.* 15 (1987) 773–778.
- [21] M.J. Ratain, R. Mick, F. Berezin, L. Janisch, R.L. Schilsky, S.F. Williams, Paradoxical relationship between acetvlator phenotype and aminafide toxicity, *Clin. Pharmacol. Ther.* 50 (1991) 573–579. <https://doi.org/10.1038/clpt.1991.183>.
- [22] M.J. Ratain, G. Rosner, S.L. Allen, M. Costanza, D.A. Van Echo, I.C. Henderson, R.L. Schilsky, Population pharmacodynamic study of amonafide: a cancer and leukemia group B study, *J. Clin. Oncol.* 13 (1995) 741–747. <https://doi.org/10.1200/JCO.1995.13.3.741>.
- [23] F. Innocenti, L. Iyer, M.J. Ratain, Pharmacogenetics of anticancer agents: lessons from amonafide and irinotecan, *Drug Metab. Dispos.* 29 (2001) 596–600.
- [24] M. Braña, A. Ramos, Naphthalimides as anticancer agents: synthesis and biological activity, *Curr. Med. Chem. Agents* 1 (2001) 237–255. <https://doi.org/10.2174/1568011013354624>.
- [25] L. Ingrassia, F. LeFranc, R. Kiss, T. Mijatovic, Naphthalimides and azonafides as promising anti-cancer agents, *Curr. Med. Chem.* 16 (2009) 1192–1213. <https://doi.org/10.2174/092986709787846659>.
- [26] M. Lv, H. Xu, Overview of naphthalimide analogs as anticancer agents, *Curr. Med. Chem.* 16 (2009) 4797–4813. <https://doi.org/10.2174/092986709789909576>.
- [27] S. Banerjee, E.B. Veale, C.M. Phelan, S.A. Murphy, G.M. Tocci, L.J. Gillespie, D.O. Frimannsson, J.M. Kelly, T. Gunnlaugsson, Recent advances in the development of 1,8-naphthalimide based DNA targeting binders, anticancer and fluorescent cellular imaging agents, *Chem. Soc. Rev.* 42 (2013) 1601–1618. <https://doi.org/10.1039/c2cs35467e>.
- [28] A. Kamal, N.R. Bolla, P.S. Srikanth, A.K. Srivastava, Naphthalimide derivatives with therapeutic characteristics: a patent review, *Expert Opin. Ther. Pat.* 23 (2013) 299–317. <https://doi.org/10.1517/13543776.2013.746313>.
- [29] G. Gellerman, Recent developments in the synthesis and applications of anticancer amonafide derivatives, A Mini Review, *Lett. Drug Des. Discov.* 13 (2016) 47–63. <https://doi.org/10.2174/1570180812666150529205049>.
- [30] E. Van Quaquebeke, T. Mahieu, P. Dumont, J. Dewelle, F. Ribaucour, G. Simon, S. Sauvage, J.F. Gaussin, J. Tuti, M. El Yazidi, F. Van Vynck, T. Mijatovic, F. LeFranc, F. Darro, R. Kiss, 2,2,2-Trichloro-N-((2-(2-(dimethylamino)ethyl)-1,3-dioxo-2, 3-dihydro-1H-benzo[de]isoquinolin-5-yl)carbonyl)acetamide



- (UNBS3157), a novel nonhematotoxic naphthalimide derivative with potent antitumor activity, *J. Med. Chem.* 50 (2007) 4122–4134. <https://doi.org/10.1021/jm070315q>.
- [31] T. Mijatovic, T. Mahieu, C. Bruyère, N. De Nève, J. Dewelle, G. Simon, M.J.M. Dehoux, E. van der Aar, B. Haibe-Kains, G. Bontempi, C. Decaestecker, E. Van Quaquebeke, F. Darro, R. Kiss, UNBS5162, a novel naphthalimide that decreases CXCL chemokine expression in experimental prostate cancers, *Neoplasia* 10 (2008) 573–586. <https://doi.org/10.1593/neo.08290>.
- [32] I. Antonini, R. Volpini, D. Dal Ben, C. Lambertucci, G. Cristalli, Design, synthesis, and biological evaluation of new mitonafide derivatives as potential antitumor drugs, *Bioorg. Med. Chem.* 16 (2008) 8440–8446. <https://doi.org/10.1016/j.bmc.2008.08.027>.
- [33] J.T. Norton, M.A. Witschic, L. Luong, A. Kawamura, S. Ghosha, M.S. Stacka, E. Sime, M.J. Avramb, D.H. Appellac, S. Huanga, Synthesis and anticancer activities of 6-amino amonafide derivatives, *Anti Canc. Drugs* 19 (2008) 23–36. <https://doi.org/10.1097/CAD.0b013e3282f00e17>.
- [34] G.N. Qazi, A.K. Saxena, S. Muthiah, D.M. Mondhe, P.R. Sharma, S.K. Singh, U. Sanyal, Novel Substituted 1H-Benz[de]isoquinoline-1,3-diones, 2008. WO 2008/084496.
- [35] L. Xie, Y. Xu, F. Wang, J. Liu, X. Qian, J. Cui, Synthesis of new amonafide analogues via coupling reaction and their cytotoxic evaluation and DNA-binding studies, *Bioorg. Med. Chem.* 17 (2009) 804–810. <https://doi.org/10.1016/j.bmc.2008.11.053>.
- [36] A. Wu, Y. Xu, X. Qian, J. Wang, J. Liu, Novel naphthalimide derivatives as potential apoptosis-inducing agents: design, synthesis and biological evaluation, *Eur. J. Med. Chem.* 44 (2009) 4674–4680. <https://doi.org/10.1016/j.ejmech.2009.07.011>.
- [37] J. Wang, A. Wu, Y. Xu, J. Liu, X. Qian, M2-A induces apoptosis and G2-M arrest via inhibiting PI3 K/Akt pathway in HL60 cells, *Canc. Lett.* 283 (2009) 193–202. <https://doi.org/10.1016/j.canlet.2009.03.039>.
- [38] A. Wu, Y. Xu, X. Qian, Novel naphthalimide-amino acid conjugates with flexible leucine moiety as side chain: design, synthesis and potential antitumor activity, *Bioorg. Med. Chem.* 17 (2009) 592–599. <https://doi.org/10.1016/j.bmc.2008.11.080>.
- [39] J.B. LePecq, C. Paoletti, A fluorescent complex between ethidium bromide and nucleic acids. Physical-chemical characterization, *J. Mol. Biol.* 27 (1967) 87–106. [https://doi.org/10.1016/0022-2836\(67\)90353-1](https://doi.org/10.1016/0022-2836(67)90353-1).
- [40] A. Mukherjee, S. Dutta, M. Shanmugavel, D.M. Mondhe, P.R. Sharma, S.K. Singh, A.K. Saxena, U. Sanyal, 6-Nitro-2-(3-hydroxypropyl)-1H-benz[de]isoquinoline-1,3-dione, a potent antitumor agent, induces cell cycle arrest and apoptosis, *J. Exp. Clin. Oncol.* 29 (2010), 175–182. <https://doi.org/10.1186/1756-9966-29-175>.
- [41] A. Mukherjee, S. Hazra, S. Dutta, S. Muthiah, D.M. Mondhe, P.R. Sharma, S.K. Singh, A.K. Saxena, G.N. Qazi, U. Sanyal, Antitumor efficacy and apoptotic activity of substituted chloroalkyl 1H-benz[de]isoquinoline-1,3-diones: a new class of potential antineoplastic agents, *Invest. N. Drugs* 29 (2011) 434–442. <https://doi.org/10.1007/s10637-009-9372-z>.
- [42] Z. Chen, X. Liang, H. Zhang, H. Xie, J. Liu, Y. Xu, W. Zhu, Y. Wang, X. Wang, S. Tan, D. Kuang, X. Qian, A new class of naphthalimide-based antitumor agents that inhibit topoisomerase II and induce lysosomal membrane permeabilization and apoptosis, *J. Med. Chem.* 53 (2010) 2589–2600. <https://doi.org/10.1021/jm100025u>.
- [43] A.R. Solitro, J.P. MacKeigan, Leaving the lysosome behind: novel developments in autophagy inhibition, *Future Med. Chem.* 8 (2016) 73–86. <https://doi.org/10.4155/fmc.15.166>.
- [44] K. Wang, Y. Wang, X. Yan, H. Chen, G. Ma, P. Zhang, J. Li, X. Li, J. Zhang, DNA binding and anticancer activity of naphthalimides with 4-hydroxyl-alkylamine side chains at different lengths, *Bioorg. Med. Chem. Lett.* 22 (2012) 937–941. <https://doi.org/10.1016/j.bmcl.2011.12.018>.
- [45] M.F. Brana, A. Gradillas, A. Gomez, N. Acero, F. Llinares, D. Munoz-Mingarro, C. Abradelo, F. Rey-Stolle, M. Yuste, J. Campos, M.A. Gallo, A. Espinosa, Synthesis, biological activity, and quantitative structure-activity relationship study of azanaphthalimide and aryl naphthalimide derivatives, *J. Med. Chem.* 47 (2004) 2236–2242. <https://doi.org/10.1021/jm0310784>.
- [46] L. Xie, J. Cui, X. Qian, Y. Xu, J. Liu, R. Xu, 5-Non-amino aromatic substituted naphthalimides as potential antitumor agents: synthesis via Suzuki reaction, antiproliferative activity, and DNA-binding behavior, *Bioorg. Med. Chem.* 19 (2011) 961–967. <https://doi.org/10.1016/j.bmc.2010.11.055>.
- [47] U.H. Sk, A.S. Prakasha Gowda, M.A. Crampsie, J.K. Yun, T.E. Spratt, S. Amin, A.K. Sharma, Development of novel naphthalimide derivatives and their evaluation as potential melanoma therapeutics, *Eur. J. Med. Chem.* 46 (2011) 3331–3338. <https://doi.org/10.1016/j.ejmech.2011.04.058>.
- [48] P. Quintana-Espinoza, J. García-Luis, Á. Amesty, P. Martín-Rodríguez, I. Lorenzo-Castrillejo, A.G. Ravelo, L. Fernández-Pérez, F. Machín, A. Estévez-Braun, Synthesis and study of antiproliferative, antitopoisomerase II, DNA-intercalating and DNA-damaging activities of aryl naphthalimides, *Bioorg. Med. Chem.* 21 (2013) 6484–6495. <https://doi.org/10.1016/j.bmc.2013.08.039>.
- [49] S. Banerjee, J.A. Kitchen, T. Gunnlaugsson, J.M. Kelly, Synthesis and photophysical evaluation of a pyridinium 4-amino-1,8-naphthalimide derivative that upon intercalation displays preference for AT-rich double-stranded DNA, *Org. Biomol. Chem.* 10 (2012) 3033–3043. <https://doi.org/10.1039/c2ob06898b>.
- [50] S. Banerjee, J.A. Kitchen, T. Gunnlaugsson, J.M. Kelly, The effect of the 4-amino functionality on the photophysical and DNA binding properties of alkyl-pyridinium derived 1,8-naphthalimides, *Org. Biomol. Chem.* 11 (2013) 5642–5655. <https://doi.org/10.1039/c3ob40037j>.
- [51] S. McMasters, L.A. Kelly, Sequence-dependent interactions of cationic naphthalimides and polynucleotides, *Photochem. Photobiol.* 83 (2007) 889–896. <https://doi.org/10.1111/j.1751-1097.2007.00155.x>.
- [52] K.-R. Wang, F. Qian, Z.-B. Yang, H.-W. An, D. Han, H. Chen, P.-Z. Zhang, X.-L. Li, Anticancer activity and DNA binding of 4-alkylenediamines modified naphthalimide derivatives, *Lett. Drug Des. Discov.* 11 (2014) 742–748. <https://doi.org/10.2174/1570180811666140121234834>.
- [53] K.R. Wang, F. Qian, X.M. Wang, G.H. Tan, R.X. Rong, Z.R. Cao, H. Chen, P.Z. Zhang, X.L. Li, Cytotoxic activity and DNA binding of naphthalimide derivatives with amino acid and dichloroacetamide functionalizations, *Chin. Chem. Lett.* 25 (2014) 1087–1093. <https://doi.org/10.1016/j.ccl.2014.04.020>.
- [54] R. Seliga, M. Pilatova, M. Sarissky, V. Víglašky, M. Walko, J. Mojzis, Novel naphthalimide polyamine derivatives as potential antitumor agents, *Mol. Biol. Rep.* 40 (2013) 4129–4137. <https://doi.org/10.1007/s11033-013-2523-5>.
- [55] Y.L. Luo, K. Baathulaa, V.K. Kannekanti, C.H. Zhou, G.X. Cai, Novel benzimidazole derived naphthalimide triazoles: synthesis, antimicrobial activity and interactions with calf thymus DNA, *Sci. China Chem.* 58 (2015) 483–494. <https://doi.org/10.1007/s11426-014-5296-3>.
- [56] X. Li, W. Zhao, Anti-tumor Compound Containing Triazole Heterocyclic Structure and Application Thereof, CN 101628912, 2010.
- [57] S. Li, S. Xu, Y. Tang, S. Ding, J. Zhang, S. Wang, G. Zhou, C. Zhou, X. Li, Synthesis, anticancer activity and DNA-binding properties of novel 4-pyrazolyl-1,8-naphthalimide derivatives, *Bioorg. Med. Chem. Lett.* 24 (2014) 586–590. <https://doi.org/10.1016/j.bmcl.2013.12.014>.
- [58] P.S. Nayab, M. Pulaganti, S.K. Chitta, M. Abid, R. Uddin, Evaluation of DNA binding, radicals scavenging and antimicrobial studies of newly synthesized N-substituted naphthalimides: spectroscopic and molecular docking investigations, *J. Fluoresc.* 25 (2015) 1905–1920. <https://doi.org/10.1007/s10895-015-1683-1>.
- [59] J. Zhou, A. Chang, L. Wang, Y. Liu, X. Liu, D. Shangguan, Effects of side chains on DNA binding, cell permeability, nuclear localization and cytotoxicity of 4-aminonaphthalimides, *Org. Biomol. Chem.* 12 (2014) 9207–9215. <https://doi.org/10.1039/c4ob01274g>.
- [60] K.-R. Wang, F. Qian, R.-X. Rong, Z.-R. Cao, X.-M. Wang, X.-L. Li, Fluorescence enhancement, cellular imaging and biological investigation of chiral pyrrolidinol modified naphthalimide derivatives, *RSC Adv.* 4 (2014) 47605–47608. <https://doi.org/10.1039/c4ra08372e>.
- [61] M. Verma, V. Luxami, K. Paul, Synthesis, in vitro evaluation and molecular modelling of naphthalimide analogue as anticancer agents, *Eur. J. Med. Chem.* 68 (2013) 352–360. <https://doi.org/10.1016/j.ejmech.2013.07.027>.
- [62] K. Kokosza, G. Andrei, D. Schols, R. Snoeck, D.G. Piotrowska, Design, antiviral and cytostatic properties of isoxazolidine-containing amonafide analogues, *Bioorg. Med. Chem.* 23 (2015) 3135–3146. <https://doi.org/10.1016/j.bmc.2015.04.079>.
- [63] J. Noro, J. Maciel, D. Duarte, A.C.D. Olival, C. Baptista, A.C.D. Silva, M.J. Alves, P. Kong Thoo Lin, Evaluation of new naphthalimides as potential anticancer agents against breast cancer MCF-7, pancreatic cancer BxPC-3 and colon cancer HCT-15 cell lines, *Org. Chem. Curr. Res.* 4 (2015). <https://doi.org/10.4172/2161-0401.1000144>.
- [64] S. Li, S. Xu, J. Zhang, S. Wang, G. Zhou, Targeted DNA (Deoxyribonucleic Acid) Naphthylidimide-structure-containing Celecoxib Derivatives with Antitumor Activity, Pharmaceutical Composition, and Preparation Method and Application Thereof, 2015. CN 104974135.
- [65] K.R. Wang, F. Qian, Q. Sun, C.L. Ma, R.X. Rong, Z.R. Cao, X.M. Wang, X.L. Li, Substituent effects on cytotoxic activity, spectroscopic property, and DNA binding property of naphthalimide derivatives, *Chem. Biol. Drug Des.* 87 (2016) 664–672. <https://doi.org/10.1111/cbdd.12698>.
- [66] I. Giowacka, R. Gulej, P. Grzonkowski, G. Andrei, D. Schols, R. Snoeck, D. Piotrowska, Synthesis and the biological activity of phosphorylated 1,2,3-triazolenaphthalimide conjugates, *Molecules* 21 (2016) 1420–1439. <https://doi.org/10.3390/molecules21111420>.
- [67] G.W. Collie, R. Promontorio, S.M. Hampel, M. Micco, S. Neidle, G.N. Parkinson, Structural basis for telomeric G-quadruplex targeting by naphthalene diimide ligands, *J. Am. Chem. Soc.* 134 (2012) 2723–2731. <https://doi.org/10.1021/ja2102423>.
- [68] S.T.G. Street, D.N. Chin, G.J. Hollingworth, M. Berry, J.C. Morales, M.C. Galan, Divalent naphthalene diimide ligands display high selectivity for the human telomeric G-quadruplex in K<sup>+</sup> buffer, *Chem. Eur. J.* 23 (2017) 6953–6958. <https://doi.org/10.1002/chem.201700140>.
- [69] Y.V. Suseela, S. Das, S.K. Pati, T. Govindaraju, Imidazolyl-naphthalenediimide-based threading intercalators of DNA, *Chembiochem* 17 (2016) 2162–2171. <https://doi.org/10.1002/cbic.201600478>.
- [70] J.-S. Lv, X.-M. Peng, B. Kishore, C.-H. Zhou, 1,2,3-Triazole-derived naphthalimides as a novel type of potential antimicrobial agents: synthesis, antimicrobial activity, interaction with calf thymus DNA and human serum albumin, *Bioorg. Med. Chem. Lett.* 24 (2014) 308–313. <https://doi.org/10.1016/j.bmcl.2013.11.013>.
- [71] Y.Y. Zhang, C.H. Zhou, Synthesis and activities of naphthalimide azoles as a new type of antibacterial and antifungal agents, *Bioorg. Med. Chem. Lett.* 21 (2011) 4349–4352. <https://doi.org/10.1016/j.bmcl.2011.05.042>.
- [72] P. Quintana-Espinoza, P. Martín-Acosta, Á. Amesty, P. Martín-Rodríguez,

- I. Lorenzo-Castrillejo, L. Fernández-Pérez, F. Machín, A. Estévez-Braun, 5-Ethynylarylnaphthalimides as antitumor agents: synthesis and biological evaluation, *Bioorg. Med. Chem.* 4 (2017) 1–8. <https://doi.org/10.1016/j.bmc.2017.02.024>.
- [73] C. Ge, L. Chang, Y. Zhao, C. Chang, X. Xu, H. He, Y. Wang, F. Dai, S. Xie, C. Wang, Design, synthesis and evaluation of naphthalimide derivatives as potential anticancer agents for hepatocellular carcinoma, *Molecules* 22 (2017) 342–359. <https://doi.org/10.3390/molecules22020342>.
- [74] Y.-T. Lu, T.-L. Chen, K.-S. Chang, C.-M. Chang, T.-Y. Wei, J.-W. Liu, C.-A. Hsiao, T.-L. Shih, Synthesis of novel C4-benzazole naphthalimide derivatives with potent anti-tumor properties against murine melanoma, *Bioorg. Med. Chem.* 25 (2017) 789–794. <https://doi.org/10.1016/j.bmc.2016.11.057>.
- [75] S.M. Sami, R.T. Dorr, D.S. Alberts, W.A. Remers, 2-Substituted 1,2-Dihydro-3H-dibenz[de,h]isoquinoline-1,3-diones. A New Class of Antitumor Agent, *J. Med. Chem.* 36 (1993) 765–770. <https://doi.org/10.1021/jm00058a014>.
- [76] S.M. Sami, R.T. Dorr, A.M. Solyom, D.S. Alberts, W.A. Remers, Amino-Substituted 2-[2'-(Dimethylamino)ethyl]-1,2-dihydro-3H-dibenz[de,h]isoquinoline-1,3-diones. Synthesis, Antitumor Activity, and Quantitative Structure-Activity Relationship, *J. Med. Chem.* 38 (1995) 983–993. <https://doi.org/10.1021/jm00006a018>.
- [77] S.M. Sami, R.T. Dorr, D.S. Alberts, A. M. Solyom, W.A. Remers, 2-[2'-(Dimethylamino)ethyl]-1,2-dihydro-3H-dibenz[de,h]isoquinoline-1,3-diones with substituents at positions 4, 8, 9, 10, and 11. Synthesis, antitumor activity, and quantitative structure-activity relationships, *J. Med. Chem.* 39 (1996) 4978–4987. <https://doi.org/10.1021/jm960623g>.
- [78] S.M. Sami, R.T. Dorr, A.M. Solyom, D.S. Alberts, B.S. Iyengar, W.A. Remers, 6- and 7-Substituted 2-[2'-(Dimethylamino)ethyl]-1,2-dihydro-3H-dibenz[de,h]isoquinoline-1,3-diones: synthesis, nucleophilic displacements, antitumor activity, and quantitative structure-activity relationships, *J. Med. Chem.* 39 (1996) 1609–1618. <https://doi.org/10.1021/jm950742g>.
- [79] M.C. Sharma, S. Sharma, P. Sharma, A. Kumar, Comparative QSAR and pharmacophore modeling of substituted 2-[2'-(dimethylamino)ethyl]-1,2-dihydro-3H-dibenz[de,h]isoquinoline-1,3-diones derivatives as anti-tumor activity, *Med. Chem. Res.* 22 (2013) 5772–5788. <https://doi.org/10.1007/s00044-013-0554-z>.
- [80] L. Ingrassia, F. Lefranc, R. Kiss, T. Mijatovic, Naphthalimides and azonafides as promising anti-cancer agents, *Curr. Med. Chem.* 16 (2009) 1192–1213. <https://doi.org/10.2174/092986709787846659>.
- [81] A. Pourpak, T.H. Landowski, R.T. Dorr, Ethonafide-induced cytotoxicity is mediated by topoisomerase II inhibition in prostate cancer cells, *J. Pharmacol. Exp. Therapeut.* 321 (2007) 1109–1117. <https://doi.org/10.1124/jpet.106.117457>.
- [82] L.M. Congdon, A. Pourpak, A.M. Escalante, R.T. Dorr, T.H. Landowski, Proteasomal inhibition stabilizes topoisomerase II $\alpha$  protein and reverses resistance to the topoisomerase II poison ethonafide (AMP-53, 6-ethoxyazonafide), *Biochem. Pharmacol.* 75 (2008) 883–890. <https://doi.org/10.1016/j.bcp.2007.10.026>.
- [83] S.M. Sami, R.T. Dorr, D.S. Alberts, A.M. Solyom, W.A. Remers, Analogues of amonafide and azonafide with novel ring systems, *J. Med. Chem.* 43 (2000) 3067–3073. <https://doi.org/10.1021/jm9905817>.
- [84] Z.-D. Xu, M. Wang, S.-L. Xiao, C.-L. Liu, M. Yang, Synthesis, biological evaluation and DNA binding properties of novel bleomycin analogues, *Bioorg. Med. Chem. Lett* 13 (2003) 2595–2599. [https://doi.org/10.1016/S0960-894X\(03\)00435-9](https://doi.org/10.1016/S0960-894X(03)00435-9).
- [85] M. Verma, V. Luxami, K. Paul, Synthesis, in vitro evaluation and molecular modelling of naphthalimide analogue as anticancer agents, *Eur. J. Med. Chem.* 68 (2013) 352–360. <https://doi.org/10.1016/j.ejmech.2013.07.027>.
- [86] A. Rozovsky, E. Regozin, M. Oron-Herman, A. Albeck, G. Gellerman, Synthesis of antitumor carbazole-amonafide structural hybrids, *Eur. J. Org. Chem.* (2015) 1811–1818, 2015. <https://doi.org/10.1002/ejoc.201403549>.
- [87] C. Ge, L. Chang, Y. Zhao, C. Chang, X. Xu, H. He, Y. Wang, F. Dai, S. Xie, C. Wang, Design, synthesis and evaluation of naphthalimide derivatives as potential anticancer agents for hepatocellular carcinoma, *Molecules* 22 (2017) 342–358. <https://doi.org/10.3390/molecules22020342>.
- [88] S. Li, W. Zhong, Z. Li, X. Meng, Unprecedented synthesis, in vitro and in vivo anti-cancer evaluation of novel triazolone naphthalimide derivatives, *Eur. J. Med. Chem.* 47 (2012) 546–552. <https://doi.org/10.1016/j.ejmech.2011.11.025>.
- [89] C. Wang, X. Zhang, Y. Wang, W. Luo, L. Chang, X. Li, X. Wu, J. Wang, Pyrimidine Naphthalimide Derivatives, and Preparation Method and Application Thereof, 2016. CN 106083850.
- [90] X. Li, R. Zhao, Imidazolium Naphthalimide Derivative Containing Indole, as Well as Synthesis and Application of Imidazolium Naphthalimide Derivative, 2016. CN 106167490.
- [91] B. Armitage, Photocleavage of nucleic acids, *Chem. Rev.* 98 (1998) 1171–1200. <https://doi.org/10.1021/cr960428+>.
- [92] X. Qian, Z. Li, Q. Yang, Highly efficient antitumor agents of heterocycles containing sulfur atom: linear and angular thiazonaphthalimides against human lung cancer cell in vitro, *Bioorg. Med. Chem.* 15 (2007) 6846–6851. <https://doi.org/10.1016/j.bmc.2007.07.008>.
- [93] Z. Li, Q. Yang, X. Qian, Novel 2-aminothiazonaphthalimides as visible light activatable photolabile nucleases: effects of intercalation, heterocyclic-fused area and side chains, *Bioorg. Med. Chem. Lett* 15 (2005) 1769–1772. <https://doi.org/10.1016/j.bmcl.2005.02.053>.
- [94] F. Li, J. Cui, L. Guo, X. Qian, W. Ren, K. Wang, F. Liu, Molecular design, chemical synthesis, and biological evaluation of “4-1” pentacyclic aryl/heteroaryl-imidazonaphthalimides, *Bioorg. Med. Chem.* 15 (2007) 5114–5121. <https://doi.org/10.1016/j.bmc.2007.05.032>.
- [95] X. Li, Y. Lin, Y. Yuan, K. Liu, X. Qian, Novel efficient anticancer agents and DNA-intercalators of 1,2,3-triazol-1,8-naphthalimides: design, synthesis, and biological activity, *Tetrahedron* 67 (2011) 2299–2304. <https://doi.org/10.1016/j.tet.2011.01.063>.
- [96] X. Li, Y. Lin, Q. Wang, Y. Yuan, H. Zhang, X. Qian, The novel anti-tumor agents of 4-triazol-1,8-naphthalimides: synthesis, cytotoxicity, DNA intercalation and photocleavage, *Eur. J. Med. Chem.* 46 (2011) 1274–1279. <https://doi.org/10.1016/j.ejmech.2011.01.050>.
- [97] Q. Yang, P. Yang, X. Qian, L. Tong, Naphthalimide intercalators with chiral amino side chains: effects of chirality on DNA binding, photodamage and antitumor cytotoxicity, *Bioorg. Med. Chem. Lett* 18 (2008) 6210–6213. <https://doi.org/10.1016/j.bmcl.2008.09.104>.
- [98] I. Ott, Y. Xu, J. Liu, M. Kokoschka, M. Harlos, W.S. Sheldrick, X. Qian, Sulfur-substituted naphthalimides as photoactivatable anticancer agents: DNA interaction, fluorescence imaging, and phototoxic effects in cultured tumor cells, *Bioorg. Med. Chem.* 16 (2008) 7107–7116. <https://doi.org/10.1016/j.bmc.2008.06.052>.
- [99] S. Tan, H. Yin, Z. Chen, X. Qian, Y. Xu, Oxo-heterocyclic fused naphthalimides as antitumor agents: synthesis and biological evaluation, *Eur. J. Med. Chem.* 62 (2013) 130–138. <https://doi.org/10.1016/j.ejmech.2012.12.039>.
- [100] J. Zhou, C. Fang, Y. Liu, Y. Zhao, N. Zhang, X. Liu, F. Wang, D. Shanguan, Visible-light-induced cleavage of 4- $\alpha$ -amino acid substituted naphthalimides and its application in DNA photocleavage, *Org. Biomol. Chem.* 13 (2015) 3931–3935. <https://doi.org/10.1039/C5OB00302D>.
- [101] A. Kamal, R. Ramu, V. Tekumalla, G.B. Ramesh Khanna, M.S. Barkume, A.S. Juvekar, S.M. Zingde, Remarkable DNA binding affinity and potential anticancer activity of pyrrolo[2,1-c][1,4]benzodiazepine-naphthalimide conjugates linked through piperazine side-armed alkane spacers, *Bioorg. Med. Chem.* 16 (2008) 7218–7224. <https://doi.org/10.1016/j.bmc.2008.06.034>.
- [102] A. Kamal, S. Azeeda, E. V. Bharathi, M.S. Malik, R.V.C.R.N.C. Shetti, Search for new and novel chemotherapeutics for the treatment of human malignancies, *Mini Rev. Med. Chem.* 10 (2010) 405–435. <https://doi.org/10.2174/138955710791330918>.
- [103] A. Kamal, B.S.N. Reddy, G.S.K. Reddy, G. Ramesh, Design and synthesis of C-8 linked pyrrolobenzodiazepine-naphthalimide hybrids as anti-tumour agents, *Bioorg. Med. Chem. Lett* 12 (2002) 1933–1935. [https://doi.org/10.1016/S0960-894X\(02\)00326-8](https://doi.org/10.1016/S0960-894X(02)00326-8).
- [104] M. Rettig, A. Kamal, R. Ramu, J. Mikolajczak, K. Weisz, Spectroscopic and calorimetric studies on the DNA recognition of pyrrolo[2,1-c][1,4]benzodiazepine hybrids, *Bioorg. Med. Chem.* 17 (2009) 919–928. <https://doi.org/10.1016/j.bmc.2008.11.033>.
- [105] M. Rettig, W. Langel, A. Kamal, K. Weisz, NMR structural studies on the covalent DNA binding of a pyrrolobenzodiazepine-naphthalimide conjugate, *Org. Biomol. Chem.* 8 (2010) 3179–3187. <https://doi.org/10.1039/c001893g>.
- [106] A. Kamal, S.F. Adil, J. Tamboli, B. Siddardha, U.S.N. Murthy, Synthesis of coumarin linked naphthalimide conjugates as potential anticancer and antimicrobial agents, *Letts. Drug Des. Discov.* 6 (2009) 201–209. <https://doi.org/10.2174/157018009787847855>.
- [107] Y.H. Kim, Management with topical nitrogen mustard in mycosis fungoides, *Dermatol. Ther.* 16 (2003) 288–298. <https://doi.org/10.1111/j.1396-0296.2003.01640.x>.
- [108] S.Q. Xie, Y.H. Zhang, Q. Li, F.H. Xu, J.W. Miao, J. Zhao, C.J. Wang, 3-Nitro-naphthalimide and nitrogen mustard conjugate NNM-25 induces hepatocellular carcinoma apoptosis via PARP-1/p53 pathway, *Apoptosis* 17 (2012) 725–734. <https://doi.org/10.1007/s10495-012-0712-7>.
- [109] Q. Lou, L. Ji, W. Zhong, S. Li, S. Yu, Z. Li, X. Meng, Synthesis and cytotoxicity evaluation of naphthalimide derived N-mustards, *Molecules* 19 (2014) 8803–8819. <https://doi.org/10.3390/molecules19078803>.
- [110] T. Brider, B. Redko, M. Oron-Herman, A. Cohen-Matzlich, G. Gerlitz, G. Gellerman, F. Grynszpan, Synthesis and in vitro anticancer evaluation of 1,8-naphthalimide N(4) and S(4)-derivatives combining DNA intercalation and alkylation capabilities, *Res. Chem. Intermed.* 42 (2016) 1741–1757. <https://doi.org/10.1007/s11164-015-2115-1>.
- [111] J. Holley, A. Mather, P. Cullis, M.R. Symons, P. Wardman, R.A. Watt, G.M. Cohen, Uptake and cytotoxicity of novel nitroimidazole-polyamine conjugates in ehrlich ascites tumour cells, *Biochem. Pharmacol.* 43 (1992) 763–769. [https://doi.org/10.1016/0006-2952\(92\)90241-A](https://doi.org/10.1016/0006-2952(92)90241-A).
- [112] S. Xie, J. Wang, Y. Zhang, C. Wang, Antitumor conjugates with polyamine vectors and their molecular mechanisms, *Exp. Opin. Drug Deliv.* 7 (2010) 1049–1061. <https://doi.org/10.1517/17425247.2010.504205>.
- [113] Z.Y. Tian, S.Q. Xie, Y.W. Du, Y.F. Ma, J. Zhao, W.Y. Gao, C.J. Wang, Synthesis, cytotoxicity and apoptosis of naphthalimide polyamine conjugates as anti-tumor agents, *Eur. J. Med. Chem.* 44 (2009) 393–399. <https://doi.org/10.1016/j.ejmech.2008.02.044>.
- [114] Z. Tian, S. Xie, Z. Mei, J. Zhao, W. Gao, C. Wang, Conjugation of substituted naphthalimides to polyamines as cytotoxic agents targeting the Akt/mTOR signal pathway, *Org. Biomol. Chem.* 7 (2009) 4651–4660. <https://doi.org/10.1039/b912685f>.
- [115] Z. Tian, Y. Huang, Y. Zhang, L. Song, Y. Qiao, X. Xu, C. Wang, Spectroscopic and molecular modeling methods to study the interaction between naphthalimide-polyamine conjugates and DNA, *J. Photochem. Photobiol. B*

- Biol. 158 (2016) 1–15. <https://doi.org/10.1016/j.jphotobiol.2016.01.017>.
- [116] Z.Y. Tian, J.H. Li, Q. Li, F.L. Zang, Z.H. Zhao, C.J. Wang, Study on the synthesis, biological activity and spectroscopy of naphthalimide-diamine conjugates, *Molecules* 19 (2014) 7646–7668. <https://doi.org/10.3390/molecules19067646>.
- [117] Z. Tian, L. Su, S. Xie, J. Zhao, C. Wang, Synthesis, biological activity and fluorescence spectroscopy of naphthalimide-polyamine conjugates, *Chin. J. Org. Chem.* 33 (2013) 1514–1521. <https://doi.org/10.6023/cjoc201301008>.
- [118] L. Yang, J. Zhao, Y. Zhu, Z. Tian, C. Wang, Reactive oxygen species (ROS) accumulation induced by mononaphthalimide-spermidine leads to intrinsic and AIF-mediated apoptosis in HeLa cells, *Oncol. Rep.* 25 (2011) 1099–1107. <https://doi.org/10.3892/or.2011.1173>.
- [119] K. Wang, H. An, Y. Wang, X. Yan, R. Li, H. Chen, P. Zhang, J. Li, X. Li, J. Zhang, Synthesis, DNA binding properties and bioactivity of naphthalimide polyethylene imine conjugates, *Chin. J. Org. Chem.* 32 (2012) 696–702. <https://doi.org/10.6023/cjoc112052>.
- [120] Y. Wang, J. Zhang, M. Li, M. Li, S. Xie, C. Wang, Synthesis and evaluation of novel amonafide-polyamine conjugates as anticancer agents, *Chem. Biol. Drug Des.* 89 (2017) 670–680. <https://doi.org/10.1111/cbdd.12888>.
- [121] M. Li, Y. Wang, J. Zhang, S. Xie, C. Wang, Y. Wu, Synthesis and biological evaluation of novel aromatic imide-polyamine conjugates, *Molecules* 21 (2016) 1637–1652. <https://doi.org/10.3390/molecules21121637>.
- [122] X. Wang, Z. Chen, L. Tong, S. Tan, W. Zhou, T. Peng, K. Han, J. Ding, H. Xie, Y. Xu, Naphthalimides exhibit in vitro antiproliferative and antiangiogenic activities by inhibiting both topoisomerase II (topo II) and receptor tyrosine kinases (RTKs), *Eur. J. Med. Chem.* 65 (2013) 477–486. <https://doi.org/10.1016/j.ejmech.2013.05.002>.
- [123] H. Ihmels, D. Otto, Intercalation of organic dye molecules into double-stranded DNA – general principles and recent developments, *Supramolecular Dye Chem.* 258 (2005) 161–204. <https://doi.org/10.1007/b135804>.
- [124] M.H. David-Cordonnier, M.P. Hildebrand, B. Baldeyrou, A. Lansiaux, C. Keuser, K. Benzschawel, T. Lemstr, U. Pindur, Design, synthesis and biological evaluation of new oligopyrrole carboxamides linked with tricyclic DNA-intercalators as potential DNA ligands or topoisomerase inhibitors, *Eur. J. Med. Chem.* 42 (2007) 752–771. <https://doi.org/10.1016/j.ejmech.2006.12.039>.
- [125] E.B. Pedersen, A.M.A. Osman, P.T. Jorgensen, N. Bomholt, Intercalating Triplexes and Duplexes Using Aryl Naphthoimidazol and Process for the Preparation Thereof, 2019. WO 2009/135890.
- [126] A. Kamal, P.P. Kumar, Novel Naphthalimide-benzimidazole Hybrids as Potential Antitumour Agents and Process for the Preparation Thereof, 2009. WO 2009/110000.
- [127] A. Wu, P. Mei, Y. Xu, X. Qian, Novel naphthalimide-benzoic acid conjugates as potential apoptosis-inducing agents: design, synthesis, and biological activity, *Chem. Biol. Drug Des.* 78 (2011) 941–947. <https://doi.org/10.1111/j.1747-0285.2011.01232.x>.
- [128] A. Wu, Y. Xu, X. Qian, Novel naphthalimide-indomethacin hybrids as potential antitumor agents: effects of linkers on hypoxic/oxic cytotoxicity and apoptosis-inducing activity, *Monatshfte Fur Chemie* 141 (2010) 893–899. <https://doi.org/10.1007/s00706-010-0337-x>.
- [129] G. Hawcroft, M. D'Amico, C. Albanese, A.F. Markham, R.G. Pestell, M. A Hull, Indomethacin induces differential expression of beta-catenin, gamma-catenin and T-cell factor target genes in human colorectal cancer cells, *Carcinogenesis* 23 (2002) 107–114. <https://doi.org/10.1093/carcin/23.1.107>.
- [130] M.K. Jones, H. Wang, B.M. Peskar, E. Levin, R.M. Itani, I.J. Sarfeh, A. S. Tarnawski, Inhibition of angiogenesis by nonsteroidal anti-inflammatory drugs: insight into mechanisms and implications for cancer growth and ulcer healing, *Nat. Med.* 5 (1999) 1418–1423. <https://doi.org/10.1038/70995>.
- [131] S. Tan, D. Sun, J. Lyu, X. Sun, F. Wu, Q. Li, Y. Yang, J. Liu, X. Wang, Z. Chen, H. Li, X. Qian, Y. Xu, Antiproliferative and apoptosis-inducing activities of novel naphthalimide-cyclam conjugates through dual topoisomerase (topo) I/II inhibition, *Bioorg. Med. Chem.* 23 (2015) 5672–5680. <https://doi.org/10.1016/j.bmc.2015.07.011>.
- [132] C.J. Anderson, R. Ferdani, Copper-64 radiopharmaceuticals for PET imaging of cancer: advances in preclinical and clinical research, *cancer biother. Radiopharm.* 24 (2009) 379–393. <https://doi.org/10.1089/cbr.2009.0674>.
- [133] N. Chitrappriya, W. Wang, Y.J. Jang, S.K. Kim, J.H. Kim, Ligand effect and cooperative role of metal ions on the DNA cleavage efficiency of mono and binuclear Cu(II) macrocyclic ligands complexes, *J. Inorg. Biochem.* 140 (2014) 153–159. <https://doi.org/10.1016/j.jinorgbio.2014.06.017>.
- [134] M. Fang, L. Wei, Z. Lin, G.Y. Lu, Synthesis and DNA cleavage properties of triazacrown derivatives, *Chin. J. Chem.* 32 (2014) 142–150. <https://doi.org/10.1002/cjoc.201300699>.
- [135] G.J. Ryan, R.B.P. Elmes, S.J. Quinn, T. Gunnlaugsson, Synthesis and photophysical evaluations of fluorescent quaternary bipyridyl-1,8-naphthalimide conjugates as nucleic acid targeting agents, *Supramol. Chem.* 24 (2012) 175–188. <https://doi.org/10.1080/10610278.2011.638381>.
- [136] A. Pain, S. Samanta, S. Dutta, A.K. Saxena, M. Shanmugavel, M. Sharma, G.N. Qazi, U. Sanyal, Synthesis and evaluation of ethylnitrosoureas of substituted naphthalimides as anticancer compounds, *Acta Pol. Pharm. – Drug Res.* 64 (2007) 27–33.
- [137] J. Kang, V.K.R. Tangadanchu, L. Gopala, W.-W. Gao, Y. Cheng, H.-B. Liu, R.-X. Geng, S. Li, C.-H. Zhou, Novel potentially antibacterial naphthalimide-derived metronidazoles: design, synthesis, biological evaluation and supramolecular interactions with DNA, human serum albumin and topoisomerase II, *Chin. Chem. Lett.* 28 (2017) 1369–1374. <https://doi.org/10.1016/j.ccl.2017.04.002>.
- [138] A. Kamal, S.F. Adil, J.R. Tamboli, B. Siddardha, U.S.N. Murthy, Synthesis and anticancer activity of phthalimido and naphthalimido substituted dihydropyrimidone conjugates, *Lett. Drug Des. Discov.* 5 (2008) 261–270. <https://doi.org/10.2174/157018008784619933>.
- [139] H.K. Hariprakash, T. Kosakowska-Cholody, C. Meyer, W.M. Cholody, S.F. Stinson, N.I. Tarasova, C.J. Michejda, Optimization of naphthalimide-imidazoacridone with potent antitumor activity leading to clinical candidate (HKH40A, RTA 502), *J. Med. Chem.* 50 (2007) 5557–5560. <https://doi.org/10.1021/jm7009777.3>.
- [140] M.C. Wieslaw, M. Sante, P.L. Jolanta, J. Konopa, 5-[(Aminoalkyl) amino]imidazo[4,5,1-d]acridine-6-ones as a novel class of antineoplastic agents – synthesis and biological activity, *J. Med. Chem.* 33 (1990) 49–52. <https://doi.org/10.1021/jm00163a009>.
- [141] T. Kosakowska-Cholody, W.M. Cholody, A. Monks, B.A. Woyrnarowska, C.J. Michejda, WMC-79, a potent agent against colon cancers, induces apoptosis through a p53-dependent pathway, *Mol. Canc. Therapeut.* 4 (2005) 1617–1627. <https://doi.org/10.1158/1535-7163.MCT-05-0170>.
- [142] W.M. Cholody, T. Kosakowska-Cholody, M.G. Hollingshead, H.K. Hariprakash, C.J. Michejda, A new synthetic agent with potent but selective cytotoxic activity against cancer, *J. Med. Chem.* 13 (2005) 4474–4481. <https://doi.org/10.1021/jm048946x>.
- [143] H.-K. Liu, P.J. Sadler, Metal complexes as DNA intercalators metal complexes as DNA intercalators liu and sadler, *Acc. Chem. Res.* 29 (2011) 349–359. <https://doi.org/10.1021/ar100140e>.
- [144] I. Ott, X. Qian, Y. Xu, D.H.W. Vlecken, I.J. Marques, D. Kubutat, J. Will, W.S. Sheldrick, P. Jesse, A. Prokop, C.P. Bagowski, A gold(I) phosphine complex containing a naphthalimide ligand functions as a TrxR inhibiting antiproliferative agent and angiogenesis inhibitor, *J. Med. Chem.* 52 (2009) 763–770. <https://doi.org/10.1021/jm8012135>.
- [145] S. Banerjee, J. a Kitchen, S. a Bright, J.E. O'Brien, D.C. Williams, J.M. Kelly, T. Gunnlaugsson, Synthesis, spectroscopic and biological studies of a fluorescent Pt(II) (terpy) based 1,8-naphthalimide conjugate as a DNA targeting agent, *Chem. Commun.* 49 (2013) 8522–8524. <https://doi.org/10.1039/c3cc44962a>.
- [146] M. Cusumano, M. Letizia, D. Pietro, A. Giannetto, Stacking surface effect in the DNA intercalation of some polypyridine platinum (II) complexes, *Inorg. Chem.* 38 (1999) 1754–1758. <https://doi.org/10.1021/ic9809759>.
- [147] L. Zhao, J. Li, Y. Li, J. Liu, T. Wirth, Z. Li, Selenium-containing naphthalimides as anticancer agents: design, synthesis and bioactivity, *Bioorg. Med. Chem.* 20 (2012) 2558–2563. <https://doi.org/10.1016/j.bmc.2012.02.049>.
- [148] D.N. Karelia, U.H. Sk, P. Singh, A.S.P. Gowda, M.K. Pandey, S.R. Ramisetty, S. Amin, A.K. Sharma, Design, synthesis, and identification of a novel naphthalimide-isoselenocyanate compound NISC-6 as a dual Topoisomerase-II $\alpha$  and Akt pathway inhibitor, and evaluation of its anti-melanoma activity, *Eur. J. Med. Chem.* 135 (2017) 282–295. <https://doi.org/10.1016/j.ejmech.2017.04.052>.
- [149] S.S. Roy, P. Chakraborty, P. Ghosh, S. Ghosh, J. Biswas, S. Bhattacharya, Influence of novel naphthalimide-based organoselenium on genotoxicity induced by an alkylating agent: the role of reactive oxygen species and selenoenzymes, *Redox Rep.* 17 (2012) 157–166. <https://doi.org/10.1179/1351000212Y.0000000018>.
- [150] S. Mati, S. Roy, S. Chall, S. Bhattacharya, Unveiling the groove binding mechanism of a biocompatible naphthalimide-based organoselenocyanate with calf thymus DNA: an “ex vivo” fluorescence imaging, *J. Phys. Chem. B* 117 (2013) 14655–14665. <https://doi.org/10.1021/jp4090553>.
- [151] P. Ghosh, S. Singha Roy, A. Basu, A. Bhattacharjee, S. Bhattacharya, Sensitization of cisplatin therapy by a naphthalimide based organoselenium compound through modulation of antioxidant enzymes and p53 mediated apoptosis, *Free Radic. Res.* 49 (2015) 453–471. <https://doi.org/10.3109/10715762.2015.1012079>.
- [152] W. Streciwilk, A. Terenzi, R. Misgeld, C. Frias, P.G. Jones, A. Prokop, B.K. Keppler, I. Ott, Metal NHC complexes with naphthalimide ligands as DNA-Interacting antiproliferative agents, *ChemMedChem* 12 (2017) 214–225. <https://doi.org/10.1002/cmdc.201600557>.
- [153] K. Ghebreyessus, A. Peralta, M. Katdare, K. Prabhakaran, S. Paranawithana, Ruthenium(II)-Arene complexes with naphthalimide-tagged N,O- and N,N-chelating ligands: synthesis and biological evaluation, *Inorg. Chim. Acta.* 434 (2015) 239–251. <https://doi.org/10.1016/j.ica.2015.05.025>.
- [154] H. Wang, Y. Liu, M. Li, H. Huang, H.M. Xu, R.J. Hong, H. Shen, Multifunctional TiO<sub>2</sub>nanowires-modified nanoparticles bilayer film for 3D dye-sensitized solar cells, *Optoelectron. Adv. Mater. Rapid Commun.* 4 (2010) 1166–1169. <https://doi.org/10.1039/c5dt00360a>.
- [155] G.J. Ryan, S. Quinn, T. Gunnlaugsson, Highly effective DNA photocleavage by novel “rigid” Ru(bpy) 3-4-nitro- and -4-amino-1,8-naphthalimide conjugates, *Inorg. Chem. Commun.* 47 (2008) 401–403. <https://doi.org/10.1021/ic700967y>.
- [156] X. Xiao, J. Liang, J. Xie, X. Liu, D. Zhu, Y. Dong, Organotin(IV) carboxylates based on 2-(1,3-dioxo-1 H -benzo[d]isoquinolin-2(3H)-yl)acetic acid: syntheses, crystal structures, luminescent properties and antitumor activities, *J. Mol. Struct.* 1146 (2017) 233–241. <https://doi.org/10.1016/j.molstruc.2017.05.141>.
- [157] K.J. Kilpin, C.M. Clavel, F. Edefe, P.J. Dyson, Naphthalimide-tagged

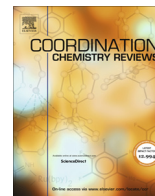
- ruthenium-arene anticancer complexes: combining coordination with intercalation, *Organometallics* 31 (2012) 7031–7039. <https://doi.org/10.1021/om3007079>.
- [158] A. Meyer, L. Oehninger, Y. Geldmacher, H. Alborzina, S. Wölfl, W.S. Sheldrick, I. Ott, Gold(I) N-heterocyclic carbene complexes with naphthalimide ligands as combined thioredoxin reductase inhibitors and DNA intercalators, *ChemMedChem* 9 (2014) 1794–1800. <https://doi.org/10.1002/cmdc.201402049>.
- [159] S. Mao, K. Shen, X. Shi, Y. Xu, H. Wu, Synthesis, crystal structures, and biological properties of a new naphthalimide Schiff base and its copper(II) complex, *J. Coord. Chem.* 70 (2017) 3677–3691. <https://doi.org/10.1080/00958972.2017.1407409>.
- [160] Y. Chen, S. Mao, X. Shi, K. Shen, H. Wu, Synthesis, crystal structure, DNA-binding properties and antioxidant activity of a copper(II) complex with naphthalimide Schiff base, *Z. Anorg. Allg. Chem.* 643 (2017) 1182–1190. <https://doi.org/10.1002/zaac.201700207>.
- [161] S. Roy, S. Saha, R. Majumdar, R.R. Dighe, A.R. Chakravarty, Photocytotoxic 3d-metal scorpionates with a 1,8-naphthalimide chromophore showing photoinduced DNA and protein cleavage activity, *Inorg. Chem.* 48 (2009) 9501–9509. <https://doi.org/10.1021/ic9015355>.
- [162] J.M. Herrera, F. Mendes, I. Santos, C.N. Ranninger, S. Cabrera, G. Quiroga, Design and biological evaluation of new platinum(II) complexes bearing ligands with DNA-targeting ability, *Inorg. Chem.* 53 (2014) 12627–12634. <https://doi.org/10.1021/ic502373n>.
- [163] F. Navas, F. Mendes, I. Santos, C. Navarro-Ranninger, S. Cabrera, A.G. Quiroga, Enhanced cytotoxicity and reactivity of a novel platinum(IV) family with DNA-targeting naphthalimide ligands, *Inorg. Chem.* 56 (2017) 6175–6183. <https://doi.org/10.1021/acs.inorgchem.7b00136>.
- [164] C.A. Davey, W.H. Ang, C.F. Chin, Platinum Complexes as Anticancer Agents, *WO* 2016/028225, 2016.
- [165] Q. Li, T. a van den Berg, B.L. Feringa, G. Roelfes, Mononuclear Fe(II)-N4Py complexes in oxidative DNA cleavage: structure, activity and mechanism, *Dalton Trans.* 39 (2010) 8012–8021. <https://doi.org/10.1039/b927145g>.
- [166] Q. Li, W.R. Browne, G. Roelfes, DNA cleavage activity of Fe(II)N4Py under photo irradiation in the presence of 1,8-naphthalimide and 9-aminoacridine: unexpected effects of reactive oxygen species scavengers, *Inorg. Chem.* 50 (2011) 8318–8325. <https://doi.org/10.1021/ic2008478>.

## **Publikacja P.6**

Cyclen-based artificial nucleases: Three decades of development (1989–2022). Part a – hydrolysis of phosphate esters.

**Tomczyk, M. D.\*; Kuźnik, N.\*; Walczak, K.**

*Coordination Chemistry Reviews* **2023**, *481*, 215047.



## Review

## Cyclen-based artificial nucleases: Three decades of development (1989–2022). Part a – Hydrolysis of phosphate esters



Mateusz D. Tomczyk\*, Nikodem Kuźnik\*, Krzysztof Walczak

Department of Organic Chemistry, Bioorganic Chemistry and Biotechnology, Silesian University of Technology, ul. Krzywoustego 4, 44-100 Gliwice, Poland

## ARTICLE INFO

## Article history:

Received 14 September 2022

Accepted 22 January 2023

## Keywords:

Cyclen complexes  
Artificial nucleases  
Artificial enzymes  
DNA hydrolysis  
Phosphate hydrolysis

## ABSTRACT

The first part of the review summarizes more than three decades of research on cyclen complexes, with a particular focus on complexes that exhibit hydrolytic (or transesterification) activity against small-molecule model phosphodiester and their larger natural counterparts, such as nucleic acids. The second part of the paper will focus on the same family of complexes that cleave phosphodiester oxidatively. The review collects results for nearly 200 examples of *f*- and *d*-block metal complexes of cyclen and its *N*-functionalized derivatives, as well as examples of metal-free catalysts based on the cyclen scaffold that show nucleolytic activity. The purpose of the review is to summarize possibly all of the complexes reported so far and to determine the impact of cyclen functionalization, particularly the effect of side arms on their application as artificial nucleases for medical purposes. In the review, we also tried to include some side topics, such as comparisons of the presented complexes to natural nucleases or closely related complexes of other azamacrocycles, in order to fully introduce the topic to readers entering this field of science.

© 2023 Elsevier B.V. All rights reserved.

## Contents

1. Introduction	2
1.1. Importance and purpose	2
1.2. Searching methodology	2
1.3. Final remarks	3
2. Mononuclear catalysts	3
2.1. Mononuclear complexes of <i>f</i> -block metals	3
2.1.1. Examples	3
2.1.2. Conclusions	8
2.2. Mononuclear complexes of <i>d</i> -block metals	11
2.2.1. Role of zinc ions in natural metalloenzymes	12
2.2.2. Effect of ligand size and structure on zinc complexes	13

**Abbreviations:** Acrcyclen, acridinylmethylcyclen; ALP, alkaline phosphatase; ATP, adenosine triphosphate; BNPP, bis(*p*-nitrophenyl) phosphate;  $\beta_{\text{nuc}}$ , Brønsted coefficient; C/BP, molar ratio of catalyst to base pairs; CPP, cyclic propylene phosphate; CHES, *N*-cyclohexyl-2-aminoethanesulfonic acid; C/S, molar ratio of catalyst to substrate; CT-DNA, calf thymus DNA; cyclen, 1,4,7,10-tetraazacyclododecane; DEP, diethyl phosphate; DENP, diethyl 2,4-dinitrophenylphosphate; DTPA, diethylenetriaminepentaacetic acid; ds-DNA, double-stranded DNA; DSC, double-strand cuts; DSP, distearoylphosphatidylcholine; EB, ethidium bromide; EDTA, ethylenediaminetetraacetic acid; ENP, ethyl 4-nitrophenyl phosphate; HEPES, 4-(2-hydroxyethyl)-1-piperazineethanesulfonic acid; HEPPS, 4-(2-Hydroxyethyl)-1-piperazinepropanesulfonic acid; HPNP, 2-hydroxypropyl-4-nitrophenyl phosphate; HPP, 2-hydroxypropylphenyl phosphate;  $k_2$ , second order rate constant;  $K_a$ , acid dissociation constant;  $K_{\text{app}}$ , Apparent rate constant;  $K_b$ , binding constant;  $K_f$ , stability constant;  $k_{\text{obs}}$ , pseudo-first-order rate constant; L, ligand; MOPS, 3-(*N*-morpholino)propanesulfonic acid; lncRNA, long non-coding RNA; mRNA, messenger RNA; miRNA, microRNA; MP, methyl phosphate; NP, 4-nitrophenyl phosphate; NP1, Nuclease P1; NTA, nitrilotriacetic acid; PAP, purple acid phosphatases; PASP, polyaspartic acid; PB, phosphate buffer;  $\text{pH}_e$ , extracellular pH;  $\text{pH}_i$ , intracellular pH; PNA, peptide nucleic acid; PP, phenyl phosphate; RFI, amount of relaxed form I DNA; *rt*, room temperature; saliden, *N,N'*-disalicylidenediethylenetriamine; SSC, single-strand cuts; ss-DNA, single-stranded DNA;  $t_{1/2}$ , time of half-life; TEA, Tris-acetate-EDTA buffer; TREN, tris(2-aminoethyl)amine; Tris, tris(hydroxymethyl)aminomethane; TRPN, tris(3-aminopropyl)amine.

\* Corresponding authors.

E-mail addresses: [mateusz.d.tomczyk@polsl.pl](mailto:mateusz.d.tomczyk@polsl.pl) (M.D. Tomczyk), [nikodem.kuznik@polsl.pl](mailto:nikodem.kuznik@polsl.pl) (N. Kuźnik).

2.2.3.	Hydrolysis of RNA-like substrates by zinc complexes	13
2.2.4.	Hydrolysis of DNA-like substrates by zinc complexes	15
2.2.5.	Examples of mononuclear <i>d</i> -block cyclen complexes	16
2.2.6.	Mononuclear <i>d</i> -block complexes with nucleic acid binders	18
2.2.7.	Free cyclen ligands with nucleolytic activity	19
2.2.8.	Recognition of thymine and uridine by Zn(II)-cyclen.	19
2.2.9.	Effect of side arms on <i>d</i> -block complexes.	21
2.2.10.	Conclusions on mononuclear <i>d</i> -block complexes.	23
3.	Multinuclear catalysts	24
3.1.	Dinuclear complexes	24
3.1.1.	Examples of <i>f</i> -block and <i>d</i> -block dinuclear complexes	24
3.1.2.	Effect of linker structure on dinuclear zinc complexes	27
3.2.	Multinuclear and supramolecular complexes	28
3.2.1.	Examples	28
3.2.2.	Conclusions	30
4.	Concluding remarks	32
	Funding	33
	Declaration of Competing Interest	33
	References	33

## 1. Introduction

### 1.1. Importance and purpose

More than three decades ago, Chin *et al.* first demonstrated that a 12-membered tetraazamacrocyclic Co(III) complex with 1,4,7,10-tetraazacyclododecane (cyclen) effectively promotes the hydrolysis of bis(*p*-nitrophenyl) phosphate (BNPP), a small-molecule model of the DNA phosphodiester backbone.[1] Cyclen has quickly become a popular scaffold for obtaining complexes that mimic the action of natural nucleases, contributing to the development of their artificial analogs that could be used for therapeutic purposes. Since then, there has been a steady increase in the number of articles and interest in cyclen-based lanthanide and transition metal complexes that promote the cleavage of phosphate esters. Due to their biological importance, the most noteworthy structures employing phosphate esters are deoxyribonucleic acid (DNA) and ribonucleic acid (RNA). Although uncatalyzed hydrolysis of nucleic acids is extremely slow (the half-life of DNA hydrolysis under physiological conditions is about 130,000 years), the rate of DNA hydrolysis *in vivo* is increased about  $10^{16}$ -fold by natural enzymes of the nuclease family, allowing DNA to be processed at a rate necessary for life.[2–4] Typically, it is the natural nucleases that are more efficient and specific in cleaving nucleic acids than their artificial mimetics, but the latter are more stable than proteins and can therefore work under a wider range of conditions. The advantages of simple structure and high stability make artificial nucleases of increasing interest in the development of new artificial systems that favor the cleavage of phosphate esters found in biological structures. From an application perspective, artificial nucleases may be highly desirable as potential therapeutics for cancer and gene therapy, both as small-molecule compounds and in combination with larger biological vectors such as antisense oligonucleotides, as well as versatile tools in molecular and genetic diagnostics.

Due to the ease of functionalization of the cyclen ring through its *N*-atoms, most research in this field naturally focuses on the introduction of side arms and the study of their effects on catalytic activity, selectivity, and stability *in vitro* and in biological systems. Functionalization of the ligand, as well as the use of a specific metal ion, can not only affect the activity of the resulting complex,

but sometimes completely change the mechanism of phosphodiester cleavage. Most papers published up to 2022 present complexes that cleave phosphodiester by hydrolysis or transesterification (depending on the form of the active nucleophile), but many papers from this period also present complexes that act oxidatively, employing various types of reactive oxygen species to cleave or damage phosphodiester. Depending on the mechanism by which the complex cleaves phosphodiester, the effect of ligand functionalization on its activity varies, as activity comes from different sources. In order to introduce systematicity in tracing the structure–activity relationship and to make it easier for the reader to get acquainted with the extensive material generated over thirty years of research, we have divided the collected material into two parts. In the first part we consider almost exclusively complexes acting through nucleophilic cleavage (hydrolysis or transesterification), while in the second – through an oxidative mechanism. We conclude each chapter with a table containing examples of the most active complexes in groups sharing the same ligands.

### 1.2. Searching methodology

We have conducted the first such comprehensive review on the progress of research and applications of cyclen-based complexes exhibiting nucleolytic activity. This review covers scientific papers and patents from the early 1980s to 2022. The first report on the nucleolytic activity of cyclen complexes that we came across dates back to 1989, but artificial nucleases based on other ligands were already known. Research on the influence of side arms on nucleolytic activity began in earnest around 1994 with the pioneering studies of Prof. Janet K. Morrow. Extensive research was conducted to collect as many articles as possible from PubMed MEDLINE and SciFinder databases. No additional filters were applied to limit the search results. The first search was conducted in the SciFinder database using a Chemical Structure query with a Substructure search type to obtain results containing the chemical structures of interest. The structure we used in the search (Fig. 1) is essentially a cyclen molecule in which all nitrogen positions are available for functionalization (we left them with no attached hydrogens), while all carbon atoms were manually “blocked” by hydrogens. The keywords used to search PubMed and SciFinder

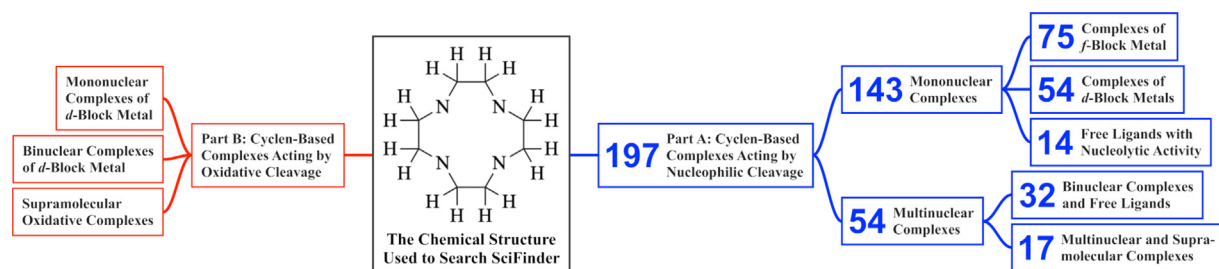


Fig. 1. Distribution and number of found cyclen complexes showing nucleolytic activity by metal type and ligand structure.

were: “artificial nucleases”, “tetraazacyclododecane complexes”, “cyclen complexes”, their combinations with “DNA hydrolysis activity”, “DNA cleavage activity” and related terms. After combining the results from the two libraries and removing duplicates, we selected 184 of them that met the purpose and scope of the review. We divided all the collected examples according to the methodology presented in Fig. 1 – we grouped the found examples primarily according to the two main cleavage mechanisms: nucleophilic cleavage or oxidative mechanism, and then according to the structure (e.g. nuclearity, metal ion type) of the complexes and the role of structural features present in them (e.g. DNA-binding molecules). To make it easier for the interested reader to compare the catalytic activity of different groups of complexes, at the end of each chapter we have included a table compiling the activities and selected features of the most active complexes, as well as conclusions about the influence of the structure of the complex on its activity.

### 1.3. Final remarks

Beginning in the section titled 2.2.5 *Examples of mononuclear d-block cyclen complexes*, we use the terms “cleavage” or “cleavage activity” to refer to the cleavage of covalently closed circular (form I) plasmid DNA. In some cases where information on DNA cleavage efficiency was missing from the original paper, but electrophoresis or other results were available, we have calculated the efficiency according to Eq. (1) and marked it with an asterisk.

$$RFI = \frac{\text{intensity of form I band}}{\text{intensity of whole line}} \times 100\% \quad (1)$$

## 2. Mononuclear catalysts

### 2.1. Mononuclear complexes of f-block metals

#### 2.1.1. Examples

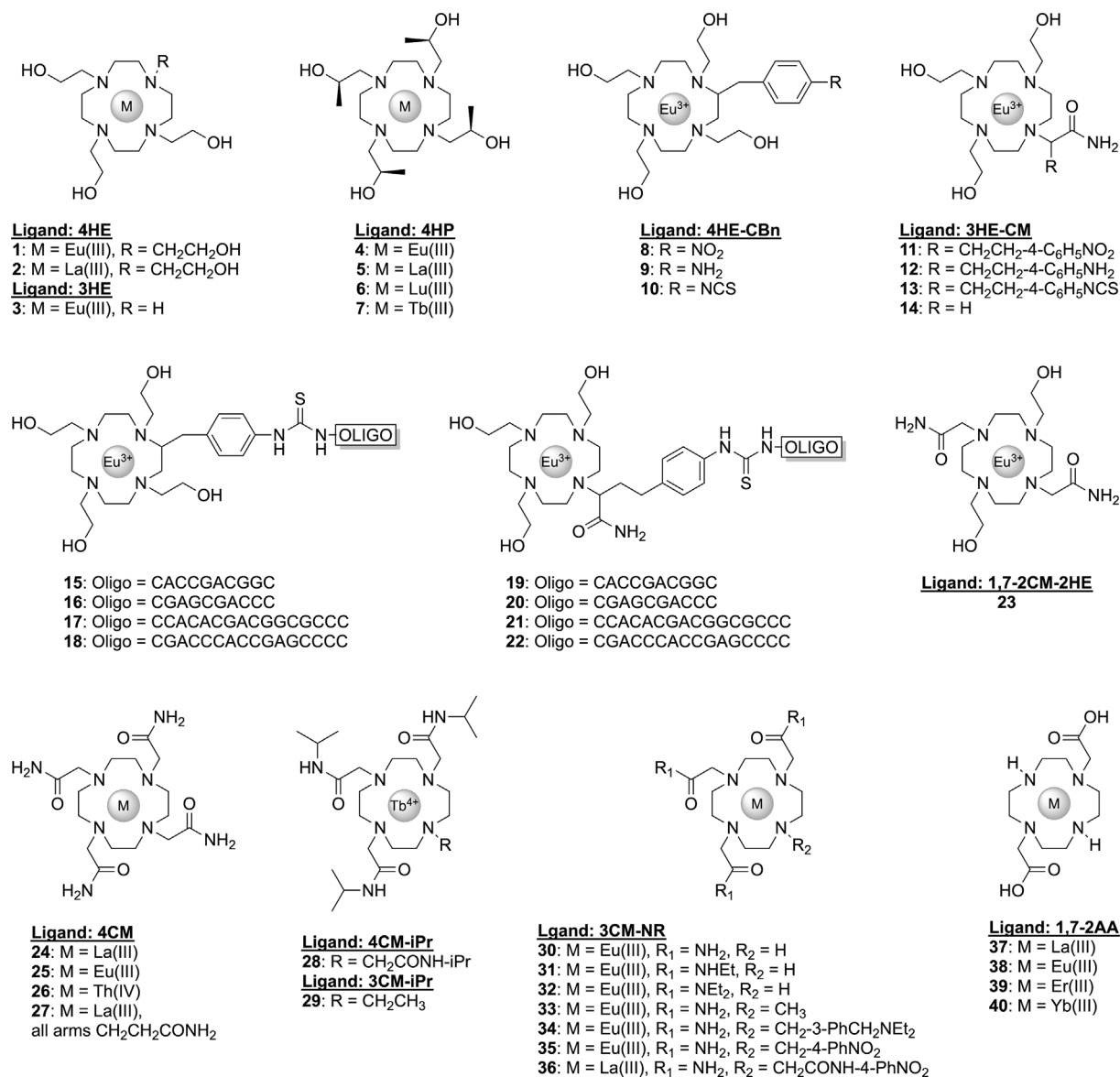
The earliest examples of f-block complexes modified with pendent arms containing donor atoms were described in 1994 by Morrow's group. Complexes **1–6** (Fig. 2) were shown to significantly accelerate the transesterification of HPNP (2-hydroxypropyl-4-nitrophenyl phosphate) in neutral aqueous media.[5–7] Under physiological-like conditions, the Eu(III) **1** complex consisting of four 2-hydroxyethyl arms is 10 times more active in cleaving BNPP than the analogous La(III) **2** complex. Eu(III) **1** with  $k_2 = 7.2 \times 10^{-2} \text{ M}^{-1} \text{ s}^{-1}$  is also several times more active than its stiffer analogs, Eu(III) **4**,  $k_2 = 1.4 \times 10^{-2} \text{ M}^{-1} \text{ s}^{-1}$ , and La(III) **5**,  $k_2 = 6.3 \times 10^{-2} \text{ M}^{-1} \text{ s}^{-1}$  (pH 7.5, 37 °C). The differences in activity between the two types of complexes were attributed to the positive effect of the more flexible 2-hydroxypropyl arms on the availability of the free coordination site needed to bind the substrate molecule. X-ray studies have shown that the 2-hydroxypropyl arms, due to the steric hindrance

resulting from the additional methyl group, form a more compact and rigid structure around the metal ion, thus limiting its accessibility to the substrate. Although Lu(III) **6** is the strongest Lewis acid in this series, resulting in the lowest  $pK_a$  of the metal-bound water, it is the least efficient promoter of transesterification. With few exceptions, usually among series with the same ligand structure, the cleavage efficiency is inversely proportional to the increase in Lewis acidity for lanthanides and decreases in the order: La(III) **5** > Eu(III) **4** > Lu(III) **6**. This behavior can be attributed to a decrease in the ionic radius in the lanthanide series by about 15% during the transition from the La(III) to Lu(III) ion (known as the lanthanide contraction effect), which translates into fewer coordination sites available for substrate binding in complexes of heavier lanthanides compared to lighter ones.[8–10].

Quite recently, Ma *et al.* showed that another complex from the 4HP ligand family, Tb(III) **7** (Fig. 2), in which Eu(III) is replaced by Tb(III), is an even more potent agent for cleaving HPNP and RNA with high selectivity toward A-specific sites.[11] The selectivity in cleaving oligonucleotide was confirmed by MALDI-TOF-MS and gel electrophoresis and decreased in the order: ApU > ApC > ApG > ApA, with an apparent preference for pyrimidine bases over purine ones. Interestingly, no reactions were observed with Tb(III) **7** within other nucleotide pairs. The exact mechanism of HPNP cleavage was further elucidated from the ESI-MS spectra and, as shown in Fig. 3a, involves the formation of an adduct between HPNP and Tb(III) **7**, accompanied by the release of a metal-bound water molecule, yielding an ion with  $m/z$  838.25. Then, an alkoxy ion derived from one of the side arms draws hydrogen from the 2'-hydroxyl group of HPNP, thereby activating an intramolecular nucleophile involved in the attack on the electrophilic phosphorus atom; the result is an ion with  $m/z$  350.33 derived from the adduct with CPP<sup>−</sup> (cyclic propylene phosphate). Dissociation of CPP<sup>−</sup> and re-coordination of the water molecule leads to full regeneration of the starting complex. HPNP cleavage studies showed that Tb(III) **7** ( $k_{\text{obs}} = 1.01 \times 10^{-2} \text{ min}^{-1}$ ; pH 7.2, 25 °C) is about 30 times more active than the analogous Eu(III) **4** ( $k_{\text{obs}} = 3.30 \times 10^{-4} \text{ min}^{-1}$ ; determined from Fig. 2 in ref. [5] for pH 7.2, 37 °C).

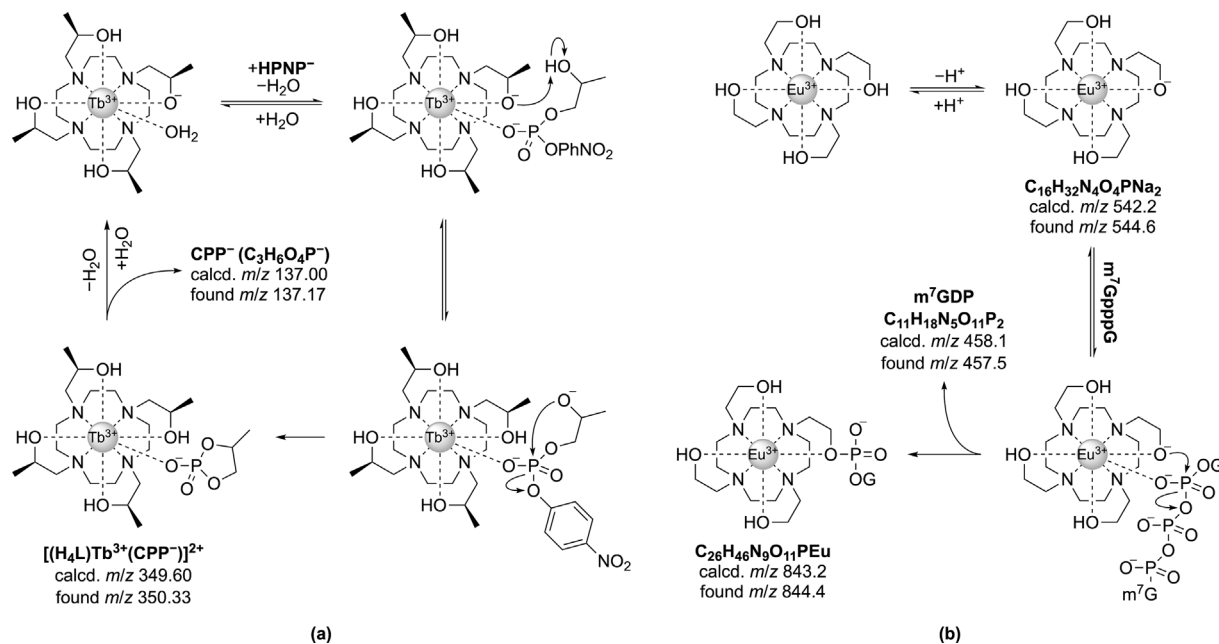
Studies on the mechanism of cleavage of 5'-capped mRNA/DNA hybrids in the presence of Eu(III) **1**, La(III) **2**, Eu(III) **4** and La(III) **24** showed that only Eu(III) **1** exhibits good reactivity toward oligonucleotides.[7,12] Using MALDI-TOF MS analysis of the reaction products of Eu(III) **1** and  $m^7\text{GpppG}$ , Baker and Morrow proposed a transesterification mechanism in which the 2-hydroxyethyl arm of Eu(III) **1** ionizes, forming a metal-bound alkoxy group, which carries out a nucleophilic attack on one of the phosphates and cleaves the 5'-capped substrate to form a covalent Eu(III) **1**- $m^7\text{GMP}$  adduct with  $m/z$  844.4 (Fig. 3b). In addition, it was shown that cleavage of the mRNA-DNA hybrid occurs only within the 5'-capped end. Similar conclusions regarding the structure of transesterification products were drawn from <sup>31</sup>P NMR analysis of the analogous reaction of Eu(III) **1** with BNPP. The product of this



Fig. 2. Examples of mononuclear *f*-block complexes 1–40.

reaction turns out to be a conjugate of Eu(III) **1** complex with a covalently bound phosphate diester (final product in Fig. 3b). Eu(III) **1** ( $k_{\text{obs}} = 2.0 \times 10^{-4} \text{ s}^{-1}$ ; pH 7.4, 37 °C) was found to be significantly more active in cleaving BNPP than the analogous La(III) **2** ( $k_{\text{obs}} = 0.27 \times 10^{-4} \text{ s}^{-1}$ ; pH 7.4, 37 °C). Lowering the reaction temperature from 37 to 25 °C reduced the activity of Eu(III) **1** to  $k_{\text{obs}} = 0.90 \times 10^{-4} \text{ s}^{-1}$ , while increasing the ionic strength by adding 0.1 M NaCl reduced its activity by almost half. Note: These are interesting results, as they clearly indicate the difficulty of directly comparing the activity of different groups of complexes, which were usually tested under different reaction conditions that differed not only in pH, but also in the catalyst-to-substrate (C/S) molar ratio. Most of the results on *f*-block metal complexes came from just a few scientific groups, so the studies were carried out under similar conditions (usually in HEPES buffer, pH 7.4, 37 °C) and their comparison should not be subject to much error. However, we observed that if the introduced modification has a clear effect on the activity of the complex, a significant increase in activity is observed, from one to several orders of magnitude, even with a lower C/S ratio; in contrast, if the modification decreases the activity of the complex, a significant decrease or even no activity is observed.

Studies on the effect of C-attached side arms (attached to the cyclen core but not as donors) on the efficiency of HPNP transesterification by Eu(III) **8–14** (Fig. 2) showed that Eu(III) **8** with four 2-hydroxyethyl arms and a C-attached 4-nitrobenzyl group is similarly active to Eu(III) **1**, but about 5-fold more active than Eu(III) **11**. [13–16] Note: We suspect that the increase in activity after the introduction of the 4-nitrobenzyl group may have a similar basis to that of Eu(III) **35**, discussed later in this chapter; the strong electron-withdrawing effect of the nitro group may lower the  $pK_a$  of the metal-bound species, probably the hydroxyl group of one of the side arms. In the case of Eu(III) **11**, the electron-withdrawing effect probably does not occur due to the greater distance from the metal ion. Replacing one hydroxyl-terminated arm of Eu(III) **1** ( $k_{\text{obs}} = 0.48 \times 10^{-4} \text{ s}^{-1}$ ; determined from Fig. 2 in ref. [5] for pH 7.3, 37 °C) with an amide-terminated arm resulted in a 5-fold reduction in the rate of HPNP cleavage by Eu(III) **14** ( $k_{\text{obs}} = 0.09 \times 10^{-4} \text{ s}^{-1}$ ; HEPES 10 mM, pH 7.3, 37 °C). The rate of HPNP cleavage by Eu(III) **14** is comparable to that by La(III) **5** ( $k_{\text{obs}} = 0.085 \times 10^{-4} \text{ s}^{-1}$ ; determined from Fig. 2 in ref. [5] for HEPES 10 mM, pH 7.3, 37 °C), however, the rate of cleavage of 3',5'-UpU by Eu(III) **14** ( $k_{\text{obs}} = 4.9 \times 10^{-8} \text{ s}^{-1}$ ) is about 10 times lower compared to La(III) **5** ( $k_{\text{obs}} = 39.8 \times 10^{-8} \text{ s}^{-1}$ ;



**Fig. 3.** Comparison of transesterification mechanisms common to lanthanide(III) complexes with a metal-bound alkoxy group. **(a)** Mechanism of HPNP cleavage, a model RNA-like substrate, derived from MALDI-TOF-MS results, ref. [11]. **(b)** Mechanism of triphosphate cleavage, a model DNA-like substrate, derived from ESI-MS results, ref. [12].

pH 8.9, 37 °C). Replacement of the second hydroxyl group in Eu(III) **14** with an amide group resulted in a further decrease in the cleavage activity of Eu(III) **23** ( $k_{\text{obs}} = 0.01 \times 10^{-4} \text{ s}^{-1}$ ). A similar order of activity was found in studies with BNPP, against which Eu(III) **11** ( $k_{\text{obs}} = 1.5 \times 10^{-4} \text{ s}^{-1}$ ; pH 7.4, 37 °C) was 4 times more active than Eu(III) **23** ( $k_{\text{obs}} = 3.5 \times 10^{-5} \text{ s}^{-1}$ ). The type of donor groups was found to have a profound effect on the  $\text{p}K_{\text{a}}$  of a metal-bound water molecule; for Eu(III) **23**  $\text{p}K_{\text{a}} = 8.1$ , while for Eu(III) **1** and Eu(III) **11**  $\text{p}K_{\text{a}} = 7.5$ , indicating that the former is a much weaker Lewis acid, which seems to be the reason for the decrease in activity.

The reason for the C-modification described above was to enable the attachment of Eu(III) complexes to antisense oligonucleotides to obtain sequence-specific artificial nucleases. Such conjugates, in addition to being a useful tool in molecular biology, may provide promising models for the development of new gene therapies. In 2000, Morrow's group presented such conjugates with sequences complementary to the codon 12 region of the Ha-ras oncogene, **15**, **17**, **19** and **21** (Fig. 2), and their scrambled analogues, **16**, **18**, **20** and **22**, and tested their cleavage activity on the 25-mer RNA corresponding to this codon.[14] Only conjugates with sequences complementary to the oncogene promoted its cleavage, while no cleavage was observed in the presence of the conjugates with scrambled sequences or metal-free conjugates (pH 7.5, 37 °C for 16 h). Under these conditions, the activity (% RNA cleavage) decreases in the order: **21** (14%) > **17** (10%) > **19** (9%) > **15** (8%). Interestingly, cleavage was observed only within the non-hybridized part of the RNA and mainly at the C19 site, while the hybridized part remained intact. In contrast, when Eu(III) **21** was reacted with RNA in the absence of salt to prevented full hybridization, non-selective cleavage was observed at several sites in the sequence.

Replacement of all hydroxyl-terminated arms with amide-terminated arms in complexes **24–27** (Fig. 2) resulted in an overall increase in the activity of La(III)-containing complexes, but a decrease in the activity of Eu(III)-containing complexes; for example La(III) **24** ( $k_{\text{obs}} = 0.16 \times 10^{-4} \text{ s}^{-1}$ ; pH 7.3, 37 °C) is significantly more active in HPNP transesterification than La(III) **5** ( $k_{\text{obs}} = 0.085 \times 10^{-4} \text{ s}^{-1}$ ; determined from Fig. 2 in ref. [5] for similar condi-

tions).[17,18] Although the radii of Th(IV) and Eu(III) ions are nearly equal, Th(IV) **26** ( $k_{\text{obs}} = 7.5 \times 10^{-4} \text{ s}^{-1}$ ) was the most active in this series, while Eu(III) **25** remains completely inactive. The reason for this surprising lack of activity of Eu(III) **25** is probably that Eu(III) in this complex cannot bind to the phosphodiester group. [19] As can be seen from the X-ray structure (Fig. 4), Eu(III) **25** is almost completely encapsulated by the macrocyclic ligand and its arms. <sup>31</sup>P NMR studies showed that Eu(III) **25**, unlike the other examples in this series, binds weakly to diethyl phosphate, a simple model phosphodiester that is inert to hydrolysis. Morrow suggested that because both Th(IV) **26** and Eu(III) **25** contain 9-coordinate ions and the same 8-dentate ligand, resulting in a single coordination site available for substrate binding, the higher activity of Th(IV) **26** is due to the higher charge and thus higher Lewis acidity of Th(IV) compared to Eu(III).[17] The binding constant of Th(IV) **26** to diethyl phosphate was determined to be  $K = 17.0 \text{ M}^{-1}$ , while the binding of the other complexes in this series was insufficient to be determined. A comparison of the X-ray structures of Eu(III) **25** with La(III) **24** (Fig. 4b–4c) provides grounds for explaining the highest activity of the latter by the higher number of free coordination sites. Both Eu(III) complexes have a 9-coordinate geometry, which gives only one free site available for substrate binding, while La(III) **24** has a 10-coordinate La(III) ion, which, in combination with the 8-dentate ligand, gives two free coordination sites. A higher number of free coordination sites results in higher activity of the La(III) complex. The optimal distance of the donor groups from the central metal ion is two carbons; shifting the donors by another carbon, as in the case of La(III) **27**, results in a drastic decrease in stability (which occurred within minutes at 37 °C, pH 6.5) compared to the analogous Eu(III) **25** (which remained intact after four days at 37 °C, neutral pH). The very low stability of La(III) **27** made it impossible to determine its cleavage activity.

Significant differences in catalytic activity were observed between the four-armed Tb(III) **28** and the triarmed Tb(III) **29** (Fig. 2).[22] X-ray crystal structure analysis indicates that the Tb(III) ion is 9-coordinated, with a square-antiprism geometry. Thus, when Tb(III) is bound by 8-dentate ligand **28**, only one coordina-

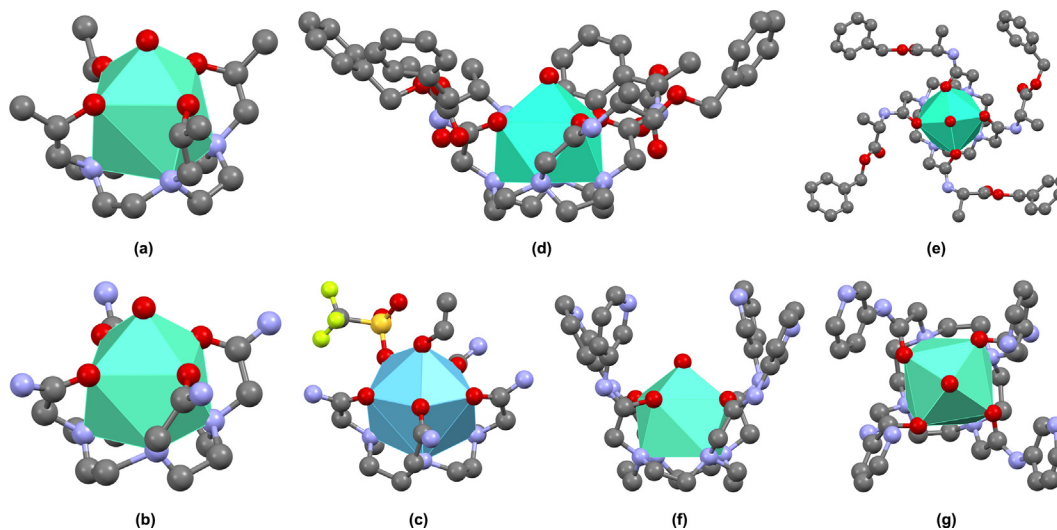


**Fig. 4.** X-ray structures for: (a) Eu(III) **4**, ref. [6]; (b) Eu(III) **25**, ref. [15]; (c) La(III) **24**, ref. [20]; (d) and (e) Eu(III) **57**, ref. [30]; (f) and (g) Eu(III) **65**, ref. [33]. Graphics were generated using Mercury software, ref. [21].

tion site is occupied by labile water and the complex remains inactive. In contrast, when Tb(III) is bound by 7-dentate ligand **29**, two coordination sites are available for substrate binding and the complex can effectively promote RNA cleavage. Tb(III) **29** significantly accelerates the transesterification of an activated RNA model, uridine-3'-(4-nitrophenylphosphate), with  $k_{\text{obs}} = 5.5 \times 10^{-2} \text{ s}^{-1}$  at 21 °C and pH 7.5, but neither Tb(III) **28** nor Tb(III) **29** was reactive towards BNPP, even at 50 °C.

By removing one of the donor arms and thus obtaining Eu(III) **30–35** and La(III) **36** complexes (Fig. 2) with 7-dentate ligands, Morrow *et al.* observed a significant increase in phosphodiester cleavage.[23] Unlike their inactive 8-dentate analog, Eu(III) **25**, the new 7-dentate complexes have two coordination sites available for substrate binding instead of one. Of these, triarmed Eu(III) **31** with monoalkylated amide donors showed the highest HPNP cleavage rate ( $k_2 = 0.12 \text{ M}^{-1} \text{ s}^{-1}$ ; pH 7.6, 25 °C), while non-alkylated Eu(III) **30** and dialkylated Eu(III) **32** showed 2.2 to 2.9-fold lower activity. These studies highlight that the hydrolytic activity is not solely related to the  $\text{pK}_a$  value of metal-bound water, which begins to decrease as the amide groups become alkylated ( $\text{pK}_a$  were > 9.0, > 8.5 and > 8.0 for Eu(III) **30**, **31** and **32**, respectively). To better understand the interaction of the complexes with the substrates and products of RNA cleavage and to shed more light on the reaction mechanism, the binding constants ( $K_i$ ) of methyl phosphate (MP) and diethyl phosphate (DEP) to the complexes were determined by competitive inhibition of HPNP cleavage. Eu(III) **30** binds more strongly to MP than to DEP ( $K_i = 0.28 \text{ mM}$  for MP, 7.50 mM for DEP), which is attributed to MP's charge and therefore stronger electrostatic interaction with the cationic metal center (referring to Pearson's concept). Another interesting observation is that all these complexes show remarkably simple speciation in solution over a wide range of pH; each complex exists in only one major form as  $[\text{Eu(III)L}(\text{H}_2\text{O})_2]^{3+}$ , which shows an almost linear  $\log k_2$  correlation with pH. Such a simple pH-rate relationship may suggest that these complexes do not ionize significantly in the pH range studied. A similar coordination environment to Eu(III) **30** was also observed for Eu(III) **33** and Eu(III) **34**, which have four side arms, but only three of them act as donors.[24] Both complexes, Eu(III) **33** and Eu(III) **34**, were shown to coordinate two water molecules and both can effectively promote HPNP transesterification. Their activity decreases in the following order: **34** ( $k_2 = 0.32 \text{ M}^{-1} \text{ s}^{-1}$ ) > **33** ( $k_2 = 0.095 \text{ M}^{-1} \text{ s}^{-1}$ ) > **30** ( $k_2 = 0.020 \text{ M}^{-1} \text{ s}^{-1}$ ; pH 7.0, 25 °C). The higher activity of these

complexes compared to Eu(III) **30** was explained by the influence of the fourth side arm containing a strongly electron-withdrawing nitro group, which results in a lower  $\text{pK}_a$  of coordinated water and a lower binding constant of Eu(III) **34** ( $K_i = 0.018 \text{ mM}$  for MP) vs Eu(III) **30** ( $K_i = 0.28 \text{ mM}$  for MP).

Morrow *et al.* choose the 4-nitrobenzyl group as the non-donor arm to provide a suitable linker for coupling complexes to oligonucleotides and thus obtained the 7-dentate complex Eu(III) **35** (Fig. 2).[25] Although the coordination structures of Eu(III) **31** and Eu(III) **35** are similar, i.e. both have two coordination sites available for binding substrates or water molecules, the cleavage activity of Eu(III) **35** towards HPNP ( $k_2 = 3.7 \text{ M}^{-1} \text{ s}^{-1}$ ; pH 7.4, 37 °C) is about 30 times higher. The authors speculate that Eu(III) **35** is more active than Eu(III) **31** because the former is a stronger Lewis acid due to the presence of the electron-withdrawing 4-nitrobenzyl arm; this results in a much lower  $\text{pK}_a$  of metal-bound water of 6.85, facilitating the formation of active hydroxide forms already at neutral pH. In comparison, the less efficient Eu(III) **31** ( $k_2 = 0.12 \text{ M}^{-1} \text{ s}^{-1}$ ; under the same conditions) has  $\text{pK}_a$  as high as 8.5.

Akkaya *et al.* obtained La(III) **36** (Fig. 2) with a terminal 4-nitrophenyl group as a suitable linker for coupling the complex to DNA.[26,27] In this approach, the complex has three unmodified amide side arms, while the fourth arm is functionalized with a terminal 4-nitrobenzyl group. The nitro group can be easily reduced to an amino group and then reacted with oligonucleotides according to known protocols. The presence of four amide donors in La(III) **36** (the modified arm also acts as an amide donor) makes this complex more inert to dissociation than Eu(III) **35** with a triarmed ligand. The 4-nitrophenyl group was found to cause a slight increase in HPNP cleavage by La(III) **36** ( $k_{\text{obs}} = 2.2 \times 10^{-5} \text{ s}^{-1}$ ; HEPES 50 mM, pH 7.4, 25 °C) compared to the analogous La(III) **24** ( $k_{\text{obs}} = 3.8 \times 10^{-5} \text{ s}^{-1}$ ).

Chang *et al.* investigated the activity of lanthanide complexes **37–40** derived from 1,7-dicarboxymethylated cyclen against cleavage of BNPP (Fig. 2).[28,29] The La(III) **37**, Eu(III) **38**, Er(III) **39** and Yb(III) **40** complexes contain three, three, two and two metal-bound water molecules, respectively. Of these, only La(III) **37** and Eu(III) **38** were able to effectively promote the hydrolysis of BNPP, but their hydrolytic activity begins to appear at pH > 8.1. Above this pH, one of the coordinated water molecules ionize, giving the active form  $[\text{Ln(III)L}(\text{H}_2\text{O})_2(\text{OH})]^{2+}$ . In the pH range studied, the rate constants of Eu(III) **38** were 1.4–10 times higher than

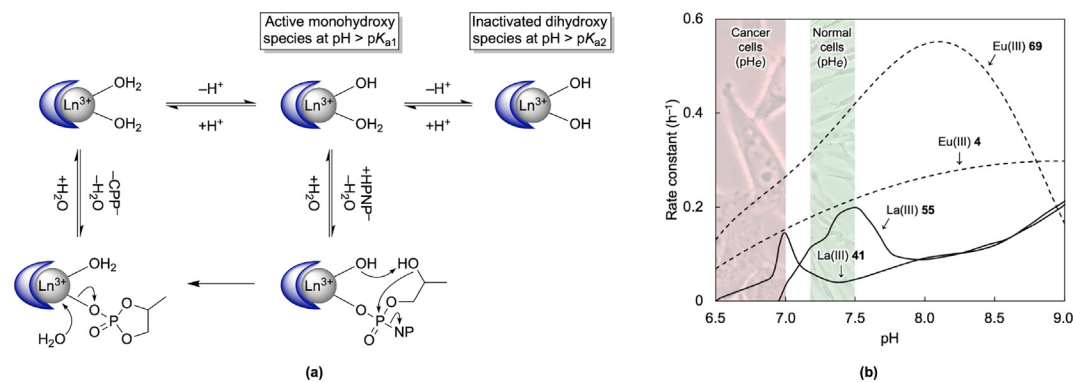


**Fig. 5.** (a) Mechanism of HPNP transesterification, a model RNA-like substrate, catalyzed by lanthanide(III) complexes with two coordination sites available to bind substrate molecules. (b) pH-rate curves of HPNP cleavage catalyzed by selected *f*-block complexes. The graph shows the characteristic sigmoidal pattern for complexes with a single free coordination site, e.g. Eu(III) **4**, and the bell-shaped pattern for complexes with two free coordination sites, e.g. Eu(III) **69**, La(III) **55** and La(III) **41**. The graph shows the differences in extracellular pH (pH<sub>e</sub>) in the environment of cancerous (red area) and normal (green area) tissues.

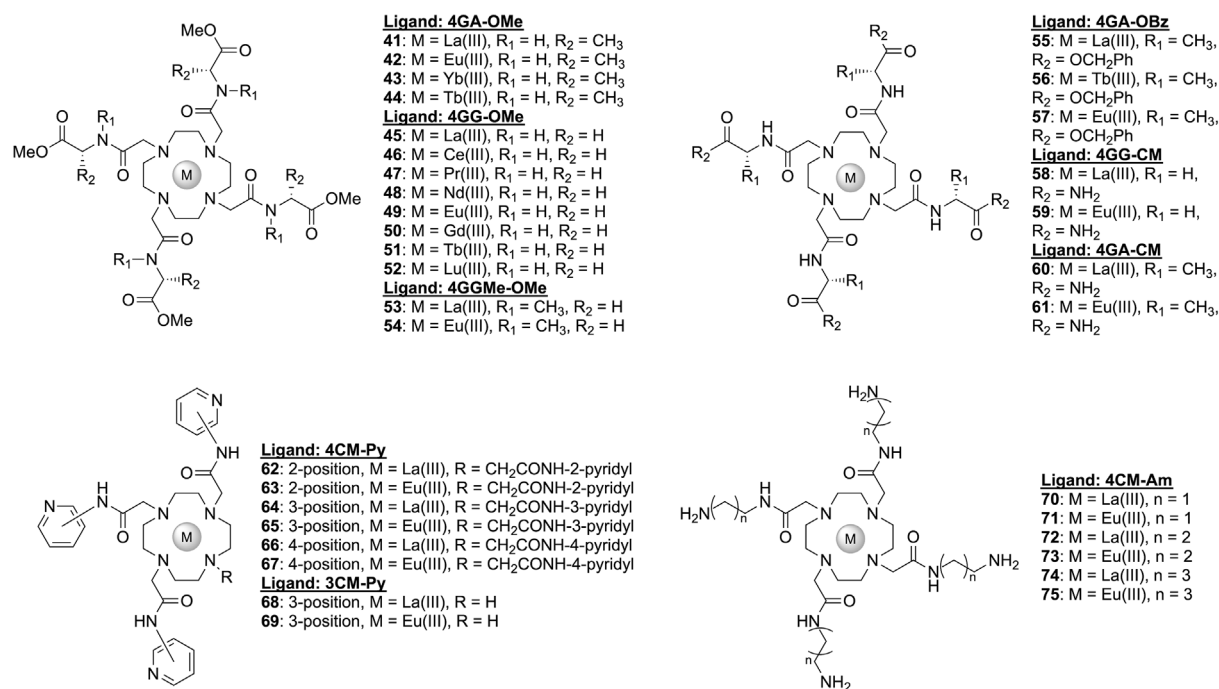


**Fig. 6.** Examples of mononuclear *f*-block complexes **41–75**.

those of La(III) **37** and about 45–92.7 times higher than those of Er(III) **39**. The rate constant of Eu(III) **38** increases linearly with pH, without reaching a clear maximum; near physiological pH,  $k_{\text{obs}} = 2.9 \times 10^{-6} \text{ s}^{-1}$  (pH 7.5, 25 °C). The significant difference between the active La(III) and Eu(III) complexes and the inactive Er(III) and Yb(III) complexes can be explained by their dimerization. Since both La(III) **37** and Eu(III) **38** have three metal-bound water molecules, they can form active catalyst  $[\text{Ln}(\text{III})_2\text{L}_2(\mu\text{-OH})_2(\text{OH}_2)_2]$  with two single coordination sites located on separate metal centers, each occupied by one water molecule, one of which can bind BNPP and the other help initiate its hydrolysis. On the other hand, Er(III) **39** and Yb(III) **40**, which initially have only two coordinated water molecules, give inactive forms of  $[\text{Ln}(\text{III})_2\text{L}_2(\mu\text{-OH})_2]$  without any coordination site available to bind the substrate.

Gunnlaugsson's group was the first to use pseudodipeptides as side arms (in which glycine has its *N*-terminus as part of the cyclen ring) to create a large hydrophobic cavity around the metal ion to better mimic the hydrophobic environment of the active centers

found in many natural nucleases.[30,31] They emphasize that the higher activity of natural enzymes compared to chemical catalysts is due to the synergistic action of several cofactors, such as the presence of basic amino acids (for a general acid-base catalysis), divalent metal cations and the hydrophobic reaction environment, which can affect the affinity for substrates and  $\text{pK}_a$  of metal-bound ligands. When in 2002 Gunnlaugsson's group reported complexes **41–46** with methyl ester AlaGly arms and **55–57** with benzyl ester AlaGly arms (Fig. 6), these complexes were among the most effective artificial nucleases in promoting HPNP hydrolysis under near-physiological conditions. The most active complex among the methyl ester family is Tb(III) **44** ( $k_{\text{obs}} = 3.9 \times 10^{-5} \text{ s}^{-1}$ ; pH 7.4, 37 °C), while among the benzyl ester family is La(III) **55** ( $k_{\text{obs}} = 5.2 \times 10^{-5} \text{ s}^{-1}$ ). The latter was even more active than its parent complex La(III) **24** ( $k_{\text{obs}} = 1.6 \times 10^{-5} \text{ s}^{-1}$ ; pH 7.3, 37 °C; ref. [17]) consisting of simpler amide side arms. An interesting property, first observed in La(III) **41** and La(III) **55** complexes, was a strong and narrow bell-shaped pH-rate curve with a local maximum at pH

7.0 and 7.5, respectively (please see Figs. 5 and 6 in ref. [30]). Although at optimum pH La(III) **41** ( $k_{\text{obs}} = 0.41 \times 10^{-4} \text{ s}^{-1}$ ; pH 7.0) is more active than Eu(III) **42** ( $k_{\text{obs}} = 0.25 \times 10^{-4} \text{ s}^{-1}$ ; pH 7.4), at pH 7.4 the former is 2.3 times less active than Eu(III) **42**. In contrast, La(III) **55** ( $k_{\text{obs}} = 0.56 \times 10^{-4} \text{ s}^{-1}$ ; pH 7.5) reaches a maximum rate much closer to physiological pH, making it more active ( $k_{\text{obs}} = 0.52 \times 10^{-4} \text{ s}^{-1}$ ; pH 7.4) than the analogous Eu(III) **57** ( $k_{\text{obs}} = 0.16 \times 10^{-4} \text{ s}^{-1}$ ; pH 7.4) at this pH. The reason for the difference in  $pK_a$  between the methyl and benzyl ester families is the difference in the hydrophobicity of the environment around the metal center; the more hydrophobic arms of the benzyl esters cause a greater increase in the  $pK_a$  of coordinated water molecules compared to the arms of methyl esters. The X-ray structure of Eu(III) **57** is shown in Fig. 4d–4e.

In a similar study, Gunnaugsson's group showed that complexes **45–52** (Fig. 6), with simpler GlyGly side arms, exhibit remarkable activity in cleaving HPNP under physiological pH,  $k_{\text{obs}} = 0.16\text{--}1.14 \times 10^{-4} \text{ s}^{-1}$  (pH 7.4, 37 °C).[32] Despite the increased activity against HPNP, none of the complexes hydrolyzed BNPP. Unlike the series with AlaGly side arms, the activity of complexes **45–52** follows the trend of increasing ion radius, with larger ions being more active than smaller ones. Due to the greater number of coordination sites in the larger ions, they bind an additional water molecule, which improves their cleavage mechanism and catalytic activity. The most active in this series is La(III) **45** ( $k_{\text{obs}} = 1.14 \times 10^{-4} \text{ s}^{-1}$ ), while the least active is Lu(III) **52** ( $k_{\text{obs}} = 0.06 \times 10^{-4} \text{ s}^{-1}$ ). As with La(III) **41** and La(III) **55**, the activity of La(III) **45** was strongly pH dependent, with the highest value of  $k_{\text{obs}} = 2.24 \times 10^{-4} \text{ s}^{-1}$  at pH 8.5 and a characteristic bell-shaped rate curve.  $^{31}\text{P}$  NMR studies with DEP showed that La(III) **45** has about 30 times lower substrate binding affinity than the less active Eu(III) **49** ( $k_{\text{obs}} = 0.04 \times 10^{-4} \text{ s}^{-1}$ ). This may explain the second reason for the increased hydrolytic activity of complexes with larger ions, which is the easier release of cleavage products from the metal center. Like the AlaGly series complexes, most GlyGly series complexes promote cleavage at each base pair of the GAG-HIV gene mRNA under physiological-like conditions.

Gunnaugsson's group presented two interesting series of La(III) and Eu(III) complexes, **53–54** and **58–61** derived from four-armed ligands with GlyGly pseudodipeptides and **68–69** from triarmed ligands containing 3-pyridyl groups (Fig. 6).[33] Both triarmed complexes, La(III) **68** ( $k_{\text{obs}} = 1.14 \times 10^{-4} \text{ s}^{-1}$ ; pH 7.4, 37 °C) and Eu(III) **69** ( $k_{\text{obs}} = 1.1 \times 10^{-4} \text{ s}^{-1}$ ), had the strongest effect on promoting HPNP cleavage under physiological-like conditions. The triarmed Eu(III) **69** was a 5-fold more efficient catalyst than its four-armed analog Eu(III) **65** (under similar conditions), while La(III) **68** and La(III) **64** (described in next paragraph) showed similar activity regardless of the number of side-arms. The pH-rate profiles of HPNP hydrolysis by La(III) **68** and Eu(III) **69** are bell-shaped with a peak at pH 8.4 and 8.0, respectively, and a decrease in rate with further increase in pH. This particular shape of the pH-rate curve is attributed to the presence of two metal-bound water molecules, which undergo subsequent ionization to form an active monohydroxyl species, followed by an inactive dihydroxyl species, as shown in Fig. 5a. The authors found that *N*-methylation of the amide bonds between GlyGly dipeptides results in an approx. 50–60% decrease in the activity of La(III) **53** ( $k_{\text{obs}} = 3.22 \times 10^{-5} \text{ s}^{-1}$ ) and Eu(III) **54** ( $k_{\text{obs}} = 0.69 \times 10^{-5} \text{ s}^{-1}$ ) compared to their unmethylated analogs, La(III) **45** and Eu(III) **49**. The presence of the methyl group near the metal ion may prevent the formation of a hydrophobic cavity around the catalytic center due to the increased steric hindrance; tertiary amides are known for their rigidity. On the other hand, the results suggest that the presence of hydrogen bond-forming groups (e.g. amide groups) near the metal center may be key to improving the cleavage activity by improving acid-base catalysis or even changing the cleavage mech-

anism. Replacing the terminal methyl ester group in La(III) **45** and Eu(III) **49** with terminal amide group in La(III) **58** ( $k_{\text{obs}} = 3.97 \times 10^{-5} \text{ s}^{-1}$ ) and Eu(III) **59** ( $k_{\text{obs}} = 0.83 \times 10^{-5} \text{ s}^{-1}$ ) resulted in a 38–51% reduction in cleavage activity. Such an effect was also observed for the Eu(III) **61** complex ( $k_{\text{obs}} = 1.56 \times 10^{-5} \text{ s}^{-1}$ ) having GlyAla side arms; after derivatization with amide functionality, its activity decreased compared to the methyl ester-terminated Eu(III) **42** ( $k_{\text{obs}} = 2.52 \times 10^{-5} \text{ s}^{-1}$ ). The opposite effect was observed for La(III) **60** ( $k_{\text{obs}} = 1.8 \times 10^{-5} \text{ s}^{-1}$ ) with GlyAla side arms; after the same derivatization, its activity was even slightly higher than that of the parent La(III) **41** ( $k_{\text{obs}} = 1.1 \times 10^{-5} \text{ s}^{-1}$ ; pH 7.4, 37 °C). The decrease in cleavage activity observed after the introduction of terminal amide functionality may be related to an increase in the number of hydrogen bonds that can be formed inside or outside the complex, which in turn may have affected the formation and shape of the hydrophobic cavity around the catalytic center.

Considering that the formation of a hydrophobic cavity has a positive effect on hydrolytic activity, Gunnaugsson's group investigated the role of pyridine groups and their substitution positions in a series of four-armed complexes **62–67** (Fig. 6).[34] Of these, only complexes with 3-pyridyl moieties promoted HPNP hydrolysis, while the others did not induce any hydrolysis (pH 7.4, 37 °C). The most active was La(III) **64** ( $k_{\text{obs}} = 5.25 \times 10^{-5} \text{ s}^{-1}$ ), followed by Eu(III) **65** ( $k_{\text{obs}} = 2.17 \times 10^{-5} \text{ s}^{-1}$ ), both consisting of 3-substituted pyridine groups. The relationship between the absence and occurrence of hydrolytic activity depending on the position of pyridyl nitrogen was attributed to its preferential participation in overall acid-base catalysis or hydrogen bonding to the substrate molecule. The X-ray structure of Eu(III) **65** is shown in Fig. 4f–4g. La(III) **64** coordinates two water molecules in aqueous environment, while Eu(III) **65** can only coordinate one water. This difference in the structure of the active forms appears to be responsible for the pH-dependent change in their activity profile. The activity of Eu(III) **65** is almost independent of pH, while that of La(III) **64** is strongly pH-dependent, reaching a local peak around pH 8.2 ( $k_{\text{obs}} = 1.97 \times 10^{-4} \text{ s}^{-1}$ ) and then dropping rapidly at pH > 8.5. The drop in rate at pH > 8.5 is likely due to dissociation of the second metal-bound water, leading to the formation of dihydroxyl forms that electrostatically prevent the substrate from binding to the metal ion; the active and inactive forms, along with the authors' proposed mechanism of action, are shown in Fig. 5a.

To the best of our knowledge, Gunnaugsson's group has so far presented the most active mononuclear lanthanide(III) complex; La(III) **70** (Fig. 6) catalyzes the hydrolysis of HPNP ( $k_{\text{obs}} = 2.59 \times 10^{-4} \text{ s}^{-1}$ ,  $k_2 = 1.41 \text{ M}^{-1} \text{ s}^{-1}$ ; pH 7.4, 37 °C) with a much higher rate constant than the parent La(III) **58** ( $k_{\text{obs}} = 3.97 \times 10^{-5} \text{ s}^{-1}$ ) containing GlyGly arms terminated with amide groups.[35] Gunnaugsson's group investigated the effect of alkyl length on the efficiency of HPNP hydrolysis by the newly prepared complexes **70–75** and found that their optimal length is two carbons, and that further chain elongation only results in lower rate constants. In all series with the same arm length, the La(III) complexes were 1.5–2.6 times more efficient than their Eu(III) analogs. While the lower activity of Eu(III) **71** compared to La(III) **70** is not surprising (one vs two free coordination sites), what may be surprising is that the four-armed Eu(III) **71** ( $k_{\text{obs}} = 1.01 \times 10^{-4} \text{ s}^{-1}$ ) with one substrate-binding site is comparably active to the triarmed Eu(III) **69** ( $k_{\text{obs}} = 1.1 \times 10^{-4} \text{ s}^{-1}$ ) with two substrate-binding sites. These results show how important the support of side-arm functional groups can be for improving the activity of artificial nucleases.

### 2.1.2. Conclusions

**The number of metal-bound water molecules is the key to hydrolytic activity.** One of the key factors determining the catalytic efficiency of *f*-block cyclen complexes is the number of metal-bound water molecules and the associated number of free coordi-

nation sites, which determine the hydrolysis mechanism. In general, complexes with two metal-bound water molecules are tens to hundreds of times more active than complexes with one metal-bound water molecule. During the reaction, the substrate molecule replaces one of the metal-bound water molecules; complexes having a second coordinated water can form an additional metal-bound hydroxide that is close enough to the phosphate group (or 2'-hydroxyl group) to carry out a nucleophilic attack on it. This additional metal-bound hydroxide is the source of the higher activity of complexes with two free coordination sites. Increasing the number of free coordination sites to three, as in the case of Eu(III) **38**, does not translate into a further increase in the cleavage activity of *f*-block complexes. A common feature of complexes with two coordinated water molecules is a bell-shaped pH-rate curve, with a local peak at the pH value corresponding to the highest concentration of the active complex (the form with one ionized water molecule), which drops sharply with a further increase in pH leading to ionization of the second water molecule (Fig. 5). This doubly ionized form is inactive due to repulsion from the negatively charged phosphate bond and the resulting limited binding to the substrate. In contrast, complexes with a single substrate-binding site show a sigmoidal pH-rate curve that flattens out after full ionization of the only metal-bound water molecule.

A higher number of coordination sites available for substrate binding can be achieved in two ways: (1) by introducing a metal with a higher coordination number while keeping the same number of ligand donor groups, or (2) by reducing the number of ligand donor groups, e.g. by reducing the number of ligand side arms (pendant donor groups) from four to three. The decrease in coordination number for successive lanthanides is associated with a decrease in their ionic radii, a phenomenon known as lanthanide contraction. With an increase in the charge of the nucleus from  $Z = 57$  for La(III) to  $Z = 71$  for Lu(III), the number of electron shells does not change, only the number of electrons on the inner 4f shell. Due to the simultaneous increase in the charge of the nucleus (number of protons) for successive lanthanides, the attraction of electrons by the nucleus increases. This phenomenon is also responsible for the decrease in catalytic activity in the series: La(III) **5** ( $k_2 = 6.3 \times 10^{-2} \text{ M}^{-1} \text{ s}^{-1}$ ) > Eu(III) **4** ( $k_2 = 1.4 \times 10^{-2} \text{ M}^{-1} \text{ s}^{-1}$ ) > Lu(III) **6** ( $k_2 = 0.088 \times 10^{-2} \text{ M}^{-1} \text{ s}^{-1}$ ). So how does Th(IV) compare to lanthanides(III)? Although the radius of its crystal ion (108 pm) is similar to that of Eu(III) (108.7 pm), [8–10] Th(IV) **26** is about 50 times more active than La(III) **24**, while Eu(III) **25** is inactive under the same conditions. This is likely due to both the higher Lewis acidity and the higher charge of Th(IV) ions, which provide stronger binding to the substrate's phosphate group. Cyclen modified with only three pendant donors forms 7-dentate ligands, allowing complexes of smaller lanthanides such as Eu(III) to have two coordination sites available for substrate binding. The importance of the number of free coordination sites for catalytic activity can be depicted on two groups of Eu(III) complexes differing in the type of side arms: (1) **25** (4 × amide arms, no activity) vs **30** (3 × amide arms,  $k_2 = 4.2 \times 10^{-2} \text{ M}^{-1} \text{ s}^{-1}$ ) and (2) **65** (4 × 3-pyridyl arms,  $k_{\text{obs}} = 2.17 \times 10^{-5} \text{ s}^{-1}$ ) vs **69** (3 × 3-pyridyl arms,  $k_{\text{obs}} = 0.11 \times 10^{-5} \text{ s}^{-1}$ ). An interesting effect accompanying the change in coordination number in the last point (2) is a change in the shape of the pH-rate curve from sigmoidal to bell-shaped with a clear local peak in activity corresponding to the active monohydroxyl form and a drop in activity corresponding to the inactive dihydroxyl form (Fig. 5b), an effect that indirectly indicates a change in the cleavage mechanism.

**For complexes with one free coordination site, the  $pK_a$  of the metal-bound species influences the cleavage activity, but is not the only or main factor.** Information on the effect of  $pK_a$  can be obtained by comparing the activity of two groups of complexes:

(1) those that have the same ligand structure but differ in the type of metal ion, and (2) those that have the same metal ion but differ in ligand structure. In the case of the complexes referred to in (1), i.e. complexes that have a single coordination site available for substrate binding, the active agent involved in the nucleophilic attack is usually a metal-bound alkoxy group derived from one of the side arms. The single water molecule initially bound to the complex is of little importance here, since it is exchanged during the substrate-binding step, and therefore cannot participate in phosphate cleavage (Fig. 3). In the case of complexes with the same metal type, e.g. 8-coordinated Eu(III), and the same number of pendant donor groups (let's ignore steric effects here), it is the type of donor that determine the cleavage activity by affecting the  $pK_a$  of the metal-bound species, e.g. the alkoxy group: Eu(III) **1** (4 × hydroxyl groups,  $k_{\text{obs}} = 0.48 \times 10^{-4} \text{ s}^{-1}$ ) > Eu(III) **14** (3 × hydroxyl groups, 1 × amide group,  $k_{\text{obs}} = 0.09 \times 10^{-4} \text{ s}^{-1}$ ) > Eu(III) **23** (2 × hydroxyl groups, 2 × amide groups,  $k_{\text{obs}} = 0.01 \times 10^{-4} \text{ s}^{-1}$ ). The above gradual decrease in rate constants is related to the  $pK_a$  of the alkoxy group; for Eu(III) **1**,  $pK_a = 7.5$ , for Eu(III) **23**,  $pK_a = 8.1$ , although the  $pK_a$  for Eu(III) **14** has not been described, it is expected to be lower than for Eu(III) **23**. [16] The 6.8-fold higher activity of Eu(III) **1** (4 × 2-hydroxyethyl arms,  $pK_a = 7.5$ ) relative to Eu(III) **4** (4 × 2-hydroxypropyl arms,  $pK_a = 7.8$ ) can be partially explained by the same principle, but in this case the flexibility of the side arms is also suspected to have a significant effect on activity. The presence of an easily ionizable hydroxyl function in 8-dentate Eu(III) complexes is important from a mechanistic point of view; once the substrate is bound to the metal center, the only nucleophile in its vicinity is the ionized alkoxy group. Therefore, replacing all 2-hydroxyethyl side arms of Eu(III) **1** with amide-terminated side arms, which are inferior nucleophiles, led to a loss of Eu(III) **25** cleavage activity.

**For complexes with two free coordination sites, fine-tuning the  $pK_a$  of the metal-bound water determines activity and selectivity under physiological conditions.** For complexes with two coordinated water molecules, characterized by a bell-shaped pH-rate curve, one would expect the stronger Lewis acid to be a better catalyst. In general, this assumption is true, but it should be kept in mind that depending on the structure of the complexes, their optimal activity may fall within different pH ranges, and since they are often developed for *in vivo* use, the specifics of physiological conditions, such as the pH difference between normal and cancer cells, should be taken into account. For example, cancer cells have a lower extracellular pH ( $pH_e$ ) of ~ 6.5–7.0 and a higher intracellular pH ( $pH_i$ ) of 7.4, while normal cells have a higher extracellular pH of ~ 7.2–7.5 and a lower intracellular pH of 7.2 (Fig. 5b). [36–38] One of the attractive and timely targets for pH-sensitive organometallic complexes may be the extracellular matrix (ECM), a tissue-specific structure responsible for transmitting extracellular signals to cells, which is a network of >300 biopolymers and molecules. [39] Data from a number of relevant studies suggest that basic behaviors of cancer cells, including altered intercellular contacts, invasive growth and metastasis, can be related to abnormal functioning of the tumor ECM. Organometallic complexes do not necessarily need to penetrate the cell to exhibit anticancer activity or to support treatment with other chemotherapeutics; the mere modification or degradation of the ECM environment by these complexes could lead to potential new anticancer therapies. We can distinguish two main types of cyclen-based complexes with two free coordination sites: (1) complexes with 10-coordinated La(III) ions and four-armed 8-dentate ligands, and (2) complexes with 9-coordinated Eu(III) ions and triarmed 7-dentate ligands.

The flagship examples from group (1) are La(III) **41** (max  $k_{\text{obs}} = 0.41 \times 10^{-4} \text{ s}^{-1}$  at pH 7.0) and La(III) **55** (max  $k_{\text{obs}} = 0.56 \times 10^{-4} \text{ s}^{-1}$  at pH 7.5), whose pH-dependent rates are shown in Fig. 5b. Overall, at optimal pH, both La(III) complexes were more active than their

Eu(III) analogues, but due to the narrow peak of optimal activity, La(III) **41** performed worse and La(III) **55** better than their Eu(III) analogues at pH 7.4. Although the authors were unable to determine the  $pK_a$  of these complexes, based on the  $pK_a$  determined for La(III) **45**, [32] we speculate that the  $pK_a$  of La(III) **41** and La(III) **55** lies near the pH corresponding to the local peak of activity. On the other hand, La(III) **41** is 4 times more active at pH 7.0 than at pH 7.4, while La(III) **55** is 6 times more active at pH 7.4 than at 7.0. Such narrow ranges and large differences in the optimal pH for nucleolytic activity are of particular interest because they can provide a viable basis for designing complexes that act selectively on a specific cell type, such as cancer cells. It is known that the pH of altered cancer tissues ( $pH_e$  6.5–7.0) is more acidic than the environment of normal cells ( $pH_e$  7.2–7.5). [40] One molecular target for pH-sensitive artificial nucleases may be genetic material secreted and stored in the ECM, such as miRNA, mRNA or lncRNA. [41,42] Research on the mutual regulation of RNA and the surrounding ECM, although still in its infancy, may be crucial to the development of strategies to prevent or treat diseases in which abnormal levels or activity of RNA and/or ECM composition and architecture are present. It is also worth noting that the highest  $k_{obs}$  of most similar complexes is usually far from physiological conditions and can be found at higher pH values, but the arms of the pH-rate curve are usually so broad that even at pH 7.4 they can still show significant activity. This is the case for La(III) **45** (max  $k_{obs} = 2.24 \times 10^{-4} \text{ s}^{-1}$  at pH 8.5,  $pK_a = 8.2, 8.5$ ), La(III) **64** (max  $k_{obs} = 3.33 \times 10^{-4} \text{ s}^{-1}$  at pH 8.4,  $pK_a = 8.6$ ) and La(III) **68** (max  $k_{obs} = 3.85 \times 10^{-4} \text{ s}^{-1}$  at pH 8.4,  $pK_a = \sim 8.6$ ).

Some 7-dentate Eu(III) complexes, such as Eu(III) **69**, consisting of a triarmed ligand, also have two coordination sites available for substrate binding and therefore show a similar bell-shaped pH-activity relationship as the analogous La(III) complexes (Fig. 5b). Again, some selectivity toward a particular cell type can be observed, although not as pronounced as in the case of La(III) complexes; Eu(III) **69** is about 1.5 times more active at  $pH_i$  of normal cells than cancer cells (Fig. 5b). However, it is difficult to state whether such pH sensitivity is sufficient to selectively affect cancer cells. The overall anticancer activity of cyclen complexes may depend mainly on other factors, such as intracellular uptake and localization, about which little is known so far. 7-dentate Eu(III) complexes generally have a shifted peak of activity toward higher pH and a flatter pH-rate curve than analogous La(III) complexes, most likely due to the higher Lewis acidity of Eu(III) ion. The complexes in group (2) are also of interest because of the possibility of tracing the effect of the fourth, non-donor arm on  $pK_a$  and catalytic activity. Although the literature reports only four such examples, and these data are not complete, a clear effect of the electron-withdrawing group on the cleavage activity can be observed; the activity decreases in the order: Eu(III) **35** (3 × amide groups, 1 × nitrobenzyl group,  $k_2 = 3.7 \text{ M}^{-1} \text{ s}^{-1}$ ,  $pK_a = 6.85$ ) > Eu(III) **33** (3 × amide groups, 1 × benzyl group,  $k_2 = 0.33 \text{ M}^{-1} \text{ s}^{-1}$ ,  $pK_a$  unknown) > Eu(III) **34** (3 × amide groups, 1 × methyl group,  $k_2 = 0.32 \text{ M}^{-1} \text{ s}^{-1}$ ,  $pK_a$  unknown) > Eu(III) **30** (3 × amide groups,  $k_2 = 0.042 \text{ M}^{-1} \text{ s}^{-1}$ ,  $pK_a > 8.0$ ). Lowering the  $pK_a$  value results in a higher number of mono-ionized complexes already at lower pH, which translates into higher activity under physiological conditions. However, it should be emphasized that this effect applies only to complexes with the same type of ligand and the same number of free coordination sites. If, on the other hand, the complexes differ in the type of pendant donors, such as triarmed Eu(III) **30–32**, among which monomethylated Eu(III) **31** ( $pK_a = 8.5$ ,  $k_2 = 0.12 \text{ M}^{-1} \text{ s}^{-1}$ ) is more active than dimethylated Eu(III) **32** ( $pK_a = 8.0$ ,  $k_2 = 0.054 \text{ M}^{-1} \text{ s}^{-1}$ ), the effect of  $pK_a$  on activity is usually of secondary importance.

**Side arms can regulate the accessibility and environment of the metal center, affecting the cleavage activity.** In the previous

paragraph we discussed the effect of functional groups in the side arms (pendant donors) on the  $pK_a$  of metal-bound water, here we will focus on examples illustrating the effect of side arm structure on  $pK_a$  and the associated cleavage activity; although this effect has not yet been fully characterized, the literature provides some important clues. Studies by Gunnlaugsson *et al.* have shown that a large increase in arm volume, accompanying the introduction of terminal methyl or benzyl esters, can result in increased cleavage activity. For most of the complexes in the methyl ester family **41–54**, as well as the benzyl ester family **55–61**, the  $pK_a$  of the coordinated water molecule(s) could not be determined, but it is suspected that the more hydrophobic benzyl arms cause a greater increase in  $pK_a$  values. There is essentially only one pair of complexes, Eu(III) **42** ( $pK_a = 6.9$ ;  $k_{obs} = 0.25 \times 10^{-4} \text{ s}^{-1}$  at pH 7.4) from the methyl ester family and Eu(III) **57** ( $pK_a = 7.8$ ;  $k_{obs} = 0.16 \times 10^{-4} \text{ s}^{-1}$  at pH 7.4) from the benzyl ester family, whose  $pK_a$  can be compared and which support the above conjecture.

The structure of the side arms can also significantly affect the cleavage mechanism, which can change from being dependent on nucleophilic activation by metal-bound hydroxides to being ligand-based, with side arms functional groups playing a major role. Therefore, for complexes whose side arms contain functional groups that can participate in the reaction via hydrogen bonding or general acid-base catalysis, the highest cleavage activity is not always observed at pH close to  $pK_a$ . An excellent example is La(III) **70** ( $k_{obs} = 2.59 \times 10^{-4} \text{ s}^{-1}$  at pH 7.4), whose side arms are terminated with primary amines and whose highest  $k_{obs}$  is observed at pH 7.4, while the  $pK_a$  values assigned for ionized water molecules oscillate around 9.21 and 9.26. The speciation diagram (please see Fig. 2 in ref. [35]) shows that the doubly protonated form  $H_2[La(III) \text{ 70}]$  is the most active species; the formation of these species may be due to the protonation of primary amines in the side arms, whose  $pK_a$  values are 10.6 and 9.7. In contrast to complexes composed of simpler amide arms, in the case of extended ester arms, the increase in cleavage activity is not exclusively associated with a decrease in  $pK_a$  values.

**What is the relationship between ligand structure, stability and activity of f-block complexes?** If the complexes are to be useful *in vivo*, it is important that they remain intact in solution containing competing ligands and under physiological conditions. The data on the stability of mononuclear f-block complexes available in the cited literature are very limited and mainly concern kinetic studies in excess of Cu(II) ions as a trapping agent. Nonetheless, some partial conclusions can be drawn from them regarding the influence of (1) steric effects, (2) ligand denticity and (3) donor type on the stability of the complexes.

(1) In the case of Eu(III) complexes **4–6** with 2-hydroxypropyl arms differing in chirality on the  $\alpha$ -carbon, the complexes of specific stereoisomers clearly differ in stability. S,S,S-complexes are the most resistant to dissociation;  $t_{1/2}$  of Eu(III) **4** = 100 d,  $t_{1/2}$  of La(III) **5** = 73 d,  $t_{1/2}$  of Lu(III) **6** = 53 d (pH 6.0, 37 °C). [6] For example, the S,S,S-isomer of Lu(III) **6** is about 60 times more resistant to dissociation than the mixture of Lu(III) **6** stereoisomers. Molecular models suggest that S,S,S-isomers are preferred for steric reasons and are likely to be the same ones observed in solution, while complexes with mixed chiral centers are less stable or do not form at all due to steric problems associated with the placement of the R-arms next to the S-arms. Moreover, the stiffer Eu(III) **4** with 2-hydroxypropyl arms is 9-fold more resistant to dissociation than the more flexible Eu(III) **1** ( $t_{1/2} = 11$  d) with 2-hydroxyethyl arms, but the latter is 1.3-fold more active in HPNP transesterification. [16,43] Thus, it appears that the arrangement of the side arms may favor a particular conformation of the cyclen ethylene groups, which modifies the rigidity of the entire macrocycle and has a profound effect on catalytic activity and resistance to dissociation.

(2) Another factor that has a significant effect on the stability of complexes is the number of side arms and pendant donors. The absence of one 2-hydroxyethyl side arm was found to significantly reduce the resistance of 7-dentate Eu(III) **3** to dissociation, which occurs almost completely within 20 h under slightly acidic conditions in the absence of competing ligands (pH 6.0, 37 °C).[16] Under natural and physiological conditions (pH 7.4, 37 °C), complexes such as 7-dentate Eu(III) **35** can be sufficiently stable (no dissociation was observed within 3 days), but they are still more susceptible to dissociation than their four-arm analogs; for example, 8-dentate Eu(III) **25** did not dissociate over 6 weeks ( $t_{1/2} = 50$  days at pH 2.0 and 60 °C).[20] The greatest difference in stability of such complexes is observed in the presence of other competing ligands. The dissociation rate of Eu(III) **35** is significantly accelerated in the presence of polycarboxylates, after 1 h of incubation with DTPA, EDTA and NTA the dissociation increased to 9.6–90.3%; under the same conditions Eu(III) **25** remained intact. For ligands with relatively small side arms (e.g., 2-hydroxyethyl), those with fewer pendant donors tend to form less stable complexes; the smaller number of arms allows competing ligands to approach and interact with the central metal ion, accelerating its dissociation. However, lower ligand denticity does not necessarily lead to a less stable complex; in fact, the opposite effect can be observed for ligands with side arms of significant size. In the case of Eu(III) complexes with 3-pyridine arms, the triarmed Eu(III) **69** ( $\log K_f = 18.6$ ) and the four-armed Eu(III) **65** ( $\log K_f = 16.5$ ), it is the former that is more stable to dissociation, as indicated by a larger formation constant.[33] This is suspected to be due to at least two reasons – on the one hand, the more flexible triarmed ligand **69** can more easily adapt to the size and high surface charge density of Eu(III) ions; on the other hand, the four-armed ligand **65** will be more positively charged at low pH than the triarmed analog, which can electrostatically destabilize the entire complex.

(3) Finally, the type of pendant donors and their distance from the metal ion are other key features that determine the stability of

*f*-block complexes. Gradual replacement of 2-hydroxyethyl arms with amide arms in series: Eu(III) **1** (4 × hydroxyl arms,  $t_{1/2} = 11$  d at pH 6.0, 37 °C), Eu(III) **14** (3 × hydroxyl arms, 1 × amide arm,  $t_{1/2} = 13$  d at pH 6.0, 37 °C), Eu(III) **23** (2 × hydroxyl arms, 2 × amide arms,  $t_{1/2} = 14$  d at pH 6.0, 37 °C) and Eu(III) **25** (4 × amide arms,  $t_{1/2} = 50$  d at pH 2.0, 60 °C) resulted in a clear increase in stability, especially for the last complex with four amide arms.[5,16,20] Among this series, we observe an inverse relationship between stability: (Eu(III) **1** < Eu(III) **14** < Eu(III) **23** < Eu(III) **25**) and cleavage activity: (Eu(III) **1** with  $k_{obs} = 0.48 \times 10^{-4} \text{ s}^{-1}$  > Eu(III) **14** with  $k_{obs} = 0.09 \times 10^{-4} \text{ s}^{-1}$  > Eu(III) **23** with  $k_{obs} = 0.01 \times 10^{-4} \text{ s}^{-1}$ ), while Eu(III) **25** was completely inactive under physiological-like conditions. Extending the amide arms by one carbon (from 2 to 3 carbons) drastically reduced the stability of La(III) **27**, which decomposes within minutes (pH 6.5, 37 °C). The complex is also inactive against HPNP under neutral conditions.[18] We conclude this chapter with Table 1 and Table 2, where we summarized the structure-activity relationships for selected lanthanide(III) complexes with various ligands.

## 2.2. Mononuclear complexes of *d*-block metals

Although our focus in this review is on functionalized complexes, it is worthwhile to lean into the history of research on Zn(II)-cyclen, which is the simplest yet best-studied transition metal cyclen complex. It is also worth to look at the structure and function of natural Zn(II)-containing metalloenzymes, which we are strenuously trying to mimic. The conclusions from these studies will give us a basis for a later discussion on the usefulness of ligand functionalization to improve the properties of artificial nucleases based on cyclen complexes. As we mentioned in the introduction to this paper, research on functionalized cyclen complexes began more than three decades ago, but the first examples of simple transition metal-azamacrocyclic complexes with known hydrolytic activity date back to the early 1950s. The first known zinc metal-

**Table 1**

Summary of rate constants for HPNP transesterification catalyzed by selected lanthanide(III) complexes along with their selected features. The activity of the complexes is given under conditions closest to physiological conditions. The table summarizes examples of the most active complexes among the series having the same ligand structure.

Complex	Ligand	$k_{obs}$ ( $10^{-4} \text{ s}^{-1}$ )	$k_2$ ( $\text{M}^{-1} \text{ s}^{-1}$ )	FCS	$\text{p}K_a$	C/S	Conditions	Ref.
Eu(III) <b>1</b>	4HE	0.48	7.2	1	7.5	10	HEPES 10 mM, pH 7.5, 37 °C, $I = 0.1 \text{ M}$ ( $\text{NaNO}_3$ )	[5]
Eu(III) <b>4</b>	4HP	0.07	1.4	1	7.4	10	HEPES 10 mM, pH 7.5, 37 °C, $I = 0.1 \text{ M}$ ( $\text{NaNO}_3$ )	[5]
La(III) <b>5</b>	4HP	0.13	6.3	2	8.1	10	HEPES 10 mM, pH 7.5, 37 °C, $I = 0.1 \text{ M}$ ( $\text{NaNO}_3$ )	[5]
Tb(III) <b>7</b>	4HP	1.68		1		10	MOPS 50 mM, pH 7.2, 25 °C, $I = 0.1 \text{ M}$ ( $\text{NaClO}_4$ )	[14]
Eu(III) <b>11</b>	3HE-CM	0.14		1	7.5	10	HEPES 10 mM, pH 7.4, 37 °C, $I = 0.1 \text{ M}$ ( $\text{NaCl}$ )	[16]
Eu(III) <b>23</b>	1,7-2HE2CM	0.01		1	8.1	10	HEPES 10 mM, pH 7.4, 37 °C, $I = 0.1 \text{ M}$ ( $\text{NaCl}$ )	[16]
La(III) <b>24</b>	4CM	0.16		2		10	HEPES 10 mM, pH 7.3, 37 °C, $I = 0.1 \text{ M}$ ( $\text{NaNO}_3$ )	[17]
Eu(III) <b>25</b>	4CM	N.A.		1	>9.0	10	HEPES 10 mM, pH 7.3, 37 °C, $I = 0.1 \text{ M}$ ( $\text{NaNO}_3$ )	[17,19]
Th(IV) <b>26</b>	4CM	7.50		1		10	HEPES 10 mM, pH 7.3, 37 °C, $I = 0.1 \text{ M}$ ( $\text{NaNO}_3$ )	[17]
Eu(III) <b>31</b>	3CM-NR		0.12	1	8.5		HEPES 20 mM, pH 7.6, 25 °C, $I = 0.1 \text{ M}$ ( $\text{NaNO}_3$ )	[23]
La(III) <b>41</b>	4GA-OMe	0.11		2		1	HEPES 50 mM, pH 7.4, 37 °C	[31]
La(III) <b>42</b>	4GA-OMe	0.25		1	6.9	1	HEPES 50 mM, pH 7.4, 37 °C	[31]
Tb(III) <b>44</b>	4GA-OMe	0.39		1		1	HEPES 50 mM, pH 7.4, 37 °C	[31]
La(III) <b>45</b>	4GG-OMe	1.14		2	8.2, 8.5	1	HEPES 50 mM (4% MeOH/ $\text{H}_2\text{O}$ ), pH 7.4, 37 °C	[32]
Eu(III) <b>49</b>	4GG-OMe	0.42		1	7.38	1	HEPES 50 mM (4% MeOH/ $\text{H}_2\text{O}$ ), pH 7.4, 37 °C	[32]
La(III) <b>53</b>	4GGMe-OMe	0.32		2		1.3	HEPES 50 mM, pH 7.4, 37 °C	[33]
Eu(III) <b>54</b>	4GGMe-OMe	0.069		1		1.3	HEPES 50 mM, pH 7.4, 37 °C	[33]
La(III) <b>55</b>	4GA-OBz	0.52		2		1	HEPES 50 mM, pH 7.4, 37 °C	[31]
Eu(III) <b>57</b>	4GA-OBz	0.16		1	7.8	1	HEPES 50 mM, pH 7.4, 37 °C	[31]
La(III) <b>58</b>	4GG-CM	0.40		2		1.3	HEPES 50 mM, pH 7.4, 37 °C	[33]
Eu(III) <b>59</b>	4GG-CM	0.083		1		1.3	HEPES 50 mM, pH 7.4, 37 °C	[33]
La(III) <b>60</b>	4GA-CM	0.18		2		1.3	HEPES 50 mM, pH 7.4, 37 °C	[33]
Eu(III) <b>61</b>	4GA-CM	0.16		1		1.3	HEPES 50 mM, pH 7.4, 37 °C	[33]
La(III) <b>64</b>	4CM-Py	0.53		2	~8.6	1	HEPES 50 mM, pH 7.4, 37 °C	[32,34]
Eu(III) <b>65</b>	4CM-Py	0.22		1		1	HEPES 50 mM, pH 7.4, 37 °C	[34]
La(III) <b>68</b>	3CM-Py	1.14		3	~8.6	1.3	HEPES 50 mM, pH 7.4, 37 °C	[33]
Eu(III) <b>69</b>	3CM-Py	1.10		2		1.3	HEPES 50 mM, pH 7.4, 37 °C	[33]
La(III) <b>70</b>	4CM-Am	2.59	1.41	2	9.21, 9.26	1.3	HEPES 50 mM, pH 7.4, 37 °C	[35]
Eu(III) <b>71</b>	4CM-Am	1.01		1	8.0	1.3	HEPES 50 mM, pH 7.4, 37 °C	[35]

FCS – free coordination sites. N.A. – no catalytic activity observed.



**Table 2**

Summary of rate constants for BNPP hydrolysis catalyzed by selected lanthanide(III) complexes along with their selected features. The activity of the complexes is given under conditions closest to physiological conditions. The table summarizes examples of the most active complexes among the series having the same ligand structure.

Complex	Ligand	$k_{\text{obs}}$ ( $10^{-4} \text{ s}^{-1}$ )	$k_2$ ( $\text{M}^{-1} \text{ s}^{-1}$ )	FCS	pK <sub>a</sub>	C/S	Conditions	Ref.
Eu(III) <b>1</b>	4HE	2.0	0.19	1	7.5	10	pH 7.4, 37 °C,	[5,7]
La(III) <b>2</b>	4HE	0.27		2	>7.5	10	pH 7.4, 37 °C,	[5,7]
Eu(III) <b>11</b>	3HE-CM	1.50		1	7.5	9.1	HEPES 10 mM, pH 7.3, 37 °C, $I = 0.1 \text{ M}$ (NaCl)	[16]
Eu(III) <b>23</b>	1,7-2HE2CM	0.035		1	8.1	9.1	HEPES 10 mM, pH 7.3, 37 °C, $I = 0.1 \text{ M}$ (NaCl)	[16]
La(III) <b>37</b>	1,7-2AA	0.012		3	8.4	10	MOPS 20 mM, pH 7.54, 25 °C, $I = 0.1 \text{ M}$ (Me <sub>4</sub> NCl)	[28]
Eu(III) <b>38</b>	1,7-2AA	0.029		2	8.4	10	MOPS 20 mM, pH 7.5, 25 °C, $I = 0.1 \text{ M}$ (Me <sub>4</sub> NCl)	[28]
La(III) <b>45</b>	4GG-OMe	N.A.		2	8.2, 8.5	1	HEPES 50 mM (4% MeOH/H <sub>2</sub> O), pH 7.4, 37 °C	[32]

FCS – free coordination sites. N.A. – no catalytic activity observed.

loenzyme, carbonic anhydrase II (CA<sup>3</sup> II, EC 4.2.1.1), was discovered by Keilin and Mann even earlier, in 1940.[44] Since then, our interest in complexes of zinc and other transition metals has grown steadily. Along with cobalt and copper complexes, it is zinc complexes that are most often studied for *in vivo* applications. This is not surprising, after all, zinc is the second most abundant trace metal in the human body after iron; each of us contains 2–4 g of this metal, mainly in the form of zinc proteins.[45].

### 2.2.1. Role of zinc ions in natural metalloenzymes

Let's first look at the active sites of enzymes that catalyze the hydrolysis of natural phosphates, such as phosphatases and nucleases. Enzymes of this group contain one to three zinc ions present in single-, doubly-, or multinuclear centers, where zinc either participates directly in opening or closing a chemical bond or interacts with other metal ions in the catalytic reaction. In enzyme active sites, zinc is usually coordinated with three or four amino acids in a slightly distorted tetrahedral symmetry; a distorted triangular bipyramid is less commonly and is mainly observed in cocatalytic and structural (noncatalytic) zinc.[46,47] With the *d* orbital filled, zinc ions do not participate in redox reactions, but rather function as Lewis acids, accepting a pair of electrons, which is crucial for catalyzing hydrolysis reactions. Thus, of the >300 Zn(II)-containing metalloenzymes found in all six classes of enzymes, zinc proteins are the most prevalent as hydrolases. In this review, we present only selected topics on the hydrolysis of phosphomonoesters and phosphodiester by natural enzymes, for more infor-

mation on the catalysis of all three phosphoesters groups, we refer the interested reader to Andrea Erxleben's review.[48].

In nature, the hydrolysis of phosphomonoesters is catalyzed by phosphomonoesterases such as alkaline phosphatase (ALP) from *E. Coli*, a homodimeric metalloenzyme with two Zn(II) and one Mg(II) in each active sites located in separate units (Fig. 7a).[49–51] In the substrate-bound structure, both Zn(II) ions adopt a tetrahedral or disordered tetrahedral geometry; The first zinc (Zn1) interacts with His331<sup>NE2</sup>, His412<sup>NE2</sup>, Asp327<sup>OD1</sup>, Asp327<sup>OD2</sup> and one of the phosphate oxygens; the second zinc (Zn2) interacts with His370<sup>NE2</sup>, Asp51<sup>OD1</sup>, Asp369<sup>OD1</sup> and one of the phosphate oxygens; the third metal site is occupied by Mg(II).[52] The average distance between zinc ions is 4.06 Å. The two Zn(II) centers play a key role in inducing catalytic hydrolysis of the phosphate bond. Hydrolysis occurs via a dissociative mechanism in which Mg(II)-activated water deprotonates the Ser102 residue to form serine alkoxide – an active nucleophile, which then directly attacks the phosphate monoester, leading to elimination of the substrate's alcohol group (Fig. 7b). While Zn2 promotes the formation of serine alkoxide; Zn1 facilitates P–O bond cleavage by stabilizing the negative charge on the oxygen atom of the leaving group in the transition state; this process can be assisted by protonation of the phosphate group by Mg(II)-coordinated water. Thus, zinc in ALP is involved in all three direct (inner sphere) modes of activation that the metal ion can provide to enhance the rate of phosphate hydrolysis, namely: (1) Lewis acid activation (phosphate oxygen coordination), (2) nucleophile activation (hydroxide coordi-

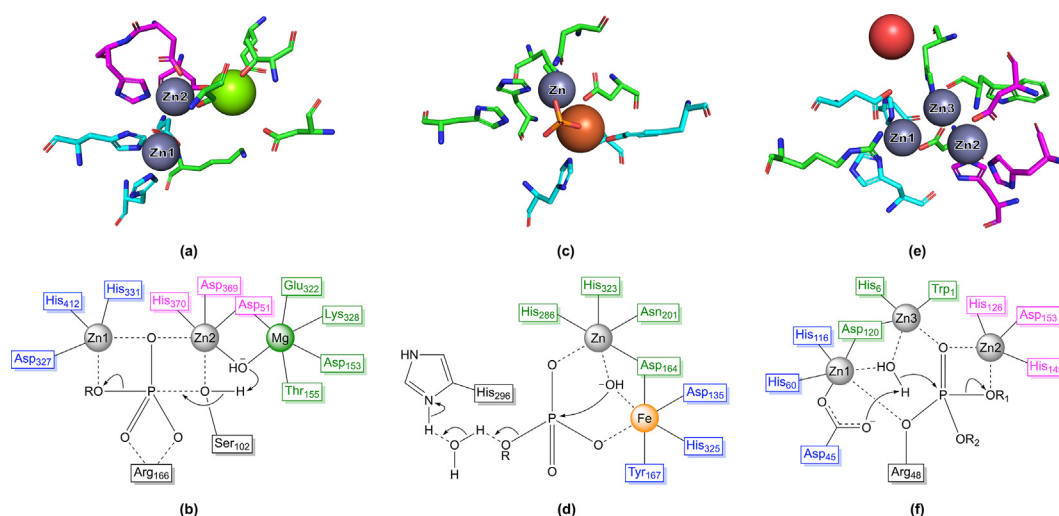


**Fig. 7.** Structure of the active center with highlighted metal-binding amino acids and mechanism of nucleophilic attack on the phosphorous atom initiating reaction by: (a–b) alkaline phosphatase from *Escherichia coli*, (c–d) purple acid phosphatase from common bean (*Phaseolus vulgaris*) and (e–f) P1 nuclease from *Penicillium citrinum*. The gray spheres represent Zn(II) ions, the green sphere represents Mg(II) ion, the orange sphere represents Fe(II) ion, the red sphere represents a water molecule. Images of active sites were created with PyMOL software (ref. [64]) using the following PDB structures: (a) PDB 1ALK, ref. [48]; (b) PDB 4KBP, ref. [53]; (c) PDB 1AK0, ref. [61].

dination) and (3) leaving group activation (leaving group oxygen coordination).

Purple acid phosphatases (PAPs) are another example of well-studied metalloenzymes found in animals, plants and fungi that catalyze the hydrolysis of phosphate esters and anhydrides, such as ATP, over a wide pH range of 4 to 7.[53] PAPs have a heterodinuclear active center occupied by Zn(II) and a redox-active pair of Fe(II/III) ions in animals or Zn(II) and Mn(II) in plants (Fig. 7c). The distance between the two metal ions is about 3.3 Å. Klabunde *et al.* showed that in PAP from common bean, both metal sites are six-coordinate in a distorted octahedral environment.[53] The phosphate group interacts via two non-esterified oxygen atoms with both metal ions, displacing previously metal-bound solvent molecules. By interacting with the Zn(II) ion, the phosphate group is oriented in-line with the attacking Fe(III)-bound hydroxide from a position opposite to the esterified oxygen. Two mechanisms have been proposed for PAP, and in both cases the reactions are consistent with the  $S_N2$  mechanism: (1) the mechanism proposed by Klabunde *et al.* involves monodentate coordination of the phosphate ester with the Zn(II) ion followed by nucleophilic attack of the Fe(III)-bound hydroxide, (2) the alternative mechanism observed for sweet potato PAP is characterized by bridging coordination of the phosphate ester and nucleophilic attack of the bridging hydroxide (Fig. 7d).[54,55] In both reactions, the phosphorous configuration is reversed. The bridging hydroxide in PAP resembles the hydroxides found in some binuclear complexes, including cyclen complexes. While the Fe(II)-bound hydroxide is a fairly efficient nucleophile, the nucleophilicity of a hydroxide that is tightly bounded to two metals should be rather low, which is why some question whether the bridging hydroxide is sufficient to participate directly in phosphate hydrolysis.[56,57] Therefore, it has been suggested that the bridging hydroxide in hydrolytic enzymes must move to a (pseudo-)terminal position after binding to the substrate in order to perform a nucleophilic attack.[58,59] On the other hand, some computational studies have shown that the nucleophilicity of bridging hydroxide is actually sufficient to be utilized in the hydrolysis reaction.[60] Similar considerations often apply to small-molecule transition metal dinuclear complexes.

Nuclease P1 (NP1) is a zinc-dependent phosphodiesterase that cleaves the P-O3' bond, but also acts as a phosphomonoesterase that cleaves the 3'-terminal phosphate groups. The active center contains a cluster of three Zn(II) ions that coordinate the substrate scissile phosphate and a water molecule (Fig. 7e). [61–63] Two zinc ions (Zn1 and Zn3) form a closely spaced dinuclear pair with a distance of 3.67 Å and are located deep in the pocket, while the third ion is further away (by about 5 Å) and exposed to the solvent. Several possible reaction mechanisms can be found in the literature, but all assume a nucleophilic attack by the zinc-activated water molecule and stabilization of the pentacovalent transition state by Arg48. The most cited mechanism assumes that the hydroxide ion (red sphere) linking Zn1 and Zn3, attacks the phosphate in line with the P-O3'-bond. At the same time, Zn2 activates and stabilizes the leaving O3'-oxyanion, while Arg48 neutralizes the additional negative charge of the transition state.

### 2.2.2. Effect of ligand size and structure on zinc complexes

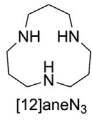
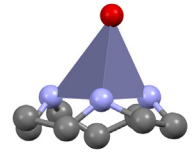
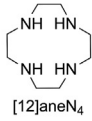
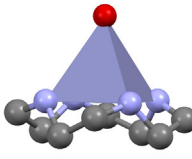
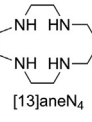
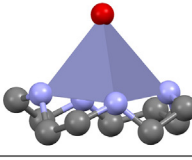
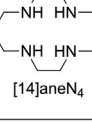
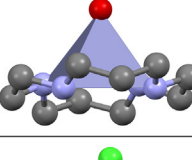
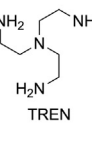
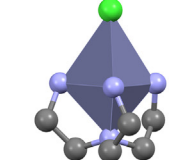
Fig. 8 shows the properties of Zn(II) complexes with some of the most described azamacrocyclic ligands, such as the 3-dentate [12]aneN<sub>3</sub>, 4-dentate [12]aneN<sub>4</sub> and [14]aneN<sub>4</sub>, and the tripodal tetraamine TREN. A key difference between ring-shaped ligands and open-chain TREN is that the latter can wrap around the metal in a trigonal pyramid geometry, leaving less room for additional ligands than in the facial coordination mode of azamacrocycles. The effect of complex geometry on catalytic activity can be readily deduced from the differences between Zn(II)-TREN and Zn(II)-[14]aneN<sub>4</sub>; although both ligands are 4-dentate and the pK<sub>a</sub> of the

metal-bound water is almost identical (pK<sub>a</sub> 9.8), Zn(II)-[14]aneN<sub>4</sub> ( $k_{\text{BNPP}} = 0.11 \times 10^{-4} \text{ M}^{-1} \text{ s}^{-1}$ ; pH 11.0) is about three times more active in BNPP hydrolysis than Zn(II)-TREN ( $k_{\text{BNPP}} = 0.039 \times 10^{-4} \text{ M}^{-1} \text{ s}^{-1}$ ; pH 11.0). As the ring size of the tetraazamacrocyclic ligand decreases, the metal-bound water becomes increasingly acidic, and the pK<sub>a</sub> decreases to 8.3 in [13]aneN<sub>4</sub> and 8.0 in [12]aneN<sub>4</sub>; this is accompanied by an increase in the hydrolytic activity of Zn(II)-[12]aneN<sub>4</sub> ( $k_{\text{BNPP}} = 0.31 \times 10^{-4} \text{ M}^{-1} \text{ s}^{-1}$ ; pH 7.4), which becomes noticeable already at physiological pH. Since all three ligands are 4-dentate and form tetrahedral complexes, they have the same coordination number and similar geometries. So what is the reason for the increase in pK<sub>a</sub> accompanying the increase in ligand ring size? In general, the coordination geometry can be characterized by the L–M–L bond angles ( $\angle\text{L–Zn–L}$ ). Linder *et al.* used  $\angle\text{H}_2\text{O–Zn–(ImH)}_n$  as a predictive tool in computational studies of imidazole (ImH) complexes of Zn(II) and showed that the proton dissociation energy and pK<sub>a</sub> of coordinated water decrease significantly with increasing average H<sub>2</sub>O–Zn–ImH angle.[65] As the angle  $\angle\text{H}_2\text{O–Zn–ImH}$  increases, the H<sub>2</sub>O–Zn bond length decreases; Mulliken charge analysis indicates that this also increases the electron density transfer from the H<sub>2</sub>O ligand to the Zn(II)(ImH)<sub>n</sub> molecule. As a result, with an increase of  $\angle\text{O–Zn–(ImH)}_{2,3}$  there is an accumulation of positive charge on the hydrogen atom, accompanied by an increase in length and decrease in dissociation energy of the H–OH bond. However, it should be noted that this regularity occurs only in complexes with the same coordination number and similar structure. Fig. 8 shows experimental and computational values of H<sub>2</sub>O–Zn bond lengths and average values of  $\angle\text{H}_2\text{O–Zn–N}$  calculated by us from the equilibrium geometries given by Kozioł *et al.*[66]. As the coordination number decreases from four to three, pK<sub>a</sub> drops further to 7.3 in [12]aneN<sub>3</sub>.

The 3-dentate ligands reduce the Lewis acidity of the metal ion to a much lesser extent than the 4-dentate ligands, as evidenced by the much lower pK<sub>a</sub> of Zn(II)-[12]aneN<sub>3</sub> (7.3) compared to Zn(II)-[12]aneN<sub>4</sub> (8.0); however, Zn(II)-[12]aneN<sub>3</sub> is about 20 times more active in hydrolyzing BNPP and HPNP than [12]aneN<sub>4</sub>, and such a difference in activity cannot be attributed solely to pK<sub>a</sub>. In fact, due to the lower denticity of [12]aneN<sub>3</sub>, its complexes have an additional free coordination site, which changes their mechanism of action and is mainly responsible for the increase in activity. On the other hand, as the denticity of ligands decreases or the ring size of ligands with the same denticity increases, their stability constant decreases. As one might expect, activity and stability are opposing characteristics of complexes, and this means that complexes with higher activity are not necessarily better suited for *in vitro* applications, as they can cause many adverse effects due to the release of metal ions in the body. The toxicity of many complexes is much lower than that of free ions, a good example being the Gd(III)-DOTA (log K<sub>f</sub> = 25.3) and Zn(III)-DOTA (log K<sub>f</sub> = 21.1) complexes, which are thermodynamically stable and kinetically inert toward dissociation, and thus considered safe for use *in vivo*. [67–69] Of the azamacrocyclic complexes shown in Fig. 8, it is Zn(II)-cyclen that exhibits the highest stability constant (log K<sub>f</sub> = 16.2), which is similar to those presented by clinically used Gd(III)-DTPA (log K<sub>f</sub> = 16.8) and its derivatives.[70].

### 2.2.3. Hydrolysis of RNA-like substrates by zinc complexes

For a long time, the Zn(II)-catalyzed hydrolysis of RNA and its model substrates, such as HPNP, was thought to proceed with metal-bound hydroxide as a general base catalyst, according to pathway A shown in Fig. 9a. Pathway A involves the transfer of a proton in the rate-determining transition state from the adjacent 2'-hydroxyl group of the substrate to the metal-bound hydroxide. In this case, the catalytically active form should be  $[\text{Zn(II)L(OH)}]^+$  formed by deprotonation of  $[\text{Zn(II)L(H}_2\text{O)}]^{2+}$ , and thus the observed increase in activity with increasing pH can be easily explained by

Ligand	Ring size	Complex geometry	$pK_a$	$\log K_f$ ( $\text{dm}^3 \text{M}^{-1}$ )	Zn-OH <sub>2</sub> (Å)	$\angle \text{H}_2\text{O-Zn-N}$ (°)	$k_{\text{BNPP}}$ ( $10^{-4} \text{M}^{-1} \text{s}^{-1}$ )	$k_{\text{HPNP}}$ ( $10^{-4} \text{M}^{-1} \text{s}^{-1}$ )
 [12]aneN <sub>3</sub>	12		7.3 <sup>a</sup>	8.25 <sup>b</sup>	2.061 (calc.) <sup>c</sup> 1.944 (exp.) <sup>d</sup>	111.21 (calc.) <sup>c</sup> 112.98 (exp.) <sup>d</sup>	0.61 (pH 7.4) <sup>e</sup>	75.6 (pH 7.4) <sup>f</sup>
 [12]aneN <sub>4</sub>	12		8.0 <sup>a</sup>	16.2 <sup>g</sup>	2.061 (calc.) <sup>c</sup> 1.971 (exp.) <sup>h</sup>	110.95 (calc.) <sup>c</sup> 110.71 (exp.) <sup>h</sup>	0.031 (pH 7.4) <sup>e</sup>	3.98 (pH 7.4) <sup>f</sup>
 [13]aneN <sub>4</sub>	13		8.3 <sup>c</sup>	15.6 <sup>g</sup>	2.094 (calc.) <sup>c</sup>	106.05 (calc.) <sup>c</sup>		
 [14]aneN <sub>4</sub>	14		9.8 <sup>a</sup>	14.5 <sup>b</sup> 15.5 <sup>g</sup>	2.147 (calc.) <sup>c</sup>	99.10 (calc.) <sup>c</sup>	0.11 (pH 11.0) <sup>i</sup>	
 TREN			9.8 <sup>b</sup>	12.1 <sup>b</sup>			0.39 (pH 11.0) <sup>i</sup>	

**Fig. 8.** Summary of the acid dissociation constants of metal-bound water ( $pK_a$ ), the formation constants ( $\log K_f$ ) for Zn(II) complexes, and the apparent second-order rate constants of BNPP ( $k_{\text{BNPP}}$ ) and HPNP ( $k_{\text{HPNP}}$ ) hydrolysis catalyzed by the respective complexes. **a** – ref. [71]; **b** – conditions:  $I = 0.1 \text{ M}$  ( $\text{NaClO}_4$ ), ref. [72]; **c** – ref. [66]; **d** – ref. [73]; **e** – determined from Fig. 3 in ref. [74], conditions: HEPES 50 mM, pH 7.4, 35 °C,  $I = 0.2 \text{ M}$  ( $\text{NaClO}_4$ ); **f** – conditions: HEPES 20 mM, pH 7.4, 25 °C,  $I = 0.1 \text{ M}$  ( $\text{NaNO}_3$ ), ref. [75]; **g** – conditions:  $I = 0.2 \text{ M}$  ( $\text{NaClO}_4$ ), 25 °C, ref. [76]; **h** – ref. [77]; **i** – conditions: CAPS buffer, pH 11.0, 25 °C, ref. [78]. Graphics of coordination polyhedra were prepared based on following works:  $[\text{Zn}(\text{II})([\text{12}] \text{aneN}_3)(\text{H}_2\text{O})]$ , ref. [73];  $[\text{Zn}(\text{II})([\text{12}] \text{aneN}_4)(\text{H}_2\text{O})]$ , ref. [79];  $[\text{Zn}(\text{II})([\text{13}] \text{aneN}_3)(\text{H}_2\text{O})]$ , ref. [66];  $[\text{Zn}(\text{II})([\text{14}] \text{aneN}_4)(\text{H}_2\text{O})]$ , ref. [80];  $[\text{Zn}(\text{II})(\text{TREN})(\text{Cl})]$ , ref. [81].

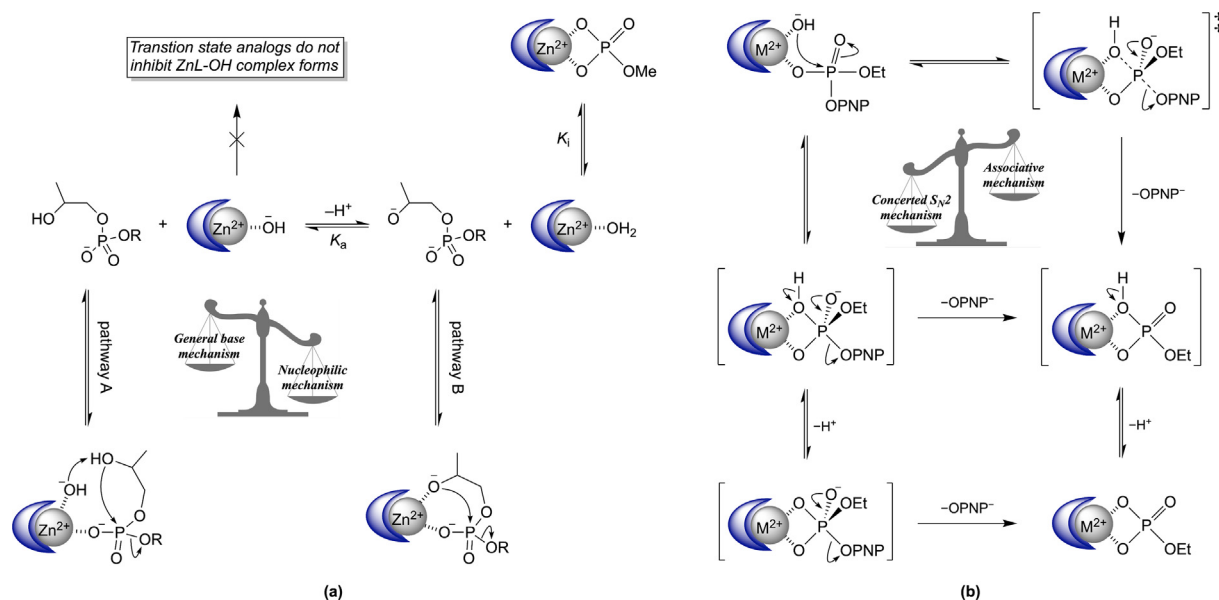


**Fig. 9.** (a) Proposed mechanisms of HPNP transesterification catalyzed by Zn(II)-azamacrocycle complexes and the ability of transition state analogs (MP<sup>2-</sup> and DEP<sup>-</sup>) to inhibit the  $[\text{Zn}(\text{II})\text{L}(\text{H}_2\text{O})]$  and  $[\text{Zn}(\text{II})\text{L}(\text{OH})]$  forms. Experimental results indicate that the reaction follows pathway B; only the  $[\text{Zn}(\text{II})\text{L}(\text{H}_2\text{O})]$  form is effectively inhibited by MP<sup>2-</sup> and DEP<sup>-</sup>, indicating that this is the actual active form of the complex.

an increase in the concentration of the active catalyst until it reaches its maximum concentration at high pH, resulting in a flattening of the pH-rate curve (please see Fig. 1 in ref. [70]). Although pathway A is widely known and accepted, increasing evidence supports the existence of a kinetically equivalent pathway B, in which  $[\text{Zn(II)L}(\text{H}_2\text{O})]^{2+}$  is the active catalyst that can be deprotonated at high pH to the inactive form  $[\text{Zn(II)L}(\text{OH})]^+$ . Pathway B involves the nucleophilic attack of the metal-bound deprotonated 2'-hydroxyl group of the substrate on the metal-activated phosphate group. Bonfá *et al.* note that even the finding that the pH-rate curve indicates the contribution of acidic functions with a  $\text{pK}_a$  very close to that of metal-bound water does not absolutely confirm pathway A.[78] In fact, it has been showed that the  $\text{pK}_a$  values of metal-bound water molecules and alcohol groups are almost identical. Since the two pathways are kinetically equivalent and differ only in the mode of proton transfer, in both cases the transesterification activity should follow the same pH-rate curve. The only difference lies in the type of kinetically active form, the associated rate-limiting mechanism for the reaction at high pH, and the way in which the transition state is stabilized. At least three arguments support the validity of pathway B:

(1) According to Morrow *et al.* the strongest evidence in favor of pathway B appears to be the lack of a primary deuterium isotope effect on the RNA-like UpPNP (uridine 3,4-nitrophenyl phosphate) cleavage catalyzed by  $\text{Zn(II)}$ -cyclen complexes.[82] If the active catalyst were formed by detaching a proton from the metal-bound water, the exchange of hydrogen for the heavier and less mobile deuterium should slow down the rate of phosphodiester cleavage in  $\text{D}_2\text{O}$  ( $^{\text{H}_2\text{O}}k_c$ ), and thus  $^{\text{H}_2\text{O}}k_c$  should increase much faster than the corresponding  $^{\text{D}_2\text{O}}k_c$  with increasing pH/pD. In fact, it was observed that in the pH/pD range of 7.1 to 9.3, the value of  $^{\text{D}}k_c = ^{\text{D}_2\text{O}}k_c/^{\text{H}_2\text{O}}k_c$  increases from 0.32 up to 1.14 at high pH. For carboxylic esters, studies have shown that  $^{\text{D}}k_c < 1.5$  indicates a nucleophilic mechanism in which no proton moves during the rate-limiting step of the reaction, while  $^{\text{D}}k_c > 2.0$  indicates a general basic catalysis:[83] similar assumptions were made by Bonfá *et al.* regarding phosphodiester cleavage, who showed that  $^{\text{D}}k_c = 4.01$  for HNPN transesterification in buffer alone at pH 9.0 indicates a general basic catalysis.[78] They also reported that  $^{\text{D}}k_c = 1.55$  for the hydroxide-assisted hydrolysis of BNPP is consistent with a nucleophilic mechanism.[84] In contrast, Morrow *et al.* reported that  $^{\text{D}}k_c = 2.0$  was obtained for bifunctional cleavage of HPNP involving general acid catalysis by a guanidinium group.[85]

(2) If the Zn-aqua form of the complex is the catalytically active form, inhibition by transition state analogs such as  $\text{MP}^{2-}$  should be stronger at lower pH, while if the Zn-hydroxyl form is active, inhibition should be weaker at lower pH. Studies by Morrow's group have shown that the  $(K_i)_{\text{obsd}}$  values for the inhibition of HPNP cleavage by the  $\text{Zn(II)}$ -(1-oxa-4,7,10-triazacyclododecane) complex (a close analogue of  $\text{Zn(II)}$ -cyclen) by  $\text{MP}^{2-}$  decrease by 50-fold as the pH is lowered from 10 to 7.6.[75] This indicates that the inhibitor binds specifically to the Zn-aqua form and does not bind tightly to the ionized Zn-hydroxyl form.

(3) There is competition in stabilizing the transition state between the two demonstrated catalytically active forms due to: (a) electrostatic interactions between the oppositely charged  $\text{Zn}^{2+}$  and the dianionic ligand  $\text{HPNP}^{2-}$ , which can interact in a bidentate manner, and (b) additional stabilization of the transition state resulting from a concerted mechanism, but with the drawback that the monoanionic  $\text{HPNP}^-$  can only binds to the metal center in a monodentate manner. According to the simplest expectation derived from Coulomb's law, electrostatic interactions between  $[\text{Zn(II)L}(\text{H}_2\text{O})]^{2+}$  and the dianionic ligand should stabilize the transition state more strongly than interactions between the partially neutralized metal ion in  $[\text{Zn(II)L}(\text{OH})]^+$  and the monoanionic ligand. This supposition is supported by the differences in the inhi-

bition constants ( $K_i$ ) of the  $\text{MP}^{2-}$  and  $\text{DEP}^-$  anions with  $\text{Zn(II)}$ -cyclen ( $K_i = 0.51$  and 46 mM, respectively) and  $\text{Zn(II)}$ -[12]ane $\text{N}_3$  ( $K_i = 0.78$  and 29 mM, respectively).[75] The dianionic  $\text{MP}^{2-}$  interacts more strongly than the monoanionic  $\text{DEP}^-$ , indicating an important role for the ligand charge. Similar conclusions can be drawn by comparing the binding constants of cyclen complexes and their analogs with various dianions with slightly different partial charges. Koike and Kimura reported that the  $\text{PP}^{2-}$  (phenyl phosphate) anion with  $\text{pK}_a = 5.8$  has a lower affinity for the  $\text{Zn(II)}$  complex, as indicated by  $\log K_{\text{ZnLA}} = 3.5 \text{ M}^{-1}$ , than  $\text{NP}^{2-}$  (4-nitrophenyl phosphate) anion with  $\text{pK}_a = 5.1$  and  $\log K_{\text{ZnLA}} = 3.1 \text{ M}^{-1}$ , and thus with a higher Lewis acidity and a higher partial negative charge.[74] These results correlate with the calculated partial charges of dihydrogen phosphate ( $e = -1.738$ ) and phenyl phosphate ( $e = -1.816$ ).[86] Sigel *et al.* also showed a similar relationship between the affinity of the phosphomonoester dianion for the  $\text{Zn(II)}$  ion and the basicity of the phosphate ligand.[87] It should be noted that the affinity of anions for azamacrocyclic complexes is not solely due to their charges or Lewis acidity. For example,  $\text{MP}^{2-}$  ( $\text{pK}_a = 1.54$ ) and  $\text{DEP}^-$  ( $\text{pK}_a = 1.29$ ) show similar inhibition of  $\text{Zn(II)}$ -cyclen and  $\text{Zn(II)}$ -[12]ane $\text{N}_3$ , while oxalate ion ( $\text{pK}_a = 1.27$ ) inhibits the latter complex ( $K_i = 0.18 \text{ mM}$ ) > 20 times more strongly than  $\text{Zn(II)}$ -cyclen ( $K_i = 4.4 \text{ mM}$ ). This shows that the structure of the anion can have a significant effect on the affinity and selectivity toward complexes of specific azamacrocycles, and this can have important implications for designing complexes for use in specific tissues or organisms.

#### 2.2.4. Hydrolysis of DNA-like substrates by zinc complexes

The main difference in the mechanism of RNA and DNA hydrolysis is the absence of the 2'-hydroxyl group in the latter substrate, which can act as an intramolecular nucleophile. It is widely believed that the mechanism of DNA-like phosphodiester hydrolysis catalyzed by *d*-block complexes involves a direct nucleophilic attack of the metal-bound hydroxide on the electrophilic phosphorous atom of the substrate, leading to the formation of a five-membered phosphate intermediate with rate-limiting loss of the leaving group (Fig. 9b). However, for metal complex-promoted hydrolysis of phosphodiester with a good leaving group, such as 4-nitrophenol, the mechanism may also be associative. This alternative pathway assumes that the formation of the pentavalent phosphate is the rate-limiting step, followed by a rapid loss of the activated leaving group, leading to the formation of the final product.

Jones *et al.* conducted an  $^{18}\text{O}$ -tracking experiment to investigate the mechanism of 4-nitrophenyl phosphate (NPP) hydrolysis catalyzed by the  $\text{Co(III)}(\text{en})_2$  complex and proved that the active nucleophile is the metal-bound hydroxide. The  $^{18}\text{O}$ -hydroxide performs an intramolecular attack on the  $[\text{Co(III)}(\text{en})_2(^{18}\text{OH})(\text{NPP})]$  complex, yielding product  $[\text{Co}(\text{en})_2(\text{PO}_4)]$  with complete retention of the label.[88] Much insight into the mechanism of the reaction was provided by Deal *et al.* in a detailed study on the hydrolysis of ENP (ethyl 4-nitrophenyl phosphate) by  $\text{Cu(II)}$ -[9]ane $\text{N}_3$ . [89] They examined primary deuterium isotope effect and found  $^{\text{D}}k_c = 1.14$ ; such a value suggests that there is no proton at the rate-limiting step of the reaction, indicating a nucleophilic attack of the  $\text{Cu(II)}$ -bound hydroxide on the phosphorus atom. They also determined the mechanism of hydrolysis based on the  $^{15}\text{N}$  isotopic effect. In the associative mechanism, the loss of 4-nitrophenol is not involved in the rate-limiting step of the reaction, so no secondary  $^{15}\text{N}$  isotopic effect is expected. In contrast, in the concerted mechanism, the bond between the phosphate and 4-nitrophenol is broken at the same time as the bond between nucleophile and phosphate is formed, so an isotope effect is expected. The secondary  $^{15}\text{N}$  isotope effect for the alkaline hydrolysis of 4-nitrophenyl phosphate  $^{15}k = 1.0028$ , for  $\text{Zn(II)}$ -[12]ane $\text{N}_3$  catalyzed

hydrolysis of ENP, the  $^{15}k = 1.0013$ . The presence of a normal isotopic effect indicates that the loss of the leaving group is the rate-limiting step in the reaction, proving that the reaction follows a concerted mechanism.

**What is the main driving force behind phosphate cleavage catalyzed by d-block metal complexes?** There are two main mechanistic limitations on phosphate hydrolysis promoted by metal complexes, namely: (1) intermolecular nucleophilic attack on the phosphate group or (2) activation of the phosphate group through coordination with metal ions to make it more susceptible to nucleophilic attack. Both effects are competitive and oppositely related to  $pK_a$ ; an increase in  $pK_a$  means a higher Lewis acidity of the metal ion, which should enhance the electrostatic interaction with the oppositely charged phosphate group, but on the other hand, the same reason leads to a decrease in the nucleophilicity of the metal-bound hydroxide. For reactions involving metal complexes, the Brønsted correlation is a reliable indicator of which effect prevails. The Brønsted coefficient ( $\beta_{\text{nuc}}$ ) obtained from the slope of rate constant for the nucleophilic reaction ( $\log k$ ) vs the  $pK_a$  of the nucleophile (eq. (2)), describes the relative sensitivity of the examined electrophile substrate to the reactivity of the nucleophile.[90]

$$\log k = \beta_{\text{nuc}} pK_a + C \quad (2)$$

As shown by Itoh *et al.* the hydrolysis of DENP (diethyl 2,4-dinitrophenylphosphate) by triamine Zn(II) complexes yields  $\beta_{\text{nuc}} = -015$  (Fig. 10).[72] A negative  $\beta_{\text{nuc}}$  can be interpreted that for phosphotriester hydrolysis, the most important role of the catalyst is to activate the substrate. On the other hand, Bonfá *et al.* reported that  $\beta_{\text{nuc}}$  values for cleavage of HPNP and BNPP by triamine Zn(II) complexes are 0.75 and 0.20, respectively (Fig. 10).[78] A positive  $\beta_{\text{nuc}}$  value indicates that for phosphodiester cleavage, nucleophile efficiency appears to be the dominant parameter controlling reaction rate. Thus, which effect dominates depends largely on the type of substrate, that is, the degree of substitution of the phosphate group, and perhaps also on the type of ligands. Complexes based on rigid triamine ligands (L9–L11, Fig. 10a), have been shown to follow a linear Brønsted correlation. So far, no similar studies have been described for a large series of tetraamine complexes; only single results can be found for Zn(II)-[14]aneN<sub>4</sub> and Zn(II)-TREN, accompanying studies of triamine complexes. Since complexes based on both systems have a similar principle of action, it can be assumed that the activity of both systems may be determined by similar effects. It should be noted, however, that in the case of phosphodiester hydrolysis, the tetraamine complexes studied so far do not fit the linear Brønsted correlation of complexes based on rigid triamine ligands, nor do complexes based on flexible triamine ligands (L4–L6 in Fig. 10).

### 2.2.5. Examples of mononuclear d-block cyclen complexes

Chang's group obtained complexes Co(III) **76–77** (Fig. 11) mono-functionalized with a benzoyl group to allow the complex to be conjugated to biomolecules containing primary amines.[91,92] The introduced benzoyl group had a negative effect on activity under mild conditions and caused a 7-fold slowdown in the hydrolysis of BNPP by Co(III) **76** ( $k_2 = 2.7 \text{ M}^{-1} \text{ min}^{-1}$ ; pH 7.3, 50 °C) relative to Co(III)-cyclen ( $k_2 = 19.0 \text{ M}^{-1} \text{ min}^{-1}$ ); however, at higher pH of 8.2, the rate constants for both complexes are almost equal with  $k_2 = 12.0$  and  $14.0 \text{ M}^{-1} \text{ min}^{-1}$ , respectively. The esterified Co(III) **77** ( $k_2 = 14.0 \text{ M}^{-1} \text{ min}^{-1}$ ) has similar activity at pH 7.3 as the parent Co(III)-cyclen, indicating that the decrease in Co(III) **76** activity is mainly due to the presence of negative charge or hydrogen bonding at higher pH. According to the speciation model, at pH 7.2 both complexes are mainly present in the mono-ionized form [Co(III)L(H<sub>2</sub>O)(OH)]. Hydrolysis of plasmid DNA catalyzed by Co(III) **77** (43%; C/BP = 30, pH 7.0, 37 °C, 16 h) yielded more of the nicked form II than the reaction with Co(III)

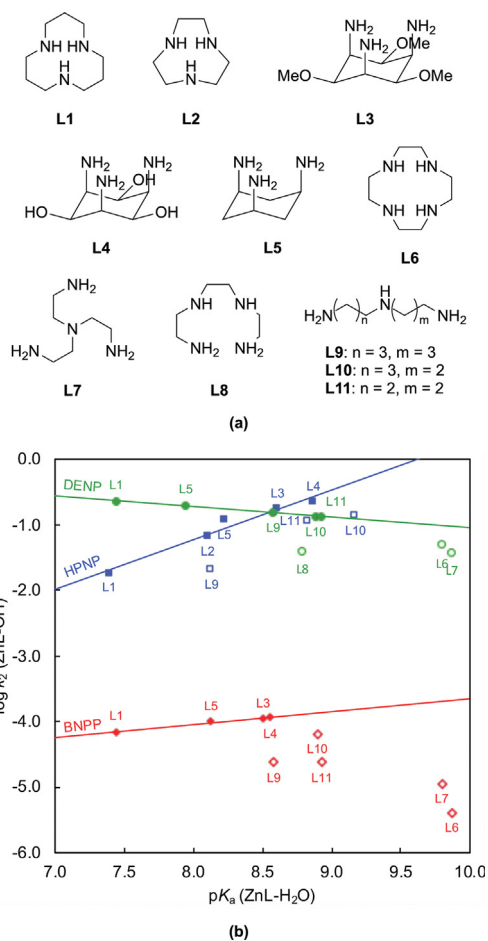


**Fig. 10.** (a) Structures of selected polyamine ligands. (b) Plot of second-order rate constant ( $\log k_2$ ) as a function of  $pK_a$  of metal-bound water for: DENP (green set), HPNP (blue set) and BNPP (red set), catalyzed by Zn(II) complexes in water at 25 °C. Full labels indicate complexes that conform to the linear fit (plain lines) of the reactivity data, empty labels indicate complexes that do not conform to the linear fit. The figure is based on data from ref. [67] and ref. [73]. The structure of the ligands is intentionally shown in an unstable conformation to show the distribution of the  $-NH_2$  groups as close as possible to that found in their complexes.

**76** (25%), but was only half as efficient as the reaction with nickase enzyme (88%). Co(III) **77** is also capable of inhibiting cell-free translation of luciferase mRNA with a relatively low  $IC_{50} = 0.13 \text{ mM}$ . A few minutes' incubation of mRNA with this complex did not result in the formation of lower-mass protein products, but a longer 24 h incubation was sufficient to hydrolyze about 96% of the mRNA. Thus, the inhibition of translation is probably not due to hydrolysis, but rather to a kinetically inert interaction between Co(III) **77** and mRNA.

A series of 1,7-dimethylcyclen complexes, **78–81** (Fig. 11), were tested by Liang *et al.* for nucleolytic and antiproliferative activity.[93] These complexes showed moderate efficiency against HeLa and A549 cell lines compared to the free ligand (results are presented later in the review). The most potent were Co(II) **78** and Ni(II) **80**, which at a concentration of  $10^{-4} \text{ M}$  inhibit A549 cell proliferation by 35.1 and 43.7%, respectively, but their activity was lower compared to the 53.6% inhibition by the free ligand. Moreover, neither complex caused significant DNA damage; here, the free ligand also showed greater activity.

Breslow *et al.* reported *N*-mesyl Zn(II) **82** and *N*-tosyl Cu(II) **83** and Zn(II) **84** (Fig. 11).[94] The *N*-tosyl complexes were more active in the hydrolysis of HPNP ( $k_{\text{obs}} = 6.07$  and  $3.15 \times 10^{-5} \text{ s}^{-1}$ , respectively) that the *N*-mesyl analog ( $k_{\text{obs}} = 2.91 \times 10^{-7} \text{ s}^{-1}$ ) and the parent Zn(II)-cyclen and Cu(II)-cyclen ( $k_{\text{obs}} = 0.90$  and  $0.23 \times 10^{-5} \text{ s}^{-1}$ ,

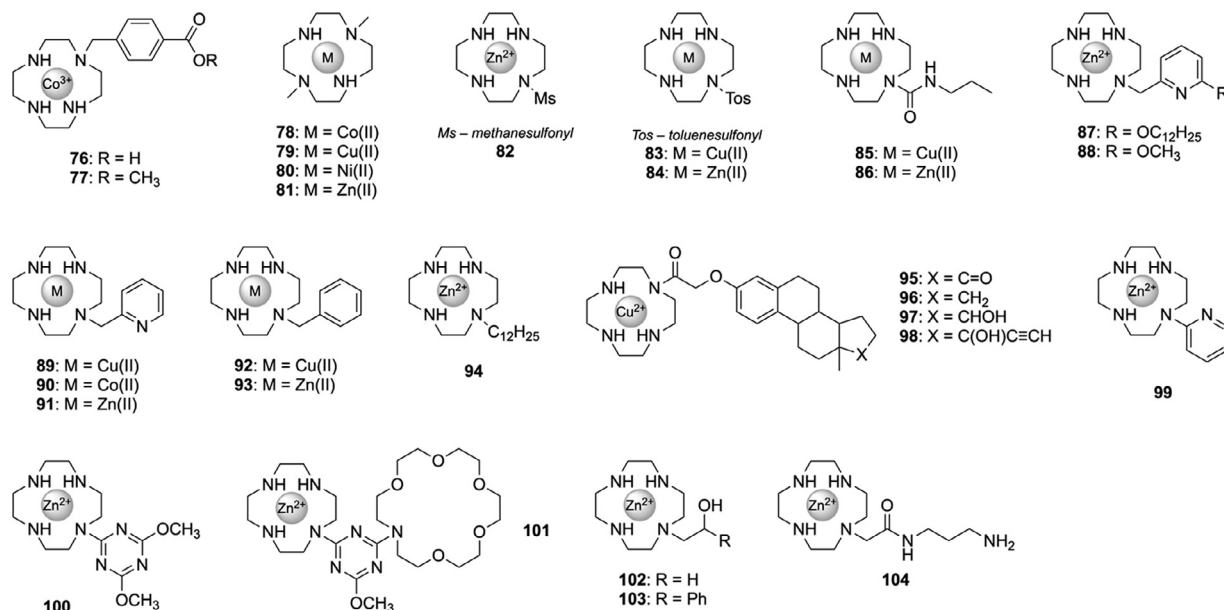


Fig. 11. Examples of mononuclear *d*-block complexes 76–104.

respectively) under the same conditions ( $C/S = 1.0$ , pH 8.0, 30 °C). These results were interpreted by the authors as evidence that hydrophobic side arms can strongly enhance the catalytic activity of transition metal cyclen complexes.

Described by König *et al.* Cu(II) **85** and Zn(II) **86** functionalized with an *N*-propylcarboxamide group (which together with the ligand's nitrogen forms a pseudourea group) show higher binding affinity ( $K_{app} = 51$  and  $4.0 \times 10^3 \text{ M}^{-1}$ , respectively; pH 7.4, rt) to calf thymus DNA (CT-DNA) compared to free-metal cyclen ( $K_{app} < 1.0 \times 10^3 \text{ M}^{-1}$ ).<sup>[95]</sup> These complexes, although binding to CT-DNA, do not show hydrolyzing activity against BNPP or CT-DNA.

Xiang *et al.* reported mono-functionalized complexes **87–94** (Fig. 11).<sup>[96]</sup> The most active against BNPP was Zn(II) **94** ( $k_{obs} = 9.0 \times 10^{-4} \text{ s}^{-1}$ ;  $C/S = 25$ , pH 7.5, 30 °C) with a long lipophilic chain, which was about 2–8 times more active than the other Zn(II) complexes in this series. The relaxation of plasmid pUC18 was strongly dependent on the type of metal ion and decreased in the order: Cu(II) **89** (100%\*) > Co(II) **90** (43%\*) > Zn(II) **91** (31%\*) when the side arm contained a lipophilic group (e.g., OPh or  $C_{12}H_{25}$ ). In all cases, only selective cleavage of plasmid form I to form II was observed. Interestingly, Cu(II) **89** was the most active in cleaving DNA, yielding almost 100%\* of form II after 3 h of incubation, while Zn(II) **94** under the same conditions yielded only 26%\* of form II ( $C/BP = 39.3$ , pH 7.1, rt, vit. C 0.041 M). *Note: The activity of the complexes was evaluated in the presence of vit. C, so it can be assumed that Cu(II) **89** may act according to an oxidative mechanism.*

Yang *et al.* prepared a series of conjugates **95–98** (Fig. 11) and showed that attachment of estrogen derivatives reduces CT-DNA binding capacity ( $K_{app} = 0.93\text{--}1.57 \times 10^7 \text{ M}^{-1}$ ) compared to unmodified Cu(II)-cyclen ( $K_{app} = 2.75 \times 10^7 \text{ M}^{-1}$ ).<sup>[97]</sup> However, in the same study, the cleavage of pUC19 by estrogen conjugates was shown to be much more efficient than by Cu(II)-cyclen (almost no activity); at the highest concentration tested and under physiological-like conditions ( $C/BP = 35.3$ , pH 7.4, 37 °C for 24 h), the ability of the conjugates to cleave plasmid DNA decreases in the order: Cu(II) **95** (~100%\*) > Cu(II) **96** (93%\*) > Cu(II) **97** (60%\*) > Cu(II) **98** (51%\*), with only selective cleavage to form II observed.

It is widely believed that additional substrate interactions next to the metal center can increase the hydrolytic activity by the attachment of functional groups to a chelate ligand. For this pur-

pose, Subat *et al.* prepared mononuclear Zn(II) **99–101** (Fig. 11) conjugated to substituted triazine or pyridine.<sup>[98]</sup> Comparison of second-order rate constants for BNPP hydrolysis catalyzed by Zn(II) **99**, Zn(II) **100**, and Zn(II) **101**, which under near-physiological conditions (pH 7.4, 25 °C,  $I = 0.1 \text{ M}$  (NaCl)) are  $1.37 \times 10^{-5}$ ,  $0.59 \times 10^{-5}$ , and  $0.64 \times 10^{-5} \text{ M}^{-1} \text{ s}^{-1}$ , respectively, show that they are even several times more active than the parent Zn(II)-cyclen ( $k_2 = 0.31 \times 10^{-5} \text{ M}^{-1} \text{ s}^{-1}$  at pH 7.5). The activity of Zn(II) **101** conjugated to polyoxamacrocycle differs little from that of Zn(II) **100**, so it can be assumed that the increase in activity relative to the initial Zn(II)-cycle comes from the presence of the aromatic substituent and possible  $\pi$ - $\pi$  interactions with the aromatic ring of the BNPP.

To shed more light on the function of Ser102 and Zn(II) ions in alkaline phosphatase, Kimura *et al.* prepared Zn(II) **102–103** (Fig. 11) with an embedded pendant nucleophile.<sup>[99]</sup> The crystallographic structure of Zn(II) **103** showed that the alkoxide derived from the hydroxyethyl group is tightly coordinated to the fifth coordination site. The pH-rate profile for the phosphoryl transfer reaction ( $k_{BNPP}$ ) from BNPP to  $[\text{Zn(II) } \mathbf{103}\text{-H}]^-$  yielded a sigmoidal curve with an inflection point at pH 7.4; the  $pK_a$  for the metal-bound alkoxide was determined to be 7.3. The second-order rate constant of  $k_{BNPP}$  is  $3.39 \times 10^{-4} \text{ M}^{-1} \text{ s}^{-1}$ . The product of the phosphoryl transfer reaction by Zn(II) **103** is the phosphorylated adduct  $[(\text{Zn(II) } \mathbf{103}\text{-BNPP})(\text{H}_2\text{O})]^-$  (Fig. 12). In the next step, the pendant phosphodiester undergoes spontaneous intramolecular nucleophilic attack by metal-bound  $\text{OH}^-$ , yielding the phosphomonoester  $[\text{Zn(II) } \mathbf{103}\text{-PO}_3]^-$ , which is stable under these conditions and does not undergo further hydrolysis. The reaction with the analogous Zn(II) **102** follows the same mechanism, but is slower (the exact results have not been published), probably due to a higher  $pK_a = 7.64$  and thus a lower concentration of the active form of the catalyst under the test conditions.

Kalesse *et al.* obtained a mono-functionalized complex Zn(II) **104** (Fig. 11), in which the carbamoyl side arm is terminated by a diamine, allowing the complex to be coupled to targeting vectors.<sup>[100]</sup> The authors found that the  $pK_a$  of the metal-bound water is 9.6 (at 25 °C), which is much higher than  $pK_a = 7.6$  for Zn(II)-cyclen (under the same conditions). Due to its high  $pK_a$ , Zn(II) **104** begins to hydrolyze HPNP efficiently only at pH > 8.0, while at pH 7.3,  $k_{obs} = 2.9 \times 10^{-4} \text{ s}^{-1}$  ( $C/S = 40$ , 50 °C). The pH-rate plot

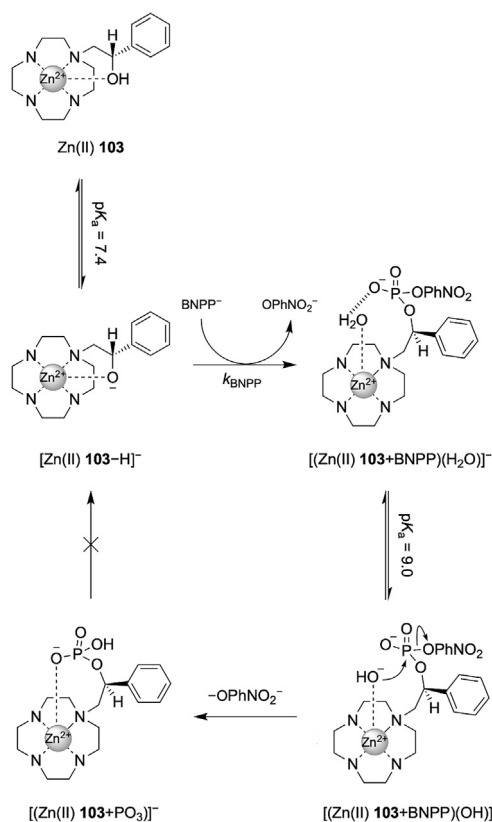


**Fig. 12.** Proposed mechanism for transesterification of BNPP by Zn(II) **103** with a reactive alkoxy arm. Experimental results shows that the metal-bound alkoxy group attacks the phosphorus atom, yielding a stable and unreactive phosphorylated adduct [Zn(II) **103**+PO<sub>3</sub>]<sup>-</sup>.

indicates that the active form of the complex is the mono-hydroxyl form [Zn(II)L(OH)]<sup>+</sup>.

### 2.2.6. Mononuclear *d*-block complexes with nucleic acid binders

In 1997, Hettich *et al.* described transition metal complexes **105.1–114.2** (Fig. 13) functionalized with single side arms with varying numbers of positively charged peralkylammonium groups to increase binding affinity to the negatively charged DNA backbone.[101] Increasing the number of positive ammonium groups from one to two and three in Co(III) **105.4**, Co(III) **110.1** and Co(III) **110.2**, provides better binding to DNA, as evidenced by an increase in  $\Delta T_m$  by 0.7, 4.2 and 8.9, respectively, and a decrease in  $C_{50}$  (the ligand concentration needed to reduce the fluorescence of the EB-DNA complex to 50%) by 1.9, 0.14 and  $0.05 \times 10^{-5}$  M, respectively. All Co(III) complexes cleaved BNPP ( $k_{obs} = 1.16\text{--}4.14 \times 10^{-3} \text{ s}^{-1}$ ; pH 7.0, 50 °C) and its monophosphate analog NP ( $k_{obs} = 1.9\text{--}3.4 \times 10^{-3} \text{ s}^{-1}$ ); Co(III) **105.2** was the most active complex in this series, but the activity of the parent Co(III)-cyclen ( $k_{obs} = 25.0 \times 10^{-3} \text{ s}^{-1}$ ) against BNPP was better. Although the additional positive charges of the polyamine chain led to a decrease in activity against small-molecule NP<sup>2-</sup> and BNPP<sup>-</sup>, due to competition in substrate binding, the same phenomenon led to a significant increase in plasmid DNA cleavage by all series of complexes; at the highest concentration tested (C/BP = 263, pH 7.0, 37 °C), activity decreases as follows: Co(III) **110.2** ( $k_{obs} = 53.7 \times 10^{-5} \text{ s}^{-1}$ ) > Co(III) **110.1** ( $k_{obs} = 40.9 \times 10^{-5} \text{ s}^{-1}$ )  $\gg$  Co(III) **105.1–105.4** ( $k_{obs} = 18.3\text{--}21.4 \times 10^{-5} \text{ s}^{-1}$ ). Addition of hydrogen peroxide did not change the cleavage efficiency of Co(III) complexes, as did radical scavengers such as DMSO or alcohol, indicating a hydrolytic pathway. The hydrolytic activity of the remaining complexes was below the measurement limits or negligible compared to Co(III) complexes. Although Cu(II) complexes were even more active than Co(III) complexes, the complete loss of their activity in the presence of radical scavengers indicates an oxidative mechanism for DNA cleavage.

Attachment of an intercalator is a well-known strategy for increasing the affinity of the resulting conjugates to ds-DNA, a strategy that was used by Kady *et al.* to obtain a series of transition metal complexes **115–122** (Fig. 13).[102] The cyclen complexes were linked to the acridine molecule by spacers of different lengths. The most active of the series was Co(III) **116**. The hydrolytic

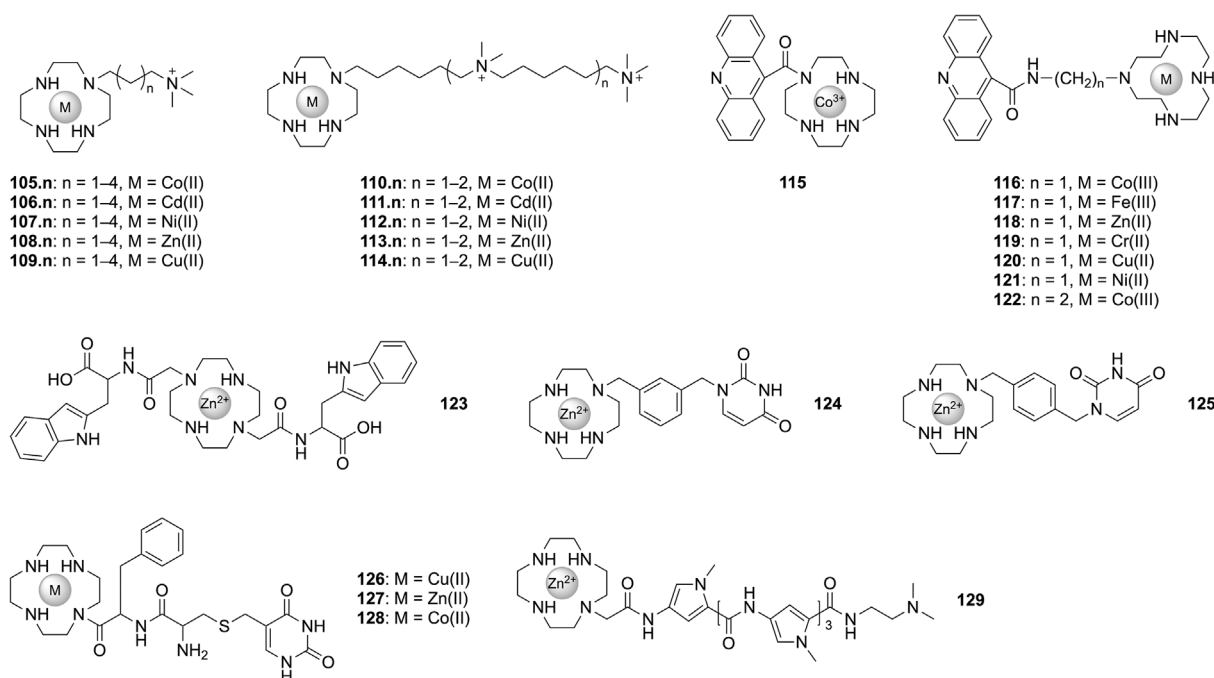


**Fig. 13.** Examples of mononuclear *d*-block complexes **105.1–129**.

tive activity of the conjugates depended both on the structure of the ligand: Co(III) **116** (85%) > Co(III) **122** (62%) > Co(III) **115** (54%), and on the type of metal ion: Co(III) **116** (85%) > Zn(II) **118** (83%) > Cr(II) **119** (78%) > Ni(II) **121** (75%) > Cu(II) **120** (65%) > Fe(III) **117** (12%). The presented conjugates selectively cleave form I of pBR322 to form II after 6 h of incubation under near-physiological conditions (C/BP = 1.0, pH 7.4, 37 °C). Interestingly, Zn(II) **118** showed a bell-shaped pH profile for DNA hydrolysis with a maximum at pH 7.4, followed by a sharp decrease in activity; as the authors state, the decrease in activity can probably be due to destabilization of the metal complex under alkaline conditions.

Adhikari *et al.* described Zn(II) **123** (Fig. 13) containing two pendant L-tryptophan molecules, which allows the complex to bind in a minor groove ( $K_b = 2.12 \times 10^5 \text{ M}^{-1}$ ) and leads to CT-DNA unwinding.[103] Zn(II) **123** cleaves plasmid pUC19 with a yield of 23–86% after 3 h of incubation under physiological-like conditions (C/BP = 0.0046–11.2, pH 7.2, 37 °C). At the highest concentration tested, Zn(II) **123** cleaved 80% of pUC19 after only 30 min of incubation. The complex was also shown to exhibit DNA cleavage activity *in vitro* and induce cell cycle changes, leading to a 4.9-fold increase in the percentage of apoptotic cells compared to the controls after 2 h of incubation. Zn(II) **123** also showed greater antiproliferative activity against U-87MG glioma cells at  $IC_{50}$  (25.0  $\mu\text{M}$ ) than against normal HEK 293 cells at the same concentration. In addition to the DNA-binding function of the L-tryptophan group, their second purpose is to improve intracellular uptake of the complex. In this case, they took advantage of the fact that cancer cells have a higher-than-normal expression of L-type amino acid transporters (LAT1), which are often used as carriers for the delivery of target compounds. The tumor specificity of the complex was confirmed using an analogous  $^{99m}\text{Tc(IV)}$ -labeled **123** in U-87 MG tumor-bearing mice. A high tumor/muscle ratio of >6 was found, clearly suggesting the specificity of the compound to the tumor. In addition, the complex was observed to be rapidly eluted from all non-target organs, such as liver, intestine, muscle, heart, and lung. These studies provide rare information on the intracellular and *in vivo* uptake of cyclen complexes and indicate the target specificity of the ligand to the tumor, demonstrating the usefulness of these complexes as tumor-specific antiproliferative agents that exhibit anticancer properties through DNA cleavage.

The combination of uracil and Zn(II)-cyclen via rigid aryl spacers gave complexes Zn(II) **124** and Zn(II) **125** (Fig. 13) with enhanced DNA recognition due to their ability to form additional Watson-Crick bonds.[104] At lower concentrations (C/BP = 0.48), both complexes catalyze the cleavage of supercoiled pUC19 selectively to form II, but at higher concentrations (C/BP = 0.8) a decrease in form II in favor of form III (linear fragments) is observed. The highest activity of Zn(II) **125** was observed at pH 8.0, which is consistent with  $pK_a = 7.8$  of metal-bound water. DNA cleavage efficiency decreased as follows: Zn(II) **124** (79%) > Zn(II) **123** (44%) > Zn(II)-cyclen (24%), under optimal conditions (C/BP = 0.48, pH 8.0, 37 °C for 3 h). The higher activity of Zn(II) **122** linked to uracil via *m*-xylene may be due to dimer formation as a result of intermolecular interaction between the N-atom of uracil and the Zn(II) ion.

Wang *et al.* obtained a series of PNA-cyclen (peptide nucleic acid) conjugates, consisting of uridine as a DNA recognition motif and phenylalanine providing additional  $\pi$ - $\pi$  interactions.[105] Complexes **126–128** (Fig. 13) promote relaxation of supercoiled pUC19, yielding 23–87% of form II after 24 h incubation under physiological-like conditions (C/BP = 12.7, pH 7.4, 37 °C). Since all the ions used have similar charge densities ( $\rho_{\text{Zn(II)}} = 112 \text{ C mm}^{-3}$ ,  $\rho_{\text{Cu(II)}} = 116 \text{ C mm}^{-3}$  and  $\rho_{\text{Co(II)}} = 155 \text{ C mm}^{-3}$ ), the highest cleavage activity observed for Cu(II) **126** was attributed to the highest ionization potential and thus the strongest Lewis acidity of the Cu(II) ion ( $I_{\text{Cu(II)}} = 20.29 \text{ eV}$ ,  $I_{\text{Zn(II)}} = 17.96 \text{ eV}$  and  $I_{\text{Co(II)}} = 17.06$

eV).[106] As the authors note, the stronger Lewis acid can more easily activate the phosphodiester bond in DNA by neutralizing its negative charge. The activity of Cu(II) **126** did not change after the addition of free radical scavengers, so cleavage most likely occurs via a hydrolytic rather than oxidative pathway.

The introduction of side arms containing oligopyrrole carboxamides makes it possible to increase the affinity and specificity of the obtained conjugates toward regions of ds-DNA rich in AT pairs. Such a strategy was used by Zhou *et al.* to obtain Zn(II) **129** conjugate, which showed excellent cleavage activity against pBR322 and pUC19 plasmids; in the pH range of 7.2–8.2 (37–40 °C), the tested DNA appeared in linear form after only 15 min of incubation.[107].

### 2.2.7. Free cyclen ligands with nucleolytic activity

As a result of our literature search, we came across several examples of metal-free cyclen derivatives (referred to here as “free ligands”) that are nucleolytically active against plasmid DNA. One example of such compounds are **130** and **131**, described by Liang *et al.*[93,95,108] Compound **130** at a concentration of  $10^{-4} \text{ M}$  was able to inhibit the proliferation of A549 and HeLa cells by 54% and 63%, respectively. The compound was found to disrupt the cell cycle and induce concentration- and time-dependent apoptosis in HeLa and A549 cells, and induce DNA fragmentation *in vitro* in HeLa cells. Further *N*-methylation of cyclen to tetramethylated **131** resulted in a significant reduction in the *in vitro* antiproliferative activity and hydrolysis of plasmid pBR322. Interestingly, **130** exhibits a bell-shaped pH-rate curve with the highest  $k_{\text{obs}} = 6.0 \times 10^{-4} \text{ s}^{-1}$  at pH 7.2 (C/BP = 10, 37 °C). *In vitro* DNA cleavage was not reduced in the presence of free radical scavengers, so it most likely occurred via a hydrolytic pathway. As suggested by potentiometric studies, protonated  $\text{H}[\mathbf{130}]^+$  and  $\text{H}_2[\mathbf{130}]^{2+}$  are the predominant forms over a wide pH range of 1.5–10, and the DNA cleavage reaction probably occurred with water molecules activated by associated these protonated forms.

Metal-free **132–133** (Fig. 13) with arginine-rich side arms and tyrosine-containing series **134–140** were designed by Kalesse *et al.* as novel RNA-binding molecules for cleaving HIV-1 TAR RNA.[109,110] The only active peptide conjugate was **133**, which showed selective and efficient RNA cleavage in the pH range 6.0–7.4 with a preference for unpaired uridines. The only cleavage site in the TAR region was between U31 and G32, but there was no cleavage when U31 was changed to A31. This remarkably selectivity was also observed for **134–135** containing tyrosine and **136–137** containing phenylalanine, but the former were more active, indicating an important role for the hydroxyl group of tyrosine in the cleavage process. The other ligands were found to be inactive. Since no dU base cleavage was observed, RNA cleavage probably occurs via transesterification involving the 2'-hydroxyl group.

Zhao *et al.* also showed free ligands **141–143** with side arms containing oligopyrrole carboxamides, analogous to the conjugate Zn(II) **129** discussed earlier.[111–113] CT-DNA binding results showed that **141** ( $\Delta T_m = 7.7$ ) as well as **143** ( $\Delta T_m = 13.8$ ) and **142** ( $\Delta T_m = 11.5$ ) strongly binds to ds-DNA, increasing its thermal stability. Previous studies show that zinc complexes based on such ligands exhibit strong nucleolytic activity. However, no observable activity was found for Zhao's free ligands.

### 2.2.8. Recognition of thymine and uridine by Zn(II)-cyclen

Metal complexes with fine-designed ligands represents a promising direction for the development of small molecules targeting nucleic acids. Among the complexes discussed so far, the role of the recognition motif has usually been played by the side arms, but it has also been found that Zn(II)-cyclen itself can selectively recognize specific nucleobases, in particular thymine (T) and uracil (U), and thus can act as a recognition motif. This discovery has evolved



over time to a new aspect of molecular recognition by Zn(II)-cyclen complexes. The action of such complexes resembles a “molecular crowbar” that can pull apart AT pairs in ds-DNA and selectively bind to T; the interaction is strong enough to alter important biochemical and ultimately biological properties of DNA, affecting transcription factors or exhibiting antimicrobial activity. Readers interested in learning more about other aspects of selective nucleobases recognition by Zn(II)-cyclen complexes are encouraged to read the 2000 paper by Kimura and Kikuta, who were the first to discover the phenomenon and develop work on it.[114] Interestingly, many of the Zn(II)-cyclen complexes known to date, in addition to the nucleolytic properties discussed mainly in this article, may in some cases exhibit nucleoprotective activity. It is also worth noting that not only Zn(II)-cyclen complexes are capable of selective recognition of T and U, but under certain conditions the free cyclen ligand can also exhibit a similar ability. In our recent work, we showed that oligonucleotide-cyclen conjugates are capable of selectively recognizing TT mismatches on the complementary strand, stabilizing the resulting duplex while destabilizing other sequences and mismatches.[115].

To get a more detailed picture of nucleoprotective activity of Zn(II)-cyclen derivatives, Kikuta *et al.* performed a DNA footprinting study using microtubule nuclease (MNase),[116] a relatively small (16.8 kDa) endonuclease, which has a preference for digesting ss-DNA and ss-RNA, particularly in AT-rich (or AU-rich) regions.[117–119] A useful feature of MNase is its ability to nick ds-DNA predominantly in areas of transiently melted base pairs, which results, for example, from DNA “breathing” (Fig. 15a). This term refers to local conformational fluctuations in ds-DNA in the form of base pair breaks at temperatures well below the melting point of DNA. The disconnection of complementary strands results in the formation of a transient region of ss-DNA within one or more bases.[120] The binding domain of MNase is quite narrow, allowing it to reach the double helix and bind one strand without much interference from the opposite strand, making it extremely useful as a model for studying the nucleoprotective effects of Zn(II)-cyclen derivatives. Kikuta *et al.* showed that the Zn(II)-acridinylmethylcyclen (Zn(II)-acrcyclen; Fig. 15b) protected pT bonds from hydrolysis by micrococcal nuclease, but at the same time does not protect pA bonds. Because the complex selectively bound to T bases within the melted AT base pair, the separated A

bases were actually more susceptible to digestion by MNase, which resulted in increased hydrolysis in the homopolymeric dA regions. However, in an analogous experiment with DNase I, which acts on double-stranded rather than single-stranded structures, both T and A partners in AT-rich regions were protected from hydrolysis in the presence of Zn(II)-cyclen complexes. The same experiment also showed that Zn(II) ions were necessary for a nucleoprotective effect; analogous complexes with Co(II) or Ni(II) ions did not exhibit such properties.

The propensity of Zn(II)-cyclen to form stable complexes with weak acids has long been known and is manifested, among other things, in large complexation constants with phosphate, oxalate, carboxyl and aromatic sulfonamide anions. The main source of stabilization in such ternary complexes is the electrostatic interaction between the positively charged metal ion and the anionic ligand, some additional stabilization may also come from hydrogen bonds between the cyclen ring and the metal-bound ligand. An analogous situation exists between deprotonated T (T<sup>-</sup>) and Zn(II)-cyclen. The carbonyl groups at T and U play a major role in stabilizing the ternary complex in two ways: (1) they pull electrons away from the neighboring nitrogen, helping Zn(II) to remove the imide proton and form a Zn<sup>2+</sup>-N<sup>-</sup> bond; (2) due to their partial negative charge, the carbonyl oxygens form hydrogen bonds with the amino groups of the cyclen ligand, thus introducing bond complementarity and helping the ligands stay in their proper positions (Fig. 15c). Zn(II)-cyclen was found to exclusively recognize the imide functionality of thymine (log K = 5.6 M<sup>-1</sup>, 25 °C) and uracil (log K = 5.2 M<sup>-1</sup>, 25 °C). Zn(II)-[12]aneN<sub>3</sub> can also form a stable 1:1 complex with dT<sup>-</sup> (log K ~ 6.0 M<sup>-1</sup>, 25 °C), but in general cyclen complexes interact with dT<sup>-</sup> more strongly than any macrocyclic triamine complexes.[121] An even stronger association was found in the ternary complex of Zn(II)-acrcyclen and deprotonated methylthymine.[122] X-ray structure revealed that the central Zn(II) ion has a tetrahedral pyramidal structure coordinated by four cyclen nitrogens and a deprotonated imide anion (Fig. 15b). The acridine moiety lies parallel to the thymine plane and is approx. 3.4 Å away from it, allowing for additional aromatic interaction between acridine and thymine (π-π stacking). The presence of acridine in the ternary complex leads to increased association with dT and U compared to the non-functionalized Zn(II)-cyclen (Fig. 15d).

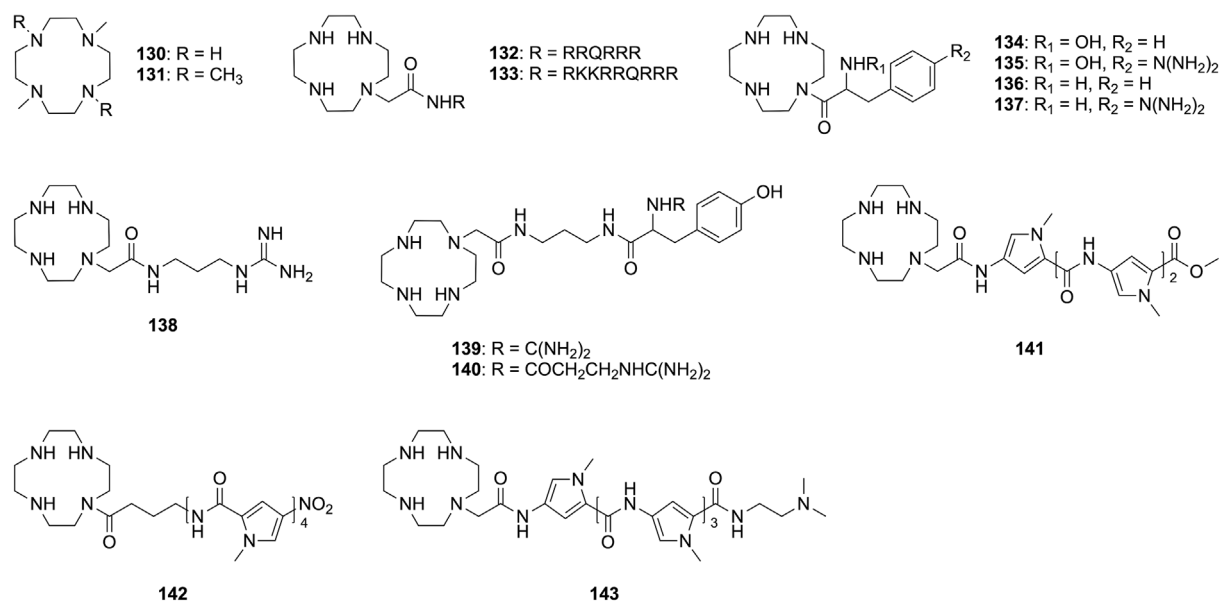
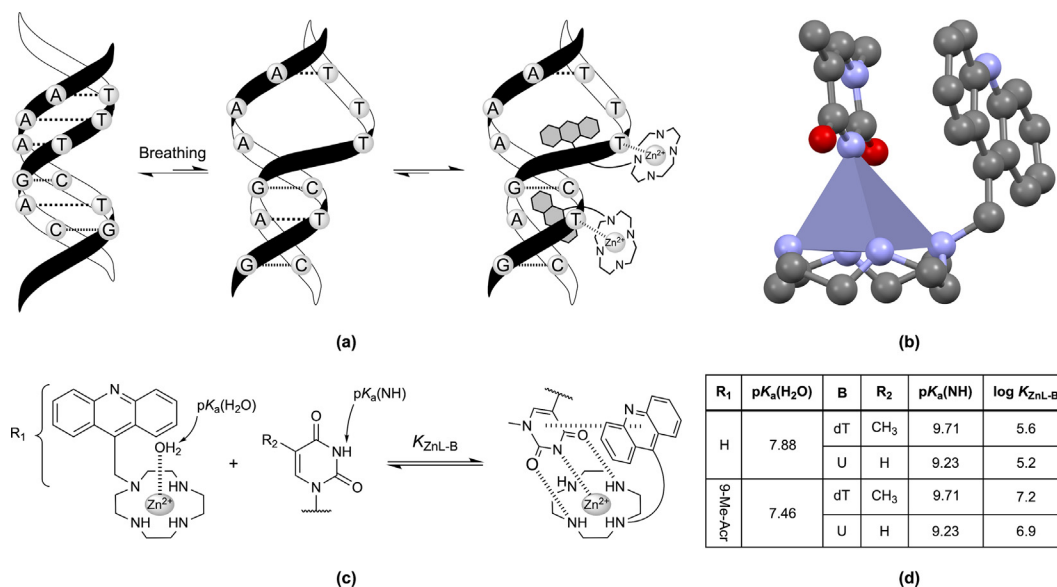


Fig. 14. Examples of mononuclear cyclen-based nucleases 130–143.



**Fig. 15.** (a) Schematic figure of breathing DNA. Zn(II)-acridinylmethylcyclen binds only to thymine groups to separate AT base pairs and expose adenine, making it more susceptible to digestion by micrococcal nuclease (MNase). (b) X-ray structure of Zn(II)-acridinylmethylcyclen. (c) Scheme of thymidine (dT, or uridine U) recognition by Zn(II)-acridinylmethylcyclen. The ternary complex is stabilized by the Zn(II) ion binding to *N*-deprotonated dT<sup>-</sup> or U<sup>-</sup> imide anions, complemented by two hydrogen bonds between the NH groups of the cyclen and the carbonyl oxygens of the imide group, and by the  $\pi$ - $\pi$  stacking interaction of the aromatic moieties. (d) Selected properties of ternary complexes.

### 2.2.9. Effect of side arms on d-block complexes

**Effect of *N*-alkylation in cyclen.** By far the simplest and most abundant side arms are alkyl chains without any appended donor functionalities that would interact with the central metal ion. Discussing the effect of *N*-alkylation on the properties of the resulting complexes will allow us to understand the influence of other types of side arms, which are most often  $\alpha$ - and  $\beta$ -functionalized alkyl chains. The conversion of cyclen amino groups from secondary to tertiary by the attachment of *N*-methyl groups results in a decrease in their metal-binding capacity, and thus a worsening decrease in the stability of the complex as the number of alkyl groups increases: Zn(II)-cyclen (log  $K_f$  = 16.2) > dimethyl Zn(II) **L12** (log  $K_f$  = 15.1) > tetramethyl Zn(II) **L14** (log  $K_f$  = 14.0). The reason for this is most likely the large increase in steric hinderance that occurs when *N*-alkyl groups are added to the complexes. Selected properties of the complexes and ligand structures are shown in Fig. 16.[123–125].

**Effect of pyridylmethyl side arms.** Pyridylmethyl arms are most often found as 2-methylpyridine or its derivatives, such as in ligands **87–91** (Fig. 11). Such isomerism of the methylpyridine group facilitates intramolecular binding of the pyridyl nitrogen atom to the central metal ion. As noted by Ghachtouli *et al.*, in the case of Cu(II)-cyclen (log  $K_f$  = 23.3)[126], the introduction of 2-methylpyridine side arm causes a slight decrease in the stability of Cu(II) **L15** (log  $K_f$  = 21.0), but the magnitude of this effect is comparable to the introduction of the benzyl group in Cu(II) **L17** (log  $K_f$  = 20.4), suggesting that in aqueous solution the pyridyl group is only weakly involved in the direct coordination of the copper ion.[127] A subtle change in the isomerism on the functional group can significantly alter the coordination properties of pyridine-functionalized ligands. El Hajj *et al.* showed that Cu(II) **L16** functionalized with a 4-methylpyridine group tends to form a coordination polymer in which the macrocyclic ligand acts as a bridging ligand.[128] Despite the lack of information on the stability of mono-substituted complexes of various transition metals, a comparison of the stability of 1,7-disubstituted complexes: Cu(II) **L18** (log  $K_f$  = 20.3) > Zn(II) **L18** (log  $K_f$  = 17.5)  $\approx$  Co(II) **L18** (log  $K_f$  = 17.5) suggests that this type of arm causes the least destabi-

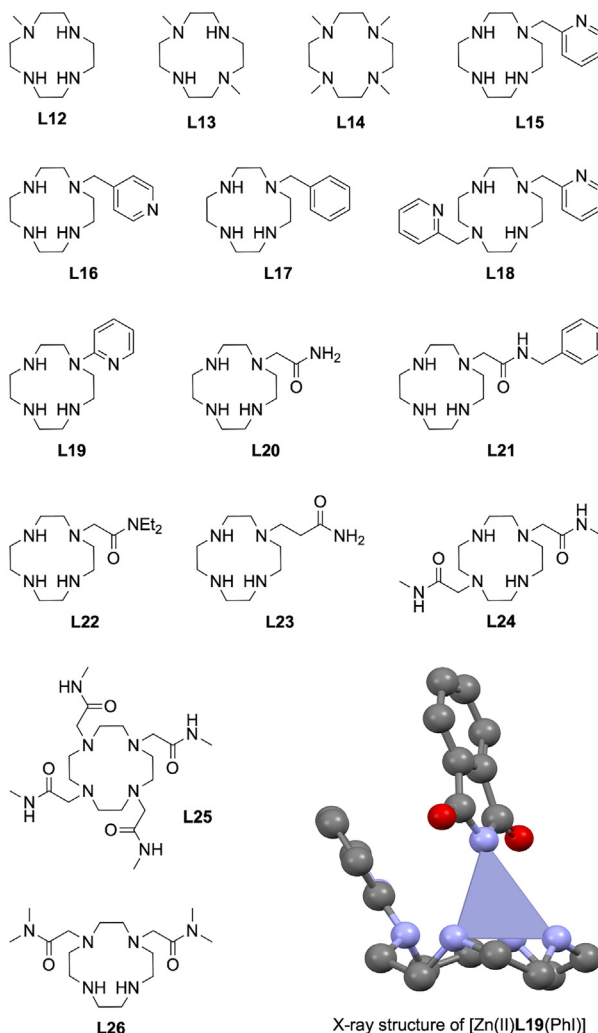
lization of the copper complex.[129] As we described in the previous section, the functionalization of cyclen complexes with aromatic side arms often leads to increased stability of ternary complexes through  $\pi$ - $\pi$  interactions with nucleic bases (Fig. 15c). In the case of Zn(II) **L15** and its derivatives, it was found that whether the guest belonged to purine or pyrimidine bases, it was recognized less effectively than by Zn(II) **L17**. [130] The main reason for the reduced stability is probably the lower  $\pi$ -electron density of the pyridine ring compared to the benzene ring, making the stacking effect of the benzene ring greater. Moreover, by interacting with the metal ion, the pyridine moiety further reduces the stability of host-guest complexes with nucleic bases.

**Effect of pyridine moiety as a side arm.** The pyridine is attached to the cyclen mainly through position 2, as in Zn(II) **99** (Fig. 11). The X-ray structure of Zn(II) **99** shows intramolecular coordination of the pyridine nitrogen to Zn(II), but only three of the four nitrogen atoms of the cyclen ring are involved in metal complexation, resulting in reduced stability of Zn(II) **L19** (log  $K_f$  = 11.3) compared to the parent Zn(II)-cyclen (log  $K_f$  = 16.2).[131] pK<sub>a</sub> of Zn(II)-bound water in Zn(II) **99** was determined to be 8.37. Like other Zn(II)-cyclen derivatives, Zn(II) **99** tends to form ternary complexes with guests having a dissociated imide group. The X-ray structure of [Zn(II)(L19)(PhI)] (Fig. 16b) shows that the ternary complex is stabilized by coordination of zinc to the deprotonated imide nitrogen and H-bonding between amine proton donors and carbonyl groups. Although the Zn(II) ion is no longer coordinated to the pyridine nitrogen, only three of the four cyclen nitrogens are still involved in Zn(II) binding.

**Effect of a single amide-containing side arm.** One of the most common ways to functionalize cyclen complexes of transition metals and *f*-metals is through amide-containing arms, especially carbamoylmethyl arms, which provide an optimal distance between the central metal ion and the donor nitrogen or oxygen atoms. Kimura *et al.* showed that depending on pH conditions, carbamoylmethyl arms can interact with zinc ions in two ways – amine oxygen binds to zinc ions at slightly acidic pH (below the pK<sub>a</sub> of the amide group), or deprotonated amide nitrogen binds to zinc ions at basic pH.[132] The pK<sub>a</sub> values of the amide group and its deriva-

Complex	log $K_f$	$pK_a$	Conditions	Ref.
Co(III)-cyclen	13.8 <sup>a</sup>	$pK_{a1} = 5.66$ <sup>b</sup> $pK_{a2} = 6.96$ <sup>b</sup>	35 °C, $I = 0.2$ (NaClO <sub>4</sub> )	135 136
Cu(II)-cyclen	23.3		25 °C, $I = 0.5$ (NaNO <sub>3</sub> )	126
Zn(II)-cyclen	16.2	8.0	25 °C, $I = 0.2$ (NaClO <sub>4</sub> )	76
	15.3	7.9	25 °C, $I = 0.1$ (NaNO <sub>3</sub> )	131
Zn(II) <b>L12</b>	15.1	7.68	25 °C, $I = 0.1$ (NaClO <sub>4</sub> )	123
Cu(II) <b>L13</b>	17.9		25 °C, $I = 0.1$ (NMe <sub>4</sub> Cl)	124
Cu(II) <b>L14</b>	18.4		25 °C, $I = 0.1$ (NaNO <sub>3</sub> )	125
Zn(II) <b>L14</b>	14.0		25 °C, $I = 0.1$ (NaNO <sub>3</sub> )	125
Cu(II) <b>L15</b>	21.0		25 °C, $I = 0.1$ (KNO <sub>3</sub> )	126
Cu(II) <b>L17</b>	20.4		25 °C, $I = 0.1$ (KNO <sub>3</sub> )	126
Co(II) <b>L18</b>	17.5		25 °C, $I = 0.1$ (NMe <sub>4</sub> NO <sub>3</sub> )	129
Cu(II) <b>L18</b>	20.3		25 °C, $I = 0.1$ (NMe <sub>4</sub> NO <sub>3</sub> )	129
Zn(II) <b>L18</b>	17.5		25 °C, $I = 0.1$ (NMe <sub>4</sub> NO <sub>3</sub> )	129
Zn(II) <b>L19</b>	11.3	8.37	25 °C, $I = 0.1$ (NaNO <sub>3</sub> )	131
Zn(II) <b>L20</b>	14.4	8.59 <sup>c</sup>	25 °C, $I = 0.1$ (NaClO <sub>4</sub> )	132
Zn(II) <b>L21</b>	14.2	7.92 <sup>c</sup>	25 °C, $I = 0.1$ (NaNO <sub>3</sub> )	132
Zn(II) <b>L22</b>	15.5	9.92	25 °C, $I = 0.1$ (NaClO <sub>4</sub> )	132
Zn(II) <b>L23</b>	14.5	8.19 <sup>c</sup>	25 °C, $I = 0.1$ (NaNO <sub>3</sub> )	132
Cu(II) <b>L24</b>	15.4	>9.0 <sup>d</sup>	25 °C, $I = 0.1$ (NMe <sub>4</sub> Cl)	123
Zn(II) <b>L24</b>	12.3	>9.0 <sup>d</sup>	25 °C, $I = 0.1$ (NMe <sub>4</sub> Cl)	123
Cu(II) <b>L25</b>	14.1		25 °C, $I = 0.1$ (NMe <sub>4</sub> Cl)	133
Zn(II) <b>L25</b>	13.0		25 °C, $I = 0.1$ (NMe <sub>4</sub> Cl)	133
Cu(II) <b>L26</b>	21.4		25 °C, $I = 0.1$ (KCl)	134
Zn(II) <b>L26</b>	15.6		25 °C, $I = 0.1$ (KCl)	134

(a)



(b)

**Fig. 16.** (a) Comparison of  $pK_a$  and stability constant of cyclen complexes due to metal type and ligand structure. (b) Model ligands with commonly used functional groups for cyclen modification. X-ray structure of ternary complex between Zn(II) **L19** and phthalimide (PhI). **a** – ref. [135]; **b** – ref. [136]; **c** –  $pK_a$  of metal-bound amide NH group; **d** – calculated from species distribution diagram, Fig. 3 in ref. [124].

tives are shown in Fig. 16a. Under neutral conditions (pH 7.0, 25 °C), zinc in Zn(II) **L20**, Zn(II) **L21** and Zn(II) **L23** complexes binds to the amidate *N*-atom along with four cyclen nitrogen atoms. The carbamoylmethyl arms form five-membered chelates and provide more stable complexes compared to non-functionalized cyclen than the carbamoylethyl arms, which form six-membered chelates. On the other hand, the carboxamide group obscures the Zn(II) active site so effectively that the catalytically active hydroxyl form of [Zn(II)L(OH)] is absent at both acidic and basic pH. The amide arms are usually present in the form of a free amide group or its mono-substituted derivatives, both of which have similar effects on the stability of complexes; the di-substituted amide groups, as in Zn(II) **L22**, leads to further stabilization of the complex (log  $K_f = 15.5$ ), and a change in the coordination mode to amide oxygen-coordination. The high  $pK_a = 9.92$  for Zn(II) **L22** has been attributed to metal-bound water and is probably so high because of competitive amide coordination; the presence of a metal-bound water molecule provides the complex with hydrolytic activity, albeit at a very low rate.

**Effect of two amide-containing side arms.** Doubly functionalized transition metal cyclen complexes are less frequently studied in the context of artificial nucleases, and the only example of such

a structure we have found is Zn(II) **L23** (Fig. 13). Although it might seem that the presence of two mono-substituted amides would contribute to the loss of catalytic activity of the corresponding complexes (after all, the presence of one such arm results in the loss of hydrolytic activity of Zn(II) **L21**), Bazzicalupi *et al.* showed that, in fact, two-armed complexes Cu(II) **L24** and Zn(II) **L24** induce the formation of hydroxyl species in alkaline solution (pH > 9.0). [123] The presence of water molecules in the first coordination sphere suggests the involvement of a low number of ligand donor atoms in the coordination of these metals ions in aqueous solution. The <sup>13</sup>C NMR results showed no shift in the characteristic signal from the C=O groups in Cu(II) **L24** and Zn(II) **L24**, which is shifted by about 2.5 ppm in complexes where the amide oxygen binds to the metal ion. This, along with low tendency to bear protonation, indicates that mainly *N*-atoms of cyclen are involved in Zn(II) and Cu(II) complexation. In addition, the stability constant of Cu(II) **L24** (log  $K_f = 15.4$ ) is lower than that found earlier for the analogous complex Cu(II) **L13** (log  $K_f = 17.9$ ), and the stability constant of Zn(II) **L24** (log  $K_f = 12.3$ ) is lower than for Zn(II) **L21** (log  $K_f = 14.2$ ), the main reason for which may be steric factors and electronegativity related to the presence of four tertiary amines in the cyclen ring, which in aqueous solution show less binding capacity

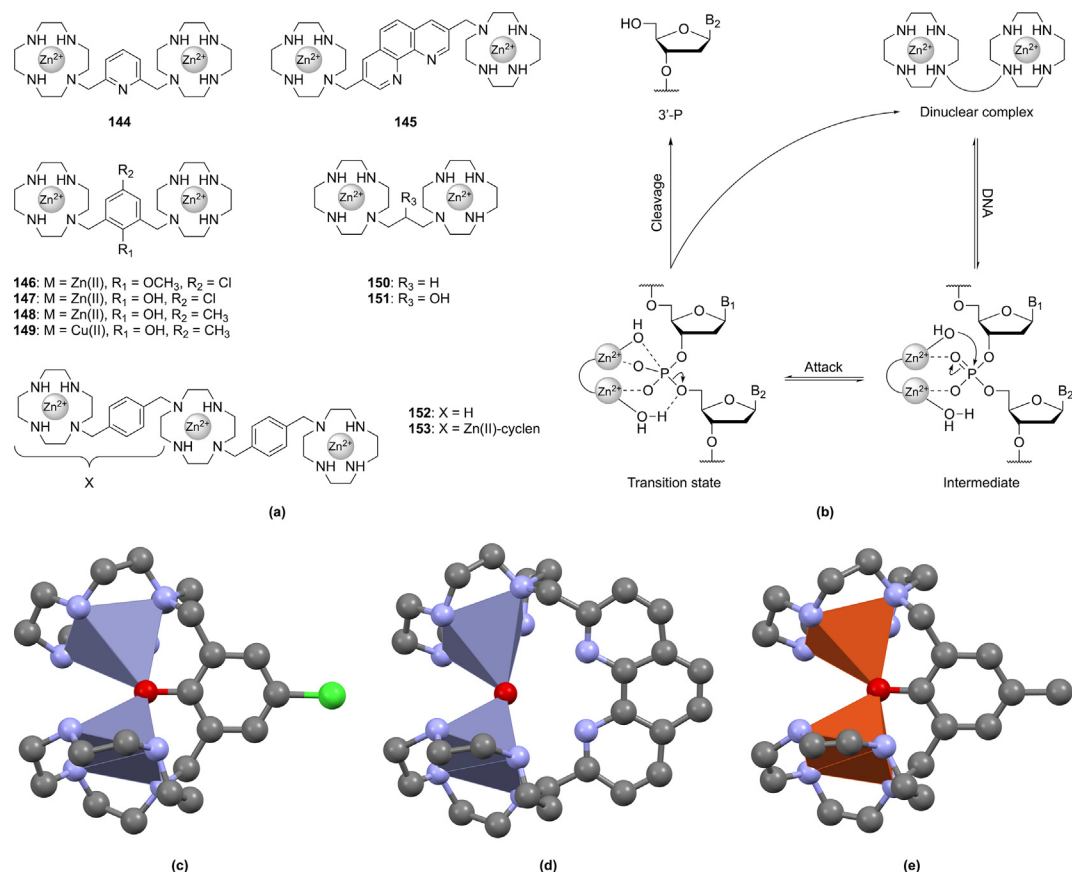


**Fig. 17.** (a) Examples of dinuclear *f*-block complexes **144–153**. (b) Proposed mechanism of DNA hydrolysis catalyzed by dinuclear Zn(II)-cyclen complexes, ref. [146]. X-ray structures for: (c) Zn(II)<sub>2</sub> **147**, ref. [146]; (d) Zn(II)<sub>2</sub> **145**, ref. [146]; (e) Zn(II)<sub>2</sub> **149**, ref. [148].

than secondary amines. The stability constants of complexes with **L24** are similar to those of analogous complexes with **L25** ( $\log K_f = 14.1$  and  $13.0$  for Cu(II) and Zn(II) complexes, respectively), indicating that side-arm donor atoms, even in greater numbers, do not contribute significantly to the stability of the complex. [133] Interestingly, the substitution pattern of the cyclen appears to have a significant effect on the stability of the resulting complexes. Forgács *et al.* reported 1,4-disubstituted Cu(II) **L26** ( $\log K_f = 21.4$ ) and Zn(II) **L26** ( $\log K_f = 15.6$ ), whose stability constants are higher than those of their 1,7-disubstituted analogs and similar to mono-substituted Zn(II) **L22** ( $\log K_f = 15.4$ ). [134].

#### 2.2.10. Conclusions on mononuclear *d*-block complexes

**Differences in design strategies between *d*-block and *f*-block complexes.** Most mononuclear *f*-block cyclen complexes have only been studied *in solution* on simple phosphodiester models such as HPNP and BNPP. While research on *f*-block complexes focuses on selecting side arms to improve the stability and activity of the complexes against model compounds, research on *d*-block complexes is mainly conducted on plasmid DNA and focuses on introducing targeting vectors and improving DNA recognition. The differences in the design strategies of the two families of cyclen complexes stem from differences in the coordination chemistry of their metal centers. Unlike *f*-block metals, which have a higher coordination number and require ligands with higher denticity to form stable complexes, *d*-block cyclen complexes are typically five-coordinated by one water molecule (or pendant donor group) and four cyclen nitrogens, and thus have only one coordination site available for substrate binding. Consequently, *d*-block cyclen complexes are more susceptible to changes in catalytic activity result-

ing from the structure of the side arms. For example, attachment of a non-nucleophilic donor, such as the carbamoylmethyl arms in Zn(II) **L20** and Zn(II) **L21** (Fig. 16), leads to a complete loss of hydrolytic activity against activated phosphodiester. Competition of the amide group with the water molecule for the only free coordination site results in a reduction in the presence of the catalytically active form [Zn(II)L(OH)]. [122] On the other hand, attachment of the rigid pyridine ring in Zn(II) **L19** (Fig. 16), directly to the cyclen nitrogen, resulted in distortion of the cyclen ring, as manifests by the lack of binding of the metal ion to the substituted cyclen nitrogen (Fig. 17b) and a significant reduction in the stability constant. The coordination and catalytic properties of such complexes fall between Zn(II)-cyclen and Zn(II)-[12]aneN<sub>3</sub>. Finally, attachment of a nucleophilic donor, such as the 2-hydroxyethyl group in Zn(II) **102** (Fig. 11), yields active complexes with the metal-bound alkoxide that catalyze phosphate transesterification to form a stable and unreactive phosphorylated adduct (Fig. 12). For these reasons, current works on *d*-block cyclen complexes are mainly focused on the introduction of targeting vectors. The targeting vectors can be biomolecules (e.g. peptides, proteins, antibodies), modified biological compounds (e.g. sugars, nucleosides, nucleotides) and other synthetic constructs (e.g. small molecules, nanoparticles, liposomes) designed to bring the complex closer to its biological target.

**Strategies for improving the selectivity and activity of mononuclear *d*-block complexes against DNA.** To date, the dominant strategy for increasing the affinity of cyclen complexes for their primary biological target has been to equip them with DNA-binding molecules. An example of this approach is Co(III) **110.2** (Fig. 13) with an attached positively charged polyamine

chain, which exhibit 2-fold higher activity against plasmid DNA than the parent Co(III)-cyclen ( $k_{\text{obs}} = 5.37$  vs  $2.2 \times 10^{-4} \text{ s}^{-1}$ ). [101] The observed increase in activity against DNA is not due to an overall increase in the activity of the metal center, since the activity of Co(III) **110.2** against BNPP is even lower than that of the parent Co(III)-cyclen ( $k_{\text{obs}} = 1.16$  vs  $25.0 \times 10^{-3} \text{ s}^{-1}$ ), but because of the conjugate's increased affinity for the negatively charged DNA backbone. In a similar manner, increased activity was obtained for complexes labeled with a DNA-intercalating dye or grafted onto a groove-binding polypyrrole chain.[137–139] Such modifications of *d*-block complexes rarely translated into increased metal center activity, and in some cases activity against model phosphodiester was even impaired due to competitive interactions of the substrate molecule with the functional groups of the side arms; but such modifications provide increased affinity for DNA, resulting in enhanced nucleolytic activity. In this context, an interesting property of Zn(II)-cyclen complexes, e.g. Zn(II)-acrcyclen (Fig. 15b), is their increased affinity for natural DNA, e.g. CT-DNA, compared to analogous complexes of other transition metals, e.g. Cu(II)-acrcyclen ( $K_{\text{app}} = 4.0$  vs  $1.2 \times 10^{-4} \text{ M}^{-1}$ ), in particular the increased affinity for poly(dA)·poly(dT) sequences ( $K_{\text{app}} = 11.0$  vs  $0.03 \times 10^{-4} \text{ M}^{-1}$ ).[140].

**Two sides of the same coin, or base sequence recognition by Zn(II)-cyclen.** Specific recognition of uracil and thymine in DNA by Zn(II)-cyclen can have a dual effect – on the one hand, it can lead to increased selectivity and susceptibility of DNA to cutting, as in the case of increased nucleolytic activity of MNase against AT-rich sequences in the presence of Zn(II)-acrcyclen conjugate;[116] on the other hand, it may inhibit nucleolytic and transcriptional activity. Adhikari *et al.* showed that cyclen molecule bound to the arginine-rich region of the HIV-1 Tat protein, **133** (Fig. 14) cleaves TAR-RNA of HIV-1 already at neutral pH and room temperature, with the only cleavage site located between the unpaired U31 on the side of the adjacent G32 in the loop region. Interestingly, the activity of **133** was completely inhibited in the presence of ions such as Zn(II) and Eu(III). Following this lead, one may come across the work of Kimura *et al.* investigating the ability of bi- and trinuclear Zn(II)-cyclen complexes to recognize and bind to TAR-RNA. The results showed that their unique ability to recognize base sequences resulted in protection of the loop region from enzymatic cleavage.[141] Our recent studies have also shown that cyclen bound to oligonucleotide can selectively recognize thymine when present as a TT base mismatch on the complementary strand and stabilize the resulting duplex.[115] Although it is not entirely clear what features of cyclen complexes determine the presence of nucleolytic or nucleoprotective effect, three cases can be distinguished: (1) a Zn(II)-cyclen complex is required for nucleoprotective effect; complexes of other transition metals, as well as free cyclen, do not form strong ternary complexes with thymine and uracil; (2) the nucleoprotective effect of Zn(II)-cyclen occurs more frequently within unpaired nucleotides; (3) while most mononuclear Zn(II)-cyclen complexes exhibit hydrolytic activity against DNA, multinuclear complexes exhibit a clear dependence of activity on ligand shape. Multinuclear complexes with a linear structure are more likely to show nucleoprotective activity, while complexes with a curved shape are more likely to show hydrolytic activity (due to synergism between the two metal ions).

**Balance between stability, activity, and selectivity of mononuclear *d*-block complexes.** One of the critical aspects determining the clinical utility of complexes is their stability under *in vivo* conditions. One of the earliest observations on the stability of transition metal complexes was that for a given set of ligands, the stability of complexes is usually in the following order: Mn(II) < Fe(II) < Co(II) < Ni(II) < Cu(II) > Zn(II), which became known as the “Irving Williams series”. [142,143] The superior stability of Cu(II) complexes in this series is due to the fact that copper's d9 orbitals

have a pronounced Jahn-Teller effect that makes them tetragonal, making Cu(II) complexes more stable than complexes of other metals whose coordination structures are closer to pure octahedral geometry.[144] Under *in vivo* conditions, an important parameter is kinetic stability, which determines the susceptibility of the complex to dissociation and transchelation by numerous competing ligands present in body fluids. An excellent source of knowledge on the *in vivo* stability of lanthanide complexes (especially macrocyclic complexes) is the study of radiopharmaceuticals. A comprehensive review on the stability of radiopharmaceutical complexes has recently been reported.[145] The strategies used to design artificial enzymes resemble those known for radiopharmaceuticals, especially the bifunctional chelate method, in which the radiometal is tightly coordinated with a bifunctional chelator containing a tumor-targeting vector. Radiopharmaceuticals often consist of macrocyclic ligands such as NOTA (1,4,7-triazacyclononano-1,4,7-tetraacetic acid), DOTA (1,4,7,10-tetraazacyclododecano-1,4,7,10-tetraacetic acid) and their derivatives, which are ideal for smaller radioactive ions such as  $^{64}\text{Cu(II)}$ . Due to the 6-dentate N3O3 coordination environment of NOTA and 8-dentate N4O4 of DOTA, the resulting complexes show excellent *in vivo* kinetic stability ( $\log K_{\text{ML}} > 20$ ), but do not exhibit nucleolytic (or any catalytic) activity, which is desirable given their application. In terms of kinetic stability, complexes based on tetraazamacrocycles perform better than triazamacrocyclic ligands, and among them it is the cyclen that forms the most stable complexes with Zn(II) and many other transition metals.

In Table 3 we have compiled examples of the most active *d*-block cyclen complexes with similar ligand structures. Although studies of *d*-block complexes have not been conducted with as much regularity as studies of *f*-block complexes, it is clear that Co(III)-cyclen and Zn(II)-cyclen derivatives are usually one to two orders of magnitude less active than *f*-block complexes. However, some of them, such as Co(III) **110.2** (Fig. 13) bound to a positively charged polyamine, may even surpass *f*-block complexes in activity. Such activity may be entirely sufficient to achieve the desirable effect *in vivo*, which, combined with the high selectivity of *d*-block complexes, makes them promising candidates for further research.

### 3. Multinuclear catalysts

#### 3.1. Dinuclear complexes

##### 3.1.1. Examples of *f*-block and *d*-block dinuclear complexes

Xiang *et al.* used two linker system – a rigid aromatic and a flexible aliphatic – in a series of dinuclear complexes Zn(II)<sub>2</sub> **144–151** (Fig. 17a) to achieve a synergistic action of the two metal ions, resulting in an unprecedented increase in the rate of DNA hydrolysis.[146] All complexes were active against plasmid pUC18 and caused its selective conversion from type I to type II in just a few minutes of incubation under near-physiological conditions, while longer incubation led to cleavage of form II into smaller fragments. Cleavage activity was strongly dependent on linker rigidity – complexes with stiffer aromatic linkers were more active (RFI = 75–100%; C/BP = 0.77, pH 7.5, 37 °C, vit. C 0.125 mM for 30 min) than the Zn(II)<sub>2</sub> **150** complex (48%\*) with a flexible propylene linker; the presence of a hydroxyl group (PhOH) in the linker also positively affects the cleavage efficiency (82%\* for Zn(II)<sub>2</sub> **151** vs 48%\* for Zn(II)<sub>2</sub> **150**), although not as much as the presence of a methoxy group (PhOCH<sub>3</sub>) (100%\* for Zn(II)<sub>2</sub> **146** vs 75–90%\* for Zn(II)<sub>2</sub> **147–148**). The activity of these bimetallic complexes far exceeds that of 2 equiv. of corresponding mononuclear complexes, e.g. Zn(II)<sub>2</sub> **144** ≫ Zn(II) **91** (RFI = 31%\*; C/BP = 39.3, pH 7.1, rt, vit. C 41 mM). According to the authors, this is due to stronger two-point binding to the substrate than in the case of mononuclear

**Table 3**

Comparison of the cleavage activity of selected mononuclear *d*-block metal complexes. The selected examples represent the most active complexes among the series with similar ligand structures.

Catalyst	Substrate	$k_{\text{obs}}$ ( $10^{-4} \text{ s}^{-1}$ )	$k_2$ ( $\text{M}^{-1} \text{ s}^{-1}$ )	RFI (%)				C/S <sup>a</sup>	Conditions	Ref.
				3 h	6 h	16 h	24 h			
Co(III) <b>77</b>	BNPP		0.23						MOPS 100 mM (15% H <sub>2</sub> O/MeOH), pH 7.3, 50 °C	[91]
Co(III) <b>77</b>	pBluescript					43		30	MOPS 100 mM, pH 7.0, 50 °C	[91]
Cu(II) <b>83</b>	HPNP	0.61						1.0	HEPES 10 mM (30% DMSO/H <sub>2</sub> O), pH 8.0, 30 °C	[94]
Zn(II) <b>94</b>	BNPP	9.0						25	Tris-HCl 10 mM, pH 7.5, 30 °C	[96]
Zn(II) <b>94</b>	pUC18				24			39.3	HEPES 41 mM, pH 7.1, rt, <i>I</i> = 0.1 M (NaNO <sub>3</sub> ) <sup>b</sup>	[96]
Cu(II) <b>95</b>	pUC19						75	6.9	Tris-HCl 100 mM, pH 7.4, 37 °C	[97]
Cu(II) <b>99</b>	BNPP		$1.37 \times 10^{-5}$						Tris-HCl 50 mM, pH 7.4, 25 °C, <i>I</i> = 0.1 M (NaCl)	[98]
Zn(II) <b>103</b>	BNPP		$3.39 \times 10^{-4}$						HEPES 20 mM, pH 7.4, 35 °C, <i>I</i> = 0.1 M (NaNO <sub>3</sub> )	[99]
Zn(II) <b>104</b>	HPNP	2.9						40	HEPES 50 mM, pH 7.3, 50 °C, <i>I</i> = 0.1 M (NaNO <sub>3</sub> )	[100]
Co(III) <b>105.2</b>	BNPP	41.4							HEPPS 10 mM, pH 7.0, 50 °C	[98]
Co(III) <b>110.2</b>	pBR322	5.4						263	HEPPS 100 mM, pH 7.0, 37 °C	[98]
Co(II) <b>116</b>	pBR322				85			1.0	Tris-HCl 20 mM, pH 7.4, 37 °C, <i>I</i> = 0.1 M (NaCl)	[99]
Zn(II) <b>123</b>	pUC19				86			11.2	TEA 100 mM, pH 7.2, 37 °C	[101]
Zn(II) <b>124</b>	pUC19				79			0.48	Tris-HCl 100 mM, pH 8.0, 37 °C for 3 h	[102]
Cu(II) <b>126</b>	pUC19						87	12.7	PB 100 mM, pH 7.4, 37 °C	[103]
<b>130</b>	pBR322	6.0						10	Tris-HCl 10 mM, pH 7.2, 37 °C	[106]

Solvent mixtures are given in volume percentages. **a** – The molar ratio of catalyst to substrate. For a small-molecule substrate, S corresponds to the molar concentration; for DNA as a substrate, S corresponds to the molar concentration of base pairs. **b** – The reaction system contains a reductant (vit. C), so DNA cleavage can proceed by an alternative oxidative mechanism.

complexes and a synergistic mechanism of hydrolysis (Fig. 17b). In the proposed catalytic cycle, the binuclear complex first binds to DNA to form an intermediate, which allows both metal ions to activate the central phosphorus atom. Then a hydroxyl anion bound to one of the zincs acts as a nucleophilic agent and attacks the phosphorus atom, leading to a transition state. Cleavage of the phosphodiester bond with simultaneous catalyst regeneration completes the DNA hydrolysis process. From the crystal structures of Zn(II)<sub>2</sub> **147** (Fig. 17c) and Zn(II)<sub>2</sub> **145** (Fig. 17d), it appears that each zinc site has the geometry of a distorted square pyramidal with four *N*-atoms of the cyclen ligand and one *O*-atom of the  $\mu$ -OPh bridge. The Zn...Zn distances in both cases are about 4.0 Å and are within the 3.3–4.5 Å range found in most natural Zn(II)-dependent nucleases (Fig. 8). *Note: These complexes appear to be active only in the presence of a reducing agent (vit. C), so DNA cleavage may proceed by a mechanism other than hydrolytic. On the other hand, results from another paper by the same authors showed that*

*cleavage of plasmid pUC19 by Zn(II)-cyclen in the presence of vit. C yields a similar degree of cleavage as control DNA.*[147].

A ligand with a similar structure is present in the complex Cu(II)<sub>2</sub> **149** (Fig. 17a), which, like the complexes Zn(II)<sub>2</sub> **147–149**, has a  $\mu$ -OPh bridge; the Cu...Cu distance is 3.9 Å, and each Cu(II) ion adopts a square pyramid geometry with four *N*-atoms of the cyclen ring and a bridging *O*-atom (Fig. 17e).[148] ESI-MS spectra show that the  $\mu$ -OPh bridge is stable at pH 5–9. This complex binds to ds-DNA mainly through H-bonds and electrostatic interaction with  $K_b = 2.63 \times 10^5 \text{ M}^{-1}$  (at pH 6) and catalyzes the hydrolysis of pUC19 at 37 °C and pH range of 5.0–6.0. After 6 h of incubation at pH 5.0, the conversion of form I to form II was about 50%, while at pH 7.4 it was only about 4% (C/BP = 0.2, 37 °C) (Table 4).

Kimura *et al.* developed the dinuclear Zn(II)<sub>2</sub> **152** and its trinuclear analog Zn(II)<sub>3</sub> **153** (Fig. 17a) linked by *p*-xylene. Such ligand structure resulted in host-type molecules that selectively and strongly interact with the “guest” – poly(dT) and poly(U)

**Table 4**

Comparison of the cleavage activity of selected dinuclear *d*-block metal complexes. The selected examples represent the most active complexes among the series with similar ligand structures.

Complex	Linker	M...M (Å)	Substrate	C/BP	RFI (%)			Conditions	Ref.
					0.5 h	6 h	12 h		
Zn(II) <sub>2</sub> <b>145</b>		3.640	pUC18	0.77	100			PB 41 mM, pH 7.5, 37 °C <sup>a</sup>	[146]
Zn(II) <sub>2</sub> <b>146</b>		3.619	pUC18	0.77	100			PB 41 mM, pH 7.5, 37 °C <sup>a</sup>	[146]
Cu(II) <sub>2</sub> <b>149</b>		3.852	pUC19	0.20	<1	4		Tris-HCl 10 mM, pH 7.4, 37 °C, <i>I</i> = 0.1 M (NaCl)	[148]
Zn(II) <sub>2</sub> <b>156</b>			pUC19	88.9			22	Tris-HCl 100 mM, pH 7.8, 37 °C	[150]
Co(II) <sub>2</sub> <b>162</b>			pUC19	17.3		51	67	PB 100 mM, pH 7.0, 37 °C	[152]
Cu(II) <sub>2</sub> <b>168</b>			pBR322	0.74		65	80	CB 5.0 mM, pH 7.0, 37 °C	[153]
Zn(II) <sub>2</sub> <b>173</b>			pUC18	1.24			42	Tris-HCl 40 mM, pH 7.7, 37 °C	[155]

**a** – The reaction system contains a reductant (vit. C), so DNA cleavage can proceed by an alternative oxidative mechanism.

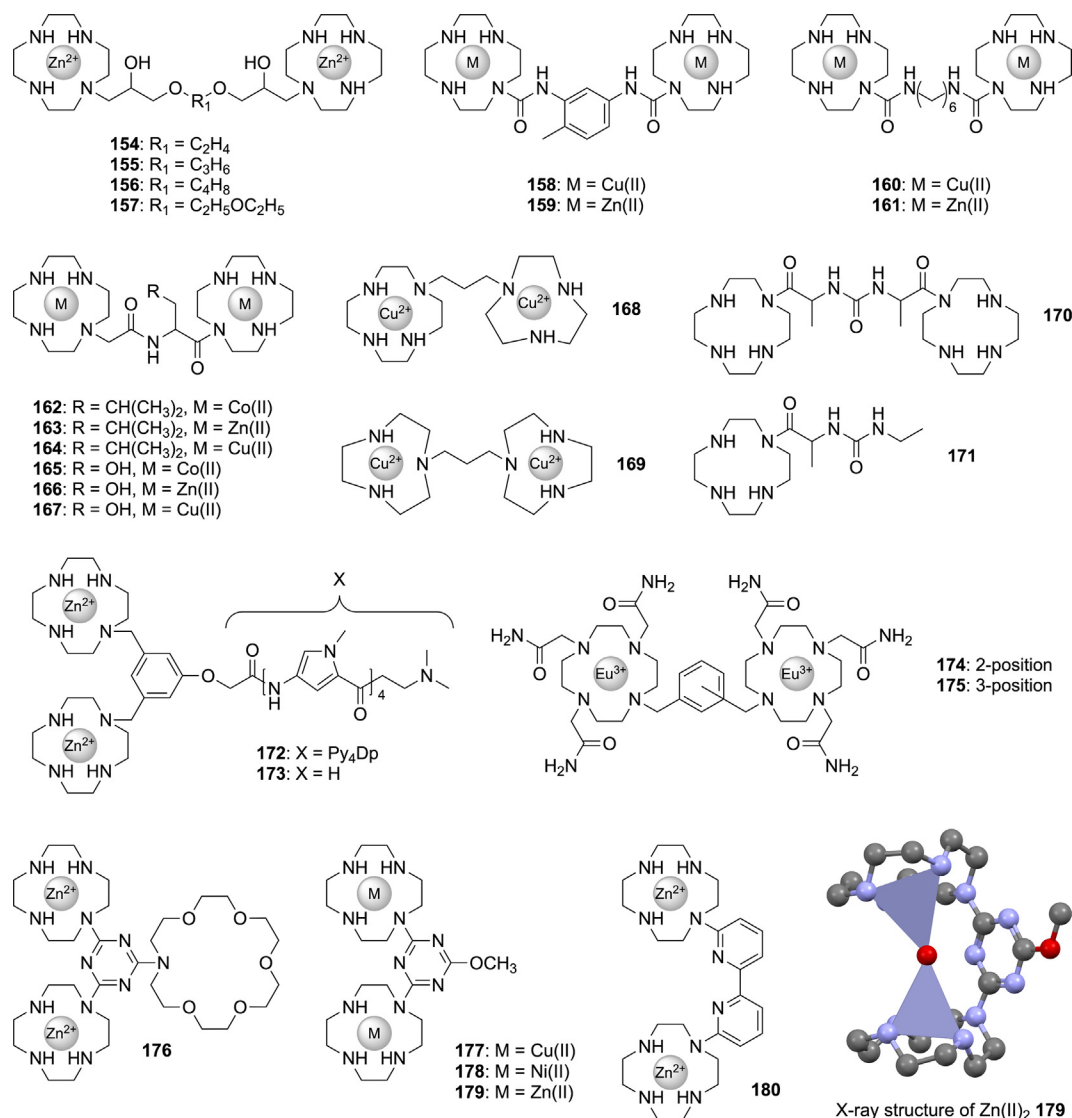


Fig. 18. Examples of dinuclear *f*-block complexes 154–180.

sequences, forming tertiary complexes with them.[149] Both multinuclear complexes,  $Zn(II)_2$  **152** ( $K_d = 6.3 \times 10^{-7}$  M for TpT) and  $Zn(II)_3$  **153** ( $K_d = 8.0 \times 10^{-10}$  M for TpTpT), show much stronger affinity for poly(T) than mononuclear  $Zn(II)$ -cyclen for single T ( $K_d = 7.9 \times 10^{-4}$  M), with the interaction constant increasing with the number of  $Zn(II)$ -cyclen units in the complexes. This unique feature, combined with the high selectivity towards thymine over other bases – e.g.  $Zn(II)_2$  **152** binds to GpT ( $K_d = 1.3 \times 10^{-5}$  M), CpT and ApT ( $K_d > 4.0 \times 10^{-4}$  M) 10–100 times weaker, makes this type of complexes an interesting tool for controlling gene expression. Both complexes were tested for DNA cleavage, but neither showed measurable activity.

Dinuclear complexes  $Zn(II)_2$  **154–157** (Fig. 18) connected by a long flexible spacer were found to be more active in hydrolyzing plasmid pUC19 than the parent  $Zn(II)$ -cyclen, although the cooperativity between two  $Zn(II)$  ions is rather weak indicating a lack of synergistic effect.[150] The highest activity for this series was observed at pH 7.8.  $Zn(II)_2$  **157** was most active with conversion of form I to II at 22% after 12 h of incubation at pH 7.8 (C/BP = 88.9, Tris-HCl 100 mM, pH 7.8, 37 °C for 12 h), while an analogous incubation with  $Zn(II)$ -cyclen yielded only 8% of form II.

König *et al.* described transition metal complexes **158–161** (Fig. 18) attached via urea functionality to rigid or flexible link-

ers.[151] Compared to metal-free ligands, the apparent binding constant ( $K_{app}$ ) of metal complexes with CT-DNA was several times higher:  $Cu(II)$  **158** ( $>1000$  M $^{-1}$ )  $>$   $Cu(II)$  **160** (650 M $^{-1}$ )  $>$   $Zn(II)$  **161**  $\sim$   $Zn(II)$  **159** (350 M $^{-1}$ )  $\gg$   $Cu(II)$ -cyclen (68 M $^{-1}$ )  $>$   $Zn(II)$ -cyclen (3.4 M $^{-1}$ ). In tests with the reactive small-molecule BNPP, none of the complexes hydrolyzed the substrate under physiological-like conditions, hence the authors' conclusion that the complexes would also be inactive against ds-DNA.

Complexes **162–167** (Fig. 18) containing chiral pseudodipeptide spacers catalyze the hydrolysis of supercoiled pUC19 to form II plasmid.[152] Among the series with GlyLeu spacers, the most active catalyst is  $Co(II)_2$  **163**, which converts 51% of form I plasmid to form II after 48 h of incubation in neutral aqueous conditions (C/BP = 17.3, pH 7.0, 37 °C). Among the series with GlySer spacers, the most active catalyst is the  $Cu(II)_2$  **168** analog, which cleaves 61% of the plasmid.

The combination of  $Cu(II)$ -cyclen with  $Cu(II)$ -[9]aneN $_3$ , known for its excellent nucleolytic properties, via a short alkyl spacer yielded an asymmetric dinuclear complex  $Cu(II)_2$  **168** (Fig. 18) capable of cleaving the pBR322 plasmid by hydrolytic or oxidative pathway, depending on the availability of an oxidant (e.g.  $H_2O_2$ ). [153] In the absence of oxidant, the hydrolytic activity of asymmetric  $Cu(II)_2$  **168** (RFI = 65%; C/BP = 0.74, pH 7.0, 37 °C, 6 h) is much lower than that of  $Cu(II)_2$  **169** (RFI = 100%) consisting of two  $Cu$

(II)-[9]aneN<sub>3</sub> units (Fig. 18). Direct comparison of the activity of the two complexes is difficult, because while Cu(II)<sub>2</sub> **168** mainly causes single-strand cuts (SSC), Cu(II)<sub>2</sub> **169** yields many double-strand cuts (DSC). Moreover, Cu(II)<sub>2</sub> **168** is a much slower catalyst than its zinc analog Zn(II)<sub>2</sub> **150** (RFI = 48%\*, pH 7.5, 30 min).

As with the mononuclear complexes discussed earlier, artificial nucleases can also be made from metal-free ligands containing multiple cyclen molecules. As might be expected, such derivatives are much less active than their analogous complexes; the bis-cyclen derivative **170** (Fig. 18; RFI ~ 100%; C/BP = 31.6, pH 7.4, 37 °C, 36 h) cleaves plasmid pUC19 much more efficiently than the mono-cyclen derivative **171** (RFI = 25%\*).[154] Both **170** ( $\Delta T_m = 1.9$ ) and **171** ( $\Delta T_m = 4.0$ ) stabilized DNA in melting temperature assays, while viscometric assays showed no significant deviation from control CT-DNA, suggesting that these compounds interact with ds-DNA most likely via electrostatic groove-binding rather than classical intercalation.

Zhao *et al.* compared the nucleolytic activity of Zn(II)<sub>2</sub> **172** (Fig. 18) containing oligopyrrole chain with its non-functionalized analog Zn(II)<sub>2</sub> **173** and showed that they differ significantly in the cleavage mechanism.[155] Both complexes act via the hydrolytic pathway, but while Zn(II)<sub>2</sub> **172** causes non-selective SSC and random DSC, yielding a mixture of form II and form III DNA, the Zn(II)<sub>2</sub> **173** oligopyrrole conjugate causes non-random DSC, as evidenced by the presence of linear fragments of 1500–2000 bp in length, which appear even after increasing the concentration of the complex. After 12 h of incubation under near-physiological conditions (C/BP = 1.24, pH 7.7, 37 °C) Zn(II)<sub>2</sub> **172** yields 32% of form II and 25% of form III, while Zn(II)<sub>2</sub> **173** yields 35% of form II and 7% of form III.

Morrow's group has made interesting observations about the cooperativity of dinuclear Eu(III)<sub>2</sub> **174–175** (Fig. 18), where each subunit contains three carbamoylmethyl side arms, and the complexes differ in the position of the xylyl linker substitution.[24] Each Eu(III) center coordinates one water molecule, each of which is later replaced by one substrate molecule. Although this behavior may indicate cooperation, in fact the two metal ions behave as two separate centers. This is evidenced by the small differences (about 11–13%) in transition state binding energies between the dinuclear complexes and the analogous mononuclear Eu(III) **30** (Fig. 2). The second-order rate constant for HPNP cleavage at pH 7.6 by Eu(III)<sub>2</sub> **174** ( $k_2 = 5.5 \text{ M}^{-1} \text{ s}^{-1}$ ) is only slightly higher than that for Eu(III)<sub>2</sub> **175** ( $k_2 = 3.5 \text{ M}^{-1} \text{ s}^{-1}$ ), but almost 9-fold higher than that for 2 equiv. of Eu(III) **30**. Note: The results of this work suggest that even a severalfold increase in the activity of binuclear complexes relative to a multiple of the activity of the parent mononuclear complexes does not always indicate the cooperativity of the metal centers. Differences in transition state binding energies are a much better indicator of the cooperativity. This is worth bearing in mind when reading the conclusions of the chapter on multinuclear complexes.

Subat *et al.* obtained binuclear analogs of the previously described complexes Zn(II) **99–101** (Fig. 11), dinuclear complexes **176–180** complexes (Fig. 18) outperformed their mononuclear analogs, and their activity was closely related to the length of the linker. [98] Zn(II)<sub>2</sub> **176** ( $k_2 = 1.28 \times 10^{-3} \text{ M}^{-1} \text{ s}^{-1}$ ) and Zn(II)<sub>2</sub> **179** ( $k_2 = 2.45 \times 10^{-3} \text{ M}^{-1} \text{ s}^{-1}$ ), having shorter spacers, were able to hydrolyze BNPP by 1 to 2 orders of magnitude faster than Zn(II)<sub>2</sub> **180** ( $k_2 = 0.24 \times 10^{-3} \text{ M}^{-1} \text{ s}^{-1}$ ) under mild conditions (pH 8.0, 25 °C). The X-ray structure of Zn(II)<sub>2</sub> **179** (Fig. 18) shows that the zinc ion is coordinated by only three of the four N-atoms of the cyclen, so the metal site structure is between Zn(II)-cyclen ( $k_2 = 2.1 \times 10^{-5} \text{ M}^{-1} \text{ s}^{-1}$ ) and Zn(II)-[12]aneN<sub>3</sub> ( $k_2 = 8.5 \times 10^{-5} \text{ M}^{-1} \text{ s}^{-1}$ ), which, together with the synergistic action of the two metal ion, may explain the increased hydrolysis rate of BNPP.[156] The complexes Zn(II)<sub>2</sub> **176** and Zn(II)<sub>2</sub> **179** exist in equilibrium in aqueous media in two forms – as the species [Zn(II)<sub>2</sub>L(μ-OH<sub>2</sub>)] (Fig. 18)

and in the “open” form [Zn<sub>2</sub>L(H<sub>2</sub>O)<sub>2</sub>] with two Zn(II)-bound water molecules. Due to the close proximity of the two metal sites, the  $pK_a = 5.96$  of the bridging water molecule in Zn(II)<sub>2</sub> **179** is lower than reported for most similar compounds, indicating increased acidity and stability of the μ-OH group. In the case of Zn(II)<sub>2</sub> **180**, the pH curve corresponds to two water molecules, each binding to one zinc ion, and two subsequent deprotonations ( $pK_{a1} = 7.45$ ,  $pK_{a2} = 8.85$ ) leading to the formation of the dihydroxyl species [Zn<sub>2</sub>L(OH<sup>-</sup>)<sub>2</sub>]. Under near-physiological conditions, Ni(II)<sub>2</sub> **178** showed no significant effect on the hydrolysis of BNPP ( $k_{obs}$  ranged from  $10^{-8}$  to  $10^{-7} \text{ s}^{-1}$ , depending on the pH of the solution), for Cu(II)<sub>2</sub> **177**, the values of  $k_{obs}$  were in the range of  $10^{-5} \text{ s}^{-1}$ .

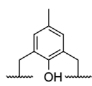
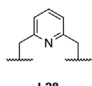
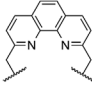
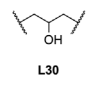
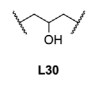
### 3.1.2. Effect of linker structure on dinuclear zinc complexes

**2,6-Dimethyl-4-nitrophenol (L27)** is a commonly used short aromatic linker characterized by having a phenoxy group “sandwiched” between two macrocycles. The aromatic spacer provides a rigid scaffold for dinuclear complexes, while the bridging phenoxy group abolishes electrostatic repulsion between the metal ions and keeps them in close proximity. A dinuclear zinc complex consisting of such a linker and two Zn(II)-[9]aneN<sub>3</sub> units was obtained and thoroughly characterized by Montagner *et al.*[157] At a 20-fold lower catalyst-to-substrate ratio, (Zn(II)-[9]aneN<sub>3</sub>)<sub>2</sub>L27 (Fig. 17) shows similar cleavage activity to its tetraamine analog (Zn(II)-cyclen)<sub>2</sub>L27, so despite the lack of uniform experimental conditions, it is clear that the former complex is much more active. Such an observation is consistent with the well-established view that macrocyclic triamine complexes are much more active in phosphate hydrolysis than their tetraamine analogs. This regularity is observed for both mononuclear and binuclear complexes. Interestingly, the distance of Zn...μ-OH is identical for both complexes, in contrast to the significant differences observed in the distances of metal-bound water (Zn...OH<sub>2</sub>) in the corresponding mononuclear complexes (Fig. 8).

In binuclear complexes connected by a short **2,6-dimethylpyridine** spacer (L28), the two metal centers are in relative proximity, which can cause significant electrostatic repulsion between them. Unlike L27 discussed above, L28 does not have a μ-OPh bridge connecting and stabilizing the two Zn<sup>2+</sup> of like sign, but pH-metric studies indicate that in the case of (Zn(II)-[9]aneN<sub>3</sub>)<sub>2</sub>L28 and (Zn(II)-cyclen)<sub>2</sub>L28 (Fig. 19) this drawback is compensated by a water molecule between the two metal centers. In fact, the formation of [M<sub>2</sub>L]<sup>4+</sup> type complexes is not observed, and binuclear complexes occur over a wide pH range only in the hydroxyl form [M<sub>2</sub>L(μ-OH)]<sup>3+</sup>. Bazzicalupi *et al.* showed that the pyridine nitrogen in (Zn(II)-[9]aneN<sub>3</sub>)<sub>2</sub>L28 is not involved in the complexation of Zn(II) ions.[158] In addition, Sheng *et al.* showed that the limiting activity of this complex is reached at 2 equiv. of zinc ions per ligand, and is only 2 times higher compared to 2 equiv. of Zn(II)-[9]aneN<sub>3</sub> ( $k_{obs} = 0.11 \times 10^{-4} \text{ M}^{-1} \text{ s}^{-1}$ ), indicating a low possibility of a cooperative mode of catalysis.[159] What significantly distinguishes the two complexes is their pH-rate profiles. Typically, macrocyclic triamine complexes exhibit optimal activity at much lower pH than the corresponding tetraamine complexes; the optimal pH for (Zn(II)-[9]aneN<sub>3</sub>)<sub>2</sub>L28 is 6.0–6.8, while at pH 7.5 the activity drops to 33%; for (Zn(II)-cyclen)<sub>2</sub>L28 one would expect an optimal pH > 7.0. As we discussed earlier, a finely tuned pH-rate optimum may be clinically relevant, as the environment of tumor tissues is known to differ significantly from that of healthy tissues. Complexes operating with maximum activity at pH < 7.4 may exhibit greater selectivity against tumor tissues and thus cause fewer side effects *in vivo*.

**2,9-dimethyl-1,10-phenanthroline (L29)** is characterized by its considerable size and the presence of two pyridine nitrogens in the vicinity of two macrocyclic units, which could in principle participate in the binding of metal ions. Arca *et al.* showed that



Linker	Ligand	Distances (Å)	pK <sub>a</sub>	log K <sub>f</sub>	Substrate	Activity	Acceleration	Conditions
 L27	[9]aneN <sub>3</sub>	Zn...Zn 3.219 <sup>a</sup> Zn...O 1.999 <sup>a</sup>	5.4 <sup>a,b</sup> 7.8 <sup>a,c</sup>		pUC19 <sup>a,d</sup>	RFI ~ 100%		C/BP = 0.031, pH 8.2, 37 °C, 3 h
	HPNP <sup>a,e</sup>				HPNP <sup>a,e</sup>	k <sub>cat</sub> = 2.60 × 10 <sup>-4</sup> s <sup>-1</sup>		C/S = 0.1, pH 8.5, 40 °C
 L28	[9]aneN <sub>3</sub>		5.2 <sup>i,j</sup>	26.2 <sup>i,k</sup>	pUC19 <sup>l</sup>	RFI = 27% k <sub>obs</sub> = 0.37 × 10 <sup>-4</sup> s <sup>-1</sup>	2.15	C/BP = 2.0, pH 6.8, 37 °C, 3 h
	Cyclen				pUC18 <sup>f,g</sup>	RFI = 86%*		C/BP = 0.77, pH 7.5, 37 °C, 0.5 h <sup>h</sup>
 L29	[9]aneN <sub>3</sub>			29.7 <sup>m</sup>	BNPP <sup>m</sup>	k <sub>2</sub> = 0.69 × 10 <sup>-4</sup> M <sup>-1</sup> s <sup>-1</sup>	1.00	pH 7.6, 35 °C
	HPNP <sup>n</sup>				HPNP <sup>n</sup>	k <sub>2</sub> = 0.89 × 10 <sup>-2</sup> M <sup>-1</sup> s <sup>-1</sup>	2.12	pH 7.6, 25 °C, I = 0.1 M (NaNO <sub>3</sub> )
 L30	[9]aneN <sub>3</sub>	Zn...Zn 3.640 <sup>f</sup> Zn...O 1.902 <sup>f</sup>			pUC18 <sup>f,g</sup>	RFI ~ 100%*		C/BP = 0.77, pH 7.5, 37 °C, 0.5 h <sup>h</sup>
	Cyclen							
 L30	[9]aneN <sub>3</sub>	Zn...Zn 3.687 <sup>o</sup> Zn...O 1.995 <sup>o</sup>	8.0 <sup>o</sup>		HPNP <sup>n</sup>	k <sub>2</sub> = 25.0 × 10 <sup>-2</sup> M <sup>-1</sup> s <sup>-1</sup>	59.5	pH 7.6, 25 °C, I = 0.1 M (NaNO <sub>3</sub> )
	Cyclen				pUC18 <sup>f,g</sup>	RFI = 82%*		C/BP = 0.77, pH 7.5, 37 °C, 0.5 h <sup>h</sup>

**Fig. 19.** Comparison of selected properties of dinuclear Zn(II) complexes depending on ligand structure. Relative acceleration is calculated as the ratio of the activity of the dinuclear complex to that of 2 equiv. of Zn(II)-[9]aneN<sub>3</sub>. **a** – ref. [157]; **b** – potentiometric pK<sub>a</sub> for [Zn<sub>2</sub>L(OH)]<sup>3+</sup>; **c** – kinetic pK<sub>a</sub> from HPNP cleavage; **d** – conditions: Tris-HCl 50 mM, NaCl 18 mM; **e** – conditions: HEPES 50 mM, I = 0.1 M (KNO<sub>3</sub>); **f** – ref. [146]; **g** – conditions: PB 0.041 mM **h** – reaction in the presence of vit. C 0.125 mM; **i** – ref. [158]; **j** – calculated from species distribution diagram; **k** – K<sub>f</sub> for 2Zn<sup>2+</sup> + L + OH<sup>-</sup> = [Zn<sub>2</sub>L(OH)]<sup>3+</sup>; **l** – conditions: Tris-HCl 50 mM, NaCl 10 mM, ref. [159]; **m** – activity calculated from pH-rate diagram at pH = 7.6, conditions: 50 mM of appropriate buffer, I = 0.1 M (NMe<sub>4</sub>NO<sub>3</sub>), ref. [160]; **n** – conditions: 20 mM of appropriate buffer, I = 0.1 M (NaNO<sub>3</sub>), ref. [165]; **o** – ref. [166].

the formation of the binuclear (Zn(II)-[9]aneN<sub>3</sub>)<sub>2</sub>**L29** does not red-shift the dipyrindine band at 283 nm, indicating that the metals are coordinated only by the macrocyclic units.[160] The X-ray structure of (Zn(II)-cyclen)<sub>2</sub>**L29** (Fig. 17d) shows that, as with the **L28**-based complexes, there is a water molecule between the two metal ions that screens electrostatic repulsion and helps keep them in close proximity. Morrow's team showed that the catalytic activity of the binuclear (Zn(II)-[9]aneN<sub>3</sub>)<sub>2</sub>**L29** in HPNP hydrolysis (k<sub>2</sub> = 89.0 × 10<sup>-4</sup> M<sup>-1</sup> s<sup>-1</sup>) is only slightly higher than that of Zn(II)-[9]aneN<sub>3</sub> (k<sub>2</sub> = 21.0 × 10<sup>-4</sup> M<sup>-1</sup> s<sup>-1</sup>).[165] These results provide strong evidence that the two subunits act almost independently. Note: Despite the results of Xiang *et al.*[146] indicating significant activity of (Zn(II)-cyclen)<sub>2</sub>**L29** compared to Zn(II)-cyclen, determination of cooperativity for the former is troublesome because it was tested in the presence of the reductant (vit. C).

**2-Hydroxypropyl (L30)** is among the most efficient linkers and is a common structural motif among many dinuclear complexes exhibiting cooperative activity. The presence of a bridging alkoxy group in the middle of the linker helps connect the two metal centers and appears to be essential for cooperative catalytic activity. It has been found that ligands containing two macrocyclic units linked by a simple propyl chain (without hydroxyl functionality) tend to form "sandwich-type" structures with metal ions, where two macrocycles bind one metal ion between them.[161–163] In the case of (Zn(II)-[9]aneN<sub>3</sub>)<sub>2</sub>**L30** (Fig. 17), Morrow's group confirmed that two zinc ions bind to the 2-hydroxy group, cause its deprotonation and the formation of a dinuclear Zn(II)-alkoxy complex.[164,165] The observation that the k<sub>2</sub> value for HPNP cleavage catalyzed by (Zn(II)-[9]aneN<sub>3</sub>)<sub>2</sub>**L30** is 43-fold higher than that for catalysis by (Zn(II)-[9]aneN<sub>3</sub>)<sub>2</sub>**L29** provides strong evidence that the former complex acts cooperatively. In a series of tetraamine ligands, (Zn(II)-cyclen)<sub>2</sub>**L30** (RFI = 82%\*) also showed significantly higher nucleolytic activity than the analogous Zn(II)<sub>2</sub>**L50** (RFI = 48%\*) with a propyl linker, suggesting cooperative effect of the former complex.

### 3.2. Multinuclear and supramolecular complexes

#### 3.2.1. Examples

Zhao *et al.* obtained Zn(II)<sub>6</sub>**181** (Fig. 20) by placing six Zn(II)-cyclen units in close proximity to each other on a star-shaped

cyclotriphosphazene scaffold.[166] This multinuclear complex selectively converts 42% of pUC19 form I to form II after 48 h of incubation under near-physiological conditions (C/BP = 0.01, pH 7.5, 37 °C).

Trinuclear Cu(II)-cyclen complexes **182–184** (Fig. 20) with different metal ions to ligand ratios have been described by Bencini *et al.*[167] Their hydrolytic activity against BNPP decreases with decreasing Cu(II) to ligand ratio: Cu(II)<sub>3</sub>**184** (k<sub>obs</sub> = 0.035 × 10<sup>-4</sup> s<sup>-1</sup>) > Cu(II)<sub>2</sub>**183** (k<sub>obs</sub> = 0.023 × 10<sup>-4</sup> s<sup>-1</sup>) > Cu(II)**182** (k<sub>obs</sub> = 0.018 × 10<sup>-4</sup> s<sup>-1</sup>). The most active complex in the series, Cu(II)<sub>3</sub>**184**, was not particularly efficient and cleaved only 1% of pBR322 after 2 h of incubation (C/BP = 52.6, pH 7.0, 37 °C). The stability of complexes decreases with increasing nuclearity: Cu(II)**182** (log K<sub>f</sub> = 21.9) > Cu(II)<sub>2</sub>**183** (log K<sub>f</sub> = 16.3) > Cu(II)<sub>3</sub>**184** (log K<sub>f</sub> = 11.5), and is lower than that of the parent Cu(II)-cyclen (log K<sub>f</sub> = 23.4).[168] The reason for this is probably the increasing electrostatic repulsion between an increasing number of metal ions. As shown by spectrophotometric studies, individual cyclen moieties bind metal ions independently, while the central nitrogen atom derived from the TREN unit is not involved in the interaction with any metal centers.

Inspired by Kimura's work on trinuclear Zn(II)<sub>3</sub>**153** (Fig. 17a), Laine *et al.* investigated whether increasing the number of Zn(II)-cyclen units in multinuclear Zn(II)<sub>3</sub>**185** (Fig. 20) would lead to increased selectivity and nucleolytic activity compared to a previously characterized trinuclear complex based on Zn(II)-cyclen units.[149,169,170] The trinuclear Zn(II)<sub>3</sub>**185** consist of two Zn(II)-cyclen units for improved U-base recognition and a Zn(II)-[9]aneN<sub>3</sub> unit to maintain nucleolytic activity at the level of demand. Experiments on UpU, ApU, and UpA dinucleotides showed that incorporation of Zn(II)-cyclen units contributes to increased recognition of consecutive UpU sites. At a C/S ratio of 20, Zn(II)<sub>3</sub>**185** was able to cleave ApU (k<sub>obs</sub> = 19.8 × 10<sup>-4</sup> s<sup>-1</sup>) and UpA (k<sub>obs</sub> = 17.7 × 10<sup>-4</sup> s<sup>-1</sup>) 3 times faster than UpU dinucleotide (k<sub>obs</sub> = 5.7 × 10<sup>-4</sup> s<sup>-1</sup>) under neutral conditions and elevated temperature (pH 6.84, 90 °C).

Li *et al.* showed that metal-free catalysts **186–189** (Fig. 20), consisting of cyclen and polyamine substituents grafted onto polyaspartic acid (PASP), exhibit high DNA-binding affinity and cleavage activity against plasmid pUC18.[171] PASP-cyclen **188**,

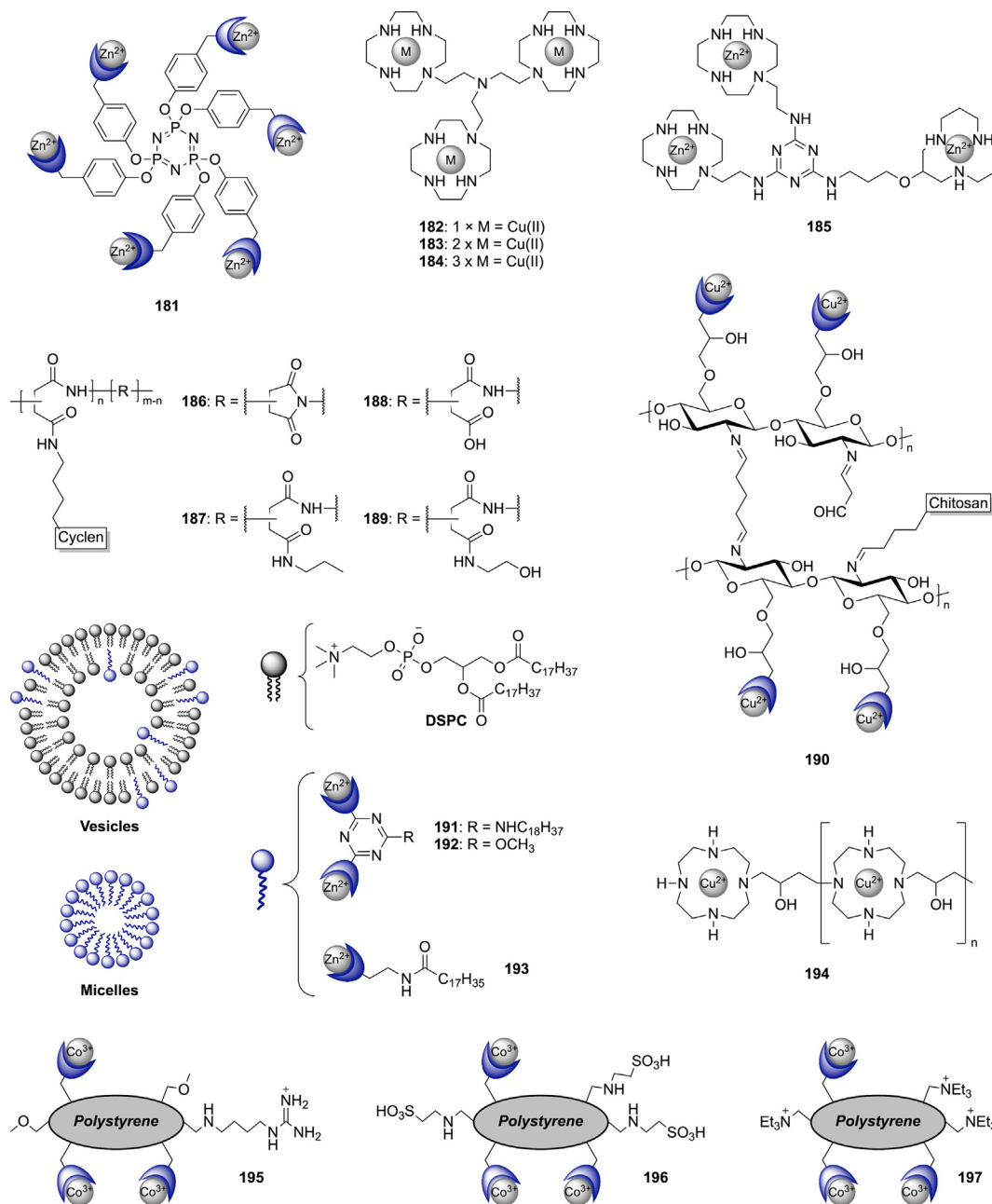


Fig. 20. Examples of multinuclear complexes **181**–**197**. Blue crescent represents cyclen molecule.

which contains both ungrafted carboxylic acid groups and cyclen moieties, shows the highest cleavage activity ( $k_{obs} = 1.63 \times 10^{-4} s^{-1}$ ) and DNA-binding affinity ( $K_{app} = 2.35 \times 10^7$ ) under near-physiological conditions ( $[C] = 38.2 \mu g ml^{-1}$ ,  $[BP] = 0.08 mM$ ,  $pH 7.4$ ,  $37^\circ C$ ). Under these conditions, at a catalyst concentration of  $9.6 \mu g ml^{-1}$ , plasmid cleavage leads to the appearance of the linear form III even before form II, while at a concentration of  $38.7 \mu g ml^{-1}$ , form III (71.2%) dominates over form II (18.2%) after just 3 h of incubation. The cleavage mechanism was identified as non-random hydrolysis, and the binding to DNA was identified as a hybrid of electrostatic interactions and hydrogen bonds, but not as classical minor groove-binding. Combinations of individual components, such as PASP+cyclen molecules, cyclen+ $Zn(II)$  ions, and PASP+ $Zn(II)$  ions, resulted in significant relaxation of pUC18 with dominance of form II (31.9–64.9%) and poor linearization of the plasmid (8.9–9.9%), while a combining of all three components

together, PASP+cyclen+ $Zn(II)$  ions, led to gel retardation. In addition, derivatives **186** and **187** with functionalized carboxyl groups showed lower cleavage activity (RFI = 12.6–15.0%), only derivative **189** containing terminal hydroxyl groups showed better activity (RFI = 31.0%), with neither derivative causing noticeable plasmid linearization.

Wang *et al.* reported a heterogeneous catalyst **190** (Fig. 20) consisting of catalytically active  $Cu(II)$ -cyclen complexes grafted onto a chitosan-based polymer, which not only provides a scaffold for the complexes, but also provides a preferred hydrophobic environment to facilitate DNA cleavage.[172] In this artificial enzyme, the ratio of cyclen to sugar is 1:3 and the ratio of  $Cu(II)$  ions to sugar is 1:2, the average hydrodynamic diameter of > 90% of the microspheres is  $353 \mu m$ . The enzyme cleaves pUC18 with  $k_{obs} = 2.78 \times 10^{-4} s^{-1}$  under near-physiological conditions ( $[C] = 0.12 mM$ ,  $[BP] = 8.1 \times 10^{-3} mM$ ,  $pH 7.2$ ,  $37^\circ C$ ). None of the components used

individually in the control experiment showed noticeable hydrolytic activity, suggesting that the activity of Cu(II) **190** is due to the cooperative action of the individual parts. Another important advantage of this design is that the heterogeneous catalyst can be easily separated from the reaction medium and reused. The discussed catalyst retained 75% of its initial activity after 4 reaction cycles.

Gruber *et al.* reported micellar and vesicular Zn(II)-cyclen catalysts formed by self-assembly of amphiphilic **191–193** and DSPC derivatives (Fig. 20).[173] Under neutral aqueous conditions ([BNPP] = 2.3 mM, [Zn] =  $4.5 \times 10^{-5}$  M; pH 7.4, 25 °C), micellar and vesicular catalysts showed an increase in second-order rate constants for BNPP hydrolysis by 4–7 orders of magnitude compared to single-molecule complexes; activities decreases in the following order: Zn(II)<sub>2</sub> **191**-vesicle ( $k_2 = 9.4 \text{ M}^{-1} \text{ s}^{-1}$ ) > Zn(II)<sub>2</sub> **191**-micelle ( $k_2 = 7.9 \text{ M}^{-1} \text{ s}^{-1}$ ) > Zn(II) **193**-vesicle ( $k_2 = 7.4 \text{ M}^{-1} \text{ s}^{-1}$ ) > Zn(II) **182**-micelle ( $k_2 = 1.8 \text{ M}^{-1} \text{ s}^{-1}$ )  $\gg$  Zn(II)<sub>2</sub> **192** and Zn(II)-cyclen (below detection limit). Both **192** and **193** micelle catalysts were  $\sim 10$  nm in diameter; the most active vesicular catalyst was Zn(II)<sub>2</sub> **191** with an average diameter of  $\sim 100$  nm and 10 mol% catalyst to DSPC. The authors explain such a significant increase in hydrolytic activity of vesicular catalysts by the high local concentration of coordinated Zn(II) ions in the tightly packed domains of complexes embedded in bilayer membranes and the reduced polarity on the vesicle surface, which facilitates nucleophilic attack on the phosphate compared to bulk water. The self-assembling catalytic systems presented here are among the most efficient catalysts for BNPP hydrolysis, but not only that, Zn(II)<sub>2</sub> **191**-vesicles are also very efficient in cleaving plasmid DNA to a mixture of form II and smaller DNA fragments of about 2.0 kb. As shown in an experiment with a commercially available 24mer oligonucleotide, even cleavage of inactivated single-stranded oligonucleotides could be significantly promoted by this catalytic system (35-fold increase in  $k_{\text{obs}}$  relative to control; pH 8.0, 40 °C).

By combining multiple Cu(II)-cyclen moieties with epichlorohydrin, a linear polymer Cu(II) **194** (Fig. 20) was obtained that catalyzes the selective cleavage of supercoiled pUC19 to form II. [174] The result of agarose gel electrophoresis showed that the highest activity was observed at pH 7.4, at which a 42% linearization of the plasmid occurred after 72 h of incubation ([C] = 1.0 mg ml<sup>-1</sup>, [BP] = 11.3 μM; 37 °C). When the pH was lowered from 7.4 to 6.6, polymer Cu(II) **194** showed almost the same catalytic effect in DNA cleavage, while no DNA cleavage was observed at pH below 6.2.

Suh's group presented a series of catalyst **195–197** (Fig. 20) based on Co(III)-cyclen complexes attached to polystyrene beads,

which accelerate the hydrolysis of supercoiled pUC18 >200-fold and its linear form >150-fold relative to the background reaction. [175,176] The resulting catalysts differ in the functional groups on the polymer surface, each providing a different microenvironment for the reaction – while methoxy groups and taurine provide a neutral and zwitterionic environment, guanidinium and TEA groups provide a cationic environment. The most active of the series is TEA-containing catalyst **197**, whose bell-shaped pH-rate curve shows maximum activity at pH 5.3 ( $k_{\text{obs}} = 3.53 \times 10^{-4} \text{ s}^{-1}$ ; [C] = 0.48 mM, 25 °C); Co(III) **195** ( $k_{\text{obs}} = 3.05 \times 10^{-4} \text{ s}^{-1}$ ; [C] = 0.81 mM) and Co(III) **196** ( $k_{\text{obs}} = 1.20 \times 10^{-4} \text{ s}^{-1}$ ; [C] = 1.0 mM) show maximum activity at pH 5.5. The DNA cleavage mechanism was shown to be hydrolytic. Co(III) **197** degraded ds-DNA into smaller fragments, mostly about 17-mer, in just a few hours at 25 °C.

### 3.2.2. Conclusions

**Why are multinuclear complexes more active than mononuclear ones?** Since the active centers in natural nucleases are coordinated structures of dinuclear or trinuclear metal complexes, it should come as no surprise that chemical catalysts based on similar multinuclear structures are also leading the way among artificial nucleases. Not only are dinuclear complexes relatively easy to prepare, but due to the cooperation between adjacent metal ions, they are tens to hundreds of times more active than their mononuclear counterparts. Therefore, in the field of artificial nucleases, special attention is paid to dinuclear metal complexes that mimic the enzymatic hydrolysis of nucleic acids. From the studies of mononuclear complexes discussed earlier, we know that at least two aspects are critical to the rate of reactions catalyzed by small-molecule complexes: (1) activation of the phosphate group of the substrate and (2) activation of the nucleophile; in the case of larger and pre-organized structures, such as enzymes or supramolecular catalysts, an additional (3) aspect that becomes important is activation of the leaving group. Multinuclear complexes have the following advantages over mononuclear complexes in these three aspects:

(1) In principle, dinuclear complexes should be able to provide double Lewis acid activation for phosphate hydrolysis by bridging two metal ions with two phosphoryl oxygens (Fig. 17b). Sargeson's group showed that the rate of intramolecular aminolysis of the bridged monophosphate [(Co(III)(NH<sub>3</sub>)<sub>5</sub>)<sub>2</sub>NP] ( $k_2 = 3.4 \times 10^{-2} \text{ M}^{-1} \text{ s}^{-1}$ ; Fig. 21a) is 50 times higher (per mole of catalyst) than the aminolysis of the mononuclear analog [(Co(III)(NH<sub>3</sub>)<sub>5</sub>)ENP] ( $k_2 = 3.6 \times 10^{-4} \text{ M}^{-1} \text{ s}^{-1}$ ).[177] The difference in the reactivity of the two systems was attributed primarily to the increased elec-

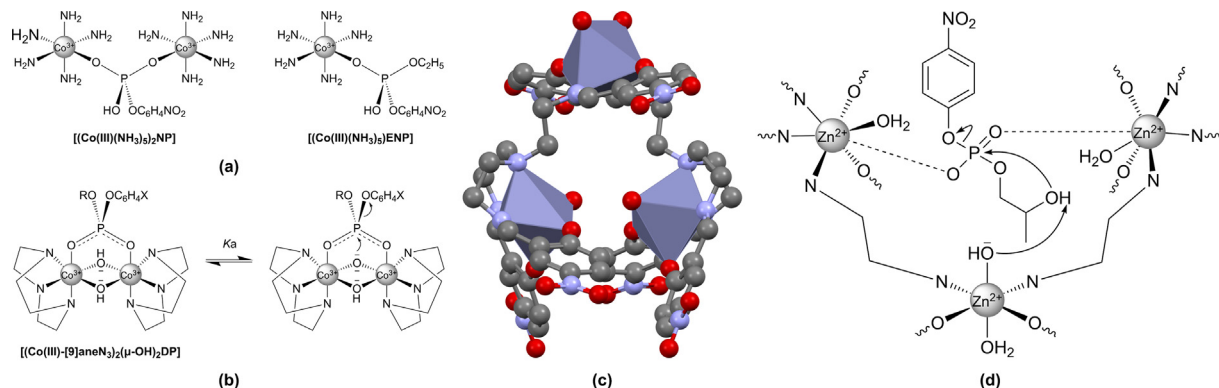


**Fig. 21.** (a) Structure of dinuclear O,O'-bridged monophosphate [(Co(III)(NH<sub>3</sub>)<sub>5</sub>)<sub>2</sub>NP] and monodentate coordinated diphosphate [(Co(III)(NH<sub>3</sub>)<sub>5</sub>)ENP]. (b) Proposed mechanism for hydrolysis of bridging phosphodiester by the bridging oxide. The mechanism involves rapid equilibrium proton transfer ( $K_a$ ) followed by rate-determining nucleophilic attack. (c) X-ray structure of [Zn(II)<sub>3</sub>(5-NO<sub>2</sub>-saldien)<sub>2</sub>(H<sub>2</sub>O)<sub>4</sub>], ref. [184]. (d) Possible mechanism for HPNP hydrolysis catalyzed by [Zn(II)<sub>3</sub>(5-NO<sub>2</sub>-saldien)<sub>2</sub>(H<sub>2</sub>O)<sub>4</sub>] showing trinuclear cooperativity.

trophilicity of the phosphorus atom due to the coordination of an additional cobalt ion. In a similar experiment, Chin's group showed that Co(III)-[9]aneN<sub>3</sub> provided an approx.  $4 \times 10^5$ -fold acceleration of HPP (2-hydroxypropylphenyl phosphate) hydrolysis relative to the background reaction.[178] This acceleration was attributed to the cooperative action of two Co(III) complexes linked by bridging hydroxides (Fig. 21b). As the authors noted, unlike single Lewis acid activation, which provides only a slight acceleration in the rate of phosphate ester cleavage, double Lewis acid activation provides a significant increase in the rate.

(2) The ability to form metal-bound hydroxyl already at physiological pH is a key feature of most hydrolytic metalloenzymes. It is estimated that coordination of a water molecule by a single metal ion can lower its  $pK_a$  from 14 in bulk solvent to as low as 9.0, while bridging a water molecule by two metal ions can lower its  $pK_a$  by as much as another 3–4 units to about 6; such lowering of  $pK_a$  can be exploited to obtain artificial nucleases that function in the low  $pH_e$  environment of cancer cell.[179,180] In some natural enzymes, such as P1 nuclease and PAP from sweet potato, the  $\mu$ -OH group is considered a key nucleophile in hydrolysis. Chin *et al.* showed that bridging (hydro)oxide can act as a very effective nucleophilic catalyst in the hydrolysis of the tertiary phosphodiester complex [(Co(III)-[9]aneN<sub>3</sub>)<sub>2</sub>( $\mu$ -OH)<sub>2</sub>DP] (Fig. 21b).[181] Overall, double Lewis acid activation combined with bridging hydroxide activation yields an approx.  $10^{11}$ -fold acceleration in the rate of phosphodiester hydrolysis relative to the background reaction.

(3) The pre-organized environment of the enzyme active site can modulate the  $pK_a$  values of the reactive groups and help modulate the reaction environment in a way that small-molecule catalysts cannot. Typically, the leaving group can be activated by coordination of the metal ion to the O-atom of the leaving group and neutralization of the negative charge formed on it during elimination, or by direct protonation of the O-atom by a general acid catalyst. In the alkaline phosphatase discussed earlier (Fig. 7), both effects are likely to occur; while one of the Zn(II) sites coordinates the O-atom of the leaving group, the water molecule coordinated by the Mg(II) ion can act as a general acid and directly protonate the leaving group, further facilitating its elimination. Model studies have shown that the rate constant of phosphodiester hydrolysis catalyzed by a small-molecule Co(III)-TRPN (TRPN – tris(3-aminopropyl)amine) is strongly dependent on the  $pK_a$  of the leaving group.[182] Lowering the  $pK_a$  of the leaving group of the substrate by 5 units resulted in a  $10^6$ -fold acceleration of the reaction. However, for reactions involving small-molecule catalysts, theoretical calculations of NPP cleavage by two Zn(II) ions suggest that metal-induced elimination of the leaving group is less favorable than proton transfer-assisted elimination of the leaving group.[183] Although it is very difficult to coordinate the leaving group directly to a small-molecule catalyst, hypothetically, in the case of multinuclear catalysts, an additional advantage can be gained by allowing one of the metal ions to bind to the O-atom of the leaving group; alternatively, introducing a functional group that acts as a general acid catalyst in the vicinity of the leaving group may also help eliminate it.

**What linker structure ensures the cooperativity of dinuclear cyclen complexes?** The cooperativity of dinuclear complexes is due to the close proximity of the two metal centers, so as one might expect, shorter linkers such as the 3 atom long 2-hydroxypropyl group in Zn(II)<sub>2</sub> **151** (Fig. 17a) help ensure the cooperativity, while longer linkers, such as the 10-atom chain in Zn(II)<sub>2</sub> **154** (Fig. 18) distance the two metals from each other enough that cooperativity disappears and such a complex shows activity at a similar level to the corresponding number of parent Zn(II)-cyclen units. The same is true for stiffer aromatic linkers, while (Zn(II)-[9]aneN<sub>3</sub>)<sub>2</sub> **L28** with a short *m*-xylene linker shows cooperativity,

resulting in 4 times more active in BNPP hydrolysis than the parent Zn(II)-[9]aneN<sub>3</sub>, (Zn(II)-[9]aneN<sub>3</sub>)<sub>2</sub> **L29** with a larger polyaromatic linker is only slightly more active than 2 equiv. of Zn(II)-[9]aneN<sub>3</sub>. [161] However, excessive proximity of the metal ions can also lead to a lack of cooperation between them and destabilization of the complex by the appearance of electrostatic repulsion. In some cases, such as Zn(II)<sub>2</sub> **145** (Fig. 17d) and (Zn(II)-[9]aneN<sub>3</sub>)<sub>2</sub> **L29** (Fig. 19), a water molecule bridges the gap between two metal ions and prevents mutual repulsion by electrostatically shielding ions of like sign; consequently, the water molecule allows the metals to approach each other and develop cooperation.[146,160] The presence of such a bridging water molecule in the crystallographic structure is usually a good indicator of the cooperativity. Another problem with the spacer strategy is that the resulting complexes are often too flexible for the metal centers to act in a highly cooperative manner. This has prompted researchers to use relatively short spacers with embedded deprotonable functional groups that link metal ions and place them at distance of about 3–6 Å, which roughly corresponds to the distance found in metalloenzymes. Such linkers, often found in dinuclear complexes, include 1,3-disubstituted-2-propanol (**L30**) and 2,6-disubstituted phenol (**L27**), which deprotonate to form an alkoxy bridge between two metal ions. A particularly large, > 50-fold acceleration of the hydrolysis rate of the model HPNP was observed for (Zn(II)-[9]aneN<sub>3</sub>)<sub>2</sub> **L30** with a 2-propanol linker relative to 2 equiv. of Zn(II)-[9]aneN<sub>3</sub>.

**Methods for increasing the activity and selectivity of multinuclear complexes towards DNA.** One of the most effective strategies for increasing the activity and selectivity of small-molecule complexes is to attach a DNA-binding molecule to them. For mononuclear complexes, the binding motif is usually attached via a side arm in such a way that it does not impede metal binding. In the case of binuclear cyclen complexes, only one example of such a strategy is known, i.e. Zn(II)<sub>2</sub> **172** with an oligopyrrole chain attached to the linker.[155] The use of a groove-binding motif in this case allowed the complex to increase its nucleolytic activity and made it less random. For multinuclear complexes, one would expect that increasing the number of Zn(II)-cyclen units should increase nucleolytic activity on a similar basis to the transition from mononuclear to dinuclear complexes. Such an effect was observed for the trinuclear complex [Zn(II)<sub>3</sub>(5-NO<sub>2</sub>-saldien)<sub>2</sub>(H<sub>2</sub>O)<sub>4</sub>] (Fig. 21c), in which all the metal centers are linked in a cup-shaped arrangement, giving the complex sufficient flexibility to develop cooperativity.[184] It has been proposed that the complex binds HPNP through three-point coordination, where two adjacent Zn(II) ions promote dual activation of the phosphoryl group, while a third central Zn(II) ion facilitate deprotonation of the 2'-hydroxyl group (Fig. 21d). This combination of promoting effects provided the complex with promising activity ( $k_{obs} = 4.1 \times 10^{-5} \text{ s}^{-1}$ ;  $C/S = 0.1$ ,  $pH > 8.5$ ,  $30 \text{ }^\circ\text{C}$ ). In the literature on cyclen-based complexes, there are only three examples of multinuclear complexes: linear Zn(II)<sub>3</sub> **153**, a series of star-shaped Cu(II) **182–184**, and six-nuclear Zn(II)<sub>6</sub> **181**. However, none of these complexes show cooperativity or such data are not available, nor did we find data on analogous complexes based on triamine ligands. The lack of cooperativity in these complexes is likely due to suboptimal linker structures; for example, Zn(II)<sub>3</sub> **153** has *p*-xylene linkers instead of *m*-xylene linkers, as in the case with most dinuclear complexes showing cooperativity; in Zn(II)<sub>6</sub> **181** the individual metal centers are too far apart to develop cooperativity; for Cu(II)<sub>3</sub> **184** complexation of a third copper ion not only fails to increase activity, but actually destabilizes the resulting trinuclear complex due to increased electrostatic repulsion. However, for multinuclear complexes based on such "suboptimal linkers", another feature of the Zn(II)-cyclen complex begins to dominate, namely the ability to recognize thymine and uridine. This feature

**Table 5**  
Comparison of ds-DNA cleavage rate constant ( $k_{\text{obs}}$ ) of selected supramolecular cyclen complexes and endonucleases.

Catalyst	Substrate	$k_{\text{obs}}$ ( $\text{h}^{-1}$ ) <sup>a</sup>	Conditions	Ref.
<b>188</b>	pUC18	0.56	Tris-HCl 40 mM, pH 7.4, 37 °C	[171]
Cu(II) <b>190</b>	pUC18	0.25	PB 200 mM, pH 7.2, 37 °C	[172]
Zn(II) <sub>2</sub> <b>191</b>	pBR322	0.022 <sup>b</sup>	HEPES 25 mM, pH 7.4, 40 °C	[173]
Cu(II) <b>194</b>	pUC19	0.015 <sup>c</sup>	Tris-HCl 100 mM, pH 7.4, 37 °C	[174]
Co(III) <b>197</b>	pUC18	3.53	pH 5.3, 25 °C	[175]
EcoRI	pBR322	43.2	Tris-HCl 20 mM, pH 7.6, 37 °C, MgCl <sub>2</sub> 5.0 mM, NaCl 25 mM, EDTA 0.05 mg/ml, BSA 0.05 mg/ml	[188]
R.Cfr9I	pUC18	40.2	Tris-HCl 10 mM, pH 7.5, 22 °C, MgCl <sub>2</sub> 7.0 mM, MSG 200 mM, DTT 1.0 mM, BSA 0.1 mg/ml	[189]
PvuII	pBR322	738	Tris-HCl 10 mM, pH 7.9, 37 °C, MgCl <sub>2</sub> 10 mM, NaCl 50 mM, DTT 1.0 mM, BSA 0.1 mg/ml	[190]

**a** – Most studies on chemical nucleases have been carried out under catalyst excess conditions (pseudo-Michaelis-Menten conditions) and do not represent true enzyme-like reactions with substrate turnover;  $k_{\text{obs}}$  is defined as  $k_{\text{cat}}[\text{catalyst}]/(K_{\text{m}} + [\text{catalyst}])$ , and the values presented are uncorrected for catalyst concentrations. Enzyme efficiencies are reported under true Michaelis-Menten conditions, where  $k_{\text{cat}}$  is defined as  $V_{\text{max}}/[\text{catalyst}]$ . **b** – Calculated from Fig. 1 in ref. [173]. **c** – Calculated from Fig. 2 in ref. [174]. BSA – bovine serum albumin. MSG – monosodium glutamate. DTT – dithiothreitol.

was exploited by Laine *et al.* to increase the selectivity of Zn(II)<sub>3</sub> **185** (Fig. 20) cleavage against non-consecutive dU sequences; in fact, Zn(II)<sub>3</sub> **185** cleaves ApU and UpA dinucleotides 3 times faster than UpU. In addition, Kimura *et al.* showed that linear Zn(II)<sub>3</sub> **153** (Fig. 17) can efficiently and selectively recognize U-rich single-stranded elements in biologically important RNA, such as TAR RNA of HIV-1, and serve as a new type of targeting motif.

**How do supramolecular complexes compare with natural enzymes?** Typically, artificial nucleases are designed to be well soluble in aqueous media, often overlooking the fact that their hydrolytic activity can be impaired by polar water molecules. The catalytic sites of natural nucleases often consist of a hydrophobic pocket with up to several metal cofactors. The general scenario for enzymatic hydrolysis is that a metal ion converts a water molecule into a metal-bound hydroxide, which then attacks the coordinated phosphodiester. These highly reactive species are solvated by water molecules in aqueous media and must desolvate to react with the substrate.[185,186] The hydrophobic environment of a supramolecular catalyst can mimic the enzymatic environment and facilitate this process. An example of a successful strategy for enhancing hydrolytic activity by increasing the hydrophobicity of the catalyst is metallomicelles **191** (Fig. 20), which combine locally concentrated Zn(II)<sub>2</sub> centers with a bilayer membrane to provide a hydrophobic reaction environment. The resulting nanoparticles not only significantly accelerated the hydrolysis of ds-DNA, but also of the less reactive ss-DNA. However, the activity of this catalyst depends on the size of the particles, further disintegration or aggregation of the catalyst induced by changing the reaction environment can result in a decrease in catalytic activity. Catalysts immobilized on polymer supports, such as Cu(II) **190** (Fig. 20) based on chitosan, Co(III) **195–197** based on polystyrene, or the metal-free series **186–189** with cyclen grafted onto a polyamide backbone, are more stable compared to noncovalent interactions in metallomicelles. The obtained catalysts were characterized not only by a significant acceleration of DNA hydrolysis, but also by high stability allowing the separation of the insoluble matrix from the reaction products. For example, Cu(II) **190** can retaining up to 75% of its original activity even after recovering from the reaction four times. Table 5 compares the activity of selected supramolecular catalysts towards ds-DNA with that of natural endonucleases. Despite the tremendous progress that has been made in the last 30 years in the field of cyclen-based artificial nucleases, it is clear that natural nucleases are still one to two orders of magnitude faster than their most efficient artificial counterparts. On the other hand, the optimal activity of most enzymes falls within a narrow temperature range from about 30 to 50 °C, beyond which their activity rapidly declines.[187] In this aspect, artificial nucleases are superior to natural proteins, and reactions involving them can be carried out at temperatures inaccessible to enzymes.

#### 4. Concluding remarks

Natural nucleases, mainly zinc metalloenzymes, are so far unsurpassed in the rate of nucleic acid hydrolysis under physiological conditions. However, the search for artificial analogs of these enzymes is contributing to the development of anticancer therapies, genetic engineering, and a better understanding of natural mechanisms. These applications are made possible by >30 years of research in this field, which has identified the most promising *d*- and *f*-block cyclen complexes. This review summarizes this vast experimental material. As a result of the above review, it can be confirmed that the metal complexes created by a generation of researchers are more durable and more stable than natural enzymes. The macrocyclic scaffold of cyclen provides the highest stability and flexibility for substitution, while allowing the complex to interact with water molecules – the source of the hydrolyzing agent. In addition, the side arms introduced on the nitrogen atoms of the cyclen ring, by tuning the  $pK_{\text{a}}$  of metal-bound water, ligand bulkiness, affinity for the central ion or biological targets, are responsible for numerous effects such as complex stability, catalytic activity, and selectivity. Studies on numerous models have shown a structure–activity relationship for metal type and ligand structure. La(III) complexes generally show the highest activity among *f*-block elements, which may be related to its largest ionic radius and thus the largest space for coordination. Among *f*-metal complexes, Tb(III) and Eu(III) are also promising candidates for further research on artificial nucleases. Typically, transition metal complexes are one order slower than lanthanide complexes. However, as shown on Co(III) complexes, providing them with DNA-binding molecules can boost their activity much over that of the *f*-block complexes. Thus, one more factor appears to be crucial for net catalytic activity in specific applications – this is selectivity and specificity. Such an effect can be achieved by proper design of ligands, and in addition, due to the supramolecular nature of the complexes, it becomes possible to mimic the natural environment of enzymes to get even closer to their activity level. The above generalizations provide a rough picture of the current state of knowledge and the development paths taken to design promising catalysts for nucleic acids hydrolysis. The last 3 decades of arduous and inquisitive research in this field provide the basis for the development of highly effective tools for the controlled and specific modification of nucleic acids.

We believe that advances in coordination compounds, especially in the form of conjugates with biomolecules and supramolecular complexes, can seriously contribute to the development of new solutions in medicine. So far, the most popular application of coordination compounds is diagnostics and imaging of cancerous lesions in the body. In addition to this conventional application, it is becoming possible to use small-molecule complexes to mimic the function of key natural enzymes and apply them to

more challenging areas, such as anticancer therapies. The history of the development of cyclen complexes as artificial nucleases, summarized in this review, has provided much knowledge of their properties under *in solution* (cell-free) conditions. What is lacking in current knowledge are the results of *in vitro* and *in vivo* studies that would help realistically assess the potential applications of the compounds in question. In particular, understanding of the intracellular and tissue distribution of cyclen complexes would be useful in elucidating the mechanism of action and *in vivo* applications. There are just a few works, such as studies of Zn(II) **123** in mouse models (see ref. [103]), which reveal the promising *in vivo* potential of transition metal cyclen complexes and may encourage further biological research.

## Funding

This work was financially supported by the Department of Chemistry, Silesian University of Technology, No. 04/020/BK-22/1035.

## Data availability

Data will be made available on request.

## Declaration of Competing Interest

The authors declare that they have no known competing financial interests or personal relationships that could have appeared to influence the work reported in this paper.

## References

- [1] J. Chin, M. Banaszczyk, V. Jubian, X. Zou, *J. Am. Chem. Soc.* 111 (1989) 186–190.
- [2] A. Radzicka, R. Wolfenden, *Science* 267 (1995) 90–93.
- [3] F.H. Westheimer, *Science* 235 (1987) 1173–1178.
- [4] T. Lindahl, *Nature* 362 (1993) 709–715.
- [5] K.O.A. Chin, J.R. Morrow, *Inorg. Chem.* 33 (1994) 5036–5041.
- [6] K.O.A. Chin, J.R. Morrow, C.H. Lake, M.R. Churchill, *Inorg. Chem.* 33 (1994) 656–664.
- [7] J.R. Morrow, K. Aures, D.J. Epstein, *Chem. Soc., Chem. Commun.* (1995) 2431–2432.
- [8] S. Siekierski, *Pol. J. Chem.* 66 (1992) 215–1000.
- [9] S. Siekierski, *Inorg. Chim. Acta.* 109 (1985) 199–1000.
- [10] R.E. Gerkin, W.J. Reppart, *Acta Crystallogr. C* 40 (1984) 781–786.
- [11] X. Ma, Y. Yin, Z. Geng, Z. Yang, J. Wen, Z. Wang, *RSC Adv.* 4 (2014) 50070–50073.
- [12] B.F. Baker, H. Khalili, N. Wei, J.R. Morrow, *J. Am. Chem. Soc.* 119 (1997) 8749–8755.
- [13] L. Huang (1999) PhD thesis. State University of New York at Buffalo.
- [14] L. Huang, L.L. Chappell, O. Iranzo, B.F. Baker, J.R. Morrow, *J. Biol. Inorg. Chem.* 5 (2000) 85–92.
- [15] J.P. Richard, J.R. Morrow, A.M.C. O'Donoghue, S.Y. Pyun, *Bull. Korean Chem. Soc.* 25 (2004) 403–406.
- [16] L.L. Chappell, D.A. Voss, W.D. Horrocks, J.R. Morrow, *Inorg. Chem.* 37 (1998) 3989–3998.
- [17] C. Wang, S. Choudhary, C.B. Vink, E.A. Secord, J.R. Morrow, *Chem. Commun.* (2000) 2509–2510.
- [18] J.R. Morrow, K.A. Kolasa, S. Amin, K.O.A. Chin, *Mech. Bioinorg. Chem., American Chemical Society*, 1996, pp. 431–447.
- [19] S. Amin, D.A. Voss, W.W.D.W. Horrocks, C.H. Lake, M.R. Churchill, J.R. Morrow, *Inorg. Chem.* 34 (1995) 3294–3300.
- [20] S. Amin, J.R. Morrow, C.H. Lake, M.R. Churchill, *Angew. Chem. Int. Ed.* 33 (1994) 773–775.
- [21] C.F. Macrae, I. Sovago, S.J. Cottrell, P.T.A. Galek, P. McCabe, E. Pidcock, M. Platings, G.P. Shields, J.S. Stevens, M. Towler, P.A. Wood, *J. Appl. Cryst.* 53 (2020) 226–235.
- [22] M.J. Belousoff, P. Ung, C.M. Forsyth, Y. Tor, L. Spiccia, B. Graham, *J. Am. Chem. Soc.* 131 (2009) 1106–1114.
- [23] K. Nwe, J.P. Richard, J.R. Morrow, *J. Chem. Soc. Dalt. Trans.* (2006) 5171–5178.
- [24] K. Nwe, C.M. Andolina, J.R. Morrow, *J. Am. Chem. Soc.* 130 (2008) 14861–14871.
- [25] S. Amin, D.A. Voss, W.D. Horrocks, J.R. Morrow, *Inorg. Chem.* 35 (1996) 7466–7467.
- [26] U. Baykal, E.U. Akkaya, *Tetrahedron Lett.* 39 (1998) 5861–5864.
- [27] U. Baykal, M.S. Akkaya, E.U. Akkaya, *J. Incl. Phenom.* 35 (1999) 311–315.
- [28] C.A. Chang, H.W. Bo, Y.K. Bu, *Inorg. Chem.* 44 (2005) 6646–6654.
- [29] C.A. Chang, B.H. Wu, C.H. Hsiao, *Eur. J. Inorg. Chem.* (2009) 1339–1346.
- [30] T. Gunnlaugsson, J.E. O'Brien, S. Mulready, *Tetrahedron Lett.* 43 (2002) 8493–8497.
- [31] T. Gunnlaugsson, R.J.H. Davies, M. Nieuwenhuyzen, J.E. O'Brien, C.S. Stevenson, S. Mulready, *Polyhedron* 22 (2003) 711–724.
- [32] T. Gunnlaugsson, R.J.H. Davies, M. Nieuwenhuyzen, C.S. Stevenson, R. Viguier, S. Mulready, *Chem. Commun.* 2 (2002) 2136–2137.
- [33] A.M. Fanning, S.E. Plush, T. Gunnlaugsson, *Org. Biomol. Chem.* 13 (2015) 5804–5816.
- [34] T. Gunnlaugsson, R.J.H. Davies, P.E. Kruger, P. Jensen, T. McCabe, S. Mulready, J.E. O'Brien, C.S. Stevenson, A.M. Fanning, *Tetrahedron Lett.* 46 (2005) 3761–3766.
- [35] A.M. Fanning, S.E. Plush, T. Gunnlaugsson, *Chem. Commun.* (2006) 3791–3793.
- [36] E. Persi, M. Duran-Frigola, M. Damaghi, W.R. Roush, P. Aloy, J.L. Cleveland, R.J. Gillies, E. Rupp, *Nat. Commun.* 9 (2018) 2997–3008.
- [37] B.A. Webb, M. Chimentì, M.P. Jacobson, D.L. Barber, *Nat. Rev. Cancer.* 11 (2011) 671–677.
- [38] J.W. Wojtkowiak, R.J. Gillies, *Autophagy* 8 (2012) 1688–1689.
- [39] R. Harisi, A. Jeney, *Onco Targets Ther.* 8 (2015) 1387–1398.
- [40] G. Hao, Z.P. Xu, L. Li, *RSC Adv.* 8 (2018) 22182–22192.
- [41] A.M. Piccinini, K.S. Midwood, *Int. J. Exp. Path.* 95 (2014) 158–180.
- [42] Y. Su, X. Li, W. Ji, B. Sun, C. Xu, Z. Li, G. Qian, C. Su, *Cancer Lett.* 344 (2014) 147–156.
- [43] J.R. Morrow, K.O.A. Chin, *Inorg. Chem.* 32 (1993) 3357–3361.
- [44] D. Keilin, T. Mann, *Biochem. J.* 34 (1940) 1163–1176.
- [45] R.A. McCance, E.M. Widdowson, *Biochem. J.* 36 (1942) 692–696.
- [46] P. Argos, R.M. Garavito, W. Eventoff, M.G. Rossman, C.I. Branden, *J. Mol. Biol.* 126 (1978) 141–158.
- [47] K.A. McCall, C.-C. Huang, C.A. Fierke, *J. Nutr.* 130 (2000) 1437–1446.
- [48] A. Erxleben, *Front. Chem.* (2019) 7.
- [49] E.E. Kim, H.W. Wyckoff, *J. Mol. Biol.* 218 (1991) 449–464.
- [50] B. Stec, K.M. Holtz, E.R. Kantrowitz, *J. Mol. Biol.* 299 (2000) 1303–1311.
- [51] J.G. Zalatan, T.D. Fenn, D. Herschlag, *J. Mol. Biol.* 384 (2008) 1174–1189.
- [52] J. Wang, K.A. Stieglitz, E.R. Kantrowitz, *Biochemistry* 44 (2005) 8378–8386.
- [53] T. Klabunde, N. Sträter, R. Fröhlich, H. Witzel, B. Krebs, *J. Mol. Biol.* 259 (1996) 737–748.
- [54] N. Lanznaster, A. Neves, A.J. Bortoluzzi, V.V.E. Aires, B. Szpoganicz, H. Terenzi, P.C. Severino, J.M. Fuller, S.C. Drew, L.R. Gahan, G.R. Hanson, M.J. Riley, G. Schenk, *J. Biol. Inorg. Chem.* 10 (2005) 319–332.
- [55] N. Mitic, S.J. Smith, A. Neves, L.W. Guddat, L.R. Gahan, G. Schenk, *Chem. Rev.* 106 (2006) 3338–3363.
- [56] N.V. Kaminskaia, C. He, S.J. Lippard, *Inorg. Chem.* 39 (2000) 3365–3373.
- [57] C. Jackson, H.-K. Kim, P.D. Carr, J.-W. Liu, D.L. Ollis, *Biochim. Biophys. Acta* 1752 (2005) 56–64.
- [58] N. Díaz, D. Suárez, T.L. Sordo, *J. Am. Chem. Soc.* 122 (2000) 6710–6719.
- [59] G. Schürer, H. Lanig, T. Clak, *Biochemistry* 43 (2004) 5414–5427.
- [60] S. Chen (2008) PhD thesis. Royal Institute of Technology in Stockholm.
- [61] C. Romier, R. Dominguez, A. Lahm, O. Dahl, D. Suck, *Proteins* 32 (1998) 414–424.
- [62] T. Kova, L.H. Stergaard, J. Lehmebeck, A. Nørgaard, P. Lipovová, J. Dušková, T. Skálová, M. Trundová, P. Kolenko, K. Fejfarová, J. Stránský, L. Švecová, J. Hašek, J. Dohnálek, *PLoS One* 11 (2016) 1–25.
- [63] T.F. Yu, N. Maestre-Reyna, C.Y. Ko, T.P. Ko, Y.J. Sun, T.Y. Lin, J.F. Shaw, A. H., J. Wang *PLoS One* 9 (2014) 1–10.
- [64] L. Schrödinger, W. DeLano Available at PyMOL (2020). <http://www.pymol.org/pymol>.
- [65] D.P. Linder, B.E. Baker, K.R. Rodgers, *Phys. Chem. Chem. Phys.* 20 (2018) 24979–24991.
- [66] L. Koziol, C.A. Valdez, S.E. Baker, E.Y. Lau, W.C. Floyd, S.E. Wong, J.H. Satcher, F. C. Lightstone, R.D. Aines, *Inorg. Chem.* 51 (2012) 6803–6812.
- [67] K. Kumar, C.A. Chang, L.C. Francesconi, D.D. Dischino, M.F. Malley, J.Z. Gougoutas, M.F. Tweedle, *Inorg. Chem.* 33 (1994) 3567–3575.
- [68] V.M. Runge, D.Y. Gelblum, S. Jacobson, *Magn. Reson. Imaging* 9 (1991) 79–87.
- [69] P. Caravan, J.J. Ellison, T.J. McMurry, R.B. Lauffer, *Chem. Rev.* 99 (1999) 2293–2352.
- [70] W.P. Cacheris, S.C. Quay, S.M. Rocklage, *Magn. Reson. Imaging* 8 (1990) 467–481.
- [71] M. Shionoy, E. Kimura, M. Shiro, *J. Am. Chem. Soc.* 115 (1993) 6730–6737.
- [72] T. Itoh, Y. Fujii, T. Tada, Y. Yuzo, H. Hisada, *Bull. Chem. Soc. Jpn.* 69 (1996) 1265–1274.
- [73] E. Kimura, T. Shiota, T. Koike, M. Shiro, M. Kodama, *J. Am. Chem. Soc.* 112 (1990) 5805–5811.
- [74] T. Koike, E. Kimura, *J. Inorg. Biochem.* 113 (1991) 8935–8941.
- [75] R.A. Mathews, C.S. Rossiter, J.R. Morrow, J.P. Richard, *Dalt. Trans.* (2007) 3804–3811.
- [76] M. Kodama, E. Kimura, *J. Chem. Soc., Dalton Trans.* (1977) 2269–2276.
- [77] Y. Ichimaru, K. Kato, H. Kurosaki, H. Fujioka, M. Sakai, Y. Yamaguchi, J. Wanchun, K. Sugiura, M. Imai, T. Koike, *IUCrData* 6 (2021), <https://doi.org/10.1107/s2414314621003977>.
- [78] L. Bonfá, M. Gatos, F. Mancin, P. Tecilla, U. Tonellato, *Inorg. Chem.* 42 (2003) 3943–3949.
- [79] S.P. Gavriš, S. Shova, Y.D. Lampeka, *Acta Crystallogr. Sect. E Crystallogr. Commun.* 77 (2021) 1185–1189.
- [80] S.P. Gavriš, S. Shovab, Y.D. Lampeka, *Acta Cryst.* 77 (2021) 1185–1189.

- [81] A. Zalkin, R.J. Sime, R.P. Dodge, D.H. Templeton, *Inorg. Chem.* 10 (1971) 537–541.
- [82] M.-Y. Yang, O. Iranzo, J.P. Richard, J.R. Morrow, *J. Am. Chem. Soc.* 127 (2005) 1064–1065.
- [83] *Advances in Physical Organic Chemistry; Gold, V., Ed.; Academic Press: New York, 1967.*
- [84] A.J. Kirby, M.J. Younas, *J. Chem. Soc. B* (1970) 510–513.
- [85] A.M. Piatek, M. Gray, M., E. V. Anslын, *J. Am. Chem. Soc.* 126 (2004) 9878–9879.
- [86] C. Margreitter, M.M. Reif, C. Oostenbrink, *J. Comput. Chem.* 38 (2017) 714–720.
- [87] S.S. Massoud, H. Sigel, *Inorg. Chem.* 27 (1988) 1447–1453.
- [88] D.R. Jones, L.F. Lindoy, A.M. Sargeson, *J. Am. Chem. Soc.* 105 (1983) 7327–7336.
- [89] K.A. Deal, A.C. Hengge, J.N. Burstyn, *J. Am. Chem. Soc.* 118 (1996) 1713–1718.
- [90] D.A. Kingery, S.A. Strobel, *Acc. Chem. Res.* 45 (2012) 495–503.
- [91] D.A. Knight, J.B. Delehanty, E.R. Goldman, J. Bongard, F. Streich, L.W. Edwards, E.L. Chang, *J. Chem. Soc. Dalton Trans.* 4 (2004) 2006–2011.
- [92] J.B. Delehanty, T.C. Stuart, D.A. Knight, E.R. Goldman, D.C. Thach, J.E. Bongard, E.L. Chang, *Rna* 11 (2005) 831–836.
- [93] L. Yang, F. Liang, M. Liu, C. Zheng, S. Wan, X. Xiong, X. Zhang, C. Shen, X. Zhou, *Bioorg. Med. Chem. Lett.* 17 (2007) 1818–1822.
- [94] M. Leivers, R. Breslow, *Bioorg. Chem.* 29 (2001) 345–356.
- [95] B. König, M. Pelka, M. Subat, I. Dix, P.G. Jones, *Eur. J. Org. Chem.* (2001) 1943–1949.
- [96] Q.X. Xiang, L.Q. Zhang, X.Q. Yu, R.G. Xie, *Chin. Chem. Lett.* 20 (2009) 523–526.
- [97] X. Bin Yang, J. Feng, J. Zhang, Z.W. Zhang, H.H. Lin, L.H. Zhou, X.Q. Yu, *Bioorg. Med. Chem.* 16 (2008) 3871–3877.
- [98] M. Subat, K. Woinaroschy, S. Anthofer, B. Malterer, B. König, *Inorg. Chem.* 46 (2007) 4336–4435.
- [99] E. Kimura, Y. Kodama, T. Koike, M. Shiro, *J. Am. Chem. Soc.* 117 (1995) 8304–8311.
- [100] M. Kalesse, A. Loos, *Liebigs Ann.* 4 (1996) 935–939.
- [101] R. Hettich, H.J. Schneider, *J. Am. Chem. Soc.* 119 (1997) 5638–5647.
- [102] J.A. Krauser, A.L. Joshi, I.O. Kady, *J. Inorg. Biochem.* 104 (2010) 877–884.
- [103] A. Adhikari, N. Kumari, M. Adhikari, N. Kumar, A.K. Tiwari, A. Shukla, A.K. Mishra, A. Datta, *Bioorg. Med. Chem.* 25 (2017) 3483–3490.
- [104] C.Q. Xia, N. Jiang, J. Zhang, S.Y. Chen, H.H. Lin, X.Y. Tan, Y. Yue, X.Q. Yu, *Bioorg. Med. Chem.* 14 (2006) 5756–5764.
- [105] X.Y. Wang, J. Zhang, K. Li, N. Jiang, S.Y. Chen, H.H. Lin, Y. Huang, L.J. Ma, X.Q. Yu, *Bioorg. Med. Chem.* 14 (2006) 6745–6751.
- [106] G. Rayner-Canham, *Descriptive inorganic chemistry*, W.H. Freeman, New York, 1996.
- [107] Y. Zhou, R. Qiao, Z. Zhang, Preparation of the metal complexes of polyamide conjugate with big nitrogen heterocyclic compound and its DNA cutting activity. CN Patent CN1560112, filed 03 March 2004.
- [108] S.H. Wan, F. Liang, X.Q. Xiong, L. Yang, X.J. Wu, P. Wang, X. Zhou, C.T. Wu, *Bioorg. Med. Chem. Lett.* 16 (2006) 2804–2806.
- [109] K. Michaelis, M. Kalesse, *Angew Chemie - Int. Ed.* 38 (1999) 2243–2245.
- [110] K. Michaelis, M. Kalesse, *ChemBioChem* 2 (2001) 79–83.
- [111] Q. Yin, Z. Zhang, Y.F. Zhao, *Spectrochim. Acta - Part A Mol. Biomol. Spectrosc.* 66 (2007) 904–908.
- [112] Q. Yin, Z. Zhang, Y. Fen Zhao, *Chem. Res. Chinese Univ.* 23 (2007) 44–47.
- [113] C. Li, C. Du, H. Tian, C. Jiang, M. Du, Y. Liu, R.Z. Qiao, Y.X. Jia, Y.F. Zhao, *Chem. - Eur. J.* 16 (2010) 12935–12940.
- [114] E. Kimura, E. Kikuta, *Prog. React. Kinet. Mech.* 25 (2000) 1–64.
- [115] M.D. Tomczyk, M. Zalewski, P.T. Jørgensen, J. Wengel, K. Walczak, *Pharmaceutics* 14 (2022) 1–16.
- [116] E. Kikuta, M. Murata, N. Katsube, T. Koike, E. Kimura, *J. Am. Chem. Soc.* 121 (1999) 5426–5436.
- [117] J. Portugal, M.J. Waring, *Biochim. Biophys. Acta* 949 (1988) 158–168.
- [118] K.R. Fox, M.J. Waring, *Biochim. Biophys. Acta* 909 (1987) 145–155.
- [119] H.R. Drew, *J. Mol. Biol.* 176 (1984) 535–557.
- [120] J. Fei, T. Ha, *Proc. Natl. Acad. Sci. U. S. A.* 110 (2013) 17173–17174.
- [121] N.C. Okoye, J.E. Baumeister, F.N. Khosroshahi, H.M. Hennkens, S.S. Jurisson, *Radiochim. Acta* 107 (2019) 1087–1120.
- [122] M. Shionoya, T. Ikeda, E. Kimura, M. Shiro, *J. Am. Chem. Soc.* 116 (1994) 3848–3859.
- [123] E. Kimura, T. Gotoh, T. Koike, M. Shiro, *J. Am. Chem. Soc.* 121 (1999) 1267–1274.
- [124] C. Bazzicalupi, A. Bianchi, E. Berni, L. Calabi, C. Giorgi, P. Mariani, P. Losi, B. Valtancoli, *Inorganica Chim. Acta* 329 (2002) 93–99.
- [125] R.D. Hancock, P.W. Wade, M.P. Ngwenya, A.S. de Sousa, K.V. Damu, *Inorg. Chem.* 29 (1990) 1968–1974.
- [126] V.J. Thöm, G.D. Hosken, R.D. Hancock, *Inorg. Chem.* 24 (1985) 3378–3381.
- [127] S. El Ghachtouli, C. Cadiou, I. Déchamps-Olivier, F. Chuburu, M. Aplincourt, T. Roisnel, *Eur. J. Inorg. Chem.* 17 (2006) 3472–3481.
- [128] F. El Hajji, V. Patinec, S. Triki, H. Handel, M. Marchivie, *Inorg. Chem. Commun.* 13 (2010) 1314–1316.
- [129] N. Bernier, J. Costa, R. Delgado, V. Felix, G. Royale, R. Tripier, *Dalton Trans.* 40 (2011) 4514–4526.
- [130] T.J. Mooibroek, S. Scheiner, H. Valkenier, *ChemPhysChem* 22 (2021) 433–434.
- [131] S. Aoki, D. Kagata, M. Shiro, K. Takeda, E. Kimura, *J. Am. Chem. Soc.* 126 (2004) 13377–13390.
- [132] E. Kimura, T. Gotoh, S. Aoki, M. Shiro, *Inorg. Chem.* 41 (2002) 3239–3248.
- [133] A. Bianchi, L. Calabi, P.L. Claudia Giorgi, P. Mariani, P. Paoli, P. Rossi, B. Valtancoli, M. Virtuani, *J. Chem. Soc. Dalton Trans.* (2000) 697–705.
- [134] A. Forgács, L. Tei, Z. Baranyai, I. Tóth, L. Zékány, M. Botta, *Eur. J. Inorg. Chem.* (2016, 2016.) 1165–1174.
- [135] M. Kodama, E. Kimura, *J. Chem. Soc., Dalton Trans.* (1980) 327–333.
- [136] H.M. Kim, B. Jang, Y.E. Cheon, M.P. Suh, J. Suh, *J. Biol. Inorg. Chem.* 14 (2009) 151–157.
- [137] U. Pindur, M. Jansen, T. Lemster, *Curr. Med. Chem.* 12 (2005) 2805–2847.
- [138] V. Sharma, M. Gupta, P. Kumar, A. Sharma, *Curr. Pharm. Des.* 27 (2020) 15–42.
- [139] M.D. Tomczyk, K.Z. Walczak, *Eur. J. Med. Chem.* 159 (2018) 393–422.
- [140] E. Kikuta, R. Matsubara, N. Katsube, T. Koike, E. Kimura, *J. Inorg. Biochem.* 82 (2000) 239–249.
- [141] E. Kikuta, S. Aoki, E. Kimura, *J. Am. Chem. Soc.* 123 (2001) 7911–7912.
- [142] H. Irving, R.J.P. Williams, *J. Chem. Soc.* (1953) 3192–3210.
- [143] R.B. Martin, *J. Chem. Educ.* 64 (1987) 402.
- [144] D. Reinen, M. Atanasov, G. St, F.S. Nikolov, *Inorg. Chem.* 27 (1988) 1678–1686.
- [145] N.C. Okoye, J.E. Baumeister, F.N. Khosroshahi, H.M. Hennkens, S.S. Jurisson, *Radiochim. Acta* 107 (2019) 1087–1120.
- [146] Q.X. Xiang, J. Zhang, P.Y. Liu, C.Q. Xia, Z.Y. Zhou, R.G. Xie, X.Q. Yu, *J. Inorg. Biochem.* 99 (2005) 1661–1669.
- [147] C.Q. Xia, N. Jiang, J. Zhang, S.Y. Chen, H.H. Lin, X.Y. Tan, Y. Yue, X.Q. Yu, *Bioorg. Med. Chem.* 14 (2006) 5756–5764.
- [148] M. Kodaera, Y. Kadoya, K. Aso, K. Fukui, A. Nomura, Y. Hitomi, H. Kitagishi, *Bull. Chem. Soc. Jpn.* 92 (2019) 739–747.
- [149] E. Kimura, M. Kikuchi, H. Kitamura, T. Koike, *Chem. Eur. J.* 5 (1999) 3113–3123.
- [150] W.Peng, P.Y. Liu, N. Jiang, H.H. Lin, G.L. Zhang, Y. Liu, X.Q. Yu, *Bioorg. Chem.* 33 (2005) 374–385.
- [151] B. König, M. Pelka, M. Subat, I. Dix, P.G. Jones, *Eur. J. Org. Chem.* 10 (2001) 1943–1949.
- [152] Y.G. Fang, J. Zhang, S.Y. Chen, N. Jiang, H.H. Lin, Y. Zhang, X.Q. Yu, *Bioorg. Med. Chem.* 15 (2007) 696–701.
- [153] N. Chitrapriya, W. Wang, Y.J. Jang, S.K. Kim, J.H. Kim, *J. Inorg. Biochem.* 140 (2014) 153–159.
- [154] J. Li, J. Zhang, Q. Sen Lu, Y. Yue, Y. Huang, D.W. Zhang, H.H. Lin, S.Y. Chen, X.Q. Yu, *Eur. J. Med. Chem.* 44 (2009) 5090–5093.
- [155] C. Li, C. Du, H. Tian, C. Jiang, M. Du, Y. Liu, R.Z. Qiao, Y.X. Jia, Y.F. Zhao, *Chem. Eur. J.* 16 (2010) 12935–12940.
- [156] M. Subat, K. Woinaroschy, S. Anthofer, B. Malterer, B. König, *Inorg. Chem.* 46 (2007) 4336–4356.
- [157] D. Montagner, V. Gandin, C. Marzano, A. Erxleben, *Eur. J. Inorg. Chem.* 25 (2014) 4084–4092.
- [158] C. Bazzicalupi, A. Bencini, E. Faggi, A. Garau, C. Giorgi, V. Lippolis, A. Perra, B. Valtancoli, *Dalt. Trans.* 6 (2006) 1409–1418.
- [159] X. Sheng, X. Guo, X.M. Lu, G.Y. Lu, Y. Shao, F. Liu, Q. Xu, *Bioconjug. Chem.* 19 (2008) 490–498.
- [160] M. Arca, A. Bencini, E. Berni, C. Caltagirone, F.A. Devillanova, F. Isaia, A. Garau, C. Giorgi, V. Lippolis, A. Perra, L. Tei, B. Valtancoli, *Inorg. Chem.* 42 (2003) 6929–6939.
- [161] R. Haidar, M. Ipek, B. DasGupta, M. Yousaf, L.J. Zompa, *Inorg. Chem. Acta.* 36 (1997) 3125–3132.
- [162] B. DasGupta, R. Haidar, W.-Y. Hsieh, L.J. Zompa, *Inorganica Chim. Acta.* 306 (2000) 78–86.
- [163] T. Moufarrej, K. Bui, L.J. Zompa, *Inorg. Chim. Acta* 340 (2002) 56–64.
- [164] O. Iranzo, A.Y. Kovalevsky, J.R. Morrow, J.P. Richard, *J. Am. Chem. Soc.* 125 (2003) 1988–1993.
- [165] O. Iranzo, T. Elmer, J.P. Richard, J.R. Morrow, *Inorg. Chem.* 42 (2003) 7737–7746.
- [166] J.H. Wang, C.C. Wang, D. Zhang, C.J. Liu, Y. Ye, Y. Zhao, *Phosphorus, Sulfur Silicon Relat. Elem.* 188 (2013) 54–58.
- [167] A. Bencini, E. Berni, A. Biancini, C. Giorgi, B. Valtancoli, D.K. Chand, H.J. Schneider, *Dalt. Trans.* (2003) 793–800.
- [168] R.D. Hancock, M. Salim Shaikjee, S.M. Dobson, J.C.A. Boeyens, *Inorganica Chim. Acta* 154 (1988) 229–238.
- [169] M. Laine, T. Lönnberg, M. Helkear, H. Lönnberg, *Inorganica Chim. Acta* 452 (2016) 111–117.
- [170] E. Kimura, M. Kikuchi, H. Kitamura, T. Koike, *T. Eur. J. Chem.* 5 (1999) 3113–3123.
- [171] C. Li, F. Zhao, Y. Huang, X. Liu, Y. Liu, R. Qiao, Y. Zhao, *Bioconjug. Chem.* 23 (2012) 1832–1837.
- [172] X. Wang, M. Ding, Z. Liu, D. Wang, *RSC Adv.* 5 (2015) 19541–19551.
- [173] B. Gruber, E. Kataev, J. Aschenbrenner, S. Stadlbauer, B. König, *J. Am. Chem. Soc.* 133 (2011) 20704–20707.
- [174] Y.Z. Xiang, L.H. Zhou, N. Jiang, H.H. Lin, X.Q. Yu, *J. Enzyme Inhib. Med. Chem.* 24 (2009) 315–319.
- [175] C.S. Jeung, C.H. Kim, K. Min, S.W. Suh, J. Suh, *Bioorg. Med. Chem. Lett.* 11 (2001) 2401–2404.
- [176] C.S. Jeung, J.B. Song, Y.H. Kim, J. Suh, *Bioorg. Med. Chem. Lett.* 11 (2001) 3061–3064.
- [177] P. Hendry, A.M. Sargeson, *Inorg. Chem.* 29 (1990) 92–97.
- [178] N.H. Williams, *J. Chin. Chem. Commun.* (1996) 131–132.
- [179] D.W. Christianson, J.D. Cox, *Annu. Rev. Biochem.* 68 (1999) 35–57.
- [180] G.A. Omburo, J.M. Kuo, L.S. Mullins, F.M. Raushel, *J. Biol. Chem.* 267 (1992) 13278–132783.
- [181] N.H. Williams, W. Cheung, J. Chin, *J. Am. Chem. Soc.* 120 (1998) 8079–8087.

- [182] MPadovani, N.H. Williams, P. Wyman, *J. Phys. Org. Chem.* 17 (2004) 472–477.
- [183] X. Zhang, Y. Zhu, X. Zheng, D.L. Philips, C. Zhao, *Inorg. Chem.* 53 (2014) 3354–3361.
- [184] P. Joshi, N. Hussain, S.R. Ali, V.K. Rishu, Bhardwaj., *New J. Chem.* 42 (2018) 2204–2215.
- [185] A. Babbie, N. Tokuriki, F. Hollfelder, *Curr. Opin. Chem. Biol.* 14 (2010) 200–207.
- [186] C.A. Fierke, T.L. Calderone, J.F. Krebs, *Biochemistry* 30 (1991) 11054–11063.
- [187] F.M. Pohl, R. Thomae, A. Karst, *Eur. J. Biochem.* 123 (1982) 141–152.
- [188] D.J. Wright, W.E. Jack, P. Modrich, *J. Biol Chem.* 274 (1999) 31896–31902, *Eur. J. Biochem.* 1982, 123, 141–152.
- [189] V. Siksnys, M. Pleckaityte, *Eur. J. Biochem.* 217 (1993) 411–419.
- [190] A. Simoncsits, M.-L. Tjörnhammar, T. Raskó, A. Kiss, S. Pongor, *J. Mol. Biol.* 309 (2001) 89–97.



**Mateusz Tomczyk** is a graduate of the Silesian University of Technology (Poland, 2017), where he received a master's degree in organic chemistry. Since November 2017 he is a Ph.D. student at the Silesian University of Technology under the supervision of Prof. Krzysztof Walczak. His research is focused on post-synthetic modification of oligonucleotides with particular use of coordination chemistry and photoactive systems. M. T. has held research internships at Loschmidt Laboratories at Masaryk University (Czech Republic, 2017) and University of Southern Denmark in the group of Prof. J. Wengel (Denmark, 2019–2021). He is the recipient of

two research grants (by NCN and NCBR), under which he leads a team working on HK2 inhibitors and combination therapies.



**Prof. Nikodem Kuźnik** is a graduate of the Silesian University of Technology (Poland, 2001), where he also received his PhD (2005). N. K. held research internships in the laboratory of J. F. Hartwig at Yale University (USA, 2000) and Lund University (Sweden, 2001), followed by a postdoctoral fellowship at Ecole Normale Supérieure Lyon (France, 2007–2008) and a research stay at the University of Strasbourg (France, 2023) as a visiting scientist. He is currently an associated professor at the Silesian University of Technology, where he leads a research group investigating coordination chemistry oriented to MRI, PET, catalysis and agriculture.



**Prof. Krzysztof Walczak** received his Ph.D. in organic chemistry from the Silesian University of Technology (Poland, 1988) under the supervision of Prof. J. Suwiński. He continued his scientific training as a postdoctoral fellow at the University of Southern Denmark (Denmark, 1989–1992, 1996) in Prof. E. Pedersen's team. In 2004, he obtained the position of professor at the Silesian University of Technology. He has been a full professor since 2011. His current research activities focus on the chemistry of heterocyclic compounds, including their sugar and nucleoside derivatives, the design and synthesis of fluorophores and monomers for optically active polymers. An important part of his research is the design and synthesis of bioactive compounds.